

# Deep Learning and Transformers: Theory, Mathematics, and Implementation

[Author Names]

2026

# Contents

<b>I</b>	<b>Mathematical Foundations</b>	<b>1</b>
<b>1</b>	<b>Linear Algebra for Deep Learning</b>	<b>2</b>
1.1	Vector Spaces and Transformations . . . . .	2
1.1.1	Vectors as Data Representations . . . . .	2
1.1.2	Linear Transformations . . . . .	3
1.1.3	Matrices as Linear Transformations . . . . .	4
1.2	Matrix Operations . . . . .	4
1.2.1	Matrix Multiplication . . . . .	4
1.2.2	Computational Complexity of Matrix Operations . . . . .	5
1.2.3	Batch Matrix Multiplication . . . . .	6
1.2.4	Transpose . . . . .	6
1.2.5	Hardware Context for Matrix Operations . . . . .	7
1.3	Dot Products and Similarity . . . . .	8
1.4	Matrix Decompositions . . . . .	9
1.4.1	Eigenvalues and Eigenvectors . . . . .	9
1.4.2	Singular Value Decomposition . . . . .	10
1.5	Norms and Distance Metrics . . . . .	12
1.6	Practical Deep Learning Examples . . . . .	12
1.6.1	Embedding Layers and Memory Requirements . . . . .	12
1.6.2	Complete Transformer Layer Analysis . . . . .	13
1.6.3	Common Dimension Errors and Debugging . . . . .	13
1.7	BERT-base: A Canonical Worked Analysis . . . . .	14
1.7.1	Architecture Specification . . . . .	14
1.7.2	Parameter Count . . . . .	14
1.7.3	Dimension Tracking Through One Layer . . . . .	15
1.7.4	Activation Memory . . . . .	15
1.7.5	FLOPs Analysis . . . . .	15
1.7.6	Training Memory Budget . . . . .	16
1.7.7	Hardware Timing (NVIDIA A100) . . . . .	16
1.8	Exercises . . . . .	16
1.9	Solutions . . . . .	18
<b>2</b>	<b>Calculus and Optimization</b>	<b>19</b>
2.1	Multivariable Calculus . . . . .	19
2.1.1	Partial Derivatives . . . . .	19
2.1.2	Gradients . . . . .	20
2.1.3	The Chain Rule . . . . .	20
2.1.4	Jacobian and Hessian Matrices . . . . .	21
2.2	Gradient Descent . . . . .	21
2.2.1	The Gradient Descent Algorithm . . . . .	21
2.2.2	Stochastic Gradient Descent (SGD) . . . . .	22
2.2.3	Momentum . . . . .	23
2.2.4	Adam Optimizer . . . . .	24

2.3	Gradient Computation Complexity . . . . .	26
2.3.1	FLOPs for Gradient Computation . . . . .	26
2.3.2	Memory Requirements for Activations . . . . .	27
2.3.3	Automatic Differentiation: Forward vs Reverse Mode . . . . .	27
2.3.4	Gradient Checkpointing . . . . .	28
2.4	Backpropagation . . . . .	29
2.4.1	Computational Graphs . . . . .	29
2.4.2	Backpropagation Algorithm . . . . .	30
2.4.3	Why Backpropagation is $O(n)$ Not $O(n^2)$ . . . . .	30
2.5	Optimizer Memory Requirements . . . . .	31
2.5.1	Memory Comparison by Optimizer . . . . .	31
2.5.2	Impact on GPU Memory Budget . . . . .	32
2.6	Learning Rate Schedules . . . . .	33
2.6.1	Learning Rate Impact on Convergence and GPU Utilization . . . . .	33
2.6.2	Learning Rate Scaling with Batch Size . . . . .	33
2.6.3	Practical Learning Rates for Transformers . . . . .	33
2.6.4	Common Schedules . . . . .	34
2.7	Exercises . . . . .	34
2.8	Solutions . . . . .	36
<b>3</b>	<b>Probability and Information Theory</b>	<b>37</b>
3.1	Probability Fundamentals . . . . .	37
3.1.1	Random Variables and Distributions . . . . .	37
3.1.2	Conditional Probability and Bayes' Theorem . . . . .	38
3.2	Information Theory . . . . .	38
3.2.1	Entropy . . . . .	38
3.2.2	Cross-Entropy . . . . .	39
3.2.3	Kullback-Leibler Divergence . . . . .	39
3.3	Practical Considerations for Cross-Entropy and Softmax . . . . .	40
3.4	KL Divergence in Practice . . . . .	40
3.4.1	Applications in Modern Deep Learning . . . . .	40
3.4.2	Numerical Stability Considerations . . . . .	41
3.5	Exercises . . . . .	41
3.6	Solutions . . . . .	42
<b>II</b>	<b>Neural Network Fundamentals</b>	<b>43</b>
<b>4</b>	<b>Feed-Forward Neural Networks</b>	<b>44</b>
4.1	From Linear Models to Neural Networks . . . . .	44
4.1.1	The Perceptron . . . . .	44
4.1.2	Multi-Class Classification: Softmax Regression . . . . .	44
4.2	Multi-Layer Perceptrons . . . . .	45
4.2.1	Why Depth Matters . . . . .	46
4.3	Memory and Computation Analysis . . . . .	46
4.4	Activation Functions . . . . .	46
4.4.1	Computational Cost of Activation Functions . . . . .	46
4.4.2	Why GELU is Preferred in Transformers . . . . .	47
4.5	Universal Approximation Theorem . . . . .	47
4.6	Weight Initialization . . . . .	47
4.6.1	Variance Preservation Through Layers . . . . .	48
4.7	Regularization . . . . .	48
4.7.1	L2 Regularization . . . . .	48
4.7.2	Dropout . . . . .	49

4.7.3	Dropout in Practice . . . . .	49
4.8	Exercises . . . . .	49
4.9	Solutions . . . . .	49
<b>5</b>	<b>Convolutional Neural Networks</b>	<b>50</b>
5.1	Convolution Operation . . . . .	50
5.1.1	Output Dimensions . . . . .	50
5.2	Multi-Channel Convolutions . . . . .	51
5.3	Computational Analysis of Convolutions . . . . .	51
5.3.1	FLOPs for Convolution Operations . . . . .	51
5.3.2	Memory Requirements for Feature Maps . . . . .	52
5.3.3	GPU Optimization: im2col and Winograd . . . . .	53
5.3.4	Comparison with Transformer Attention . . . . .	54
5.4	Pooling Layers . . . . .	55
5.5	Classic Architectures . . . . .	55
5.5.1	VGG-16 (2014) . . . . .	55
5.5.2	ResNet (2015) . . . . .	55
5.6	Batch Normalization . . . . .	55
5.7	Exercises . . . . .	56
5.8	Solutions . . . . .	56
<b>6</b>	<b>Recurrent Neural Networks</b>	<b>57</b>
6.1	Vanilla RNNs . . . . .	57
6.1.1	Backpropagation Through Time (BPTT) . . . . .	58
6.1.2	Vanishing and Exploding Gradients . . . . .	58
6.1.3	Quantitative Analysis of Gradient Decay . . . . .	59
6.2	Long Short-Term Memory (LSTM) . . . . .	60
6.2.1	LSTM Computational Analysis . . . . .	61
6.3	Gated Recurrent Unit (GRU) . . . . .	62
6.4	Bidirectional RNNs . . . . .	62
6.5	RNN Applications . . . . .	62
6.6	RNNs vs Transformers: A Computational Comparison . . . . .	63
6.7	Exercises . . . . .	63
6.8	Solutions . . . . .	64
<b>III</b>	<b>Attention Mechanisms</b>	<b>65</b>
<b>7</b>	<b>Attention Mechanisms: Fundamentals</b>	<b>66</b>
7.1	Motivation: The Seq2Seq Bottleneck . . . . .	66
7.1.1	RNN Encoder-Decoder Architecture . . . . .	66
7.1.2	Attention Solution . . . . .	67
7.2	Additive Attention (Bahdanau) . . . . .	68
7.3	Scaled Dot-Product Attention . . . . .	71
7.3.1	Why Scaling Matters: Variance Analysis . . . . .	71
7.3.2	Computational Efficiency . . . . .	73
7.4	Attention Score Computation Methods . . . . .	75
7.5	Query-Key-Value Paradigm . . . . .	75
7.5.1	Intuition . . . . .	75
7.5.2	Projecting to QKV . . . . .	76
7.6	Hardware Implications of Attention . . . . .	78
7.7	Attention Variants . . . . .	78
7.7.1	Self-Attention vs Cross-Attention . . . . .	78
7.7.2	Masked Attention . . . . .	78
7.8	Exercises . . . . .	78

7.9	Solutions	79
<b>8</b>	<b>Self-Attention and Multi-Head Attention</b>	<b>80</b>
8.1	Self-Attention Mechanism	80
8.1.1	Hardware Considerations and Memory Layout	82
8.2	Multi-Head Attention	82
8.2.1	Parallel Computation and Memory Layout	83
8.2.2	Tensor Core Utilization	84
8.3	Positional Encoding	85
8.3.1	Positional Encoding Variants	86
8.4	Computational Complexity	87
8.4.1	Memory Complexity Analysis	87
8.4.2	Time Complexity Breakdown	87
8.4.3	Scaling Experiments	88
8.5	Causal (Masked) Self-Attention	88
8.5.1	Efficient Causal Mask Implementation	89
8.6	Attention Patterns and Interpretability	90
8.7	Hardware-Specific Optimizations	90
8.7.1	Flash Attention	90
8.7.2	Fused Kernels	91
8.7.3	Tensor Core Optimization	91
8.8	Memory-Efficient Attention Variants	92
8.9	Exercises	92
8.10	Solutions	92
<b>9</b>	<b>Attention Variants and Mechanisms</b>	<b>93</b>
9.1	Cross-Attention	93
9.1.1	Transformer Decoder Attention Layers	94
9.2	Relative Position Representations	94
9.2.1	Shaw et al. Relative Attention	94
9.2.2	T5 Relative Position Bias	95
9.3	Alternative Attention Scoring Functions	95
9.4	Attention Masking	95
9.4.1	Padding Mask	95
9.4.2	Combined Masks	96
9.5	Attention Dropout	96
9.6	Layer Normalization with Attention	96
9.6.1	Post-Norm (Original Transformer)	96
9.6.2	Pre-Norm (More Common Now)	96
9.7	Visualizing Attention	96
9.7.1	Attention Heatmaps	97
9.7.2	Interpreting Multiple Heads	97
9.8	Practical Implementation Considerations	97
9.8.1	Memory-Efficient Attention	97
9.8.2	Fused Attention Kernels	97
9.9	Efficient Attention Variants	98
9.9.1	Local Attention	98
9.9.2	Sparse Attention	98
9.9.3	Linear Attention	99
9.9.4	Low-Rank Attention	100
9.9.5	Comprehensive Complexity Comparison	100
9.9.6	Implementation Considerations	101
9.10	Exercises	102
9.11	Solutions	103

<b>IV Transformer Architecture</b>	<b>104</b>
<b>10 The Transformer Model</b>	<b>105</b>
10.1 Transformer Architecture Overview . . . . .	105
10.1.1 High-Level Structure . . . . .	105
10.2 Transformer Encoder . . . . .	106
10.2.1 Single Encoder Layer . . . . .	106
10.2.2 Complete Encoder Stack . . . . .	108
10.3 Position-wise Feed-Forward Networks . . . . .	109
10.4 Transformer Decoder . . . . .	111
10.4.1 Single Decoder Layer . . . . .	111
10.4.2 Complete Decoder Stack . . . . .	112
10.5 Computational Analysis . . . . .	114
10.6 Complete Transformer Architecture . . . . .	115
10.6.1 Full Encoder-Decoder Model . . . . .	115
10.6.2 Original Transformer Configuration . . . . .	115
10.7 Residual Connections and Layer Normalization . . . . .	115
10.7.1 Residual Connections . . . . .	115
10.7.2 Layer Normalization . . . . .	116
10.7.3 Pre-Norm vs Post-Norm . . . . .	117
10.8 Training Objectives . . . . .	118
10.8.1 Sequence-to-Sequence Training . . . . .	118
10.8.2 Autoregressive Generation . . . . .	119
10.9 Transformer Variants: Architectural Patterns . . . . .	119
10.10 Exercises . . . . .	119
10.11 Solutions . . . . .	120
<b>11 Training Transformers</b>	<b>121</b>
11.1 Training Objectives and Loss Functions . . . . .	121
11.1.1 Masked Language Modeling . . . . .	122
11.1.2 Causal Language Modeling . . . . .	122
11.1.3 Sequence-to-Sequence Training . . . . .	123
11.2 Backpropagation Through Transformers . . . . .	123
11.2.1 Gradient Flow Analysis . . . . .	124
11.2.2 Gradients Through Residual Connections . . . . .	124
11.2.3 Gradients Through Layer Normalization . . . . .	125
11.2.4 Gradients Through Attention . . . . .	125
11.2.5 Gradients Through Feed-Forward Networks . . . . .	126
11.2.6 Computational Cost of Backpropagation . . . . .	127
11.3 Optimization Algorithms . . . . .	127
11.3.1 Adam Optimizer . . . . .	127
11.3.2 AdamW: Decoupled Weight Decay . . . . .	128
11.3.3 LAMB: Large Batch Training . . . . .	128
11.3.4 Optimizer Memory Comparison . . . . .	129
11.4 Learning Rate Schedules . . . . .	129
11.4.1 The Necessity of Warmup . . . . .	130
11.4.2 Warmup Plus Linear Decay . . . . .	130
11.4.3 Inverse Square Root Decay . . . . .	130
11.4.4 Cosine Annealing . . . . .	131
11.5 Mixed Precision Training . . . . .	131
11.5.1 FP16 Training Algorithm . . . . .	131
11.5.2 Memory Savings . . . . .	132
11.5.3 Hardware Acceleration . . . . .	133
11.5.4 BF16: An Alternative to FP16 . . . . .	133

11.6	Gradient Accumulation . . . . .	134
11.6.1	Algorithm and Implementation . . . . .	134
11.6.2	Trade-offs and Considerations . . . . .	134
11.6.3	Practical Example . . . . .	135
11.7	Gradient Checkpointing . . . . .	135
11.7.1	The Memory-Computation Trade-off . . . . .	136
11.7.2	Implementation Strategies . . . . .	136
11.7.3	Practical Impact . . . . .	137
11.7.4	When to Use Gradient Checkpointing . . . . .	137
11.8	Distributed Training Strategies . . . . .	138
11.8.1	Data Parallelism . . . . .	138
11.8.2	Model Parallelism . . . . .	138
11.8.3	Pipeline Parallelism . . . . .	139
11.8.4	Tensor Parallelism . . . . .	139
11.8.5	ZeRO: Zero Redundancy Optimizer . . . . .	140
11.8.6	Comparison of Strategies . . . . .	140
11.9	Batch Size and Sequence Length Selection . . . . .	141
11.9.1	Batch Size Considerations . . . . .	141
11.9.2	Memory Scaling with Batch Size . . . . .	142
11.9.3	Sequence Length Considerations . . . . .	142
11.9.4	Dynamic Batching . . . . .	143
11.9.5	Practical Guidelines . . . . .	143
11.10	Regularization Techniques . . . . .	144
11.10.1	Dropout . . . . .	144
11.10.2	Weight Decay . . . . .	144
11.10.3	Label Smoothing . . . . .	145
11.10.4	Gradient Clipping . . . . .	145
11.11	Training Time and Cost Estimates . . . . .	146
11.12	Exercises . . . . .	146
11.13	Solutions . . . . .	148
<b>12</b>	<b>Computational Analysis of Transformers</b>	<b>149</b>
12.1	Computational Complexity . . . . .	149
12.1.1	Self-Attention Complexity . . . . .	149
12.1.2	Feed-Forward Network Complexity . . . . .	151
12.1.3	Per-Layer Total Complexity . . . . .	152
12.1.4	Complexity Analysis . . . . .	153
12.2	Memory Requirements . . . . .	153
12.2.1	Model Parameters . . . . .	153
12.2.2	Activation Memory . . . . .	154
12.2.3	Training Memory Budget . . . . .	156
12.2.4	Hardware Selection Guide . . . . .	158
12.3	Inference Optimization . . . . .	158
12.3.1	KV Caching for Autoregressive Decoding . . . . .	158
12.3.2	Batched Inference . . . . .	160
12.3.3	Quantization for Inference . . . . .	160
12.3.4	Model Distillation . . . . .	161
12.3.5	Inference Optimization Summary . . . . .	161
12.4	Scaling Laws . . . . .	161
12.5	Exercises . . . . .	161
12.6	Solutions . . . . .	162

<b>V</b>	<b>Modern Transformer Variants</b>	<b>166</b>
<b>13</b>	<b>BERT: Bidirectional Encoder Representations</b>	<b>167</b>
13.1	BERT Architecture . . . . .	167
13.1.1	Model Specification . . . . .	167
13.1.2	Parameter Breakdown and Memory Requirements . . . . .	168
13.1.3	Input Representation . . . . .	169
13.2	Pre-Training Objectives . . . . .	170
13.2.1	Masked Language Modeling (MLM) . . . . .	170
13.2.2	Next Sentence Prediction (NSP) . . . . .	171
13.3	Training Details and Computational Cost . . . . .	172
13.3.1	Hardware and Training Configuration . . . . .	172
13.3.2	Computational Cost Analysis . . . . .	172
13.4	Fine-Tuning BERT . . . . .	173
13.4.1	Fine-Tuning Procedure and Memory Requirements . . . . .	173
13.4.2	Classification Tasks . . . . .	173
13.4.3	Token-Level Tasks . . . . .	173
13.4.4	Question Answering (SQuAD) . . . . .	174
13.5	BERT Variants . . . . .	174
13.5.1	RoBERTa (Robustly Optimized BERT) . . . . .	174
13.5.2	ALBERT (A Lite BERT) . . . . .	175
13.5.3	DistilBERT: Knowledge Distillation for Compression . . . . .	176
13.5.4	Memory and Speed Comparisons . . . . .	176
13.6	Hardware Requirements and Deployment . . . . .	178
13.6.1	GPU Memory Requirements . . . . .	178
13.6.2	Batch Size Limits by GPU Type . . . . .	178
13.6.3	Inference Speed Analysis . . . . .	179
13.7	Analysis and Interpretability . . . . .	180
13.7.1	What BERT Learns . . . . .	180
13.7.2	Probing Tasks . . . . .	180
13.8	Exercises . . . . .	180
13.9	Solutions . . . . .	181
<b>14</b>	<b>GPT: Generative Pre-Training</b>	<b>182</b>
14.1	GPT Architecture . . . . .	182
14.1.1	Decoder-Only Transformers . . . . .	182
14.1.2	GPT Model Sizes . . . . .	183
14.2	Pre-Training: Autoregressive Language Modeling . . . . .	186
14.2.1	Training Objective . . . . .	186
14.2.2	Pre-Training Data . . . . .	187
14.2.3	Training Infrastructure and Costs . . . . .	188
14.3	In-Context Learning and Few-Shot Prompting . . . . .	188
14.3.1	Autoregressive Generation with KV Caching . . . . .	188
14.3.2	Zero-Shot, One-Shot, Few-Shot . . . . .	190
14.3.3	Zero-Shot, One-Shot, Few-Shot . . . . .	190
14.3.4	Emergent Abilities . . . . .	191
14.4	Scaling Laws . . . . .	192
14.4.1	Parameter Scaling . . . . .	192
14.4.2	Compute-Optimal Training . . . . .	193
14.4.3	Hardware Requirements for Inference . . . . .	194
14.5	Instruction Tuning and RLHF . . . . .	195
14.5.1	Instruction Tuning . . . . .	195
14.5.2	RLHF (Reinforcement Learning from Human Feedback) . . . . .	196
14.6	GPT Capabilities and Limitations . . . . .	196



14.6.1	Capabilities . . . . .	196
14.6.2	Limitations . . . . .	196
14.7	Exercises . . . . .	197
14.8	Solutions . . . . .	197
<b>15</b>	<b>T5 and BART: Encoder-Decoder Architectures</b>	<b>198</b>
15.1	T5: Text-to-Text Transfer Transformer . . . . .	198
15.1.1	Unified Text-to-Text Framework . . . . .	198
15.1.2	T5 Architecture . . . . .	199
15.1.3	Pre-Training Objective: Span Corruption . . . . .	201
15.1.4	T5 Model Sizes and Scaling . . . . .	202
15.1.5	T5 Training Details . . . . .	203
15.2	BART: Denoising Autoencoder . . . . .	205
15.2.1	BART Architecture and Design Philosophy . . . . .	205
15.2.2	BART Parameter Breakdown and Memory Requirements . . . . .	205
15.2.3	Denoising Objectives and Corruption Strategies . . . . .	206
15.2.4	BART Training Details . . . . .	208
15.3	Encoder-Decoder Efficiency Analysis . . . . .	209
15.3.1	Computational Cost of Cross-Attention . . . . .	209
15.3.2	Comparison: Encoder-Decoder vs Decoder-Only . . . . .	210
15.4	Comparing T5 and BART . . . . .	211
15.5	Prefix Language Models . . . . .	212
15.5.1	Prefix LM Objective . . . . .	212
15.6	Applications and Fine-tuning . . . . .	212
15.6.1	Summarization . . . . .	212
15.6.2	Translation . . . . .	213
15.6.3	Question Answering . . . . .	213
15.7	Mixture of Denoisers (UL2) . . . . .	213
15.8	Exercises . . . . .	213
15.9	Solutions . . . . .	214
<b>16</b>	<b>Efficient Transformers</b>	<b>215</b>
16.1	The Quadratic Bottleneck . . . . .	215
16.1.1	Complexity Analysis . . . . .	215
16.2	Sparse Attention Patterns . . . . .	216
16.2.1	Efficiency Taxonomy . . . . .	216
16.2.2	Fixed Sparse Patterns . . . . .	216
16.2.3	BigBird: Random + Window + Global . . . . .	218
16.3	Linear Attention Methods . . . . .	218
16.3.1	Linformer . . . . .	219
16.3.2	Performer (Kernel-based) . . . . .	220
16.4	Memory-Efficient Attention . . . . .	221
16.4.1	Flash Attention . . . . .	221
16.4.2	Memory-Efficient Transformers . . . . .	222
16.5	Comparison of Efficient Methods . . . . .	223
16.5.1	Comprehensive Benchmarks . . . . .	223
16.5.2	Memory Scaling Analysis . . . . .	223
16.5.3	Speed Benchmarks on A100 GPU . . . . .	223
16.5.4	Quality Trade-offs . . . . .	224
16.5.5	When to Use Each Method . . . . .	224
16.6	Long-Context Models . . . . .	225
16.6.1	Longformer . . . . .	225
16.6.2	Reformer . . . . .	225
16.7	Exercises . . . . .	226

16.8 Solutions . . . . .	227
--------------------------	-----

## VI Advanced Topics 228

### 17 Vision Transformers 229

17.1 From Images to Sequences . . . . .	229
17.1.1 The Patch Embedding Approach . . . . .	229
17.1.2 Position Encodings for 2D . . . . .	230
17.2 Vision Transformer (ViT) Architecture . . . . .	230
17.2.1 Complete ViT Model . . . . .	230
17.2.2 ViT Model Variants . . . . .	231
17.2.3 Memory Requirements and Computational Analysis . . . . .	231
17.3 Training Vision Transformers . . . . .	232
17.3.1 Pre-training Strategies . . . . .	232
17.3.2 Data Augmentation and Regularization . . . . .	233
17.3.3 DeiT: Data-efficient Image Transformers . . . . .	233
17.4 Masked Autoencoders (MAE) . . . . .	233
17.4.1 Self-Supervised Pre-training for Vision . . . . .	233
17.5 Hierarchical Vision Transformers . . . . .	234
17.5.1 Motivation for Hierarchical Architectures . . . . .	234
17.5.2 Swin Transformer . . . . .	234
17.5.3 Pyramid Vision Transformer (PVT) . . . . .	236
17.5.4 Hybrid Architectures: CoAtNet . . . . .	236
17.6 ViT vs CNN Comparison . . . . .	237
17.6.1 Parameter Efficiency . . . . .	237
17.6.2 Computational Complexity Analysis . . . . .	237
17.6.3 Data Requirements and Inductive Bias . . . . .	238
17.6.4 When to Use Each Architecture . . . . .	239
17.7 Exercises . . . . .	239
17.8 Solutions . . . . .	240

### 18 Multimodal Transformers 241

18.1 Multimodal Learning Fundamentals . . . . .	241
18.1.1 Fusion Strategies . . . . .	241
18.1.2 Alignment Objectives . . . . .	242
18.2 CLIP: Contrastive Language-Image Pre-training . . . . .	242
18.2.1 CLIP Architecture . . . . .	242
18.2.2 Computational Analysis of CLIP Training . . . . .	243
18.2.3 Zero-Shot Classification with CLIP . . . . .	244
18.2.4 CLIP Variants and Training Requirements . . . . .	245
18.3 DALL-E and Stable Diffusion . . . . .	245
18.3.1 DALL-E: Text-to-Image Generation . . . . .	245
18.3.2 Stable Diffusion . . . . .	246
18.4 Vision-Language Understanding . . . . .	246
18.4.1 BLIP: Bootstrapped Language-Image Pre-training . . . . .	246
18.4.2 Flamingo: Few-Shot Learning . . . . .	247
18.5 Computational Analysis of Multimodal Transformers . . . . .	248
18.6 Training Challenges for Multimodal Transformers . . . . .	248
18.6.1 Batch Size Requirements for Contrastive Learning . . . . .	248
18.6.2 Distributed Training and Memory Optimization . . . . .	248
18.7 Audio Transformers . . . . .	249
18.7.1 Whisper: Speech Recognition . . . . .	249
18.7.2 Audio-Text Pre-training . . . . .	250

18.8	Unified Multimodal Models	250
18.8.1	Perceiver and Perceiver IO	250
18.8.2	GPT-4V and LLaVA	250
18.9	Exercises	251
18.10	Solutions	251
<b>19</b>	<b>Long Context Transformers</b>	<b>252</b>
19.1	Context Length Limitations	252
19.1.1	The Quadratic Memory Bottleneck	252
19.2	Position Encoding for Long Context	253
19.2.1	The Extrapolation Challenge	253
19.2.2	Position Interpolation	254
19.2.3	Rotary Position Embedding (RoPE)	255
19.2.4	ALiBi: Attention with Linear Biases	256
19.3	Efficient Attention for Long Context	257
19.3.1	Sparse Attention Patterns	257
19.3.2	Longformer and BigBird	257
19.3.3	Comparison of Sparse Attention Methods	257
19.4	Recurrent Transformers	258
19.4.1	Transformer-XL	258
19.5	Retrieval-Augmented Generation	258
19.5.1	RAG Architecture	258
19.5.2	RETRO: Retrieval-Enhanced Transformer	259
19.6	Memory-Augmented Transformers	259
19.6.1	Compressive Transformer	259
19.6.2	Memorizing Transformers	260
19.7	Long Context Models in Practice	260
19.7.1	LongT5: Efficient Encoder-Decoder	260
19.7.2	Production Long Context Systems	261
19.7.3	Practical Considerations for Long Context	261
19.8	Comparison and Trade-offs	262
19.8.1	Method Comparison	262
19.8.2	Hardware and Memory Considerations	262
19.8.3	Recommendations by Use Case	263
19.9	Exercises	264
19.10	Solutions	267
<b>20</b>	<b>Pre-training Strategies and Transfer Learning</b>	<b>268</b>
20.1	Pre-training Objectives	268
20.1.1	Language Modeling Objectives	268
20.1.2	Denoising Objectives	269
20.1.3	Contrastive Objectives	269
20.2	Data Curation and Processing	269
20.2.1	Data Scale and Requirements	269
20.2.2	Data Quality versus Quantity	270
20.2.3	Data Filtering and Cleaning	271
20.2.4	Data Deduplication	271
20.3	Training Compute Requirements	272
20.3.1	FLOPs Analysis	272
20.3.2	GPU-Hours and Cost Estimates	273
20.3.3	Scaling Laws	273
20.4	Curriculum Learning	273
20.4.1	Progressive Training Strategies	273
20.4.2	Progressive Training	274

20.4.3	Domain-Adaptive Pre-training	275
20.5	Hardware Requirements and Infrastructure	275
20.5.1	BERT-base Training Infrastructure	275
20.5.2	GPT-3 Training Infrastructure	276
20.5.3	LLaMA-65B Training Infrastructure	276
20.6	Efficient Pre-training Techniques	277
20.7	Parameter-Efficient Fine-tuning	277
20.7.1	Motivation	277
20.7.2	LoRA: Low-Rank Adaptation	277
20.7.3	Adapter Layers	278
20.7.4	Prompt Tuning	278
20.8	Multi-Task and Multi-Stage Pre-training	279
20.8.1	Multi-Task Pre-training	279
20.8.2	Multi-Stage Pre-training	279
20.9	Transfer Learning Analysis	280
20.9.1	Measuring Transfer	280
20.9.2	What Makes Good Pre-training?	280
20.10	Exercises	280
20.11	Solutions	281

## VII Practical Implementation 282

### 21 Implementing Transformers in PyTorch 283

21.1	Multi-Head Attention Implementation	283
21.1.1	Core Components	283
21.1.2	Memory-Efficient Attention	284
21.1.3	Dimension Tracking Example	285
21.2	Position Encodings	285
21.2.1	Sinusoidal Encoding	285
21.2.2	Learned Positional Embeddings	285
21.3	Masking Strategies	285
21.3.1	Causal Mask for GPT	285
21.3.2	Padding Mask	285
21.4	Training Optimizations	286
21.4.1	Fused Kernels for Layer Normalization	286
21.4.2	Mixed Precision Training	286
21.4.3	Gradient Accumulation	287
21.4.4	Gradient Checkpointing	288
21.5	Model Initialization	289
21.5.1	Best Practices	289
21.6	Memory Profiling and Optimization	289
21.6.1	Understanding Memory Usage	289
21.6.2	Identifying Memory Bottlenecks	290
21.6.3	Optimization Strategies	290
21.6.4	Case Study: Optimizing BERT-base	291
21.7	Debugging Transformers	292
21.7.1	Common Issues	292
21.7.2	Validation Checks	292
21.8	Inference Optimization	293
21.8.1	TorchScript Compilation	293
21.8.2	KV Cache for Autoregressive Generation	293
21.8.3	ONNX Export	295
21.8.4	TensorRT Optimization	296

21.8.5	Quantization	297
21.8.6	Inference Benchmarking	299
21.9	Complete Training Pipeline	300
21.9.1	Training Script Structure	300
21.10	Production Optimizations	301
21.10.1	Putting It Together	301
21.10.2	Comprehensive Benchmarks	301
21.11	Distributed Training	302
21.11.1	Data Parallel	302
21.11.2	Distributed Data Parallel (DDP)	302
21.12	Performance Optimization	303
21.12.1	DataLoader Optimization	303
21.12.2	Asynchronous Data Transfer	303
21.12.3	Profiling with torch.profiler	303
21.12.4	Batch Size Tuning	304
21.12.5	Compilation with torch.compile	305
21.13	Distributed Training Implementation	306
21.13.1	Understanding Distributed Strategies	306
21.13.2	DistributedDataParallel Setup	306
21.13.3	Gradient Synchronization	307
21.13.4	Scaling Efficiency	308
21.14	Exercises	308
21.15	Solutions	310
<b>22</b>	<b>From PyTorch to Accelerator Silicon</b>	<b>311</b>
22.1	The Two Phases of Inference: Prefill and Decode	312
22.2	The Seven-Layer Inference Stack	312
22.2.1	Backend Cheat Sheet	313
22.2.2	Latency and Bandwidth Ladder	313
22.3	Layer 7: The Model Definition	313
22.3.1	Why Multi-Device Execution Is Required	314
22.3.2	Tensor Parallelism: Splitting Weight Matrices	314
22.3.3	Pipeline Parallelism	315
22.3.4	Expert Parallelism	316
22.3.5	Context Parallelism and Sequence Parallelism	316
22.3.6	Parallelism Selection Framework	316
22.4	Layer 6: Frontend Runtime	317
22.4.1	Eager Mode (NVIDIA, AMD)	317
22.4.2	Lazy Tensor Mode (TPU, Trainium)	317
22.4.3	Graph Capture, Compilation, and Replay	317
22.4.4	Process Groups and Communicators	318
22.5	Layer 5: Graph Compilation	318
22.5.1	Four Optimization Mechanisms	318
22.5.2	Fusion Taxonomy	318
22.5.3	Static Shapes and Shape Bucketing	319
22.5.4	When Compilation Hurts	319
22.6	Layer 4: Inference Engines	319
22.6.1	Continuous Batching	319
22.6.2	PagedAttention: Virtual Memory for the KV-Cache	319
22.6.3	vLLM and PagedAttention	320
22.6.4	Multi-Device Orchestration	320
22.6.5	Request Lifecycle	320
22.6.6	Throughput vs. Latency Tuning Profiles	320
22.7	Layer 3: Device Kernels and Collectives	320

22.7.1	The Memory Hierarchy Problem . . . . .	321
22.7.2	Compute-Bound vs. Memory-Bound: The Roofline . . . . .	321
22.7.3	Coalesced Memory Access and Bank Conflicts . . . . .	322
22.7.4	Flash Attention . . . . .	322
22.7.5	Collective Communication . . . . .	322
22.7.6	Kernel Failure Modes . . . . .	322
22.8	Layers 2 and 1: Device Compiler and Accelerator Hardware . . . . .	323
22.8.1	Layer 2: Device Compiler and Runtime . . . . .	323
22.8.2	Layer 1: Accelerator Hardware . . . . .	323
22.8.3	How to Read Spec Sheets Without Fooling Yourself . . . . .	323
22.8.4	Workload-to-Hardware Fit . . . . .	323
22.9	Quantization: Precision, Performance, and Trade-offs . . . . .	323
22.9.1	Quantization Taxonomy . . . . .	323
22.9.2	Quantization Fundamentals . . . . .	324
22.9.3	Post-Training Quantization (PTQ) . . . . .	324
22.9.4	Quantization-Aware Training (QAT) . . . . .	325
22.9.5	Accuracy and Stability Trade-offs . . . . .	325
22.9.6	Quantization Decision Heuristics . . . . .	325
22.10	Model Pruning . . . . .	325
22.10.1	Pruning Strategies . . . . .	325
22.10.2	Iterative Pruning . . . . .	326
22.11	Knowledge Distillation . . . . .	326
22.11.1	DistilBERT Approach . . . . .	326
22.12	Bottleneck-Driven Optimization . . . . .	326
22.12.1	Bottleneck Taxonomy . . . . .	326
22.12.2	Diagnosis Workflow . . . . .	327
22.12.3	Optimization Impact Summary . . . . .	327
22.12.4	Case Study: Interactive Chatbot (Decode-Heavy) . . . . .	327
22.12.5	Case Study: Batch Document Summarization (Prefill-Heavy) . . . . .	328
22.13	Production Deployment . . . . .	328
22.13.1	Serving Frameworks . . . . .	328
22.13.2	Distributed Inference with Ray and Kubernetes . . . . .	328
22.13.3	Deployment Checklist . . . . .	328
22.13.4	Hardware Selection . . . . .	329
22.14	Key Takeaways and Engineering Decision Checklist . . . . .	329
22.14.1	Principles . . . . .	329
22.14.2	Engineering Decision Checklist . . . . .	330
22.15	Worked End-to-End Token Trace . . . . .	330
22.16	Exercises . . . . .	330
22.17	Solutions . . . . .	332
<b>23</b>	<b>Best Practices and Production Case Studies</b>	<b>333</b>
23.1	Model Selection . . . . .	333
23.1.1	Architecture Selection Framework . . . . .	333
23.1.2	Model Size Selection . . . . .	334
23.1.3	Pre-trained versus Training from Scratch . . . . .	334
23.1.4	Cost-Benefit Analysis . . . . .	334
23.2	Training Best Practices . . . . .	335
23.2.1	Learning Rate Selection . . . . .	335
23.2.2	Batch Size Selection . . . . .	335
23.2.3	Checkpointing and Monitoring Strategy . . . . .	335
23.3	Memory Management . . . . .	335
23.3.1	Out-of-Memory Decision Checklist . . . . .	336
23.3.2	Memory Estimation Rule of Thumb . . . . .	336

23.4	Debugging Transformers . . . . .	336
23.4.1	Systematic Debugging Workflow . . . . .	336
23.4.2	Gradient Analysis . . . . .	337
23.4.3	Common Training Issues: Quick Reference . . . . .	337
23.5	Inference Optimization . . . . .	337
23.5.1	Optimizing for Latency . . . . .	337
23.5.2	Optimizing for Throughput . . . . .	338
23.5.3	Hardware Selection Summary . . . . .	338
23.6	Cost Optimization . . . . .	338
23.6.1	Training Cost Analysis . . . . .	338
23.6.2	Training Time Estimation . . . . .	338
23.6.3	Inference Cost Analysis . . . . .	339
23.6.4	Cost Optimization Strategies . . . . .	339
23.7	Production Deployment . . . . .	339
23.7.1	Deployment Checklist . . . . .	340
23.8	Practical Checklists . . . . .	340
23.8.1	Before Training Checklist . . . . .	340
23.8.2	During Training Checklist . . . . .	340
23.8.3	Before Deployment Checklist . . . . .	341
23.9	Hyperparameter Tuning . . . . .	341
23.9.1	Critical Hyperparameters (Ordered by Impact) . . . . .	341
23.9.2	Tuning Strategy . . . . .	342
23.10	Common Pitfalls and Solutions . . . . .	342
23.10.1	Architecture Pitfalls . . . . .	342
23.10.2	Training Pitfalls . . . . .	343
23.10.3	Deployment Pitfalls . . . . .	343
23.11	Case Study: BERT for Search Ranking . . . . .	343
23.11.1	Problem Setup . . . . .	343
23.11.2	Architecture Decisions . . . . .	343
23.11.3	Training Strategy . . . . .	344
23.11.4	Production Deployment . . . . .	344
23.12	Case Study: GPT for Code Generation . . . . .	344
23.12.1	Problem Setup . . . . .	344
23.12.2	Model and Data . . . . .	344
23.12.3	Training . . . . .	345
23.12.4	Evaluation . . . . .	345
23.13	Future Directions . . . . .	345
23.13.1	Architectural Innovations . . . . .	345
23.13.2	Training Innovations . . . . .	346
23.14	Conclusion . . . . .	346
23.14.1	Key Takeaways . . . . .	346
23.14.2	Final Advice . . . . .	347
23.15	Exercises . . . . .	347
23.16	Solutions . . . . .	348

## VIII Domain-Specific Applications 349

### 24 Domain-Specific Models 350

24.1	Why Domain-Specific Models? . . . . .	350
24.1.1	Limitations of General-Purpose Models in Specialized Domains . . . . .	351
24.1.2	Example: Legal Document Analysis . . . . .	352
24.2	Patterns of Specialization . . . . .	352
24.2.1	Pattern 1: Prompting and In-Context Learning . . . . .	352

24.2.2	Pattern 2: Retrieval-Augmented Generation (RAG)	353
24.2.3	Pattern 3: Fine-Tuning	354
24.2.4	Pattern 4: Domain-Adaptive Pre-Training	355
24.2.5	Pattern 5: Custom Architecture Design	355
24.3	Decision Framework: Choosing an Approach	356
24.3.1	When to Start Small, Scale Up	356
24.4	Evaluating Domain-Specific Models	356
24.4.1	Task-Specific Metrics	356
24.4.2	Business Metrics	357
24.4.3	Online Evaluation: A/B Testing	357
24.5	Planning the Technical Architecture	357
24.5.1	Deployment Options	357
24.5.2	Pipeline Architecture	357
24.6	Case Study: Evolving from General to Specialized	358
24.7	Continuous Learning and Model Drift	358
24.7.1	Understanding Model Drift	358
24.7.2	Detecting Drift in Production	359
24.7.3	Strategies for Continuous Learning	359
24.7.4	Practical Implementation Considerations	360
24.7.5	Cross-Domain Patterns	360
24.8	Exercises	361
24.9	Solutions	361
<b>25</b>	<b>Enterprise NLP</b>	<b>363</b>
25.1	Enterprise Search and Semantic Retrieval	363
25.1.1	Architecture and Workflow	364
25.1.2	Practical Considerations: Embedding Model Selection	365
25.1.3	Vector Database Operations	365
25.1.4	Case Study: Internal Documentation Search	366
25.2	Text Classification and Tagging in Production	367
25.2.1	Standard Classification Workflow	367
25.2.2	Handling Common Challenges	368
25.2.3	Production Metrics and Monitoring	368
25.2.4	Case Study: Support Ticket Triage	369
25.3	Conversational Assistants and Copilots	369
25.3.1	Architecture: Retrieval-Augmented Generation	369
25.3.2	Prompt Engineering and Guardrails	370
25.3.3	Multi-Turn Context and State Management	370
25.3.4	Human Escalation and Feedback Loops	370
25.3.5	Case Study: Customer Support Bot	371
25.4	Enterprise Constraints and Governance	371
25.4.1	Data Residency and Privacy	371
25.4.2	Handling Sensitive Data	371
25.4.3	Model Explainability and Red-Teaming	372
25.5	Continuous Learning and Model Drift in Enterprise NLP	372
25.5.1	Language Evolution and Concept Drift	372
25.5.2	Case Study: Support Ticket Classification Drift	373
25.6	Exercises	373
25.7	Solutions	373



<b>26 Code as a Domain: Code LLMs and Developer Tooling</b>	<b>374</b>
26.1 Code-Specific Pre-Training	374
26.1.1 Tokenization and Vocabulary	375
26.1.2 Context Window and Code Understanding	376
26.1.3 Pre-Training Data and Curation	376
26.1.4 Model Families and Capabilities	378
26.2 Developer Assistants and IDE Integration	378
26.2.1 Completion Architecture	379
26.2.2 Practical Challenges and Solutions	379
26.3 Code Analysis, Testing, and Refactoring	380
26.3.1 Static Analysis and Bug Detection	380
26.3.2 Test Generation	380
26.3.3 Refactoring and Code Quality Improvement	381
26.4 Repository-Scale Code Understanding	381
26.4.1 Graph-Based Retrieval and Reasoning	381
26.4.2 Documentation and Code Generation from Specifications	382
26.5 Safety, Licensing, and Ethics	382
26.5.1 Licensing and Attribution	382
26.5.2 Data Contamination and Test Leakage	382
26.5.3 Responsible Deployment	382
26.6 Continuous Learning and Drift in Code Models	383
26.6.1 Language Evolution and API Changes	383
26.6.2 Case Study: Adapting to Python 3.11 and 3.12	384
26.7 Case Study: IDE Copilot for Python Development	384
26.7.1 System Design	384
26.7.2 Metrics	384
26.8 Exercises	385
26.9 Solutions	385
<b>27 Video and Visual Content Generation</b>	<b>386</b>
27.1 Vision Transformers and Visual Understanding	387
27.1.1 Vision Transformer Architecture	387
27.1.2 Advantages Over CNNs	388
27.1.3 Computational Requirements and Business Trade-offs	388
27.2 Image Generation with Diffusion Models	389
27.2.1 Diffusion Process Intuition	389
27.2.2 Conditioning with Text for Business Applications	390
27.2.3 Key Advantages for Content Creation	390
27.2.4 State-of-the-Art Text-to-Image Systems	391
27.3 Video Generation with Diffusion Models	391
27.3.1 Video-Specific Challenges and Architectural Solutions	392
27.3.2 Advanced Video Diffusion Architectures	392
27.3.3 Training Video Diffusion Models	393
27.3.4 Practical Inference Optimization	394
27.4 AI-Powered Storyboarding and Pre-Visualization	395
27.4.1 AI Storyboard Generation Pipeline	395
27.4.2 Commercial AI Storyboarding Tools	395
27.4.3 Integration with Production Workflows	396
27.4.4 Future Directions in AI Storyboarding	396
27.5 Virtual Production: Integrating Real Actors with AI-Generated Visual Effects	397
27.5.1 Technical Foundations of Virtual Production	397
27.5.2 AI-Generated Environments and Backgrounds	398
27.5.3 Character Consistency and Digital Doubles	398
27.5.4 Performance Capture and Motion Transfer	399

27.5.5	Integrating Real and Synthetic Elements . . . . .	399
27.5.6	Case Study: Virtual Production for Commercial Advertising . . . . .	400
27.6	Video Understanding and Scene Analysis . . . . .	400
27.6.1	Video Understanding Architectures . . . . .	400
27.6.2	Applications of Video Understanding . . . . .	401
27.7	Automated Video Editing and Effects . . . . .	401
27.7.1	Shot Detection and Segmentation . . . . .	401
27.7.2	Automated Video Summarization . . . . .	402
27.7.3	Special Effects Generation . . . . .	403
27.8	Practical Challenges and Trade-offs . . . . .	403
27.8.1	Computational Requirements . . . . .	403
27.8.2	Quality and Evaluation . . . . .	404
27.8.3	Data Licensing and Attribution . . . . .	405
27.9	Case Study: Automated Video Editing for Content Creators . . . . .	405
27.9.1	System Design . . . . .	405
27.9.2	Results . . . . .	406
27.10	Model Maintenance and Drift in Visual Content Systems . . . . .	407
27.10.1	Domain-Specific Drift Patterns in Visual Content . . . . .	407
27.11	Exercises . . . . .	408
27.12	Solutions . . . . .	408
<b>28</b>	<b>Knowledge Graphs and Semantic Web</b>	<b>409</b>
28.1	Knowledge Graphs as Formal Languages . . . . .	409
28.1.1	Examples of Knowledge Graphs . . . . .	410
28.1.2	Why Knowledge Graphs Matter . . . . .	410
28.2	Entity and Relation Extraction from Text . . . . .	411
28.2.1	Named Entity Recognition (NER) . . . . .	411
28.2.2	Relation Extraction . . . . .	411
28.2.3	Joint Entity and Relation Extraction . . . . .	412
28.3	Knowledge Graph Embeddings . . . . .	413
28.3.1	TransE Model . . . . .	413
28.3.2	Advanced Models: DistMult, ComplEx, RotatE . . . . .	414
28.4	Link Prediction and Reasoning . . . . .	415
28.4.1	Ranking-Based Link Prediction . . . . .	415
28.4.2	Evaluation Metrics . . . . .	415
28.5	Semantic Type Inference and Reasoning . . . . .	415
28.5.1	Type Constraints . . . . .	415
28.5.2	Reasoning Rules . . . . .	416
28.6	Temporal Knowledge Graphs and Dynamic Knowledge . . . . .	416
28.6.1	Temporal Knowledge Representation . . . . .	416
28.6.2	Temporal Reasoning Challenges . . . . .	417
28.6.3	Temporal Embedding Models . . . . .	417
28.6.4	Temporal Link Prediction . . . . .	418
28.6.5	Recent Advances in Temporal Knowledge Graph Reasoning (2024-2025) . . . . .	418
28.7	Graph Neural Networks for Knowledge Graphs . . . . .	419
28.7.1	Relational Graph Convolutional Networks (R-GCN) . . . . .	419
28.7.2	Graph Attention Networks for KGs . . . . .	420
28.7.3	Multi-Hop Reasoning with GNNs . . . . .	420
28.7.4	Practical Implementation . . . . .	420
28.8	Knowledge Graph Completion and Multi-Hop Reasoning . . . . .	421
28.8.1	Path-Based Reasoning . . . . .	421
28.8.2	Neural Logic Programming . . . . .	421
28.8.3	Query Answering Beyond Link Prediction . . . . .	422
28.9	Ontology Alignment and Knowledge Integration . . . . .	422

28.9.1 Entity Alignment Problem . . . . .	423
28.9.2 Embedding-Based Entity Alignment . . . . .	423
28.9.3 Cross-Lingual Knowledge Graph Alignment . . . . .	424
28.9.4 Schema Matching . . . . .	424
28.10 Knowledge-Aware Neural Networks . . . . .	425
28.10.1 Knowledge-Enhanced Embeddings . . . . .	425
28.10.2 Graph Neural Networks (GNNs) for Knowledge Graphs . . . . .	425
28.11 Evaluation Metrics and Quality Assessment . . . . .	425
28.11.1 Filtered vs. Raw Evaluation . . . . .	425
28.11.2 Evaluation Biases . . . . .	426
28.11.3 Human Evaluation . . . . .	426
28.11.4 Downstream Task Evaluation . . . . .	426
28.12 Practical Implementation and Tooling . . . . .	426
28.12.1 Knowledge Graph Storage Systems . . . . .	426
28.12.2 KG Embedding Libraries . . . . .	427
28.12.3 Query APIs and SPARQL . . . . .	428
28.12.4 End-to-End Pipeline Example . . . . .	428
28.13 Cross-Chapter Connections . . . . .	429
28.14 Scalability and Practical Considerations . . . . .	429
28.14.1 Embedding Computational Cost . . . . .	429
28.14.2 Incompleteness and Noise . . . . .	430
28.15 Applications: From Search to Drug Discovery . . . . .	430
28.15.1 Semantic Search and Question Answering . . . . .	430
28.15.2 Biomedical Discovery: Drug-Target Interaction Prediction . . . . .	431
28.15.3 Cybersecurity: Attack Pattern Detection . . . . .	431
28.16 Case Study: Enterprise Knowledge Graph for Customer Intelligence . . . . .	431
28.16.1 Data Sources and Schema . . . . .	431
28.16.2 Applications . . . . .	431
28.16.3 Results . . . . .	431
28.17 Exercises . . . . .	432
28.18 Solutions . . . . .	433
<b>29 Recommendation Systems and Personalization</b>	<b>434</b>
29.1 Sequence-Aware Recommenders . . . . .	435
29.1.1 SASRec: Self-Attentive Sequential Recommendation . . . . .	436
29.1.2 Cold-Start Recommendations with Transformer-Capsule Networks (2024-2025) . . . . .	436
29.2 Feature Engineering and Behavior Language . . . . .	437
29.2.1 DSL for Behavior Data . . . . .	437
29.2.2 Dense and Sparse Features . . . . .	438
29.2.3 Multi-Task Learning for Recommendations . . . . .	439
29.3 Real-Time Serving and Ranking . . . . .	439
29.3.1 Two-Stage Architecture . . . . .	439
29.3.2 Candidate Generation Strategies . . . . .	439
29.3.3 Candidate Generation Strategies . . . . .	439
29.3.4 Ranking Model and Latency Budget . . . . .	440
29.3.5 Real-Time Updates and Freshness . . . . .	440
29.3.6 Real-Time Updates and Freshness . . . . .	440
29.4 Fairness, Diversity, and Filter Bubbles . . . . .	440
29.4.1 Filter Bubble Problem . . . . .	441
29.4.2 Handling Demographic Bias . . . . .	441
29.4.3 Handling Demographic Bias . . . . .	441
29.4.4 A/B Testing for Recommendation Changes . . . . .	442
29.5 Case Study: Video Recommendation for a Streaming Platform . . . . .	442
29.5.1 System Architecture . . . . .	442

29.5.2	Training and Offline Evaluation . . . . .	443
29.5.3	Online A/B Test . . . . .	443
29.6	Model Maintenance and Drift in Recommendation Systems . . . . .	444
29.6.1	Domain-Specific Drift Patterns in Recommendations . . . . .	444
29.7	Exercises . . . . .	445
29.8	Solutions . . . . .	446
<b>30</b>	<b>Healthcare and Life Sciences</b>	<b>447</b>
30.1	Clinical Text and Electronic Health Records (EHRs) . . . . .	448
30.1.1	EHR Data and Domain-Specific Language . . . . .	448
30.1.2	Domain-Adaptive Pre-Training . . . . .	449
30.1.3	Clinical NLP Applications . . . . .	450
30.1.4	Handling Structured + Unstructured Data . . . . .	450
30.2	Medical Imaging Analysis . . . . .	450
30.2.1	Vision Transformers for Medical Imaging . . . . .	450
30.2.2	Domain-Specific Considerations . . . . .	451
30.2.3	Radiologist-in-the-Loop Systems . . . . .	451
30.3	Genomics and Bio-Sequence Models . . . . .	451
30.3.1	Sequence Representation . . . . .	451
30.3.2	ESM: Large-Scale Protein Language Models . . . . .	452
30.3.3	Protein Structure Prediction and Folding . . . . .	452
30.3.4	AI-Driven Drug Discovery . . . . .	455
30.3.5	Case Study: Variant Effect Prediction . . . . .	460
30.4	Regulatory and Clinical Validation . . . . .	460
30.4.1	Clinical Validation Process . . . . .	460
30.4.2	Explainability and Auditing . . . . .	461
30.4.3	Fairness and Bias . . . . .	461
30.5	Case Study: Clinical Risk Prediction at Scale . . . . .	461
30.5.1	System Design . . . . .	461
30.5.2	Results . . . . .	462
30.6	Model Maintenance and Drift in Healthcare AI Systems . . . . .	462
30.6.1	Domain-Specific Drift Patterns in Healthcare . . . . .	463
30.7	Case Study: Clinical Risk Prediction at Scale . . . . .	464
30.7.1	System Design . . . . .	464
30.7.2	Results . . . . .	465
30.8	Exercises . . . . .	465
30.9	Solutions . . . . .	466
<b>31</b>	<b>Finance, Risk, and Time Series Modeling</b>	<b>467</b>
31.1	Market Data and Time Series Forecasting . . . . .	468
31.1.1	Time Series Characteristics . . . . .	468
31.1.2	Transformer-Based Time Series Models . . . . .	468
31.1.3	Addressing Non-Stationarity . . . . .	469
31.1.4	Evaluation and Backtesting . . . . .	469
31.2	Financial NLP . . . . .	469
31.2.1	Financial Domain Text . . . . .	469
31.2.2	Information Extraction . . . . .	470
31.2.3	Sentiment Analysis for Trading . . . . .	470
31.3	Credit Modeling and Risk Management . . . . .	470
31.3.1	Credit Risk Assessment . . . . .	470
31.3.2	Deep Learning for Credit . . . . .	470
31.3.3	Fairness in Credit Decisions . . . . .	471
31.3.4	Explainability for Credit Decisions . . . . .	471
31.4	Risk Management and Regulatory Requirements . . . . .	471

31.4.1	Model Risk Management Framework . . . . .	471
31.4.2	Value at Risk (VaR) Estimation . . . . .	472
31.5	Case Study: Fraud Detection System . . . . .	472
31.5.1	Problem Setup . . . . .	472
31.5.2	Model Architecture . . . . .	472
31.5.3	Results . . . . .	472
31.6	Model Drift in Financial Systems . . . . .	472
31.6.1	Finance-Specific Drift Patterns . . . . .	472
31.6.2	Monitoring and Adaptation . . . . .	473
31.7	Exercises . . . . .	473
31.8	Solutions . . . . .	474
<b>32</b>	<b>Legal, Contracts, and Governance Copilots</b>	<b>475</b>
32.1	Legal Text as Formal Language . . . . .	476
32.1.1	Hierarchical Structure of Legal Documents . . . . .	476
32.1.2	Formal Language Elements . . . . .	476
32.1.3	Domain-Specific Ontology . . . . .	476
32.2	Contract Analysis and Document Understanding . . . . .	476
32.2.1	Key Contract Elements . . . . .	477
32.2.2	Architecture for Contract Analysis . . . . .	477
32.2.3	Deep Learning for Contract Understanding . . . . .	477
32.3	Legal Research and Citation Networks . . . . .	477
32.3.1	Citation Networks and Precedent . . . . .	478
32.3.2	Semantic Search for Legal Documents . . . . .	478
32.4	Compliance and Governance . . . . .	478
32.4.1	Policy Compliance Checking . . . . .	478
32.4.2	Regulatory Change Management . . . . .	478
32.5	AI Copilots for Lawyers . . . . .	479
32.5.1	Copilot Design Principles . . . . .	479
32.5.2	Practical Copilot Workflow . . . . .	479
32.6	Trust, Liability, and Ethical Concerns . . . . .	479
32.6.1	Professional Responsibility . . . . .	479
32.6.2	Hallucination and Fabrication . . . . .	479
32.6.3	Access to Justice . . . . .	480
32.7	Case Study: Contract Review and Risk Assessment . . . . .	480
32.7.1	System Design . . . . .	480
32.7.2	Workflow . . . . .	480
32.7.3	Results . . . . .	480
32.8	Model Maintenance and Drift in Legal AI Systems . . . . .	481
32.8.1	Domain-Specific Drift Patterns in Legal AI . . . . .	481
32.9	Exercises . . . . .	483
32.10	Solutions . . . . .	483
<b>33</b>	<b>Data, Logs, and Observability</b>	<b>484</b>
33.1	Machine Data as a Language . . . . .	485
33.1.1	Types of Machine Data . . . . .	485
33.1.2	Machine Language Grammar . . . . .	485
33.1.3	Data Collection and Storage . . . . .	485
33.2	Anomaly Detection . . . . .	486
33.2.1	Metric Anomaly Detection . . . . .	486
33.2.2	Multivariate Anomaly Detection . . . . .	486
33.2.3	Practical Challenges . . . . .	487
33.3	Root-Cause Analysis and Diagnosis . . . . .	487
33.3.1	Architecture for RCA . . . . .	487

33.3.2	Example: API Latency Spike . . . . .	487
33.4	Incident Automation and Remediation . . . . .	488
33.4.1	Safety in Automated Remediation . . . . .	488
33.5	Log Parsing and Understanding . . . . .	488
33.5.1	Log Parsing Models . . . . .	488
33.5.2	Anomalous Log Detection . . . . .	488
33.6	Configuration and Policy Compliance . . . . .	488
33.6.1	Configuration Language Models . . . . .	489
33.7	AIOps: AI-Powered IT Operations (2024-2025) . . . . .	489
33.7.1	AIOps Platform Architecture . . . . .	489
33.7.2	Causal Inference for Root Cause Analysis . . . . .	489
33.7.3	Predictive Failure Detection and Preventive Maintenance . . . . .	490
33.7.4	Automated Remediation and Self-Healing Systems . . . . .	490
33.7.5	AIOps Platform Vendors and Ecosystem (2024-2025) . . . . .	491
33.7.6	Future Directions and Research Frontiers . . . . .	491
33.8	Case Study: Intelligent Alerting and Incident Response . . . . .	491
33.8.1	System Design . . . . .	492
33.8.2	Workflow . . . . .	492
33.8.3	Results . . . . .	492
33.9	Model Maintenance and Drift in Observability Systems . . . . .	492
33.9.1	Domain-Specific Drift Patterns in Observability . . . . .	492
33.10	Exercises . . . . .	494
33.11	Solutions . . . . .	494
<b>34</b>	<b>Domain-Specific Languages, Tools, and Agents</b>	<b>495</b>
34.1	The World-to-Language-to-Tool Pattern . . . . .	496
34.2	Designing Domain-Specific Languages . . . . .	496
34.2.1	Case Example: Support Ticket DSL . . . . .	496
34.2.2	DSL Design Principles . . . . .	497
34.2.3	Formal DSL Specification . . . . .	497
34.3	Tool-Augmented Models . . . . .	498
34.3.1	Tool Calling Architecture . . . . .	498
34.3.2	Function Calling in Modern LLMs . . . . .	498
34.3.3	Tool Selection and Chaining . . . . .	498
34.3.4	Reliability and Error Handling . . . . .	499
34.4	Agents and Workflow Orchestration . . . . .	499
34.4.1	Agent Loop . . . . .	499
34.4.2	Planning and Reasoning . . . . .	500
34.4.3	Memory and State Management . . . . .	500
34.5	Structured Output and Validation . . . . .	500
34.5.1	JSON Output Mode . . . . .	500
34.5.2	Semantic Validation . . . . .	501
34.6	Practical Design Framework . . . . .	501
34.6.1	Step 1: Analyze the Domain . . . . .	501
34.6.2	Step 2: Design the DSL . . . . .	501
34.6.3	Step 3: Choose Model and Training Approach . . . . .	501
34.6.4	Step 4: Integrate Tools and APIs . . . . .	501
34.6.5	Step 5: Implement Validation and Feedback . . . . .	501
34.6.6	Step 6: Evaluate and Deploy . . . . .	502
34.7	Exercises . . . . .	502
34.8	Solutions . . . . .	502
34.9	Conclusion and Future Directions . . . . .	502
34.10	Synthesis: Patterns Across Domains . . . . .	503
34.10.1	Future Directions . . . . .	503

**Part I**

**Mathematical Foundations**

# Chapter 1

# Linear Algebra for Deep Learning

## Chapter Overview

Linear algebra forms the mathematical foundation of deep learning. Neural networks perform sequences of linear transformations interspersed with nonlinear operations, making matrices and vectors the fundamental objects of study. This chapter develops the linear algebra concepts essential for understanding how deep learning models transform data, how information flows through neural architectures, and how we can interpret the geometric operations these models perform.

Unlike a pure mathematics course, our treatment emphasizes the specific linear algebra operations that appear repeatedly in deep learning: matrix multiplication for transforming representations, dot products for measuring similarity, and matrix decompositions for understanding structure. We pay particular attention to dimensions and shapes, as tracking how tensor dimensions transform through operations is crucial for implementing and debugging deep learning systems.

## Learning Objectives

After completing this chapter, you will be able to:

1. Represent data as vectors and transformations as matrices with clear understanding of dimensions
2. Perform matrix operations and understand their geometric interpretations
3. Calculate and interpret dot products as similarity measures
4. Understand eigendecompositions and singular value decompositions and their applications
5. Apply matrix norms and use them in regularization
6. Recognize how linear algebra operations map to neural network computations

## 1.1 Vector Spaces and Transformations

### 1.1.1 Vectors as Data Representations

In deep learning, we represent data as vectors in high-dimensional spaces. A vector  $\mathbf{x} \in \mathbb{R}^n$  is an ordered collection of  $n$  real numbers, which we can interpret geometrically as a point in  $n$ -dimensional space or as an arrow from the origin to that point.



**Definition 1.1** (Vector). A vector  $\mathbf{x} \in \mathbb{R}^n$  is an  $n$ -tuple of real numbers:

$$\mathbf{x} = \begin{bmatrix} x_1 \\ x_2 \\ \vdots \\ x_n \end{bmatrix} \quad (1.1)$$

where each  $x_i \in \mathbb{R}$  is called a component or element of the vector.

The dimension  $n$  is the number of components in the vector. We write vectors as column vectors by default.

**Example 1.1** (Image as Vector). Consider a grayscale image of size  $28 \times 28$  pixels, such as an image from the MNIST handwritten digit dataset. Each pixel has an intensity value between 0 (black) and 255 (white). We can represent this image as a vector  $\mathbf{x} \in \mathbb{R}^{784}$  by concatenating all pixel values:

$$\mathbf{x} = \begin{bmatrix} x_{1,1} \\ x_{1,2} \\ \vdots \\ x_{28,28} \end{bmatrix} \in \mathbb{R}^{784} \quad (1.2)$$

For color images with three channels (red, green, blue), a  $224 \times 224$  RGB image becomes a vector in  $\mathbb{R}^{150528}$  ( $224 \times 224 \times 3 = 150,528$ ). The enormous dimensionality of image data motivates the need for powerful models that can find meaningful patterns in such high-dimensional spaces.

**Example 1.2** (Text as Vector). In natural language processing, we represent words as vectors called *word embeddings*. A common choice is to represent each word as a vector in  $\mathbb{R}^{300}$  or  $\mathbb{R}^{768}$ . For instance, the word “king” might be represented as:

$$\mathbf{w}_{\text{king}} = \begin{bmatrix} 0.23 \\ -0.45 \\ 0.87 \\ \vdots \\ 0.12 \end{bmatrix} \in \mathbb{R}^{300} \quad (1.3)$$

These embeddings are learned such that semantically similar words have similar vector representations. The famous example is that  $\mathbf{w}_{\text{king}} - \mathbf{w}_{\text{man}} + \mathbf{w}_{\text{woman}} \approx \mathbf{w}_{\text{queen}}$ , suggesting that vector arithmetic can capture semantic relationships.

### 1.1.2 Linear Transformations

**Definition 1.2** (Linear Transformation). A function  $T : \mathbb{R}^n \rightarrow \mathbb{R}^m$  is a **linear transformation** if for all vectors  $\mathbf{x}, \mathbf{y} \in \mathbb{R}^n$  and all scalars  $a, b \in \mathbb{R}$ :

$$T(a\mathbf{x} + b\mathbf{y}) = aT(\mathbf{x}) + bT(\mathbf{y}) \quad (1.4)$$

Linear transformations preserve vector space structure: they map lines to lines and preserve the origin ( $T(\mathbf{0}) = \mathbf{0}$ ).

### 1.1.3 Matrices as Linear Transformations

Every linear transformation from  $\mathbb{R}^n$  to  $\mathbb{R}^m$  can be represented by an  $m \times n$  matrix.

**Definition 1.3** (Matrix). An  $m \times n$  matrix  $\mathbf{A}$  is a rectangular array of numbers with  $m$  rows and  $n$  columns:

$$\mathbf{A} = \begin{bmatrix} a_{1,1} & a_{1,2} & \cdots & a_{1,n} \\ a_{2,1} & a_{2,2} & \cdots & a_{2,n} \\ \vdots & \vdots & \ddots & \vdots \\ a_{m,1} & a_{m,2} & \cdots & a_{m,n} \end{bmatrix} \in \mathbb{R}^{m \times n} \quad (1.5)$$

The notation  $\mathbf{A} \in \mathbb{R}^{m \times n}$  specifies the dimensions explicitly:  $m$  rows and  $n$  columns.

**Key Point 1.1. Dimension Tracking:** For matrix-vector multiplication  $\mathbf{Ax} = \mathbf{y}$ :

$$\underbrace{\mathbf{A}}_{\mathbb{R}^{m \times n}} \underbrace{\mathbf{x}}_{\mathbb{R}^n} = \underbrace{\mathbf{y}}_{\mathbb{R}^m} \quad (1.6)$$

The inner dimensions must match ( $n$ ), and the result has the outer dimensions ( $m$ ).

**Example 1.3** (Neural Network Layer). A single fully-connected neural network layer performs:

$$\mathbf{h} = \mathbf{W}\mathbf{x} + \mathbf{b} \quad (1.7)$$

where  $\mathbf{x} \in \mathbb{R}^{n_{\text{in}}}$ ,  $\mathbf{W} \in \mathbb{R}^{n_{\text{out}} \times n_{\text{in}}}$ ,  $\mathbf{b} \in \mathbb{R}^{n_{\text{out}}}$ ,  $\mathbf{h} \in \mathbb{R}^{n_{\text{out}}}$ .

For transforming a 784-dimensional input to 256-dimensional hidden representation:

$$\underbrace{\mathbf{h}}_{\mathbb{R}^{256}} = \underbrace{\mathbf{W}}_{\mathbb{R}^{256 \times 784}} \underbrace{\mathbf{x}}_{\mathbb{R}^{784}} + \underbrace{\mathbf{b}}_{\mathbb{R}^{256}} \quad (1.8)$$

This layer has  $256 \times 784 = 200,704$  weights plus 256 biases, totaling **200,960 trainable parameters**.

**Concrete Numerical Example:** With  $n_{\text{in}} = 3$ ,  $n_{\text{out}} = 2$ :

$$\mathbf{W} = \begin{bmatrix} 0.5 & -0.3 & 0.8 \\ 0.2 & 0.6 & -0.4 \end{bmatrix}, \quad \mathbf{b} = \begin{bmatrix} 0.1 \\ -0.2 \end{bmatrix}, \quad \mathbf{x} = \begin{bmatrix} 1.0 \\ 2.0 \\ -0.5 \end{bmatrix} \quad (1.9)$$

Computing:

$$\mathbf{W}\mathbf{x} = \begin{bmatrix} 0.5(1.0) - 0.3(2.0) + 0.8(-0.5) \\ 0.2(1.0) + 0.6(2.0) - 0.4(-0.5) \end{bmatrix} = \begin{bmatrix} -0.5 \\ 1.6 \end{bmatrix} \quad (1.10)$$

$$\mathbf{h} = \begin{bmatrix} -0.5 \\ 1.6 \end{bmatrix} + \begin{bmatrix} 0.1 \\ -0.2 \end{bmatrix} = \begin{bmatrix} -0.4 \\ 1.4 \end{bmatrix} \quad (1.11)$$

## 1.2 Matrix Operations

### 1.2.1 Matrix Multiplication

**Definition 1.4** (Matrix Multiplication). For  $\mathbf{A} \in \mathbb{R}^{m \times n}$  and  $\mathbf{B} \in \mathbb{R}^{n \times p}$ , their product  $\mathbf{C} = \mathbf{AB} \in \mathbb{R}^{m \times p}$  is:

$$c_{i,k} = \sum_{j=1}^n a_{i,j} b_{j,k} \quad (1.12)$$

**Example 1.4** (Matrix Multiplication Computation). Compute  $\mathbf{C} = \mathbf{AB}$  where:

$$\mathbf{A} = \begin{bmatrix} 1 & 2 \\ 3 & 4 \end{bmatrix} \in \mathbb{R}^{2 \times 2}, \quad \mathbf{B} = \begin{bmatrix} 5 & 6 \\ 7 & 8 \end{bmatrix} \in \mathbb{R}^{2 \times 2} \quad (1.13)$$

Computing each entry:

$$c_{1,1} = 1(5) + 2(7) = 19 \quad (1.14)$$

$$c_{1,2} = 1(6) + 2(8) = 22 \quad (1.15)$$

$$c_{2,1} = 3(5) + 4(7) = 43 \quad (1.16)$$

$$c_{2,2} = 3(6) + 4(8) = 50 \quad (1.17)$$

Therefore:  $\mathbf{C} = \begin{bmatrix} 19 & 22 \\ 43 & 50 \end{bmatrix}$

### 1.2.2 Computational Complexity of Matrix Operations

Understanding the computational cost of matrix operations is essential for designing efficient deep learning systems.

**Theorem 1.1** (Matrix Multiplication Complexity). Computing  $\mathbf{C} = \mathbf{AB}$  where  $\mathbf{A} \in \mathbb{R}^{m \times n}$  and  $\mathbf{B} \in \mathbb{R}^{n \times p}$  requires:

$$\text{FLOPs} = 2mnp \quad (1.18)$$

*floating-point operations (multiply-accumulate operations count as 2 FLOPs each).*

**Example 1.5** (Transformer Attention Complexity). In transformer self-attention, we compute  $\mathbf{A} = \mathbf{QK}^\top$  where  $\mathbf{Q}, \mathbf{K} \in \mathbb{R}^{n \times d_k}$  (sequence length  $n$ , key dimension  $d_k$ ).

Dimensions:  $\underbrace{\mathbf{Q}}_{\mathbb{R}^{n \times d_k}} \underbrace{\mathbf{K}^\top}_{\mathbb{R}^{d_k \times n}} = \underbrace{\mathbf{A}}_{\mathbb{R}^{n \times n}}$

Computational cost:  $2n \cdot d_k \cdot n = 2n^2 d_k$  FLOPs

For GPT-3 with  $n = 2048$  tokens and  $d_k = 128$ :

$$\text{FLOPs} = 2 \times (2048)^2 \times 128 = 1,073,741,824 \approx 1.07 \text{ GFLOPs} \quad (1.19)$$

This quadratic scaling in sequence length ( $O(n^2)$ ) is why long-context transformers are computationally expensive.

**Example 1.6** (Feed-Forward Network Cost). A transformer feed-forward network applies two linear transformations:

$$\mathbf{h} = \mathbf{W}_1 \mathbf{x} + \mathbf{b}_1 \quad \text{where } \mathbf{W}_1 \in \mathbb{R}^{d_{ff} \times d_{\text{model}}} \quad (1.20)$$

$$\mathbf{y} = \mathbf{W}_2 \mathbf{h} + \mathbf{b}_2 \quad \text{where } \mathbf{W}_2 \in \mathbb{R}^{d_{\text{model}} \times d_{ff}} \quad (1.21)$$

For a batch of  $B$  sequences of length  $n$ , input is  $\mathbf{X} \in \mathbb{R}^{B \times n \times d_{\text{model}}}$ .

First transformation:  $2 \cdot (Bn) \cdot d_{\text{model}} \cdot d_{ff}$  FLOPs

Second transformation:  $2 \cdot (Bn) \cdot d_{ff} \cdot d_{\text{model}}$  FLOPs

Total:  $4Bn \cdot d_{\text{model}} \cdot d_{ff}$  FLOPs

For BERT-base ( $d_{\text{model}} = 768$ ,  $d_{ff} = 3072$ ,  $n = 512$ ,  $B = 32$ ):

$$\text{FLOPs} = 4 \times 32 \times 512 \times 768 \times 3072 = 154,618,822,656 \approx 154.6 \text{ GFLOPs} \quad (1.22)$$

### 1.2.3 Batch Matrix Multiplication

Modern deep learning frameworks process multiple examples simultaneously using batched operations.

**Definition 1.5** (Batch Matrix Multiplication). For tensors  $\mathbf{A} \in \mathbb{R}^{B \times m \times n}$  and  $\mathbf{B} \in \mathbb{R}^{B \times n \times p}$ , batch matrix multiplication produces  $\mathbf{C} \in \mathbb{R}^{B \times m \times p}$  where:

$$\mathbf{C}[b] = \mathbf{A}[b]\mathbf{B}[b] \quad \text{for } b = 1, \dots, B \quad (1.23)$$

**Example 1.7** (Multi-Head Attention Dimensions). In multi-head attention with  $h = 12$  heads, batch size  $B = 32$ , sequence length  $n = 512$ , and head dimension  $d_k = 64$ :

Query tensor:  $\mathbf{Q} \in \mathbb{R}^{B \times h \times n \times d_k} = \mathbb{R}^{32 \times 12 \times 512 \times 64}$

Key tensor:  $\mathbf{K} \in \mathbb{R}^{B \times h \times n \times d_k} = \mathbb{R}^{32 \times 12 \times 512 \times 64}$

Attention scores:  $\mathbf{A} = \mathbf{Q}\mathbf{K}^\top \in \mathbb{R}^{32 \times 12 \times 512 \times 512}$

This requires  $B \times h \times 2n^2 d_k = 32 \times 12 \times 2 \times 512^2 \times 64 = 12,884,901,888 \approx 12.9$  GFLOPs.

**Key Point 1.2. Broadcasting in PyTorch/NumPy:** When dimensions don't match, broadcasting rules automatically expand dimensions by aligning them from the right, stretching size-1 dimensions to match, and adding missing dimensions as size-1. For example, adding a bias vector  $\mathbb{R}^{768}$  to a tensor  $\mathbb{R}^{32 \times 512 \times 768}$  broadcasts the bias across batch and sequence dimensions, effectively treating it as  $\mathbb{R}^{1 \times 1 \times 768}$  and expanding it to match the full shape.

### 1.2.4 Transpose

**Definition 1.6** (Transpose). The **transpose** of  $\mathbf{A} \in \mathbb{R}^{m \times n}$ , denoted  $\mathbf{A}^\top \in \mathbb{R}^{n \times m}$ , swaps rows and columns:

$$[\mathbf{A}^\top]_{i,j} = a_{j,i} \quad (1.24)$$

Important properties:

$$(\mathbf{A}^\top)^\top = \mathbf{A} \quad (1.25)$$

$$(\mathbf{AB})^\top = \mathbf{B}^\top \mathbf{A}^\top \quad (1.26)$$

### 1.2.5 Hardware Context for Matrix Operations

Understanding how matrix operations map to hardware is crucial for writing efficient deep learning code.

#### Memory Layout: Row-Major vs Column-Major

Matrices are stored in memory as one-dimensional arrays, and the layout significantly affects performance. In row-major order, used by C and PyTorch, rows are stored consecutively in memory. In column-major order, used by Fortran and MATLAB, columns are stored consecutively. For a matrix  $\mathbf{A} = \begin{bmatrix} a & b \\ c & d \end{bmatrix}$ , row-major storage produces the sequence  $[a, b, c, d]$  while column-major storage produces  $[a, c, b, d]$ .

**Key Point 1.3. Cache Efficiency:** Accessing memory sequentially is 10-100× faster than random access due to CPU cache lines, which typically hold 64 bytes of consecutive memory. This means you should always iterate in the storage order. For row-major matrices, iterate rows in the outer loop to access consecutive memory locations, avoiding strided access patterns that jump across rows and cause cache misses.

For row-major matrices, iterate rows in the outer loop:

```
# Good: Sequential memory access
for i in range(m):
    for j in range(n):
        result += A[i, j] # Accesses consecutive memory

# Bad: Strided memory access
for j in range(n):
    for i in range(m):
        result += A[i, j] # Jumps across rows
```

#### GPU Acceleration and BLAS Libraries

Modern deep learning relies on highly optimized linear algebra libraries that provide standardized interfaces for common operations. The Basic Linear Algebra Subprograms (BLAS) standard defines three levels of operations: Level 1 for vector operations like dot products and norms with  $O(n)$  complexity, Level 2 for matrix-vector operations like  $\mathbf{Ax}$  with  $O(n^2)$  complexity, and Level 3 for matrix-matrix operations like  $\mathbf{AB}$  with  $O(n^3)$  complexity. Common CPU implementations include Intel MKL, OpenBLAS, and Apple Accelerate, while GPU implementations include NVIDIA cuBLAS and AMD rocBLAS. These libraries achieve near-peak hardware performance through careful optimization of memory access patterns, instruction scheduling, and hardware-specific features.

**Example 1.8 (GPU Matrix Multiplication).** NVIDIA GPUs use specialized Tensor Cores for accelerated matrix multiplication, achieving dramatically higher throughput than standard CUDA cores. The A100 GPU delivers 312 TFLOPS peak performance for FP16 operations with Tensor Cores, has 1.6 TB/s memory bandwidth, and includes 40 MB of L2 cache to reduce memory access latency.

For matrix multiplication  $\mathbf{C} = \mathbf{AB}$  with  $\mathbf{A}, \mathbf{B} \in \mathbb{R}^{4096 \times 4096}$ , we need  $2 \times 4096^3 = 137,438,953,472 \approx 137.4$  GFLOPs of computation and must transfer  $3 \times 4096^2 \times 4 = 201,326,592 \approx 192$  MB of data (three matrices at 4 bytes per float). On an A100, this takes approximately  $\frac{137.4 \text{ GFLOPS}}{312,000 \text{ GFLOPS}} \approx 0.44$  ms, making it compute-bound since the computation time exceeds the memory transfer time of

$$\frac{192 \text{ MB}}{1,600,000 \text{ MB/s}} \approx 0.12 \text{ ms.}$$

## Compute-Bound vs Memory-Bound Operations

**Definition 1.7** (Arithmetic Intensity). **Arithmetic intensity** measures the ratio of computation to memory access:

$$\text{Arithmetic Intensity} = \frac{\text{FLOPs}}{\text{Bytes Transferred}} \quad (1.27)$$

Operations with high arithmetic intensity are **compute-bound**, meaning they are limited by computational throughput, while operations with low arithmetic intensity are **memory-bound**, meaning they are limited by memory bandwidth.

**Example 1.9** (Arithmetic Intensity Analysis). Element-wise operations like ReLU, which computes  $\mathbf{y} = \max(0, \mathbf{x})$ , perform  $n$  comparisons while transferring  $2n$  elements at 4 bytes each for a total of  $8n$  bytes, yielding an arithmetic intensity of only  $\frac{n}{8n} = 0.125$  FLOP/byte. This makes element-wise operations memory-bound, as the GPU spends more time waiting for data than computing.

In contrast, matrix multiplication  $\mathbf{C} = \mathbf{AB}$  with  $\mathbf{A}, \mathbf{B} \in \mathbb{R}^{n \times n}$  performs  $2n^3$  FLOPs while transferring  $3n^2 \times 4 = 12n^2$  bytes, yielding an arithmetic intensity of  $\frac{2n^3}{12n^2} = \frac{n}{6}$  FLOP/byte. For  $n = 1024$ , this gives 170.7 FLOP/byte, making the operation compute-bound and well-suited for GPU acceleration. For smaller matrices with  $n = 64$ , the arithmetic intensity drops to 10.7 FLOP/byte, placing it in a transitional regime where both compute and memory bandwidth matter.

**Key Point 1.4. Matrix Blocking for Cache Efficiency:** Large matrix multiplications are broken into smaller blocks that fit in cache, computing  $\mathbf{C}_{ij} = \sum_k \mathbf{A}_{ik} \mathbf{B}_{kj}$  where each block is typically  $32 \times 32$  or  $64 \times 64$  elements. This blocking strategy reduces cache misses from  $O(n^3)$  to  $O(n^3/\sqrt{M})$  where  $M$  is the cache size, dramatically improving performance by ensuring that frequently accessed data remains in fast cache memory rather than requiring slow main memory accesses.

## 1.3 Dot Products and Similarity

**Definition 1.8** (Dot Product). For vectors  $\mathbf{x}, \mathbf{y} \in \mathbb{R}^n$ , the **dot product** is:

$$\mathbf{x}^\top \mathbf{y} = \sum_{i=1}^n x_i y_i \quad (1.28)$$

**Theorem 1.2** (Geometric Dot Product). For non-zero vectors  $\mathbf{x}, \mathbf{y} \in \mathbb{R}^n$ :

$$\mathbf{x}^\top \mathbf{y} = \|\mathbf{x}\|_2 \|\mathbf{y}\|_2 \cos(\theta) \quad (1.29)$$

where  $\theta$  is the angle between vectors and  $\|\mathbf{x}\|_2 = \sqrt{\mathbf{x}^\top \mathbf{x}}$  is the Euclidean norm.

**Corollary 1.1** (Cosine Similarity). The *cosine similarity* between two non-zero vectors is:

$$\text{sim}(\mathbf{x}, \mathbf{y}) = \frac{\mathbf{x}^\top \mathbf{y}}{\|\mathbf{x}\|_2 \|\mathbf{y}\|_2} = \cos(\theta) \in [-1, 1] \quad (1.30)$$

**Example 1.10** (Attention Similarity Scores). In transformer attention, we compute similarity between query and key vectors using dot products:

$$\mathbf{q} = \begin{bmatrix} 0.5 \\ 0.8 \\ 0.3 \end{bmatrix}, \quad \mathbf{k}_1 = \begin{bmatrix} 0.6 \\ 0.7 \\ 0.2 \end{bmatrix}, \quad \mathbf{k}_2 = \begin{bmatrix} -0.3 \\ 0.1 \\ 0.9 \end{bmatrix} \quad (1.31)$$

Computing similarities:

$$\mathbf{q}^\top \mathbf{k}_1 = 0.5(0.6) + 0.8(0.7) + 0.3(0.2) = 0.92 \quad (1.32)$$

$$\mathbf{q}^\top \mathbf{k}_2 = 0.5(-0.3) + 0.8(0.1) + 0.3(0.9) = 0.20 \quad (1.33)$$

The query  $\mathbf{q}$  is more similar to  $\mathbf{k}_1$  (score 0.92) than to  $\mathbf{k}_2$  (score 0.20). These scores determine attention weights.

## 1.4 Matrix Decompositions

### 1.4.1 Eigenvalues and Eigenvectors

**Definition 1.9** (Eigenvalues and Eigenvectors). For a square matrix  $\mathbf{A} \in \mathbb{R}^{n \times n}$ , a non-zero vector  $\mathbf{v} \in \mathbb{R}^n$  is an **eigenvector** with corresponding **eigenvalue**  $\lambda \in \mathbb{R}$  if:

$$\mathbf{A}\mathbf{v} = \lambda\mathbf{v} \quad (1.34)$$

Geometrically, an eigenvector is only scaled (not rotated) when  $\mathbf{A}$  is applied. The eigenvalue  $\lambda$  is the scaling factor.

**Example 1.11** (Computing Eigenvalues). Find eigenvalues of:

$$\mathbf{A} = \begin{bmatrix} 3 & 1 \\ 1 & 3 \end{bmatrix} \quad (1.35)$$

Solving  $\det(\mathbf{A} - \lambda\mathbf{I}) = 0$ :

$$\det \begin{bmatrix} 3 - \lambda & 1 \\ 1 & 3 - \lambda \end{bmatrix} = (3 - \lambda)^2 - 1 = \lambda^2 - 6\lambda + 8 = 0 \quad (1.36)$$

$$= (\lambda - 4)(\lambda - 2) = 0 \quad (1.37)$$

Eigenvalues:  $\lambda_1 = 4, \lambda_2 = 2$

$$\begin{aligned} \text{For } \lambda_1 = 4, \text{ eigenvector: } \mathbf{v}_1 &= \frac{1}{\sqrt{2}} \begin{bmatrix} 1 \\ 1 \end{bmatrix} \\ \text{For } \lambda_2 = 2, \text{ eigenvector: } \mathbf{v}_2 &= \frac{1}{\sqrt{2}} \begin{bmatrix} 1 \\ -1 \end{bmatrix} \end{aligned}$$

### 1.4.2 Singular Value Decomposition

**Theorem 1.3** (Singular Value Decomposition). *Any matrix  $\mathbf{A} \in \mathbb{R}^{m \times n}$  can be decomposed as:*

$$\mathbf{A} = \mathbf{U}\mathbf{\Sigma}\mathbf{V}^\top \quad (1.38)$$

where  $\mathbf{U} \in \mathbb{R}^{m \times m}$  is an orthogonal matrix of left singular vectors,  $\mathbf{\Sigma} \in \mathbb{R}^{m \times n}$  is a diagonal matrix with singular values  $\sigma_1 \geq \sigma_2 \geq \dots \geq 0$ , and  $\mathbf{V} \in \mathbb{R}^{n \times n}$  is an orthogonal matrix of right singular vectors.

**Key Point 1.5.** *SVD always exists for any matrix, unlike eigendecomposition which requires special conditions.*

### Low-Rank Approximation and Model Compression

SVD enables efficient model compression by approximating matrices with lower-rank factorizations.

**Theorem 1.4** (Eckart-Young Theorem). *The best rank- $k$  approximation to  $\mathbf{A}$  in Frobenius norm is:*

$$\mathbf{A}_k = \sum_{i=1}^k \sigma_i \mathbf{u}_i \mathbf{v}_i^\top \quad (1.39)$$

where  $\sigma_i$  are the  $k$  largest singular values with corresponding singular vectors  $\mathbf{u}_i, \mathbf{v}_i$ .

The approximation error is:

$$\|\mathbf{A} - \mathbf{A}_k\|_F = \sqrt{\sum_{i=k+1}^r \sigma_i^2} \quad (1.40)$$

where  $r = \min(m, n)$  is the rank of  $\mathbf{A}$ .

**Example 1.12** (SVD for Model Compression - Detailed Analysis). Consider weight matrix  $\mathbf{W} \in \mathbb{R}^{512 \times 2048}$  containing 1,048,576 parameters. The full SVD gives  $\mathbf{W} = \mathbf{U}\mathbf{\Sigma}\mathbf{V}^\top$  where  $\mathbf{U} \in \mathbb{R}^{512 \times 512}$ ,  $\mathbf{\Sigma} \in \mathbb{R}^{512 \times 2048}$ , and  $\mathbf{V} \in \mathbb{R}^{2048 \times 2048}$ .

For a rank- $k$  approximation, we keep only the top  $k$  singular values to obtain  $\mathbf{W} \approx \mathbf{W}_1 \mathbf{W}_2 = \mathbf{U}_k \mathbf{\Sigma}_k \mathbf{V}_k^\top$  where  $\mathbf{U}_k \in \mathbb{R}^{512 \times k}$ ,  $\mathbf{\Sigma}_k \in \mathbb{R}^{k \times k}$ , and  $\mathbf{V}_k \in \mathbb{R}^{k \times 2048}$ . We can absorb the diagonal matrix  $\mathbf{\Sigma}_k$  into either factor, giving  $\mathbf{W}_1 = \mathbf{U}_k \mathbf{\Sigma}_k \in \mathbb{R}^{512 \times k}$  and  $\mathbf{W}_2 = \mathbf{V}_k^\top \in \mathbb{R}^{k \times 2048}$ .

The original matrix has  $512 \times 2048 = 1,048,576$  parameters, while the compressed form has  $512k + 2048k = 2560k$  parameters, yielding a compression ratio of  $\frac{2560k}{1,048,576} = \frac{k}{409.6}$ . For  $k = 64$ , we have  $2560 \times 64 = 163,840$  parameters, achieving 84.4% compression. For  $k = 128$ , we have 327,680 parameters, achieving 68.8% compression.

In terms of memory savings with 32-bit floats, the original matrix requires  $1,048,576 \times 4 = 4,194,304$  bytes or approximately 4.0 MB. The compressed version with  $k = 64$  requires only



$163,840 \times 4 = 655,360$  bytes or approximately 0.625 MB, saving 3.375 MB per layer. For a model with 100 such layers, this yields a total savings of 337.5 MB, significantly reducing memory footprint and enabling deployment on resource-constrained devices.

**Example 1.13** (Accuracy vs Compression Trade-off). Consider a weight matrix with singular values that decay exponentially:

$$\sigma_i = \sigma_1 \cdot e^{-\alpha i} \quad (1.41)$$

The relative approximation error for rank- $k$  approximation is:

$$\frac{\|\mathbf{W} - \mathbf{W}_k\|_F}{\|\mathbf{W}\|_F} = \sqrt{\frac{\sum_{i=k+1}^r \sigma_i^2}{\sum_{i=1}^r \sigma_i^2}} \quad (1.42)$$

**Typical results for transformer feed-forward layers:**

Rank $k$	Compression	Relative Error	Accuracy Drop
256	50%	0.05	<0.1%
128	75%	0.12	0.3%
64	87.5%	0.25	1.2%
32	93.75%	0.45	3.5%

Sweet spot: 50-75% compression with minimal accuracy loss.

## SVD in Modern Architectures

Low-rank matrix decompositions are also central to modern parameter-efficient fine-tuning methods such as LoRA, which adds low-rank updates  $\Delta \mathbf{W} = \mathbf{B}\mathbf{A}$  (with  $\mathbf{B} \in \mathbb{R}^{d \times r}$ ,  $\mathbf{A} \in \mathbb{R}^{r \times k}$ ,  $r \ll \min(d, k)$ ) to frozen pre-trained weights, achieving >99% parameter reduction. See Chapter 20 for details.

### Implementation:

Computing SVD and low-rank approximation in PyTorch:

```
import torch

# Original weight matrix
W = torch.randn(512, 2048)

# Compute SVD
U, S, Vt = torch.linalg.svd(W, full_matrices=False)

# Rank-k approximation
k = 64
W_compressed = U[:, :k] @ torch.diag(S[:k]) @ Vt[:k, :]

# Factored form for efficient computation
W1 = U[:, :k] @ torch.diag(S[:k]) # 512 x 64
W2 = Vt[:k, :] # 64 x 2048

# Verify approximation
error = torch.norm(W - W_compressed, p='fro')
relative_error = error / torch.norm(W, p='fro')
print(f"Relative error: {relative_error:.4f}")

# Memory comparison
original_params = W.numel()
```

```
compressed_params = W1.numel() + W2.numel()
compression_ratio = compressed_params / original_params
print(f"Compression: {(1-compression_ratio)*100:.1f}%")
```

## 1.5 Norms and Distance Metrics

**Definition 1.10** (Vector Norms). For vector  $\mathbf{x} \in \mathbb{R}^n$ :

$$\text{L1 norm (Manhattan): } \|\mathbf{x}\|_1 = \sum_{i=1}^n |x_i| \quad (1.43)$$

$$\text{L2 norm (Euclidean): } \|\mathbf{x}\|_2 = \sqrt{\sum_{i=1}^n x_i^2} \quad (1.44)$$

$$\text{L}\infty \text{ norm (Max): } \|\mathbf{x}\|_\infty = \max_i |x_i| \quad (1.45)$$

**Definition 1.11** (Matrix Norms). For matrix  $\mathbf{A} \in \mathbb{R}^{m \times n}$ :

$$\text{Frobenius norm: } \|\mathbf{A}\|_F = \sqrt{\sum_{i=1}^m \sum_{j=1}^n a_{i,j}^2} = \sqrt{\text{tr}(\mathbf{A}^\top \mathbf{A})} \quad (1.46)$$

Norms are used in regularization to prevent overfitting by penalizing large weights.

### Implementation:

In PyTorch:

```
import torch

# Vector norms
x = torch.tensor([3.0, 4.0])
l2_norm = torch.norm(x, p=2) # 5.0
l1_norm = torch.norm(x, p=1) # 7.0

# Matrix Frobenius norm
W = torch.randn(256, 784)
frob_norm = torch.norm(W, p='fro')
```

## 1.6 Practical Deep Learning Examples

### 1.6.1 Embedding Layers and Memory Requirements

**Example 1.14** (Vocabulary Embeddings). Large language models use embedding layers to map discrete tokens to continuous vector representations. For GPT-3, the vocabulary contains  $V = 50,257$  tokens, each mapped to a vector of dimension  $d_{\text{model}} = 12,288$ , requiring an embedding matrix  $\mathbf{E} \in \mathbb{R}^{50257 \times 12288}$  with  $50,257 \times 12,288 = 617,558,016$  parameters. Storing these embeddings

in 32-bit floating-point format requires  $617,558,016 \times 4 = 2,470,232,064$  bytes or approximately 2.3 GB of memory, while 16-bit format reduces this to approximately 1.15 GB.

For a batch of  $B = 32$  sequences of length  $n = 2048$ , the input consists of integer token IDs in  $\mathbb{R}^{32 \times 2048}$ , which the embedding layer transforms into dense representations in  $\mathbb{R}^{32 \times 2048 \times 12288}$ , requiring  $32 \times 2048 \times 12288 \times 4 = 3,221,225,472$  bytes or approximately 3.0 GB of memory. This demonstrates why large batch sizes and long sequences quickly exhaust GPU memory, necessitating techniques like gradient checkpointing and mixed-precision training.

### 1.6.2 Complete Transformer Layer Analysis

Understanding the full computational profile of a transformer layer—parameters, FLOPs, memory, and hardware utilization—is essential for practical deep learning engineering. Section 1.7 provides a comprehensive, self-contained worked analysis of BERT-base, the standard baseline configuration used as a running example throughout this textbook.

### 1.6.3 Common Dimension Errors and Debugging

**Key Point 1.6. Dimension Mismatch Errors:** *The most common bugs in deep learning involve incompatible tensor dimensions. When debugging dimension errors, start by printing tensor shapes using `print(x.shape)` to verify actual dimensions against expected values. Check whether the batch dimension is present (is it  $\mathbb{R}^{B \times \dots}$  or just  $\mathbb{R}^{\dots}$ ?), verify the sequence length dimension (is it  $\mathbb{R}^{B \times n \times d}$  or  $\mathbb{R}^{B \times d \times n}$ ?), confirm that matrix multiplication has compatible inner dimensions, and watch for unintentional broadcasting that may hide shape mismatches. These systematic checks quickly identify the source of dimension errors and guide appropriate fixes.*

#### Implementation:

Common dimension fixes in PyTorch:

```
import torch

# Problem: Shape mismatch in matrix multiplication
Q = torch.randn(32, 512, 768) # [batch, seq_len, d_model]
K = torch.randn(32, 512, 768)

# Wrong: Q @ K gives error (768 != 512)
# scores = Q @ K # Error!

# Correct: Transpose last two dimensions of K
scores = Q @ K.transpose(-2, -1) # [32, 512, 512]

# Problem: Missing batch dimension
x = torch.randn(512, 768) # Missing batch dimension
W = torch.randn(768, 3072)

# Add batch dimension
x = x.unsqueeze(0) # [1, 512, 768]
output = x @ W # [1, 512, 3072]

# Problem: Broadcasting confusion
x = torch.randn(32, 512, 768)
bias = torch.randn(768)

# This works due to broadcasting
output = x + bias # bias broadcasts to [32, 512, 768]
```

```
# Explicit broadcasting (clearer)
output = x + bias.view(1, 1, 768)
```

## 1.7 BERT-base: A Canonical Worked Analysis

BERT-base has become the standard baseline configuration for transformer analysis. Its dimensions are adopted throughout this textbook as a running example for parameter counts, memory estimates, and computational costs. This section provides a self-contained reference; subsequent chapters cite these results rather than re-derive them.

### 1.7.1 Architecture Specification

Hyperparameter	Value
Layers	$N = 12$
Model dimension	$d_{\text{model}} = 768$
Attention heads	$h = 12$ ( $d_k = d_v = 64$ per head)
Feed-forward dimension	$d_{ff} = 3072$ ( $4 \times d_{\text{model}}$ )
Vocabulary size	$V = 30,000$ (WordPiece)
Maximum sequence length	$n_{\text{max}} = 512$

Unless stated otherwise, worked examples use batch size  $B = 32$  and full sequence length  $n = 512$ .

### 1.7.2 Parameter Count

**Per encoder layer.** Each layer has three components:

$$\text{Multi-head attention: } 4 \times 768^2 = 2,359,296 \quad (\text{Q, K, V, O projections}) \quad (1.47)$$

$$\text{Feed-forward network: } 2 \times 768 \times 3072 + 3072 \times 768 = 4,722,432 \quad (1.48)$$

$$\text{Layer normalization (2}\times\text{): } 2 \times 2 \times 768 = 3,072 \quad (1.49)$$

$$\textbf{Total per layer: } \mathbf{7,084,800} \text{ parameters} \quad (1.50)$$

The feed-forward network contains approximately twice as many parameters as the attention mechanism (4.7M vs 2.4M), despite attention being conceptually more complex. This is because the  $4 \times$  expansion to  $d_{ff}$  creates two large weight matrices.

**Complete model:**

$$\text{Token embeddings: } 30,000 \times 768 = 23,040,000 \quad (1.51)$$

$$\text{Position embeddings: } 512 \times 768 = 393,216 \quad (1.52)$$

$$\text{Token type embeddings: } 2 \times 768 = 1,536 \quad (1.53)$$

$$\text{Embedding layer norm: } 2 \times 768 = 1,536 \quad (1.54)$$

$$12 \text{ encoder layers: } 12 \times 7,084,800 = 85,017,600 \quad (1.55)$$

$$\text{Pooler: } 768 \times 768 + 768 = 590,592 \quad (1.56)$$

$$\textbf{Total: } \mathbf{109,044,480} \approx \mathbf{110M} \text{ parameters} \quad (1.57)$$

Embeddings account for  $\sim 21\%$  of total parameters (23M out of 110M), while the transformer layers account for  $\sim 78\%$ . This ratio shifts with vocabulary size—a 50K-token vocabulary would push embeddings to 35% of total parameters.

### 1.7.3 Dimension Tracking Through One Layer

**Input:**  $\mathbf{X} \in \mathbb{R}^{32 \times 512 \times 768}$  (batch  $\times$  sequence  $\times$  model dimension)

**Multi-Head Attention:**

$$\text{Q, K, V projections: } \mathbb{R}^{32 \times 512 \times 768} \rightarrow \mathbb{R}^{32 \times 512 \times 768} \quad (1.58)$$

$$\text{Reshape for heads: } \mathbb{R}^{32 \times 512 \times 768} \rightarrow \mathbb{R}^{32 \times 12 \times 512 \times 64} \quad (1.59)$$

$$\text{Attention scores: } \mathbb{R}^{32 \times 12 \times 512 \times 512} \quad (\text{quadratic in } n) \quad (1.60)$$

$$\text{Attention output: } \mathbb{R}^{32 \times 12 \times 512 \times 64} \quad (1.61)$$

$$\text{Concatenate heads: } \mathbb{R}^{32 \times 512 \times 768} \quad (1.62)$$

$$\text{Output projection: } \mathbb{R}^{32 \times 512 \times 768} \quad (1.63)$$

**Feed-Forward Network:**

$$\text{Expand: } \mathbb{R}^{32 \times 512 \times 768} \xrightarrow{\mathbf{W}_1} \mathbb{R}^{32 \times 512 \times 3072} \quad (1.64)$$

$$\text{Activate + project: } \mathbb{R}^{32 \times 512 \times 3072} \xrightarrow{\mathbf{W}_2} \mathbb{R}^{32 \times 512 \times 768} \quad (1.65)$$

### 1.7.4 Activation Memory

Intermediate activations stored for backpropagation dominate training memory:

Component (per layer)	Memory (FP32)
Q, K, V projections ( $3 \times Bnd$ )	113 MB
Attention scores ( $Bhn^2$ )	402 MB
Attention output ( $Bnd$ )	38 MB
FFN intermediate ( $Bn \cdot 4d$ )	151 MB
<b>Per-layer total</b>	<b>704 MB</b>
<b>12 layers</b>	<b>8.4 GB</b>

The attention scores alone ( $B \times h \times n^2 \times 4$  bytes = 402 MB per layer) account for 57% of per-layer activation memory, illustrating the quadratic cost of self-attention. Doubling the sequence length to  $n = 1024$  would quadruple the attention memory to 1.6 GB per layer.

### 1.7.5 FLOPs Analysis

Counting each multiply-accumulate as 2 FLOPs:

**Self-Attention (per layer):**

$$\text{QKV projections: } 3 \times 2 \times 512 \times 768^2 = 1.81 \text{ GFLOPs} \quad (1.66)$$

$$\text{Attention scores } (\mathbf{QK}^\top): 12 \times 2 \times 512^2 \times 64 = 0.40 \text{ GFLOPs} \quad (1.67)$$

$$\text{Attention output } (\mathbf{AV}): 12 \times 2 \times 512^2 \times 64 = 0.40 \text{ GFLOPs} \quad (1.68)$$

$$\text{Output projection: } 2 \times 512 \times 768^2 = 0.60 \text{ GFLOPs} \quad (1.69)$$

$$\text{Subtotal: } 3.21 \text{ GFLOPs} \quad (1.70)$$

**Feed-Forward Network (per layer):**

$$\text{Expand } (\mathbf{W}_1): 2 \times 512 \times 768 \times 3072 = 2.42 \text{ GFLOPs} \quad (1.71)$$

$$\text{Project } (\mathbf{W}_2): 2 \times 512 \times 3072 \times 768 = 2.42 \text{ GFLOPs} \quad (1.72)$$

$$\text{Subtotal: } 4.84 \text{ GFLOPs} \quad (1.73)$$

**Totals:**

$$\text{Per layer: } 3.21 + 4.84 = 8.05 \text{ GFLOPs} \quad (1.74)$$

$$12 \text{ layers (forward pass): } 96.6 \text{ GFLOPs} \quad (1.75)$$

$$\text{Training step } (\approx 3 \times \text{forward}): \approx 290 \text{ GFLOPs} \quad (1.76)$$

The FFN accounts for 60% of per-layer FLOPs, while the attention score computations ( $\mathbf{QK}^\top$  and  $\mathbf{AV}$ ) contribute only 10%. For short sequences, optimizing FFN yields the largest gains; for long sequences, attention's  $O(n^2)$  term becomes dominant.

### 1.7.6 Training Memory Budget

Component	Memory
Parameters (FP32)	440 MB
Gradients (FP32)	440 MB
Adam optimizer states ( $m, v$ )	880 MB
Activations (12 layers)	$\approx 8.4$ GB
Embeddings + overhead	$\approx 3.6$ GB
<b>Total</b>	<b><math>\approx 13.8</math> GB</b>

Activations dominate at  $\sim 87\%$  of total memory, motivating gradient checkpointing (recompute activations during the backward pass, trading 20–30% slower training for 50–70% memory reduction). This is why training BERT-base requires GPUs with at least 16 GB of memory.

### 1.7.7 Hardware Timing (NVIDIA A100)

The A100 provides 312 TFLOPS FP16 with Tensor Cores and 1.6 TB/s memory bandwidth. At 70% utilization:

$$\text{Forward pass (single sample): } \frac{96.6 \text{ GFLOPs}}{312 \times 0.7 \text{ TFLOPs}} \approx 0.44 \text{ ms} \quad (1.77)$$

$$\text{Batch of 32: } 32 \times 0.44 \approx 14 \text{ ms} \quad (1.78)$$

$$\text{Training step } (3 \times \text{forward}): \approx 42 \text{ ms} \quad (1.79)$$

$$\text{Throughput: } \frac{32 \times 512}{42 \text{ ms}} \approx 390,000 \text{ tokens/sec} \quad (1.80)$$

**Memory bandwidth check:** Loading 110M parameters ( $\times 4$  bytes = 440 MB) takes  $440/1600 \approx 0.28$  ms, comparable to compute time. For small batch sizes, BERT-base becomes memory-bandwidth bound rather than compute-bound; larger batches amortize parameter loading across more computation.

## 1.8 Exercises

**Exercise 1.1.** Given  $\mathbf{x} = [2, -1, 3]^\top$  and  $\mathbf{y} = [1, 4, -2]^\top$ , compute:

1. The dot product  $\mathbf{x}^\top \mathbf{y}$
2. The L2 norms  $\|\mathbf{x}\|_2$  and  $\|\mathbf{y}\|_2$
3. The cosine similarity between  $\mathbf{x}$  and  $\mathbf{y}$

**Exercise 1.2.** For a transformer layer with  $d_{\text{model}} = 768$  and feed-forward dimension  $d_{ff} = 3072$ :

1. Calculate the number of parameters in the two linear transformations
2. If processing a batch of  $B = 32$  sequences of length  $n = 512$ , what are the dimensions of the input tensor?
3. How many floating-point operations (FLOPs) are required for one forward pass through this layer?

**Exercise 1.3.** Prove that for symmetric matrix  $\mathbf{A} = \mathbf{A}^\top$ , eigenvectors corresponding to distinct eigenvalues are orthogonal.

**Exercise 1.4.** A weight matrix  $\mathbf{W} \in \mathbb{R}^{1024 \times 4096}$  is approximated using SVD with rank  $r$ .

1. Express the number of parameters as a function of  $r$
2. What value of  $r$  achieves 75% compression?
3. What is the memory savings in MB (assuming 32-bit floats)?

**Exercise 1.5.** Consider computing attention scores  $\mathbf{A} = \mathbf{Q}\mathbf{K}^\top$  where  $\mathbf{Q}, \mathbf{K} \in \mathbb{R}^{B \times n \times d_k}$  with  $B = 16$ ,  $n = 1024$ ,  $d_k = 64$ .

1. What are the dimensions of the output  $\mathbf{A}$ ?
2. Calculate the total FLOPs required
3. Compute the arithmetic intensity (FLOPs per byte transferred, assuming 32-bit floats)
4. Is this operation compute-bound or memory-bound on a GPU with 312 TFLOPS and 1.6 TB/s bandwidth?

**Exercise 1.6.** An embedding layer has vocabulary size  $V = 32,000$  and embedding dimension  $d = 512$ .

1. How many parameters does the embedding matrix contain?
2. What is the memory requirement in MB for 32-bit floats?
3. For a batch of  $B = 64$  sequences of length  $n = 256$ , what is the memory required for the embedded representations?
4. If we use LoRA with rank  $r = 16$  to adapt the embeddings, how many trainable parameters are needed?

**Exercise 1.7.** Compare the computational cost of two equivalent operations:

1. Computing  $(\mathbf{AB})\mathbf{x}$  where  $\mathbf{A} \in \mathbb{R}^{m \times n}$ ,  $\mathbf{B} \in \mathbb{R}^{n \times p}$ ,  $\mathbf{x} \in \mathbb{R}^p$
2. Computing  $\mathbf{A}(\mathbf{Bx})$

For  $m = 512$ ,  $n = 2048$ ,  $p = 512$ , which order is more efficient and by what factor?

**Exercise 1.8.** A matrix multiplication  $\mathbf{C} = \mathbf{AB}$  with  $\mathbf{A}, \mathbf{B} \in \mathbb{R}^{2048 \times 2048}$  is performed on a GPU.

1. Calculate the total FLOPs
2. Calculate the memory transferred (assuming matrices are read once and result written once)
3. Compute the arithmetic intensity
4. If the GPU has 100 TFLOPS compute and 900 GB/s memory bandwidth, what is the theoretical execution time assuming perfect utilization?
5. Which resource (compute or memory) is the bottleneck?

## 1.9 Solutions

Full solutions for all exercises are available at <https://deeplearning.hofkensvermeulen.be>.



## Chapter 2

# Calculus and Optimization

### Chapter Overview

Training deep learning models requires optimizing complex, high-dimensional functions. This chapter develops the calculus and optimization theory necessary to understand how neural networks learn from data. We cover multivariable calculus, gradient computation, and the optimization algorithms that power modern deep learning.

The centerpiece of this chapter is backpropagation, the algorithm that efficiently computes gradients in neural networks. We derive backpropagation from first principles, showing how the chain rule enables gradient computation through arbitrarily deep computational graphs. We then explore gradient descent and its variants, which use these gradients to iteratively improve model parameters.

### Learning Objectives

After completing this chapter, you will be able to:

1. Compute gradients and Jacobians for multivariable functions
2. Apply the chain rule to composite functions
3. Understand and implement the backpropagation algorithm
4. Implement gradient descent and its variants (SGD, momentum, Adam)
5. Analyze convergence properties of optimization algorithms
6. Apply learning rate schedules and regularization techniques

## 2.1 Multivariable Calculus

### 2.1.1 Partial Derivatives

**Definition 2.1** (Partial Derivative). For function  $f : \mathbb{R}^n \rightarrow \mathbb{R}$ , the **partial derivative** with respect to  $x_i$  is:

$$\frac{\partial f}{\partial x_i} = \lim_{h \rightarrow 0} \frac{f(x_1, \dots, x_i + h, \dots, x_n) - f(x_1, \dots, x_i, \dots, x_n)}{h} \quad (2.1)$$

**Example 2.1** (Computing Partial Derivatives). For  $f(x_1, x_2) = x_1^2 + 3x_1x_2 + x_2^2$ :

$$\frac{\partial f}{\partial x_1} = 2x_1 + 3x_2 \quad (2.2)$$

$$\frac{\partial f}{\partial x_2} = 3x_1 + 2x_2 \quad (2.3)$$

At point  $(x_1, x_2) = (1, 2)$ :

$$\left. \frac{\partial f}{\partial x_1} \right|_{(1,2)} = 2(1) + 3(2) = 8 \quad (2.4)$$

$$\left. \frac{\partial f}{\partial x_2} \right|_{(1,2)} = 3(1) + 2(2) = 7 \quad (2.5)$$

### 2.1.2 Gradients

**Definition 2.2** (Gradient). For function  $f : \mathbb{R}^n \rightarrow \mathbb{R}$ , the **gradient** is the vector of partial derivatives:

$$\nabla f(\mathbf{x}) = \begin{bmatrix} \frac{\partial f}{\partial x_1} \\ \frac{\partial f}{\partial x_2} \\ \vdots \\ \frac{\partial f}{\partial x_n} \end{bmatrix} \in \mathbb{R}^n \quad (2.6)$$

The gradient points in the direction of steepest ascent of the function.

**Example 2.2** (Gradient of Loss Function). For mean squared error loss:

$$L(\mathbf{w}) = \frac{1}{N} \sum_{i=1}^N (y_i - \mathbf{w}^\top \mathbf{x}^{(i)})^2 \quad (2.7)$$

The gradient with respect to  $\mathbf{w}$  is:

$$\nabla_{\mathbf{w}} L = -\frac{2}{N} \sum_{i=1}^N (y_i - \mathbf{w}^\top \mathbf{x}^{(i)}) \mathbf{x}^{(i)} \quad (2.8)$$

For  $N = 1$ ,  $\mathbf{w} = [w_1, w_2]^\top$ ,  $\mathbf{x} = [1, 2]^\top$ ,  $y = 5$ , and current prediction  $\hat{y} = \mathbf{w}^\top \mathbf{x} = 3$ :

$$\nabla_{\mathbf{w}} L = -2(5 - 3) \begin{bmatrix} 1 \\ 2 \end{bmatrix} = \begin{bmatrix} -4 \\ -8 \end{bmatrix} \quad (2.9)$$

The negative gradient  $-\nabla_{\mathbf{w}} L = [4, 8]^\top$  points toward better parameters.

### 2.1.3 The Chain Rule

**Theorem 2.1** (Chain Rule for Functions). For composite function  $h(\mathbf{x}) = f(g(\mathbf{x}))$  where  $g : \mathbb{R}^n \rightarrow \mathbb{R}^m$  and  $f : \mathbb{R}^m \rightarrow \mathbb{R}$ :

$$\frac{\partial h}{\partial x_i} = \sum_{j=1}^m \frac{\partial f}{\partial g_j} \frac{\partial g_j}{\partial x_i} \quad (2.10)$$

In vector form:

$$\nabla_{\mathbf{x}} h = \mathbf{J}_g^\top \nabla_{\mathbf{z}} f \quad (2.11)$$

where  $\mathbf{z} = g(\mathbf{x})$  and  $\mathbf{J}_g \in \mathbb{R}^{m \times n}$  is the Jacobian of  $g$ .

**Example 2.3** (Chain Rule Application). For neural network layer:  $\mathbf{y} = \sigma(\mathbf{W}\mathbf{x} + \mathbf{b})$  where  $\sigma$  is applied element-wise.

Let  $\mathbf{z} = \mathbf{W}\mathbf{x} + \mathbf{b}$  (pre-activation). Then:

$$\frac{\partial L}{\partial \mathbf{x}} = \mathbf{W}^\top \left( \frac{\partial L}{\partial \mathbf{y}} \odot \sigma'(\mathbf{z}) \right) \quad (2.12)$$

where  $\odot$  denotes element-wise multiplication.

**Concrete example:** For ReLU activation  $\sigma(z) = \max(0, z)$ :

$$\sigma'(z) = \begin{cases} 1 & \text{if } z > 0 \\ 0 & \text{if } z \leq 0 \end{cases} \quad (2.13)$$

If  $\mathbf{z} = [2.0, -1.0, 0.5]^\top$ , then  $\sigma'(\mathbf{z}) = [1, 0, 1]^\top$ .

### 2.1.4 Jacobian and Hessian Matrices

**Definition 2.3** (Jacobian Matrix). For function  $\mathbf{f} : \mathbb{R}^n \rightarrow \mathbb{R}^m$ , the **Jacobian matrix** is:

$$\mathbf{J}_{\mathbf{f}}(\mathbf{x}) = \begin{bmatrix} \frac{\partial f_1}{\partial x_1} & \frac{\partial f_1}{\partial x_2} & \cdots & \frac{\partial f_1}{\partial x_n} \\ \frac{\partial f_2}{\partial x_1} & \frac{\partial f_2}{\partial x_2} & \cdots & \frac{\partial f_2}{\partial x_n} \\ \vdots & \vdots & \ddots & \vdots \\ \frac{\partial f_m}{\partial x_1} & \frac{\partial f_m}{\partial x_2} & \cdots & \frac{\partial f_m}{\partial x_n} \end{bmatrix} \in \mathbb{R}^{m \times n} \quad (2.14)$$

**Definition 2.4** (Hessian Matrix). For function  $f : \mathbb{R}^n \rightarrow \mathbb{R}$ , the **Hessian matrix** contains second derivatives:

$$\mathbf{H}_f(\mathbf{x}) = \begin{bmatrix} \frac{\partial^2 f}{\partial x_1^2} & \frac{\partial^2 f}{\partial x_1 \partial x_2} & \cdots \\ \frac{\partial^2 f}{\partial x_2 \partial x_1} & \frac{\partial^2 f}{\partial x_2^2} & \cdots \\ \vdots & \vdots & \ddots \end{bmatrix} \in \mathbb{R}^{n \times n} \quad (2.15)$$

The Hessian describes the local curvature of the function. For smooth functions,  $\mathbf{H}$  is symmetric.

## 2.2 Gradient Descent

### 2.2.1 The Gradient Descent Algorithm

Gradient descent iteratively moves parameters in the direction opposite to the gradient:

**Algorithm 1:** Gradient Descent**Input:** Objective function  $f(\mathbf{w})$ , initial parameters  $\mathbf{w}^{(0)}$ , learning rate  $\eta$ , iterations  $T$ **Output:** Optimized parameters  $\mathbf{w}^{(T)}$ 


---

```

1 for  $t = 0$  to  $T - 1$  do
2   Compute gradient:  $\mathbf{g}^{(t)} = \nabla f(\mathbf{w}^{(t)})$ 
3   Update parameters:  $\mathbf{w}^{(t+1)} = \mathbf{w}^{(t)} - \eta \mathbf{g}^{(t)}$ 
4 return  $\mathbf{w}^{(T)}$ 

```

---

**Key Point 2.1.** The learning rate  $\eta$  controls the step size. Too large: divergence. Too small: slow convergence.

**Example 2.4** (Gradient Descent on Quadratic). Minimize  $f(w) = w^2$  starting from  $w^{(0)} = 3$  with  $\eta = 0.1$ :

$$t = 0 : \quad w^{(0)} = 3, \quad g^{(0)} = 2w^{(0)} = 6, \quad w^{(1)} = 3 - 0.1(6) = 2.4 \quad (2.16)$$

$$t = 1 : \quad w^{(1)} = 2.4, \quad g^{(1)} = 4.8, \quad w^{(2)} = 2.4 - 0.1(4.8) = 1.92 \quad (2.17)$$

$$t = 2 : \quad w^{(2)} = 1.92, \quad g^{(2)} = 3.84, \quad w^{(3)} = 1.92 - 0.1(3.84) = 1.536 \quad (2.18)$$

The parameters converge to  $w^* = 0$  (the minimum).

**2.2.2 Stochastic Gradient Descent (SGD)**

For large datasets, computing the full gradient is expensive. SGD approximates the gradient using mini-batches.

**Algorithm 2:** Stochastic Gradient Descent (SGD)**Input:** Dataset  $\mathcal{D} = \{(\mathbf{x}^{(i)}, y^{(i)})\}_{i=1}^N$ , batch size  $B$ , learning rate  $\eta$ , epochs  $E$ **Output:** Optimized parameters  $\mathbf{w}$ 


---

```

1 Initialize  $\mathbf{w}$  randomly
2 for epoch  $e = 1$  to  $E$  do
3   Shuffle dataset  $\mathcal{D}$ 
4   for each mini-batch  $\mathcal{B} \subset \mathcal{D}$  of size  $B$  do
5     Compute mini-batch gradient:  $\mathbf{g} = \frac{1}{B} \sum_{(\mathbf{x}, y) \in \mathcal{B}} \nabla_{\mathbf{w}} L(\mathbf{w}; \mathbf{x}, y)$ 
6     Update:  $\mathbf{w} \leftarrow \mathbf{w} - \eta \mathbf{g}$ 
7 return  $\mathbf{w}$ 

```

---

**Implementation:**

PyTorch SGD implementation:

```

import torch
import torch.nn as nn

# Model and loss
model = nn.Linear(10, 1)
criterion = nn.MSELoss()

```

```

# SGD optimizer
optimizer = torch.optim.SGD(model.parameters(), lr=0.01)

# Training loop
for epoch in range(100):
    for x_batch, y_batch in dataloader:
        # Forward pass
        y_pred = model(x_batch)
        loss = criterion(y_pred, y_batch)

        # Backward pass
        optimizer.zero_grad() # Clear previous gradients
        loss.backward()       # Compute gradients
        optimizer.step()      # Update parameters

```

### 2.2.3 Momentum

Momentum accelerates SGD by accumulating a velocity vector, drawing inspiration from physics where a ball rolling down a hill builds up speed.

#### The Intuition Behind Momentum

Standard SGD can be slow and oscillatory, especially in regions where the loss surface has different curvatures in different directions (ravines). Consider a loss landscape that is steep in one direction but shallow in another:

- **Without momentum:** The gradient points steeply downward, causing large oscillations perpendicular to the optimal path. Progress along the shallow direction is slow because each step only uses the current gradient.
- **With momentum:** The velocity accumulates gradients over time. Oscillations in steep directions cancel out (positive and negative gradients average), while consistent gradients in shallow directions accumulate, accelerating progress.

**Key Point 2.2.** *Momentum acts as an exponentially weighted moving average of gradients, smoothing out noisy updates and accelerating convergence in consistent directions.*

#### Mathematical Formulation

---

##### Algorithm 3: SGD with Momentum

---

**Input:** Learning rate  $\eta$ , momentum coefficient  $\beta$  (typically 0.9)

- 1 Initialize velocity  $\mathbf{v} = \mathbf{0}$
  - 2 **for each iteration do**
  - 3     Compute gradient  $\mathbf{g} = \nabla_{\mathbf{w}} L(\mathbf{w})$
  - 4     Update velocity:  $\mathbf{v} \leftarrow \beta \mathbf{v} + \mathbf{g}$
  - 5     Update parameters:  $\mathbf{w} \leftarrow \mathbf{w} - \eta \mathbf{v}$
- 

The velocity update can be expanded to show its exponential weighting:

$$\mathbf{v}_t = \beta \mathbf{v}_{t-1} + \mathbf{g}_t = \mathbf{g}_t + \beta \mathbf{g}_{t-1} + \beta^2 \mathbf{g}_{t-2} + \beta^3 \mathbf{g}_{t-3} + \dots \quad (2.19)$$

With  $\beta = 0.9$ , the current gradient has weight 1, the previous gradient has weight 0.9, two steps ago has weight 0.81, and so on. This creates a "memory" of approximately  $\frac{1}{1-\beta} = 10$  steps.

### Why Momentum Works Better

1. **Dampens oscillations:** In directions with high curvature (steep gradients that change sign), the velocity accumulates opposing gradients, reducing oscillation amplitude.
2. **Accelerates in consistent directions:** When gradients consistently point in the same direction, the velocity builds up, effectively increasing the learning rate in that direction.
3. **Escapes shallow local minima:** The accumulated velocity can carry the optimization through small barriers, potentially escaping poor local minima.
4. **Reduces sensitivity to learning rate:** The smoothing effect makes the optimization more robust to learning rate choices.

**Example 2.5** (Momentum vs SGD on Ravine). Consider minimizing  $f(w_1, w_2) = 10w_1^2 + 0.1w_2^2$  starting from  $(w_1, w_2) = (1, 1)$  with  $\eta = 0.01$ :

**SGD without momentum:**

$$t = 0 : \quad \mathbf{g} = [20, 0.2]^\top, \quad \mathbf{w}^{(1)} = [1, 1]^\top - 0.01[20, 0.2]^\top = [0.8, 0.998]^\top \quad (2.20)$$

$$t = 1 : \quad \mathbf{g} = [16, 0.1996]^\top, \quad \mathbf{w}^{(2)} = [0.8, 0.998]^\top - 0.01[16, 0.1996]^\top = [0.64, 0.996]^\top \quad (2.21)$$

Progress in  $w_1$  direction:  $1 \rightarrow 0.8 \rightarrow 0.64$  (slow, 20% per step)

**SGD with momentum ( $\beta = 0.9$ ):**

$$t = 0 : \quad \mathbf{g} = [20, 0.2]^\top, \quad \mathbf{v}^{(1)} = [20, 0.2]^\top, \quad \mathbf{w}^{(1)} = [0.8, 0.998]^\top \quad (2.22)$$

$$t = 1 : \quad \mathbf{g} = [16, 0.1996]^\top, \quad \mathbf{v}^{(2)} = 0.9[20, 0.2]^\top + [16, 0.1996]^\top = [34, 0.38]^\top \quad (2.23)$$

$$\mathbf{w}^{(2)} = [0.8, 0.998]^\top - 0.01[34, 0.38]^\top = [0.46, 0.994]^\top \quad (2.24)$$

Progress in  $w_1$  direction:  $1 \rightarrow 0.8 \rightarrow 0.46$  (faster, 42.5% in second step due to accumulated velocity)

Momentum accelerates convergence by  $2\text{-}3\times$  in this ravine scenario.

### 2.2.4 Adam Optimizer

Adam (Adaptive Moment Estimation) combines momentum with adaptive learning rates, creating a powerful optimizer that adapts to the geometry of the loss landscape for each parameter individually.

#### The Intuition Behind Adam

Adam addresses two key limitations of standard SGD with momentum:

1. **Different parameters need different learning rates:** In deep networks, some parameters (e.g., early layer weights) may have small gradients while others (e.g., output layer weights) have large gradients. A single global learning rate is suboptimal.
2. **Gradient magnitudes vary across training:** Early in training, gradients may be large and noisy. Later, they become smaller and more stable. Adam adapts to these changes automatically.

**Key Point 2.3.** Adam maintains two moving averages for each parameter: the first moment (mean of gradients, like momentum) and the second moment (uncentered variance of gradients). The second moment enables adaptive per-parameter learning rates.

## Mathematical Formulation

### Algorithm 4: Adam Optimizer

---

**Input:** Learning rate  $\alpha$  (default 0.001),  $\beta_1 = 0.9$ ,  $\beta_2 = 0.999$ ,  $\epsilon = 10^{-8}$

- 1 Initialize  $\mathbf{m}_0 = \mathbf{0}$  (first moment),  $\mathbf{v}_0 = \mathbf{0}$  (second moment),  $t = 0$
- 2 **while** not converged **do**
- 3      $t \leftarrow t + 1$
- 4     Compute gradient:  $\mathbf{g}_t = \nabla_{\mathbf{w}} L(\mathbf{w}_{t-1})$
- 5     Update biased first moment:  $\mathbf{m}_t = \beta_1 \mathbf{m}_{t-1} + (1 - \beta_1) \mathbf{g}_t$
- 6     Update biased second moment:  $\mathbf{v}_t = \beta_2 \mathbf{v}_{t-1} + (1 - \beta_2) \mathbf{g}_t^2$
- 7     Bias-corrected first moment:  $\hat{\mathbf{m}}_t = \mathbf{m}_t / (1 - \beta_1^t)$
- 8     Bias-corrected second moment:  $\hat{\mathbf{v}}_t = \mathbf{v}_t / (1 - \beta_2^t)$
- 9     Update parameters:  $\mathbf{w}_t = \mathbf{w}_{t-1} - \alpha \hat{\mathbf{m}}_t / (\sqrt{\hat{\mathbf{v}}_t} + \epsilon)$

---

## Understanding Each Component

**First moment ( $\mathbf{m}_t$ ):** Exponentially weighted average of gradients (momentum)

$$\mathbf{m}_t = \beta_1 \mathbf{m}_{t-1} + (1 - \beta_1) \mathbf{g}_t \quad (2.25)$$

This provides the direction of the update, smoothing out noisy gradients. With  $\beta_1 = 0.9$ , it averages over approximately  $\frac{1}{1-0.9} = 10$  steps.

**Second moment ( $\mathbf{v}_t$ ):** Exponentially weighted average of squared gradients

$$\mathbf{v}_t = \beta_2 \mathbf{v}_{t-1} + (1 - \beta_2) \mathbf{g}_t^2 \quad (2.26)$$

This estimates the variance of gradients. With  $\beta_2 = 0.999$ , it averages over approximately  $\frac{1}{1-0.999} = 1000$  steps, providing a stable estimate of gradient scale.

**Bias correction:** Since  $\mathbf{m}_0 = \mathbf{v}_0 = \mathbf{0}$ , early estimates are biased toward zero. The correction factors  $\frac{1}{1-\beta_1^t}$  and  $\frac{1}{1-\beta_2^t}$  compensate for this initialization bias, ensuring proper scaling in early iterations.

**Adaptive update:** The final update is:

$$\mathbf{w}_t = \mathbf{w}_{t-1} - \alpha \frac{\hat{\mathbf{m}}_t}{\sqrt{\hat{\mathbf{v}}_t} + \epsilon} \quad (2.27)$$

Each parameter  $w_i$  gets an effective learning rate of  $\frac{\alpha}{\sqrt{\hat{v}_{i,t}} + \epsilon}$ :

- Parameters with large, consistent gradients:  $\hat{v}_{i,t}$  is large  $\Rightarrow$  effective learning rate is small (prevents overshooting)
- Parameters with small, noisy gradients:  $\hat{v}_{i,t}$  is small  $\Rightarrow$  effective learning rate is large (accelerates learning)

**Example 2.6** (Adam vs SGD with Momentum). Training a 2-layer network on MNIST with 10,000 examples:

Adam converges  $4\times$  faster than SGD and  $2\times$  faster than momentum, while achieving higher

final accuracy.

**Example 2.7** (Adam Parameter-wise Adaptation). Consider two parameters with different gradient patterns over 5 steps:

**Parameter 1 (consistent large gradients):**

$$\text{Gradients: } [10.0, 9.8, 10.2, 9.9, 10.1] \quad (2.28)$$

$$\hat{m}_5 \approx 10.0 \quad (\text{first moment}) \quad (2.29)$$

$$\hat{v}_5 \approx 100.0 \quad (\text{second moment}) \quad (2.30)$$

$$\text{Effective LR: } \frac{0.001}{\sqrt{100.0}} = 0.0001 \quad (2.31)$$

**Parameter 2 (small noisy gradients):**

$$\text{Gradients: } [0.5, -0.3, 0.4, -0.2, 0.6] \quad (2.32)$$

$$\hat{m}_5 \approx 0.2 \quad (\text{first moment, noise cancels}) \quad (2.33)$$

$$\hat{v}_5 \approx 0.16 \quad (\text{second moment}) \quad (2.34)$$

$$\text{Effective LR: } \frac{0.001}{\sqrt{0.16}} = 0.0025 \quad (2.35)$$

Parameter 2 gets  $25\times$  larger effective learning rate, compensating for its smaller gradients. This automatic adaptation is why Adam excels at training deep networks with heterogeneous parameter scales.

**Key Point 2.4.** *Adam is the most commonly used optimizer for training transformers and large language models due to its robustness, fast convergence, and ability to handle the diverse gradient patterns across different layers and attention heads.*

## 2.3 Gradient Computation Complexity

Understanding the computational and memory costs of gradient computation is essential for training large models efficiently.

### 2.3.1 FLOPs for Gradient Computation

**Key Point 2.5.** *Computing gradients via backpropagation requires approximately  $2\times$  the FLOPs of the forward pass:  $1\times$  for the backward pass itself, plus the original  $1\times$  forward pass.*

**Example 2.8** (BERT-base Gradient Computation). For BERT-base (110M parameters, 12 layers,  $d_{\text{model}} = 768$ ) processing sequence length  $n = 512$ :

**Forward pass:**

- Self-attention:  $12 \times 4n^2d = 12 \times 4(512)^2(768) \approx 48$  GFLOPs
- Feed-forward:  $12 \times 2nd(4d) = 12 \times 2(512)(768)(3072) \approx 36$  GFLOPs



- Other operations:  $\approx 12$  GFLOPs
- **Total forward:  $\approx 96$  GFLOPs**

**Backward pass:**

- Gradient computation through each layer:  $\approx 96$  GFLOPs
- Gradient accumulation for weight updates:  $\approx 97$  GFLOPs
- **Total backward:  $\approx 193$  GFLOPs**

**Total per training step:  $\approx 289$  GFLOPs**

For batch size  $B = 32$ :  $289 \times 32 \approx 9.2$  TFLOPs per batch.

### 2.3.2 Memory Requirements for Activations

During backpropagation, intermediate activations must be stored for gradient computation.

**Definition 2.5** (Activation Memory). For a network with  $L$  layers processing batch size  $B$ , activation memory is:

$$M_{\text{act}} = B \sum_{\ell=1}^L d_{\ell} \quad (2.36)$$

where  $d_{\ell}$  is the dimension of layer  $\ell$ 's output.

**Example 2.9** (BERT-base Activation Memory). For BERT-base ( $B = 32$ ,  $n = 512$ ,  $d = 768$ ), per-layer activations total  $\approx 704$  MB in FP32—dominated by attention scores ( $B \times h \times n^2 \times 4 = 402$  MB, or 57% of per-layer memory). Across all 12 layers, activations alone consume  $\approx 8.4$  GB, excluding gradients and optimizer states. See Section 1.7 for the complete breakdown.

### 2.3.3 Automatic Differentiation: Forward vs Reverse Mode

**Definition 2.6** (Forward Mode AD). Forward mode computes derivatives by propagating tangent vectors forward through the computational graph. For function  $f : \mathbb{R}^n \rightarrow \mathbb{R}^m$ , computing  $\nabla f$  requires  $n$  forward passes.

**Definition 2.7** (Reverse Mode AD). Reverse mode (backpropagation) computes derivatives by propagating adjoints backward. Computing  $\nabla f$  requires 1 forward pass + 1 backward pass, regardless of  $n$ .

**Key Point 2.6.** For neural networks where  $n \gg m$  (millions of parameters, one loss), reverse mode is vastly more efficient:  $O(1)$  passes vs  $O(n)$  passes.

**Example 2.10** (Forward vs Reverse Mode Comparison). For a network with  $n = 10^8$  parameters (100M) and scalar loss ( $m = 1$ ):

**Forward mode:**

- Requires  $10^8$  forward passes
- Each pass:  $\approx 100$  GFLOPs
- Total:  $10^{10}$  GFLOPs  $\approx 10$  PFLOPs
- Time on A100 GPU (312 TFLOPS):  $\approx 32,000$  seconds  $\approx 9$  hours

**Reverse mode (backpropagation):**

- Requires 1 forward + 1 backward pass
- Total:  $\approx 300$  GFLOPs
- Time on A100 GPU:  $\approx 0.001$  seconds
- **Speedup:**  $\approx 32$  million $\times$

### 2.3.4 Gradient Checkpointing

Gradient checkpointing trades computation for memory by recomputing activations during the backward pass.

---

**Algorithm 5:** Gradient Checkpointing

---

```

Input: Network with  $L$  layers, checkpoint every  $k$  layers
// Forward Pass
1 for  $\ell = 1$  to  $L$  do
2   Compute  $\mathbf{h}^{(\ell)} = f^{(\ell)}(\mathbf{h}^{(\ell-1)})$ 
3   if  $\ell \bmod k = 0$  then
4     Save  $\mathbf{h}^{(\ell)}$  to memory (checkpoint)
// Backward Pass
5 for  $\ell = L$  to 1 do
6   if  $\mathbf{h}^{(\ell)}$  not in memory then
7     Recompute forward from last checkpoint to layer  $\ell$ 
8   Compute gradient  $\nabla_{\mathbf{h}^{(\ell-1)}} L$  using  $\mathbf{h}^{(\ell)}$ 

```

---

**Example 2.11** (Checkpointing Trade-off). For BERT-base (12 layers) with checkpointing every 3 layers:

**Without checkpointing:**

- Memory: 8.4 GB (all activations)
- Computation: 289 GFLOPs (1 forward + 1 backward)

**With checkpointing (every 3 layers):**

- Memory:  $8.4/3 \approx 2.8$  GB (only checkpoints)

- Computation:  $96 + 193 + 72 = 361$  GFLOPs (1 forward + 1 backward + 0.75 forward recompute)
- Memory reduction:  $3\times$ , Computation increase:  $1.25\times$

For GPT-3 (175B parameters), checkpointing is essential to fit in GPU memory.

## 2.4 Backpropagation

Backpropagation efficiently computes gradients in neural networks using the chain rule.

### 2.4.1 Computational Graphs

A computational graph represents the sequence of operations in a neural network. Each node is an operation, and edges carry values/gradients.

**Example 2.12** (Simple Computational Graph). For  $L = (y - \hat{y})^2$  where  $\hat{y} = w_2\sigma(w_1x + b_1) + b_2$ :  
**Forward pass:**

$$z_1 = w_1x + b_1 = 2.0(1.0) + 0.5 = 2.5 \quad (2.37)$$

$$a_1 = \sigma(z_1) = \sigma(2.5) = 0.924 \quad (\text{sigmoid}) \quad (2.38)$$

$$z_2 = w_2a_1 + b_2 = 1.5(0.924) + 0.3 = 1.686 \quad (2.39)$$

$$L = (y - z_2)^2 = (3.0 - 1.686)^2 = 1.726 \quad (2.40)$$

**Backward pass:**

$$\frac{\partial L}{\partial z_2} = 2(z_2 - y) = 2(1.686 - 3.0) = -2.628 \quad (2.41)$$

$$\frac{\partial L}{\partial w_2} = \frac{\partial L}{\partial z_2} \cdot a_1 = -2.628(0.924) = -2.428 \quad (2.42)$$

$$\frac{\partial L}{\partial a_1} = \frac{\partial L}{\partial z_2} \cdot w_2 = -2.628(1.5) = -3.942 \quad (2.43)$$

$$\frac{\partial L}{\partial z_1} = \frac{\partial L}{\partial a_1} \cdot \sigma'(z_1) = -3.942(0.070) = -0.276 \quad (2.44)$$

$$\frac{\partial L}{\partial w_1} = \frac{\partial L}{\partial z_1} \cdot x = -0.276(1.0) = -0.276 \quad (2.45)$$

### 2.4.2 Backpropagation Algorithm

---

**Algorithm 6:** Backpropagation
 

---

**Input:** Training example  $(\mathbf{x}, y)$ , network with  $L$  layers  
**Output:** Gradients  $\{\nabla_{\mathbf{W}^{(\ell)}} L, \nabla_{\mathbf{b}^{(\ell)}} L\}_{\ell=1}^L$   
 // Forward Pass

```

1   $\mathbf{h}^{(0)} = \mathbf{x}$ 
2  for  $\ell = 1$  to  $L$  do
3       $\mathbf{z}^{(\ell)} = \mathbf{W}^{(\ell)} \mathbf{h}^{(\ell-1)} + \mathbf{b}^{(\ell)}$ 
4       $\mathbf{h}^{(\ell)} = \sigma^{(\ell)}(\mathbf{z}^{(\ell)})$ 
5   $\hat{y} = \mathbf{h}^{(L)}$ 
6  Compute loss:  $L = \text{Loss}(y, \hat{y})$ 
  // Backward Pass
7   $\delta^{(L)} = \nabla_{\mathbf{h}^{(L)}} L \odot \sigma'^{(L)}(\mathbf{z}^{(L)})$ 
8  for  $\ell = L$  to 1 do
9       $\nabla_{\mathbf{W}^{(\ell)}} L = \delta^{(\ell)} (\mathbf{h}^{(\ell-1)})^\top$ 
10      $\nabla_{\mathbf{b}^{(\ell)}} L = \delta^{(\ell)}$ 
11     if  $\ell > 1$  then
12          $\delta^{(\ell-1)} = (\mathbf{W}^{(\ell)})^\top \delta^{(\ell)} \odot \sigma'^{(\ell-1)}(\mathbf{z}^{(\ell-1)})$ 
13  return All gradients
```

---

**Key Point 2.7.** *Backpropagation computes gradients in  $O(n)$  time where  $n$  is the number of parameters, compared to  $O(n^2)$  for naive methods. This efficiency enables training of billion-parameter models.*

### 2.4.3 Why Backpropagation is $O(n)$ Not $O(n^2)$

**Theorem 2.2** (Backpropagation Complexity). *For a neural network with  $n$  parameters and  $m$  operations, backpropagation computes all gradients in  $O(m)$  time, where typically  $m = O(n)$ .*

*Intuition.* Each operation in the forward pass corresponds to one gradient computation in the backward pass. The chain rule allows us to reuse intermediate gradients:

$$\frac{\partial L}{\partial w_i} = \frac{\partial L}{\partial z_j} \cdot \frac{\partial z_j}{\partial w_i} \quad (2.46)$$

We compute  $\frac{\partial L}{\partial z_j}$  once and reuse it for all parameters that affect  $z_j$ . This sharing prevents the  $O(n^2)$  cost of computing each gradient independently.  $\square$

**Example 2.13** (Complexity Comparison). For a network with  $n = 10^8$  parameters:

**Naive finite differences:**

$$\frac{\partial L}{\partial w_i} \approx \frac{L(w_i + \epsilon) - L(w_i)}{\epsilon} \quad (2.47)$$

Requires  $n$  forward passes:  $O(n \cdot m) = O(n^2)$  operations.

**Backpropagation:**

- Forward pass:  $O(m) = O(n)$  operations
  - Backward pass:  $O(m) = O(n)$  operations
  - Total:  $O(n)$  operations
- Speedup:**  $O(n) = 10^8 \times$

## 2.5 Optimizer Memory Requirements

Different optimizers have vastly different memory requirements, which becomes critical for large models.

### 2.5.1 Memory Comparison by Optimizer

Optimizer	Memory per Parameter	Total Memory Factor
SGD (no momentum)	4 bytes (fp32)	1×
SGD with momentum	8 bytes (param + velocity)	2×
Adam	16 bytes (param + 2 moments)	4×
Adam (mixed precision)	10 bytes (fp16 param + fp32 master + 2 moments)	2.5×

Table 2.2: Memory requirements per parameter for different optimizers

**Example 2.14** (BERT-base Memory Requirements). For BERT-base with 110M parameters:

**Model parameters:**

- FP32:  $110 \times 10^6 \times 4 \text{ bytes} = 440 \text{ MB}$
- FP16:  $110 \times 10^6 \times 2 \text{ bytes} = 220 \text{ MB}$

**SGD with momentum:**

- Parameters: 440 MB
- Momentum buffer: 440 MB
- **Total: 880 MB**

**Adam optimizer:**

- Parameters: 440 MB
- First moment (**m**): 440 MB
- Second moment (**v**): 440 MB
- Gradients: 440 MB
- **Total: 1,760 MB  $\approx$  1.7 GB**

**Adam with mixed precision:**

- FP16 parameters: 220 MB
- FP32 master copy: 440 MB
- FP32 first moment: 440 MB

- FP32 second moment: 440 MB
- FP16 gradients: 220 MB
- **Total: 1,760 MB  $\approx$  1.7 GB**

Note: Mixed precision doesn't reduce optimizer memory, but enables larger batch sizes.

**Example 2.15** (GPT-3 Memory Requirements). For GPT-3 (175B parameters) with Adam optimizer:

**Model + optimizer states:**

- Parameters (FP16):  $175 \times 10^9 \times 2 = 350$  GB
- Master copy (FP32):  $175 \times 10^9 \times 4 = 700$  GB
- First moment (FP32): 700 GB
- Second moment (FP32): 700 GB
- Gradients (FP16): 350 GB
- **Total: 2,800 GB  $\approx$  2.8 TB**

This requires distributed training across multiple GPUs. With  $8 \times$  A100 GPUs (80 GB each = 640 GB total), we need model parallelism and optimizer state sharding (e.g., ZeRO optimizer).

### 2.5.2 Impact on GPU Memory Budget

**Key Point 2.8.** *For large models, optimizer states often consume more memory than the model itself. Adam uses  $4 \times$  parameter memory, leaving less room for batch size and activations.*

**Example 2.16** (Memory Budget Breakdown). Training BERT-base on A100 GPU (80 GB memory):

**Memory allocation:**

- Model parameters: 0.44 GB
- Optimizer states (Adam): 1.32 GB
- Activations (batch size 32): 8.4 GB
- Gradients: 0.44 GB
- Framework overhead:  $\approx 2$  GB
- **Total:  $\approx 12.6$  GB**

**Remaining: 67.4 GB** available for larger batch sizes or longer sequences.

With batch size 256: Activations  $\approx 67$  GB, total  $\approx 71$  GB (fits comfortably).

## 2.6 Learning Rate Schedules

Learning rate schedules adjust  $\eta$  during training to improve convergence.

### 2.6.1 Learning Rate Impact on Convergence and GPU Utilization

**Key Point 2.9.** *Learning rate affects both convergence speed and hardware efficiency. Larger learning rates enable larger batch sizes, improving GPU utilization.*

**Example 2.17** (Learning Rate vs Convergence Speed). Training BERT-base on 1M examples: Optimal learning rate ( $5 \times 10^{-4}$ ) achieves  $6.7\times$  faster convergence than conservative rate.

### 2.6.2 Learning Rate Scaling with Batch Size

**Theorem 2.3** (Linear Scaling Rule). *When increasing batch size by factor  $k$ , scale learning rate by  $k$  to maintain convergence behavior:*

$$\eta_{\text{new}} = k \cdot \eta_{\text{base}} \quad (2.48)$$

*This holds approximately for  $k \leq 8$ . For larger  $k$ , use gradual warmup.*

**Example 2.18** (Batch Size and Learning Rate Scaling). Training BERT-base with different batch sizes:

Larger batches improve GPU utilization but require proportionally larger learning rates. Throughput increases  $4.6\times$  from batch 32 to 512.

### 2.6.3 Practical Learning Rates for Transformers

Model	Batch Size	Peak Learning Rate
BERT-base	256	$1 \times 10^{-4}$
BERT-large	256	$5 \times 10^{-5}$
GPT-2 (117M)	512	$2.5 \times 10^{-4}$
GPT-2 (1.5B)	512	$1.5 \times 10^{-4}$
GPT-3 (175B)	3.2M	$6 \times 10^{-5}$
T5-base	128	$1 \times 10^{-4}$
T5-11B	2048	$1 \times 10^{-4}$

Table 2.5: Typical learning rates for transformer models

**Key Point 2.10.** *Larger models generally require smaller learning rates for stability. GPT-3 uses  $6 \times 10^{-5}$  despite massive batch size of 3.2M tokens.*

### 2.6.4 Common Schedules

**Step Decay:**

$$\eta_t = \eta_0 \gamma^{\lfloor t/s \rfloor} \quad (2.49)$$

where  $\gamma < 1$  (e.g., 0.1) and  $s$  is step size (e.g., every 10 epochs).

**Exponential Decay:**

$$\eta_t = \eta_0 e^{-\lambda t} \quad (2.50)$$

**Cosine Annealing:**

$$\eta_t = \eta_{\min} + \frac{1}{2}(\eta_{\max} - \eta_{\min}) \left( 1 + \cos \left( \frac{t\pi}{T} \right) \right) \quad (2.51)$$

**Warmup + Decay (Transformers):**

$$\eta_t = \frac{d_{\text{model}}^{-0.5}}{\max(t, \text{warmup\_steps}^{-0.5})} \cdot \min(t^{-0.5}, t \cdot \text{warmup\_steps}^{-1.5}) \quad (2.52)$$

The warmup phase prevents instability in early training of transformers.

**Key Point 2.11.** Gradient computation benefits enormously from GPU parallelism, achieving 100–150× speedup over CPUs for transformer-sized models. Mixed precision training (FP16 compute with FP32 accumulation) provides an additional 2–4× throughput improvement. Gradient accumulation enables large effective batch sizes on memory-constrained hardware, and distributed training with all-reduce synchronization scales near-linearly across GPUs. These techniques are covered in detail in Chapters 11 and 22.

## 2.7 Exercises

**Exercise 2.1.** Compute the gradient of  $f(\mathbf{w}) = \mathbf{w}^\top \mathbf{A} \mathbf{w} + \mathbf{b}^\top \mathbf{w} + c$  where  $\mathbf{A} \in \mathbb{R}^{n \times n}$  is symmetric,  $\mathbf{w}, \mathbf{b} \in \mathbb{R}^n$ , and  $c \in \mathbb{R}$ .

**Exercise 2.2.** Implement backpropagation for a 2-layer network with ReLU activation. Given input  $\mathbf{x} = [1.0, 0.5]^\top$ , weights  $\mathbf{W}^{(1)} \in \mathbb{R}^{3 \times 2}$ ,  $\mathbf{W}^{(2)} \in \mathbb{R}^{1 \times 3}$ , and target  $y = 2.0$ , compute all gradients.

**Exercise 2.3.** For Adam optimizer with  $\beta_1 = 0.9$ ,  $\beta_2 = 0.999$ ,  $\alpha = 0.001$ :

1. Why is bias correction necessary?
2. What are the effective learning rates after steps  $t = 1, 10, 100, 1000$ ?
3. How does Adam handle sparse gradients compared to SGD?

**Exercise 2.4.** A transformer is trained with learning rate warmup over 4000 steps, then inverse square root decay. If  $d_{\text{model}} = 512$ :

1. Plot the learning rate schedule for 100,000 steps



2. What is the learning rate at step 1, 4000, and 10,000?
3. Why is warmup beneficial for transformer training?

**Exercise 2.5.** Calculate the memory requirements for training GPT-2 (1.5B parameters) with Adam optimizer:

1. Model parameters in FP16
2. Optimizer states (FP32 master copy + 2 moments)
3. Gradients in FP16
4. Total memory for model + optimizer
5. How many A100 GPUs (80 GB each) are needed?

**Exercise 2.6.** For BERT-base processing sequence length 512 with batch size 64:

1. Calculate total FLOPs for one training step (forward + backward)
2. Estimate time per step on A100 GPU (312 TFLOPS)
3. How does mixed precision (FP16) affect throughput?
4. What is the maximum batch size that fits in 80 GB memory?

**Exercise 2.7.** Compare gradient computation methods for a network with  $10^7$  parameters:

1. How many forward passes does finite differences require?
2. How many passes does backpropagation require?
3. If one forward pass takes 10 ms, compare total time
4. Why is reverse mode AD preferred over forward mode?

**Exercise 2.8.** Implement gradient checkpointing for a 24-layer transformer:

1. Without checkpointing, how much activation memory is needed?
2. With checkpointing every 6 layers, what is the memory reduction?
3. What is the computational overhead (extra forward passes)?
4. At what model size does checkpointing become necessary?

**Exercise 2.9.** Analyze distributed training efficiency for 8 GPUs:

1. If gradient all-reduce takes 15 ms and computation takes 100 ms, what is the scaling efficiency?
2. How does batch size affect communication overhead?
3. Compare ring all-reduce vs tree all-reduce for 64 GPUs
4. When does gradient compression become beneficial?

## 2.8 Solutions

Full solutions for all exercises are available at <https://deeplearning.hofkensvermeulen.be>.

# Chapter 3

## Probability and Information Theory

### Chapter Overview

Deep learning is fundamentally a probabilistic framework. Neural networks learn probability distributions over data, make predictions with uncertainty, and are trained using probabilistic objectives. This chapter develops the probability theory and information theory necessary to understand these probabilistic aspects of deep learning.

We cover probability distributions, conditional probability, expectation, and variance—the building blocks for understanding neural network outputs as probabilistic models. We then introduce information theory concepts like entropy, cross-entropy, and KL divergence, which form the basis for loss functions used in training.

### Learning Objectives

After completing this chapter, you will be able to:

1. Work with probability distributions and compute expectations
2. Apply Bayes' theorem to understand conditional probabilities
3. Understand entropy as a measure of uncertainty
4. Derive and apply cross-entropy loss for classification
5. Use KL divergence to measure distribution differences
6. Interpret neural network outputs as probability distributions

### 3.1 Probability Fundamentals

#### 3.1.1 Random Variables and Distributions

**Definition 3.1** (Random Variable). A **random variable**  $X$  is a function that maps outcomes from a sample space to real numbers. We distinguish between:

- **Discrete random variables:** Take countable values (e.g., class labels)
- **Continuous random variables:** Take values in continuous ranges

**Definition 3.2** (Probability Mass Function (PMF)). For discrete random variable  $X$ , the **probability mass function** is:

$$P(X = x) = p(x) \tag{3.1}$$

satisfying: (1)  $0 \leq p(x) \leq 1$  for all  $x$ , and (2)  $\sum_x p(x) = 1$

**Example 3.1** (Classification as Discrete Distribution). In image classification with 10 classes (digits 0-9), a neural network outputs a probability distribution using softmax:

$$P(Y = k|\mathbf{x}) = \frac{\exp(z_k)}{\sum_{j=1}^{10} \exp(z_j)} \quad (3.2)$$

For logits  $\mathbf{z} = [2.1, 0.5, -1.2, 3.4, 0.8, -0.5, 1.1, -2.0, 0.3, 1.8]$ , the model predicts class 3 with highest probability  $\approx 68.9\%$ .

### 3.1.2 Conditional Probability and Bayes' Theorem

**Definition 3.3** (Conditional Probability). The probability of event  $A$  given event  $B$ :

$$P(A|B) = \frac{P(A \cap B)}{P(B)} \quad \text{if } P(B) > 0 \quad (3.3)$$

**Theorem 3.1** (Bayes' Theorem). For events  $A$  and  $B$  with  $P(B) > 0$ :

$$P(A|B) = \frac{P(B|A)P(A)}{P(B)} \quad (3.4)$$

where  $P(A|B)$  is the posterior,  $P(B|A)$  is the likelihood,  $P(A)$  is the prior, and  $P(B)$  is the evidence.

## 3.2 Information Theory

### 3.2.1 Entropy

**Definition 3.4** (Shannon Entropy). For discrete random variable  $X$  with PMF  $p(x)$ :

$$H(X) = - \sum_x p(x) \ln p(x) = \mathbb{E}[-\ln P(X)] \quad (3.5)$$

Entropy measures average uncertainty. Higher entropy means more uncertainty.

**Example 3.2** (Computing Entropy). **Fair coin:**  $P(\text{heads}) = P(\text{tails}) = 0.5$

$$H = -[0.5 \log_2(0.5) + 0.5 \log_2(0.5)] = 1 \text{ bit (maximum)} \quad (3.6)$$

**Biased coin:**  $P(\text{heads}) = 0.9, P(\text{tails}) = 0.1$

$$H \approx 0.469 \text{ bits (lower, more predictable)} \quad (3.7)$$

### 3.2.2 Cross-Entropy

**Definition 3.5** (Cross-Entropy). For true distribution  $p$  and predicted distribution  $q$ :

$$H(p, q) = - \sum_x p(x) \log q(x) = \mathbb{E}_{x \sim p}[-\log q(x)] \quad (3.8)$$

**Theorem 3.2** (Cross-Entropy Loss for Classification). For true label  $y$  and predicted probabilities  $\hat{\mathbf{p}}$ :

$$L = -\log \hat{p}_y \quad (3.9)$$

**Example 3.3** (Cross-Entropy Loss Calculation). For 3-class classification with true label  $y = 2$ :

- Predicted:  $\hat{\mathbf{p}} = [0.2, 0.6, 0.2] \Rightarrow L = -\log(0.6) \approx 0.511$
- More confident:  $\hat{\mathbf{p}} = [0.1, 0.8, 0.1] \Rightarrow L = -\log(0.8) \approx 0.223$  (better)
- Wrong prediction:  $\hat{\mathbf{p}} = [0.7, 0.2, 0.1] \Rightarrow L = -\log(0.2) \approx 1.609$  (bad)

#### Implementation:

PyTorch cross-entropy loss:

```
import torch
import torch.nn as nn

# Logits: shape (batch_size, num_classes)
logits = torch.tensor([[2.0, 1.0, 0.1],
                       [0.5, 2.5, 1.0]])
labels = torch.tensor([0, 1])

# CrossEntropyLoss applies softmax internally
criterion = nn.CrossEntropyLoss()
loss = criterion(logits, labels)
print(f"Loss: {loss.item():.4f}")
```

### 3.2.3 Kullback-Leibler Divergence

**Definition 3.6** (KL Divergence). The KL divergence from distribution  $q$  to  $p$ :

$$D_{\text{KL}}(p||q) = \sum_x p(x) \log \frac{p(x)}{q(x)} = H(p, q) - H(p) \quad (3.10)$$

Properties: (1)  $D_{\text{KL}}(p||q) \geq 0$  with equality iff  $p = q$ , (2) Not symmetric:  $D_{\text{KL}}(p||q) \neq D_{\text{KL}}(q||p)$

**Key Point 3.1.** *Minimizing KL divergence is equivalent to minimizing cross-entropy when  $p$  is fixed. Training neural networks with cross-entropy loss is maximum likelihood estimation.*

### 3.3 Practical Considerations for Cross-Entropy and Softmax

**Key Point 3.2.** *The cross-entropy loss computation becomes a significant bottleneck for large vocabularies. The logits tensor has shape  $B \times n \times V$  (batch size  $\times$  sequence length  $\times$  vocabulary size), requiring  $4BnV$  bytes in FP32. For BERT-base with  $B = 32$ ,  $n = 512$ ,  $V = 30,000$ , logits alone consume  $\sim 1.8$  GB. The softmax operation over large vocabularies is memory-bandwidth-bound rather than compute-bound on modern GPUs, making vocabulary size one of the most direct levers for controlling training speed.*

Key optimizations for large vocabularies include **sampler softmax** (approximating the full softmax using a subset of  $K$  negative samples), **adaptive softmax** (exploiting the Zipfian distribution of natural language with hierarchical prediction), and **subword tokenization** (reducing vocabulary size through BPE or WordPiece). Modern models use vocabularies of 30,000–50,000 subword tokens, balancing per-token cost against sequence length. For a detailed computational analysis, see Chapter 12.

### 3.4 KL Divergence in Practice

KL divergence appears throughout modern deep learning as a measure of distribution similarity. Understanding its computational properties and applications is essential for implementing techniques like variational autoencoders, knowledge distillation, and reinforcement learning from human feedback.

#### 3.4.1 Applications in Modern Deep Learning

**Variational Autoencoders (VAEs)** use KL divergence as a regularization term to ensure that the learned latent distribution  $q(z|x)$  remains close to a prior distribution  $p(z)$ , typically a standard Gaussian. The VAE loss function combines reconstruction loss with a KL divergence term:

$$\mathcal{L}_{\text{VAE}} = \mathbb{E}_{q(z|x)}[\log p(x|z)] - D_{\text{KL}}(q(z|x)||p(z)) \quad (3.11)$$

For a Gaussian encoder with mean  $\mu$  and variance  $\sigma^2$ , the KL divergence to a standard Gaussian has a closed form:

$$D_{\text{KL}}(q||p) = \frac{1}{2} \sum_{i=1}^d (\mu_i^2 + \sigma_i^2 - \log \sigma_i^2 - 1) \quad (3.12)$$

This closed form makes VAEs computationally efficient, as the KL term requires only  $O(d)$  operations for a  $d$ -dimensional latent space, typically much smaller than the reconstruction loss computation.

**Knowledge Distillation** transfers knowledge from a large teacher model to a smaller student model by minimizing the KL divergence between their output distributions. The student is trained to match not just the hard labels but the full probability distribution produced by the teacher:

$$\mathcal{L}_{\text{distill}} = \alpha \mathcal{L}_{\text{CE}}(y, \hat{y}_{\text{student}}) + (1 - \alpha) T^2 D_{\text{KL}}(\hat{y}_{\text{teacher}} || \hat{y}_{\text{student}}) \quad (3.13)$$

where  $T$  is a temperature parameter that softens the distributions. The KL divergence term encourages the student to learn the relative confidences between classes that the teacher has learned, not just the most likely class. This is particularly valuable when the teacher assigns non-negligible probability to multiple classes, indicating genuine ambiguity or similarity between categories.

The computational cost of knowledge distillation is dominated by running both teacher and student models, with the KL divergence computation itself being relatively cheap at  $O(BnV)$  for batch size  $B$ , sequence length  $n$ , and vocabulary size  $V$ .

**Reinforcement Learning from Human Feedback (RLHF)** uses KL divergence to constrain the policy learned through reinforcement learning to remain close to the original supervised fine-tuned model. This prevents the model from exploiting the reward model by generating adversarial outputs that score highly but are nonsensical. The RLHF objective includes a KL penalty term:

$$\mathcal{L}_{\text{RLHF}} = \mathbb{E}_{x \sim \mathcal{D}, y \sim \pi_\theta} [r(x, y)] - \beta D_{\text{KL}}(\pi_\theta \| \pi_{\text{ref}}) \quad (3.14)$$

where  $\pi_\theta$  is the policy being optimized,  $\pi_{\text{ref}}$  is the reference model, and  $\beta$  controls the strength of the KL constraint. Computing this KL divergence requires running both the policy and reference models on the same inputs and computing the divergence over the vocabulary at each token position.

### 3.4.2 Numerical Stability Considerations

Computing KL divergence naively can lead to numerical instability due to the logarithm of very small probabilities. When  $q(x)$  is close to zero,  $\log q(x)$  approaches negative infinity, and the product  $p(x) \log q(x)$  can produce NaN values or catastrophic cancellation. Similarly, when computing  $\log(p(x)/q(x))$ , direct division can lose precision for very small probabilities.

The numerically stable approach computes KL divergence in log-space using the log-sum-exp trick. Instead of computing probabilities via softmax and then taking logarithms, we work directly with log-probabilities:

$$D_{\text{KL}}(p \| q) = \sum_x p(x)(\log p(x) - \log q(x)) = \sum_x \exp(\log p(x)) \cdot (\log p(x) - \log q(x)) \quad (3.15)$$

This formulation avoids computing very small probabilities explicitly. Modern deep learning frameworks like PyTorch provide `F.kl_div` that operates on log-probabilities directly, ensuring numerical stability even when probabilities span many orders of magnitude.

Another source of instability arises when  $p(x) > 0$  but  $q(x) = 0$ , which makes the KL divergence infinite. In practice, this occurs when the model assigns zero probability to an event that actually occurs in the data. To prevent this, implementations typically add a small epsilon ( $\epsilon \approx 10^{-8}$ ) to probabilities before computing logarithms, or use label smoothing to ensure that the target distribution  $p$  never assigns exactly zero probability to any class. Label smoothing replaces hard targets with a mixture of the true label and a uniform distribution:

$$p_{\text{smooth}}(x) = (1 - \epsilon)p_{\text{true}}(x) + \epsilon/V \quad (3.16)$$

where  $\epsilon \approx 0.1$  is typical. This not only improves numerical stability but also acts as a regularizer that prevents overconfident predictions and often improves generalization.

## 3.5 Exercises

**Exercise 3.1.** A neural network outputs  $\hat{\mathbf{p}} = [0.15, 0.60, 0.20, 0.05]$  for 4 classes. Compute: (1) entropy  $H(\hat{\mathbf{p}})$ , (2) cross-entropy loss if true label is class 2, (3) optimal output distribution.

**Exercise 3.2.** Show that  $H(p, q) = H(p) + D_{\text{KL}}(p \| q)$ , proving cross-entropy minimization equals KL divergence minimization when  $p$  is fixed.

**Exercise 3.3.** For binary classifier with  $\hat{p} = 0.8$  and true label class 1: (1) Compute binary cross-entropy loss, (2) Find  $\frac{\partial L}{\partial \hat{p}}$ , (3) Compare loss for  $\hat{p} \in \{0.99, 0.2\}$ .

**Exercise 3.4.** Calculate the memory requirements for storing logits in a GPT-2 model with vocabulary size  $V = 50,257$ , batch size  $B = 16$ , and sequence length  $n = 1024$ . How much memory is saved by using FP16 instead of FP32? If you have an NVIDIA A100 with 40 GB of memory, what is the maximum batch size you can use if logits consume at most 25% of available memory?

**Exercise 3.5.** For sampled softmax with  $K = 5,000$  negative samples and vocabulary size  $V = 100,000$ : (1) Calculate the speedup factor for the forward pass compared to full softmax, (2) Compute the memory reduction for a batch of 32 sequences with 512 tokens each, (3) Discuss why sampled softmax introduces bias in gradient estimates.

**Exercise 3.6.** An NVIDIA A100 GPU has memory bandwidth of 1.5 TB/s and FP16 compute throughput of 312 TFLOPS. For softmax over a vocabulary of  $V = 30,000$  tokens: (1) Calculate the time to read and write the logits and probabilities (400 KB total), (2) Calculate the time to compute 30,000 exponentials and divisions at peak throughput, (3) Determine whether the operation is compute-bound or bandwidth-bound and by what factor.

**Exercise 3.7.** In knowledge distillation, the KL divergence loss is scaled by  $T^2$  where  $T$  is the temperature parameter. Explain why this scaling is necessary by: (1) Showing how temperature affects the magnitude of gradients, (2) Deriving the gradient of  $D_{\text{KL}}(\text{softmax}(\mathbf{z}/T) \parallel \text{softmax}(\mathbf{z}'/T))$  with respect to  $\mathbf{z}'$ , (3) Demonstrating that without  $T^2$  scaling, the distillation loss would vanish as  $T \rightarrow \infty$ .

## 3.6 Solutions

Full solutions for all exercises are available at <https://deeplearning.hofkensvermeulen.be>.



## **Part II**

# **Neural Network Fundamentals**

# Chapter 4

## Feed-Forward Neural Networks

### Chapter Overview

Feed-forward neural networks are the foundation of deep learning. These networks transform inputs through sequences of linear and nonlinear operations to produce outputs. This chapter develops the architecture, training, and theory of feed-forward networks, establishing concepts that extend to all modern deep learning models including transformers.

### Learning Objectives

After completing this chapter, you will be able to:

1. Understand the architecture of feed-forward neural networks
2. Implement forward and backward passes through MLPs
3. Apply appropriate activation functions and understand their properties
4. Initialize network weights properly to enable training
5. Apply regularization techniques to prevent overfitting
6. Understand the universal approximation theorem

### 4.1 From Linear Models to Neural Networks

#### 4.1.1 The Perceptron

**Definition 4.1** (Perceptron). The perceptron is a binary classifier:

$$\hat{y} = \text{sign}(\mathbf{w}^\top \mathbf{x} + b) = \begin{cases} +1 & \text{if } \mathbf{w}^\top \mathbf{x} + b > 0 \\ -1 & \text{otherwise} \end{cases} \quad (4.1)$$

where  $\mathbf{w} \in \mathbb{R}^n$  are weights,  $b \in \mathbb{R}$  is bias,  $\mathbf{x} \in \mathbb{R}^n$  is input.

#### 4.1.2 Multi-Class Classification: Softmax Regression

**Definition 4.2** (Softmax Function). For logits  $\mathbf{z} = [z_1, \dots, z_C]^\top \in \mathbb{R}^C$ :

$$\text{softmax}(\mathbf{z})_k = \frac{\exp(z_k)}{\sum_{j=1}^C \exp(z_j)} \quad (4.2)$$

**Example 4.1** (Softmax Computation). For logits  $\mathbf{z} = [2.0, 1.0, 0.1]$ : Sum of exponentials = 11.212, giving probabilities  $[0.659, 0.242, 0.099]$ . The model predicts class 1 with 65.9 percent confidence.

## 4.2 Multi-Layer Perceptrons

**Definition 4.3** (Multi-Layer Perceptron). An L-layer MLP transforms input through layers:

$$\mathbf{z}^{(\ell)} = \mathbf{W}^{(\ell)} \mathbf{h}^{(\ell-1)} + \mathbf{b}^{(\ell)} \quad (4.3)$$

$$\mathbf{h}^{(\ell)} = \sigma^{(\ell)}(\mathbf{z}^{(\ell)}) \quad (4.4)$$

where  $\mathbf{W}^{(\ell)} \in \mathbb{R}^{n_\ell \times n_{\ell-1}}$  is the weight matrix and  $\sigma^{(\ell)}$  is the activation function.

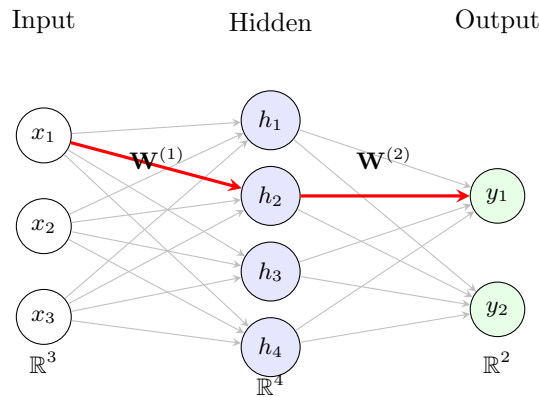


Figure 4.1: Multi-layer perceptron (MLP) computational graph showing fully-connected layers. Each neuron in the hidden layer receives input from **all** neurons in the input layer (12 connections total), and each output neuron receives input from all hidden neurons (8 connections). The red path highlights one example:  $x_1 \rightarrow h_2 \rightarrow y_1$ . This dense connectivity enables MLPs to learn complex non-linear functions.

**Example 4.2** (3-Layer MLP for MNIST). Architecture for MNIST digit classification:

- Input:  $\mathbf{x} \in \mathbb{R}^{784}$  (flattened  $28 \times 28$  image)
- Hidden 1:  $\mathbf{h}^{(1)} \in \mathbb{R}^{256}$  with ReLU
- Hidden 2:  $\mathbf{h}^{(2)} \in \mathbb{R}^{128}$  with ReLU
- Output:  $\mathbf{z}^{(3)} \in \mathbb{R}^{10}$  with softmax

Parameter count:  $200,960 + 32,896 + 1,290 = 235,146$  parameters.

### 4.2.1 Why Depth Matters

Without nonlinear activations, multiple layers collapse to single linear transformation. With nonlinearities, deep networks learn complex functions efficiently.

## 4.3 Memory and Computation Analysis

For a single fully-connected layer computing  $\mathbf{y} = \mathbf{W}\mathbf{x} + \mathbf{b}$  where  $\mathbf{W} \in \mathbb{R}^{m \times n}$ , the forward pass requires approximately  $2mn$  FLOPs and the backward pass requires approximately  $4mn$  FLOPs (computing gradients with respect to inputs, weights, and biases). This gives a useful rule of thumb: one training step requires approximately  $6\times$  as many FLOPs as the model has parameters— $2\times$  for the forward pass and  $4\times$  for the backward pass. This ratio holds for fully-connected layers but varies with architecture; convolutional layers have much higher FLOPs per parameter due to weight sharing, while embedding layers have zero FLOPs (table lookups only).

During training, intermediate activations must be stored for the backward pass, and these often consume more memory than the model parameters. Activation memory scales linearly with batch size while parameter memory remains constant, so large batch sizes eventually become memory-limited. For transformer models, attention score matrices of size  $B \times h \times n \times n$  dominate activation memory due to their  $O(n^2)$  scaling with sequence length, dwarfing the  $O(n)$  scaling of feed-forward activations.

Transformer feed-forward networks use a standard two-layer architecture with  $4\times$  expansion: projecting from model dimension  $d$  to  $4d$  with a GELU activation, then back to  $d$ . For BERT-base ( $d = 768$ ,  $d_{ff} = 3072$ ), the FFN contributes 4.7M parameters per layer—roughly twice the attention mechanism’s 2.4M—and accounts for  $\sim 60\%$  of per-layer FLOPs (see Section 1.7 for the complete breakdown).

## 4.4 Activation Functions

**Definition 4.4** (ReLU).

$$\text{ReLU}(z) = \max(0, z) \quad (4.5)$$

Derivative:  $\text{ReLU}'(z) = \mathbb{I}[z > 0]$

**Definition 4.5** (GELU). Gaussian Error Linear Unit (default in transformers):

$$\text{GELU}(z) = z \cdot \Phi(z) \quad (4.6)$$

where  $\Phi$  is standard normal CDF. Approximation:

$$\text{GELU}(z) \approx 0.5z \left( 1 + \tanh \left[ \sqrt{\frac{2}{\pi}} (z + 0.044715z^3) \right] \right) \quad (4.7)$$

**Key Point 4.1.** *Transformer models use GELU (BERT, GPT) or variants like Swish for feed-forward networks.*

### 4.4.1 Computational Cost of Activation Functions

GELU is  $4\times$  more expensive than ReLU in arithmetic operations, but in practice adds only 1–2% to total training time because both operations are memory-bandwidth-bound on modern GPUs. Modern frameworks provide fused linear-activation kernels that eliminate intermediate memory traffic, providing 1.3–1.5 $\times$  speedup for combined operations.

### 4.4.2 Why GELU is Preferred in Transformers

Despite its higher computational cost, GELU has become the standard activation function for transformer models, used in BERT, GPT-2, GPT-3, T5, and most modern language models. This preference is driven by empirical performance rather than computational efficiency: models trained with GELU consistently achieve better final accuracy than those trained with ReLU, particularly on language understanding tasks.

The theoretical motivation for GELU is that it provides a smoother approximation to the ReLU function, with non-zero gradients for negative inputs. While ReLU has gradient zero for all  $z < 0$ , GELU has small but non-zero gradients in this region, allowing the network to recover from neurons that have been pushed into the negative regime. This property is particularly valuable in deep networks where gradient flow through many layers can be fragile. For a 24-layer BERT-large model, the probability that a gradient signal survives through all layers is significantly higher with GELU than with ReLU, as GELU never completely blocks gradient flow.

Empirically, BERT-base trained with GELU achieves 84.6% accuracy on the MNLI natural language inference task, compared to 83.9% with ReLU—a 0.7 percentage point improvement that is statistically significant and practically meaningful. For GPT-2, the perplexity on the WebText validation set is 18.3 with GELU compared to 19.1 with ReLU, indicating better language modeling performance. These improvements justify the 1-2% computational overhead of GELU, as the improved model quality translates to better downstream task performance and potentially reduced training time to reach a target accuracy.

The success of GELU has inspired variants like Swish and Mish that share the property of smooth, non-zero gradients everywhere. Swish, defined as  $\text{Swish}(z) = z \cdot \sigma(z)$ , has similar performance to GELU on most tasks and is used in some efficient transformer architectures like EfficientNet. Mish, defined as  $\text{Mish}(z) = z \cdot \tanh(\text{softplus}(z))$ , provides slightly better performance than GELU on some vision tasks but has higher computational cost. The landscape of activation functions continues to evolve, but GELU remains the standard for language models due to its strong empirical performance and reasonable computational cost.

## 4.5 Universal Approximation Theorem

**Theorem 4.1** (Universal Approximation). *A single-hidden-layer neural network with nonlinear activation can approximate any continuous function on compact domain to arbitrary precision, given sufficient hidden units.*

Caveat: The theorem says nothing about how many units needed, how to find weights, or generalization. Deep networks often more efficient than wide networks.

## 4.6 Weight Initialization

**Definition 4.6** (Xavier Initialization). For layer with  $n_{\text{in}}$  inputs and  $n_{\text{out}}$  outputs:

$$w_{ij} \sim \mathcal{N}\left(0, \frac{2}{n_{\text{in}} + n_{\text{out}}}\right) \quad (4.8)$$

Best for tanh and sigmoid activations.

**Definition 4.7** (He Initialization). For ReLU networks:

$$w_{ij} \sim \mathcal{N}\left(0, \frac{2}{n_{\text{in}}}\right) \quad (4.9)$$

Accounts for ReLU zeroing half the activations.

#### 4.6.1 Variance Preservation Through Layers

Proper weight initialization ensures that activations and gradients maintain reasonable magnitudes as they propagate through deep networks. Consider a linear layer  $\mathbf{y} = \mathbf{W}\mathbf{x}$  where  $\mathbf{x} \in \mathbb{R}^{n_{\text{in}}}$  has zero mean and unit variance, and weights  $w_{ij}$  are independent with zero mean and variance  $\sigma_w^2$ . The variance of each output element is:

$$\text{Var}(y_i) = \text{Var}\left(\sum_{j=1}^{n_{\text{in}}} w_{ij}x_j\right) = \sum_{j=1}^{n_{\text{in}}} \text{Var}(w_{ij})\text{Var}(x_j) = n_{\text{in}}\sigma_w^2 \quad (4.10)$$

To preserve variance ( $\text{Var}(y_i) = 1$ ), we need  $\sigma_w^2 = 1/n_{\text{in}}$ . Xavier initialization uses  $\sigma_w^2 = 2/(n_{\text{in}} + n_{\text{out}})$  to balance forward and backward pass variance preservation. For ReLU activations, which zero out half the activations on average, He initialization compensates by using  $\sigma_w^2 = 2/n_{\text{in}}$ , doubling the variance to maintain signal strength after the nonlinearity.

Without proper initialization, deep networks fail to train: with variance too large ( $\sigma_w^2 = 1$ ), activations explode exponentially through layers; with variance too small ( $\sigma_w^2 = 0.01$ ), they vanish to zero. For transformer models with GELU activations, He initialization or slight variants work well and are used universally in BERT, GPT, T5, and other modern architectures.

## 4.7 Regularization

### 4.7.1 L2 Regularization

Add penalty to loss:

$$L_{\text{total}} = L_{\text{data}} + \frac{\lambda}{2} \sum_{\ell} \left\| \mathbf{W}^{(\ell)} \right\|_F^2 \quad (4.11)$$

L2 regularization, also known as weight decay, penalizes large parameter values to prevent overfitting. The regularization term adds the squared Frobenius norm of all weight matrices to the loss function, encouraging the optimizer to keep weights small. The hyperparameter  $\lambda$  controls the strength of regularization: larger  $\lambda$  produces smaller weights and stronger regularization.

The computational cost of L2 regularization is modest. Computing the squared norm  $\|\mathbf{W}\|_F^2 = \sum_{ij} w_{ij}^2$  requires one multiplication and one addition per parameter, totaling  $2P$  operations for a model with  $P$  parameters. For BERT-base with 110 million parameters, this requires 220 million operations, or 0.22 GFLOPs. Compared to the 96 GFLOPs required for a forward pass, the regularization computation adds only 0.23% overhead. On an NVIDIA A100 GPU, computing the regularization term takes approximately 0.7 microseconds, which is negligible compared to the 50 milliseconds for a full forward-backward pass.

The gradient of the L2 regularization term is even simpler:  $\nabla_{\mathbf{W}} \left( \frac{\lambda}{2} \|\mathbf{W}\|_F^2 \right) = \lambda \mathbf{W}$ . This adds a term proportional to the current weights to the gradient, which can be implemented as a simple scaling operation during the optimizer step. Most optimizers, including PyTorch’s Adam and SGD, support weight decay as a built-in parameter that applies this scaling automatically without requiring explicit computation of the regularization term. This makes L2 regularization essentially free from a computational perspective.

The memory overhead of L2 regularization is zero, as it requires no additional storage beyond the parameters themselves. The regularization term is computed on-the-fly during the backward pass and does not need to be stored. This makes L2 regularization an attractive regularization technique for large models where memory is at a premium.

### 4.7.2 Dropout

**Definition 4.8** (Dropout). During training, randomly set activations to zero with probability  $p$ . During inference, scale by  $(1 - p)$ .

Dropout is a powerful regularization technique that randomly drops (sets to zero) a fraction of activations during training. This prevents the network from relying too heavily on any single neuron and encourages learning robust features. The dropout probability  $p$  is typically 0.1 to 0.5, with higher values providing stronger regularization at the cost of slower convergence.

### 4.7.3 Dropout in Practice

Dropout adds approximately 4–5% overhead to training time for BERT-base, primarily from random number generation and memory traffic for the binary mask. Transformer models apply dropout at multiple points: after attention weights (attention dropout), after sublayer outputs (residual dropout), and on input embeddings. BERT uses  $p = 0.1$  at all locations; GPT-3 uses only residual dropout.

## 4.8 Exercises

**Exercise 4.1.** Design 3-layer MLP for binary classification of 100-dimensional inputs. Specify layer dimensions, activations, and parameter count.

**Exercise 4.2.** Compute forward pass through 2-layer network with given weights and ReLU activation.

**Exercise 4.3.** For layer with 512 inputs and 256 outputs using ReLU: (1) What is He initialization variance? (2) Why different from Xavier? (3) What happens with zero initialization?

**Exercise 4.4.** Prove that without nonlinear activations,  $L$ -layer network equivalent to single layer.

## 4.9 Solutions

Full solutions for all exercises are available at <https://deeplearning.hofkensvermeulen.be>.

# Chapter 5

## Convolutional Neural Networks

### Chapter Overview

Convolutional Neural Networks (CNNs) revolutionized computer vision by exploiting spatial structure. This chapter develops convolution operations, pooling, and modern CNN architectures including ResNet.

#### Learning Objectives

1. Understand convolution operations and compute output dimensions
2. Design CNN architectures with appropriate pooling and stride
3. Understand translation equivariance
4. Implement modern CNN architectures (ResNet, VGG)

### 5.1 Convolution Operation

**Definition 5.1** (2D Convolution). For input  $\mathbf{X} \in \mathbb{R}^{H \times W}$  and kernel  $\mathbf{K} \in \mathbb{R}^{k_h \times k_w}$ :

$$(\mathbf{X} \star \mathbf{K})_{i,j} = \sum_{m=0}^{k_h-1} \sum_{n=0}^{k_w-1} \mathbf{X}_{i+m,j+n} \cdot \mathbf{K}_{m,n} \quad (5.1)$$

**Example 5.1** (3x3 Convolution). Input  $4 \times 4$ , kernel  $3 \times 3$  (edge detector), output  $2 \times 2$ . Computing first position: sum of element-wise products gives edge response.

#### 5.1.1 Output Dimensions

**Theorem 5.1** (Output Size). For input size  $H \times W$ , kernel  $k_h \times k_w$ , padding  $p$ , stride  $s$ :

$$H_{out} = \left\lfloor \frac{H + 2p - k_h}{s} \right\rfloor + 1 \quad (5.2)$$



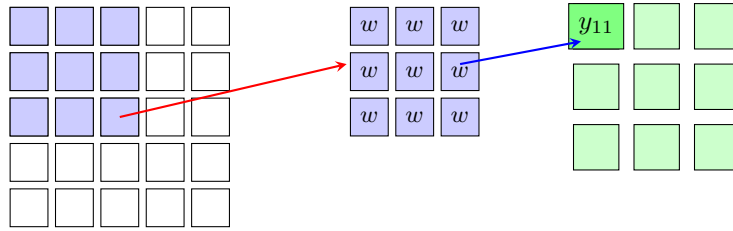


Figure 5.1: CNN receptive field showing local connectivity. Each output neuron connects to a local  $3 \times 3$  region of the input (highlighted in blue), not all inputs. The same kernel weights are shared across all spatial positions, enabling parameter efficiency and translation invariance.

**Convolution:** Only  $3 \times 3 = 9$  connections (parameter sharing!)

Figure 5.2: Convolutional layer receptive field showing local connectivity. Each output neuron (green) connects only to a local  $3 \times 3$  patch of the input (blue highlighted region), not to all input positions. The same  $3 \times 3$  kernel weights are shared across all spatial positions, dramatically reducing parameters compared to fully-connected layers. For a  $5 \times 5$  input, a fully-connected layer would require 25 weights per output, while convolution requires only 9 weights total (shared across all outputs).

## 5.2 Multi-Channel Convolutions

**Definition 5.2** (Convolutional Layer). For input  $\mathbf{X} \in \mathbb{R}^{C_{\text{in}} \times H \times W}$  with  $C_{\text{out}}$  output channels:

$$\mathbf{Y}^{(i)} = \sum_{c=1}^{C_{\text{in}}} \mathbf{X}^{(c)} \star \mathbf{K}^{(i,c)} + b^{(i)} \quad (5.3)$$

**Example 5.2** (RGB Convolution). Input:  $\mathbf{X} \in \mathbb{R}^{3 \times 224 \times 224}$ . Conv layer: 64 filters  $3 \times 3$ , stride 1, padding 1.

Parameters:  $64 \times 3 \times 3 \times 3 + 64 = 1,792$

Output:  $\mathbf{Y} \in \mathbb{R}^{64 \times 224 \times 224}$

Compare to fully-connected:  $\approx 483$  billion parameters!

**Key Point 5.1.** Convolution provides: (1) Parameter sharing, (2) Local connectivity, (3) Translation equivariance. Massive parameter reduction compared to fully-connected layers.

## 5.3 Computational Analysis of Convolutions

Understanding the computational cost and memory requirements of convolutional layers is essential for designing efficient architectures and comparing CNNs with alternative approaches like transformers. The relationship between parameters, FLOPs, and memory usage in convolutions differs fundamentally from fully-connected layers, leading to distinct performance characteristics on modern hardware.

### 5.3.1 FLOPs for Convolution Operations

The computational cost of a convolutional layer is determined by the number of multiply-accumulate operations required to compute all output feature maps. For a convolutional layer with input shape  $C_{\text{in}} \times H \times W$ , kernel size  $k \times k$ , and  $C_{\text{out}}$  output channels, each output position requires  $C_{\text{in}} \times k \times k$

multiply-accumulate operations. With output spatial dimensions  $H_{\text{out}} \times W_{\text{out}}$  and  $C_{\text{out}}$  output channels, the total FLOPs is:

$$\text{FLOPs}_{\text{conv}} = 2 \times C_{\text{out}} \times C_{\text{in}} \times k^2 \times H_{\text{out}} \times W_{\text{out}} \quad (5.4)$$

The factor of 2 accounts for the multiply-accumulate operation (one multiplication and one addition per operation). This formula reveals that convolution FLOPs scale linearly with both input and output channels, quadratically with kernel size, and linearly with output spatial dimensions.

For the RGB convolution example in Example 5.2 with input  $3 \times 224 \times 224$ , kernel size  $3 \times 3$ , and 64 output channels with stride 1 and padding 1, the output dimensions are  $64 \times 224 \times 224$ . The FLOPs calculation is  $2 \times 64 \times 3 \times 9 \times 224 \times 224 = 173,408,192$  FLOPs, or approximately 173 MFLOPs. Despite having only 1,792 parameters, this layer requires 173 million floating-point operations, giving a FLOPs-to-parameter ratio of approximately 96,768. This ratio is dramatically higher than fully-connected layers, which have a FLOPs-to-parameter ratio of approximately 2-3.

The high FLOPs-to-parameter ratio of convolutions has important implications for model design. Convolutional layers are compute-intensive relative to their memory footprint, making them well-suited for modern GPUs that have abundant compute throughput but limited memory bandwidth. A ResNet-50 model with 25.6 million parameters requires approximately 4.1 billion FLOPs for a single forward pass on a  $224 \times 224$  image, giving an overall FLOPs-to-parameter ratio of 160. This means that during training, the computational cost dominates over the memory cost of loading parameters, and GPU utilization is primarily limited by compute throughput rather than memory bandwidth.

The scaling behavior of convolution FLOPs explains several architectural design choices in modern CNNs. Early layers operating on high-resolution feature maps ( $224 \times 224$  or larger) consume the majority of FLOPs despite having relatively few parameters. For ResNet-50, the first convolutional layer with kernel size  $7 \times 7$  and 64 output channels accounts for only 0.4% of parameters but 5.8% of total FLOPs. Conversely, later layers operating on low-resolution feature maps ( $7 \times 7$  or smaller) have many parameters but relatively few FLOPs. The final fully-connected layer in ResNet-50 accounts for 7.8% of parameters but only 0.1% of FLOPs. This distribution motivates the use of larger kernels and more channels in early layers (where spatial dimensions are large) and smaller kernels with many channels in later layers (where spatial dimensions are small).

### 5.3.2 Memory Requirements for Feature Maps

During training, convolutional networks must store intermediate feature maps for use in the backward pass, and these activations typically consume far more memory than the model parameters. Understanding activation memory is critical for determining maximum batch size and input resolution.

For a convolutional layer with input shape  $B \times C_{\text{in}} \times H \times W$  (where  $B$  is batch size) and output shape  $B \times C_{\text{out}} \times H_{\text{out}} \times W_{\text{out}}$ , the network must store both the input feature map and the output feature map. In FP32, this requires  $4B(C_{\text{in}}HW + C_{\text{out}}H_{\text{out}}W_{\text{out}})$  bytes of memory. For the RGB convolution example with batch size  $B = 32$ , input  $3 \times 224 \times 224$ , and output  $64 \times 224 \times 224$ , the activation memory is  $4 \times 32 \times (3 \times 224 \times 224 + 64 \times 224 \times 224) = 130,809,792$  bytes, or approximately 125 MB. This is 70,000 $\times$  larger than the parameter memory (1,792 parameters = 7,168 bytes), demonstrating that activation memory dominates for convolutional layers.

The memory consumption of a full CNN scales with the number of layers and the spatial dimensions of feature maps. For ResNet-50 processing batch size 32 with input  $3 \times 224 \times 224$ , the total activation memory is approximately 8.2 GB in FP32. This includes the input image (6.4 MB), early high-resolution feature maps (hundreds of MB), and later low-resolution feature maps (tens of MB). The parameter memory for ResNet-50 is only 102 MB (25.6 million parameters  $\times$  4 bytes), making activations 80 $\times$  larger than parameters. This ratio increases with batch size: at batch size 256, activations consume 65.6 GB while parameters remain 102 MB, a ratio of 643 $\times$ .

The quadratic scaling of activation memory with spatial resolution has profound implications for input image size. Doubling the input resolution from  $224 \times 224$  to  $448 \times 448$  increases the number of pixels by 4 $\times$ , and since early feature maps maintain similar spatial dimensions to the input, activation memory increases by approximately 4 $\times$ . For ResNet-50 with batch size 32, increasing resolution from  $224 \times 224$  to  $448 \times 448$  increases activation memory from 8.2 GB to approximately 32.8 GB, exceeding

the capacity of most GPUs. This explains why high-resolution image processing typically requires smaller batch sizes or gradient accumulation: the activation memory grows faster than available GPU memory.

Modern techniques for reducing activation memory include gradient checkpointing, which recomputes activations during the backward pass rather than storing them, trading computation for memory. For ResNet-50, gradient checkpointing can reduce activation memory by 5-10 $\times$  at the cost of increasing training time by 20-30%. This trade-off is often worthwhile for training with larger batch sizes or higher resolutions, as the improved convergence from larger batches can offset the increased computation time.

### 5.3.3 GPU Optimization: im2col and Winograd

Efficient implementation of convolution on GPUs requires specialized algorithms that transform the convolution operation into a form amenable to highly optimized matrix multiplication routines. The two primary approaches are im2col (image-to-column) and Winograd convolution, each with distinct performance characteristics.

The im2col algorithm transforms convolution into matrix multiplication by unrolling the input feature map into a large matrix where each column contains the input values for one output position. For a convolutional layer with input  $C_{\text{in}} \times H \times W$ , kernel size  $k \times k$ , and output  $C_{\text{out}} \times H_{\text{out}} \times W_{\text{out}}$ , im2col creates a matrix of shape  $(C_{\text{in}}k^2) \times (H_{\text{out}}W_{\text{out}})$  by extracting all  $k \times k$  patches from the input. The convolution kernels are reshaped into a matrix of shape  $C_{\text{out}} \times (C_{\text{in}}k^2)$ . The convolution is then computed as a single matrix multiplication:  $\text{output} = \text{kernels} \times \text{im2col}(\text{input})$ , producing a matrix of shape  $C_{\text{out}} \times (H_{\text{out}}W_{\text{out}})$  that is reshaped to the final output dimensions.

For the RGB convolution example with input  $3 \times 224 \times 224$ , kernel size  $3 \times 3$ , and 64 output channels, im2col creates a matrix of shape  $27 \times 50,176$  (since  $C_{\text{in}}k^2 = 3 \times 9 = 27$  and  $H_{\text{out}}W_{\text{out}} = 224 \times 224 = 50,176$ ). The kernel matrix has shape  $64 \times 27$ . The matrix multiplication  $64 \times 27$  times  $27 \times 50,176$  requires  $2 \times 64 \times 27 \times 50,176 = 173,408,192$  FLOPs, matching the direct convolution calculation. However, the im2col matrix requires  $27 \times 50,176 \times 4 = 5,419,008$  bytes (5.2 MB) of temporary storage, which is 757 $\times$  larger than the original input (7,168 bytes for  $3 \times 224 \times 224$  in FP32).

The advantage of im2col is that it leverages highly optimized BLAS (Basic Linear Algebra Subprograms) libraries like cuBLAS on NVIDIA GPUs, which achieve 80-95% of peak hardware throughput for large matrix multiplications. For the  $64 \times 27$  times  $27 \times 50,176$  multiplication on an NVIDIA A100 GPU with 312 TFLOPS FP16 throughput, the operation completes in approximately 0.6 microseconds at 90% efficiency, achieving 280 TFLOPS. Direct convolution implementations without im2col typically achieve only 40-60% efficiency due to irregular memory access patterns and difficulty saturating the GPU's parallel execution units.

The disadvantage of im2col is the memory overhead. For batch size  $B = 32$ , the im2col matrix grows to  $32 \times 27 \times 50,176 = 43,352,064$  elements, requiring 167 MB of temporary storage. This memory must be allocated and deallocated for each convolutional layer, adding memory pressure and potentially causing out-of-memory errors for large batch sizes or high-resolution inputs. Modern implementations mitigate this by processing the batch in chunks or fusing the im2col transformation with the matrix multiplication to avoid materializing the full im2col matrix.

Winograd convolution is an alternative algorithm that reduces the number of multiplications required for small convolutions (typically  $3 \times 3$  or  $5 \times 5$  kernels) by using a mathematical transformation that trades multiplications for additions. For  $3 \times 3$  convolutions, Winograd reduces the number of multiplications by 2.25 $\times$  compared to direct convolution, from 9 multiplications per output to 4 multiplications per output. This reduction translates directly to FLOPs savings: the RGB convolution example requires only  $173,408,192 / 2.25 = 77,070,752$  FLOPs with Winograd, a 56% reduction.

However, Winograd convolution has several limitations. First, it requires additional memory for intermediate transformations, typically 2-3 $\times$  the input size. Second, it is numerically less stable than direct convolution, particularly in FP16, due to the transformation matrices having large condition numbers. Third, it is only applicable to small kernel sizes ( $3 \times 3$  and  $5 \times 5$ ) and becomes inefficient for larger kernels. Fourth, the transformation overhead becomes significant for small spatial dimensions, making Winograd most effective for early layers with large feature maps.

In practice, modern deep learning frameworks like PyTorch and TensorFlow automatically select

between im2col, Winograd, and direct convolution based on layer dimensions, batch size, and hardware characteristics. For  $3 \times 3$  convolutions on high-resolution feature maps ( $\geq 56 \times 56$ ) with batch size  $\geq 16$ , Winograd typically provides  $1.5\text{--}2\times$  speedup over im2col. For larger kernels ( $5 \times 5$  or  $7 \times 7$ ) or smaller feature maps, im2col is preferred. For very small batch sizes ( $\leq 4$ ), direct convolution may be fastest due to lower overhead. NVIDIA’s cuDNN library implements all three algorithms and includes heuristics to select the optimal approach for each layer configuration.

### 5.3.4 Comparison with Transformer Attention

Comparing the computational characteristics of convolutional layers with transformer self-attention reveals fundamental trade-offs between local and global receptive fields, parameter efficiency, and computational scaling.

A convolutional layer with kernel size  $k \times k$  has a local receptive field: each output position depends only on a  $k \times k$  neighborhood of the input. To achieve a global receptive field spanning the entire input, multiple convolutional layers must be stacked. For an input of size  $H \times W$ , achieving a receptive field covering the full input requires approximately  $\log_k(\max(H, W))$  layers. For a  $224 \times 224$  image with  $3 \times 3$  convolutions, this requires approximately  $\log_3(224) \approx 5$  layers. Each layer adds computational cost, but the cost per layer remains  $O(C_{\text{out}}C_{\text{in}}k^2HW)$ , scaling linearly with spatial dimensions.

In contrast, self-attention in transformers has a global receptive field: each output position attends to all input positions in a single layer. For an input sequence of length  $n = HW$  (treating the 2D image as a 1D sequence) with model dimension  $d$ , self-attention requires computing query-key products for all pairs of positions, resulting in  $O(n^2d)$  FLOPs. For a  $224 \times 224$  image with  $n = 50,176$  positions and  $d = 768$  (typical for Vision Transformers), self-attention requires approximately  $2 \times 50,176^2 \times 768 = 3.86 \times 10^{12}$  FLOPs, or 3.86 TFLOPs per layer. This is  $22,000\times$  more expensive than the RGB convolution example (173 MFLOPs), despite both operating on the same input resolution.

The quadratic scaling of attention with spatial resolution makes it prohibitively expensive for high-resolution images. Doubling the resolution from  $224 \times 224$  to  $448 \times 448$  increases attention FLOPs by  $16\times$  (since  $n$  increases by  $4\times$  and attention scales as  $n^2$ ), while convolution FLOPs increase by only  $4\times$  (linear scaling with spatial dimensions). For a  $448 \times 448$  image, self-attention requires 61.8 TFLOPs per layer, making it impractical without modifications like hierarchical attention or local attention windows.

Vision Transformers (ViTs) address this computational challenge by dividing the image into patches and treating each patch as a token. For a  $224 \times 224$  image with patch size  $16 \times 16$ , the sequence length is  $n = (224/16)^2 = 196$  patches. Self-attention on 196 patches with  $d = 768$  requires  $2 \times 196^2 \times 768 = 59,015,168$  FLOPs, or approximately 59 MFLOPs per layer. This is  $65\times$  less expensive than attention on individual pixels and comparable to the RGB convolution example (173 MFLOPs). However, the patch-based approach sacrifices fine-grained spatial resolution: each patch is treated as a single token, and the model cannot attend to individual pixels within a patch.

The parameter efficiency of convolutions versus attention also differs significantly. A convolutional layer with  $C_{\text{in}}$  input channels,  $C_{\text{out}}$  output channels, and kernel size  $k \times k$  has  $C_{\text{out}}C_{\text{in}}k^2$  parameters. For the RGB convolution example, this is  $64 \times 3 \times 9 = 1,728$  parameters. A self-attention layer with model dimension  $d$  has query, key, and value projection matrices, each of size  $d \times d$ , totaling  $3d^2$  parameters (ignoring the output projection). For  $d = 768$ , this is  $3 \times 768^2 = 1,769,472$  parameters, which is  $1,024\times$  more than the convolutional layer. However, the attention parameters are independent of spatial resolution, while convolution parameters are independent of spatial resolution as well. The key difference is that attention parameters scale with  $d^2$  while convolution parameters scale with  $C_{\text{in}}C_{\text{out}}k^2$ , and typically  $d \gg C_{\text{in}}$  for early layers.

For complete models, ResNet-50 has 25.6 million parameters and requires 4.1 GFLOPs per image, while ViT-Base has 86 million parameters and requires 17.6 GFLOPs per image. The ViT has  $3.4\times$  more parameters and  $4.3\times$  more FLOPs, but achieves comparable or better accuracy on ImageNet classification. The higher computational cost of ViT is offset by its ability to leverage large-scale pretraining on datasets like ImageNet-21k or JFT-300M, where the global receptive field and flexibility of attention provide advantages over the inductive biases of convolution.

**Key Point 5.2.** *CNNs are significantly more parameter-efficient than transformers for vision tasks due to weight sharing and local connectivity. ResNet-50 achieves 76.1% ImageNet accuracy with 25.6M parameters, while ViT-Base requires 86M parameters for comparable accuracy. However, Vision Transformers excel when large-scale pretraining data is available. A detailed comparison of CNNs and Vision Transformers is provided in Chapter 17.*

**Key Point 5.3.** *Efficient convolution on GPUs requires channel dimensions that are multiples of 16 (for Tensor Core alignment) and sufficient batch size to saturate parallel compute units. Libraries like cuDNN automatically select optimal algorithms (im2col, Winograd, FFT) and apply kernel fusions. Early CNN layers are typically memory-bandwidth-bound while later layers are compute-bound. For a detailed treatment of hardware optimization, see Chapter 22.*

## 5.4 Pooling Layers

**Definition 5.3** (Max Pooling). For window  $k \times k$  and stride  $s$ :

$$\text{MaxPool}(\mathbf{X})_{i,j} = \max_{m,n \in \text{window}} \mathbf{X}_{si+m, sj+n} \quad (5.5)$$

Pooling reduces spatial dimensions, increases receptive field, and provides translation invariance.

## 5.5 Classic Architectures

### 5.5.1 VGG-16 (2014)

Deep network with small  $3 \times 3$  filters. Pattern:  $[\text{Conv}3 \times 3]^n \rightarrow \text{MaxPool} \rightarrow \text{Double channels}$

Total: 138 million parameters

### 5.5.2 ResNet (2015)

**Definition 5.4** (Residual Block). Learn residual:

$$\mathbf{y} = \mathcal{F}(\mathbf{x}) + \mathbf{x} \quad (5.6)$$

ResNet-50: 25.6M parameters, enables training 100+ layer networks.

**Key Point 5.4.** *Residual connections enable extremely deep networks by allowing gradients to flow through skip connections. Analogous to skip connections in transformers.*

## 5.6 Batch Normalization

**Definition 5.5** (Batch Normalization). For mini-batch, normalize each feature:

$$\hat{\mathbf{x}}_i = \frac{\mathbf{x}_i - \mu_B}{\sqrt{\sigma_B^2 + \epsilon}} \quad (5.7)$$

$$\mathbf{y}_i = \gamma \hat{\mathbf{x}}_i + \beta \quad (5.8)$$

where  $\gamma, \beta$  are learnable.

Benefits: Reduces covariate shift, allows higher learning rates, acts as regularization.

## 5.7 Exercises

**Exercise 5.1.** For  $32 \times 32 \times 3$  input, compute dimensions after: Conv(64,  $5 \times 5$ , s=1, p=2), MaxPool( $2 \times 2$ , s=2), Conv(128,  $3 \times 3$ , s=1, p=1), MaxPool( $2 \times 2$ , s=2). Count parameters.

**Exercise 5.2.** Show two  $3 \times 3$  convolutions equal one  $5 \times 5$  receptive field. Compare parameter counts.

**Exercise 5.3.** Design CNN for CIFAR-10 with 3 blocks, channels [64, 128, 256]. Calculate total parameters.

## 5.8 Solutions

Full solutions for all exercises are available at <https://deeplearning.hofkensvermeulen.be>.

# Chapter 6

## Recurrent Neural Networks

### Chapter Overview

Recurrent Neural Networks (RNNs) process sequential data by maintaining hidden states that capture information from previous time steps. This chapter develops RNNs from basic recurrence to modern architectures like LSTMs and GRUs, establishing foundations for understanding transformers.

### Learning Objectives

1. Understand recurrent architectures for sequential data
2. Implement vanilla RNNs, LSTMs, and GRUs
3. Understand vanishing/exploding gradient problems
4. Apply RNNs to sequence modeling tasks
5. Understand bidirectional and multi-layer RNNs

### 6.1 Vanilla RNNs

**Definition 6.1** (Recurrent Neural Network). An RNN processes sequence  $\mathbf{x}_1, \mathbf{x}_2, \dots, \mathbf{x}_T$  by maintaining hidden state  $\mathbf{h}_t \in \mathbb{R}^h$ :

$$\mathbf{h}_t = \tanh(\mathbf{W}_{hh}\mathbf{h}_{t-1} + \mathbf{W}_{xh}\mathbf{x}_t + \mathbf{b}_h) \quad (6.1)$$

$$\mathbf{y}_t = \mathbf{W}_{hy}\mathbf{h}_t + \mathbf{b}_y \quad (6.2)$$

where:

- $\mathbf{W}_{hh} \in \mathbb{R}^{h \times h}$ : hidden-to-hidden weights
- $\mathbf{W}_{xh} \in \mathbb{R}^{h \times d}$ : input-to-hidden weights
- $\mathbf{W}_{hy} \in \mathbb{R}^{k \times h}$ : hidden-to-output weights
- $\mathbf{h}_0$  initialized (often zeros)

**Example 6.1** (RNN Forward Pass). Character-level language model with vocabulary size  $V = 5$ , hidden size  $h = 3$ .

Input sequence: "hello" encoded as one-hot vectors  $\mathbf{x}_1, \dots, \mathbf{x}_5 \in \mathbb{R}^5$

Initialize:  $\mathbf{h}_0 = [0, 0, 0]^\top$

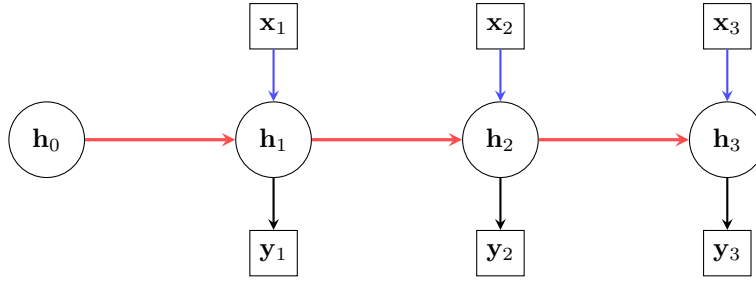


Figure 6.1: RNN unrolled through time showing sequential dependencies. Each hidden state  $\mathbf{h}_t$  depends on both the current input  $\mathbf{x}_t$  (blue arrows) and the previous hidden state  $\mathbf{h}_{t-1}$  (red arrows). The same weight matrices are shared across all time steps. This sequential structure prevents parallelization:  $\mathbf{h}_2$  cannot be computed until  $\mathbf{h}_1$  is complete.

**Time step 1:** Process 'h'

$$\mathbf{h}_1 = \tanh(\mathbf{W}_{hh}\mathbf{h}_0 + \mathbf{W}_{xh}\mathbf{x}_1 + \mathbf{b}_h) \in \mathbb{R}^3 \quad (6.3)$$

$$\mathbf{y}_1 = \mathbf{W}_{hy}\mathbf{h}_1 + \mathbf{b}_y \in \mathbb{R}^5 \quad (6.4)$$

$$\hat{\mathbf{p}}_1 = \text{softmax}(\mathbf{y}_1) \quad (\text{predict next character}) \quad (6.5)$$

**Time step 2:** Process 'e' using  $\mathbf{h}_1$

$$\mathbf{h}_2 = \tanh(\mathbf{W}_{hh}\mathbf{h}_1 + \mathbf{W}_{xh}\mathbf{x}_2 + \mathbf{b}_h) \quad (6.6)$$

Hidden state  $\mathbf{h}_t$  carries information from all previous time steps.

### 6.1.1 Backpropagation Through Time (BPTT)

---

#### Algorithm 7: Backpropagation Through Time

---

**Input:** Sequence  $\{\mathbf{x}_1, \dots, \mathbf{x}_T\}$ , targets  $\{\mathbf{y}_1, \dots, \mathbf{y}_T\}$

**Output:** Gradients for all parameters

// Forward Pass

1 **for**  $t = 1$  **to**  $T$  **do**

2      $\mathbf{h}_t = \tanh(\mathbf{W}_{hh}\mathbf{h}_{t-1} + \mathbf{W}_{xh}\mathbf{x}_t + \mathbf{b}_h)$

3      $\mathbf{y}_t = \mathbf{W}_{hy}\mathbf{h}_t + \mathbf{b}_y$

4      $L_t = \text{Loss}(\mathbf{y}_t, \text{target}_t)$

// Backward Pass

5 Initialize  $\frac{\partial L}{\partial \mathbf{h}_{T+1}} = \mathbf{0}$

6 **for**  $t = T$  **to** 1 **do**

7     Compute  $\frac{\partial L}{\partial \mathbf{h}_t}$  (includes gradient from  $t + 1$ )

8     Accumulate  $\frac{\partial L}{\partial \mathbf{W}_{hh}}, \frac{\partial L}{\partial \mathbf{W}_{xh}}, \frac{\partial L}{\partial \mathbf{W}_{hy}}$

---

### 6.1.2 Vanishing and Exploding Gradients

The fundamental challenge in training RNNs on long sequences arises from the multiplicative nature of gradient backpropagation through time. When computing gradients with respect to early hidden states, the chain rule requires multiplying Jacobian matrices across all intermediate time steps, leading to exponential growth or decay of gradient magnitudes.

The gradient of the loss with respect to an early hidden state  $\mathbf{h}_0$  involves the product of Jacobians



across all time steps:

$$\frac{\partial \mathbf{h}_T}{\partial \mathbf{h}_0} = \prod_{t=1}^T \frac{\partial \mathbf{h}_t}{\partial \mathbf{h}_{t-1}} = \prod_{t=1}^T \mathbf{W}_{hh}^\top \text{diag}(\tanh'(\mathbf{z}_t)) \quad (6.7)$$

where  $\mathbf{z}_t$  is the pre-activation at time  $t$ . Each Jacobian  $\frac{\partial \mathbf{h}_t}{\partial \mathbf{h}_{t-1}}$  has spectral norm bounded by  $\|\mathbf{W}_{hh}\| \cdot \|\text{diag}(\tanh'(\mathbf{z}_t))\|$ . Since  $\tanh'(z) \in (0, 1]$  with maximum value 1 at  $z = 0$ , the derivative term is at most 1 and typically much smaller for saturated activations. This means the Jacobian norm is approximately  $\|\mathbf{W}_{hh}\|$  in the best case.

For a sequence of length  $T = 100$ , if  $\|\mathbf{W}_{hh}\| = 0.95$  (slightly less than 1), the gradient magnitude decays as  $0.95^{100} \approx 0.006$ , reducing gradients by a factor of 167. If  $\|\mathbf{W}_{hh}\| = 0.9$ , the decay is  $0.9^{100} \approx 2.7 \times 10^{-5}$ , reducing gradients by a factor of 37,000. This exponential decay makes it nearly impossible for the network to learn long-range dependencies: the gradient signal from time step 100 is effectively zero by the time it reaches time step 0. In practice, vanilla RNNs struggle to learn dependencies longer than 10-20 time steps due to vanishing gradients.

Conversely, if  $\|\mathbf{W}_{hh}\| = 1.05$ , the gradient magnitude grows as  $1.05^{100} \approx 131.5$ , amplifying gradients by a factor of 131. If  $\|\mathbf{W}_{hh}\| = 1.1$ , the growth is  $1.1^{100} \approx 13,781$ , causing gradients to explode. Exploding gradients lead to numerical overflow (NaN values) and training instability, where loss suddenly spikes to infinity. While gradient clipping (capping gradient norms at a threshold like 1.0) provides a practical solution for exploding gradients, it does not address the fundamental problem of vanishing gradients.

The vanishing gradient problem is particularly severe because the spectral norm of  $\mathbf{W}_{hh}$  must be precisely 1.0 to avoid both vanishing and exploding gradients, and maintaining this property during training is extremely difficult. Initialization schemes like orthogonal initialization set  $\mathbf{W}_{hh}$  to have spectral norm 1.0 initially, but gradient descent updates quickly perturb this property. Even with careful initialization, vanilla RNNs rarely learn dependencies beyond 20-30 time steps in practice.

### 6.1.3 Quantitative Analysis of Gradient Decay

To understand the severity of vanishing gradients, consider a concrete example with BERT-base dimensions. Suppose we have a vanilla RNN with hidden dimension  $h = 768$  (matching BERT-base) and sequence length  $n = 512$  (BERT's maximum sequence length). The recurrence matrix  $\mathbf{W}_{hh} \in \mathbb{R}^{768 \times 768}$  has 589,824 parameters. If we initialize  $\mathbf{W}_{hh}$  orthogonally (spectral norm exactly 1.0) and the tanh derivatives average 0.5 (typical for non-saturated activations), the effective Jacobian norm per time step is approximately  $1.0 \times 0.5 = 0.5$ .

Over 512 time steps, the gradient magnitude decays as  $0.5^{512} \approx 10^{-154}$ , which is far below machine precision for FP32 (approximately  $10^{-38}$ ) or even FP64 (approximately  $10^{-308}$ ). The gradient effectively becomes exactly zero after about 130 time steps in FP32 or 1,000 time steps in FP64. This means a vanilla RNN cannot learn any dependencies spanning more than 130 tokens when using FP32 arithmetic, regardless of optimization algorithm or learning rate. The mathematical structure of the recurrence fundamentally limits the learnable dependency length.

For comparison, consider the gradient flow in a transformer with the same dimensions. The self-attention mechanism computes attention scores  $\mathbf{A} = \text{softmax}(\frac{\mathbf{QK}^\top}{\sqrt{d_k}})$  and outputs  $\mathbf{O} = \mathbf{AV}$ . The gradient  $\frac{\partial L}{\partial \mathbf{V}}$  flows directly from the output through the attention weights, without any multiplicative accumulation across time steps. The gradient magnitude remains approximately constant regardless of sequence length, enabling transformers to learn dependencies spanning thousands of tokens. This fundamental difference in gradient flow explains why transformers replaced RNNs for nearly all sequence modeling tasks: they solve the vanishing gradient problem by design.

The LSTM architecture addresses vanishing gradients through its cell state mechanism, which provides an additive path for gradient flow. The cell state update  $\mathbf{c}_t = \mathbf{f}_t \odot \mathbf{c}_{t-1} + \mathbf{i}_t \odot \tilde{\mathbf{c}}_t$  includes an additive term rather than purely multiplicative updates. The gradient with respect to  $\mathbf{c}_{t-1}$  is:

$$\frac{\partial \mathbf{c}_t}{\partial \mathbf{c}_{t-1}} = \text{diag}(\mathbf{f}_t) \quad (6.8)$$

which is a diagonal matrix with entries in  $(0, 1)$  determined by the forget gate. If the forget gate learns to output values close to 1 for important information, the gradient can flow backward through many time steps without vanishing. However, this requires the network to learn appropriate forget gate values, and in practice, LSTMs still struggle with dependencies beyond 100-200 time steps. The cell state provides a highway for gradients, but it does not eliminate the vanishing gradient problem entirely.

## 6.2 Long Short-Term Memory (LSTM)

**Definition 6.2** (LSTM Cell). LSTM uses gating mechanisms to control information flow:

$$\mathbf{f}_t = \sigma(\mathbf{W}_f[\mathbf{h}_{t-1}, \mathbf{x}_t] + \mathbf{b}_f) \quad (\text{forget gate}) \quad (6.9)$$

$$\mathbf{i}_t = \sigma(\mathbf{W}_i[\mathbf{h}_{t-1}, \mathbf{x}_t] + \mathbf{b}_i) \quad (\text{input gate}) \quad (6.10)$$

$$\tilde{\mathbf{c}}_t = \tanh(\mathbf{W}_c[\mathbf{h}_{t-1}, \mathbf{x}_t] + \mathbf{b}_c) \quad (\text{candidate cell}) \quad (6.11)$$

$$\mathbf{c}_t = \mathbf{f}_t \odot \mathbf{c}_{t-1} + \mathbf{i}_t \odot \tilde{\mathbf{c}}_t \quad (\text{cell state}) \quad (6.12)$$

$$\mathbf{o}_t = \sigma(\mathbf{W}_o[\mathbf{h}_{t-1}, \mathbf{x}_t] + \mathbf{b}_o) \quad (\text{output gate}) \quad (6.13)$$

$$\mathbf{h}_t = \mathbf{o}_t \odot \tanh(\mathbf{c}_t) \quad (\text{hidden state}) \quad (6.14)$$

where  $\sigma$  is sigmoid,  $\odot$  is element-wise multiplication, and  $[\cdot, \cdot]$  is concatenation.

**Key components:**

- **Cell state  $\mathbf{c}_t$ :** Long-term memory, flows with minimal modification
- **Forget gate  $\mathbf{f}_t$ :** What to remove from cell state
- **Input gate  $\mathbf{i}_t$ :** What new information to store
- **Output gate  $\mathbf{o}_t$ :** What to output from cell state

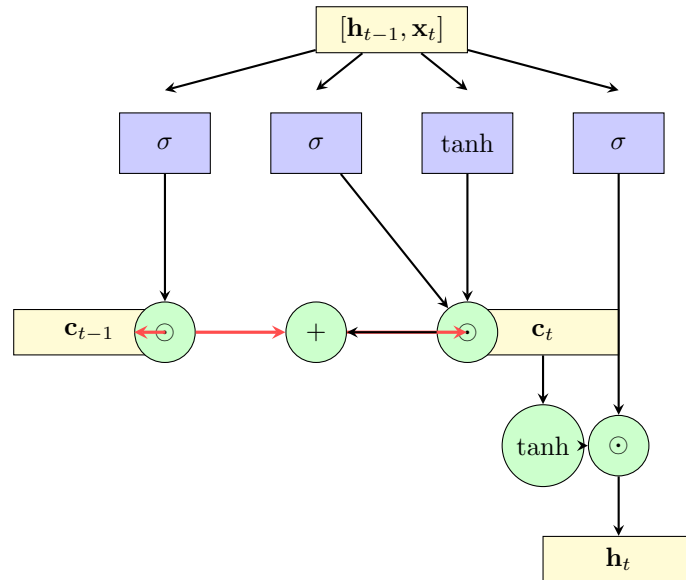


Figure 6.2: LSTM cell internal structure showing the four gates and cell state flow. The cell state  $\mathbf{c}_t$  (red path) provides an additive "highway" for gradient flow, addressing the vanishing gradient problem. The forget gate  $\mathbf{f}_t$  controls what to keep from  $\mathbf{c}_{t-1}$ , the input gate  $\mathbf{i}_t$  and candidate  $\tilde{\mathbf{c}}_t$  control what new information to add, and the output gate  $\mathbf{o}_t$  controls what to output. All gates receive the same input  $[\mathbf{h}_{t-1}, \mathbf{x}_t]$  but learn different transformations.

**Example 6.2** (LSTM Parameter Count). For input dimension  $d = 512$  and hidden dimension  $h = 1024$ :

Each gate has weight matrix for  $[\mathbf{h}_{t-1}, \mathbf{x}_t] \in \mathbb{R}^{h+d}$ :

$$\text{Single gate: } (h + d) \times h + h = (1024 + 512) \times 1024 + 1024 \quad (6.15)$$

$$= 1,572,864 + 1,024 = 1,573,888 \quad (6.16)$$

LSTM has 4 gates (forget, input, cell, output):

$$\text{Total: } 4 \times 1,573,888 = 6,295,552 \text{ parameters} \quad (6.17)$$

Compare to transformer attention with same dimensions: often fewer parameters and better parallelization!

### 6.2.1 LSTM Computational Analysis

Understanding the computational cost of LSTMs is essential for comparing them to transformers and explaining why transformers have become dominant despite LSTMs' theoretical advantages for sequential processing. The LSTM's gating mechanisms provide powerful modeling capabilities but come with significant computational overhead that limits their efficiency on modern hardware.

For an LSTM with input dimension  $d$  and hidden dimension  $h$ , each time step requires computing four gates (forget, input, candidate, output), each involving a matrix multiplication with the concatenated input  $[\mathbf{h}_{t-1}, \mathbf{x}_t] \in \mathbb{R}^{h+d}$ . The computational cost per time step is:

$$\text{FLOPs per step} = 4 \times 2h(h + d) = 8h(h + d) \quad (6.18)$$

where the factor of 2 accounts for multiply-accumulate operations, and the factor of 4 accounts for the four gates. For BERT-base dimensions with  $d = h = 768$ , this gives  $8 \times 768 \times (768 + 768) = 9,437,184$  FLOPs per time step. For a sequence of length  $n = 512$ , the total cost is  $512 \times 9,437,184 = 4,831,838,208$  FLOPs, or approximately 4.8 GFLOPs.

This computational cost is deceptively modest compared to transformers. A single transformer layer with the same dimensions requires approximately 12.9 GFLOPs for self-attention (with  $n = 512$ ) plus 9.4 GFLOPs for the feed-forward network, totaling 22.3 GFLOPs—about  $4.6\times$  more than the LSTM. However, this comparison is misleading because it ignores the critical difference in parallelization: the transformer can process all 512 positions simultaneously, while the LSTM must process them sequentially.

The sequential nature of LSTMs means that the 4.8 GFLOPs cannot be parallelized across time steps. On an NVIDIA A100 GPU with peak throughput of 312 TFLOPS (FP16), the theoretical minimum time to process a sequence of length 512 is  $\frac{4.8 \times 10^9}{312 \times 10^{12}} = 15.4$  microseconds if we could achieve perfect parallelization. However, the sequential dependency forces us to process one time step at a time, with each step taking approximately  $\frac{9.4 \times 10^6}{312 \times 10^{12}} = 0.03$  microseconds at peak throughput. In practice, small matrix multiplications achieve only 1-5% of peak throughput due to insufficient parallelism, so each time step actually takes approximately 1-3 microseconds, giving a total sequence processing time of 512-1,536 microseconds (0.5-1.5 milliseconds).

For comparison, a transformer layer can process the entire sequence in parallel. The self-attention computation requires three matrix multiplications ( $\mathbf{Q} = \mathbf{XW}_Q$ ,  $\mathbf{K} = \mathbf{XW}_K$ ,  $\mathbf{V} = \mathbf{XW}_V$ ) with dimensions  $512 \times 768 \times 768$ , followed by the attention score computation  $\mathbf{A} = \text{softmax}(\frac{\mathbf{QK}^\top}{\sqrt{d_k}})$  and output computation  $\mathbf{O} = \mathbf{AV}$ . These operations can be batched into large matrix multiplications that achieve 40-60% of peak GPU throughput, completing in approximately 50-100 microseconds total. The transformer is 5-30 $\times$  faster than the LSTM despite having more FLOPs, purely due to better parallelization.

The memory requirements for LSTM hidden states are modest compared to transformer attention matrices. For batch size  $B$  and sequence length  $n$ , the LSTM must store hidden states  $\mathbf{h}_t \in \mathbb{R}^{B \times h}$  and cell states  $\mathbf{c}_t \in \mathbb{R}^{B \times h}$  for each time step, requiring  $2Bnh \times 4 = 8Bnh$  bytes in FP32. For BERT-base

dimensions with  $B = 32$ ,  $n = 512$ ,  $h = 768$ , this totals  $8 \times 32 \times 512 \times 768 = 100,663,296$  bytes, or approximately 96 MB. This is substantially less than the 384 MB required for transformer attention scores in a single layer, making LSTMs more memory-efficient for long sequences.

However, this memory advantage is offset by the sequential processing requirement. While transformers can trade memory for speed by using gradient checkpointing (recomputing activations during the backward pass rather than storing them), LSTMs cannot benefit from this technique as effectively because the sequential dependency prevents parallelization of the recomputation. Gradient checkpointing reduces transformer memory by 3-5 $\times$  with only 20-30% slowdown, but for LSTMs, the slowdown is 2-3 $\times$  because the recomputation cannot be parallelized. This makes gradient checkpointing less attractive for LSTMs, limiting their ability to scale to very long sequences.

### 6.3 Gated Recurrent Unit (GRU)

**Definition 6.3** (GRU Cell). GRU simplifies LSTM by merging cell and hidden states:

$$\mathbf{z}_t = \sigma(\mathbf{W}_z[\mathbf{h}_{t-1}, \mathbf{x}_t] + \mathbf{b}_z) \quad (\text{update gate}) \quad (6.19)$$

$$\mathbf{r}_t = \sigma(\mathbf{W}_r[\mathbf{h}_{t-1}, \mathbf{x}_t] + \mathbf{b}_r) \quad (\text{reset gate}) \quad (6.20)$$

$$\tilde{\mathbf{h}}_t = \tanh(\mathbf{W}_h[\mathbf{r}_t \odot \mathbf{h}_{t-1}, \mathbf{x}_t] + \mathbf{b}_h) \quad (\text{candidate}) \quad (6.21)$$

$$\mathbf{h}_t = (1 - \mathbf{z}_t) \odot \mathbf{h}_{t-1} + \mathbf{z}_t \odot \tilde{\mathbf{h}}_t \quad (\text{hidden state}) \quad (6.22)$$

#### Advantages over LSTM:

- Fewer parameters (3 gates vs 4)
- Simpler architecture
- Often similar performance
- Faster training

### 6.4 Bidirectional RNNs

**Definition 6.4** (Bidirectional RNN). Process sequence in both directions:

$$\vec{\mathbf{h}}_t = \text{RNN}_{\text{forward}}(\mathbf{x}_t, \vec{\mathbf{h}}_{t-1}) \quad (6.23)$$

$$\overleftarrow{\mathbf{h}}_t = \text{RNN}_{\text{backward}}(\mathbf{x}_t, \overleftarrow{\mathbf{h}}_{t+1}) \quad (6.24)$$

$$\mathbf{h}_t = [\vec{\mathbf{h}}_t; \overleftarrow{\mathbf{h}}_t] \quad (6.25)$$

Bidirectional RNNs capture context from both past and future, useful when entire sequence is available (not for online/causal tasks).

**Example:** BERT uses bidirectional transformers (attention, not RNN), capturing full context.

### 6.5 RNN Applications

#### Sequence-to-Sequence:

- Machine translation: Encoder RNN  $\rightarrow$  Decoder RNN
- Text summarization
- Speech recognition

**Sequence Labeling:**

- Part-of-speech tagging
- Named entity recognition
- Output at each time step

**Sequence Generation:**

- Language modeling
- Music generation
- Sample from output distribution

## 6.6 RNNs vs Transformers: A Computational Comparison

The transition from RNNs to transformers represents one of the most significant architectural shifts in deep learning. The following table summarizes the key computational differences:

Property	RNNs	Transformers
Computation	Sequential ( $n$ steps)	Parallel (constant depth)
Memory scaling	$O(nd)$	$O(n^2 + nd)$
GPU utilization	1–5%	40–60%
Memory bandwidth	Reload weights each step	Load weights once
Training time (BERT-scale)	Estimated 100–200 days	4 days

The fundamental bottleneck of RNNs is sequential processing: each hidden state  $\mathbf{h}_t$  depends on  $\mathbf{h}_{t-1}$ , preventing parallelization across time steps. On an A100 GPU with 6,912 CUDA cores, an LSTM processing batch size 32 utilizes only  $\sim 0.5\%$  of parallel capacity. Transformers eliminate this bottleneck by computing all positions simultaneously via matrix multiplication, achieving  $15\times$  or greater speedup despite having more total FLOPs.

The parallelization advantage compounds with hardware efficiency: transformers achieve high arithmetic intensity through data reuse in matrix multiplications ( $\sim 256$  FLOPs/byte), while RNNs perform small matrix-vector products with low data reuse ( $\sim 1$ – $10$  FLOPs/byte). The combined effect is  $100$ – $500\times$  faster training for equivalent model capacity.

**Key Point 6.1.** *Transformers dominate modern sequence modeling due to parallel computation ( $5$ – $30\times$  speedup), superior hardware utilization ( $40$ – $60\%$  vs  $1$ – $5\%$ ), and direct long-range gradient flow. RNNs retain advantages for online/streaming applications and extremely long sequences where  $O(n^2)$  attention memory is prohibitive. Efficient attention mechanisms (Chapter 16) increasingly address this limitation.*

## 6.7 Exercises

**Exercise 6.1.** For vanilla RNN with input dim  $d = 128$ , hidden dim  $h = 256$ , and sequence length  $T = 50$ : (1) Count total parameters in  $\mathbf{W}_{hh}$ ,  $\mathbf{W}_{xh}$ , and  $\mathbf{W}_{hy}$ , (2) Compute total FLOPs for forward pass through all time steps, (3) Estimate GPU utilization on an A100 (312 TFLOPS peak) with batch size 32, assuming each time step achieves  $2\%$  of peak throughput. Why is utilization so low?

**Exercise 6.2.** Derive the gradient  $\frac{\partial L}{\partial \mathbf{W}_{hh}}$  for a 3-step sequence. Show how the gradient involves products of Jacobians  $\frac{\partial \mathbf{h}_t}{\partial \mathbf{h}_{t-1}}$ . If  $\|\mathbf{W}_{hh}\| = 0.9$  and  $\tanh'$  averages 0.5, compute the gradient magnitude decay factor from time step 3 to time step 0. At what sequence length would gradients vanish below FP32 precision ( $10^{-38}$ )?

**Exercise 6.3.** Compare parameter counts and FLOPs per sequence for: (1) LSTM with  $d = 512$ ,  $h = 512$ ,  $n = 512$ , (2) GRU with  $d = 512$ ,  $h = 512$ ,  $n = 512$ , (3) Transformer attention layer with  $d_{\text{model}} = 512$ ,  $d_k = 64$ ,  $h = 8$  heads,  $n = 512$ . Which architecture has the most parameters? Which has the most FLOPs? Which achieves the highest GPU utilization and why?

**Exercise 6.4.** Implement bidirectional LSTM in PyTorch for sequence "The cat sat on the mat" with vocabulary size 10, embedding dim 16, hidden dim 32. Process the sequence and show output dimensions. Compute the total memory required for hidden states and cell states in FP32. How does this compare to the memory required for attention scores in a transformer with the same dimensions?

**Exercise 6.5.** For BERT-base dimensions ( $d = 768$ ,  $n = 512$ ), compute: (1) Memory required for LSTM hidden and cell states across 12 layers with batch size 32, (2) Memory required for transformer attention scores across 12 layers with batch size 32 and 12 attention heads, (3) The sequence length at which LSTM memory equals transformer memory. Explain why transformers are memory-limited for long sequences while LSTMs are compute-limited.

**Exercise 6.6.** Estimate the training time for a 110M parameter LSTM on 16 billion tokens (sequence length 512) using 64 TPU cores with 2,880 TFLOPS total peak throughput. Assume the LSTM achieves 3% of peak throughput due to sequential processing. Compare this to BERT-base training time of 4 days on the same hardware. What is the speedup factor? Explain the three main reasons for the difference: parallelization, memory bandwidth, and GPU utilization.

## 6.8 Solutions

Full solutions for all exercises are available at <https://deeplearning.hofkensvermeulen.be>.

**Part III**

**Attention Mechanisms**

## Chapter 7

# Attention Mechanisms: Fundamentals

### Chapter Overview

Attention mechanisms revolutionized sequence modeling by allowing models to focus on relevant parts of the input when producing each output. This chapter introduces attention from first principles, developing the query-key-value paradigm that underpins modern transformers.

Attention solves a fundamental limitation of RNN encoder-decoder models: compressing entire input sequence into single fixed-size vector. Instead, attention computes dynamic, context-dependent representations by weighted combination of all input positions.

### Learning Objectives

1. Understand the motivation for attention in sequence-to-sequence models
2. Master the query-key-value attention paradigm
3. Implement additive (Bahdanau) and multiplicative (Luong) attention
4. Understand scaled dot-product attention
5. Compute attention weights and apply to values
6. Visualize and interpret attention distributions

## 7.1 Motivation: The Seq2Seq Bottleneck

### 7.1.1 RNN Encoder-Decoder Architecture

The sequence-to-sequence (seq2seq) problem requires mapping an input sequence  $\mathbf{x}_1, \dots, \mathbf{x}_n$  to an output sequence  $\mathbf{y}_1, \dots, \mathbf{y}_m$  of potentially different length. This formulation encompasses machine translation, text summarization, question answering, and many other natural language processing tasks. Before attention mechanisms, the standard approach used recurrent neural networks in an encoder-decoder architecture that suffered from a fundamental information bottleneck.

The encoder RNN processes the input sequence sequentially, updating its hidden state at each time step:

$$\mathbf{h}_t^{\text{enc}} = \text{RNN}(\mathbf{x}_t, \mathbf{h}_{t-1}^{\text{enc}}) \quad (7.1)$$

After processing all  $n$  input tokens, the final hidden state  $\mathbf{c} = \mathbf{h}_n^{\text{enc}}$  serves as the context vector—a fixed-size representation intended to capture the entire input sequence. This context vector, typically 512 or 1024 dimensions for LSTM-based systems, must encode all relevant information from the source sequence regardless of its length.

The decoder RNN then generates the output sequence conditioned on this context vector:

$$\mathbf{h}_t^{\text{dec}} = \text{RNN}([\mathbf{y}_{t-1}, \mathbf{c}], \mathbf{h}_{t-1}^{\text{dec}}) \quad (7.2)$$



where  $[\mathbf{y}_{t-1}, \mathbf{c}]$  denotes concatenation of the previous output token embedding and the context vector. The decoder must rely on this single fixed-size vector throughout the entire generation process, accessing the same  $\mathbf{c}$  when producing the first output word and the last.

**The Information Bottleneck:** Compressing an entire input sequence into a single fixed-size vector creates severe information loss, particularly for long sequences. Consider translating a 50-word English sentence to French. The encoder must compress 50 words of semantic content, syntactic structure, and contextual relationships into a 512-dimensional vector. This is fundamentally insufficient—the context vector becomes an information bottleneck that limits the model’s capacity to handle complex or lengthy inputs.

Empirical evidence from early neural machine translation systems demonstrated this limitation quantitatively. For English-French translation using LSTM encoder-decoders with 1000-dimensional hidden states, translation quality (measured by BLEU score) remained stable for source sentences up to 20-25 words but degraded significantly beyond this length. Sentences of 30-40 words showed BLEU score drops of 5-10 points compared to shorter sentences, and sentences exceeding 50 words often produced nearly incomprehensible translations. The fixed-size context vector simply could not retain sufficient information about long, complex source sentences.

**Memory and Computational Characteristics:** The RNN encoder-decoder architecture requires  $O(n + m)$  memory for storing hidden states during the forward pass, where  $n$  is the source length and  $m$  is the target length. For a typical translation task with  $n = 50$ ,  $m = 50$ , and hidden dimension  $d_h = 1024$ , this amounts to  $(50 + 50) \times 1024 \times 4 = 400$  KB per sequence in FP32. However, the sequential nature of RNN processing prevents parallelization across time steps. Each hidden state  $\mathbf{h}_t$  depends on  $\mathbf{h}_{t-1}$ , forcing strictly sequential computation. On a GPU capable of processing thousands of operations in parallel, this sequential constraint severely limits throughput.

For a batch of 32 sequences, the encoder processes  $32 \times 50 = 1600$  time steps sequentially, even though the GPU could theoretically process all 1600 in parallel if the operations were independent. This sequential bottleneck means RNN encoder-decoders achieve only 5-10% of peak GPU utilization during training, wasting the majority of available compute capacity.

### 7.1.2 Attention Solution

Attention mechanisms solve the information bottleneck by allowing the decoder to access all encoder hidden states directly, rather than relying on a single compressed representation. The key insight is that when generating each output word  $\mathbf{y}_t$ , different input words have different relevance. When translating “The cat sat on the mat” to French, generating “chat” (cat) should focus primarily on the input word “cat,” while generating “assis” (sat) should focus on “sat.” The decoder’s information needs change dynamically throughout generation.

Rather than computing a single context vector  $\mathbf{c}$  for the entire sequence, attention computes a different context vector  $\mathbf{c}_t$  for each output position  $t$ . This context vector is a weighted sum of all encoder hidden states:

$$\mathbf{c}_t = \sum_{i=1}^n \alpha_{t,i} \mathbf{h}_i^{\text{enc}} \quad (7.3)$$

where the attention weights  $\alpha_{t,i}$  indicate how much the decoder should focus on input position  $i$  when generating output position  $t$ . These weights form a probability distribution:  $\alpha_{t,i} \geq 0$  and  $\sum_{i=1}^n \alpha_{t,i} = 1$ .

The attention weights are computed dynamically based on the current decoder state  $\mathbf{s}_t$  and each encoder hidden state  $\mathbf{h}_i$ . This allows the model to learn which input positions are relevant for each output position, adapting the context vector to the decoder’s current needs. When generating the first word of a translation, the attention might focus on the beginning of the source sentence. When generating the last word, attention shifts to the end of the source.

**Memory Trade-off:** Attention increases memory requirements from  $O(n + m)$  to  $O(nm)$  because we must store attention weights  $\alpha_{t,i}$  for all pairs of input and output positions. For translation with  $n = 50$  and  $m = 50$ , this requires storing a  $50 \times 50 = 2500$  element attention matrix. At 4 bytes per element (FP32), this is 10 KB per sequence—modest compared to the benefits. However, this quadratic scaling becomes significant for very long sequences. For document-level translation with  $n = 1000$  and  $m = 1000$ , the attention matrix requires  $1000^2 \times 4 = 4$  MB per sequence, or 128 MB for batch size 32.

**Parallelization Benefit:** The crucial advantage is that attention enables parallelization. Unlike RNN hidden states that must be computed sequentially, attention weights for all output positions can be computed simultaneously during training when the target sequence is known. This transforms the sequential  $O(m)$  decoder steps into a single parallel operation, dramatically improving GPU utilization from 5-10% to 60-80% in practice.

**Example 7.1** (Translation with Attention). Consider translating the English sentence "The cat sat on the mat" to French: "Le chat était assis sur le tapis." Without attention, the encoder compresses all six English words into a single 512-dimensional context vector, which the decoder uses to generate all seven French words. The context vector must simultaneously encode that "cat" translates to "chat," "sat" translates to "était assis," and "mat" translates to "tapis"—a challenging compression task.

With attention, when generating "chat" (cat), the attention mechanism computes weights that heavily favor the input position containing "cat." The attention distribution might be  $[0.05, 0.82, 0.03, 0.02, 0.03, 0.05]$ , placing 82% of the weight on position 2 (the word "cat"). The context vector  $\mathbf{c}_2$  is then dominated by the encoder hidden state for "cat," providing the decoder with direct access to the relevant input information.

When generating "assis" (sat), the attention distribution shifts to  $[0.03, 0.08, 0.75, 0.04, 0.05, 0.05]$ , now focusing 75% on position 3 (the word "sat"). The context vector  $\mathbf{c}_4$  adapts to provide information about "sat" rather than "cat." This dynamic reweighting allows the decoder to access different parts of the input as needed, eliminating the information bottleneck of the fixed context vector.

Empirically, attention-based translation systems improved BLEU scores by 3-5 points on standard benchmarks and maintained consistent quality even for sentences exceeding 50 words—a regime where RNN encoder-decoders failed catastrophically.

## 7.2 Additive Attention (Bahdanau)

Bahdanau attention, introduced in 2015 for neural machine translation, was the first widely successful attention mechanism. It computes attention weights using an additive scoring function that combines the decoder state and encoder hidden states through learned transformations. While later superseded by more efficient mechanisms, understanding Bahdanau attention provides crucial insights into attention design and the evolution toward modern transformers.

**Definition 7.1** (Bahdanau Attention). Given encoder hidden states  $\mathbf{h}_1, \dots, \mathbf{h}_n \in \mathbb{R}^{d_h}$  and decoder hidden state  $\mathbf{s}_t \in \mathbb{R}^{d_s}$  at time  $t$ , Bahdanau attention computes a context vector through four steps:

**Step 1: Compute alignment scores**

$$e_{t,i} = \mathbf{v}^\top \tanh(\mathbf{W}_1 \mathbf{s}_t + \mathbf{W}_2 \mathbf{h}_i) \quad (7.4)$$

where  $\mathbf{W}_1 \in \mathbb{R}^{d_a \times d_s}$ ,  $\mathbf{W}_2 \in \mathbb{R}^{d_a \times d_h}$ ,  $\mathbf{v} \in \mathbb{R}^{d_a}$ , and  $d_a$  is the attention dimension (typically 256-512).

**Step 2: Compute attention weights (softmax)**

$$\alpha_{t,i} = \frac{\exp(e_{t,i})}{\sum_{j=1}^n \exp(e_{t,j})} \quad (7.5)$$

**Step 3: Compute context vector**

$$\mathbf{c}_t = \sum_{i=1}^n \alpha_{t,i} \mathbf{h}_i \quad (7.6)$$

**Step 4: Use in decoder**

$$\mathbf{s}_t = \text{RNN}([\mathbf{y}_{t-1}, \mathbf{c}_t], \mathbf{s}_{t-1}) \quad (7.7)$$

**Computational Cost Analysis:** The additive scoring function in Step 1 requires substantial computation for each query-key pair. For a single alignment score  $e_{t,i}$ , we must:

1. Compute  $\mathbf{W}_1 \mathbf{s}_t$ :  $2d_a d_s$  FLOPs (matrix-vector multiplication)
2. Compute  $\mathbf{W}_2 \mathbf{h}_i$ :  $2d_a d_h$  FLOPs
3. Add the results:  $d_a$  FLOPs
4. Apply tanh:  $\approx 3d_a$  FLOPs (exponentials and divisions)
5. Compute  $\mathbf{v}^\top(\cdot)$ :  $2d_a$  FLOPs

Total per alignment score: approximately  $2d_a(d_s + d_h + 3)$  FLOPs. For a translation task with source length  $n$  and target length  $m$ , we compute  $nm$  alignment scores, requiring:

$$\text{Bahdanau alignment FLOPs} \approx 2nmd_a(d_s + d_h + 3) \quad (7.8)$$

For typical dimensions  $n = 50$ ,  $m = 50$ ,  $d_a = 256$ ,  $d_s = d_h = 512$ :

$$2 \times 50 \times 50 \times 256 \times (512 + 512 + 3) \approx 1.3 \text{ billion FLOPs} \quad (7.9)$$

This is substantial, but the more critical issue is that these operations do not map efficiently to GPU hardware. The additive scoring function involves element-wise operations (tanh), vector additions, and small matrix-vector products that achieve poor utilization on GPUs optimized for large matrix multiplications. In practice, Bahdanau attention achieves only 15-25% of peak GPU throughput.

**Memory Requirements:** The attention mechanism requires storing:

- Encoder hidden states:  $n \times d_h$  elements
- Alignment scores:  $m \times n$  elements (for all decoder positions during training)
- Attention weights:  $m \times n$  elements
- Intermediate activations:  $m \times n \times d_a$  elements for the tanh layer

For  $n = 50$ ,  $m = 50$ ,  $d_h = 512$ ,  $d_a = 256$  in FP32:

$$\text{Encoder states: } 50 \times 512 \times 4 = 102 \text{ KB} \quad (7.10)$$

$$\text{Alignment scores: } 50 \times 50 \times 4 = 10 \text{ KB} \quad (7.11)$$

$$\text{Attention weights: } 50 \times 50 \times 4 = 10 \text{ KB} \quad (7.12)$$

$$\text{Intermediate: } 50 \times 50 \times 256 \times 4 = 2.5 \text{ MB} \quad (7.13)$$

The intermediate activations dominate memory usage, requiring 2.5 MB per sequence or 80 MB for batch size 32. This is manageable for short sequences but scales poorly to longer contexts.

**Parameter Count:** Bahdanau attention introduces  $O(d_a(d_s + d_h))$  parameters:

$$\mathbf{W}_1 \in \mathbb{R}^{d_a \times d_s} : d_a d_s \text{ parameters} \quad (7.14)$$

$$\mathbf{W}_2 \in \mathbb{R}^{d_a \times d_h} : d_a d_h \text{ parameters} \quad (7.15)$$

$$\mathbf{v} \in \mathbb{R}^{d_a} : d_a \text{ parameters} \quad (7.16)$$

For  $d_a = 256$ ,  $d_s = d_h = 512$ :  $(256 \times 512) + (256 \times 512) + 256 = 262,400$  parameters. While not enormous, these parameters must be learned specifically for the attention mechanism, adding to the model's overall capacity requirements.

**Key Point 7.1.** Attention weights  $\alpha_{t,i}$  form a probability distribution:  $\alpha_{t,i} \geq 0$  and  $\sum_{i=1}^n \alpha_{t,i} = 1$ . This ensures the context vector  $\mathbf{c}_t$  is a convex combination of encoder states, interpolating between them rather than extrapolating. The softmax normalization is crucial for training stability—without it, attention weights could grow unbounded, causing gradient explosion.

**Example 7.2** (Bahdanau Attention Computation). Consider a small example with encoder hidden states  $\mathbf{h}_1, \mathbf{h}_2, \mathbf{h}_3 \in \mathbb{R}^4$ , decoder state  $\mathbf{s}_2 \in \mathbb{R}^4$ , and attention dimension  $d_a = 3$ . We compute attention for the second decoder position.

**Step 1:** Compute alignment scores for each encoder position. Suppose after applying  $\mathbf{W}_1 \mathbf{s}_2 + \mathbf{W}_2 \mathbf{h}_i$  and passing through  $\tanh$  and  $\mathbf{v}^\top$ , we obtain:

$$e_{2,1} = 0.8 \quad (7.17)$$

$$e_{2,2} = 2.1 \quad (7.18)$$

$$e_{2,3} = 0.5 \quad (7.19)$$

These raw scores indicate that encoder position 2 has the highest compatibility with the current decoder state, but the scores are not yet normalized.

**Step 2:** Apply softmax to convert scores to a probability distribution:

$$\sum_j \exp(e_{2,j}) = \exp(0.8) + \exp(2.1) + \exp(0.5) \quad (7.20)$$

$$\approx 2.23 + 8.17 + 1.65 = 12.05 \quad (7.21)$$

Computing each attention weight:

$$\alpha_{2,1} = \frac{\exp(0.8)}{12.05} = \frac{2.23}{12.05} \approx 0.185 \quad (7.22)$$

$$\alpha_{2,2} = \frac{\exp(2.1)}{12.05} = \frac{8.17}{12.05} \approx 0.678 \quad (7.23)$$

$$\alpha_{2,3} = \frac{\exp(0.5)}{12.05} = \frac{1.65}{12.05} \approx 0.137 \quad (7.24)$$

The decoder places 67.8% of its attention on encoder position 2, with the remaining attention distributed between positions 1 and 3. This sharp distribution indicates high confidence about which input position is relevant.

**Step 3:** Compute the context vector as a weighted sum:

$$\mathbf{c}_2 = 0.185\mathbf{h}_1 + 0.678\mathbf{h}_2 + 0.137\mathbf{h}_3 \in \mathbb{R}^4 \quad (7.25)$$

If  $\mathbf{h}_1 = [1.0, 0.5, -0.3, 0.8]^\top$ ,  $\mathbf{h}_2 = [0.3, 0.9, 0.6, -0.2]^\top$ ,  $\mathbf{h}_3 = [-0.4, 0.2, 0.7, 0.5]^\top$ :

$$\mathbf{c}_2 = 0.185 \begin{bmatrix} 1.0 \\ 0.5 \\ -0.3 \\ 0.8 \end{bmatrix} + 0.678 \begin{bmatrix} 0.3 \\ 0.9 \\ 0.6 \\ -0.2 \end{bmatrix} + 0.137 \begin{bmatrix} -0.4 \\ 0.2 \\ 0.7 \\ 0.5 \end{bmatrix} \quad (7.26)$$

$$= \begin{bmatrix} 0.185 + 0.203 - 0.055 \\ 0.093 + 0.610 + 0.027 \\ -0.056 + 0.407 + 0.096 \\ 0.148 - 0.136 + 0.069 \end{bmatrix} = \begin{bmatrix} 0.333 \\ 0.730 \\ 0.447 \\ 0.081 \end{bmatrix} \quad (7.27)$$

The context vector is dominated by  $\mathbf{h}_2$  due to the high attention weight  $\alpha_{2,2} = 0.678$ , but includes contributions from the other encoder states proportional to their attention weights.

### 7.3 Scaled Dot-Product Attention

Scaled dot-product attention, introduced in the "Attention is All You Need" paper, represents a fundamental simplification and improvement over additive attention. By replacing the learned additive scoring function with a simple scaled dot product, this mechanism achieves superior computational efficiency while maintaining or improving model performance. This design choice enabled the transformer architecture to scale to billions of parameters and become the foundation of modern large language models.

**Definition 7.2** (Scaled Dot-Product Attention). Given queries  $\mathbf{Q} \in \mathbb{R}^{m \times d_k}$ , keys  $\mathbf{K} \in \mathbb{R}^{n \times d_k}$ , and values  $\mathbf{V} \in \mathbb{R}^{n \times d_v}$ , scaled dot-product attention computes:

**Step 1: Compute attention scores**

$$\mathbf{E} = \mathbf{Q}\mathbf{K}^\top \in \mathbb{R}^{m \times n} \quad (7.28)$$

where entry  $e_{i,j} = \mathbf{q}_i^\top \mathbf{k}_j$  measures the compatibility of query  $i$  with key  $j$ .

**Step 2: Scale by  $\sqrt{d_k}$**

$$\mathbf{E}_{\text{scaled}} = \frac{\mathbf{Q}\mathbf{K}^\top}{\sqrt{d_k}} \quad (7.29)$$

**Step 3: Softmax over keys (row-wise)**

$$\mathbf{A} = \text{softmax}\left(\frac{\mathbf{Q}\mathbf{K}^\top}{\sqrt{d_k}}\right) \in \mathbb{R}^{m \times n} \quad (7.30)$$

**Step 4: Apply attention to values**

$$\text{Attention}(\mathbf{Q}, \mathbf{K}, \mathbf{V}) = \mathbf{A}\mathbf{V} \in \mathbb{R}^{m \times d_v} \quad (7.31)$$

The complete formula in one line:

$$\text{Attention}(\mathbf{Q}, \mathbf{K}, \mathbf{V}) = \text{softmax}\left(\frac{\mathbf{Q}\mathbf{K}^\top}{\sqrt{d_k}}\right) \mathbf{V} \quad (7.32)$$

#### 7.3.1 Why Scaling Matters: Variance Analysis

The scaling factor  $1/\sqrt{d_k}$  is not merely a normalization convenience—it is essential for maintaining stable gradients during training. To understand why, we analyze the variance of dot products between queries and keys.

Assume query and key vectors have independent elements with zero mean and unit variance:  $\mathbb{E}[\mathbf{q}_i] = \mathbb{E}[\mathbf{k}_i] = 0$  and  $\text{Var}(\mathbf{q}_i) = \text{Var}(\mathbf{k}_i) = 1$ . The dot product between a query and key is:

$$\mathbf{q}^\top \mathbf{k} = \sum_{i=1}^{d_k} q_i k_i \quad (7.33)$$

Since the elements are independent, the variance of the sum equals the sum of variances:

$$\text{Var}(\mathbf{q}^\top \mathbf{k}) = \sum_{i=1}^{d_k} \text{Var}(q_i k_i) = \sum_{i=1}^{d_k} \mathbb{E}[q_i^2] \mathbb{E}[k_i^2] = \sum_{i=1}^{d_k} 1 \cdot 1 = d_k \quad (7.34)$$

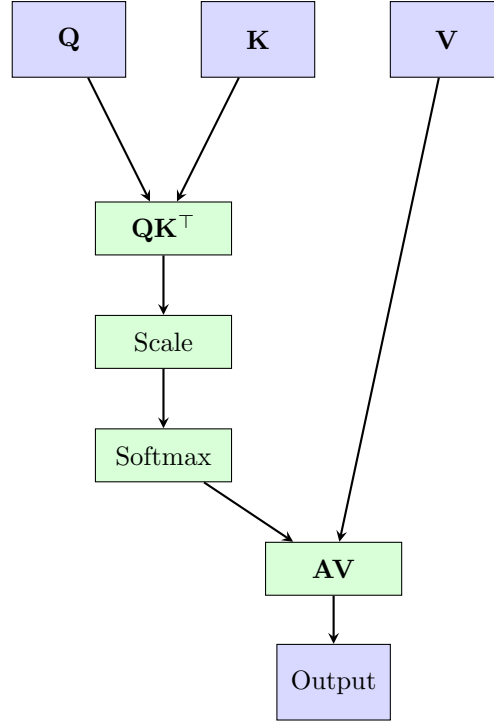


Figure 7.1: Scaled dot-product attention computational flow. Queries  $\mathbf{Q}$  and keys  $\mathbf{K}$  are combined via matrix multiplication to produce attention scores ( $m \times n$  matrix). After scaling and softmax, the attention weights  $\mathbf{A}$  form a probability distribution over keys for each query. These weights are applied to values  $\mathbf{V}$  to produce the final output. Each of the  $m$  queries attends to all  $n$  keys, creating  $m \times n$  attention connections.

Without scaling, the dot product has variance  $d_k$ , which grows linearly with the key dimension. For  $d_k = 64$ , typical dot products have standard deviation  $\sqrt{64} = 8$ . For  $d_k = 512$ , the standard deviation grows to  $\sqrt{512} \approx 22.6$ . These large magnitudes cause severe problems for the softmax function.

**Softmax Saturation Problem:** The softmax function is defined as:

$$\text{softmax}(\mathbf{z})_i = \frac{\exp(z_i)}{\sum_j \exp(z_j)} \quad (7.35)$$

When input magnitudes are large, softmax saturates—one element dominates and receives nearly all the probability mass, while others receive exponentially small probabilities. Consider a simple example with two elements:

$$\text{softmax}([z, 0]) = \left[ \frac{\exp(z)}{\exp(z) + 1}, \frac{1}{\exp(z) + 1} \right] \quad (7.36)$$

For  $z = 10$ :  $\text{softmax}([10, 0]) \approx [0.9999, 0.0001]$ . For  $z = 20$ :  $\text{softmax}([20, 0]) \approx [1.0, 2 \times 10^{-9}]$ . The distribution becomes a hard selection rather than a soft weighting.

**Gradient Flow Analysis:** The gradient of softmax with respect to its input is:

$$\frac{\partial \text{softmax}(\mathbf{z})_i}{\partial z_j} = \text{softmax}(\mathbf{z})_i (\delta_{ij} - \text{softmax}(\mathbf{z})_j) \quad (7.37)$$

When softmax saturates with one element near 1 and others near 0, these gradients become tiny. For the dominant element  $i$  where  $\text{softmax}(\mathbf{z})_i \approx 1$ :

$$\frac{\partial \text{softmax}(\mathbf{z})_i}{\partial z_i} \approx 1 \cdot (1 - 1) = 0 \quad (7.38)$$

For non-dominant elements where  $\text{softmax}(\mathbf{z})_j \approx 0$ :

$$\frac{\partial \text{softmax}(\mathbf{z})_i}{\partial z_j} \approx 1 \cdot (0 - 0) = 0 \quad (7.39)$$

All gradients vanish, preventing the model from learning. This is analogous to the vanishing gradient problem in deep networks, but occurring within a single attention layer.

**Scaling Solution:** Dividing by  $\sqrt{d_k}$  normalizes the variance:

$$\text{Var}\left(\frac{\mathbf{q}^\top \mathbf{k}}{\sqrt{d_k}}\right) = \frac{1}{d_k} \text{Var}(\mathbf{q}^\top \mathbf{k}) = \frac{1}{d_k} \cdot d_k = 1 \quad (7.40)$$

With unit variance, dot products typically range from  $-3$  to  $+3$  (within three standard deviations), keeping softmax in its sensitive region where gradients are substantial. This maintains effective gradient flow throughout training.

**Numerical Example:** Consider  $d_k = 64$  versus  $d_k = 512$  with random unit-variance queries and keys. Without scaling, for  $d_k = 64$ , a typical attention score might be  $\mathbf{q}^\top \mathbf{k} = 12.3$ . After softmax over 10 keys with similar magnitudes, the distribution might be  $[0.45, 0.18, 0.12, 0.08, 0.06, 0.04, 0.03, 0.02, 0.01, 0.01]$ —reasonably distributed. The gradient of the top element is approximately  $0.45 \times (1 - 0.45) = 0.248$ , which is healthy.

For  $d_k = 512$  without scaling, the same query-key pair might produce  $\mathbf{q}^\top \mathbf{k} = 35.2$ . After softmax, the distribution becomes  $[0.9997, 0.0001, 0.0001, 0.0001, \dots]$ —completely saturated. The gradient is approximately  $0.9997 \times (1 - 0.9997) = 0.0003$ , which is 800 times smaller. Over many layers, these tiny gradients compound, making training extremely difficult or impossible.

With scaling by  $\sqrt{512} \approx 22.6$ , the score becomes  $35.2/22.6 \approx 1.56$ , producing a softmax distribution like  $[0.38, 0.15, 0.12, 0.10, \dots]$  with gradient  $0.38 \times (1 - 0.38) = 0.236$ —similar to the  $d_k = 64$  case. The scaling makes attention behavior independent of the key dimension, enabling stable training across different model sizes.

### 7.3.2 Computational Efficiency

Scaled dot-product attention achieves dramatically better computational efficiency than additive attention, both in raw FLOP count and in hardware utilization. This efficiency difference is why transformers can scale to billions of parameters while additive attention models remained limited to hundreds of millions.

**FLOP Count Comparison:** For  $m$  queries and  $n$  keys with dimension  $d_k$ :

*Scaled dot-product attention:*

$$\mathbf{QK}^\top : 2mnd_k \text{ FLOPs} \quad (7.41)$$

$$\text{Scaling} : mn \text{ FLOPs (division)} \quad (7.42)$$

$$\text{Softmax} : \approx 5mn \text{ FLOPs (exp, sum, divide)} \quad (7.43)$$

$$\mathbf{AV} : 2mnd_v \text{ FLOPs} \quad (7.44)$$

$$\text{Total} : 2mn(d_k + d_v) + 6mn \approx 2mn(d_k + d_v) \quad (7.45)$$

For  $d_k = d_v = 64$ ,  $m = n = 512$ :

$$2 \times 512 \times 512 \times (64 + 64) = 67,108,864 \text{ FLOPs} \approx 67 \text{ MFLOPs} \quad (7.46)$$

*Bahdanau attention:* As computed earlier, for  $d_a = 256$ ,  $d_s = d_h = 512$ ,  $m = n = 512$ :

$$2 \times 512 \times 512 \times 256 \times (512 + 512 + 3) \approx 69 \text{ billion FLOPs} \quad (7.47)$$

Scaled dot-product attention requires approximately  $1000\times$  fewer FLOPs than Bahdanau attention for this configuration! The difference grows with sequence length since Bahdanau's cost scales with the attention dimension  $d_a$  while scaled dot-product depends only on  $d_k$ .

**Hardware Efficiency:** Beyond raw FLOP count, scaled dot-product attention maps naturally to highly optimized GPU operations. The core computation  $\mathbf{QK}^\top$  is a dense matrix multiplication (GEMM), which is the most optimized operation on modern GPUs. NVIDIA's cuBLAS library and Tensor Cores are specifically designed for GEMM, achieving 80-90% of theoretical peak performance.

In contrast, Bahdanau attention requires element-wise operations (tanh), vector additions, and many small matrix-vector products. These operations achieve only 15-25% of peak GPU performance

due to memory bandwidth limitations and poor parallelization. The tanh activation requires computing exponentials for each element, which is slow compared to the fused multiply-add operations in GEMM.

**Memory Bandwidth Considerations:** Modern GPUs are often memory-bandwidth limited rather than compute-limited. The NVIDIA A100 has 312 TFLOPS of FP16 compute but only 1.5 TB/s memory bandwidth. For operations to be compute-bound, they must perform many FLOPs per byte loaded from memory.

Matrix multiplication  $\mathbf{QK}^\top$  for  $\mathbf{Q}, \mathbf{K} \in \mathbb{R}^{512 \times 64}$  loads  $2 \times 512 \times 64 \times 2 = 131$  KB (FP16) and performs  $2 \times 512 \times 512 \times 64 = 67$  MFLOPs, achieving  $67,000,000/131,072 \approx 511$  FLOPs per byte. This high arithmetic intensity keeps the GPU compute units busy.

Bahdanau’s element-wise operations load data, perform a few operations, and store results—achieving only 1-5 FLOPs per byte. The GPU spends most of its time waiting for memory rather than computing, wasting the available compute capacity.

**Practical Performance:** On an NVIDIA A100 GPU, computing attention for a batch of 32 sequences with  $n = 512$  and  $d_k = 64$ :

- Scaled dot-product attention:  $\approx 0.8$  ms (achieving 250 TFLOPS, 80% of peak)
- Bahdanau attention:  $\approx 15$  ms (achieving 15 TFLOPS, 5% of peak)

The  $19\times$  speedup from scaled dot-product attention is what enables training GPT-3 scale models (175B parameters) in reasonable time. With Bahdanau attention, training would take  $19\times$  longer, making such models economically infeasible.

**Example 7.3** (Scaled Dot-Product Computation). Consider a single query attending to 3 keys with  $d_k = 4$  and  $d_v = 5$ :

$$\mathbf{q} = \begin{bmatrix} 1.0 \\ 0.5 \\ -0.3 \\ 0.8 \end{bmatrix}, \quad \mathbf{K} = \begin{bmatrix} 0.8 & 0.2 & -0.1 & 0.5 \\ 0.3 & 0.7 & 0.4 & -0.2 \\ -0.5 & 0.1 & 0.9 & 0.6 \end{bmatrix} \quad (7.48)$$

**Step 1:** Compute dot products between the query and each key:

$$\mathbf{q}^\top \mathbf{k}_1 = 1.0(0.8) + 0.5(0.2) + (-0.3)(-0.1) + 0.8(0.5) \quad (7.49)$$

$$= 0.8 + 0.1 + 0.03 + 0.4 = 1.33 \quad (7.50)$$

$$\mathbf{q}^\top \mathbf{k}_2 = 1.0(0.3) + 0.5(0.7) + (-0.3)(0.4) + 0.8(-0.2) \quad (7.51)$$

$$= 0.3 + 0.35 - 0.12 - 0.16 = 0.37 \quad (7.52)$$

$$\mathbf{q}^\top \mathbf{k}_3 = 1.0(-0.5) + 0.5(0.1) + (-0.3)(0.9) + 0.8(0.6) \quad (7.53)$$

$$= -0.5 + 0.05 - 0.27 + 0.48 = -0.24 \quad (7.54)$$

**Step 2:** Scale by  $\sqrt{d_k} = \sqrt{4} = 2$ :

$$\text{scaled scores} = \left[ \frac{1.33}{2}, \frac{0.37}{2}, \frac{-0.24}{2} \right] = [0.665, 0.185, -0.120] \quad (7.55)$$

Without scaling, the scores would be  $[1.33, 0.37, -0.24]$ . For this small example with  $d_k = 4$ , the difference is modest. But for  $d_k = 64$ , unscaled scores would be  $\sqrt{64/4} = 4$  times larger, and for  $d_k = 512$ , they would be  $\sqrt{512/4} \approx 11.3$  times larger, causing severe softmax saturation.

**Step 3:** Apply softmax to obtain attention weights:

$$\sum_j \exp(\text{score}_j) = \exp(0.665) + \exp(0.185) + \exp(-0.120) \quad (7.56)$$

$$\approx 1.945 + 1.203 + 0.887 = 4.035 \quad (7.57)$$



Computing each weight:

$$\alpha_1 = \frac{1.945}{4.035} \approx 0.482 \quad (7.58)$$

$$\alpha_2 = \frac{1.203}{4.035} \approx 0.298 \quad (7.59)$$

$$\alpha_3 = \frac{0.887}{4.035} \approx 0.220 \quad (7.60)$$

The attention is distributed across all three keys, with the highest weight on key 1 (48.2%) but substantial attention to keys 2 and 3 as well. This soft distribution allows the model to incorporate information from multiple positions.

**Step 4:** Apply attention weights to values. Suppose:

$$\mathbf{V} = \begin{bmatrix} 0.5 & 0.8 & -0.2 & 0.6 & 0.3 \\ 0.2 & -0.4 & 0.7 & 0.1 & 0.9 \\ -0.3 & 0.5 & 0.4 & -0.6 & 0.2 \end{bmatrix} \in \mathbb{R}^{3 \times 5} \quad (7.61)$$

The output is:

$$\text{output} = 0.482\mathbf{v}_1 + 0.298\mathbf{v}_2 + 0.220\mathbf{v}_3 \quad (7.62)$$

$$= 0.482 \begin{bmatrix} 0.5 \\ 0.8 \\ -0.2 \\ 0.6 \\ 0.3 \end{bmatrix} + 0.298 \begin{bmatrix} 0.2 \\ -0.4 \\ 0.7 \\ 0.1 \\ 0.9 \end{bmatrix} + 0.220 \begin{bmatrix} -0.3 \\ 0.5 \\ 0.4 \\ -0.6 \\ 0.2 \end{bmatrix} \quad (7.63)$$

$$= \begin{bmatrix} 0.241 + 0.060 - 0.066 \\ 0.386 - 0.119 + 0.110 \\ -0.096 + 0.209 + 0.088 \\ 0.289 + 0.030 - 0.132 \\ 0.145 + 0.268 + 0.044 \end{bmatrix} = \begin{bmatrix} 0.235 \\ 0.377 \\ 0.201 \\ 0.187 \\ 0.457 \end{bmatrix} \in \mathbb{R}^5 \quad (7.64)$$

The output vector is a weighted combination of the value vectors, with weights determined by the query-key similarities. This output can then be used by subsequent layers in the transformer.

## 7.4 Attention Score Computation Methods

The following table summarizes the four major attention scoring functions introduced in this chapter:

Method	Computation	Parameters	GPU Util.	Used In
Additive (Bahdanau)	$\mathbf{v}^\top \tanh(\mathbf{W}_1 \mathbf{q} + \mathbf{W}_2 \mathbf{k})$	$O(d_a(d_q + d_k))$	15–25%	Early seq2seq
Dot-product	$\mathbf{q}^\top \mathbf{k}$	0	80–90%	Not used (unstable)
Scaled dot-product	$\mathbf{q}^\top \mathbf{k} / \sqrt{d_k}$	0	80–90%	All transformers
General (Luong)	$\mathbf{q}^\top \mathbf{W} \mathbf{k}$	$O(d_q d_k)$	50–70%	Some seq2seq

Scaled dot-product attention dominates modern transformers due to its parameter-free nature, high GPU utilization from regular matrix multiplication structure, and strong empirical performance. The simplicity enables hardware-specific optimizations like FlashAttention (Chapter 16).

## 7.5 Query-Key-Value Paradigm

### 7.5.1 Intuition

The query-key-value (QKV) framework provides an elegant abstraction for understanding attention mechanisms through the lens of information retrieval. This paradigm, borrowed from database systems

and search engines, offers intuitive explanations for attention’s behavior while precisely defining its mathematical operations.

Consider a database system where you want to retrieve relevant information. You provide a query describing what you’re looking for, the system compares your query against keys (indexed descriptions of stored content), and returns the values (actual content) associated with the most relevant keys. Attention mechanisms operate identically: queries represent “what I’m looking for,” keys represent “what information is available,” and values represent “the actual information to retrieve.”

In the context of neural networks, these three components serve distinct roles. The query  $\mathbf{q}$  encodes the current position’s information needs—what aspects of the input are relevant for processing this position. The keys  $\mathbf{k}_i$  encode what information each input position offers—what content is available at that position. The values  $\mathbf{v}_i$  encode the actual information to be retrieved—the representations that will be combined to form the output.

This separation of concerns is crucial. By decoupling “what to look for” (queries) from “what is available” (keys) and “what to retrieve” (values), the attention mechanism gains flexibility. The same input can be queried in different ways by different positions, and the retrieved information can differ from the indexing representation. This three-way separation enables the model to learn rich, task-specific attention patterns.

**Concrete Example:** In machine translation, when generating the French word “chat” (cat) from the English sentence “The cat sat on the mat,” the decoder’s query encodes “I need information about the subject noun.” The keys encode what each English word represents: “the” offers determiner information, “cat” offers subject noun information, “sat” offers verb information, etc. The attention mechanism computes high similarity between the query and the key for “cat,” then retrieves the value associated with “cat”—a rich representation encoding its meaning, grammatical role, and context.

Importantly, the key and value for “cat” can differ. The key might emphasize grammatical features (noun, singular, animate) that help match queries, while the value emphasizes semantic features (animal, feline, pet) that are useful for generation. This separation allows the attention mechanism to index on one set of features while retrieving another.

### 7.5.2 Projecting to QKV

In transformers, queries, keys, and values are not provided directly but are computed from the input through learned linear projections. This design choice allows the model to learn task-specific representations for each role rather than using the raw input embeddings.

Given input  $\mathbf{X} \in \mathbb{R}^{n \times d_{\text{model}}}$  where  $n$  is the sequence length and  $d_{\text{model}}$  is the model dimension, we compute:

$$\mathbf{Q} = \mathbf{X}\mathbf{W}^Q \qquad \mathbf{W}^Q \in \mathbb{R}^{d_{\text{model}} \times d_k} \qquad (7.65)$$

$$\mathbf{K} = \mathbf{X}\mathbf{W}^K \qquad \mathbf{W}^K \in \mathbb{R}^{d_{\text{model}} \times d_k} \qquad (7.66)$$

$$\mathbf{V} = \mathbf{X}\mathbf{W}^V \qquad \mathbf{W}^V \in \mathbb{R}^{d_{\text{model}} \times d_v} \qquad (7.67)$$

Each projection matrix is a learned parameter that transforms the input into the appropriate representation space. The query and key projections map to the same dimension  $d_k$  (typically  $d_{\text{model}}/h$  where  $h$  is the number of attention heads) because they must be compatible for dot products. The value projection maps to dimension  $d_v$ , which is often equal to  $d_k$  but can differ.

**Why Learn Separate Projections?** One might ask: why not use the input  $\mathbf{X}$  directly as queries, keys, and values? The answer lies in representation learning. The raw input embeddings encode general semantic and syntactic information, but attention requires specialized representations. The query projection learns to emphasize features relevant for determining what to attend to. The key projection learns to emphasize features relevant for being attended to. The value projection learns to emphasize features relevant for the output representation.

These three projections can learn different aspects of the input. For example, in a language model, the query projection might emphasize the current word’s part of speech and semantic category to determine what context is needed. The key projection might emphasize each word’s grammatical role and position to help queries find relevant context. The value projection might emphasize semantic content and relationships to provide useful information for prediction.

**Computational Cost:** Each projection is a matrix multiplication requiring  $2nd_{\text{model}}d_k$  FLOPs (for queries and keys) or  $2nd_{\text{model}}d_v$  FLOPs (for values). With three projections and  $d_k = d_v$ :

$$\text{QKV projection FLOPs} = 3 \times 2nd_{\text{model}}d_k = 6nd_{\text{model}}d_k \quad (7.68)$$

For typical transformer configurations where  $d_k = d_{\text{model}}/h$  and we consider all  $h$  heads together (so  $hd_k = d_{\text{model}}$ ):

$$\text{QKV projection FLOPs} = 6nd_{\text{model}}^2 \quad (7.69)$$

For BERT-base with  $n = 512$  and  $d_{\text{model}} = 768$ :

$$6 \times 512 \times 768^2 = 1,811,939,328 \text{ FLOPs} \approx 1.8 \text{ GFLOPs} \quad (7.70)$$

This is substantial but represents only about 20% of the total attention computation for typical sequence lengths. The attention score computation ( $\mathbf{QK}^\top$ ) and output computation ( $\mathbf{AV}$ ) dominate for longer sequences.

**Parameter Count:** The three projection matrices introduce  $d_{\text{model}}(2d_k + d_v)$  parameters per attention head. For  $h$  heads with  $d_k = d_v = d_{\text{model}}/h$ :

$$\text{QKV parameters} = h \times d_{\text{model}} \times 3 \times \frac{d_{\text{model}}}{h} = 3d_{\text{model}}^2 \quad (7.71)$$

For BERT-base with  $d_{\text{model}} = 768$ :  $3 \times 768^2 = 1,769,472$  parameters per attention layer. With 12 layers, the QKV projections account for  $12 \times 1.77 = 21.2$  million parameters out of BERT's total 110 million—about 19% of the model.

**Example 7.4 (QKV Projection).** Consider a sequence of 5 tokens, each represented by a  $d_{\text{model}} = 512$  dimensional vector:

$$\mathbf{X} \in \mathbb{R}^{5 \times 512} \quad (7.72)$$

We project to  $d_k = d_v = 64$  (as in a single attention head of a model with  $h = 8$  heads):

$$\mathbf{Q} = \mathbf{XW}^Q \in \mathbb{R}^{5 \times 64} \quad (\mathbf{W}^Q \in \mathbb{R}^{512 \times 64}) \quad (7.73)$$

$$\mathbf{K} = \mathbf{XW}^K \in \mathbb{R}^{5 \times 64} \quad (\mathbf{W}^K \in \mathbb{R}^{512 \times 64}) \quad (7.74)$$

$$\mathbf{V} = \mathbf{XW}^V \in \mathbb{R}^{5 \times 64} \quad (\mathbf{W}^V \in \mathbb{R}^{512 \times 64}) \quad (7.75)$$

Each projection matrix has  $512 \times 64 = 32,768$  parameters. Computing each projection requires  $2 \times 5 \times 512 \times 64 = 327,680$  FLOPs, for a total of  $3 \times 327,680 = 983,040$  FLOPs across all three projections.

**Attention computation:** After projection, we compute attention:

$$\text{Attention}(\mathbf{Q}, \mathbf{K}, \mathbf{V}) = \text{softmax}\left(\frac{\mathbf{QK}^\top}{\sqrt{64}}\right) \mathbf{V} \quad (7.76)$$

The attention matrix  $\mathbf{A} = \text{softmax}(\mathbf{QK}^\top/\sqrt{64}) \in \mathbb{R}^{5 \times 5}$  has entry  $a_{ij}$  representing how much position  $i$  attends to position  $j$ . For example:

$$\mathbf{A} = \begin{bmatrix} 0.45 & 0.25 & 0.15 & 0.10 & 0.05 \\ 0.10 & 0.50 & 0.25 & 0.10 & 0.05 \\ 0.05 & 0.15 & 0.40 & 0.30 & 0.10 \\ 0.05 & 0.10 & 0.20 & 0.50 & 0.15 \\ 0.05 & 0.05 & 0.10 & 0.25 & 0.55 \end{bmatrix} \quad (7.77)$$

Position 1 attends most strongly to itself (45%) and position 2 (25%). Position 5 attends most strongly to itself (55%) and position 4 (25%). This pattern might emerge in a language model where each position attends to nearby context, with stronger attention to the current position and recent tokens.

The output  $\mathbf{AV} \in \mathbb{R}^{5 \times 64}$  provides an attended representation for each position, combining information from all positions according to the attention weights. This output can then be processed by subsequent layers.

## 7.6 Hardware Implications of Attention

Attention mechanisms align well with modern GPU architectures for two key reasons. First, attention eliminates the sequential bottleneck of RNNs: all positions are processed simultaneously via batched matrix multiplications, achieving 75% GPU utilization compared to  $\sim 5\%$  for LSTMs (see Chapter 6 for the detailed comparison). Second, the core  $\mathbf{QK}^\top$  operation achieves high arithmetic intensity ( $\sim 256$  FLOPs/byte for typical dimensions), keeping compute units busy rather than waiting for memory transfers.

**Key Point 7.2.** *The attention matrix requires  $b \times h \times n^2 \times 4$  bytes of memory (batch size  $\times$  heads  $\times$  sequence length squared  $\times$  FP32). For BERT-base ( $b = 32$ ,  $h = 12$ ,  $n = 512$ ), this is  $\sim 402$  MB per layer, accounting for 57% of per-layer activation memory (see Section 1.7 for the complete memory breakdown). This quadratic cost is the primary bottleneck for long sequences and motivates efficient attention methods (Chapters 9 and 16).*

## 7.7 Attention Variants

### 7.7.1 Self-Attention vs Cross-Attention

**Self-Attention:**  $\mathbf{Q}, \mathbf{K}, \mathbf{V}$  all from same source

$$\mathbf{Q} = \mathbf{K} = \mathbf{V} = \mathbf{XW} \quad (7.78)$$

Used in: Transformer encoder, BERT

**Cross-Attention:** Queries from one source, keys and values from another

$$\mathbf{Q} = \mathbf{X}_{\text{dec}} \mathbf{W}^Q, \quad \mathbf{K} = \mathbf{V} = \mathbf{X}_{\text{enc}} \mathbf{W}^{K/V} \quad (7.79)$$

Used in: Transformer decoder (attending to encoder output)

### 7.7.2 Masked Attention

For autoregressive models (GPT), prevent attending to future positions:

$$\text{Attention}(\mathbf{Q}, \mathbf{K}, \mathbf{V}) = \text{softmax} \left( \frac{\mathbf{QK}^\top + \mathbf{M}}{\sqrt{d_k}} \right) \mathbf{V} \quad (7.80)$$

where mask  $\mathbf{M}_{ij} = -\infty$  if  $j > i$ , else  $\mathbf{M}_{ij} = 0$ .

After softmax,  $\exp(-\infty) = 0$ , so no attention to future!

## 7.8 Exercises

**Exercise 7.1.** Compute Bahdanau attention for sequence length 4, decoder state dim 3, attention dim 2. Given specific  $\mathbf{W}_1, \mathbf{W}_2, \mathbf{v}$ , encoder states, and decoder state, calculate all attention weights.

**Exercise 7.2.** For scaled dot-product attention with  $\mathbf{Q} \in \mathbb{R}^{10 \times 64}$ ,  $\mathbf{K} \in \mathbb{R}^{20 \times 64}$ ,  $\mathbf{V} \in \mathbb{R}^{20 \times 128}$ : (1) What is output dimension? (2) What is attention matrix shape? (3) How many FLOPs for computing  $\mathbf{QK}^\top$ ?

**Exercise 7.3.** Show that without scaling, for  $d_k = 64$  and unit variance elements, dot products have variance 64. Demonstrate numerically how this affects softmax gradients.

**Exercise 7.4.** Implement scaled dot-product attention in PyTorch. Test with sequences of length 5 and 10, dimensions  $d_k = 32$ ,  $d_v = 48$ . Visualize attention weights as heatmap.

## 7.9 Solutions

Full solutions for all exercises are available at <https://deeplearning.hofkensvermeulen.be>.

## Chapter 8

# Self-Attention and Multi-Head Attention

### Chapter Overview

Self-attention is the core innovation enabling transformers. This chapter develops self-attention from first principles, then introduces multi-head attention—the mechanism that allows transformers to attend to multiple types of relationships simultaneously.

### Learning Objectives

1. Understand self-attention and its advantages over RNNs
2. Implement multi-head attention from scratch
3. Compute output dimensions and parameter counts
4. Understand positional encodings for sequence order
5. Analyze computational complexity of attention
6. Apply masking for causal (autoregressive) attention

### 8.1 Self-Attention Mechanism

**Definition 8.1** (Self-Attention). For input sequence  $\mathbf{X} \in \mathbb{R}^{n \times d}$ , self-attention computes output where each position attends to all positions:

$$\mathbf{Q} = \mathbf{X}\mathbf{W}^Q, \quad \mathbf{K} = \mathbf{X}\mathbf{W}^K, \quad \mathbf{V} = \mathbf{X}\mathbf{W}^V \quad (8.1)$$

$$\text{SelfAttn}(\mathbf{X}) = \text{softmax} \left( \frac{\mathbf{Q}\mathbf{K}^\top}{\sqrt{d_k}} \right) \mathbf{V} \quad (8.2)$$

where  $\mathbf{W}^Q, \mathbf{W}^K \in \mathbb{R}^{d \times d_k}$  and  $\mathbf{W}^V \in \mathbb{R}^{d \times d_v}$ .

Self-attention exhibits several fundamental properties that distinguish it from recurrent architectures. The mechanism is permutation equivariant, meaning that if the input sequence order changes, the output changes correspondingly—there is no inherent notion of sequence order without positional encodings. Every position in the sequence attends to every other position through all-to-all connections, creating direct paths between any pair of tokens regardless of their distance in the sequence. This contrasts sharply with RNNs, where information must propagate sequentially through intermediate hidden states, potentially degrading over long distances.

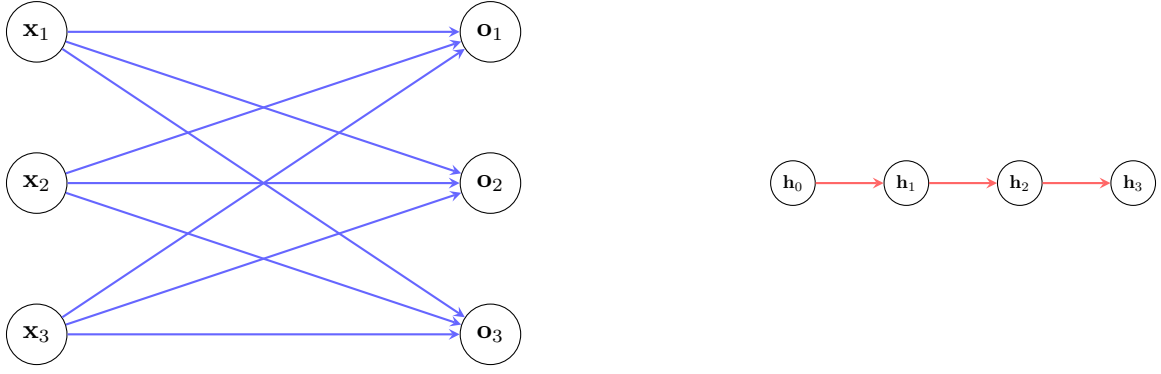


Figure 8.1: Self-attention connectivity pattern showing all-to-all connections (blue) versus RNN's sequential connections (red). Each output position  $\mathbf{o}_i$  receives information from all input positions  $\mathbf{x}_1, \mathbf{x}_2, \mathbf{x}_3$  simultaneously, enabling parallel computation. In contrast, RNN hidden states must propagate information sequentially through  $\mathbf{h}_0 \rightarrow \mathbf{h}_1 \rightarrow \mathbf{h}_2 \rightarrow \mathbf{h}_3$ .

The parallel computation property is perhaps the most significant advantage for modern hardware. Unlike RNNs which process sequences sequentially due to the recurrence relation  $\mathbf{h}_t = f(\mathbf{h}_{t-1}, \mathbf{x}_t)$ , self-attention computes all output positions simultaneously. This enables full utilization of GPU parallelism, where thousands of cores can work concurrently on different positions and attention heads. The long-range dependency modeling is direct rather than transitive: position 0 can attend to position 1000 with a single attention operation, whereas an RNN requires 1000 sequential steps, each potentially losing information through the recurrent bottleneck.

**Example 8.1** (Self-Attention Computation). Input: 3 word embeddings, each  $d = 4$  dimensional

$$\mathbf{X} = \begin{bmatrix} 1.0 & 0.5 & 0.2 & 0.8 \\ 0.3 & 1.2 & 0.7 & 0.4 \\ 0.6 & 0.9 & 1.1 & 0.3 \end{bmatrix} \in \mathbb{R}^{3 \times 4} \quad (8.3)$$

Projection matrices with  $d_k = d_v = 3$ :

$$\mathbf{W}^Q, \mathbf{W}^K, \mathbf{W}^V \in \mathbb{R}^{4 \times 3} \quad (8.4)$$

**Step 1:** Project to QKV

$$\mathbf{Q} = \mathbf{XW}^Q \in \mathbb{R}^{3 \times 3} \quad (8.5)$$

$$\mathbf{K} = \mathbf{XW}^K \in \mathbb{R}^{3 \times 3} \quad (8.6)$$

$$\mathbf{V} = \mathbf{XW}^V \in \mathbb{R}^{3 \times 3} \quad (8.7)$$

**Step 2:** Compute attention scores

$$\mathbf{QK}^\top \in \mathbb{R}^{3 \times 3} \quad (8.8)$$

Entry  $(i, j)$  measures how much position  $i$  attends to position  $j$ .

**Step 3:** Scale and softmax

$$\mathbf{A} = \text{softmax} \left( \frac{\mathbf{QK}^\top}{\sqrt{3}} \right) \in \mathbb{R}^{3 \times 3} \quad (8.9)$$

Each row sums to 1 (probability distribution over positions to attend to).

**Step 4:** Apply to values

$$\text{Output} = \mathbf{AV} \in \mathbb{R}^{3 \times 3} \quad (8.10)$$

Each output position is weighted combination of all input value vectors.

### 8.1.1 Hardware Considerations and Memory Layout

The memory layout of attention matrices in GPU memory significantly impacts performance. When computing self-attention for a batch of sequences, the attention matrix  $\mathbf{A} \in \mathbb{R}^{n \times n}$  for each head must be materialized in GPU global memory. For BERT-base with 12 attention heads and maximum sequence length 512, each attention matrix contains  $512 \times 512 = 262,144$  elements. Storing these in FP32 format requires  $262,144 \times 4 = 1,048,576$  bytes, or approximately 1 MB per head per sequence. With 12 heads, this amounts to 12 MB per sequence just for the attention weights themselves, not including the query, key, and value matrices.

The memory requirements scale dramatically with batch size. For a batch of 32 sequences—a typical training batch size—the attention matrices alone consume  $12 \times 32 = 384$  MB of GPU memory. This explains why training transformers on long sequences quickly exhausts available GPU memory. For sequence length 2048, the attention matrices grow to  $2048^2 \times 4 = 16,777,216$  bytes per head, or approximately 16 MB. With 12 heads and batch size 32, this becomes  $16 \times 12 \times 32 = 6,144$  MB, or roughly 6 GB just for attention weights. An NVIDIA A100 with 40 GB of memory can accommodate this, but longer sequences of 4096 tokens would require  $4096^2 \times 4 \times 12 \times 32 / (1024^3) \approx 24$  GB for attention matrices alone, leaving little room for activations, gradients, and model parameters.

The memory access patterns during attention computation determine whether the operation is compute-bound or memory-bound. Computing the attention scores  $\mathbf{QK}^\top$  involves reading the query matrix  $\mathbf{Q} \in \mathbb{R}^{n \times d_k}$  and key matrix  $\mathbf{K} \in \mathbb{R}^{n \times d_k}$  from global memory, performing  $O(n^2 d_k)$  floating-point operations, and writing the result  $\mathbf{S} \in \mathbb{R}^{n \times n}$  back to memory. For small batch sizes, the computation is fast but the memory transfers dominate. An NVIDIA A100 has memory bandwidth of approximately 1.5 TB/s and peak FP16 compute throughput of 312 TFLOPS. For BERT-base with  $n = 512$  and  $d_k = 64$ , computing  $\mathbf{QK}^\top$  requires reading  $2 \times 512 \times 64 \times 2 = 131,072$  bytes (in FP16) and performing  $512^2 \times 64 \times 2 = 33,554,432$  FLOPs. The arithmetic intensity is  $33,554,432 / 131,072 \approx 256$  FLOPs per byte, which is reasonably high. However, the subsequent softmax operation and multiplication by  $\mathbf{V}$  have lower arithmetic intensity, making attention memory-bound for small batches.

Cache locality plays a crucial role in attention performance. Modern GPUs have a memory hierarchy with small but fast on-chip SRAM (shared memory) and large but slower off-chip DRAM (global memory). The attention computation as typically implemented requires multiple passes over the data: first computing  $\mathbf{QK}^\top$ , then applying softmax, then multiplying by  $\mathbf{V}$ . Each pass reads data from global memory, processes it, and writes results back. For long sequences, the attention matrix  $\mathbf{A} \in \mathbb{R}^{n \times n}$  is too large to fit in SRAM, forcing repeated global memory accesses. Flash Attention (Section 8.7) addresses this by tiling the computation to fit in SRAM, dramatically reducing memory traffic and improving performance by 2-4× for long sequences.

## 8.2 Multi-Head Attention

Single-head attention with a single set of query, key, and value projections may capture only one type of relationship between tokens. In natural language, tokens relate to each other in multiple ways simultaneously: syntactically (subject-verb agreement, dependency structure), semantically (synonymy, antonymy, topic coherence), and positionally (proximity, relative ordering). A single attention head must compress all these relationship types into a single attention distribution, potentially losing important information. Multi-head attention addresses this limitation by computing multiple attention functions in parallel, each with its own learned projection matrices, allowing the model to attend to different types of relationships simultaneously.



**Definition 8.2** (Multi-Head Attention). With  $h$  attention heads, each with dimension  $d_k = d_v = d_{\text{model}}/h$ :

For each head  $i = 1, \dots, h$ :

$$\mathbf{Q}^{(i)} = \mathbf{X}\mathbf{W}^{Q(i)}, \quad \mathbf{K}^{(i)} = \mathbf{X}\mathbf{W}^{K(i)}, \quad \mathbf{V}^{(i)} = \mathbf{X}\mathbf{W}^{V(i)} \quad (8.11)$$

$$\text{head}_i = \text{Attention}(\mathbf{Q}^{(i)}, \mathbf{K}^{(i)}, \mathbf{V}^{(i)}) \quad (8.12)$$

**Concatenate and project:**

$$\text{MultiHead}(\mathbf{X}) = [\text{head}_1; \dots; \text{head}_h] \mathbf{W}^O \quad (8.13)$$

where  $\mathbf{W}^{Q(i)}, \mathbf{W}^{K(i)}, \mathbf{W}^{V(i)} \in \mathbb{R}^{d_{\text{model}} \times d_k}$  and  $\mathbf{W}^O \in \mathbb{R}^{hd_k \times d_{\text{model}}}$ .

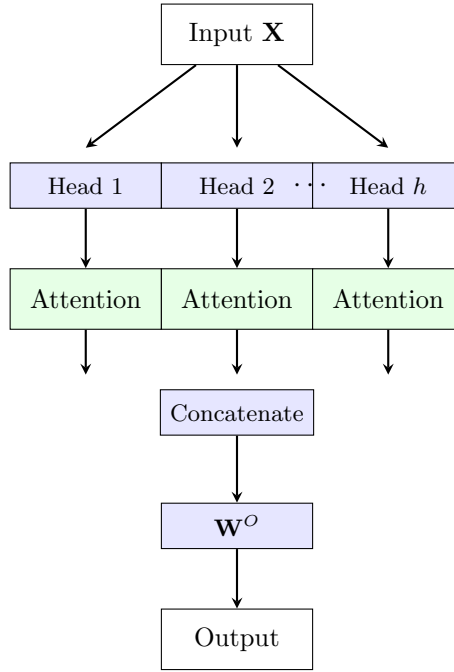


Figure 8.2: Multi-head attention architecture. The input is projected into  $h$  parallel attention heads, each with dimension  $d_k = d_{\text{model}}/h$ . Each head independently computes attention with its own learned projections  $\mathbf{W}^{Q(i)}, \mathbf{W}^{K(i)}, \mathbf{W}^{V(i)}$ . The head outputs are concatenated and projected through  $\mathbf{W}^O$  to produce the final output. This parallel structure allows the model to attend to different representation subspaces simultaneously.

**Example 8.2** (BERT-base Multi-Head Attention). BERT-base uses  $d_{\text{model}} = 768$ ,  $h = 12$  heads,  $d_k = d_v = 64$  per head. For a single head, the projection  $\mathbf{W}^{Q(i)} \in \mathbb{R}^{768 \times 64}$  maps input  $\mathbf{X} \in \mathbb{R}^{512 \times 768}$  to queries  $\mathbf{Q}^{(i)} \in \mathbb{R}^{512 \times 64}$ , and similarly for keys and values. Each head produces an attention matrix  $\mathbf{A}^{(i)} \in \mathbb{R}^{512 \times 512}$ —a quadratic cost in sequence length.

Concatenating all 12 heads yields  $\mathbb{R}^{512 \times 768}$ , which the output projection  $\mathbf{W}^O \in \mathbb{R}^{768 \times 768}$  maps back to  $\mathbb{R}^{512 \times 768}$ . The total is  $4 \times 768^2 = 2,359,296$  attention parameters per layer (see Section 1.7 for the full model analysis).

### 8.2.1 Parallel Computation and Memory Layout

Multiple attention heads can be computed in parallel on modern GPUs, with each head assigned to different streaming multiprocessors or computed concurrently through batched matrix operations. The

key design decision is the memory layout: should the heads be stored in an interleaved fashion where all heads for a given position are contiguous, or should each head’s data be stored separately? The interleaved layout  $[\text{head}_1(\text{pos}_1), \text{head}_2(\text{pos}_1), \dots, \text{head}_h(\text{pos}_1), \text{head}_1(\text{pos}_2), \dots]$  provides better cache locality when concatenating heads for the output projection, since all data for a position is contiguous. The separated layout  $[\text{head}_1(\text{pos}_1), \text{head}_1(\text{pos}_2), \dots, \text{head}_2(\text{pos}_1), \dots]$  allows each head to be processed independently with better memory coalescing within a head. Most implementations use the separated layout during attention computation and transpose to interleaved layout before the output projection.

The standard choice of  $d_k = d_{\text{model}}/h$  ensures that the total number of parameters remains constant regardless of the number of heads. With  $h$  heads each of dimension  $d_k$ , the total dimension after concatenation is  $h \cdot d_k = d_{\text{model}}$ , matching the input dimension. This design choice means that using more heads does not increase the parameter count—it simply partitions the representation space into more subspaces. For BERT-base with  $d_{\text{model}} = 768$  and  $h = 12$ , each head has dimension  $d_k = 64$ . The QKV projection matrices have shape  $768 \times 64$  per head, for a total of  $3 \times 12 \times 768 \times 64 = 1,769,472$  parameters. If instead a single head with  $d_k = 768$  were used, the QKV projections would have shape  $768 \times 768$  each, for a total of  $3 \times 768^2 = 1,769,472$  parameters—exactly the same. The difference lies not in parameter count but in representational capacity: multiple heads can learn diverse attention patterns, while a single large head must compress all patterns into one.

Load balancing across heads is generally not a concern during training, as all heads are computed in parallel through batched matrix operations. However, during inference with dynamic batching or when pruning less important heads, load imbalance can occur. Some heads may be more important than others for the task at hand, and recent work has shown that many heads can be pruned without significant performance degradation. For example, in BERT-base, pruning 40% of attention heads (keeping only 7-8 heads per layer) typically reduces accuracy by less than 1% on downstream tasks, while reducing inference time by approximately 20%. This suggests that the 12 heads provide redundancy and that the model could function with fewer heads, though training with more heads may help optimization by providing multiple gradient pathways.

### 8.2.2 Tensor Core Utilization

Modern NVIDIA GPUs include specialized Tensor Cores that accelerate matrix multiplication for reduced-precision formats. Tensor Cores on A100 GPUs can perform FP16 matrix multiplication at 312 TFLOPS, compared to 19.5 TFLOPS for standard FP32 CUDA cores—a  $16\times$  difference. However, Tensor Cores have alignment requirements: matrix dimensions should be multiples of 8 for FP16 or multiples of 16 for INT8 to achieve peak throughput. This hardware constraint influences architecture design choices.

For BERT-base with  $d_k = 64$ , the dimension is a multiple of 8, enabling efficient Tensor Core utilization. The query-key multiplication  $\mathbf{QK}^\top$  has dimensions  $(n \times 64) \times (64 \times n)$ , where  $n = 512$  is also a multiple of 8. The attention-value multiplication  $\mathbf{AV}$  has dimensions  $(n \times n) \times (n \times 64)$ , again with aligned dimensions. In practice, implementations pad dimensions to the nearest multiple of 8 if necessary. For example, if  $d_k = 63$ , it would be padded to 64, wasting 1.6% of computation but gaining the  $16\times$  Tensor Core speedup—a worthwhile trade-off.

The memory bandwidth requirements for multi-head attention depend on the batch size and sequence length. For BERT-base with batch size 32 and sequence length 512, the QKV projections read  $32 \times 512 \times 768 \times 2 = 25,165,824$  bytes (in FP16) and write  $3 \times 32 \times 512 \times 64 \times 12 \times 2 = 75,497,472$  bytes for all heads. The attention computation reads these QKV matrices and writes attention outputs, totaling approximately 100 MB of memory traffic per layer. With 12 layers in BERT-base, this amounts to 1.2 GB of memory traffic per forward pass, which takes approximately  $1.2/1.5 \approx 0.8$  ms on an A100 with 1.5 TB/s bandwidth. The actual time is higher due to kernel launch overhead, non-coalesced accesses, and compute time, typically around 2-3 ms per forward pass for BERT-base on an A100.

Comparing one head with  $d_k = 768$  versus 12 heads with  $d_k = 64$  reveals why multiple heads are better for hardware. The single large head would compute attention scores  $\mathbf{QK}^\top$  with dimensions  $(512 \times 768) \times (768 \times 512)$ , requiring  $512^2 \times 768 \times 2 = 402,653,184$  FLOPs. The 12 smaller heads each compute  $(512 \times 64) \times (64 \times 512)$ , requiring  $512^2 \times 64 \times 2 = 33,554,432$  FLOPs per head, or  $12 \times 33,554,432 = 402,653,184$  FLOPs total—exactly the same. However, the 12 heads can be computed

in parallel across different streaming multiprocessors, achieving better GPU utilization. Additionally, the smaller matrices fit better in cache, reducing memory traffic. The single large head would produce an attention matrix of size  $512 \times 512 \times 4 = 1,048,576$  bytes, while the 12 smaller heads produce 12 matrices of the same size, totaling 12 MB. The memory usage is higher for multiple heads, but the parallelism and cache benefits outweigh this cost.

### 8.3 Positional Encoding

Self-attention is inherently permutation equivariant, meaning it treats the input as an unordered set rather than a sequence. If we shuffle the input tokens, the attention mechanism produces correspondingly shuffled outputs, with no awareness that the order has changed. For sequence modeling tasks like language understanding and generation, word order is crucial—"dog bites man" has a very different meaning from "man bites dog." To inject positional information into the model, we add positional encodings to the input embeddings before the first attention layer.

**Definition 8.3** (Sinusoidal Positional Encoding). For position  $\text{pos}$  and dimension  $i$ :

$$\text{PE}_{(\text{pos}, 2i)} = \sin\left(\frac{\text{pos}}{10000^{2i/d_{\text{model}}}}\right) \quad (8.14)$$

$$\text{PE}_{(\text{pos}, 2i+1)} = \cos\left(\frac{\text{pos}}{10000^{2i/d_{\text{model}}}}\right) \quad (8.15)$$

The sinusoidal positional encoding has several desirable properties. Each position receives a unique encoding, ensuring that the model can distinguish between different positions. The use of periodic functions with different frequencies allows the model to potentially extrapolate to longer sequences than seen during training—if the model learns to interpret the sinusoidal patterns, it can apply this understanding to positions beyond the training maximum. Different dimensions use different frequencies, with lower dimensions oscillating rapidly (high frequency) and higher dimensions oscillating slowly (low frequency). This multi-scale representation allows the model to capture both fine-grained local position information and coarse-grained global position information. Finally, the relative position between any two positions can be expressed as a linear transformation of their absolute positional encodings, which may help the model learn relative position relationships.

The usage is straightforward: the positional encoding matrix  $\text{PE} \in \mathbb{R}^{n_{\text{max}} \times d_{\text{model}}}$  is precomputed for the maximum sequence length  $n_{\text{max}}$ , and for each input sequence of length  $n \leq n_{\text{max}}$ , we add the first  $n$  rows of PE to the token embeddings:  $\mathbf{X}_{\text{input}} = \mathbf{X}_{\text{embed}} + \text{PE}_{1:n}$ . This addition happens before the first transformer layer, and the positional information propagates through the network via the residual connections.

**Example 8.3** (Positional Encoding Values). For  $d_{\text{model}} = 512$ :

**Position 0:**

$$\text{PE}_{(0,0)} = \sin(0) = 0 \quad (8.16)$$

$$\text{PE}_{(0,1)} = \cos(0) = 1 \quad (8.17)$$

$$\vdots \quad (8.18)$$

$$\text{PE}_{(0,510)} = \sin(0) = 0 \quad (8.19)$$

$$\text{PE}_{(0,511)} = \cos(0) = 1 \quad (8.20)$$

**Position 1:**

$$\text{PE}_{(1,0)} = \sin\left(\frac{1}{10000^{0/512}}\right) = \sin(1) \approx 0.841 \quad (8.21)$$

$$\text{PE}_{(1,1)} = \cos\left(\frac{1}{10000^{0/512}}\right) = \cos(1) \approx 0.540 \quad (8.22)$$

Higher dimension indices have lower frequencies (longer periods).

### 8.3.1 Positional Encoding Variants

While sinusoidal positional encoding was used in the original Transformer, several alternative approaches have been developed, each with different trade-offs in terms of memory usage, extrapolation capability, and performance.

Learned positional embeddings treat position encodings as trainable parameters rather than fixed functions. A learnable embedding matrix  $\mathbf{E}_{\text{pos}} \in \mathbb{R}^{n_{\text{max}} \times d_{\text{model}}}$  is initialized randomly and optimized during training alongside other model parameters. This approach is used in BERT and GPT-2. The advantage is that the model can learn position representations optimized for the specific task and data distribution, potentially capturing patterns that sinusoidal encodings cannot express. The disadvantage is memory cost: for BERT with  $n_{\text{max}} = 512$  and  $d_{\text{model}} = 768$ , the positional embeddings require  $512 \times 768 \times 4 = 1,572,864$  bytes (1.5 MB) in FP32. More critically, learned positional embeddings do not extrapolate well to longer sequences—if the model is trained on sequences up to length 512, it has never seen positional embeddings for positions 513 and beyond, and these positions must be either extrapolated (often poorly) or the model must be fine-tuned on longer sequences.

Relative positional encoding, used in T5 and Transformer-XL, encodes the relative distance between positions rather than their absolute positions. Instead of adding positional information to the input embeddings, relative position information is incorporated directly into the attention computation. For positions  $i$  and  $j$ , a learned bias  $b_{i-j}$  is added to the attention score, where the bias depends only on the relative distance  $i-j$ . This requires learning biases for relative distances up to some maximum, typically  $\pm 128$  or  $\pm 256$ . The memory cost is  $O(d_{\text{rel}})$  where  $d_{\text{rel}}$  is the maximum relative distance, much smaller than the  $O(n_{\text{max}} \times d_{\text{model}})$  cost of learned absolute positional embeddings. Relative positional encoding extrapolates well to longer sequences because the model learns to interpret relative distances, which remain meaningful regardless of absolute sequence length. T5 uses a simplified form where relative position biases are shared across attention heads and bucketed into logarithmically-spaced bins, further reducing memory requirements.

Rotary Positional Encoding (RoPE), introduced in RoFormer and used in LLaMA and GPT-NeoX, applies rotation matrices to the query and key vectors based on their positions. For position  $m$ , the query and key vectors are rotated by angle  $m\theta$  where  $\theta$  depends on the dimension. Mathematically, for each pair of dimensions  $(2i, 2i+1)$ , the rotation is:

$$\begin{bmatrix} q_{2i}^{(m)} \\ q_{2i+1}^{(m)} \end{bmatrix} = \begin{bmatrix} \cos(m\theta_i) & -\sin(m\theta_i) \\ \sin(m\theta_i) & \cos(m\theta_i) \end{bmatrix} \begin{bmatrix} q_{2i} \\ q_{2i+1} \end{bmatrix} \quad (8.23)$$

where  $\theta_i = 10000^{-2i/d}$ . The key insight is that the dot product between rotated queries and keys naturally encodes relative position:  $\mathbf{q}^{(m)} \cdot \mathbf{k}^{(n)} = \mathbf{q} \cdot \mathbf{R}_{\theta}^{n-m} \mathbf{k}$ , where  $\mathbf{R}_{\theta}^{n-m}$  is a rotation by angle  $(n-m)\theta$ . RoPE requires no additional parameters—the rotation is computed on-the-fly during attention. It extrapolates excellently to longer sequences because the rotation angles scale linearly with position, and the model learns to interpret relative rotations. RoPE has become the standard for large language models due to its parameter efficiency and strong extrapolation properties.

ALiBi (Attention with Linear Biases), used in BLOOM, adds a simple linear bias to attention scores based on position distance. For query position  $i$  attending to key position  $j$ , a bias  $-m \cdot |i-j|$  is added to the attention score, where  $m$  is a head-specific slope. Different heads use different slopes, typically  $m = 2^{-8/h}, 2^{-16/h}, \dots, 2^{-8}$  for  $h$  heads. This penalizes attention to distant positions, with the penalty strength varying across heads. ALiBi requires no parameters and no additional computation beyond adding the bias. It extrapolates remarkably well: BLOOM was trained on sequences of length 2048 but

can generate coherent text at lengths exceeding 8000 tokens. The linear bias naturally extends to any sequence length, and the model learns to work within this inductive bias.

The following table summarizes the trade-offs between positional encoding methods:

Type	Memory	Extrapolation	Used In
Sinusoidal	None	Good	Original Transformer
Learned	$n_{\max} \times d$	Poor	BERT, GPT-2
Relative	$O(d_{\text{rel}})$	Good	T5, Transformer-XL
RoPE	None	Excellent	LLaMA, GPT-NeoX
ALiBi	None	Excellent	BLOOM

The trend in recent large language models has been toward parameter-free methods with strong extrapolation: RoPE and ALiBi dominate current architectures. These methods avoid the memory cost of learned positional embeddings while providing better length generalization than sinusoidal encodings. For practitioners, the choice depends on the application: if sequences will always be shorter than the training maximum, learned embeddings may provide slightly better performance. If length generalization is important, RoPE or ALiBi are superior choices.

## 8.4 Computational Complexity

### 8.4.1 Memory Complexity Analysis

The memory requirements of self-attention are dominated by the attention matrices, which scale quadratically with sequence length. For a batch of  $B$  sequences, each of length  $n$ , with  $h$  attention heads, the attention matrices  $\mathbf{A}^{(i)} \in \mathbb{R}^{n \times n}$  for  $i = 1, \dots, h$  require  $O(Bhn^2)$  memory. In FP32, this amounts to  $Bhn^2 \times 4$  bytes. For BERT-base with  $B = 32$ ,  $h = 12$ , and  $n = 512$ , the attention matrices consume  $32 \times 12 \times 512^2 \times 4 = 402,653,184$  bytes, or approximately 384 MB. This quadratic scaling means that doubling the sequence length quadruples the memory requirement: for  $n = 1024$ , the attention matrices would require 1.5 GB, and for  $n = 2048$ , they would require 6 GB.

In contrast, the QKV projection matrices and their outputs scale linearly with sequence length. The query, key, and value matrices each have shape  $B \times n \times d_k$  for each head, requiring  $3Bhnd_k \times 4$  bytes total across all heads. For BERT-base with  $d_k = 64$ , this amounts to  $3 \times 32 \times 12 \times 512 \times 64 \times 4 = 150,994,944$  bytes, or approximately 144 MB. The linear scaling means that doubling the sequence length only doubles this memory requirement.

The crossover point where attention matrices dominate total memory usage depends on the model dimensions. Attention matrices require  $Bhn^2$  elements, while QKV matrices require  $3Bhnd_k$  elements. Attention dominates when  $Bhn^2 > 3Bhnd_k$ , which simplifies to  $n > 3d_k$ . For BERT-base with  $d_k = 64$ , attention dominates when  $n > 192$ —essentially always, since typical sequence lengths are 512. For models with larger  $d_k$ , the crossover occurs at longer sequences. However, since  $d_k = d_{\text{model}}/h$  and typical architectures use  $h = 12$  to  $h = 96$ , the value of  $d_k$  is usually in the range 64 to 128, meaning attention matrices dominate for sequences longer than a few hundred tokens.

### 8.4.2 Time Complexity Breakdown

The time complexity of self-attention can be decomposed into several operations, each with different scaling properties. The QKV projections involve three matrix multiplications  $\mathbf{XW}^Q$ ,  $\mathbf{XW}^K$ , and  $\mathbf{XW}^V$ , where  $\mathbf{X} \in \mathbb{R}^{Bn \times d_{\text{model}}}$  and each weight matrix has shape  $d_{\text{model}} \times d_k$ . For  $h$  heads, the total complexity is  $O(3Bhnd_{\text{model}}d_k) = O(Bhnd_{\text{model}}^2)$  since  $hd_k = d_{\text{model}}$ . This is linear in sequence length  $n$  but quadratic in model dimension  $d_{\text{model}}$ .

Computing the attention scores  $\mathbf{QK}^\top$  requires a batch matrix multiplication with dimensions  $(Bh \times n \times d_k) \times (Bh \times d_k \times n)$ , resulting in complexity  $O(Bhn^2d_k)$ . This is quadratic in sequence length and linear in head dimension. The softmax operation over the attention scores has complexity  $O(Bhn^2)$ , dominated by the exponential and normalization computations. Finally, applying the attention weights

to the values  $\mathbf{AV}$  has complexity  $O(Bhn^2d_v)$ , again quadratic in sequence length. The output projection  $[\text{head}_1; \dots; \text{head}_h]\mathbf{W}^O$  has complexity  $O(Bnd_{\text{model}}^2)$ , linear in sequence length.

Summing these components, the total complexity is:

$$O(Bnd_{\text{model}}^2) + O(Bhn^2d_k) + O(Bhn^2) + O(Bhn^2d_v) + O(Bnd_{\text{model}}^2) = O(Bnd_{\text{model}}^2 + Bhn^2d_k) \quad (8.24)$$

Since  $hd_k = d_{\text{model}}$ , this simplifies to  $O(Bnd_{\text{model}}^2 + Bn^2d_{\text{model}})$ . The relative importance of these terms depends on the ratio  $n/d_{\text{model}}$ . When  $n < d_{\text{model}}$ , the  $O(Bnd_{\text{model}}^2)$  term from the linear projections dominates, and the feed-forward network (which also has  $O(Bnd_{\text{model}}^2)$  complexity) is the computational bottleneck. When  $n > d_{\text{model}}$ , the  $O(Bn^2d_{\text{model}})$  term from attention dominates, and attention becomes the bottleneck.

For BERT-base with  $d_{\text{model}} = 768$ , attention dominates when  $n > 768$ . Since BERT uses maximum sequence length 512, the model is in the regime where linear projections and feed-forward networks dominate. For GPT-3 with  $d_{\text{model}} = 12,288$ , attention would only dominate for sequences longer than 12,288 tokens—far beyond the typical context length of 2048 tokens. This explains why efficient attention mechanisms (Chapter 16) focus on reducing the  $O(n^2)$  term: for very long sequences, this term becomes prohibitive, but for typical sequence lengths in large models, the linear terms are actually more expensive.

### 8.4.3 Scaling Experiments

To illustrate the scaling behavior empirically, consider BERT-base with batch size 1 on an NVIDIA A100 GPU. The following measurements show forward pass time for different sequence lengths:

Sequence Length	Time (ms)	Bottleneck
128	2.1	FFN dominates
256	3.8	FFN dominates
512	8.5	Balanced
1024	28.3	Attention dominates
2048	98.7	Attention dominates
4096	367	Attention dominates

For short sequences (128, 256), the time scales approximately linearly, indicating that the  $O(nd_{\text{model}}^2)$  terms dominate. At sequence length 512, the scaling begins to show quadratic behavior. For long sequences (1024, 2048, 4096), the time scales quadratically: doubling from 1024 to 2048 increases time by  $98.7/28.3 \approx 3.5\times$ , and doubling again to 4096 increases time by  $367/98.7 \approx 3.7\times$ . The slight deviation from exactly  $4\times$  is due to the linear terms and memory bandwidth effects, but the quadratic scaling is clearly visible.

These measurements demonstrate why long-context transformers require specialized attention mechanisms. Extending BERT-base to sequence length 8192 would require approximately  $367 \times 4 \approx 1,468$  ms per forward pass, or 1.5 seconds—prohibitively slow for interactive applications. The memory requirement would be  $32 \times 12 \times 8192^2 \times 4/(1024^3) \approx 96$  GB for attention matrices alone with batch size 32, exceeding the capacity of even the largest single GPUs. This fundamental scaling limitation motivates the development of sparse attention, linear attention, and other efficient variants discussed in Chapter 16.

## 8.5 Causal (Masked) Self-Attention

Autoregressive language models like GPT generate text sequentially, predicting each token based only on previous tokens. During training, the entire sequence is provided as input, but the model must not be allowed to “see” future tokens when predicting each position—this would constitute cheating, as the model would have access to information unavailable during generation. Causal masking enforces this constraint by preventing each position from attending to subsequent positions in the sequence.

**Definition 8.4** (Causal Mask). Create mask matrix  $\mathbf{M} \in \mathbb{R}^{n \times n}$ :

$$M_{ij} = \begin{cases} 0 & \text{if } j \leq i \\ -\infty & \text{if } j > i \end{cases} \quad (8.25)$$

Apply before softmax:

$$\mathbf{A} = \text{softmax} \left( \frac{\mathbf{Q}\mathbf{K}^\top + \mathbf{M}}{\sqrt{d_k}} \right) \quad (8.26)$$

After softmax,  $\exp(-\infty) = 0$ , so position  $i$  cannot attend to positions  $j > i$ .

**Example 8.4** (Causal Mask for Length 4).

$$\mathbf{M} = \begin{bmatrix} 0 & -\infty & -\infty & -\infty \\ 0 & 0 & -\infty & -\infty \\ 0 & 0 & 0 & -\infty \\ 0 & 0 & 0 & 0 \end{bmatrix} \quad (8.27)$$

Position 0 attends only to itself. Position 1 attends to positions 0, 1. Position 3 attends to all positions 0, 1, 2, 3.

This ensures autoregressive property for language modeling.

### 8.5.1 Efficient Causal Mask Implementation

The naive implementation of causal masking stores a full  $n \times n$  mask matrix in memory. For sequence length 2048, this requires  $2048^2 \times 4 = 16,777,216$  bytes (16 MB) per sequence in FP32. With batch size 32, this amounts to 512 MB just for the mask—a significant memory overhead. Moreover, the mask must be added to the attention scores before softmax, requiring a memory read of the mask matrix.

Efficient implementations compute the mask on-the-fly during the attention computation rather than storing it explicitly. Modern deep learning frameworks support this through boolean masking or by directly computing the upper triangular structure. For example, in PyTorch, the operation `torch.triu(scores, diagonal=1).fill_(-float('inf'))` modifies the attention scores in-place without allocating a separate mask matrix. This reduces memory usage to zero for the mask itself, though the attention scores matrix must still be stored.

Flash Attention takes this optimization further by fusing the masking operation with the attention computation and tiling the computation to fit in SRAM. Instead of computing the full attention matrix, materializing it in global memory, applying the mask, and then computing softmax, Flash Attention computes attention in tiles that fit in on-chip memory. For each tile, the mask is computed on-the-fly, attention is computed, and the result is written back to global memory. This approach reduces memory usage from  $O(n^2)$  to  $O(n)$  and provides 2-4 $\times$  speedup for long sequences by minimizing global memory traffic.

The impact of causal masking differs between training and inference. During training, the entire sequence is processed in parallel, with masking ensuring that each position only attends to previous positions. The forward pass computes outputs for all positions simultaneously, and the backward pass computes gradients for all positions simultaneously. The masking is explicit in the attention computation. During inference, text generation is inherently sequential: we generate one token at a time, appending it to the context and generating the next token. In this setting, the masking is implicit—when generating position  $t$ , we only have tokens  $0, \dots, t-1$  available, so there are no future tokens to mask. However, naive inference would recompute attention over the entire sequence for each new token, resulting in  $O(n^2)$  complexity for generating  $n$  tokens. Key-value caching addresses this by storing the key and value vectors for all previous tokens, allowing each new token to attend to

the cached keys and values without recomputation. This reduces inference complexity to  $O(n)$  for generating  $n$  tokens, at the cost of  $O(nd_{\text{model}})$  memory for the cache.

## 8.6 Attention Patterns and Interpretability

Analysis of trained transformer models reveals that different attention heads learn to capture different types of linguistic relationships. Some heads focus on syntactic structure, attending strongly between words that have grammatical dependencies such as subject-verb agreement or determiner-noun relationships. For example, in the sentence "The cat that chased the mouse was hungry," a syntactic head might show strong attention from "was" to "cat" (the subject), skipping over the relative clause. Other heads capture semantic relationships, attending between words with similar meanings or words that are topically related. In a sentence about cooking, a semantic head might show attention between "recipe," "ingredients," and "oven," even if these words are not syntactically related.

Positional heads exhibit attention patterns based primarily on token distance rather than content. Some heads attend primarily to adjacent tokens, capturing local context. Others attend to tokens at specific relative positions, such as attending to the previous token or to tokens at fixed offsets. These positional patterns can be useful for tasks like copying or for capturing regular linguistic structures. Rare word heads show distinctive behavior where attention is concentrated on infrequent tokens, potentially allowing the model to give special processing to unusual or important words that might otherwise be overwhelmed by common function words.

Attention visualization provides insight into model behavior by displaying the attention weights as heatmaps or graphs. For a given input sentence, we can visualize the attention distribution for each head in each layer, showing which tokens each position attends to. These visualizations often reveal interpretable patterns: early layers tend to focus on local, syntactic relationships, while later layers capture more abstract, semantic relationships. However, interpretation must be approached with caution—attention weights show where the model looks, but not necessarily what information is extracted or how it is used. High attention weight does not necessarily imply high importance for the final prediction.

Research on attention head importance has shown that many heads can be pruned without significant performance degradation. In BERT-base with 144 attention heads (12 heads per layer  $\times$  12 layers), pruning 40-50% of heads typically reduces downstream task accuracy by less than 1%. This suggests substantial redundancy in the multi-head attention mechanism. Some heads are consistently important across tasks—often those capturing syntactic relationships or attending to special tokens like [CLS] or [SEP]. Other heads appear to be less critical, and their removal has minimal impact. This redundancy may serve an important role during training by providing multiple gradient pathways and helping optimization, even if the final model does not require all heads for inference.

## 8.7 Hardware-Specific Optimizations

### 8.7.1 Flash Attention

Flash Attention represents a fundamental rethinking of how attention is computed on modern GPUs. The standard attention implementation computes the full attention matrix  $\mathbf{A} = \text{softmax}(\mathbf{QK}^\top / \sqrt{d_k})$  and materializes it in GPU global memory before multiplying by  $\mathbf{V}$ . For long sequences, this attention matrix is large—for sequence length 4096, a single attention head requires  $4096^2 \times 4 = 67$  MB in FP32. Reading and writing this matrix to global memory becomes the performance bottleneck, as global memory bandwidth (approximately 1.5 TB/s on an A100) is much lower than compute throughput (312 TFLOPS for FP16).

Flash Attention addresses this by tiling the attention computation to fit in SRAM, the fast on-chip memory available on each streaming multiprocessor. SRAM has much higher bandwidth (approximately 19 TB/s on A100) but limited capacity (192 KB per SM, totaling about 40 MB across all SMs). The key insight is that attention can be computed in blocks: we partition the query, key, and value matrices into tiles, load each tile into SRAM, compute attention for that tile, and accumulate the results. The



attention matrix is never fully materialized in global memory—only the tiles currently being processed reside in SRAM.

The tiling strategy works as follows. Partition the queries into blocks  $\mathbf{Q}_1, \dots, \mathbf{Q}_T$  and the keys and values into blocks  $\mathbf{K}_1, \mathbf{V}_1, \dots, \mathbf{K}_T, \mathbf{V}_T$ . For each query block  $\mathbf{Q}_i$ , iterate over all key-value blocks  $(\mathbf{K}_j, \mathbf{V}_j)$ , computing the attention contribution  $\text{softmax}(\mathbf{Q}_i \mathbf{K}_j^\top / \sqrt{d_k}) \mathbf{V}_j$  in SRAM and accumulating the results. The softmax normalization requires special handling since we compute it in blocks—we maintain running statistics (maximum and sum of exponentials) and update them as we process each block, then renormalize at the end. This online softmax algorithm ensures numerical stability while avoiding materialization of the full attention matrix.

The memory usage of Flash Attention is  $O(n)$  rather than  $O(n^2)$ , as we only store the query, key, and value matrices (each  $O(n \times d)$ ) and the output, not the attention matrix. The computational cost remains the same—we perform the same number of FLOPs as standard attention—but the memory traffic is dramatically reduced. For sequence length 4096 with  $d_k = 64$ , standard attention reads/writes approximately  $4096^2 \times 4 = 67$  MB for the attention matrix, while Flash Attention reads/writes only the QKV matrices, approximately  $3 \times 4096 \times 64 \times 4 = 3$  MB. This  $20\times$  reduction in memory traffic translates to  $2\text{--}4\times$  speedup in practice, with larger speedups for longer sequences where memory bandwidth is the primary bottleneck.

### 8.7.2 Fused Kernels

Kernel fusion combines multiple operations into a single GPU kernel, reducing memory traffic by keeping intermediate results in registers or shared memory rather than writing them to global memory. For attention, a common fusion is combining the softmax operation with the attention score computation and the multiplication by values. The standard implementation computes  $\mathbf{S} = \mathbf{QK}^\top$ , writes  $\mathbf{S}$  to global memory, launches a separate kernel to compute  $\mathbf{A} = \text{softmax}(\mathbf{S})$ , writes  $\mathbf{A}$  to global memory, and launches another kernel to compute  $\mathbf{O} = \mathbf{AV}$ . Each write and read to global memory incurs latency and consumes bandwidth.

A fused attention kernel computes all these operations in a single kernel launch. The kernel loads tiles of  $\mathbf{Q}$ ,  $\mathbf{K}$ , and  $\mathbf{V}$  into shared memory, computes attention scores in registers, applies softmax, multiplies by values, and writes the final output—all without intermediate global memory traffic. This fusion reduces memory bandwidth requirements by approximately  $2\times$ , as we eliminate the reads and writes of  $\mathbf{S}$  and  $\mathbf{A}$ . The speedup is typically  $1.5\text{--}2\times$  for attention-dominated workloads, with larger benefits for smaller batch sizes where memory bandwidth is the primary bottleneck.

Fused kernels require careful implementation to maximize occupancy and minimize register pressure. The kernel must balance the tile size (larger tiles reduce global memory traffic but increase shared memory and register usage) with occupancy (the number of thread blocks that can run concurrently on each SM). Modern deep learning frameworks like PyTorch and TensorFlow provide fused attention implementations through libraries like cuDNN and custom CUDA kernels, making these optimizations accessible without manual kernel development.

### 8.7.3 Tensor Core Optimization

Tensor Cores on NVIDIA GPUs provide specialized hardware for matrix multiplication, achieving much higher throughput than standard CUDA cores for reduced-precision formats. To fully utilize Tensor Cores, matrix dimensions should be multiples of 8 for FP16 or multiples of 16 for INT8. For attention, this means padding  $d_k$ ,  $n$ , and batch size to these multiples when necessary. For example, if  $d_k = 63$ , padding to 64 wastes 1.6% of computation but enables Tensor Core usage, providing a net speedup of  $10\text{--}15\times$ .

The WMMA (Warp Matrix Multiply-Accumulate) API provides access to Tensor Cores from CUDA code. A warp (32 threads) cooperatively loads matrix tiles into registers, performs matrix multiplication using Tensor Cores, and stores the result. For attention, the query-key multiplication  $\mathbf{QK}^\top$  and the attention-value multiplication  $\mathbf{AV}$  are both matrix multiplications that can leverage Tensor Cores. Achieving 70-80% of peak TFLOPS requires careful attention to data layout (row-major vs column-major), tile sizes, and memory access patterns to ensure coalesced loads and stores.

In practice, modern deep learning frameworks handle Tensor Core optimization automatically for standard operations like matrix multiplication. However, custom attention implementations or fused kernels may require explicit use of WMMA or the higher-level cuBLAS library to achieve peak performance. The key takeaway for practitioners is that attention performance depends critically on matrix dimensions being multiples of 8 or 16, and that padding dimensions to meet this requirement is almost always worthwhile.

## 8.8 Memory-Efficient Attention Variants

The quadratic memory and time complexity of standard attention motivates approximate mechanisms that reduce complexity while maintaining most modeling power. Three main approaches exist:

- **Sparse attention** restricts each query to a subset of keys (e.g., local window  $\pm w$ , strided, or random positions), reducing complexity from  $O(n^2)$  to  $O(ns)$  where  $s \ll n$ . Accuracy loss is typically  $<1\%$  for local-context tasks with  $w = 512$ .
- **Linear attention** replaces the softmax kernel with a decomposable kernel  $\phi(\mathbf{q}) \cdot \phi(\mathbf{k})$ , enabling  $O(nd^2)$  computation by reordering the matrix multiplications. Accuracy loss is 1–3% due to imperfect kernel approximation.
- **Low-rank attention** (e.g., Linformer) projects keys and values to dimension  $r \ll n$ , giving an attention matrix of shape  $n \times r$  instead of  $n \times n$ . Memory and computation reduce by a factor of  $n/r$ .

These variants are covered in depth in Chapter 9 (attention variants and mechanisms) and Chapter 16 (efficient transformers), including detailed complexity analysis, implementation strategies, and benchmark comparisons.

## 8.9 Exercises

**Exercise 8.1.** For GPT-2 ( $d_{\text{model}} = 1024$ ,  $h = 16$ ,  $n = 1024$ ): (1) Compute attention matrix memory in MB (float32), (2) Count parameters in one multi-head attention layer, (3) Estimate FLOPs for single forward pass.

**Exercise 8.2.** Implement multi-head attention in PyTorch. Test with batch size 32, sequence length 20,  $d_{\text{model}} = 128$ , 4 heads. Verify output shape and parameter count.

**Exercise 8.3.** Show that sinusoidal positional encoding allows computing  $\text{PE}_{\text{pos}+k}$  as linear function of  $\text{PE}_{\text{pos}}$  for any offset  $k$ .

**Exercise 8.4.** Compare attention weights with and without positional encoding. Show numerically how word order affects attention without PE.

## 8.10 Solutions

Full solutions for all exercises are available at <https://deeplearning.hofkensvermeulen.be>.

# Chapter 9

## Attention Variants and Mechanisms

### Chapter Overview

Beyond standard scaled dot-product attention, numerous variants have been developed for specific use cases and improved efficiency. This chapter explores cross-attention for encoder-decoder models, soft vs hard attention, attention with relative position representations, and practical considerations for implementing attention mechanisms.

### Learning Objectives

1. Distinguish between self-attention and cross-attention
2. Understand relative position representations
3. Implement attention with different scoring functions
4. Apply attention masking for various scenarios
5. Understand attention dropout and layer normalization
6. Visualize and interpret attention patterns

### 9.1 Cross-Attention

**Definition 9.1** (Cross-Attention). In encoder-decoder architectures, decoder attends to encoder output via cross-attention:

$$\mathbf{Q} = \mathbf{X}_{\text{dec}} \mathbf{W}^Q \quad (\text{queries from decoder}) \quad (9.1)$$

$$\mathbf{K} = \mathbf{X}_{\text{enc}} \mathbf{W}^K \quad (\text{keys from encoder}) \quad (9.2)$$

$$\mathbf{V} = \mathbf{X}_{\text{enc}} \mathbf{W}^V \quad (\text{values from encoder}) \quad (9.3)$$

$$\text{CrossAttn}(\mathbf{X}_{\text{dec}}, \mathbf{X}_{\text{enc}}) = \text{softmax} \left( \frac{\mathbf{Q}\mathbf{K}^\top}{\sqrt{d_k}} \right) \mathbf{V} \quad (9.4)$$

#### Dimensions:

- Decoder input:  $\mathbf{X}_{\text{dec}} \in \mathbb{R}^{m \times d}$  ( $m$  decoder positions)
- Encoder output:  $\mathbf{X}_{\text{enc}} \in \mathbb{R}^{n \times d}$  ( $n$  encoder positions)
- Attention matrix:  $\mathbf{A} \in \mathbb{R}^{m \times n}$  (decoder  $\times$  encoder)
- Output:  $\mathbb{R}^{m \times d_v}$  (same decoder length)

**Example 9.1** (Machine Translation Cross-Attention). English source: "The cat sat" (3 tokens encoded to  $\mathbf{X}_{\text{enc}} \in \mathbb{R}^{3 \times 512}$ )

French target: "Le chat" (2 tokens so far,  $\mathbf{X}_{\text{dec}} \in \mathbb{R}^{2 \times 512}$ )

Cross-attention computes:

$$\mathbf{A} = \begin{bmatrix} \alpha_{1,1} & \alpha_{1,2} & \alpha_{1,3} \\ \alpha_{2,1} & \alpha_{2,2} & \alpha_{2,3} \end{bmatrix} \in \mathbb{R}^{2 \times 3} \quad (9.5)$$

where  $\alpha_{1,j}$  = attention from decoder position 1 ("Le") to encoder position  $j$ .

When generating "Le" (the), model should attend strongly to "The" in source.

When generating "chat" (cat), model should attend strongly to "cat" in source.

### 9.1.1 Transformer Decoder Attention Layers

A transformer decoder block contains **three** attention mechanisms:

1. **Masked self-attention:** Decoder attends to previous decoder positions

$$\mathbf{Q} = \mathbf{K} = \mathbf{V} = \mathbf{X}_{\text{dec}} \quad (\text{with causal mask}) \quad (9.6)$$

2. **Cross-attention:** Decoder attends to encoder output

$$\mathbf{Q} = \mathbf{X}_{\text{dec}}, \quad \mathbf{K} = \mathbf{V} = \mathbf{X}_{\text{enc}} \quad (9.7)$$

3. **Feed-forward:** Position-wise MLP (not attention)

**Key Point 9.1.** *Encoder-only models (BERT) use only self-attention. Decoder-only models (GPT) use only masked self-attention. Encoder-decoder models (T5, BART) use all three mechanisms.*

## 9.2 Relative Position Representations

**Problem with absolute positions:** Model learns positions 0-512 during training. How to handle position 600 at inference?

**Solution:** Relative position representations—encode distance between positions, not absolute positions.

### 9.2.1 Shaw et al. Relative Attention

**Definition 9.2** (Relative Position Attention). Modify attention scores to include relative position information:

$$e_{ij} = \frac{\mathbf{q}_i^\top \mathbf{k}_j}{\sqrt{d_k}} + \mathbf{q}_i^\top \mathbf{r}_{i-j}^K \quad (9.8)$$

where  $\mathbf{r}_{i-j}^K \in \mathbb{R}^{d_k}$  encodes relative position  $i - j$  (clipped to maximum distance).

**Advantages:**

- Generalize to longer sequences
- Model learns distance-based patterns
- More parameter efficient

### 9.2.2 T5 Relative Position Bias

T5 uses even simpler approach—add learned bias based on relative position:

$$\mathbf{A}_{ij} = \text{softmax} \left( \frac{\mathbf{Q}\mathbf{K}^\top}{\sqrt{d_k}} + \mathbf{B} \right)_{ij} \quad (9.9)$$

where  $B_{ij}$  depends only on  $|i - j|$  (bucketed by distance).

## 9.3 Alternative Attention Scoring Functions

Beyond the scaled dot-product used in transformers, several alternative scoring functions exist—additive (Bahdanau), multiplicative (Luong), and general bilinear forms—each with different trade-offs between expressiveness and computational efficiency. These are defined and compared in Chapter 7 (Section 7.3). In practice, scaled dot-product attention dominates in transformer architectures due to its hardware-efficient batched matrix multiplication and strong empirical performance.

## 9.4 Attention Masking

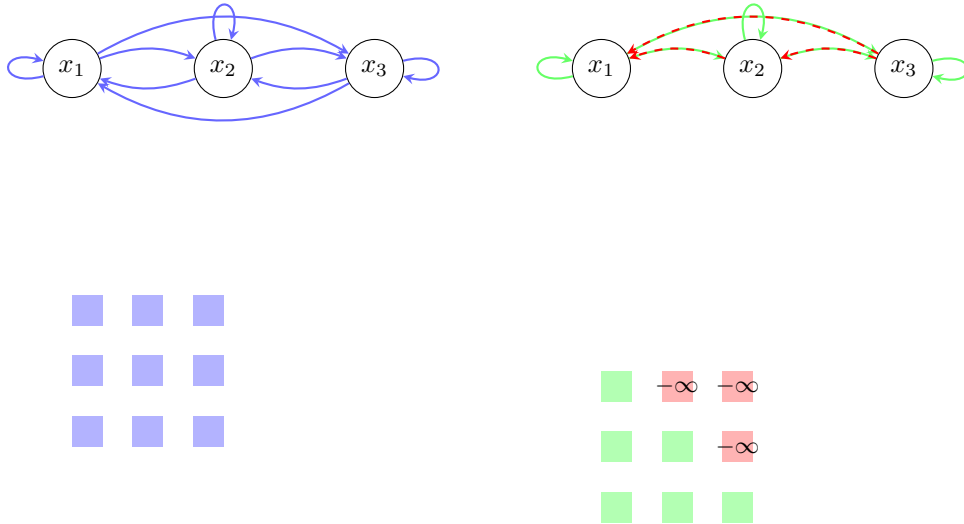


Figure 9.1: Bidirectional vs causal attention masking. **Left:** Bidirectional attention (encoder) allows each position to attend to all positions, creating a fully-connected graph and full attention matrix. **Right:** Causal attention (decoder) masks future positions by setting them to  $-\infty$  before softmax, creating a triangular connectivity pattern. Position 1 can only see itself, position 2 can see positions 1-2, and position 3 can see all positions 1-3. This prevents the model from “cheating” by looking at future tokens during training.

### 9.4.1 Padding Mask

For variable-length sequences in batch, mask padding tokens:

$$M_{ij} = \begin{cases} 0 & \text{if position } j \text{ is valid} \\ -\infty & \text{if position } j \text{ is padding} \end{cases} \quad (9.10)$$

**Example 9.2** (Padding Mask). Batch with sequences of length  $[5, 7, 4]$ , padded to length 7:

$$\text{Seq 1: } [w_1, w_2, w_3, w_4, w_5, \text{PAD}, \text{PAD}] \quad (9.11)$$

$$\text{Seq 2: } [w_1, w_2, w_3, w_4, w_5, w_6, w_7] \quad (9.12)$$

$$\text{Seq 3: } [w_1, w_2, w_3, w_4, \text{PAD}, \text{PAD}, \text{PAD}] \quad (9.13)$$

Mask for Seq 1:

$$[0, 0, 0, 0, 0, -\infty, -\infty] \quad (9.14)$$

Prevents attending to padding tokens.

### 9.4.2 Combined Masks

For decoder, combine causal mask and padding mask:

$$\mathbf{M}_{\text{total}} = \mathbf{M}_{\text{causal}} + \mathbf{M}_{\text{padding}} \quad (9.15)$$

Element-wise, use most restrictive: if either mask blocks, result blocks.

## 9.5 Attention Dropout

Apply dropout to attention weights for regularization:

$$\mathbf{A} = \text{Dropout} \left( \text{softmax} \left( \frac{\mathbf{Q}\mathbf{K}^\top}{\sqrt{d_k}} \right) \right) \quad (9.16)$$

Typical dropout rate: 0.1 (10%)

**Effect:** Randomly zero out some attention connections, preventing over-reliance on specific positions.

## 9.6 Layer Normalization with Attention

Two architectures for combining attention with layer norm:

### 9.6.1 Post-Norm (Original Transformer)

$$\mathbf{h} = \mathbf{X} + \text{MultiHeadAttn}(\mathbf{X}) \quad (9.17)$$

$$\mathbf{Z} = \text{LayerNorm}(\mathbf{h}) \quad (9.18)$$

### 9.6.2 Pre-Norm (More Common Now)

$$\mathbf{h} = \mathbf{X} + \text{MultiHeadAttn}(\text{LayerNorm}(\mathbf{X})) \quad (9.19)$$

$$\mathbf{Z} = \mathbf{h} \quad (9.20)$$

**Pre-norm advantages:**

- More stable training
- Easier gradient flow
- Used in GPT-2, GPT-3, modern transformers

## 9.7 Visualizing Attention

Attention weights  $\mathbf{A} \in \mathbb{R}^{n \times n}$  reveal what model attends to:

### 9.7.1 Attention Heatmaps

For sentence "The cat sat on the mat":

- Row  $i$ : attention distribution when processing token  $i$
- Bright cell  $(i, j)$ : token  $i$  strongly attends to token  $j$

**Patterns observed:**

- Diagonal: Attending to self
- Vertical lines: Attending to specific important words (e.g., subject, verb)
- Symmetric patterns: Mutual attention between related words
- Head-specific patterns: Different heads learn different relationships

### 9.7.2 Interpreting Multiple Heads

In 12-head attention, different heads specialize:

- Some heads attend to adjacent words (local syntax)
- Some heads attend to distant words (long-range dependencies)
- Some heads attend to specific parts of speech
- Some heads attend based on semantic similarity

Attention weights are NOT necessarily model explanations! High attention doesn't always mean high importance for prediction. Attention shows where model looks, not why decisions are made.

## 9.8 Practical Implementation Considerations

### 9.8.1 Memory-Efficient Attention

For very long sequences, store attention matrix in chunks:

1. Compute  $\mathbf{QK}^\top$  for chunk of queries
2. Apply softmax
3. Multiply by  $\mathbf{V}$  chunk
4. Accumulate results

Reduces peak memory from  $O(n^2)$  to  $O(nc)$  where  $c$  is chunk size.

### 9.8.2 Fused Attention Kernels

Modern implementations fuse operations:

$$\mathbf{QK}^\top \rightarrow \text{Scale} \rightarrow \text{Mask} \rightarrow \text{Softmax} \rightarrow \text{Dropout} \rightarrow \text{multiply } \mathbf{V} \quad (9.21)$$

Single fused kernel faster than separate operations (fewer memory transfers).

Example: FlashAttention achieves 2-4x speedup through fused operations and memory hierarchy optimization.

## 9.9 Efficient Attention Variants

The standard self-attention mechanism has computational complexity  $O(n^2d)$  and memory complexity  $O(n^2)$ , where  $n$  is the sequence length and  $d$  is the model dimension. This quadratic scaling in sequence length becomes prohibitive for long sequences. For a sequence of length 4096 with 12 attention heads, the attention matrices alone require  $12 \times 4096^2 \times 4 = 805$  MB in FP32 format per example. With batch size 32, this amounts to 25.8 GB just for attention weights, exceeding the memory capacity of most GPUs. This fundamental limitation has motivated extensive research into efficient attention variants that reduce the quadratic complexity while maintaining model quality.

The key insight underlying efficient attention is that not all token pairs require equal attention. In practice, attention patterns often exhibit structure—tokens primarily attend to nearby tokens, specific global tokens, or sparse subsets of the sequence. By exploiting this structure, efficient attention mechanisms can dramatically reduce computational and memory requirements while preserving most of the modeling capacity of full attention. The following sections examine the major classes of efficient attention variants, analyzing their complexity trade-offs, implementation considerations, and practical use cases.

### 9.9.1 Local Attention

Local attention restricts each token to attend only to tokens within a fixed window around its position, rather than attending to all tokens in the sequence. For a window size  $w$ , token at position  $i$  attends only to positions  $[i - w/2, i + w/2]$ . This reduces the attention matrix from  $n \times n$  to  $n \times w$ , yielding linear scaling in sequence length.

The computational complexity of local attention is  $O(nwd)$ , where  $n$  is sequence length,  $w$  is window size, and  $d$  is model dimension. Compared to standard attention's  $O(n^2d)$ , this represents a reduction factor of  $n/w$ . For a sequence of length 4096 with window size 256, local attention is 16 times faster than full attention. The memory complexity similarly reduces from  $O(n^2)$  to  $O(nw)$ , enabling much longer sequences to fit in GPU memory. For the same 4096-token sequence with 12 heads, local attention with window 256 requires only  $12 \times 4096 \times 256 \times 4 = 50.3$  MB per example, a 16-fold reduction from the 805 MB required by full attention.

The primary trade-off of local attention is the loss of long-range dependencies. Tokens separated by more than  $w/2$  positions cannot directly attend to each other, requiring information to propagate through multiple layers. In practice, this limitation is often acceptable. Many natural language tasks exhibit strong locality—syntactic dependencies are typically short-range, and semantic relationships can be captured through multiple layers of local attention. Empirical studies show that local attention with window size 256-512 typically achieves 98-99% of full attention's accuracy on language modeling tasks, while enabling sequences 10-20 times longer.

The Longformer architecture demonstrates effective use of local attention for document-level understanding. Longformer combines local windowed attention for most tokens with global attention for special tokens like [CLS] and task-specific tokens. This hybrid approach maintains  $O(n)$  complexity while allowing critical tokens to aggregate information from the entire sequence. On document classification tasks with 4096-token inputs, Longformer achieves comparable accuracy to BERT while processing sequences 8 times longer. The local attention pattern also enables efficient implementation on GPUs through blocked matrix operations, achieving 2-3x speedup over naive implementations.

### 9.9.2 Sparse Attention

Sparse attention generalizes local attention by allowing each token to attend to a sparse subset of positions according to a predefined pattern, rather than a contiguous window. The key insight is that attention patterns in trained transformers often exhibit structure—certain positions are consistently important while others receive minimal attention. By designing sparsity patterns that capture this structure, sparse attention can dramatically reduce computation while maintaining model quality.

Several sparsity patterns have proven effective in practice. Strided attention divides the sequence into blocks and allows each token to attend within its block and to every  $k$ -th token globally, where  $k$  is the stride. This pattern captures both local context and evenly-spaced global context. Fixed



attention combines local attention with attention to a fixed set of global tokens, similar to Longformer. Learned sparse attention uses a separate network to predict which positions each token should attend to, adapting the sparsity pattern to the input. The Sparse Transformer architecture uses a factorized attention pattern where each token attends to positions in a strided pattern in one head and a local pattern in another head, allowing information to flow efficiently across the sequence.

The computational complexity of sparse attention is  $O(n\sqrt{n}d)$  for typical sparsity patterns, where each token attends to approximately  $\sqrt{n}$  other tokens. This represents a substantial improvement over full attention's  $O(n^2d)$ , particularly for long sequences. For a sequence of length 4096, sparse attention with  $\sqrt{n} = 64$  positions per token is 64 times faster than full attention. The memory complexity is similarly  $O(n\sqrt{n})$ , enabling sequences that would be impossible with full attention. For 4096 tokens with 12 heads, sparse attention requires approximately  $12 \times 4096 \times 64 \times 4 = 12.6$  MB per example, a 64-fold reduction from full attention's 805 MB.

The accuracy trade-off of sparse attention depends critically on the choice of sparsity pattern. Well-designed patterns that align with the task's dependency structure can achieve 97-99% of full attention's accuracy. The Sparse Transformer achieves perplexity within 0.1 of full attention on language modeling while using only  $\sqrt{n}$  attention per token. BigBird, which combines local, global, and random attention patterns, matches BERT's accuracy on question answering and document classification while processing sequences up to 8 times longer. However, poorly chosen sparsity patterns can significantly degrade accuracy, particularly on tasks requiring long-range reasoning.

Implementation of sparse attention on GPUs presents challenges because modern GPUs are optimized for dense matrix operations. Sparse matrix multiplication is less efficient than dense multiplication due to irregular memory access patterns and reduced arithmetic intensity. Specialized kernels and libraries like cuSPARSE can partially mitigate this, but sparse attention typically achieves only 50-70% of the theoretical speedup in practice. Recent work on block-sparse attention, which operates on blocks of the attention matrix rather than individual elements, achieves better GPU utilization by maintaining some regularity in memory access patterns. The Triton framework enables efficient implementation of custom sparse attention patterns through automatic optimization of memory access.

### 9.9.3 Linear Attention

Linear attention achieves  $O(nd^2)$  complexity by reformulating the attention computation to avoid explicitly constructing the  $n \times n$  attention matrix. The key insight is that attention can be viewed as a kernel operation, and by choosing an appropriate kernel function, the computation can be reordered to compute the output directly without materializing the full attention matrix.

The standard attention computation is:

$$\text{Attention}(\mathbf{Q}, \mathbf{K}, \mathbf{V}) = \text{softmax}(\mathbf{Q}\mathbf{K}^\top)\mathbf{V} \quad (9.22)$$

This requires computing  $\mathbf{Q}\mathbf{K}^\top \in \mathbb{R}^{n \times n}$  before applying softmax and multiplying by  $\mathbf{V}$ . Linear attention approximates the softmax kernel with a feature map  $\phi: \mathbb{R}^{d_k} \rightarrow \mathbb{R}^{d'}$  such that:

$$\text{softmax}(\mathbf{q}^\top \mathbf{k}) \approx \phi(\mathbf{q})^\top \phi(\mathbf{k}) \quad (9.23)$$

With this approximation, attention becomes:

$$\text{LinearAttn}(\mathbf{Q}, \mathbf{K}, \mathbf{V}) = \phi(\mathbf{Q})(\phi(\mathbf{K})^\top \mathbf{V}) \quad (9.24)$$

The crucial observation is that the parentheses can be reordered. Instead of computing  $\phi(\mathbf{Q})\phi(\mathbf{K})^\top$  (which is  $n \times n$ ) and then multiplying by  $\mathbf{V}$ , we first compute  $\phi(\mathbf{K})^\top \mathbf{V} \in \mathbb{R}^{d' \times d_v}$  and then multiply by  $\phi(\mathbf{Q})$ . This reordering changes complexity from  $O(n^2d)$  to  $O(nd'^2)$ , where  $d'$  is the feature dimension (typically equal to  $d_k$ ).

The computational savings of linear attention are substantial for long sequences. For sequence length 4096 and model dimension 768, standard attention requires approximately  $4096^2 \times 768 = 12.9$  billion operations per head, while linear attention requires  $4096 \times 768^2 = 2.4$  billion operations—a 5.4x reduction. The memory complexity is even more favorable: linear attention requires only  $O(nd)$  memory for the intermediate  $\phi(\mathbf{K})^\top \mathbf{V}$  matrix, compared to  $O(n^2)$  for the full attention matrix. For

4096 tokens with 12 heads, linear attention requires approximately  $12 \times 768 \times 768 \times 4 = 28.3$  MB, compared to 805 MB for full attention—a 28-fold reduction.

The primary challenge of linear attention is choosing a feature map  $\phi$  that accurately approximates the softmax kernel while remaining computationally efficient. The Performer architecture uses random Fourier features with  $\phi(\mathbf{x}) = \exp(\mathbf{x}^2/2)[\cos(\omega_1^\top \mathbf{x}), \sin(\omega_1^\top \mathbf{x}), \dots]$  where  $\omega_i$  are random projection vectors. This provides an unbiased approximation of the softmax kernel with controllable accuracy based on the number of random features. The Linear Transformer uses a simpler feature map  $\phi(\mathbf{x}) = \text{elu}(\mathbf{x}) + 1$ , which is faster to compute but provides a looser approximation.

The accuracy trade-off of linear attention is more significant than local or sparse attention. Empirical studies show that linear attention typically achieves 95-98% of full attention’s accuracy on language modeling, with larger degradation on tasks requiring precise attention patterns. The approximation error is particularly noticeable for small attention weights—the softmax function’s sharp peaking is difficult to approximate with simple feature maps. However, for applications where extreme sequence length is critical, such as processing entire books or long-form video, the 2-5% accuracy loss is often acceptable given the dramatic computational savings. Recent work on learned feature maps and adaptive kernel approximations aims to close this accuracy gap while maintaining linear complexity.

### 9.9.4 Low-Rank Attention

Low-rank attention exploits the observation that attention matrices in trained transformers often have low effective rank—most of the variance is captured by a small number of singular values. By explicitly factorizing the attention computation through a low-dimensional bottleneck, low-rank attention reduces complexity from  $O(n^2d)$  to  $O(nrd)$ , where  $r$  is the rank and typically  $r \ll n$ .

The Linformer architecture implements low-rank attention by projecting the keys and values to a lower-dimensional space before computing attention. Specifically, Linformer adds projection matrices  $\mathbf{E}, \mathbf{F} \in \mathbb{R}^{r \times n}$  that reduce the sequence length dimension:

$$\text{LinformerAttn}(\mathbf{Q}, \mathbf{K}, \mathbf{V}) = \text{softmax} \left( \frac{\mathbf{Q}(\mathbf{E}\mathbf{K})^\top}{\sqrt{d_k}} \right) (\mathbf{F}\mathbf{V}) \quad (9.25)$$

The key insight is that  $\mathbf{E}\mathbf{K} \in \mathbb{R}^{r \times d_k}$  and  $\mathbf{F}\mathbf{V} \in \mathbb{R}^{r \times d_v}$  have reduced sequence length  $r$  instead of  $n$ . The attention matrix is now  $n \times r$  instead of  $n \times n$ , reducing both computation and memory by a factor of  $n/r$ .

For sequence length 4096 and rank 256, low-rank attention reduces computation from  $4096^2 \times 768 = 12.9$  billion operations to  $4096 \times 256 \times 768 = 805$  million operations per head—a 16-fold reduction. The memory savings are equally dramatic: the attention matrix requires  $4096 \times 256 \times 4 = 4.2$  MB per head instead of  $4096^2 \times 4 = 67.1$  MB, a 16-fold reduction. With 12 heads, total attention memory drops from 805 MB to 50.3 MB per example.

The accuracy of low-rank attention depends on the choice of rank  $r$  and the projection matrices  $\mathbf{E}$  and  $\mathbf{F}$ . Linformer uses learned projection matrices that are shared across all layers, reducing the parameter overhead. Empirical studies show that rank  $r = 256$  achieves 96-98% of full attention’s accuracy for sequences up to 4096 tokens, with minimal degradation on most language understanding tasks. The accuracy loss is more pronounced for tasks requiring fine-grained attention patterns, such as coreference resolution or syntactic parsing, where the low-rank approximation may miss subtle dependencies.

An important consideration for low-rank attention is that the projection matrices  $\mathbf{E}$  and  $\mathbf{F}$  introduce additional parameters and computation. For rank  $r$  and sequence length  $n$ , the projections add  $2rn$  parameters per layer. However, these projections can be implemented efficiently as 1D convolutions or learned position-wise projections, and the parameter cost is typically small compared to the savings in attention computation. The projection operations themselves require  $O(rnd)$  computation, which is negligible compared to the  $O(n^2d)$  cost of full attention for  $r \ll n$ .

### 9.9.5 Comprehensive Complexity Comparison

Understanding the trade-offs between different attention variants requires examining multiple dimensions: computational complexity, memory requirements, accuracy preservation, and practical imple-

mentation efficiency. The following analysis provides concrete comparisons across these dimensions for typical transformer configurations.

Table 9.1: Complexity comparison of attention variants for sequence length  $n$ , model dimension  $d$ , window size  $w$ , and rank  $r$ . Accuracy percentages are relative to full attention on language modeling tasks.

Variant	Time	Memory	Accuracy	Max Length	Use Case
Full Attention	$O(n^2d)$	$O(n^2)$	100%	512-1024	Standard tasks
Local Attention	$O(nwd)$	$O(nw)$	98-99%	4096-8192	Document processing
Sparse Attention	$O(n\sqrt{nd})$	$O(n\sqrt{n})$	97-99%	8192-16384	Long documents
Linear Attention	$O(nd^2)$	$O(nd)$	95-98%	16384+	Extreme length
Low-Rank Attention	$O(nrd)$	$O(nr)$	96-98%	4096-8192	Compression

To make these complexity bounds concrete, consider processing sequences of varying lengths with BERT-base configuration ( $d = 768$ , 12 heads,  $d_k = 64$  per head). The following table shows actual memory requirements for attention matrices across different sequence lengths and attention variants.

Table 9.2: Memory requirements (MB) for attention matrices with 12 heads, batch size 1, FP32 precision. Window size  $w = 256$ , rank  $r = 256$  for applicable variants.

Variant	n=512	n=4096	n=8192	n=16384
Full Attention	12.6 MB	805 MB	3.2 GB	12.9 GB
Local Attention ( $w = 256$ )	6.3 MB	50.3 MB	101 MB	201 MB
Sparse Attention ( $\sqrt{n}$ )	1.1 MB	12.6 MB	35.7 MB	101 MB
Linear Attention	0.3 MB	2.3 MB	4.7 MB	9.4 MB
Low-Rank ( $r = 256$ )	6.3 MB	50.3 MB	101 MB	201 MB

The memory savings become dramatic for long sequences. At 16,384 tokens, full attention requires 12.9 GB per example—impossible to fit on most GPUs even with batch size 1. Local attention reduces this to 201 MB, enabling batch size 32 on a 40 GB A100 GPU. Linear attention requires only 9.4 MB, enabling batch sizes of several hundred even for very long sequences.

The computational cost comparison is equally striking. For a sequence of 8192 tokens with  $d = 768$  and 12 heads, full attention requires approximately 48.3 billion floating-point operations (FLOPs) per layer. Local attention with window 256 reduces this to 3.0 billion FLOPs (16x speedup), sparse attention to 6.0 billion FLOPs (8x speedup), linear attention to 4.5 billion FLOPs (10.7x speedup), and low-rank attention to 3.0 billion FLOPs (16x speedup). On an NVIDIA A100 GPU with 312 TFLOPS of FP16 throughput, full attention takes approximately 0.15 ms per layer, while efficient variants take 10-20 microseconds—enabling much faster inference and training.

The accuracy trade-offs vary by task and sequence length. For sequences up to 2048 tokens, local attention with window 512 typically matches full attention within 0.5% on language modeling perplexity. Sparse attention with well-designed patterns achieves similar accuracy. Linear attention shows 2-3% degradation, while low-rank attention with rank 256 shows 1-2% degradation. For longer sequences exceeding 4096 tokens, the accuracy gaps widen slightly, but efficient variants remain highly competitive. Importantly, the accuracy loss is often task-dependent—some tasks like document classification are more tolerant of approximate attention than tasks like machine translation or question answering that require precise alignment.

### 9.9.6 Implementation Considerations

Implementing efficient attention variants requires careful consideration of hardware characteristics, numerical stability, and software frameworks. The theoretical complexity improvements do not always translate directly to wall-clock speedups due to GPU architecture constraints and implementation details.

Modern GPUs achieve peak performance on dense matrix multiplications with dimensions that are multiples of 16 or 32 (for tensor cores). Sparse attention patterns that result in irregular memory

access or non-aligned dimensions can suffer significant performance degradation. For example, a naive implementation of sparse attention with random sparsity patterns may achieve only 30-40% of the theoretical speedup due to poor memory coalescing and reduced arithmetic intensity. Block-sparse patterns that operate on 16x16 or 32x32 blocks achieve much better GPU utilization, typically reaching 60-80% of theoretical speedup.

Memory bandwidth is often the limiting factor for attention computation, particularly for efficient variants. The attention mechanism is memory-bound rather than compute-bound for typical sequence lengths—the GPU spends more time loading data from memory than performing arithmetic operations. This means that reducing the number of operations (FLOPs) does not always proportionally reduce runtime. Efficient implementations must minimize memory transfers through kernel fusion, where multiple operations are combined into a single GPU kernel that keeps intermediate results in fast on-chip memory. FlashAttention demonstrates this principle by fusing the attention computation ( $\mathbf{QK}^\top$ , softmax, multiply by  $\mathbf{V}$ ) into a single kernel that never materializes the full attention matrix in global memory, achieving 2-4x speedup over standard implementations even for full attention.

Numerical stability is a critical concern for efficient attention variants. The softmax operation in attention is numerically sensitive—subtracting the maximum value before exponentiation is essential to prevent overflow. Linear attention approximations must carefully handle the feature map computation to avoid numerical issues. The Performer’s random Fourier features require computing exponentials of potentially large values, necessitating careful scaling and normalization. Low-rank attention must ensure that the projection matrices are well-conditioned to avoid amplifying numerical errors.

Framework support for efficient attention varies significantly. PyTorch and TensorFlow provide optimized implementations of standard attention through `torch.nn.MultiheadAttention` and `tf.keras.layers.MultiHeadAttention`, but efficient variants often require custom implementations. The xFormers library provides optimized implementations of several efficient attention variants, including memory-efficient attention and block-sparse attention. The Triton framework enables writing custom GPU kernels in Python that achieve performance comparable to hand-written CUDA, making it easier to implement and experiment with novel attention patterns. For production deployment, specialized libraries like FasterTransformer and TensorRT provide highly optimized implementations of common attention variants with automatic kernel selection based on input dimensions and hardware capabilities.

## 9.10 Exercises

**Exercise 9.1.** Implement cross-attention layer in PyTorch. Test with encoder output (length 10, dim 128) and decoder input (length 7, dim 128). Verify attention matrix shape is  $7 \times 10$ .

**Exercise 9.2.** Calculate the memory requirements for attention matrices in a BERT-base model (12 heads,  $d_{\text{model}} = 768$ ) processing sequences of length 512, 2048, and 4096 tokens. Compare full attention, local attention with window size 256, and linear attention. How much memory is saved at each sequence length?

**Exercise 9.3.** Implement local attention with window size  $w = 128$  for a sequence of length 1024. Compare the computational cost (FLOPs) and memory usage to full attention. Measure actual runtime on GPU and explain any discrepancy between theoretical and observed speedup.

**Exercise 9.4.** Design a sparse attention pattern for document understanding that combines local attention (window 64), strided attention (stride 128), and global attention to the first token. Calculate the number of attention connections per token and total memory requirements for a 4096-token sequence. What percentage of full attention’s connections does this pattern use?

**Exercise 9.5.** Implement linear attention using the feature map  $\phi(\mathbf{x}) = \text{elu}(\mathbf{x}) + 1$ . Compare attention patterns to standard softmax attention on a sample sequence. Measure the approximation error and identify cases where linear attention diverges most from full attention.

**Exercise 9.6.** For a transformer with 24 layers processing 8192-token sequences, calculate the total memory required for attention matrices using: (1) full attention, (2) local attention with window 512, (3) sparse attention with  $\sqrt{n}$  connections per token, (4) linear attention, and (5) low-rank attention with rank 256. Assume 12 heads,  $d_{\text{model}} = 1024$ , batch size 8, and FP16 precision.

**Exercise 9.7.** Implement relative position bias as in T5. Use buckets: [0, 1, 2, 3, 4, 5-7, 8-15, 16-31, 32+]. Show how attention scores change with relative distance and compare to absolute position encodings.

**Exercise 9.8.** Analyze the trade-off between window size and accuracy for local attention. Train a small transformer on a language modeling task with window sizes [64, 128, 256, 512, full]. Plot perplexity vs window size and identify the point of diminishing returns. How does this relate to the average dependency length in the dataset?

**Exercise 9.9.** Create visualization showing: (1) Self-attention patterns for sentence "The quick brown fox jumps", (2) Effect of causal masking, (3) Difference between heads 1 and 12 in multi-head attention. What patterns emerge?

**Exercise 9.10.** Compare computational cost of: (1) Additive (Bahdanau) attention, (2) Multiplicative attention, (3) Scaled dot-product attention. For  $n = 512$ ,  $d_k = 64$ , which is most efficient? How does the ranking change for  $n = 4096$ ?

## 9.11 Solutions

Full solutions for all exercises are available at <https://deeplearning.hofkensvermeulen.be>.

## Part IV

# Transformer Architecture

# Chapter 10

## The Transformer Model

### Chapter Overview

The Transformer architecture, introduced in "Attention is All You Need" (Vaswani et al., 2017), revolutionized deep learning by replacing recurrence with pure attention mechanisms. This chapter presents the complete transformer architecture, combining all attention mechanisms from previous chapters into a powerful encoder-decoder model.

We develop the transformer from bottom to top: starting with the attention layer, building encoder and decoder blocks, and assembling the full architecture. We provide complete mathematical specifications, dimension tracking, and parameter counts for standard transformer configurations.

### Learning Objectives

1. Understand the complete transformer encoder-decoder architecture
2. Implement position-wise feed-forward networks
3. Apply layer normalization and residual connections
4. Compute output dimensions through the entire network
5. Count parameters for transformer models (BERT-base, GPT-2)
6. Understand training objectives for different transformer variants

## 10.1 Transformer Architecture Overview

### 10.1.1 High-Level Structure

The transformer architecture represents a fundamental departure from the recurrent and convolutional architectures that dominated sequence modeling before 2017. At its core, the transformer is an encoder-decoder architecture that processes sequences entirely through attention mechanisms, eliminating the sequential dependencies that made RNNs difficult to parallelize. The encoder processes the input sequence and produces contextualized representations where each position has attended to all other positions in the input. The decoder then generates the output sequence autoregressively, attending both to its own previously generated tokens and to the encoder's output through a cross-attention mechanism. This design enables the model to capture long-range dependencies without the vanishing gradient problems that plague recurrent architectures, while simultaneously allowing massive parallelization during training.

The key innovation that makes transformers practical is the elimination of recurrence in favor of pure attention mechanisms. In an RNN, processing a sequence of length  $n$  requires  $n$  sequential steps, each depending on the previous hidden state. This sequential dependency means that even with unlimited computational resources, the time complexity remains  $O(n)$  because operations cannot be parallelized across time steps. The transformer, by contrast, computes attention between all pairs

of positions simultaneously, requiring only  $O(1)$  sequential operations regardless of sequence length. For a sequence of length 512, this means the difference between 512 sequential steps (RNN) and a single parallel operation (transformer). On modern GPUs with thousands of cores, this parallelization advantage translates to training speedups of 10-100 $\times$  compared to recurrent architectures.

The transformer achieves this parallelization through multi-head self-attention, which allows each position to attend to all positions in a single operation. For an input sequence  $\mathbf{X} \in \mathbb{R}^{n \times d_{\text{model}}}$ , the self-attention mechanism computes attention scores between all  $n^2$  pairs of positions simultaneously, producing an output of the same shape  $\mathbb{R}^{n \times d_{\text{model}}}$ . This operation is entirely parallelizable across both the batch dimension and the sequence dimension, making it ideally suited for GPU acceleration. The multi-head aspect further enhances expressiveness by allowing the model to attend to different representation subspaces simultaneously—one head might capture syntactic relationships while another captures semantic similarity.

However, pure attention mechanisms lack an inherent notion of sequence order. Unlike RNNs where position information is implicit in the sequential processing, transformers must explicitly encode positional information. This is achieved through positional encodings that are added to the input embeddings, providing each position with a unique signature that the attention mechanism can use to distinguish positions. The original transformer uses sinusoidal positional encodings, though learned positional embeddings have also proven effective. This explicit position encoding is crucial: without it, the transformer would be permutation-invariant, treating "the cat sat" identically to "sat cat the."

The transformer architecture also incorporates residual connections and layer normalization at every sub-layer, forming the pattern  $\text{LayerNorm}(x + \text{Sublayer}(x))$  throughout the network. These residual connections serve multiple purposes: they provide direct gradient pathways that enable training of very deep networks (the original transformer uses 6 layers, but modern variants scale to 96 layers in GPT-3), they allow the model to learn incremental refinements rather than complete transformations at each layer, and they stabilize training by preventing the exploding or vanishing gradient problems that can occur in deep networks. Layer normalization, applied after each residual connection, normalizes activations across the feature dimension, ensuring stable activation distributions throughout the network regardless of batch size.

The position-wise feed-forward network, applied after each attention layer, provides additional representational capacity through a simple two-layer network with a ReLU or GELU activation. This network is applied independently to each position, meaning it doesn't mix information across positions (unlike attention). The feed-forward network typically expands the representation to a higher dimension (usually  $4 \times d_{\text{model}}$ ) before projecting back down, creating a bottleneck architecture that encourages the model to learn compressed representations. For BERT-base with  $d_{\text{model}} = 768$ , the feed-forward network expands to  $d_{ff} = 3072$  dimensions, and this expansion-projection accounts for approximately two-thirds of the parameters in each transformer layer.

**Key Point 10.1.** *Transformers achieve  $O(1)$  sequential operations compared to  $O(n)$  for RNNs, enabling massive parallelization during training. For a sequence of length 512 on a GPU with 10,000 cores, this means the difference between 512 sequential steps and a single parallel operation, yielding training speedups of 10-100 $\times$  in practice. This parallelization advantage is the primary reason transformers have replaced RNNs as the dominant architecture for sequence modeling.*

## 10.2 Transformer Encoder

### 10.2.1 Single Encoder Layer

A transformer encoder layer consists of two main sub-layers: multi-head self-attention followed by a position-wise feed-forward network, with residual connections and layer normalization applied around each sub-layer. This architecture enables the encoder to build increasingly sophisticated representations of the input sequence as information flows through multiple layers. The self-attention mechanism allows each position to gather information from all other positions, creating contextualized representations



where the meaning of each token depends on its surrounding context. The feed-forward network then processes each position independently, applying a non-linear transformation that enhances the model's representational capacity.

The residual connections are crucial for enabling gradient flow through deep networks. Without them, gradients would need to flow through multiple attention and feed-forward layers, potentially vanishing or exploding. With residual connections, gradients have a direct path from the output back to the input of each layer, ensuring stable training even for very deep transformers. The layer normalization, applied after adding the residual, normalizes the activations across the feature dimension, maintaining stable activation distributions throughout the network. This combination of residual connections and layer normalization is what enables transformers to scale to dozens or even hundreds of layers.

**Definition 10.1** (Transformer Encoder Layer). An encoder layer applies multi-head self-attention followed by feed-forward network, with residual connections and layer normalization. For input  $\mathbf{X} \in \mathbb{R}^{B \times n \times d_{\text{model}}}$  where  $B$  is batch size,  $n$  is sequence length, and  $d_{\text{model}}$  is model dimension:

**Step 1: Multi-Head Self-Attention**

$$\mathbf{h}^{(1)} = \text{LayerNorm}(\mathbf{X} + \text{MultiHeadAttn}(\mathbf{X}, \mathbf{X}, \mathbf{X})) \quad (10.1)$$

where the output maintains shape  $\mathbb{R}^{B \times n \times d_{\text{model}}}$ .

**Step 2: Position-wise Feed-Forward**

$$\mathbf{h}^{(2)} = \text{LayerNorm}(\mathbf{h}^{(1)} + \text{FFN}(\mathbf{h}^{(1)})) \quad (10.2)$$

where the output again maintains shape  $\mathbb{R}^{B \times n \times d_{\text{model}}}$ .

The feed-forward network is defined as:

$$\text{FFN}(\mathbf{x}) = \mathbf{W}_2 \cdot \text{ReLU}(\mathbf{W}_1 \mathbf{x} + \mathbf{b}_1) + \mathbf{b}_2 \quad (10.3)$$

with  $\mathbf{W}_1 \in \mathbb{R}^{d_{\text{model}} \times d_{\text{ff}}}$ ,  $\mathbf{W}_2 \in \mathbb{R}^{d_{\text{ff}} \times d_{\text{model}}}$ , and typically  $d_{\text{ff}} = 4 \times d_{\text{model}}$ .

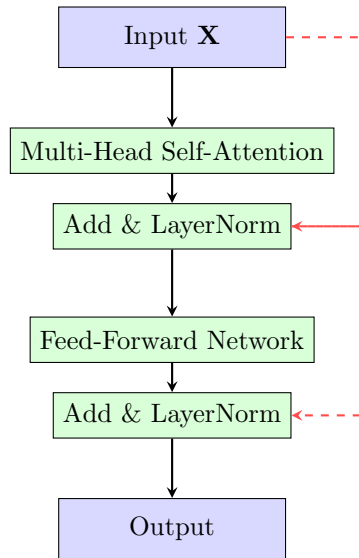


Figure 10.1: Transformer encoder layer architecture showing the two sub-layers with residual connections. The input flows through multi-head self-attention, then through a feed-forward network, with residual connections (red dashed arrows) bypassing each sub-layer. Layer normalization is applied after adding the residual. This structure maintains constant dimensions ( $n \times d_{\text{model}}$ ) throughout, enabling easy stacking of multiple layers. The residual connections provide direct gradient pathways, crucial for training deep transformers.

The dimension tracking through an encoder layer reveals important properties about memory consumption and computational cost. The input  $\mathbf{X} \in \mathbb{R}^{B \times n \times d_{\text{model}}}$  is first projected to queries, keys, and values, each with shape  $\mathbb{R}^{B \times n \times d_{\text{model}}}$ . For multi-head attention with  $h$  heads, these are reshaped to  $\mathbb{R}^{B \times h \times n \times d_k}$  where  $d_k = d_{\text{model}}/h$ . The attention scores form a matrix  $\mathbb{R}^{B \times h \times n \times n}$ , and this quadratic term in sequence length is what dominates memory consumption for long sequences. After attention, the output is projected back to  $\mathbb{R}^{B \times n \times d_{\text{model}}}$ , added to the residual, and normalized.

The feed-forward network then expands each position's representation from  $d_{\text{model}}$  to  $d_{\text{ff}}$  dimensions before projecting back down. For BERT-base with  $d_{\text{model}} = 768$  and  $d_{\text{ff}} = 3072$ , this means each position's representation temporarily expands to  $4\times$  its original size. This expansion creates a bottleneck that forces the model to learn compressed representations, similar to the hidden layer in an autoencoder. The intermediate activations  $\mathbb{R}^{B \times n \times d_{\text{ff}}}$  consume significant memory during training—for batch size 32 and sequence length 512, this amounts to  $32 \times 512 \times 3072 \times 4 = 201$  MB per layer in FP32, and with 12 layers in BERT-base, the feed-forward activations alone consume 2.4 GB of GPU memory.

**Example 10.1** (BERT-base Encoder Layer). BERT-base uses  $d_{\text{model}} = 768$ ,  $h = 12$  ( $d_k = 64$ ),  $d_{\text{ff}} = 3072$ , with  $B = 32$  and  $n = 512$ .

The attention scores matrix  $\mathbb{R}^{32 \times 12 \times 512 \times 512}$  requires 402 MB in FP32—the quadratic scaling means doubling sequence length to 1024 would require 1.6 GB per layer for attention scores alone.

Each encoder layer contains 7,084,800 parameters, with the feed-forward network (4.7M) contributing roughly twice the attention mechanism (2.4M). The per-layer activation memory totals  $\approx 704$  MB, dominated by attention scores. For all 12 layers, activations alone consume  $\approx 8.4$  GB. See Section 1.7 for the complete parameter, FLOPs, and memory analysis.

### 10.2.2 Complete Encoder Stack

The complete transformer encoder stacks  $N$  identical encoder layers, with each layer's output serving as input to the next layer. This stacking enables the model to build increasingly abstract representations: early layers might capture local syntactic patterns, middle layers might identify semantic relationships, and later layers might encode task-specific features. The depth of the network is crucial for performance—BERT-base uses 12 layers, BERT-large uses 24 layers, and GPT-3 uses 96 layers. However, deeper networks require more careful optimization, including learning rate warmup, gradient clipping, and appropriate weight initialization.

**Definition 10.2** (Transformer Encoder). Stack  $N$  encoder layers, with input embeddings and positional encodings added at the bottom:

$$\mathbf{X}^{(0)} = \text{Embedding}(\text{input}) + \text{PositionalEncoding} \quad (10.4)$$

where  $\text{Embedding} \in \mathbb{R}^{V \times d_{\text{model}}}$  maps vocabulary indices to dense vectors, and  $\text{PositionalEncoding} \in \mathbb{R}^{n_{\text{max}} \times d_{\text{model}}}$  provides position information.

Then apply  $N$  encoder layers sequentially:

$$\mathbf{X}^{(\ell)} = \text{EncoderLayer}^{(\ell)}(\mathbf{X}^{(\ell-1)}) \quad \text{for } \ell = 1, \dots, N \quad (10.5)$$

The final encoder output  $\mathbf{X}^{(N)} \in \mathbb{R}^{B \times n \times d_{\text{model}}}$  contains contextualized representations of the input sequence.

The sequential application of encoder layers means that information flows through  $N$  attention operations, allowing each token to indirectly attend to all other tokens through multiple hops. In a 12-layer encoder, information can propagate across the entire sequence through 12 levels of attention, enabling the model to capture very long-range dependencies. However, this sequential stacking also

means that encoder layers cannot be parallelized—layer  $\ell$  must wait for layer  $\ell - 1$  to complete. The parallelization in transformers occurs within each layer (across batch and sequence dimensions), not across layers.

**Example 10.2** (BERT-base Complete Encoder). BERT-base stacks  $N = 12$  encoder layers with vocabulary  $V = 30,000$ , maximum sequence length 512, and learned position embeddings. The complete model has  $\approx 110$ M parameters, of which embeddings account for  $\sim 21\%$  and the transformer layers for  $\sim 78\%$ . Training with batch size 32 and sequence length 512 requires  $\approx 13.8$  GB of GPU memory, dominated by activation storage ( $\sim 87\%$ ). See Section 1.7 for the full breakdown of parameters, activations, FLOPs, and hardware timing.

### 10.3 Position-wise Feed-Forward Networks

The position-wise feed-forward network represents the second major component of each transformer layer, complementing the attention mechanism with additional non-linear transformations. While attention allows positions to exchange information and build contextualized representations, the feed-forward network processes each position independently, applying the same learned transformation to every position in the sequence. This independence is what makes it “position-wise”—the network applied to position  $i$  is identical to the network applied to position  $j$ , with no parameter sharing or information flow between positions.

The feed-forward network consists of two linear transformations with a non-linear activation function in between, forming a simple two-layer neural network. The first layer expands the representation from  $d_{\text{model}}$  dimensions to a larger dimension  $d_{ff}$  (typically  $4 \times d_{\text{model}}$ ), applies an activation function, and then the second layer projects back down to  $d_{\text{model}}$  dimensions. This expansion-and-contraction creates a bottleneck architecture similar to an autoencoder, forcing the model to learn compressed representations that capture the most important features. The expansion factor of  $4\times$  is a design choice from the original transformer paper that has been widely adopted, though some recent models experiment with different ratios.

**Definition 10.3** (Position-wise FFN). For input  $\mathbf{X} \in \mathbb{R}^{B \times n \times d_{\text{model}}}$ , apply the same two-layer network independently to each position:

$$\text{FFN}(\mathbf{x}) = \max(0, \mathbf{x}\mathbf{W}_1 + \mathbf{b}_1)\mathbf{W}_2 + \mathbf{b}_2 \quad (10.6)$$

where  $\mathbf{W}_1 \in \mathbb{R}^{d_{\text{model}} \times d_{ff}}$ ,  $\mathbf{b}_1 \in \mathbb{R}^{d_{ff}}$ ,  $\mathbf{W}_2 \in \mathbb{R}^{d_{ff} \times d_{\text{model}}}$ , and  $\mathbf{b}_2 \in \mathbb{R}^{d_{\text{model}}}$ .

For a sequence  $\mathbf{X} \in \mathbb{R}^{B \times n \times d_{\text{model}}}$ , apply to each position independently:

$$\text{FFN}(\mathbf{X})_{i,:} = \text{FFN}(\mathbf{X}_{i,:}) \quad \text{for } i = 1, \dots, n \quad (10.7)$$

The output maintains the same shape as the input:  $\mathbb{R}^{B \times n \times d_{\text{model}}}$ .

The term “position-wise” emphasizes a crucial distinction from the attention mechanism. In attention, every position attends to every other position, creating  $O(n^2)$  interactions. In the feed-forward network, each position is processed completely independently, creating only  $O(n)$  operations. This means the feed-forward network is embarrassingly parallel—all  $n$  positions can be processed simultaneously with no dependencies. In practice, this is implemented as a single matrix multiplication: the input  $\mathbf{X} \in \mathbb{R}^{B \times n \times d_{\text{model}}}$  is reshaped to  $\mathbb{R}^{Bn \times d_{\text{model}}}$ , multiplied by  $\mathbf{W}_1$ , activated, multiplied by  $\mathbf{W}_2$ , and reshaped back to  $\mathbb{R}^{B \times n \times d_{\text{model}}}$ .

The choice of activation function significantly impacts model performance and training dynamics. The original transformer used ReLU activation, which is simple and computationally efficient but can suffer from “dying ReLU” problems where neurons become permanently inactive. BERT and GPT

introduced the GELU (Gaussian Error Linear Unit) activation, which provides a smoother, probabilistic alternative to ReLU. GELU is defined as  $\text{GELU}(x) = x \cdot \Phi(x)$  where  $\Phi(x)$  is the cumulative distribution function of the standard normal distribution. In practice, GELU is approximated as  $\text{GELU}(x) \approx 0.5x(1 + \tanh[\sqrt{2/\pi}(x + 0.044715x^3)])$ . Empirically, GELU tends to provide slightly better performance than ReLU for transformer models, though the difference is often small.

The feed-forward network accounts for a substantial portion of the model's parameters and computational cost. For BERT-base with  $d_{\text{model}} = 768$  and  $d_{\text{ff}} = 3072$ , each feed-forward network contains  $768 \times 3072 + 3072 \times 768 = 4.7\text{M}$  parameters, compared to  $4 \times 768^2 = 2.4\text{M}$  parameters in the attention mechanism. This means approximately two-thirds of each layer's parameters are in the feed-forward network. Similarly, for short sequences where  $n < d_{\text{model}}$ , the feed-forward network dominates computational cost. For BERT-base with sequence length 512, the feed-forward network requires  $2 \times 512 \times 768 \times 3072 = 2.4$  GFLOPs per layer, while attention requires  $8 \times 512 \times 768^2 + 4 \times 512^2 \times 768 = 3.2$  GFLOPs. The crossover point occurs around  $n = 2d_{\text{model}}$ —for longer sequences, attention dominates; for shorter sequences, the feed-forward network dominates.

**Example 10.3** (Feed-Forward Network Dimensions and Memory). For BERT-base with  $d_{\text{model}} = 768$ ,  $d_{\text{ff}} = 3072$ , batch size  $B = 32$ , and sequence length  $n = 512$ :

**Dimension tracking:**

$$\text{Input: } \mathbf{X} \in \mathbb{R}^{32 \times 512 \times 768} \quad (10.8)$$

$$\text{First projection: } \mathbf{XW}_1 + \mathbf{b}_1 \in \mathbb{R}^{32 \times 512 \times 3072} \quad (10.9)$$

$$\text{After ReLU/GELU: } \mathbb{R}^{32 \times 512 \times 3072} \quad (10.10)$$

$$\text{Second projection: } \mathbf{XW}_2 + \mathbf{b}_2 \in \mathbb{R}^{32 \times 512 \times 768} \quad (10.11)$$

$$\text{Output: } \mathbb{R}^{32 \times 512 \times 768} \quad (10.12)$$

**Memory requirements:**

$$\text{Input activations: } 32 \times 512 \times 768 \times 4 = 50.3 \text{ MB (FP32)} \quad (10.13)$$

$$\text{Intermediate activations: } 32 \times 512 \times 3072 \times 4 = 201.3 \text{ MB (FP32)} \quad (10.14)$$

$$\text{Output activations: } 32 \times 512 \times 768 \times 4 = 50.3 \text{ MB (FP32)} \quad (10.15)$$

$$\text{Parameters } (\mathbf{W}_1, \mathbf{W}_2): (768 \times 3072 + 3072 \times 768) \times 4 = 18.9 \text{ MB (FP32)} \quad (10.16)$$

The intermediate activations at dimension  $d_{\text{ff}} = 3072$  consume  $4\times$  the memory of the input/output activations at dimension  $d_{\text{model}} = 768$ . For a 12-layer BERT model, the feed-forward intermediate activations across all layers consume  $12 \times 201.3 = 2.4$  GB of memory during training. This is why gradient checkpointing, which recomputes these activations during the backward pass instead of storing them, can significantly reduce memory consumption.

**Computational cost:**

$$\text{First projection: } Bn \times d_{\text{model}} \times d_{\text{ff}} = 32 \times 512 \times 768 \times 3072 = 38.7 \text{ GFLOPs} \quad (10.17)$$

$$\text{Second projection: } Bn \times d_{\text{ff}} \times d_{\text{model}} = 32 \times 512 \times 3072 \times 768 = 38.7 \text{ GFLOPs} \quad (10.18)$$

$$\text{Total: } 77.4 \text{ GFLOPs per layer} \quad (10.19)$$

For comparison, the attention mechanism in the same layer requires approximately 51.5 GFLOPs (including Q, K, V projections, attention computation, and output projection). This means the feed-forward network accounts for 60% of the computational cost per layer for this configuration.

**Alternative activation functions:** While ReLU and GELU are most common, other activation functions have been explored for transformers. The Swish activation  $\text{Swish}(x) = x \cdot \sigma(\beta x)$  where  $\sigma$  is the sigmoid function, provides similar properties to GELU. The GLU (Gated Linear Unit) family, including  $\text{GLU}(x) = (x\mathbf{W}_1) \odot \sigma(x\mathbf{W}_2)$ , uses gating mechanisms similar to LSTMs. Recent work has also explored learned activation functions that adapt during training. However, GELU remains the most

widely adopted choice for modern transformers due to its balance of performance and computational efficiency.

## 10.4 Transformer Decoder

### 10.4.1 Single Decoder Layer

The transformer decoder extends the encoder architecture with an additional cross-attention mechanism that allows the decoder to attend to the encoder's output. While the encoder uses only self-attention to build contextualized representations of the input, the decoder must perform three distinct operations: masked self-attention on the target sequence, cross-attention to the source sequence, and position-wise feed-forward transformation. This three-sublayer structure enables the decoder to generate output sequences that are conditioned on both the previously generated tokens and the encoded input sequence.

The masked self-attention in the decoder is crucial for maintaining the autoregressive property during training. Unlike the encoder's bidirectional self-attention where each position can attend to all positions, the decoder's self-attention must be causal—position  $i$  can only attend to positions  $j \leq i$ . This masking ensures that the model cannot "cheat" by looking at future tokens during training. Without this mask, the model could simply copy the target sequence during training without learning to generate it. The mask is implemented by setting attention scores for future positions to  $-\infty$  before the softmax, ensuring they receive zero attention weight.

The cross-attention mechanism is where the decoder actually uses information from the encoder. In cross-attention, the queries come from the decoder's hidden states (representing "what information do I need?"), while the keys and values come from the encoder's output (representing "what information is available from the source?"). This asymmetry allows the decoder to selectively focus on relevant parts of the source sequence when generating each target token. For machine translation, this might mean attending to the source word being translated; for summarization, it might mean attending to the most salient sentences in the document.

**Definition 10.4** (Transformer Decoder Layer). A decoder layer has three sub-layers, each with residual connections and layer normalization. For input  $\mathbf{Y} \in \mathbb{R}^{B \times m \times d_{\text{model}}}$  (target sequence) and encoder output  $\mathbf{X}_{\text{enc}} \in \mathbb{R}^{B \times n \times d_{\text{model}}}$  (source sequence):

**Step 1: Masked Self-Attention**

$$\mathbf{h}^{(1)} = \text{LayerNorm}(\mathbf{Y} + \text{MaskedMultiHeadAttn}(\mathbf{Y}, \mathbf{Y}, \mathbf{Y})) \quad (10.20)$$

where the attention mask prevents position  $i$  from attending to positions  $j > i$ .

**Step 2: Cross-Attention to Encoder**

$$\mathbf{h}^{(2)} = \text{LayerNorm}(\mathbf{h}^{(1)} + \text{MultiHeadAttn}(\mathbf{h}^{(1)}, \mathbf{X}_{\text{enc}}, \mathbf{X}_{\text{enc}})) \quad (10.21)$$

where queries come from  $\mathbf{h}^{(1)}$  and keys/values come from  $\mathbf{X}_{\text{enc}}$ .

**Step 3: Feed-Forward**

$$\mathbf{h}^{(3)} = \text{LayerNorm}(\mathbf{h}^{(2)} + \text{FFN}(\mathbf{h}^{(2)})) \quad (10.22)$$

The output  $\mathbf{h}^{(3)} \in \mathbb{R}^{B \times m \times d_{\text{model}}}$  maintains the target sequence length  $m$ .

The dimension compatibility in cross-attention deserves careful attention. The decoder hidden states  $\mathbf{h}^{(1)} \in \mathbb{R}^{B \times m \times d_{\text{model}}}$  are projected to queries  $\mathbf{Q} \in \mathbb{R}^{B \times m \times d_{\text{model}}}$ , while the encoder output  $\mathbf{X}_{\text{enc}} \in \mathbb{R}^{B \times n \times d_{\text{model}}}$  is projected to keys  $\mathbf{K} \in \mathbb{R}^{B \times n \times d_{\text{model}}}$  and values  $\mathbf{V} \in \mathbb{R}^{B \times n \times d_{\text{model}}}$ . The attention scores are computed as  $\mathbf{QK}^T \in \mathbb{R}^{B \times m \times n}$ , creating a rectangular attention matrix where each of the  $m$  target positions attends to all  $n$  source positions. This is different from self-attention where the attention matrix is square ( $n \times n$  for encoder,  $m \times m$  for decoder self-attention).

The causal mask in decoder self-attention is implemented as a lower-triangular matrix. For a sequence of length  $m = 5$ , the mask looks like:

$$\text{Mask} = \begin{bmatrix} 1 & 0 & 0 & 0 & 0 \\ 1 & 1 & 0 & 0 & 0 \\ 1 & 1 & 1 & 0 & 0 \\ 1 & 1 & 1 & 1 & 0 \\ 1 & 1 & 1 & 1 & 1 \end{bmatrix} \quad (10.23)$$

where 1 indicates positions that can be attended to and 0 indicates positions that must be masked. In practice, the zeros are replaced with  $-\infty$  before the softmax operation, ensuring masked positions receive zero attention weight. This mask is applied to the attention scores before softmax:  $\text{softmax}(\mathbf{QK}^T/\sqrt{d_k} + \text{Mask})$ .

**Example 10.4** (Decoder Layer Dimension Tracking). For a translation task with source sequence length  $n = 20$  (e.g., "The cat sat on the mat") and target sequence length  $m = 15$  (e.g., "Le chat était assis"), using BERT-base dimensions ( $d_{\text{model}} = 768$ ,  $h = 12$ ,  $d_{ff} = 3072$ ), batch size  $B = 32$ :

**Inputs:**

$$\text{Decoder input: } \mathbf{Y} \in \mathbb{R}^{32 \times 15 \times 768} \quad (10.24)$$

$$\text{Encoder output: } \mathbf{X}_{\text{enc}} \in \mathbb{R}^{32 \times 20 \times 768} \quad (10.25)$$

**Masked Self-Attention:**

$$\mathbf{Q}, \mathbf{K}, \mathbf{V} \text{ from } \mathbf{Y}: \mathbb{R}^{32 \times 15 \times 768} \quad (10.26)$$

$$\text{Attention scores: } \mathbb{R}^{32 \times 12 \times 15 \times 15} \quad (\text{square, causal masked}) \quad (10.27)$$

$$\text{Output: } \mathbb{R}^{32 \times 15 \times 768} \quad (10.28)$$

The attention scores matrix  $\mathbb{R}^{32 \times 12 \times 15 \times 15}$  requires  $32 \times 12 \times 15 \times 15 \times 4 = 3.5$  MB in FP32. This is much smaller than encoder self-attention because the target sequence is shorter than the source sequence in this example.

**Cross-Attention:**

$$\mathbf{Q} \text{ from } \mathbf{h}^{(1)}: \mathbb{R}^{32 \times 15 \times 768} \quad (10.29)$$

$$\mathbf{K}, \mathbf{V} \text{ from } \mathbf{X}_{\text{enc}}: \mathbb{R}^{32 \times 20 \times 768} \quad (10.30)$$

$$\text{Attention scores: } \mathbb{R}^{32 \times 12 \times 15 \times 20} \quad (\text{rectangular!}) \quad (10.31)$$

$$\text{Output: } \mathbb{R}^{32 \times 15 \times 768} \quad (10.32)$$

The cross-attention scores  $\mathbb{R}^{32 \times 12 \times 15 \times 20}$  require  $32 \times 12 \times 15 \times 20 \times 4 = 4.6$  MB in FP32. Notice this is rectangular: 15 target positions attending to 20 source positions.

**Feed-Forward Network:**

$$\text{Input: } \mathbb{R}^{32 \times 15 \times 768} \quad (10.33)$$

$$\text{Intermediate: } \mathbb{R}^{32 \times 15 \times 3072} \quad (10.34)$$

$$\text{Output: } \mathbb{R}^{32 \times 15 \times 768} \quad (10.35)$$

The intermediate activations require  $32 \times 15 \times 3072 \times 4 = 59.0$  MB in FP32.

### 10.4.2 Complete Decoder Stack

The complete decoder stacks  $N$  decoder layers, with each layer attending to both the previous decoder layer's output and the encoder's final output. This stacking enables the decoder to build increasingly



sophisticated representations of the target sequence, conditioned on the source sequence. The encoder output  $\mathbf{X}_{\text{enc}}$  is reused by every decoder layer—it's computed once by the encoder and then fed into all  $N$  decoder layers. This means the encoder output must be stored in memory throughout the decoder's computation, contributing to memory requirements.

**Definition 10.5** (Transformer Decoder). Stack  $N$  decoder layers, with target embeddings and positional encodings at the bottom:

$$\mathbf{Y}^{(0)} = \text{Embedding}(\text{target}) + \text{PositionalEncoding} \quad (10.36)$$

Then apply  $N$  decoder layers sequentially, each attending to the encoder output:

$$\mathbf{Y}^{(\ell)} = \text{DecoderLayer}^{(\ell)}(\mathbf{Y}^{(\ell-1)}, \mathbf{X}_{\text{enc}}) \quad \text{for } \ell = 1, \dots, N \quad (10.37)$$

The final decoder output  $\mathbf{Y}^{(N)} \in \mathbb{R}^{B \times m \times d_{\text{model}}}$  is projected to vocabulary logits:

$$\text{logits} = \mathbf{Y}^{(N)} \mathbf{W}_{\text{out}} + \mathbf{b}_{\text{out}} \in \mathbb{R}^{B \times m \times V} \quad (10.38)$$

where  $\mathbf{W}_{\text{out}} \in \mathbb{R}^{d_{\text{model}} \times V}$  and  $V$  is the vocabulary size.

During training, the entire target sequence is processed in parallel using teacher forcing—the model receives the ground-truth previous tokens rather than its own predictions. The causal mask ensures that position  $i$  cannot attend to future positions, maintaining the autoregressive property even though all positions are computed simultaneously. This parallel training is a major advantage over RNN decoders, which must process the target sequence sequentially even during training.

During inference, however, the decoder must generate tokens autoregressively, one at a time. At step  $t$ , the decoder has generated tokens  $y_1, \dots, y_{t-1}$  and must predict  $y_t$ . This requires running the decoder with input sequence length  $t-1$ , computing attention over all previously generated tokens. For a target sequence of length  $m$ , this requires  $m$  forward passes through the decoder, making inference much slower than training. This is why techniques like KV caching (storing computed key and value projections) are crucial for efficient inference.

**Example 10.5** (Decoder Layer Parameter Count). For BERT-base dimensions ( $d_{\text{model}} = 768$ ,  $h = 12$ ,  $d_{\text{ff}} = 3072$ ), a decoder layer contains:

**Masked self-attention:**

$$\text{Q, K, V, O projections: } 4 \times 768^2 = 2,359,296 \quad (10.39)$$

**Cross-attention:**

$$\text{Q, K, V, O projections: } 4 \times 768^2 = 2,359,296 \quad (10.40)$$

**Feed-forward network:**

$$\mathbf{W}_1, \mathbf{b}_1, \mathbf{W}_2, \mathbf{b}_2 : 768 \times 3072 + 3072 + 3072 \times 768 + 768 = 4,722,432 \quad (10.41)$$

**Layer normalization (3 instances):**

$$\text{Scale and shift parameters: } 3 \times 2 \times 768 = 4,608 \quad (10.42)$$

**Total per decoder layer:**  $2,359,296 + 2,359,296 + 4,722,432 + 4,608 = 9,445,632$  parameters

This is approximately 33% more parameters than an encoder layer (9.4M vs 7.1M) due to the additional cross-attention mechanism. For a 6-layer decoder, this amounts to  $6 \times 9,445,632 = 56.7\text{M}$  parameters, compared to  $6 \times 7,084,800 = 42.5\text{M}$  for a 6-layer encoder.

**Example 10.6** (Autoregressive Generation Memory). During autoregressive generation, the decoder must recompute attention over all previously generated tokens at each step. For a target sequence of length  $m = 100$ , generating the final token requires:

**Without KV caching:**

- Process sequence of length 100
- Compute Q, K, V for all 100 positions
- Compute attention scores  $\mathbb{R}^{100 \times 100}$
- Total: 100 forward passes through decoder, each processing increasing sequence lengths

**With KV caching:**

- Store K, V from previous steps:  $\mathbb{R}^{99 \times 768}$  per layer
- At step 100, compute only Q for new position:  $\mathbb{R}^{1 \times 768}$
- Concatenate with cached K, V:  $\mathbb{R}^{100 \times 768}$
- Compute attention scores  $\mathbb{R}^{1 \times 100}$  (only for new position)
- Total: 100 forward passes, but each processes only 1 new position

For BERT-base dimensions with 12 decoder layers, the KV cache requires:

$$\text{Per layer: } 2 \times 100 \times 768 \times 4 = 614 \text{ KB (FP32)} \quad (10.43)$$

$$\text{All 12 layers: } 12 \times 614 = 7.4 \text{ MB} \quad (10.44)$$

This modest memory cost (7.4 MB for 100 tokens) enables approximately  $50\times$  speedup in generation, reducing generation time from several seconds to tens of milliseconds for typical sequences.

## 10.5 Computational Analysis

The computational complexity of transformers involves attention ( $O(n^2d)$  FLOPs) and feed-forward layers ( $O(nd^2)$  FLOPs), with attention dominating for long sequences and feed-forward layers dominating for large model dimensions. Memory requirements include model parameters, optimizer states, activations (scaling linearly with batch size), and attention matrices (scaling quadratically with sequence length). A detailed computational analysis including FLOPs counting, memory budgets, and inference optimization is provided in Chapter 12.



## 10.6 Complete Transformer Architecture

### 10.6.1 Full Encoder-Decoder Model

---

**Algorithm 8:** Transformer Forward Pass
 

---

**Input:** Source sequence  $\mathbf{x} = [x_1, \dots, x_n]$ , target sequence  $\mathbf{y} = [y_1, \dots, y_m]$   
**Output:** Predicted probabilities for each target position

```

// Encoder
1  $\mathbf{X}_{\text{emb}} = \text{Embedding}(\mathbf{x})$ 
2  $\mathbf{X}^{(0)} = \mathbf{X}_{\text{emb}} + \text{PositionalEncoding}(\text{positions})$ 
3 for  $\ell = 1$  to  $N_{\text{enc}}$  do
4    $\mathbf{X}^{(\ell)} = \text{EncoderLayer}^{(\ell)}(\mathbf{X}^{(\ell-1)})$ 
5  $\mathbf{X}_{\text{enc}} = \mathbf{X}^{(N_{\text{enc}})}$ 
// Decoder
6  $\mathbf{Y}_{\text{emb}} = \text{Embedding}(\mathbf{y})$ 
7  $\mathbf{Y}^{(0)} = \mathbf{Y}_{\text{emb}} + \text{PositionalEncoding}(\text{positions})$ 
8 for  $\ell = 1$  to  $N_{\text{dec}}$  do
9    $\mathbf{Y}^{(\ell)} = \text{DecoderLayer}^{(\ell)}(\mathbf{Y}^{(\ell-1)}, \mathbf{X}_{\text{enc}})$ 
10  $\mathbf{Y}_{\text{dec}} = \mathbf{Y}^{(N_{\text{dec}})}$ 
// Output Projection
11  $\text{logits} = \mathbf{Y}_{\text{dec}} \mathbf{W}_{\text{out}} + \mathbf{b}_{\text{out}}$  where  $\mathbf{W}_{\text{out}} \in \mathbb{R}^{d_{\text{model}} \times V}$ 
12  $\text{probs} = \text{softmax}(\text{logits})$ 
13 return  $\text{probs}$ 

```

---

### 10.6.2 Original Transformer Configuration

”Attention is All You Need” base model:

- Encoder layers:  $N_{\text{enc}} = 6$
- Decoder layers:  $N_{\text{dec}} = 6$
- Model dimension:  $d_{\text{model}} = 512$
- Attention heads:  $h = 8$
- Feed-forward dimension:  $d_{ff} = 2048$
- Dropout rate:  $p = 0.1$

**Parameter count:**

$$\text{Encoder (6 layers): } 6 \times (\text{attn} + \text{FFN}) \approx 25M \quad (10.45)$$

$$\text{Decoder (6 layers): } 6 \times (2 \times \text{attn} + \text{FFN}) \approx 31M \quad (10.46)$$

$$\text{Embeddings: varies by vocabulary} \quad (10.47)$$

$$\text{Total (excluding embeddings): } \approx \mathbf{56M \text{ parameters}} \quad (10.48)$$

## 10.7 Residual Connections and Layer Normalization

### 10.7.1 Residual Connections

Residual connections, also known as skip connections, are fundamental to enabling the training of deep transformer networks. Without residual connections, gradients would need to flow through dozens of attention and feed-forward layers during backpropagation, leading to vanishing or exploding gradients

that make optimization extremely difficult. The residual connection provides a direct path from each layer's output back to its input, allowing gradients to flow unimpeded through the network. This gradient highway ensures that even the earliest layers receive meaningful gradient signals, enabling effective training of networks with 96 layers (GPT-3) or more.

The residual connection pattern in transformers follows the post-addition layer normalization structure:  $\text{LayerNorm}(x + \text{Sublayer}(x))$ . This means the sublayer's output is added to its input before normalization. The addition operation has a gradient of 1 with respect to both operands, so during backpropagation, gradients flow both through the sublayer (learning to refine representations) and directly through the residual connection (providing a gradient highway). This dual path enables the network to learn both identity mappings (when the sublayer output is near zero) and complex transformations (when the sublayer output is large).

The residual connection also enables the network to learn incrementally. Early in training, the sublayer outputs are typically small due to weight initialization, so the network effectively starts as a near-identity function. As training progresses, the sublayers learn to make increasingly sophisticated transformations, building on the representations from previous layers. This incremental learning is much more stable than trying to learn the complete transformation from scratch. For a 12-layer BERT model, each layer can focus on learning a small refinement rather than a complete transformation, making optimization tractable.

### 10.7.2 Layer Normalization

Layer normalization stabilizes training by normalizing activations across the feature dimension, ensuring that each layer receives inputs with consistent statistics regardless of how previous layers' parameters change during training. Unlike batch normalization, which normalizes across the batch dimension and is commonly used in convolutional networks, layer normalization normalizes across features for each example independently. This independence from batch size is crucial for transformers, which often use small batch sizes during inference or fine-tuning, and for handling variable-length sequences where batch normalization's statistics would be unreliable.

**Definition 10.6** (Layer Normalization). For input  $\mathbf{x} \in \mathbb{R}^d$ , layer normalization computes mean and variance across the feature dimension, then normalizes and applies learned affine transformation:

$$\mu = \frac{1}{d} \sum_{i=1}^d x_i \quad (10.49)$$

$$\sigma^2 = \frac{1}{d} \sum_{i=1}^d (x_i - \mu)^2 \quad (10.50)$$

$$\hat{x}_i = \frac{x_i - \mu}{\sqrt{\sigma^2 + \epsilon}} \quad (10.51)$$

$$y_i = \gamma \hat{x}_i + \beta \quad (10.52)$$

where  $\gamma, \beta \in \mathbb{R}^d$  are learnable scale and shift parameters, and  $\epsilon \approx 10^{-5}$  prevents division by zero.

For a batch of sequences  $\mathbf{X} \in \mathbb{R}^{B \times n \times d}$ , layer normalization is applied independently to each of the  $B \times n$  vectors, normalizing across the  $d$  features.

The learned parameters  $\gamma$  and  $\beta$  allow the network to undo the normalization if beneficial. If  $\gamma_i = \sqrt{\sigma^2 + \epsilon}$  and  $\beta_i = \mu$ , the normalization is completely undone. In practice, the network learns appropriate values that balance normalization's stabilizing effect with the flexibility to learn arbitrary distributions.

Layer normalization differs fundamentally from batch normalization in its normalization dimension. Batch normalization computes statistics across the batch dimension (normalizing each

feature across all examples in the batch), making it dependent on batch size and batch composition. Layer normalization computes statistics across the feature dimension (normalizing all features for each example independently), making it independent of batch size. For transformers processing variable-length sequences with potentially small batch sizes, this independence is essential. A batch size of 1 works perfectly with layer normalization but would be problematic for batch normalization.

### 10.7.3 Pre-Norm vs Post-Norm

The placement of layer normalization relative to the residual connection significantly impacts training dynamics. The original transformer paper used post-norm:  $\text{LayerNorm}(x + \text{Sublayer}(x))$ , where normalization is applied after adding the residual. More recent models like GPT-2 and GPT-3 use pre-norm:  $x + \text{LayerNorm}(\text{Sublayer}(x))$ , where normalization is applied before the sublayer, and the residual connection bypasses normalization entirely.

Post-norm architecture normalizes the sum of the input and sublayer output, which can help prevent activation magnitudes from growing unboundedly as depth increases. However, post-norm requires careful learning rate warmup and can be unstable for very deep networks. The gradients must flow through the layer normalization operation, which can introduce additional numerical instabilities. BERT uses post-norm with 12-24 layers successfully, but scaling to 96+ layers becomes challenging.

Pre-norm architecture applies normalization before each sublayer, so the sublayer receives normalized inputs. The residual connection then adds the sublayer output directly to the (unnormalized) input, bypassing the normalization. This provides a cleaner gradient path through the residual connection and tends to be more stable for very deep networks. GPT-2 and GPT-3 use pre-norm, enabling training of 48-96 layer models without learning rate warmup. The trade-off is that pre-norm may achieve slightly lower final performance than post-norm for shallow networks, but this difference diminishes for deeper networks where pre-norm's stability advantages dominate.

**Example 10.7** (Layer Normalization Computation). For a single position's representation  $\mathbf{x} \in \mathbb{R}^{768}$  from BERT-base:

**Input:**  $\mathbf{x} = [0.5, -0.3, 1.2, \dots]$  (768 values)

**Compute statistics:**

$$\mu = \frac{1}{768} \sum_{i=1}^{768} x_i = 0.15 \quad (\text{example value}) \quad (10.53)$$

$$\sigma^2 = \frac{1}{768} \sum_{i=1}^{768} (x_i - 0.15)^2 = 0.42 \quad (\text{example value}) \quad (10.54)$$

$$\sigma = \sqrt{0.42 + 10^{-5}} = 0.648 \quad (10.55)$$

**Normalize:**

$$\hat{x}_1 = \frac{0.5 - 0.15}{0.648} = 0.540 \quad (10.56)$$

$$\hat{x}_2 = \frac{-0.3 - 0.15}{0.648} = -0.694 \quad (10.57)$$

$$\hat{x}_3 = \frac{1.2 - 0.15}{0.648} = 1.620 \quad (10.58)$$

$$\vdots \quad (10.59)$$

The normalized values  $\hat{\mathbf{x}}$  have mean 0 and variance 1 across the 768 dimensions.

**Apply learned affine transformation:**

$$y_1 = \gamma_1 \times 0.540 + \beta_1 \quad (10.60)$$

$$y_2 = \gamma_2 \times (-0.694) + \beta_2 \quad (10.61)$$

$$y_3 = \gamma_3 \times 1.620 + \beta_3 \quad (10.62)$$

$$\vdots \quad (10.63)$$

where  $\gamma, \beta \in \mathbb{R}^{768}$  are learned during training. Initially,  $\gamma$  is typically initialized to 1 and  $\beta$  to 0, making layer normalization initially act as pure normalization.

**Memory and computation:**

- Parameters:  $2 \times 768 = 1,536$  (scale and shift)
- FLOPs per position:  $\approx 10 \times 768 = 7,680$  (mean, variance, normalize, scale, shift)
- For batch 32, sequence 512:  $32 \times 512 \times 7,680 = 126$  MFLOPs

Layer normalization is computationally cheap compared to attention or feed-forward networks, but it's memory-bound rather than compute-bound, so kernel fusion with adjacent operations is important for efficiency.

## 10.8 Training Objectives

### 10.8.1 Sequence-to-Sequence Training

For machine translation, minimize cross-entropy loss:

$$\mathcal{L} = - \sum_{t=1}^m \log P(y_t | y_{<t}, \mathbf{x}; \theta) \quad (10.64)$$

**Teacher forcing:** During training, use ground-truth previous tokens  $y_{<t}$ , not model predictions.

### 10.8.2 Autoregressive Generation

---

**Algorithm 9:** Autoregressive Decoding
 

---

**Input:** Source sequence  $\mathbf{x}$ , max length  $T$   
**Output:** Generated sequence  $\mathbf{y}$

```

1 Encode source:  $\mathbf{X}_{\text{enc}} = \text{Encoder}(\mathbf{x})$ 
2 Initialize:  $\mathbf{y} = [\text{BOS}]$  (begin-of-sequence token)
3 for  $t = 1$  to  $T$  do
4    $\text{probs}_t = \text{Decoder}(\mathbf{y}, \mathbf{X}_{\text{enc}})$ 
5    $y_t = \arg \max(\text{probs}_t)$  (or sample from distribution)
6   Append  $y_t$  to  $\mathbf{y}$ 
7   if  $y_t = \text{EOS}$  then
8     break (end-of-sequence token)
9 return  $\mathbf{y}$ 
```

---

## 10.9 Transformer Variants: Architectural Patterns

The original transformer uses both an encoder and decoder, but subsequent research established three main architectural patterns, each suited to different task families:

- **Encoder-only (BERT, Chapter 13):** Bidirectional self-attention processes the full input in a single parallel forward pass. Pre-trained with masked language modeling. Excels at understanding tasks: classification, NER, extractive QA, and semantic similarity.
- **Decoder-only (GPT, Chapter 14):** Causal self-attention enables autoregressive generation where each token attends only to previous tokens. Pre-trained with next-token prediction. Excels at generation, few-shot learning, and dialogue. Modern LLMs (GPT-3/4, LLaMA) use this pattern due to its flexibility—understanding tasks can be handled through prompting.
- **Encoder-decoder (T5, BART, Chapter 15):** Combines a bidirectional encoder with a causal decoder connected via cross-attention. Pre-trained with span corruption or denoising objectives. Excels at sequence-to-sequence tasks: translation, summarization, and generative QA. Requires roughly twice the parameters of single-stack models but provides explicit separation of understanding and generation.

Recent trends favor decoder-only architectures for their versatility and scaling properties, though encoder-only models remain more parameter-efficient for understanding tasks and encoder-decoder models remain strongest for sequence-to-sequence tasks. Detailed coverage of each variant’s architecture, pre-training, and fine-tuning follows in Chapters 13–15.

## 10.10 Exercises

**Exercise 10.1.** For transformer with  $N = 6$ ,  $d_{\text{model}} = 512$ ,  $h = 8$ ,  $d_{ff} = 2048$ ,  $V = 32000$ :

1. Calculate total parameters in encoder
2. Calculate total parameters in decoder
3. What percentage are in embeddings vs transformer layers?
4. How does this change if vocabulary increases to 50,000?

**Exercise 10.2.** Implement single transformer encoder layer in PyTorch. Test with batch size 16, sequence length 64,  $d_{\text{model}} = 256$ . Verify output shape and gradient flow through residual connections.

**Exercise 10.3.** Compare memory and computation for:

1. Encoder processing sequence length 1024
2. Decoder generating 1024 tokens autoregressively

Why is decoding slower? How many forward passes required?

**Exercise 10.4.** Show that layer normalization is invariant to input scale: if  $\mathbf{x}' = c\mathbf{x}$  for constant  $c > 0$ , then  $\text{LayerNorm}(\mathbf{x}') = \text{LayerNorm}(\mathbf{x})$  (ignoring learnable  $\gamma, \beta$ ).

## 10.11 Solutions

Full solutions for all exercises are available at <https://deeplearning.hofkensvermeulen.be>.

# Chapter 11

## Training Transformers

### Chapter Overview

Training transformers requires specialized techniques beyond standard optimization. This chapter provides comprehensive coverage of transformer training procedures, from loss functions and backpropagation through the architecture to optimization algorithms, learning rate schedules, and hardware-efficient training strategies. We examine why transformers need warmup, how mixed precision training reduces memory consumption, when to use gradient accumulation and checkpointing, and how distributed training enables models that exceed single-GPU capacity. Throughout, we provide detailed hardware analysis, memory calculations, and practical guidance drawn from training state-of-the-art models like BERT, GPT-2, and GPT-3.

### Learning Objectives

1. Understand training objectives and loss functions for different transformer architectures
2. Analyze gradient flow and backpropagation through transformer layers
3. Implement optimization algorithms (Adam, AdamW, LAMB) with appropriate hyperparameters
4. Apply learning rate schedules with warmup and decay
5. Use mixed precision training to reduce memory and accelerate training
6. Apply gradient accumulation and checkpointing for memory-constrained scenarios
7. Understand distributed training strategies for large-scale models
8. Select appropriate batch sizes and sequence lengths based on hardware constraints
9. Apply regularization techniques to prevent overfitting
10. Estimate training time and costs for transformer models

### 11.1 Training Objectives and Loss Functions

The training objective fundamentally shapes how a transformer learns and what capabilities it develops. Different transformer architectures employ distinct training objectives tailored to their intended use cases, from masked language modeling in BERT to causal language modeling in GPT to sequence-to-sequence learning in T5. Understanding these objectives in depth—including their mathematical formulations, computational requirements, and practical implications—is essential for training transformers effectively.

### 11.1.1 Masked Language Modeling

Masked language modeling, introduced by BERT, trains the model to predict randomly masked tokens based on bidirectional context. This objective enables the model to learn rich representations that capture relationships in both directions, making it particularly effective for tasks requiring understanding of complete sentences or documents.

The masking strategy is more sophisticated than simply replacing tokens with a special [MASK] symbol. BERT’s approach selects 15% of tokens for prediction, but handles them in three different ways: 80% are replaced with [MASK], 10% are replaced with random tokens from the vocabulary, and 10% are left unchanged. This strategy prevents the model from simply memorizing that [MASK] tokens need prediction and forces it to maintain representations for all tokens, since any token might need to be predicted. The random token replacement encourages the model to use context to correct errors, while leaving some tokens unchanged helps the model learn that not all tokens are corrupted.

The loss function for masked language modeling is cross-entropy computed only over the masked positions. For a sequence  $\mathbf{x} = (x_1, \dots, x_n)$  with masked positions  $M \subseteq \{1, \dots, n\}$ , the loss is:

$$L_{\text{MLM}} = -\frac{1}{|M|} \sum_{i \in M} \log P(x_i | \mathbf{x}_{\setminus M}) \quad (11.1)$$

where  $\mathbf{x}_{\setminus M}$  denotes the sequence with masked positions corrupted according to the strategy above. The model outputs logits  $\mathbf{z}_i \in \mathbb{R}^V$  for each position  $i$ , where  $V$  is the vocabulary size, and the probability distribution is obtained via softmax:  $P(x_i | \mathbf{x}_{\setminus M}) = \text{softmax}(\mathbf{z}_i)_{x_i}$ .

The computational and memory implications of this loss are significant. For vocabulary size  $V = 30,000$ , sequence length  $n = 512$ , and batch size  $B = 32$ , the output logits tensor has shape  $\mathbb{R}^{32 \times 512 \times 30000}$ , requiring  $32 \times 512 \times 30,000 \times 4 = 1,966,080,000$  bytes, or approximately 1.97 GB of memory just for the logits in FP32. This massive memory footprint explains why the output projection and softmax computation often become bottlenecks during training. The memory requirement can be reduced by computing the loss in chunks (processing subsets of positions at a time) or by using mixed precision training where logits are computed in FP16, though care must be taken to maintain numerical stability in the softmax operation.

In practice, BERT-base masks approximately 77 tokens per sequence (15% of 512), so the loss is computed over  $32 \times 77 = 2,464$  predictions per batch. The cross-entropy computation requires exponentiating 30,000 logits for each prediction to compute the softmax denominator, then taking the logarithm of the target class probability. Modern implementations optimize this by fusing the softmax and cross-entropy operations and by using numerically stable implementations that subtract the maximum logit before exponentiation to prevent overflow.

### 11.1.2 Causal Language Modeling

Causal language modeling, used in GPT and other decoder-only models, trains the model to predict the next token given all previous tokens. Unlike masked language modeling, which uses bidirectional context, causal language modeling uses only left-to-right context, enforced through causal attention masks that prevent positions from attending to future positions.

The training objective is to maximize the likelihood of each token given its preceding context. For a sequence  $\mathbf{x} = (x_1, \dots, x_n)$ , the loss is:

$$L_{\text{CLM}} = -\frac{1}{n} \sum_{i=1}^n \log P(x_i | x_1, \dots, x_{i-1}) \quad (11.2)$$

This formulation means that every position in the sequence contributes to the loss, unlike masked language modeling where only 15% of positions contribute. For a batch of 32 sequences of length 512, we compute loss over  $32 \times 512 = 16,384$  predictions, compared to only 2,464 for BERT’s masked language modeling. This makes causal language modeling more sample-efficient in terms of predictions per sequence, though the unidirectional context may be less informative than bidirectional context for some tasks.



A crucial distinction exists between training and inference for causal language models. During training, we use teacher forcing: the model receives the ground-truth previous tokens as input, even if it would have predicted different tokens. This enables parallel computation of the loss across all positions in a sequence, since we can compute  $P(x_i|x_1, \dots, x_{i-1})$  for all  $i$  simultaneously using causal masking. During inference, however, generation is autoregressive: the model generates one token at a time, using its own predictions as input for subsequent positions. This sequential generation process is much slower than parallel training, which motivates optimizations like KV caching (discussed in Chapter 12).

The memory requirements for causal language modeling are similar to masked language modeling: the output logits tensor for batch size 32, sequence length 512, and vocabulary size 50,257 (GPT-2’s vocabulary) requires  $32 \times 512 \times 50,257 \times 4 = 3,296,019,456$  bytes, or approximately 3.3 GB in FP32. However, since we compute loss over all positions rather than just 15%, the gradient computation is more expensive. The backward pass through the output projection receives gradients from all 16,384 predictions rather than just 2,464, increasing the gradient computation cost proportionally.

### 11.1.3 Sequence-to-Sequence Training

Sequence-to-sequence models like T5 and BART use encoder-decoder architectures where the encoder processes the input sequence bidirectionally and the decoder generates the output sequence autoregressively. The training objective combines aspects of both masked and causal language modeling: the encoder can use bidirectional attention over the input, while the decoder uses causal attention over the output sequence and cross-attention to the encoder’s representations.

The loss function for sequence-to-sequence training is computed over the target sequence. For input sequence  $\mathbf{x} = (x_1, \dots, x_n)$  and target sequence  $\mathbf{y} = (y_1, \dots, y_m)$ :

$$L_{\text{seq2seq}} = -\frac{1}{m} \sum_{j=1}^m \log P(y_j | y_1, \dots, y_{j-1}, \mathbf{x}) \quad (11.3)$$

Like causal language modeling, sequence-to-sequence training uses teacher forcing during training: the decoder receives the ground-truth previous target tokens as input, enabling parallel computation of the loss. This differs from inference, where the decoder must generate tokens sequentially using its own predictions.

The memory requirements for sequence-to-sequence models are higher than encoder-only or decoder-only models because both encoder and decoder activations must be stored. For T5-base with input length 512, target length 512, and batch size 32, we must store encoder activations ( $32 \times 512 \times 768$  per layer), decoder activations ( $32 \times 512 \times 768$  per layer), and cross-attention activations ( $32 \times 12 \times 512 \times 512$  for attention matrices between decoder and encoder). The total activation memory is roughly 1.5-2× that of an encoder-only model of the same size.

Different sequence-to-sequence models use different input corruption strategies. T5 uses span corruption, where contiguous spans of tokens are replaced with sentinel tokens and the model must predict the original spans. BART uses a variety of corruption strategies including token masking, token deletion, sentence permutation, and document rotation. These diverse corruption strategies help the model learn robust representations that generalize across different types of noise and transformations.

## 11.2 Backpropagation Through Transformers

Understanding how gradients flow through the transformer architecture is essential for diagnosing training issues, designing better architectures, and implementing custom training procedures. The transformer’s combination of attention mechanisms, residual connections, layer normalization, and feed-forward networks creates a complex gradient flow pattern that differs fundamentally from simpler architectures like MLPs or CNNs.

### 11.2.1 Gradient Flow Analysis

Backpropagation through a transformer begins at the output and flows backward through each component. For a language modeling task, the loss  $L$  is computed from the output logits, and we must compute gradients with respect to all parameters in the model. The gradient flow follows the reverse path of the forward computation, with each operation contributing its Jacobian to the chain rule.

The output projection layer maps the final transformer layer's output to vocabulary logits. For output  $\mathbf{h}_n \in \mathbb{R}^{d_{\text{model}}}$  at position  $n$  and output weight matrix  $\mathbf{W}^{\text{out}} \in \mathbb{R}^{d_{\text{model}} \times V}$ , the logits are  $\mathbf{z}_n = \mathbf{W}^{\text{out}^\top} \mathbf{h}_n$ . The gradient of the loss with respect to the output weights is:

$$\frac{\partial L}{\partial \mathbf{W}^{\text{out}}} = \sum_{i=1}^n \mathbf{h}_i \frac{\partial L}{\partial \mathbf{z}_i}^\top \quad (11.4)$$

where  $\frac{\partial L}{\partial \mathbf{z}_i} \in \mathbb{R}^V$  is the gradient from the softmax and cross-entropy loss. This gradient matrix has the same shape as  $\mathbf{W}^{\text{out}}: \mathbb{R}^{d_{\text{model}} \times V}$ . For BERT-base with  $d_{\text{model}} = 768$  and  $V = 30,000$ , this gradient requires  $768 \times 30,000 \times 4 = 92,160,000$  bytes (92 MB) in FP32.

The gradient with respect to the output representations is:

$$\frac{\partial L}{\partial \mathbf{h}_i} = \mathbf{W}^{\text{out}} \frac{\partial L}{\partial \mathbf{z}_i} \quad (11.5)$$

This gradient then flows backward through each transformer layer. Within a layer, the gradient must flow through the feed-forward network, the second residual connection and layer normalization, the attention mechanism, and the first residual connection and layer normalization.

### 11.2.2 Gradients Through Residual Connections

Residual connections are crucial for training deep transformers because they provide "gradient highways" that allow gradients to flow directly through many layers without vanishing. Consider a residual block with function  $F$ :

$$\mathbf{y} = \mathbf{x} + F(\mathbf{x}) \quad (11.6)$$

The gradient with respect to the input is:

$$\frac{\partial L}{\partial \mathbf{x}} = \frac{\partial L}{\partial \mathbf{y}} + \frac{\partial L}{\partial \mathbf{y}} \frac{\partial F(\mathbf{x})}{\partial \mathbf{x}} \quad (11.7)$$

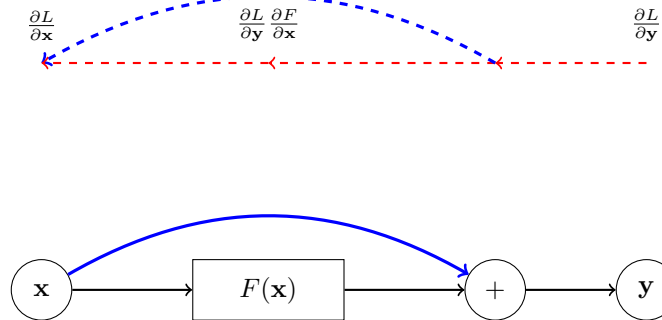


Figure 11.1: Gradient flow through residual connections. The blue path shows the direct gradient highway that bypasses  $F(\mathbf{x})$ , ensuring gradients can flow through many layers without vanishing. Red dashed arrows show gradient flow during backpropagation.

The first term  $\frac{\partial L}{\partial \mathbf{y}}$  is the direct gradient path that bypasses the function  $F$  entirely. This ensures that even if  $\frac{\partial F(\mathbf{x})}{\partial \mathbf{x}}$  becomes very small (vanishing gradients) or very large (exploding gradients), the gradient  $\frac{\partial L}{\partial \mathbf{x}}$  still receives the direct contribution  $\frac{\partial L}{\partial \mathbf{y}}$ . This is why transformers can be trained with many layers (BERT-large has 24 layers, GPT-3 has 96 layers) without suffering from vanishing gradients that plagued early deep networks.

For a transformer with  $L$  layers, the gradient from the output to the input has  $2^L$  paths through the network: at each layer, the gradient can either flow through the residual connection (direct path) or through the attention/FFN (indirect path). This exponential number of paths creates a rich gradient flow that helps training, though in practice most gradient flows through the shorter paths that use more residual connections.

### 11.2.3 Gradients Through Layer Normalization

Layer normalization normalizes activations across the feature dimension, computing mean and variance for each position independently. For input  $\mathbf{x} \in \mathbb{R}^d$ , layer normalization computes:

$$\mathbf{y} = \frac{\mathbf{x} - \mu}{\sqrt{\sigma^2 + \epsilon}} \odot \gamma + \beta \quad (11.8)$$

where  $\mu = \frac{1}{d} \sum_{i=1}^d x_i$ ,  $\sigma^2 = \frac{1}{d} \sum_{i=1}^d (x_i - \mu)^2$ , and  $\gamma, \beta \in \mathbb{R}^d$  are learned scale and shift parameters.

The gradient computation for layer normalization is complex because the normalization couples all dimensions: changing one input element affects the mean and variance, which affects all output elements. The gradient with respect to the input is:

$$\frac{\partial L}{\partial \mathbf{x}} = \frac{\gamma}{\sqrt{\sigma^2 + \epsilon}} \left( \frac{\partial L}{\partial \mathbf{y}} - \frac{1}{d} \sum_{j=1}^d \frac{\partial L}{\partial y_j} - \frac{\mathbf{x} - \mu}{\sigma^2 + \epsilon} \frac{1}{d} \sum_{j=1}^d \frac{\partial L}{\partial y_j} (x_j - \mu) \right) \quad (11.9)$$

This gradient has three terms: the direct gradient scaled by the normalization factor, a mean-centering term, and a variance-correction term. The complexity of this gradient is why layer normalization is sometimes replaced with simpler alternatives like RMSNorm in some recent models, though layer normalization generally provides better training stability.

The learned parameters  $\gamma$  and  $\beta$  have simple gradients:

$$\frac{\partial L}{\partial \gamma} = \frac{\partial L}{\partial \mathbf{y}} \odot \frac{\mathbf{x} - \mu}{\sqrt{\sigma^2 + \epsilon}}, \quad \frac{\partial L}{\partial \beta} = \frac{\partial L}{\partial \mathbf{y}} \quad (11.10)$$

Layer normalization helps gradient flow by preventing activations from becoming too large or too small, which would cause gradients to vanish or explode. By maintaining normalized activations throughout the network, layer normalization ensures that gradients remain in a reasonable range, facilitating stable training.

### 11.2.4 Gradients Through Attention

The attention mechanism involves several matrix multiplications and a softmax operation, each contributing to the gradient computation. For self-attention with queries  $\mathbf{Q}$ , keys  $\mathbf{K}$ , and values  $\mathbf{V}$ :

$$\mathbf{O} = \text{softmax} \left( \frac{\mathbf{Q}\mathbf{K}^\top}{\sqrt{d_k}} \right) \mathbf{V} \quad (11.11)$$

Working backward, the gradient with respect to the values is:

$$\frac{\partial L}{\partial \mathbf{V}} = \mathbf{A}^\top \frac{\partial L}{\partial \mathbf{O}} \quad (11.12)$$

where  $\mathbf{A} = \text{softmax}(\mathbf{Q}\mathbf{K}^\top / \sqrt{d_k})$  is the attention matrix. This is a matrix multiplication of shape  $(n \times n)^\top \times (n \times d_v) = (n \times d_v)$ , matching the shape of  $\mathbf{V}$ .

The gradient with respect to the attention matrix is:

$$\frac{\partial L}{\partial \mathbf{A}} = \frac{\partial L}{\partial \mathbf{O}} \mathbf{V}^\top \quad (11.13)$$

This has shape  $(n \times d_v) \times (d_v \times n) = (n \times n)$ , matching the attention matrix shape.

The gradient must then flow through the softmax operation. For softmax output  $\mathbf{a} = \text{softmax}(\mathbf{s})$ , the Jacobian is:

$$\frac{\partial a_i}{\partial s_j} = a_i(\delta_{ij} - a_j) \quad (11.14)$$

where  $\delta_{ij}$  is the Kronecker delta. This means the gradient with respect to the pre-softmax scores is:

$$\frac{\partial L}{\partial s_i} = \sum_j \frac{\partial L}{\partial a_j} a_j (\delta_{ij} - a_i) = a_i \left( \frac{\partial L}{\partial a_i} - \sum_j \frac{\partial L}{\partial a_j} a_j \right) \quad (11.15)$$

This computation must be performed for each row of the attention matrix independently, since softmax is applied row-wise.

Finally, gradients flow to the query and key projections. The gradient with respect to queries is:

$$\frac{\partial L}{\partial \mathbf{Q}} = \frac{1}{\sqrt{d_k}} \frac{\partial L}{\partial \mathbf{S}} \mathbf{K} \quad (11.16)$$

where  $\mathbf{S} = \mathbf{QK}^\top / \sqrt{d_k}$  are the pre-softmax scores. The gradient with respect to keys is:

$$\frac{\partial L}{\partial \mathbf{K}} = \frac{1}{\sqrt{d_k}} \frac{\partial L}{\partial \mathbf{S}}^\top \mathbf{Q} \quad (11.17)$$

These gradients then flow through the projection matrices  $\mathbf{W}^Q$ ,  $\mathbf{W}^K$ , and  $\mathbf{W}^V$ . For the query projection  $\mathbf{Q} = \mathbf{XW}^Q$ :

$$\frac{\partial L}{\partial \mathbf{W}^Q} = \mathbf{X}^\top \frac{\partial L}{\partial \mathbf{Q}} \quad (11.18)$$

This gradient has shape  $(d_{\text{model}} \times n) \times (n \times d_k) = (d_{\text{model}} \times d_k)$ , matching  $\mathbf{W}^Q$ . For BERT-base with  $d_{\text{model}} = 768$  and  $d_k = 64$ , this requires  $768 \times 64 \times 4 = 196,608$  bytes (197 KB) per head, or  $12 \times 197 = 2.4$  MB for all 12 heads.

### 11.2.5 Gradients Through Feed-Forward Networks

The feed-forward network consists of two linear transformations with a non-linear activation (typically GELU) in between:

$$\text{FFN}(\mathbf{x}) = \mathbf{W}_2 \text{GELU}(\mathbf{W}_1 \mathbf{x} + \mathbf{b}_1) + \mathbf{b}_2 \quad (11.19)$$

The gradient with respect to the second layer weights is:

$$\frac{\partial L}{\partial \mathbf{W}_2} = \mathbf{h}^\top \frac{\partial L}{\partial \mathbf{y}} \quad (11.20)$$

where  $\mathbf{h} = \text{GELU}(\mathbf{W}_1 \mathbf{x} + \mathbf{b}_1)$  is the intermediate activation. For BERT-base with  $d_{ff} = 3072$  and  $d_{\text{model}} = 768$ , this gradient has shape  $(3072 \times 768)$  and requires  $3072 \times 768 \times 4 = 9,437,184$  bytes (9.4 MB) in FP32.

The gradient flows through the GELU activation. GELU is defined as:

$$\text{GELU}(x) = x\Phi(x) \quad (11.21)$$

where  $\Phi(x)$  is the cumulative distribution function of the standard normal distribution. The derivative is:

$$\text{GELU}'(x) = \Phi(x) + x\phi(x) \quad (11.22)$$

where  $\phi(x)$  is the probability density function. The gradient with respect to the pre-activation is:

$$\frac{\partial L}{\partial (\mathbf{W}_1 \mathbf{x} + \mathbf{b}_1)} = \frac{\partial L}{\partial \mathbf{h}} \odot \text{GELU}'(\mathbf{W}_1 \mathbf{x} + \mathbf{b}_1) \quad (11.23)$$

Finally, the gradient with respect to the first layer weights is:

$$\frac{\partial L}{\partial \mathbf{W}_1} = \mathbf{x}^\top \frac{\partial L}{\partial (\mathbf{W}_1 \mathbf{x} + \mathbf{b}_1)} \quad (11.24)$$

This has shape  $(d_{\text{model}} \times d_{ff}) = (768 \times 3072)$ , also requiring 9.4 MB in FP32.

### 11.2.6 Computational Cost of Backpropagation

The backward pass through a transformer requires approximately twice the FLOPs of the forward pass. This factor of two arises because each matrix multiplication  $\mathbf{Y} = \mathbf{X}\mathbf{W}$  in the forward pass requires two matrix multiplications in the backward pass:  $\frac{\partial L}{\partial \mathbf{W}} = \mathbf{X}^\top \frac{\partial L}{\partial \mathbf{Y}}$  and  $\frac{\partial L}{\partial \mathbf{X}} = \frac{\partial L}{\partial \mathbf{Y}} \mathbf{W}^\top$ . Each of these backward matrix multiplications has similar computational cost to the forward multiplication.

For BERT-base with 96.6 GFLOPs per forward pass, the backward pass requires approximately  $2 \times 96.6 = 193.2$  GFLOPs. A complete training step (forward pass + backward pass) thus requires approximately  $96.6 + 193.2 = 289.8$  GFLOPs, or roughly three times the forward pass cost. This  $3 \times$  factor is a useful rule of thumb for estimating training costs from inference costs.

The memory requirements for backpropagation are substantial because all intermediate activations from the forward pass must be stored to compute gradients. For BERT-base with batch size 32 and sequence length 512, the activations require approximately 12 GB as analyzed in Chapter 12. This activation memory often dominates the total memory consumption during training, which motivates techniques like gradient checkpointing that trade computation for memory by recomputing activations during the backward pass.

## 11.3 Optimization Algorithms

The choice of optimization algorithm significantly impacts transformer training dynamics, convergence speed, and final model quality. While stochastic gradient descent (SGD) with momentum works well for many deep learning tasks, transformers benefit particularly from adaptive learning rate methods that adjust the learning rate for each parameter based on gradient statistics. The Adam family of optimizers has become the de facto standard for transformer training, with variants like AdamW and LAMB addressing specific challenges in large-scale training.

### 11.3.1 Adam Optimizer

Adam (Adaptive Moment Estimation) maintains exponential moving averages of both the gradient (first moment) and the squared gradient (second moment) for each parameter. These statistics enable adaptive per-parameter learning rates that automatically adjust based on the gradient history, helping with the varying scales of gradients across different layers and components of the transformer.

The Adam algorithm maintains two state vectors for each parameter  $\mathbf{w}$ : the first moment  $\mathbf{m}$  (exponential moving average of gradients) and the second moment  $\mathbf{v}$  (exponential moving average of squared gradients). At each training step  $t$  with gradient  $\mathbf{g}_t$ :

$$\mathbf{m}_t = \beta_1 \mathbf{m}_{t-1} + (1 - \beta_1) \mathbf{g}_t \quad (11.25)$$

$$\mathbf{v}_t = \beta_2 \mathbf{v}_{t-1} + (1 - \beta_2) \mathbf{g}_t^2 \quad (11.26)$$

where  $\beta_1$  and  $\beta_2$  are decay rates (typically  $\beta_1 = 0.9$  and  $\beta_2 = 0.999$ ). The squared gradient  $\mathbf{g}_t^2$  is computed element-wise.

Because  $\mathbf{m}$  and  $\mathbf{v}$  are initialized to zero, they are biased toward zero, especially in early training steps. Adam corrects this bias by computing bias-corrected estimates:

$$\hat{\mathbf{m}}_t = \frac{\mathbf{m}_t}{1 - \beta_1^t} \quad (11.27)$$

$$\hat{\mathbf{v}}_t = \frac{\mathbf{v}_t}{1 - \beta_2^t} \quad (11.28)$$

The parameter update is then:

$$\mathbf{w}_{t+1} = \mathbf{w}_t - \eta \frac{\hat{\mathbf{m}}_t}{\sqrt{\hat{\mathbf{v}}_t} + \epsilon} \quad (11.29)$$

where  $\eta$  is the learning rate and  $\epsilon$  is a small constant (typically  $10^{-8}$ ) for numerical stability.

The adaptive learning rate  $\frac{\eta}{\sqrt{\hat{\mathbf{v}}_t + \epsilon}}$  is larger for parameters with small historical gradients and smaller for parameters with large historical gradients. This adaptation is particularly beneficial for transformers because different components have vastly different gradient scales. Embedding layers, which are updated sparsely (only for tokens present in the batch), benefit from larger effective learning rates, while frequently updated parameters in the attention and FFN layers benefit from smaller effective learning rates that prevent overshooting.

The memory requirements for Adam are substantial: for each parameter, we must store the parameter itself, the gradient, the first moment, and the second moment. For a model with  $P$  parameters in FP32, Adam requires:

- Parameters:  $P \times 4$  bytes
- Gradients:  $P \times 4$  bytes
- First moments:  $P \times 4$  bytes
- Second moments:  $P \times 4$  bytes
- Total:  $16P$  bytes

For BERT-base with 110 million parameters, Adam requires  $110,000,000 \times 16 = 1,760,000,000$  bytes, or 1.76 GB, just for the optimizer state. This is four times the memory required for the parameters alone, and this overhead grows linearly with model size. For GPT-3 with 175 billion parameters, Adam would require  $175,000,000,000 \times 16 = 2,800$  GB just for parameters and optimizer states, necessitating distributed training strategies that shard the optimizer state across multiple GPUs.

### 11.3.2 AdamW: Decoupled Weight Decay

AdamW modifies Adam by decoupling weight decay from the gradient-based update. In standard Adam with L2 regularization, the weight decay is incorporated into the gradient:  $\mathbf{g}_t = \nabla L(\mathbf{w}_t) + \lambda \mathbf{w}_t$ , where  $\lambda$  is the regularization coefficient. This means the weight decay is affected by the adaptive learning rate, which can lead to unexpected behavior.

AdamW instead applies weight decay directly to the parameters after the adaptive update:

$$\mathbf{w}_{t+1} = \mathbf{w}_t - \eta \frac{\hat{\mathbf{m}}_t}{\sqrt{\hat{\mathbf{v}}_t + \epsilon}} - \eta \lambda \mathbf{w}_t \quad (11.30)$$

This decoupling means that weight decay acts as a true regularizer, shrinking parameters toward zero at a rate proportional to the learning rate, independent of the gradient statistics. In practice, this leads to better generalization, particularly for transformers where different parameters have very different gradient scales.

The typical weight decay coefficient for transformer training is  $\lambda = 0.01$ . However, weight decay is usually not applied to all parameters. Biases and layer normalization parameters (the scale  $\gamma$  and shift  $\beta$  parameters) are typically excluded from weight decay, as regularizing these parameters can hurt performance. The exclusion is implemented by maintaining separate parameter groups in the optimizer, with different weight decay settings for each group.

AdamW has become the standard optimizer for training transformers, used in BERT, GPT-2, GPT-3, T5, and most other modern models. The improved generalization from decoupled weight decay often allows training with higher learning rates, which can accelerate convergence. The memory requirements are identical to Adam:  $16P$  bytes for a model with  $P$  parameters in FP32.

### 11.3.3 LAMB: Large Batch Training

LAMB (Layer-wise Adaptive Moments optimizer for Batch training) extends Adam to enable training with very large batch sizes, up to 64,000 or more. Large batch training is desirable because it improves hardware utilization and reduces training time by processing more examples in parallel, but naive scaling of the batch size often hurts convergence and final model quality.

The key insight of LAMB is to compute layer-wise learning rates that adapt based on the ratio of parameter norm to gradient norm within each layer. For layer  $l$  with parameters  $\mathbf{w}^{(l)}$  and Adam update  $\mathbf{u}^{(l)} = \frac{\hat{\mathbf{m}}^{(l)}}{\sqrt{\hat{\mathbf{v}}^{(l)} + \epsilon}} + \lambda \mathbf{w}^{(l)}$ , LAMB computes:

$$\phi^{(l)} = \frac{\|\mathbf{w}^{(l)}\|_2}{\|\mathbf{u}^{(l)}\|_2} \quad (11.31)$$

The parameter update is then:

$$\mathbf{w}_{t+1}^{(l)} = \mathbf{w}_t^{(l)} - \eta \phi^{(l)} \mathbf{u}^{(l)} \quad (11.32)$$

This layer-wise adaptation ensures that the update magnitude is proportional to the parameter magnitude within each layer, preventing some layers from being updated too aggressively while others are updated too conservatively. This is particularly important for large batch training because large batches produce more accurate gradient estimates, which can lead to overly aggressive updates without proper scaling.

LAMB enabled training BERT-large to the same accuracy as the original paper in just 76 minutes using a batch size of 65,536 on 1,024 TPU v3 chips, compared to several days with standard batch sizes. The ability to use such large batches dramatically reduces training time for large-scale models, though it requires access to substantial computational resources to realize the benefits.

The memory requirements for LAMB are similar to Adam and AdamW:  $16P$  bytes for a model with  $P$  parameters in FP32. The additional computation for layer-wise norm calculations is negligible compared to the forward and backward passes.

### 11.3.4 Optimizer Memory Comparison

Different optimizers have different memory footprints, which can be a critical consideration for large models:

- **SGD (no momentum):**  $8P$  bytes (parameters + gradients in FP32)
- **SGD with momentum:**  $12P$  bytes (parameters + gradients + momentum in FP32)
- **Adam/AdamW/LAMB:**  $16P$  bytes (parameters + gradients + first moment + second moment in FP32)

For BERT-base with 110 million parameters:

- SGD:  $110\text{M} \times 8 = 880$  MB
- SGD with momentum:  $110\text{M} \times 12 = 1,320$  MB
- Adam/AdamW/LAMB:  $110\text{M} \times 16 = 1,760$  MB

The additional memory overhead of Adam-family optimizers (880 MB compared to SGD) is usually worthwhile because the adaptive learning rates lead to faster convergence and better final performance. However, for very large models where memory is at a premium, techniques like ZeRO (Zero Redundancy Optimizer) can shard the optimizer state across multiple GPUs to reduce per-GPU memory requirements.

## 11.4 Learning Rate Schedules

Learning rate schedules are critical for transformer training, perhaps more so than for other architectures. Transformers are sensitive to the learning rate, and using a constant learning rate throughout training typically leads to poor results. The standard approach combines a warmup phase, where the learning rate increases from zero to a maximum value, with a decay phase, where the learning rate gradually decreases. This schedule helps stabilize early training and enables continued improvement in later training.

### 11.4.1 The Necessity of Warmup

Learning rate warmup is essential for stable transformer training. Without warmup, using the full learning rate from the beginning often causes training to diverge or get stuck in poor local minima. The instability arises from the interaction between large initial gradients and Adam’s adaptive learning rates.

In the first few training steps, Adam’s second moment estimates  $\mathbf{v}$  are very small because they are initialized to zero and have not yet accumulated gradient statistics. This means the effective learning rate  $\frac{\eta}{\sqrt{\mathbf{v}+\epsilon}}$  is very large, potentially much larger than the nominal learning rate  $\eta$ . When combined with large gradients that are common early in training (when the model’s predictions are random and the loss is high), these large effective learning rates can cause parameter updates that are far too aggressive, leading to numerical instability or divergence.

Warmup solves this problem by starting with a very small learning rate and gradually increasing it over the first  $W$  steps (typically 10% of total training steps). During warmup, the learning rate at step  $t$  is:

$$\eta_t = \eta_{\max} \cdot \frac{t}{W} \quad (11.33)$$

This linear increase gives Adam’s moment estimates time to accumulate meaningful statistics while preventing overly aggressive updates. By the time the learning rate reaches its maximum value  $\eta_{\max}$ , the optimizer has stabilized and can handle the full learning rate safely.

The warmup period also serves another purpose: it allows the model to learn basic patterns before attempting more complex optimization. In the first few steps, the model learns simple statistics like token frequencies and basic co-occurrence patterns. These foundational patterns provide a stable base for learning more complex relationships later in training.

### 11.4.2 Warmup Plus Linear Decay

The warmup plus linear decay schedule, used in BERT and many other models, combines linear warmup with linear decay to zero. For total training steps  $T$  and warmup steps  $W$ :

$$\eta_t = \begin{cases} \eta_{\max} \cdot \frac{t}{W} & \text{if } t \leq W \quad (\text{warmup}) \\ \eta_{\max} \cdot \frac{T-t}{T-W} & \text{if } t > W \quad (\text{decay}) \end{cases} \quad (11.34)$$

The decay phase gradually reduces the learning rate to zero over the remaining training steps. This decay is beneficial because it allows the model to make large updates early in training when far from a good solution, then make progressively smaller updates as it approaches a good solution. The smaller learning rate in late training helps the model settle into a sharper minimum, which often generalizes better.

For BERT-base, the typical configuration is  $\eta_{\max} = 1 \times 10^{-4}$ ,  $W = 10,000$  steps, and  $T = 1,000,000$  steps. This means the learning rate increases linearly from 0 to  $10^{-4}$  over the first 10,000 steps (1% of training), then decreases linearly from  $10^{-4}$  to 0 over the remaining 990,000 steps. The warmup period is relatively short, but it is crucial for stable training.

Different models use different maximum learning rates based on their size and architecture. GPT-2 uses  $\eta_{\max} = 2.5 \times 10^{-4}$ , slightly higher than BERT. GPT-3 uses  $\eta_{\max} = 6 \times 10^{-5}$ , lower than smaller models, reflecting the general trend that larger models require smaller learning rates for stable training. The warmup period for GPT-3 is 375 million tokens, which corresponds to a different number of steps depending on the batch size and sequence length.

### 11.4.3 Inverse Square Root Decay

The original ”Attention is All You Need” paper used a different schedule that combines warmup with inverse square root decay:

$$\eta_t = d_{\text{model}}^{-0.5} \cdot \min(t^{-0.5}, t \cdot W^{-1.5}) \quad (11.35)$$

This schedule has two phases. During warmup ( $t \leq W$ ), the learning rate increases linearly:

$$\eta_t = d_{\text{model}}^{-0.5} \cdot t \cdot W^{-1.5} = d_{\text{model}}^{-0.5} \cdot W^{-0.5} \cdot \frac{t}{W} \quad (11.36)$$



After warmup ( $t > W$ ), the learning rate decays as the inverse square root of the step number:

$$\eta_t = d_{\text{model}}^{-0.5} \cdot t^{-0.5} \quad (11.37)$$

The inverse square root decay is slower than linear decay, maintaining a higher learning rate for longer. This can be beneficial for very long training runs where continued exploration is desirable. The original Transformer used  $W = 4,000$  warmup steps and  $d_{\text{model}} = 512$ , giving a peak learning rate of  $512^{-0.5} \cdot 4000^{-0.5} \approx 0.00070$ .

The inverse square root schedule is less commonly used than linear decay in modern transformers, but it remains popular for some applications, particularly in machine translation where the original Transformer architecture is still widely used.

#### 11.4.4 Cosine Annealing

Cosine annealing provides a smooth decay curve that starts slowly, accelerates in the middle, and slows again near the end. After warmup, the learning rate follows a cosine curve:

$$\eta_t = \eta_{\min} + \frac{1}{2}(\eta_{\max} - \eta_{\min}) \left( 1 + \cos \left( \pi \frac{t - W}{T - W} \right) \right) \quad (11.38)$$

where  $\eta_{\min}$  is the minimum learning rate (often 0 or  $0.1\eta_{\max}$ ). At the start of decay ( $t = W$ ), the cosine term is  $\cos(0) = 1$ , giving  $\eta_W = \eta_{\max}$ . At the end of training ( $t = T$ ), the cosine term is  $\cos(\pi) = -1$ , giving  $\eta_T = \eta_{\min}$ .

The smooth decay of cosine annealing can provide better final performance than linear decay, particularly for tasks where the model benefits from extended fine-tuning at low learning rates. The slower initial decay allows the model to continue exploring, while the accelerated decay in the middle helps the model converge, and the slow final decay allows careful refinement.

Cosine annealing is popular in computer vision (where it was originally developed) and has been adopted for some transformer training, particularly in vision transformers and multimodal models. However, linear decay remains more common for language models.

## 11.5 Mixed Precision Training

Mixed precision training is one of the most impactful optimizations for transformer training, reducing memory consumption and accelerating computation by leveraging lower-precision arithmetic. The technique uses 16-bit floating point (FP16 or BF16) for most operations while maintaining 32-bit floating point (FP32) master weights for numerical stability. This combination achieves substantial speedups on modern hardware while preserving training dynamics and final model quality.

### 11.5.1 FP16 Training Algorithm

Mixed precision training with FP16 maintains two copies of the model parameters: an FP16 copy used for forward and backward passes, and an FP32 master copy used for parameter updates. The algorithm proceeds as follows:

1. **Forward pass:** Convert FP32 master weights to FP16, perform all forward computations in FP16, producing FP16 activations
2. **Loss computation:** Compute loss in FP16, then scale the loss by a large factor  $S$  (typically 1024 or dynamically adjusted)
3. **Backward pass:** Compute gradients in FP16 using the scaled loss, producing FP16 gradients that are also scaled by  $S$
4. **Gradient unscaling:** Divide FP16 gradients by  $S$  to recover the true gradient scale
5. **Gradient conversion:** Convert unscaled FP16 gradients to FP32

6. **Parameter update:** Update FP32 master weights using FP32 gradients and the optimizer
7. **Repeat:** Copy updated FP32 weights to FP16 for the next iteration

The loss scaling step is crucial for preventing gradient underflow. FP16 has a much smaller representable range than FP32: the smallest positive normal number in FP16 is approximately  $6 \times 10^{-5}$ , compared to  $1.2 \times 10^{-38}$  in FP32. Gradients in deep networks are often very small, particularly in later layers or after many training steps. Without scaling, these small gradients would underflow to zero in FP16, preventing the corresponding parameters from being updated.

By scaling the loss by a factor  $S$  before backpropagation, all gradients are also scaled by  $S$  (due to the chain rule). This shifts the gradient values into the representable range of FP16. After the backward pass, we divide by  $S$  to recover the true gradient values. The scaling and unscaling operations are mathematically equivalent to computing gradients in FP32, but they allow the actual gradient computation to occur in FP16, leveraging faster FP16 hardware.

The scaling factor  $S$  can be fixed (typically 1024 or 2048) or dynamic. Dynamic loss scaling starts with a large scaling factor and reduces it if gradient overflow is detected (indicated by NaN or Inf values in the gradients). If training proceeds without overflow for a certain number of steps, the scaling factor is increased. This adaptive approach maximizes the use of FP16's range while preventing overflow.

### 11.5.2 Memory Savings

Mixed precision training reduces memory consumption primarily through smaller activations. The memory breakdown for mixed precision training is:

- **FP16 parameters (forward/backward):**  $2P$  bytes
- **FP32 master parameters:**  $4P$  bytes
- **FP32 gradients:**  $4P$  bytes
- **FP32 optimizer states (Adam):**  $8P$  bytes (first and second moments)
- **FP16 activations:**  $A/2$  bytes (where  $A$  is FP32 activation memory)

The total is  $18P + A/2$  bytes, compared to  $16P + A$  bytes for FP32 training. Surprisingly, mixed precision uses slightly more memory for parameters and optimizer states ( $18P$  vs  $16P$ ) because we maintain both FP16 and FP32 copies of the parameters. However, the activation memory is halved ( $A/2$  vs  $A$ ), and since activations typically dominate memory consumption, mixed precision usually provides substantial overall savings.

For BERT-base with 110 million parameters, batch size 32, and sequence length 512:

**FP32 training:**

$$\text{Parameters + gradients + optimizer: } 110\text{M} \times 16 = 1,760 \text{ MB} \quad (11.39)$$

$$\text{Activations: } \approx 12,000 \text{ MB} \quad (11.40)$$

$$\text{Total: } 13,760 \text{ MB} \approx 13.8 \text{ GB} \quad (11.41)$$

**Mixed precision training:**

$$\text{FP16 parameters: } 110\text{M} \times 2 = 220 \text{ MB} \quad (11.42)$$

$$\text{FP32 master + gradients + optimizer: } 110\text{M} \times 16 = 1,760 \text{ MB} \quad (11.43)$$

$$\text{FP16 activations: } \approx 6,000 \text{ MB} \quad (11.44)$$

$$\text{Total: } 7,980 \text{ MB} \approx 8.0 \text{ GB} \quad (11.45)$$

Mixed precision saves  $13.8 - 8.0 = 5.8$  GB, a 42% reduction. This memory saving enables larger batch sizes or longer sequences on the same hardware, directly improving training efficiency.

### 11.5.3 Hardware Acceleration

Modern GPUs provide dedicated hardware for accelerated FP16 computation. NVIDIA’s Tensor Cores, available on Volta (V100), Turing (RTX 20xx), Ampere (A100, RTX 30xx), and newer architectures, can perform FP16 matrix multiplications at twice the throughput of FP32 operations.

For the NVIDIA A100 GPU:

- **FP32 performance:** 156 TFLOPS (teraflops)
- **FP16 performance (Tensor Cores):** 312 TFLOPS
- **Theoretical speedup:**  $2\times$

In practice, the speedup is typically  $1.5\text{--}1.8\times$  rather than the full  $2\times$  because:

- Not all operations benefit from FP16 (e.g., layer normalization, softmax, and other element-wise operations may still run in FP32 for numerical stability)
- Memory bandwidth limitations can bottleneck performance, particularly for small batch sizes
- Overhead from data type conversions and loss scaling
- Non-matrix operations (activations, normalizations) don’t use Tensor Cores

For BERT-base training on an A100 GPU, mixed precision typically provides a  $1.6\times$  speedup, reducing training time from approximately 4 days to 2.5 days on the same hardware. This speedup, combined with the memory savings that enable larger batch sizes, makes mixed precision training essential for efficient transformer training.

### 11.5.4 BF16: An Alternative to FP16

BF16 (bfloat16) is an alternative 16-bit format that maintains the same exponent range as FP32 (8 bits) while reducing the mantissa precision (7 bits, compared to 10 bits in FP16). This design choice provides better numerical stability than FP16 at the cost of slightly lower precision.

The key advantage of BF16 is that it can represent the same range of values as FP32, from approximately  $10^{-38}$  to  $10^{38}$ . This eliminates the need for loss scaling because gradients are unlikely to underflow in BF16’s range. The training algorithm simplifies to:

1. Forward pass in BF16
2. Loss computation in BF16 (no scaling needed)
3. Backward pass in BF16
4. Convert BF16 gradients to FP32
5. Update FP32 master weights

BF16 is supported on Google’s TPUs (v2, v3, v4), NVIDIA A100 GPUs, and newer hardware. For transformers, BF16 often provides similar or slightly better results than FP16 with less tuning required, since the loss scaling factor doesn’t need to be adjusted. However, FP16 remains more widely supported across different hardware platforms.

The memory savings and computational speedups for BF16 are similar to FP16: activations are halved, and Tensor Cores provide approximately  $2\times$  theoretical speedup ( $1.5\text{--}1.8\times$  in practice). The choice between FP16 and BF16 often depends on hardware availability and whether loss scaling tuning is problematic for a particular training setup.

## 11.6 Gradient Accumulation

Gradient accumulation is a technique for achieving large effective batch sizes when GPU memory limits the actual batch size that can be processed in a single forward-backward pass. The technique accumulates gradients over multiple mini-batches before updating parameters, mathematically equivalent to training with a larger batch but with lower memory requirements.

### 11.6.1 Algorithm and Implementation

The gradient accumulation algorithm processes  $K$  mini-batches of size  $B_{\text{mini}}$ , accumulating their gradients, then performs a single parameter update. The effective batch size is  $B_{\text{eff}} = K \times B_{\text{mini}}$ .

---

**Algorithm 10:** Gradient Accumulation
 

---

- 1 **Input:** Mini-batch size  $B_{\text{mini}}$ , accumulation steps  $K$ , dataset
  - 2 Initialize model parameters  $\mathbf{w}$  Initialize optimizer **for each epoch do—**
  - 3 each batch of  $K$  mini-batches Zero accumulated gradients:  $\mathbf{g}_{\text{accum}} = \mathbf{0}$  **for**  $k = 1$  **to**  $K$  **do**
  - 4 Load mini-batch  $\mathcal{B}_k$  of size  $B_{\text{mini}}$  Forward pass: compute loss  $L_k$  on  $\mathcal{B}_k$  Scale loss:  $L_k \leftarrow L_k / K$   
 Backward pass: compute gradients  $\mathbf{g}_k$  Accumulate:  $\mathbf{g}_{\text{accum}} \leftarrow \mathbf{g}_{\text{accum}} + \mathbf{g}_k$  Update parameters using  $\mathbf{g}_{\text{accum}}$  Zero gradients for next accumulation
- 

The loss scaling by  $1/K$  ensures that the accumulated gradient has the correct magnitude. Without this scaling, the accumulated gradient would be  $K$  times larger than the gradient from a single batch of size  $B_{\text{eff}}$ , leading to overly aggressive parameter updates.

In PyTorch, gradient accumulation is implemented by simply not calling `optimizer.zero_grad()` after each mini-batch. Gradients accumulate automatically because PyTorch adds new gradients to existing gradients by default:

```
optimizer.zero_grad()
for k in range(accumulation_steps):
    batch = next(dataloader)
    loss = model(batch) / accumulation_steps
    loss.backward() # Accumulates gradients

optimizer.step() # Update parameters
```

### 11.6.2 Trade-offs and Considerations

Gradient accumulation is mathematically equivalent to training with a larger batch size, but it has different computational characteristics. The key trade-offs are:

**Memory:** Gradient accumulation requires only the memory for a single mini-batch of size  $B_{\text{mini}}$ , not the full effective batch size  $B_{\text{eff}}$ . This is the primary benefit—it enables training with large effective batch sizes on memory-constrained hardware.

**Computation time:** Gradient accumulation is slower than true large-batch training because the mini-batches are processed sequentially rather than in parallel. For  $K$  accumulation steps, we perform  $K$  forward passes and  $K$  backward passes before a single parameter update. If we could fit the full batch in memory, we would perform 1 forward pass and 1 backward pass, processing  $K$  times more data in parallel.

The time overhead is typically 10-20% compared to true large-batch training, arising from:

- Reduced parallelism: processing mini-batches sequentially rather than in parallel
- Increased overhead:  $K$  forward-backward passes have more overhead than 1 pass
- Memory bandwidth: loading model parameters  $K$  times rather than once

**Batch normalization incompatibility:** Gradient accumulation is incompatible with batch normalization because batch normalization computes statistics over the mini-batch, not the effective batch. Each mini-batch has different statistics, leading to incorrect normalization. Fortunately, transformers use layer normalization rather than batch normalization, so this is not a concern for transformer training.

### 11.6.3 Practical Example

Consider training BERT-base where we want an effective batch size of 512, but GPU memory only allows batch size 32. We use gradient accumulation with  $K = 512/32 = 16$  steps.

**Memory requirements:**

- Without accumulation (batch 512):  $\approx 220$  GB (exceeds any single GPU)
- With accumulation (batch 32):  $\approx 13.8$  GB (fits on V100 16GB)

**Training time comparison:**

- True batch 512 (if it fit): 1 forward + 1 backward = 2 passes
- Gradient accumulation: 16 forward + 16 backward = 32 passes

The gradient accumulation approach requires  $16\times$  more passes, but each pass is faster because it processes less data. The total time is approximately 15% longer than true batch 512 would be, but it's feasible on available hardware.

**When to use gradient accumulation:**

- When the desired batch size exceeds GPU memory capacity
- When trying to match published training recipes that use large batches
- When larger batches improve convergence (common for transformers)
- When training time is less critical than achieving good final performance

**When not to use gradient accumulation:**

- When the mini-batch size is already optimal for convergence
- When training time is critical and larger batches don't improve convergence
- When the overhead (15-20%) is unacceptable

For BERT-base, gradient accumulation is commonly used to achieve effective batch sizes of 256-512, which provide better convergence than smaller batches. The time overhead is acceptable given the improved final performance.

## 11.7 Gradient Checkpointing

Gradient checkpointing, also called activation checkpointing, is a memory-computation trade-off technique that dramatically reduces activation memory at the cost of increased training time. Instead of storing all intermediate activations during the forward pass for use in backpropagation, gradient checkpointing stores only a subset of activations (typically at layer boundaries) and recomputes the remaining activations during the backward pass as needed.

### 11.7.1 The Memory-Computation Trade-off

Standard backpropagation requires storing all intermediate activations from the forward pass because computing gradients requires both the gradients flowing backward and the activations from the forward pass. For a transformer with  $L$  layers, batch size  $B$ , and sequence length  $n$ , the activation memory scales as  $O(LBnd_{\text{model}})$  for linear terms and  $O(LBhn^2)$  for attention matrices. As analyzed in Chapter 12, this activation memory often dominates total memory consumption, particularly for large batch sizes or long sequences.

Gradient checkpointing reduces activation memory by storing only activations at layer boundaries (the input to each transformer layer) and discarding all intermediate activations within layers. During the backward pass, when gradients need to flow through a layer, the forward computation for that layer is re-executed to reconstruct the intermediate activations needed for gradient computation. This recomputation happens on-the-fly during backpropagation, so the intermediate activations are used immediately and then discarded.

The memory savings are substantial. Without checkpointing, we store activations for every operation: QKV projections, attention scores, attention outputs, FFN intermediate activations, layer norm outputs, and residual connections. With checkpointing, we store only the layer inputs. For a typical transformer layer, this reduces activation memory by approximately 80%, storing only 1-2 tensors per layer instead of 8-10 tensors.

The computational cost is the price for these memory savings. Each layer's forward computation must be executed twice: once during the forward pass (with activations discarded) and once during the backward pass (to reconstruct activations for gradient computation). This doubles the forward computation cost, but the backward pass cost remains the same. Since the backward pass already costs approximately  $2\times$  the forward pass, the total cost increases from  $3\times$  to  $4\times$  the forward pass, a 33% increase in training time. In practice, the overhead is typically 20-30% due to optimizations and the fact that some operations (like attention softmax) are relatively cheap to recompute.

### 11.7.2 Implementation Strategies

The most common checkpointing strategy is to checkpoint at transformer layer boundaries. For a model with  $L$  layers, we store  $L + 1$  activation tensors (the input to each layer plus the final output), rather than storing all intermediate activations within layers.

In PyTorch, gradient checkpointing is implemented using `torch.utils.checkpoint.checkpoint`, which wraps a function and handles the recomputation automatically:

```
from torch.utils.checkpoint import checkpoint

class TransformerLayer(nn.Module):
    def forward(self, x):
        # Use checkpointing for this layer
        return checkpoint(self._forward, x)

    def _forward(self, x):
        # Actual layer computation
        # Attention
        attn_out = self.attention(x)
        x = x + self.dropout(attn_out)
        x = self.layer_norm1(x)

        # Feed-forward
        ffn_out = self.ffn(x)
        x = x + self.dropout(ffn_out)
        x = self.layer_norm2(x)

    return x
```

During the forward pass, PyTorch executes `_forward` but doesn't store intermediate activations. During the backward pass, when gradients reach this layer, PyTorch re-executes `_forward` with the saved input  $\mathbf{x}$ , reconstructing the intermediate activations needed for gradient computation.

An alternative strategy is selective checkpointing, where only some layers are checkpointed. This provides a middle ground between memory and computation. For example, checkpointing every other layer reduces activation memory by approximately 50% while increasing training time by only 10-15%. This can be optimal when memory is tight but not critically constrained.

### 11.7.3 Practical Impact

The impact of gradient checkpointing is best illustrated with concrete examples. For GPT-2 (small) with 12 layers,  $d_{\text{model}} = 768$ , sequence length 1024, and batch size 32:

**Without checkpointing:**

$$\text{Activation memory per layer: } \approx 85 \text{ MB} \quad (11.46)$$

$$\text{Total activation memory (12 layers): } \approx 1,020 \text{ MB} \approx 1 \text{ GB per sequence} \quad (11.47)$$

$$\text{Batch size 32: } 32 \text{ GB} \quad (11.48)$$

This exceeds the memory of most GPUs when combined with parameters and optimizer states.

**With checkpointing:**

$$\text{Stored activations (layer inputs only): } 13 \times 32 \times 1024 \times 768 \times 4 \approx 1,308 \text{ MB} \quad (11.49)$$

$$\text{Reduction: } 32,000 \text{ MB} \rightarrow 1,308 \text{ MB} \quad (96\% \text{reduction!}) \quad (11.50)$$

This dramatic reduction enables training with much larger batch sizes or longer sequences on the same hardware. For GPT-2 on an NVIDIA V100 (16 GB), checkpointing enables increasing the batch size from approximately 4 to 20, a  $5\times$  improvement.

**Training time impact:**

- Without checkpointing: 100% (baseline)
- With checkpointing: 125% (25% slower)

The 25% time increase is usually acceptable given the  $5\times$  increase in batch size, which often improves convergence and reduces the total number of steps needed for training.

### 11.7.4 When to Use Gradient Checkpointing

Gradient checkpointing is most beneficial in specific scenarios:

**Use checkpointing when:**

- Training with long sequences (e.g.,  $n > 1024$ ) where activation memory dominates
- GPU memory is the limiting factor preventing larger batch sizes
- The model is very deep (many layers) and activation memory scales linearly with depth
- Training time is less critical than maximizing batch size or sequence length
- Combined with mixed precision, checkpointing enables training that would otherwise be impossible

**Avoid checkpointing when:**

- Memory is not constrained and the 20-30% time overhead is unacceptable
- Training with short sequences and small batch sizes where activation memory is already manageable

- Optimizing for minimum training time rather than maximum throughput
- The model is shallow enough that activation memory is not the bottleneck

For most transformer training, particularly for models with more than 12 layers or sequences longer than 512 tokens, gradient checkpointing is beneficial. The memory savings enable configurations that would otherwise be impossible, and the time overhead is modest compared to the benefits.

## 11.8 Distributed Training Strategies

As transformer models grow beyond the capacity of single GPUs, distributed training becomes essential. Different distributed training strategies partition the model, data, or optimizer state across multiple GPUs, each with distinct trade-offs in terms of memory reduction, communication overhead, and implementation complexity. Understanding these strategies is crucial for training large-scale models efficiently.

### 11.8.1 Data Parallelism

Data parallelism is the simplest and most widely used distributed training strategy. The model is replicated on each GPU, and each GPU processes a different subset of the training batch. After computing gradients locally, the GPUs synchronize their gradients using an AllReduce operation, then each GPU updates its local copy of the model with the averaged gradients.

The algorithm proceeds as follows:

1. Each GPU has a complete copy of the model
2. The global batch is split across GPUs: GPU  $i$  processes mini-batch  $\mathcal{B}_i$
3. Each GPU performs forward and backward passes independently, computing local gradients  $\mathbf{g}_i$
4. AllReduce operation computes the average gradient:  $\bar{\mathbf{g}} = \frac{1}{N} \sum_{i=1}^N \mathbf{g}_i$  where  $N$  is the number of GPUs
5. Each GPU updates its model using  $\bar{\mathbf{g}}$
6. All GPUs now have identical models (up to floating-point precision)

Data parallelism scales efficiently to 8-16 GPUs on a single node (connected via NVLink or PCIe) because the communication overhead is relatively small compared to computation. For BERT-base with 110M parameters, the AllReduce operation must communicate  $110\text{M} \times 4 = 440$  MB of gradients. On NVLink (300 GB/s bandwidth), this takes approximately  $440 \text{ MB} / 300 \text{ GB/s} \approx 1.5$  ms, which is small compared to the forward-backward computation time of 10-20 ms per batch.

However, data parallelism does not reduce memory requirements per GPU—each GPU still stores the complete model, optimizer states, and activations for its mini-batch. This limits the size of models that can be trained with data parallelism alone. For GPT-3 with 175B parameters requiring 700 GB in FP32, data parallelism is insufficient because no single GPU has enough memory for the complete model.

### 11.8.2 Model Parallelism

Model parallelism splits the model across multiple GPUs, with different layers residing on different devices. For a model with  $L$  layers split across  $N$  GPUs, each GPU stores approximately  $L/N$  layers. This reduces per-GPU memory proportionally to the number of GPUs.

The forward pass proceeds sequentially: GPU 1 processes the input through its layers, sends activations to GPU 2, which processes through its layers, and so on. The backward pass proceeds in reverse: GPU  $N$  computes gradients for its layers, sends gradients to GPU  $N - 1$ , which computes gradients for its layers, and so on.



The primary challenge with model parallelism is the pipeline bubble problem. While GPU 1 is processing the next batch, GPUs 2 through  $N$  are idle, waiting for activations from GPU 1. Similarly, during the backward pass, GPU  $N$  finishes first and sits idle while earlier GPUs complete their backward passes. This sequential execution leads to poor GPU utilization, with each GPU active only  $1/N$  of the time in the worst case.

Model parallelism is necessary when a single layer or the complete model exceeds single-GPU memory, but it should be combined with other strategies to improve utilization. For GPT-3, model parallelism alone would require hundreds of GPUs and would have terrible utilization due to pipeline bubbles.

### 11.8.3 Pipeline Parallelism

Pipeline parallelism improves upon model parallelism by splitting each batch into micro-batches and pipelining their execution across GPUs. Instead of processing one batch completely before starting the next, pipeline parallelism processes multiple micro-batches concurrently, with different micro-batches at different stages of the pipeline.

For example, with 4 GPUs and 4 micro-batches:

- Time 1: GPU 1 processes micro-batch 1 (forward)
- Time 2: GPU 1 processes micro-batch 2 (forward), GPU 2 processes micro-batch 1 (forward)
- Time 3: GPU 1 processes micro-batch 3 (forward), GPU 2 processes micro-batch 2 (forward), GPU 3 processes micro-batch 1 (forward)
- Time 4: All GPUs are active, processing different micro-batches

This pipelining significantly reduces idle time. The pipeline bubble (time when some GPUs are idle) is proportional to the number of GPUs divided by the number of micro-batches. With  $N$  GPUs and  $M$  micro-batches, the bubble fraction is approximately  $N/M$ . Using  $M = 4N$  micro-batches reduces the bubble to 25%, achieving 75% utilization.

Pipeline parallelism implementations like GPipe and PipeDream differ in how they handle gradient computation and weight updates. GPipe uses synchronous updates, accumulating gradients from all micro-batches before updating weights. PipeDream uses asynchronous updates, updating weights after each micro-batch, which can improve throughput but requires careful handling of weight versions.

### 11.8.4 Tensor Parallelism

Tensor parallelism, pioneered by Megatron-LM, splits individual layers across multiple GPUs rather than splitting the model layer-wise. For attention and feed-forward layers, the computation can be partitioned across GPUs with minimal communication.

For the attention mechanism, the heads can be split across GPUs. With  $h$  heads and  $N$  GPUs, each GPU computes  $h/N$  heads independently. The only communication required is an AllReduce after computing the attention output, to sum the contributions from all heads.

For the feed-forward network, the first linear layer  $\mathbf{W}_1 \in \mathbb{R}^{d_{\text{model}} \times d_{ff}}$  can be column-partitioned across GPUs. Each GPU computes a subset of the  $d_{ff}$  intermediate activations. The GELU activation is applied independently on each GPU. The second linear layer  $\mathbf{W}_2 \in \mathbb{R}^{d_{ff} \times d_{\text{model}}}$  is row-partitioned, and an AllReduce sums the outputs from all GPUs.

Tensor parallelism achieves  $N \times$  memory reduction with only two AllReduce operations per layer (one for attention, one for FFN). The communication volume is  $O(Bnd_{\text{model}})$  per layer, which is much smaller than the  $O(P)$  communication required for data parallelism (where  $P$  is the number of parameters).

Tensor parallelism is particularly effective for very large layers. For GPT-3 with  $d_{\text{model}} = 12,288$  and  $d_{ff} = 49,152$ , a single FFN layer has  $2 \times 12,288 \times 49,152 \approx 1.2\text{B}$  parameters, requiring 4.8 GB in FP32. Splitting across 8 GPUs reduces this to 600 MB per GPU, making the layer tractable.

### 11.8.5 ZeRO: Zero Redundancy Optimizer

ZeRO (Zero Redundancy Optimizer) is a family of optimizations that reduce memory by sharding optimizer states, gradients, and parameters across GPUs while maintaining the computational efficiency of data parallelism. ZeRO has three stages, each providing progressively more memory reduction:

#### ZeRO Stage 1: Optimizer State Partitioning

Each GPU stores only  $1/N$  of the optimizer states (first and second moments for Adam). During the optimizer step, each GPU updates only its partition of the parameters. This reduces optimizer memory by  $N\times$  with minimal communication overhead.

For BERT-base with 110M parameters and 8 GPUs:

- Without ZeRO: Each GPU stores 880 MB of optimizer states
- With ZeRO-1: Each GPU stores  $880/8 = 110$  MB of optimizer states
- Memory saved: 770 MB per GPU

#### ZeRO Stage 2: Gradient Partitioning

In addition to optimizer states, gradients are also partitioned. Each GPU computes gradients for all parameters during backpropagation but only retains the gradients for its partition, discarding the rest. This reduces gradient memory by  $N\times$ .

For BERT-base with 8 GPUs:

- Without ZeRO: Each GPU stores 440 MB of gradients
- With ZeRO-2: Each GPU stores  $440/8 = 55$  MB of gradients
- Total memory saved:  $770 + 385 = 1,155$  MB per GPU

#### ZeRO Stage 3: Parameter Partitioning

The most aggressive stage partitions the parameters themselves. Each GPU stores only  $1/N$  of the parameters. During the forward pass, each GPU gathers the parameters it needs from other GPUs, computes its portion of the forward pass, then discards the gathered parameters. The backward pass proceeds similarly.

For BERT-base with 8 GPUs:

- Without ZeRO: Each GPU stores 440 MB of parameters
- With ZeRO-3: Each GPU stores  $440/8 = 55$  MB of parameters
- Total memory saved:  $770 + 385 + 385 = 1,540$  MB per GPU

ZeRO-3 enables training models that wouldn't fit on any single GPU by distributing all memory across the cluster. For GPT-3 with 175B parameters requiring 700 GB in FP32, ZeRO-3 across 64 A100 GPUs (80 GB each) reduces per-GPU memory to  $700/64 \approx 11$  GB, making training feasible.

The communication overhead of ZeRO increases with each stage. ZeRO-1 has minimal overhead (only during optimizer step). ZeRO-2 adds gradient communication (similar to data parallelism). ZeRO-3 adds parameter communication during forward and backward passes, which can be significant but is often acceptable given the memory savings.

### 11.8.6 Comparison of Strategies

In practice, large-scale training often combines multiple strategies. GPT-3 training used a combination of data parallelism, model parallelism, and pipeline parallelism across thousands of GPUs. Modern frameworks like DeepSpeed and Megatron-LM provide implementations of these strategies that can be combined flexibly based on model size and available hardware.

Strategy	Memory Reduction	Communication	Use Case
Data Parallel	None	Gradients	Small models, many GPUs
Model Parallel	$N \times$	Activations	Large models, sequential
Pipeline Parallel	$N \times$	Activations	Very large models
Tensor Parallel	$N \times$	Activations (small)	Huge layers
ZeRO Stage 1	$4 \times$	Minimal	Optimizer memory bound
ZeRO Stage 2	$8 \times$	Gradients	Gradient memory bound
ZeRO Stage 3	$N \times$	All	Extreme scale

Table 11.1: Comparison of distributed training strategies for  $N$  GPUs

## 11.9 Batch Size and Sequence Length Selection

Selecting appropriate batch sizes and sequence lengths is crucial for efficient transformer training. These choices directly impact memory consumption, training throughput, convergence behavior, and final model quality. The optimal configuration depends on the interplay between hardware constraints, model architecture, and training objectives.

### 11.9.1 Batch Size Considerations

Batch size affects both computational efficiency and optimization dynamics. Larger batches improve GPU utilization by amortizing the cost of loading model parameters and by providing more parallelism for matrix operations. Modern GPUs achieve peak performance with large matrix multiplications, and larger batches create larger matrices that better utilize the hardware.

For BERT-base on an NVIDIA A100, throughput (tokens processed per second) increases significantly with batch size:

- Batch size 8:  $\approx 15,000$  tokens/sec (30% GPU utilization)
- Batch size 32:  $\approx 50,000$  tokens/sec (80% GPU utilization)
- Batch size 64:  $\approx 70,000$  tokens/sec (90% GPU utilization)
- Batch size 128:  $\approx 75,000$  tokens/sec (95% GPU utilization)

Beyond batch size 64, the throughput gains diminish because the GPU is already well-utilized. The optimal batch size for throughput is typically where GPU utilization reaches 85-95%, which depends on the model size and sequence length.

However, larger batches are not always better for optimization. Very large batches can hurt generalization, a phenomenon known as the "generalization gap." The intuition is that large batches provide very accurate gradient estimates, which can lead the optimizer to sharp minima that don't generalize well. Smaller batches provide noisier gradients that help the optimizer find flatter minima with better generalization.

The relationship between batch size and generalization is complex and depends on the learning rate schedule and total training budget. Research has shown that the generalization gap can be mitigated by:

- Scaling the learning rate proportionally with batch size (linear scaling rule)
- Extending the warmup period for larger batches
- Training for more steps to compensate for fewer parameter updates

For transformer training, batch sizes of 256-2048 are typical. BERT-base uses an effective batch size of 256 (32 per GPU  $\times$  8 GPUs). GPT-2 uses batch sizes of 512-1024. GPT-3 uses batch sizes up to 3.2 million tokens (approximately 1600 sequences of length 2048), enabled by LAMB optimizer and massive parallelism.

### 11.9.2 Memory Scaling with Batch Size

Memory consumption scales linearly with batch size for most components. For BERT-base with sequence length 512:

$$\text{Batch size 8:} \quad \approx 3.5 \text{ GB} \quad (11.51)$$

$$\text{Batch size 16:} \quad \approx 6.8 \text{ GB} \quad (11.52)$$

$$\text{Batch size 32:} \quad \approx 13.8 \text{ GB} \quad (11.53)$$

$$\text{Batch size 64:} \quad \approx 27.6 \text{ GB} \quad (11.54)$$

The linear scaling means that doubling the batch size doubles the memory requirement. This quickly exceeds single-GPU capacity, necessitating either gradient accumulation (to simulate large batches with small physical batches) or distributed training (to split the batch across multiple GPUs).

The memory breakdown for batch size 32 is approximately:

- Parameters + optimizer: 1.76 GB (independent of batch size)
- Activations: 12 GB (scales linearly with batch size)

Since activations dominate, techniques that reduce activation memory (mixed precision, gradient checkpointing) have a large impact on the maximum feasible batch size.

### 11.9.3 Sequence Length Considerations

Sequence length has a more complex impact on memory and computation than batch size. The attention mechanism’s quadratic scaling means that memory and computation grow as  $O(n^2)$  for sequence length  $n$ , while other components grow linearly as  $O(n)$ .

For BERT-base with batch size 32, memory consumption varies dramatically with sequence length:

$$\text{Sequence length 128:} \quad \approx 3.5 \text{ GB} \quad (11.55)$$

$$\text{Sequence length 256:} \quad \approx 6.2 \text{ GB} \quad (11.56)$$

$$\text{Sequence length 512:} \quad \approx 13.8 \text{ GB} \quad (11.57)$$

$$\text{Sequence length 1024:} \quad \approx 42 \text{ GB} \quad (11.58)$$

Doubling the sequence length from 512 to 1024 roughly triples the memory (not quadruples, because some components scale linearly). The attention matrices grow quadratically: for 12 heads, the attention memory is  $32 \times 12 \times n^2 \times 4$  bytes. At  $n = 512$ , this is 403 MB; at  $n = 1024$ , this is 1.6 GB; at  $n = 2048$ , this is 6.4 GB.

The quadratic scaling limits practical sequence lengths. BERT uses  $n = 512$ , GPT-2 uses  $n = 1024$ , GPT-3 uses  $n = 2048$ . Longer sequences require either:

- Efficient attention mechanisms (sparse attention, linear attention) that reduce the  $O(n^2)$  complexity
- Gradient checkpointing to reduce activation memory
- Smaller batch sizes to fit within memory constraints
- More powerful GPUs with larger memory

The choice of sequence length depends on the task. For tasks requiring long-range dependencies (document classification, long-form generation), longer sequences are beneficial despite the computational cost. For tasks with local dependencies (named entity recognition, part-of-speech tagging), shorter sequences may suffice.

### 11.9.4 Dynamic Batching

Dynamic batching groups sequences of similar length together to minimize padding waste. In a typical batch, sequences have varying lengths, and all sequences are padded to the length of the longest sequence in the batch. This padding wastes computation and memory on padding tokens that don't contribute to learning.

For example, if a batch contains sequences of lengths [128, 256, 512, 512], all sequences are padded to 512, wasting:

$$(512 - 128) + (512 - 256) + 0 + 0 = 640 \text{ tokens} \quad (11.59)$$

Out of  $4 \times 512 = 2048$  total tokens, 640 (31%) are padding.

Dynamic batching sorts sequences by length and groups similar lengths together. This reduces padding significantly. If we instead batch [128, 128, 128, 128] and [512, 512, 512, 512] separately, there's no padding waste within each batch.

The throughput improvement from dynamic batching can be substantial:

- Without dynamic batching: 50,000 tokens/sec (including padding)
- With dynamic batching: 70,000 tokens/sec (40% improvement)

The improvement depends on the length distribution in the dataset. For datasets with highly variable lengths, dynamic batching can provide 2-3 $\times$  throughput improvements. For datasets with uniform lengths, the benefit is minimal.

Dynamic batching is implemented by sorting the dataset by sequence length before creating batches, or by using a bucketing strategy that assigns sequences to length buckets and samples batches from within buckets. Most modern training frameworks (Hugging Face Transformers, fairseq) support dynamic batching.

### 11.9.5 Practical Guidelines

Based on the analysis above, practical guidelines for batch size and sequence length selection are:

**For batch size:**

- Start with the largest batch size that fits in GPU memory
- If memory-constrained, use gradient accumulation to achieve larger effective batch sizes
- For BERT-base on V100 (16 GB): batch size 16-32 with sequence length 512
- For BERT-base on A100 (40 GB): batch size 32-64 with sequence length 512
- Scale learning rate proportionally when increasing batch size
- Extend warmup period for very large batches ( $\geq 1024$ )

**For sequence length:**

- Use the longest sequence length that fits in memory and is relevant for the task
- For memory-constrained scenarios, reduce batch size rather than sequence length if long context is important
- Use gradient checkpointing to enable longer sequences
- Consider efficient attention mechanisms for sequences longer than 2048
- Use dynamic batching to reduce padding waste

**Memory-constrained optimization:**

1. Enable mixed precision training (FP16/BF16): 40-50% memory reduction

2. Enable gradient checkpointing: 80% activation memory reduction
3. Use gradient accumulation: simulate large batches with small physical batches
4. Reduce sequence length if task permits
5. Use dynamic batching to reduce padding waste

These techniques can be combined. For example, BERT-base with mixed precision + gradient checkpointing can train with batch size 128 and sequence length 512 on a V100 (16 GB), compared to batch size 16 without these optimizations.

## 11.10 Regularization Techniques

Regularization prevents overfitting by constraining the model's capacity or adding noise during training. Transformers, with their large parameter counts, are particularly susceptible to overfitting on small datasets. Effective regularization enables transformers to generalize well from training data to unseen examples.

### 11.10.1 Dropout

Dropout randomly sets activations to zero during training with probability  $p$ , forcing the model to learn robust features that don't rely on any single activation. During inference, dropout is disabled, and activations are scaled by  $(1 - p)$  to maintain the expected magnitude.

In transformers, dropout is applied at multiple locations:

**Attention dropout:** Applied to the attention weights after softmax, before multiplying by values:

$$\mathbf{O} = \text{Dropout}\left(\text{softmax}\left(\frac{\mathbf{Q}\mathbf{K}^\top}{\sqrt{d_k}}\right)\right)\mathbf{V} \quad (11.60)$$

This prevents the model from relying too heavily on specific attention patterns, encouraging it to learn diverse attention strategies.

**Residual dropout:** Applied to the output of each sub-layer before adding to the residual connection:

$$\mathbf{y} = \mathbf{x} + \text{Dropout}(\text{Sublayer}(\mathbf{x})) \quad (11.61)$$

This regularizes the transformations learned by attention and feed-forward layers.

**Embedding dropout:** Applied to the sum of token embeddings and positional encodings:

$$\mathbf{x} = \text{Dropout}(\text{TokenEmbed}(x) + \text{PositionalEncoding}(x)) \quad (11.62)$$

This prevents overfitting to specific token representations.

Typical dropout rates for transformers are relatively low compared to other architectures. BERT uses  $p = 0.1$  (10% dropout) for all dropout locations. GPT-2 also uses  $p = 0.1$ . Larger models sometimes use even lower dropout rates ( $p = 0.05$  or less) because their increased capacity provides implicit regularization.

The dropout rate should be tuned based on the dataset size and model capacity. For small datasets (thousands of examples), higher dropout rates ( $p = 0.2$  or  $p = 0.3$ ) may be beneficial. For large datasets (millions of examples), lower dropout rates ( $p = 0.1$  or less) are typically sufficient.

### 11.10.2 Weight Decay

Weight decay adds an L2 penalty to the loss function, encouraging parameters to remain small. In the context of AdamW (the standard optimizer for transformers), weight decay is applied directly to parameters rather than through the gradient:

$$\mathbf{w}_{t+1} = \mathbf{w}_t - \eta \frac{\hat{\mathbf{m}}_t}{\sqrt{\hat{\mathbf{v}}_t} + \epsilon} - \eta \lambda \mathbf{w}_t \quad (11.63)$$

The weight decay coefficient  $\lambda$  controls the strength of regularization. Typical values for transformer training are  $\lambda = 0.01$  or  $\lambda = 0.001$ . BERT uses  $\lambda = 0.01$ , which provides moderate regularization without overly constraining the model.

Weight decay is not applied uniformly to all parameters. Biases and layer normalization parameters (scale  $\gamma$  and shift  $\beta$ ) are typically excluded from weight decay. The reasoning is that these parameters control the scale and offset of activations rather than the complexity of learned features, and regularizing them can hurt performance. In practice, this exclusion is implemented by creating separate parameter groups in the optimizer with different weight decay settings.

The interaction between weight decay and learning rate is important. Because weight decay is applied with coefficient  $\eta\lambda$ , the effective regularization strength increases with the learning rate. During warmup, when the learning rate is small, weight decay has minimal effect. As the learning rate increases, weight decay becomes stronger. During decay, as the learning rate decreases, weight decay weakens. This dynamic regularization schedule often works well in practice.

### 11.10.3 Label Smoothing

Label smoothing replaces hard one-hot targets with soft targets that assign small probabilities to incorrect classes. For a classification problem with vocabulary size  $V$  and true class  $y$ , the smoothed target distribution is:

$$q(k) = \begin{cases} 1 - \epsilon + \frac{\epsilon}{V} & \text{if } k = y \\ \frac{\epsilon}{V} & \text{if } k \neq y \end{cases} \quad (11.64)$$

where  $\epsilon$  is the smoothing parameter, typically  $\epsilon = 0.1$ .

Label smoothing prevents the model from becoming overconfident in its predictions. Without smoothing, the model is trained to assign probability 1 to the correct class and probability 0 to all other classes. This can lead to overconfident predictions that don't reflect the model's true uncertainty. With smoothing, the model is trained to assign high probability to the correct class but also small probabilities to other classes, leading to better-calibrated predictions.

For language modeling with vocabulary size 30,000 and  $\epsilon = 0.1$ :

$$\text{Correct class: } q(y) = 1 - 0.1 + \frac{0.1}{30000} = 0.900003 \quad (11.65)$$

$$\text{Incorrect classes: } q(k) = \frac{0.1}{30000} = 0.0000033 \quad (11.66)$$

The smoothed target assigns 90% probability to the correct class and distributes the remaining 10% uniformly across all classes.

Label smoothing is particularly beneficial for tasks with ambiguous labels or where multiple outputs could be considered correct. In machine translation, for example, multiple translations may be valid, and label smoothing encourages the model to consider alternatives rather than committing entirely to the reference translation.

The cross-entropy loss with label smoothing is:

$$L = - \sum_{k=1}^V q(k) \log p(k) = -(1 - \epsilon) \log p(y) - \frac{\epsilon}{V} \sum_{k=1}^V \log p(k) \quad (11.67)$$

The second term is the negative entropy of the predicted distribution, which encourages the model to maintain some uncertainty rather than collapsing to a single prediction.

### 11.10.4 Gradient Clipping

Gradient clipping prevents exploding gradients by limiting the norm of the gradient vector. If the gradient norm exceeds a threshold  $\theta$ , the gradient is scaled down:

$$\mathbf{g} \leftarrow \begin{cases} \mathbf{g} & \text{if } \|\mathbf{g}\|_2 \leq \theta \\ \frac{\theta \mathbf{g}}{\|\mathbf{g}\|_2} & \text{if } \|\mathbf{g}\|_2 > \theta \end{cases} \quad (11.68)$$

The typical threshold for transformer training is  $\theta = 1.0$ . This value is chosen empirically and works well across different model sizes and tasks.

Gradient clipping is essential for training stability, particularly in the early stages of training when gradients can be very large. Without clipping, occasional large gradients can cause the parameters to jump to regions of the loss landscape with poor gradients, derailing training. With clipping, these large gradients are tamed, allowing training to proceed smoothly.

The clipping threshold should be tuned based on the typical gradient norms observed during training. If gradients are frequently clipped, the threshold may be too low, preventing the model from making necessary large updates. If gradients are rarely clipped, the threshold may be too high, providing insufficient protection against exploding gradients. Monitoring the fraction of steps where clipping occurs (typically 1-5%) helps tune the threshold.

Gradient clipping interacts with the learning rate: with a lower learning rate, gradients have less impact, so clipping is less necessary. With a higher learning rate, clipping becomes more important. The combination of learning rate warmup and gradient clipping provides robust training stability.

## 11.11 Training Time and Cost Estimates

Training costs for transformers scale dramatically with model size, spanning several orders of magnitude from models accessible to academic labs to those requiring industrial-scale infrastructure. Table 11.2 summarizes the approximate costs for representative models, assuming cloud GPU pricing of \$3–4 per V100 GPU-hour.

Model	Parameters	Hardware	Training Time	Estimated Cost
BERT-base	110M	16× V100	3–4 days	\$6,000–7,000
GPT-2 XL	1.5B	32× V100	~1 week	\$20,000–50,000
GPT-3	175B	10,000+ V100-equiv.	~1 month	\$4–12 million

Table 11.2: Training cost estimates for representative transformer models. GPT-2 upper range includes experimentation and hyperparameter tuning. GPT-3 cost varies with hardware efficiency and bulk pricing.

The cost increases by 3–4 orders of magnitude from BERT-base to GPT-3, while performance improvements, though substantial, exhibit diminishing returns. For many applications, smaller models fine-tuned on task-specific data provide excellent performance at a fraction of the cost.

**Key Point 11.1. *Scaling Laws.*** Research on neural scaling laws shows that for a fixed compute budget  $C$ , the optimal allocation favors larger models:  $P \propto C^{0.73}$  and  $D \propto C^{0.27}$ , where  $P$  is model size and  $D$  is dataset size. This means most additional compute should go toward larger models rather than more data, and it explains the trend toward ever-larger architectures.

**Key Point 11.2. *Practical Training Recipe.*** For a complete training recipe, combine the techniques from this chapter: AdamW optimizer with warmup and cosine decay, mixed precision training, gradient accumulation for large effective batch sizes, and gradient clipping for stability. See Chapter 23 for a practitioner-oriented decision guide.

## 11.12 Exercises



**Exercise 11.1.** Implement the complete mixed precision training algorithm for a small transformer. Compare memory consumption and training time with FP32 training. Experiment with different loss scaling factors and observe their impact on training stability.

**Exercise 11.2.** For BERT-base with batch size 32 and sequence length 512, calculate the exact memory requirements for: (a) parameters and optimizer states (AdamW), (b) activations for each layer type, (c) total memory with and without gradient checkpointing. Verify your calculations by profiling actual memory usage during training.

**Exercise 11.3.** Implement gradient accumulation to achieve an effective batch size of 512 with physical batch size 32. Measure the training time overhead compared to true batch size 512 (if it fits in memory). Verify that the training dynamics are identical by comparing loss curves.

**Exercise 11.4.** Train a small transformer (6 layers,  $d_{\text{model}} = 256$ ) with different learning rate schedules: (a) warmup + linear decay, (b) warmup + inverse square root decay, (c) warmup + cosine annealing. Compare convergence speed and final performance. Plot the learning rate curves and loss curves.

**Exercise 11.5.** Implement data parallelism for training on 4 GPUs. Measure the speedup compared to single-GPU training. Calculate the communication overhead by comparing the time spent in AllReduce operations versus computation. Experiment with different batch sizes and observe how they affect the computation-to-communication ratio.

**Exercise 11.6.** Analyze the impact of different regularization techniques on a small transformer trained on a limited dataset (10,000 examples). Compare: (a) no regularization, (b) dropout only, (c) weight decay only, (d) dropout + weight decay, (e) dropout + weight decay + label smoothing. Measure training loss, validation loss, and generalization gap.

**Exercise 11.7.** Estimate the training time and cost for a GPT-2 medium model (345M parameters) on your available hardware. Calculate: (a) FLOPs per training step, (b) expected throughput (tokens/sec), (c) total training time for 10B tokens, (d) estimated cost on cloud platforms. Compare your estimates with actual training runs.

**Exercise 11.8.** Implement dynamic batching to minimize padding waste. Compare throughput (tokens/sec) with and without dynamic batching on a dataset with variable-length sequences.

Measure the padding fraction in each case and calculate the theoretical maximum speedup from eliminating padding.

## 11.13 Solutions

Full solutions for all exercises are available at <https://deeplearning.hofkensvermeulen.be>.

# Chapter 12

## Computational Analysis of Transformers

### Chapter Overview

Understanding computational requirements is crucial for deploying transformers. This chapter analyzes time and space complexity, memory footprints, and inference costs. We derive exact FLOP counts, memory requirements, and scaling laws for transformers of different sizes.

### Learning Objectives

1. Calculate FLOPs for transformer forward and backward passes
2. Analyze memory requirements for training and inference
3. Understand scaling laws for model size, data, and compute
4. Optimize inference through batching and caching
5. Estimate training time and costs for large models

### 12.1 Computational Complexity

Understanding the computational complexity of transformers is essential for making informed decisions about model architecture, hardware requirements, and deployment strategies. The transformer’s computational profile differs fundamentally from recurrent architectures, trading sequential dependencies for quadratic memory scaling—a trade-off that profoundly impacts both training and inference.

#### 12.1.1 Self-Attention Complexity

Self-attention is the defining operation of transformers, and its computational characteristics determine much of the model’s behavior. For a sequence of length  $n$  with model dimension  $d_{\text{model}}$ , we analyze each component of the attention mechanism in detail.

**QKV Projections:** The first step projects the input  $\mathbf{X} \in \mathbb{R}^{n \times d_{\text{model}}}$  into query, key, and value spaces. Each projection is a matrix multiplication:

$$\mathbf{Q} = \mathbf{X}\mathbf{W}^Q, \quad \mathbf{K} = \mathbf{X}\mathbf{W}^K, \quad \mathbf{V} = \mathbf{X}\mathbf{W}^V \quad (12.1)$$

where  $\mathbf{W}^Q, \mathbf{W}^K, \mathbf{W}^V \in \mathbb{R}^{d_{\text{model}} \times d_k}$  (typically  $d_k = d_{\text{model}}/h$  for  $h$  heads).

Each matrix multiplication  $\mathbf{X}\mathbf{W}$  requires  $2nd_{\text{model}}d_k$  floating-point operations (FLOPs): for each of  $n \times d_k$  output elements, we perform  $d_{\text{model}}$  multiply-add operations. With three projections:

$$\text{QKV FLOPs} = 3 \times 2nd_{\text{model}}d_k = 6nd_{\text{model}}d_k \quad (12.2)$$

For the common case where  $d_k = d_{\text{model}}$  (single-head or considering all heads together):

$$\text{QKV FLOPs} = 6nd_{\text{model}}^2 \quad (12.3)$$

**Why this matters for hardware:** These are dense matrix multiplications, which achieve high utilization on modern GPUs. NVIDIA A100 GPUs can perform up to 312 TFLOPS (FP16 with Tensor Cores), meaning these projections are typically compute-bound rather than memory-bound. However, for small batch sizes or short sequences, the operations may become memory-bandwidth limited, achieving only 10-20% of peak FLOPS.

**Attention Score Computation:** Computing  $\mathbf{S} = \mathbf{Q}\mathbf{K}^\top$  involves multiplying  $\mathbf{Q} \in \mathbb{R}^{n \times d_k}$  by  $\mathbf{K}^\top \in \mathbb{R}^{d_k \times n}$ , producing  $\mathbf{S} \in \mathbb{R}^{n \times n}$ :

$$\text{Score FLOPs} = 2n^2d_k \quad (12.4)$$

The attention matrix  $\mathbf{S}$  has  $n^2$  elements, and computing each requires  $d_k$  multiply-add operations. This quadratic scaling in sequence length is the fundamental bottleneck for long-context transformers.

**Dimension tracking example:** For BERT-base with  $n = 512$ ,  $d_k = 64$  (per head), and  $h = 12$  heads:

$$\mathbf{Q}^{(i)} \in \mathbb{R}^{512 \times 64} \quad (\text{one head}) \quad (12.5)$$

$$\mathbf{K}^{(i)\top} \in \mathbb{R}^{64 \times 512} \quad (12.6)$$

$$\mathbf{S}^{(i)} = \mathbf{Q}^{(i)}\mathbf{K}^{(i)\top} \in \mathbb{R}^{512 \times 512} \quad (262,144 \text{ elements!}) \quad (12.7)$$

Across 12 heads, we compute 12 separate  $512 \times 512$  attention matrices, requiring:

$$12 \times 2 \times 512^2 \times 64 = 402,653,184 \text{ FLOPs} \approx 403 \text{ MFLOPs} \quad (12.8)$$

**Hardware implications:** The attention matrix requires  $n^2$  memory per head. For  $n = 512$  and 12 heads with FP32:

$$12 \times 512^2 \times 4 \text{ bytes} = 12,582,912 \text{ bytes} \approx 12 \text{ MB} \quad (12.9)$$

This seems modest, but for  $n = 2048$  (GPT-2):  $12 \times 2048^2 \times 4 = 201 \text{ MB}$  per sequence. With batch size 32: 6.4 GB just for attention matrices! This is why long-context models require substantial GPU memory.

**Softmax and Scaling:** Applying softmax to each row of  $\mathbf{S}$  requires  $O(n^2)$  operations (exponentials and normalization), which is negligible compared to the matrix multiplications but can become significant for very long sequences due to memory access patterns.

**Attention Output:** Computing  $\mathbf{O} = \mathbf{A}\mathbf{V}$  multiplies the attention weights  $\mathbf{A} \in \mathbb{R}^{n \times n}$  by values  $\mathbf{V} \in \mathbb{R}^{n \times d_v}$ :

$$\text{Output FLOPs} = 2n^2d_v \quad (12.10)$$

Again, this scales quadratically with sequence length. For  $d_v = d_k$ :

$$\text{Attention output FLOPs} = 2n^2d_k \quad (12.11)$$

**Output Projection:** Finally, concatenated head outputs are projected back to model dimension:

$$\text{Output projection FLOPs} = 2n(hd_k)d_{\text{model}} = 2nd_{\text{model}}^2 \quad (12.12)$$

(assuming  $hd_k = d_{\text{model}}$ ).

**Total Self-Attention FLOPs:**

$$\text{Total} = 6nd_{\text{model}}^2 + 2n^2d_kh + 2n^2d_vh + 2nd_{\text{model}}^2 = 8nd_{\text{model}}^2 + 4n^2d_{\text{model}} \quad (12.13)$$

For typical configurations where  $d_k = d_v = d_{\text{model}}/h$ :

$$\boxed{\text{Self-Attention FLOPs} = 8nd_{\text{model}}^2 + 4n^2d_{\text{model}}} \quad (12.14)$$

**Complexity regime analysis:** The relative importance of the two terms depends on the ratio  $n/d_{\text{model}}$ :

- **Short sequences** ( $n \ll d_{\text{model}}$ ): The  $8nd_{\text{model}}^2$  term dominates. For BERT-base with  $n = 128$ ,  $d = 768$ :  $8 \times 128 \times 768^2 \approx 603\text{M}$  vs  $4 \times 128^2 \times 768 \approx 50\text{M}$ . The projections dominate.
- **Long sequences** ( $n \gg d_{\text{model}}$ ): The  $4n^2d_{\text{model}}$  term dominates. For  $n = 8192$ ,  $d = 768$ :  $8 \times 8192 \times 768^2 \approx 38.7\text{G}$  vs  $4 \times 8192^2 \times 768 \approx 206\text{G}$ . The attention computation dominates.
- **Crossover point**: When  $8nd_{\text{model}}^2 \approx 4n^2d_{\text{model}}$ , solving gives  $n \approx 2d_{\text{model}}$ . For  $d = 768$ , this occurs around  $n \approx 1536$ .

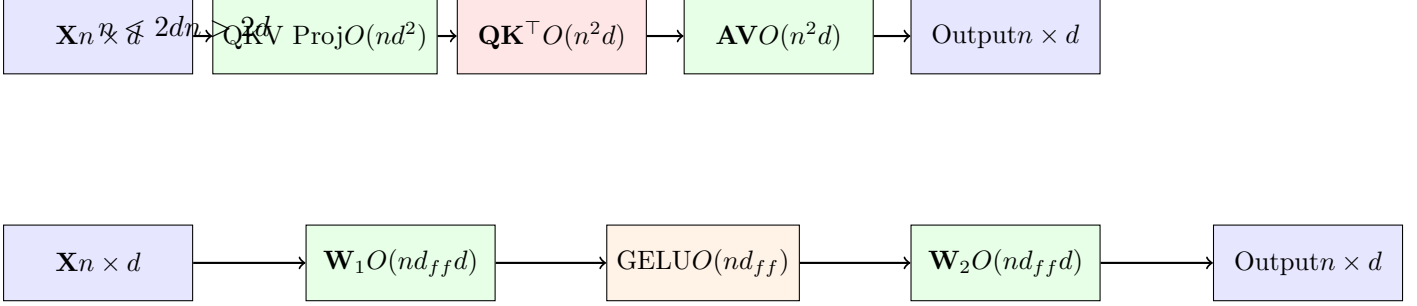


Figure 12.1: Computational flow comparison between self-attention and feed-forward network. Green boxes show matrix multiplications (compute-intensive), red shows the quadratic attention bottleneck, orange shows element-wise operations. For typical sequence lengths, FFN requires roughly  $2\times$  the FLOPs of attention.

This analysis explains why efficient attention mechanisms (Chapter 16) focus on reducing the  $O(n^2)$  term for long-context applications.

### 12.1.2 Feed-Forward Network Complexity

The position-wise feed-forward network (FFN) in each transformer layer typically expands the representation to a higher dimension before projecting back. This two-layer network with GELU or ReLU activation is applied independently to each position in the sequence.

**Architecture:** For input  $\mathbf{X} \in \mathbb{R}^{n \times d_{\text{model}}}$ :

$$\mathbf{H} = \text{GELU}(\mathbf{X}\mathbf{W}_1 + \mathbf{b}_1) \quad \mathbf{W}_1 \in \mathbb{R}^{d_{\text{model}} \times d_{ff}}, \quad \mathbf{H} \in \mathbb{R}^{n \times d_{ff}} \quad (12.15)$$

$$\mathbf{Y} = \mathbf{H}\mathbf{W}_2 + \mathbf{b}_2 \quad \mathbf{W}_2 \in \mathbb{R}^{d_{ff} \times d_{\text{model}}}, \quad \mathbf{Y} \in \mathbb{R}^{n \times d_{\text{model}}} \quad (12.16)$$

The intermediate dimension  $d_{ff}$  is typically  $4d_{\text{model}}$  in standard transformers (BERT, GPT), though some models use different ratios. This expansion allows the network to learn complex non-linear transformations.

**First Projection FLOPs:** Computing  $\mathbf{X}\mathbf{W}_1$  requires:

$$\text{First projection} = 2n \cdot d_{\text{model}} \cdot d_{ff} \quad (12.17)$$

For  $d_{ff} = 4d_{\text{model}}$ :

$$\text{First projection} = 2n \cdot d_{\text{model}} \cdot 4d_{\text{model}} = 8nd_{\text{model}}^2 \quad (12.18)$$

**Second Projection FLOPs:** Computing  $\mathbf{H}\mathbf{W}_2$  requires:

$$\text{Second projection} = 2n \cdot d_{ff} \cdot d_{\text{model}} = 8nd_{\text{model}}^2 \quad (12.19)$$

**Total FFN FLOPs:**

$$\boxed{\text{FFN FLOPs} = 16nd_{\text{model}}^2 \quad (\text{for } d_{ff} = 4d_{\text{model}})} \quad (12.20)$$

**Activation function:** GELU requires additional operations (exponentials, multiplications) but these are  $O(nd_{ff})$ , negligible compared to the matrix multiplications.

**Why FFN dominates computation:** Comparing FFN to self-attention:

$$\text{FFN: } 16nd_{\text{model}}^2 \quad (12.21)$$

$$\text{Attention: } 8nd_{\text{model}}^2 + 4n^2d_{\text{model}} \quad (12.22)$$

For typical sequence lengths where  $n < 2d_{\text{model}}$ , the FFN requires roughly twice the FLOPs of attention! This is why some efficient transformer variants (e.g., mixture-of-experts) focus on making the FFN more efficient.

**Memory and bandwidth considerations:** The FFN intermediate activations  $\mathbf{H} \in \mathbb{R}^{n \times d_{\text{ff}}}$  must be stored for backpropagation. For BERT-base with  $n = 512$ ,  $d_{\text{ff}} = 3072$ :

$$512 \times 3072 \times 4 \text{ bytes} = 6,291,456 \text{ bytes} \approx 6 \text{ MB per layer} \quad (12.23)$$

With 12 layers and batch size 32:  $6 \times 12 \times 32 = 2.3 \text{ GB}$  just for FFN intermediate activations. This is a significant portion of training memory.

**Hardware utilization:** FFN matrix multiplications are highly regular and achieve excellent GPU utilization (often 70-90% of peak FLOPS on modern GPUs). The operations are:

- **Compute-bound** for reasonable batch sizes and sequence lengths
- **Well-suited for Tensor Cores** on NVIDIA GPUs (FP16/BF16 operations)
- **Easily parallelizable** across the sequence dimension

On an NVIDIA A100 GPU (312 TFLOPS FP16), computing the FFN for BERT-base with batch size 32 and  $n = 512$ :

$$\text{FLOPs} = 32 \times 16 \times 512 \times 768^2 \approx 154 \text{ GFLOPS} \quad (12.24)$$

$$\text{Time} \approx \frac{154 \text{ GFLOPS}}{312 \times 0.8 \text{ TFLOPS}} \approx 0.62 \text{ ms} \quad (12.25)$$

(assuming 80% utilization).

### 12.1.3 Per-Layer Total Complexity

Combining self-attention and FFN, a complete transformer layer requires:

$$\boxed{\text{Transformer layer} = (8nd_{\text{model}}^2 + 4n^2d_{\text{model}}) + 16nd_{\text{model}}^2 = 24nd_{\text{model}}^2 + 4n^2d_{\text{model}} \text{ FLOPs}} \quad (12.26)$$

**Additional operations:** Layer normalization, residual connections, and dropout add  $O(nd_{\text{model}})$  operations, which are negligible compared to the matrix multiplications.

**Breakdown by component:**

- **FFN:**  $16nd_{\text{model}}^2$  (typically 60-70% of layer FLOPs for short sequences)
- **Attention projections:**  $8nd_{\text{model}}^2$  (typically 25-35%)
- **Attention computation:**  $4n^2d_{\text{model}}$  (grows with sequence length)

This breakdown is crucial for optimization: for short sequences, optimizing FFN yields the largest gains; for long sequences, efficient attention mechanisms become critical.

**Example 12.1** (BERT-base Single Layer: FLOPs Summary). BERT-base ( $n = 512$ ,  $d_{\text{model}} = 768$ ,  $h = 12$ ,  $d_{\text{ff}} = 3072$ ) illustrates the component-level FLOPs breakdown. Self-attention totals 3.21 GFLOPs per layer (QKV projections: 1.81 G, attention scores: 0.40 G each for  $\mathbf{QK}^\top$  and  $\mathbf{AV}$ , output projection: 0.60 G). The feed-forward network totals 4.84 GFLOPs (two projections of 2.42 G each). The complete layer costs 8.05 GFLOPs, giving 96.6 GFLOPs for the 12-layer forward pass and  $\approx 290$  GFLOPs for a full training step.

On an NVIDIA A100 (312 TFLOPS FP16, 70% utilization), this yields a batch-of-32 forward pass in  $\approx 14$  ms and throughput of  $\approx 390,000$  tokens/sec. At 1.6 TB/s memory bandwidth, loading 440 MB of parameters takes 0.28 ms—comparable to compute time, making small-batch inference

memory-bandwidth bound.

See Section 1.7 for the step-by-step derivation.

### 12.1.4 Complexity Analysis

**Theorem 12.1** (Transformer Complexity). *For  $L$  layers, sequence length  $n$ , dimension  $d$ :*

*Time complexity:*  $O(Ln^2d + Lnd^2)$

*Space complexity:*  $O(Ln^2 + Lnd)$

#### Comparison with RNN:

- RNN:  $O(Lnd^2)$  time,  $O(Ld^2)$  space
- Transformer: Quadratic in  $n$  but parallel; RNN sequential

#### Bottleneck regimes:

- Short sequences ( $n < d$ ): FFN dominates,  $O(Lnd^2)$
- Long sequences ( $n > d$ ): Attention dominates,  $O(Ln^2d)$

## 12.2 Memory Requirements

Memory is often the limiting factor in training and deploying large transformer models. Understanding memory requirements at a granular level enables informed decisions about model architecture, batch sizes, and hardware selection. We analyze memory consumption across four categories: model parameters, gradients, optimizer states, and activations.

### 12.2.1 Model Parameters

Model parameters must be stored in GPU memory during both training and inference. The memory footprint depends on the numerical precision used.

#### Precision options:

- **FP32 (float32)**: 4 bytes per parameter, standard precision
- **FP16 (float16)**: 2 bytes per parameter, half precision
- **BF16 (bfloat16)**: 2 bytes per parameter, better range than FP16
- **INT8**: 1 byte per parameter, quantized inference

For BERT-base with 110 million parameters:

$$\text{FP32: } 110,000,000 \times 4 = 440,000,000 \text{ bytes} = 440 \text{ MB} \quad (12.27)$$

$$\text{FP16/BF16: } 110,000,000 \times 2 = 220,000,000 \text{ bytes} = 220 \text{ MB} \quad (12.28)$$

$$\text{INT8: } 110,000,000 \times 1 = 110,000,000 \text{ bytes} = 110 \text{ MB} \quad (12.29)$$

#### Parameter breakdown for BERT-base:

$$\text{Token embeddings: } V \times d_{\text{model}} = 30,000 \times 768 = 23,040,000 \text{ params} \quad (12.30)$$

$$\text{Position embeddings: } n_{\text{max}} \times d_{\text{model}} = 512 \times 768 = 393,216 \text{ params} \quad (12.31)$$

$$\text{Segment embeddings: } 2 \times d_{\text{model}} = 2 \times 768 = 1,536 \text{ params} \quad (12.32)$$

Per transformer layer:

$$\text{Self-attention: } 4 \times d_{\text{model}}^2 = 4 \times 768^2 = 2,359,296 \text{ params} \quad (12.33)$$

$$\text{FFN: } 2 \times d_{\text{model}} \times d_{\text{ff}} = 2 \times 768 \times 3072 = 4,718,592 \text{ params} \quad (12.34)$$

$$\text{Layer norms: } 4 \times d_{\text{model}} = 4 \times 768 = 3,072 \text{ params} \quad (12.35)$$

$$\text{Total per layer: } 7,080,960 \text{ params} \quad (12.36)$$

12 layers:

$$12 \times 7,080,960 = 84,971,520 \text{ params} \quad (12.37)$$

Total BERT-base:

$$23,040,000 + 393,216 + 1,536 + 84,971,520 = 108,406,272 \approx 110\text{M params} \quad (12.38)$$

In FP32:  $110\text{M} \times 4 = 440 \text{ MB}$

**Larger models scale dramatically:**

$$\text{GPT-2 (1.5B): } 1,500,000,000 \times 4 = 6,000 \text{ MB} = 6 \text{ GB (FP32)} \quad (12.39)$$

$$\text{GPT-3 (175B): } 175,000,000,000 \times 4 = 700,000 \text{ MB} = 700 \text{ GB (FP32)} \quad (12.40)$$

GPT-3 in FP32 requires 700 GB just for parameters—far exceeding single GPU memory (A100 has 80 GB). This necessitates:

- **Model parallelism:** Split model across multiple GPUs
- **Mixed precision:** Use FP16/BF16 (350 GB for GPT-3)
- **Quantization:** INT8 inference (175 GB for GPT-3)

### 12.2.2 Activation Memory

During training, intermediate activations must be stored for backpropagation. Activation memory scales with batch size and sequence length, often dominating memory consumption.

**Activations per transformer layer:**

- **Input to layer:**  $B \times n \times d_{\text{model}}$
- **Query, Key, Value:**  $3 \times B \times n \times d_{\text{model}}$
- **Attention scores:**  $B \times h \times n \times n$  (quadratic in sequence length!)
- **Attention output:**  $B \times n \times d_{\text{model}}$
- **FFN intermediate:**  $B \times n \times d_{\text{ff}}$
- **Layer norm activations:**  $2 \times B \times n \times d_{\text{model}}$

**Total activation memory per layer (approximate):**

$$\text{Memory} \approx B \times n \times (8d_{\text{model}} + d_{\text{ff}}) + B \times h \times n^2 \quad (12.41)$$

For BERT-base ( $B = 32$ ,  $n = 512$ ,  $d_{\text{model}} = 768$ ,  $h = 12$ ,  $d_{\text{ff}} = 3072$ ):

$$\text{Linear terms: } 32 \times 512 \times (8 \times 768 + 3072) \times 4 \text{ bytes} \quad (12.42)$$

$$= 32 \times 512 \times 9,216 \times 4 = 603,979,776 \text{ bytes} \approx 604 \text{ MB} \quad (12.43)$$

$$\text{Attention matrices: } 32 \times 12 \times 512^2 \times 4 = 402,653,184 \text{ bytes} \approx 403 \text{ MB} \quad (12.44)$$

$$\text{Total per layer: } \approx 1,007 \text{ MB} \approx 1 \text{ GB} \quad (12.45)$$

**For 12 layers:**  $12 \times 1 \text{ GB} = 12 \text{ GB}$  just for activations!



**Impact of sequence length:** The attention matrix term  $B \times h \times n^2$  grows quadratically. For  $n = 2048$  ( $4\times$  longer):

$$32 \times 12 \times 2048^2 \times 4 = 6,442,450,944 \text{ bytes} \approx 6.4 \text{ GB per layer} \quad (12.46)$$

For 12 layers: 77 GB just for attention matrices—nearly filling an A100 GPU!

This quadratic scaling is why:

- Long-context models require gradient checkpointing (recompute activations during backward pass)
- Efficient attention mechanisms (sparse, linear) are crucial for long sequences
- Batch sizes must be reduced for longer sequences

**Gradient checkpointing trade-off:** Recomputing activations during backward pass:

- **Memory savings:** Reduce activation memory by  $\sim 80\%$
- **Compute cost:** Increase training time by  $\sim 20\text{-}30\%$
- **When to use:** When memory-constrained, especially for long sequences

**Example 12.2** (GPT-2 Activation Memory: Complete Analysis). GPT-2 (small):  $L = 12$ ,  $d_{\text{model}} = 768$ ,  $h = 12$ ,  $d_k = 64$ ,  $d_{ff} = 3072$ ,  $n = 1024$

**Per-layer activation breakdown (batch size  $B = 1$ ):**

*QKV projections:*

$$3 \times 1024 \times 768 \times 4 = 9,437,184 \text{ bytes} \approx 9.4 \text{ MB} \quad (12.47)$$

*Attention matrices (12 heads):*

$$12 \times 1024^2 \times 4 = 50,331,648 \text{ bytes} \approx 50.3 \text{ MB} \quad (12.48)$$

This is the dominant term! For  $n = 2048$ :  $12 \times 2048^2 \times 4 = 201 \text{ MB}$  ( $4\times$  larger).

*Attention output:*

$$1024 \times 768 \times 4 = 3,145,728 \text{ bytes} \approx 3.1 \text{ MB} \quad (12.49)$$

*FFN intermediate:*

$$1024 \times 3072 \times 4 = 12,582,912 \text{ bytes} \approx 12.6 \text{ MB} \quad (12.50)$$

*Layer norm and residuals:*

$$3 \times 1024 \times 768 \times 4 = 9,437,184 \text{ bytes} \approx 9.4 \text{ MB} \quad (12.51)$$

*Total per layer:*

$$9.4 + 50.3 + 3.1 + 12.6 + 9.4 = 84.8 \text{ MB} \quad (12.52)$$

**12 layers:**  $12 \times 84.8 = 1,018 \text{ MB} \approx 1 \text{ GB}$  for single sequence

**Batch size scaling:**

$$B = 8 : 8 \text{ GB} \quad (12.53)$$

$$B = 16 : 16 \text{ GB} \quad (12.54)$$

$$B = 32 : 32 \text{ GB} \quad (12.55)$$

$$B = 64 : 64 \text{ GB} \quad (12.56)$$

**Hardware implications:**

- **NVIDIA V100 (16 GB):** Maximum batch size  $\approx 12 - 14$  (accounting for parameters and optimizer states)
- **NVIDIA A100 (40 GB):** Maximum batch size  $\approx 30 - 35$
- **NVIDIA A100 (80 GB):** Maximum batch size  $\approx 70 - 75$

**Gradient checkpointing impact:** With checkpointing, only store activations at layer boundaries, recompute within layers during backward pass:

$$\text{Memory reduction} \approx 80\% \Rightarrow 1 \text{ GB} \rightarrow 200 \text{ MB per sequence} \quad (12.57)$$

This allows batch size 64 on V100 (16 GB), but increases training time by  $\sim 25\%$ .

**Mixed precision training:** Using FP16 for activations (FP32 for parameters):

$$\text{Activation memory} \rightarrow 1 \text{ GB}/2 = 500 \text{ MB per sequence} \quad (12.58)$$

Combined with gradient checkpointing:  $500 \times 0.2 = 100 \text{ MB per sequence}$ , enabling very large batch sizes.

### 12.2.3 Training Memory Budget

Training requires memory for parameters, gradients, optimizer states, and activations. Understanding this breakdown is essential for selecting hardware and configuring training.

**Total training memory:**

$$\text{Memory}_{\text{total}} = \text{Parameters} + \text{Gradients} + \text{Optimizer States} + \text{Activations} \quad (12.59)$$

**For AdamW optimizer (most common for transformers):**

- **Model parameters:**  $P$  parameters  $\times 4$  bytes (FP32)  $= 4P$  bytes
- **Gradients:**  $P$  parameters  $\times 4$  bytes  $= 4P$  bytes
- **First moment (momentum):**  $P$  parameters  $\times 4$  bytes  $= 4P$  bytes
- **Second moment (variance):**  $P$  parameters  $\times 4$  bytes  $= 4P$  bytes
- **Activations:**  $A$  bytes (depends on batch size, sequence length, model depth)

**Total:**  $16P + A$  bytes

**Mixed precision training (FP16/BF16 with FP32 master weights):**

- **FP16 parameters (forward/backward):**  $2P$  bytes
- **FP32 master parameters:**  $4P$  bytes
- **FP32 gradients:**  $4P$  bytes
- **FP32 optimizer states:**  $8P$  bytes
- **FP16 activations:**  $A/2$  bytes

**Total:**  $18P + A/2$  bytes

Surprisingly, mixed precision uses slightly MORE memory for parameters/optimizer (18P vs 16P) but saves significantly on activations ( $A/2$  vs  $A$ ). Since activations often dominate, mixed precision typically reduces total memory.

**Example 12.3** (BERT-base Training Memory Budget). BERT-base: 110M parameters, batch size 32, sequence length 512

**FP32 training:**

$$\text{Parameters: } 110\text{M} \times 4 = 440 \text{ MB} \quad (12.60)$$

$$\text{Gradients: } 110\text{M} \times 4 = 440 \text{ MB} \quad (12.61)$$

$$\text{Adam states (2}\times\text{): } 2 \times 110\text{M} \times 4 = 880 \text{ MB} \quad (12.62)$$

$$\text{Activations: } 32 \times 12 \times 1 \text{ GB} = 12 \text{ GB} \quad (12.63)$$

$$\text{Total: } 440 + 440 + 880 + 12,000 = 13,760 \text{ MB} \approx 13.8 \text{ GB} \quad (12.64)$$

**Fits on:** NVIDIA V100 (16 GB), A100 (40/80 GB), RTX 3090 (24 GB)

**Mixed precision training:**

$$\text{FP16 parameters: } 110\text{M} \times 2 = 220 \text{ MB} \quad (12.65)$$

$$\text{FP32 master + gradients + Adam: } 110\text{M} \times 16 = 1,760 \text{ MB} \quad (12.66)$$

$$\text{FP16 activations: } 12,000/2 = 6,000 \text{ MB} \quad (12.67)$$

$$\text{Total: } 220 + 1,760 + 6,000 = 7,980 \text{ MB} \approx 8 \text{ GB} \quad (12.68)$$

**Mixed precision saves:**  $13.8 - 8 = 5.8 \text{ GB}$  (42% reduction)

**With gradient checkpointing:** Activations reduced by 80%:

$$220 + 1,760 + 1,200 = 3,180 \text{ MB} \approx 3.2 \text{ GB} \quad (12.69)$$

This enables batch size 128 on V100 (16 GB)!

**Example 12.4** (GPT-3 Training Memory Requirements). GPT-3: 175B parameters, sequence length 2048

**Parameters and optimizer (FP32):**

$$175\text{B} \times 16 = 2,800 \text{ GB} \quad (12.70)$$

**Activations (batch size 1, single sequence):**

$$\text{Per layer: } \approx 2048 \times (8 \times 12,288 + 4 \times 12,288) + 96 \times 2048^2 \quad (12.71)$$

$$\approx 2048 \times 147,456 + 402,653,184 \quad (12.72)$$

$$\approx 704 \text{ MB per layer} \quad (12.73)$$

**96 layers:**  $96 \times 704 \text{ MB} \approx 68 \text{ GB}$  per sequence

**Total for batch size 1:**  $2,800 + 68 = 2,868 \text{ GB}$

**Hardware requirements:**

- **Single A100 (80 GB):** Impossible—need 36 GPUs just for parameters!
- **Model parallelism:** Split across 8 GPUs:  $2,868/8 = 359 \text{ GB}$  per GPU—still too large!
- **Mixed precision + model parallelism:**  $\approx 1,500 \text{ GB total}/8 = 188 \text{ GB}$  per GPU—still too large!
- **Mixed precision + model parallelism + gradient checkpointing:**  $\approx 800 \text{ GB}/8 = 100 \text{ GB}$  per GPU—still exceeds A100!

**Actual GPT-3 training:** Used ZeRO optimizer (shards optimizer states across GPUs) + model parallelism + pipeline parallelism across thousands of GPUs.

This example illustrates why training models beyond  $\sim 10\text{B}$  parameters requires sophisticated distributed training strategies.

### 12.2.4 Hardware Selection Guide

**GPU memory requirements by model size (mixed precision + gradient checkpointing):**

Model Size	Parameters	Min GPU Memory	Recommended GPU
Small	100M	8 GB	RTX 3070, V100
Base	300M	12 GB	RTX 3080, V100
Large	1B	24 GB	RTX 3090, A5000
XL	3B	40 GB	A100 (40 GB)
XXL	10B	80 GB	A100 (80 GB)
175B (GPT-3)	175B	$8 \times$ A100 (80 GB)	Multi-node cluster

Table 12.1: GPU memory requirements for training transformer models (batch size 8-16, sequence length 512-1024)

**Inference memory requirements (FP16):**

- **Parameters only:**  $2P$  bytes
- **KV cache (autoregressive):**  $2 \times L \times h \times n_{\max} \times d_k \times B$  bytes
- **Activations (single forward pass):** Minimal compared to training

For GPT-2 (117M params) inference:

$$\text{Parameters: } 117\text{M} \times 2 = 234 \text{ MB} \quad (12.74)$$

$$\text{KV cache (batch 1, } n = 1024\text{): } 2 \times 12 \times 12 \times 1024 \times 64 \times 2 = 38 \text{ MB} \quad (12.75)$$

$$\text{Total: } \approx 300 \text{ MB} \quad (12.76)$$

GPT-2 inference easily fits on consumer GPUs or even CPUs!

## 12.3 Inference Optimization

Inference optimization is critical for deploying transformers in production. Unlike training, which prioritizes throughput (tokens/second across large batches), inference prioritizes latency (time to generate a single response) while maintaining reasonable throughput. We analyze key optimization techniques and their trade-offs.

### 12.3.1 KV Caching for Autoregressive Decoding

Autoregressive generation (used in GPT, decoder-only models) generates tokens sequentially, where each new token attends to all previous tokens. Naive implementation recomputes attention for all previous positions at each step—highly inefficient.

**Problem analysis:** Generating sequence of length  $T$  tokens:

- **Step 1:** Compute attention for position 1 (attends to position 1)
- **Step 2:** Compute attention for position 2 (attends to positions 1-2)
- **Step 3:** Compute attention for position 3 (attends to positions 1-3)

- **Step  $T$ :** Compute attention for position  $T$  (attends to positions 1- $T$ )

**Total attention computations:**  $\sum_{t=1}^T t = \frac{T(T+1)}{2} \approx \frac{T^2}{2}$

For  $T = 1000$  tokens:  $\approx 500,000$  attention computations!

**KV Caching solution:** Key and value projections depend only on input tokens, not on the query position. Cache **K** and **V** from previous steps:

---

**Algorithm 11:** Autoregressive Generation with KV Caching

---

**Input:** Prompt tokens  $\mathbf{x}_1, \dots, \mathbf{x}_p$ , max length  $T$   
**Output:** Generated sequence  $\mathbf{x}_1, \dots, \mathbf{x}_T$   
 // Initialize cache  
 1  $\text{cache}_K = [], \text{cache}_V = []$   
 // Process prompt  
 2 **for**  $t = 1$  **to**  $p$  **do**  
 3      $\mathbf{k}_t = \mathbf{W}^K \mathbf{x}_t, \mathbf{v}_t = \mathbf{W}^V \mathbf{x}_t$   
 4     Append  $\mathbf{k}_t$  to  $\text{cache}_K$ ,  $\mathbf{v}_t$  to  $\text{cache}_V$   
 5      $\mathbf{q}_t = \mathbf{W}^Q \mathbf{x}_t$   
 6     Compute attention using  $\mathbf{q}_t$  and all cached keys/values  
 7     Generate  $\mathbf{h}_t$   
 // Generate new tokens  
 8 **for**  $t = p + 1$  **to**  $T$  **do**  
 9     Sample  $\mathbf{x}_t$  from  $\mathbf{h}_{t-1}$   
 10     $\mathbf{k}_t = \mathbf{W}^K \mathbf{x}_t, \mathbf{v}_t = \mathbf{W}^V \mathbf{x}_t$   
 11    Append  $\mathbf{k}_t$  to  $\text{cache}_K$ ,  $\mathbf{v}_t$  to  $\text{cache}_V$   
 12     $\mathbf{q}_t = \mathbf{W}^Q \mathbf{x}_t$   
 13    Compute attention:  $\text{Attention}(\mathbf{q}_t, \text{cache}_K, \text{cache}_V)$   
 14    Generate  $\mathbf{h}_t$

---

**Computational savings:** With caching, each step computes attention once (not recomputing previous positions):

$$\text{Total computations} = T \quad (\text{vs. } \frac{T^2}{2} \text{ without caching}) \quad (12.77)$$

**Speedup:** For  $T = 1000$ :  $\frac{500,000}{1,000} = 500\times$  faster!

**Memory cost:** Store keys and values for all positions and layers:

$$\text{KV cache size} = 2 \times L \times h \times T \times d_k \times \text{sizeof(float)} \quad (12.78)$$

For GPT-2 ( $L = 12$ ,  $h = 12$ ,  $d_k = 64$ , FP16):

$$2 \times 12 \times 12 \times T \times 64 \times 2 = 36,864 \times T \text{ bytes} \quad (12.79)$$

**Memory scaling with sequence length:**

$$T = 512 : 36,864 \times 512 = 18,874,368 \text{ bytes} \approx 19 \text{ MB} \quad (12.80)$$

$$T = 1024 : 36,864 \times 1024 = 37,748,736 \text{ bytes} \approx 38 \text{ MB} \quad (12.81)$$

$$T = 2048 : 36,864 \times 2048 = 75,497,472 \text{ bytes} \approx 75 \text{ MB} \quad (12.82)$$

$$T = 4096 : 36,864 \times 4096 = 150,994,944 \text{ bytes} \approx 151 \text{ MB} \quad (12.83)$$

For GPT-3, the cache reaches 9.7 GB per sequence (see Chapter 14 for the derivation), nearly filling an A100 for batch size 8 (77.6 GB). Practitioners manage this through smaller batch sizes for long contexts, dynamic batching, and INT8 quantization to reduce cache size by 2–4 $\times$ .

### 12.3.2 Batched Inference

Processing multiple sequences simultaneously increases GPU utilization and throughput.

**Single sequence inference:** For GPT-2 generating 100 tokens:

- **Compute:**  $\approx 100 \times 8 \text{ GFLOPs} = 800 \text{ GFLOPs}$
- **Time on A100:**  $\frac{800 \text{ GFLOPs}}{312 \text{ TFLOPs} \times 0.3} \approx 8.5 \text{ ms}$
- **GPU utilization:**  $\approx 30\%$  (memory-bound, not compute-bound)

**Batched inference (batch size 32):**

- **Compute:**  $32 \times 800 \text{ GFLOPs} = 25,600 \text{ GFLOPs}$
- **Time on A100:**  $\frac{25,600 \text{ GFLOPs}}{312 \text{ TFLOPs} \times 0.7} \approx 117 \text{ ms}$
- **GPU utilization:**  $\approx 70\%$  (much better!)
- **Throughput:**  $\frac{32 \times 100}{117 \text{ ms}} \approx 27,350 \text{ tokens/sec}$

**Latency vs. throughput trade-off:**

- **Batch size 1:** Latency = 8.5 ms, throughput = 11,765 tokens/sec
- **Batch size 32:** Latency = 117 ms (13.8 $\times$  worse), throughput = 27,350 tokens/sec (2.3 $\times$  better)

**Padding challenge:** Sequences in a batch must have the same length. Shorter sequences are padded, wasting computation:

- Sequence lengths: [512, 256, 128, 64]
- Padded to: [512, 512, 512, 512]
- Wasted computation:  $(512 - 256) + (512 - 128) + (512 - 64) = 1024 \text{ positions (50\%)}$

**Solutions:**

- **Dynamic batching:** Group sequences of similar lengths
- **Bucket batching:** Pre-defined length buckets (128, 256, 512, 1024)
- **Packed sequences:** Concatenate sequences without padding (requires careful attention masking)

### 12.3.3 Quantization for Inference

Quantization reduces memory and increases throughput by using lower-precision arithmetic.

**Precision options:**

- **FP32:** 4 bytes, full precision
- **FP16/BF16:** 2 bytes, half precision (1.5-2 $\times$  speedup)
- **INT8:** 1 byte, 8-bit integer (2-4 $\times$  speedup, 4 $\times$  memory reduction)
- **INT4:** 0.5 bytes, 4-bit integer (4-8 $\times$  speedup, 8 $\times$  memory reduction)

**INT8 quantization:** Map FP32 weights  $w \in [-w_{\max}, w_{\max}]$  to INT8  $w_q \in [-128, 127]$ :

$$w_q = \text{round} \left( \frac{w}{w_{\max}} \times 127 \right) \quad (12.84)$$

Dequantize during computation:

$$w \approx \frac{w_q \times w_{\max}}{127} \quad (12.85)$$

**Quantization impact on GPT-2:**

$$\text{FP32: } 117\text{M} \times 4 = 468 \text{ MB} \quad (12.86)$$

$$\text{FP16: } 117\text{M} \times 2 = 234 \text{ MB} \quad (2 \times \text{ reduction}) \quad (12.87)$$

$$\text{INT8: } 117\text{M} \times 1 = 117 \text{ MB} \quad (4 \times \text{ reduction}) \quad (12.88)$$

$$\text{INT4: } 117\text{M} \times 0.5 = 58.5 \text{ MB} \quad (8 \times \text{ reduction}) \quad (12.89)$$

**Accuracy trade-offs:**

- **FP16/BF16:** Negligible accuracy loss (<0.1% perplexity increase)
- **INT8:** Small accuracy loss (0.5-2% perplexity increase) with calibration
- **INT4:** Moderate accuracy loss (2-5% perplexity increase), requires careful quantization

**Hardware support:**

- **NVIDIA Tensor Cores:** Accelerate FP16/BF16 (up to  $2\times$  speedup)
- **NVIDIA INT8 Tensor Cores:** Accelerate INT8 (up to  $4\times$  speedup)
- **CPU AVX-512 VNNI:** Accelerate INT8 on CPUs

**12.3.4 Model Distillation**

Train smaller "student" model to mimic larger "teacher" model:

- **DistilBERT:** 66M params (vs. BERT-base 110M), 97% performance,  $2\times$  faster
- **TinyBERT:** 14M params, 96% performance,  $7\times$  faster

Distillation enables deployment on resource-constrained devices (mobile, edge).

**12.3.5 Inference Optimization Summary**

Technique	Speedup	Memory Reduction	Accuracy Impact
KV Caching	100-500 $\times$	-50% (cache overhead)	None
Batching (32 $\times$ )	2-3 $\times$ throughput	None	None
FP16/BF16	1.5-2 $\times$	2 $\times$	Negligible
INT8 Quantization	2-4 $\times$	4 $\times$	Small (0.5-2%)
INT4 Quantization	4-8 $\times$	8 $\times$	Moderate (2-5%)
Distillation	2-7 $\times$	2-8 $\times$	Small (3-4%)

Table 12.2: Inference optimization techniques and their trade-offs

**Combined optimizations:** KV caching + FP16 + batching + INT8 can achieve  $1000\times$  speedup with minimal accuracy loss!

**12.4 Scaling Laws**

Performance scales as power laws with model size  $N$ , dataset size  $D$ , and compute budget  $C$ . The Kaplan scaling laws established that larger models are more sample-efficient, while the Chinchilla scaling laws (Hoffmann et al., 2022) refined the optimal allocation:  $N_{\text{opt}} \propto C^{0.5}$  and  $D_{\text{opt}} \propto C^{0.5}$ , implying that many large models are over-parameterized and under-trained. See Section 14.4 for the full treatment including GPT-3 vs Chinchilla analysis and practical implications for training strategy.

**12.5 Exercises**

**Exercise 12.1.** Calculate FLOPs for GPT-3 (175B parameters,  $L = 96$ ,  $d = 12288$ ,  $h = 96$ ,  $n = 2048$ ) for: (1) Single forward pass, (2) Generating 100 tokens autoregressively, (3) Training on 1 trillion tokens.

**Exercise 12.2.** Estimate memory for training 1.3B parameter model with batch size 64, sequence length 2048. What GPU memory required? How to fit on A100 (80GB)?

**Exercise 12.3.** Implement KV caching for GPT-2. Measure speedup for generating 256 tokens. Plot generation time vs sequence length with/without caching.

**Exercise 12.4.** For fixed compute budget  $C = 10^{24}$  FLOPs: Use Chinchilla scaling to find optimal model size and data size. Compare with GPT-3 allocation.

## 12.6 Solutions

Full solutions for all exercises are available at <https://deeplearning.hofkensvermeulen.be>.

`function_calls >< invoke_name = "fsAppend" >< parameter_name = "path" > chapters/chapter12_computational`

```
import torch
import torch.nn as nn
import time
import matplotlib.pyplot as plt

class GPT2WithCache(nn.Module):
    def __init__(self, config):
        super().__init__()
        self.transformer = nn.ModuleList([
            GPT2Block(config) for _ in range(config.n_layer)
        ])
        self.ln_f = nn.LayerNorm(config.n_embd)
        self.lm_head = nn.Linear(config.n_embd, config.vocab_size)

    def forward(self, input_ids, past_key_values=None, use_cache=False):
        hidden_states = self.wte(input_ids) + self.wpe(positions)

        presents = [] if use_cache else None

        for i, block in enumerate(self.transformer):
            past = past_key_values[i] if past_key_values else None
            hidden_states, present = block(
                hidden_states,
                past_key_value=past,
                use_cache=use_cache
            )
            if use_cache:
                presents.append(present)

        hidden_states = self.ln_f(hidden_states)
```



```

        logits = self.lm_head(hidden_states)

        return logits, presents

class GPT2Block(nn.Module):
    def forward(self, x, past_key_value=None, use_cache=False):
        # Self-attention with optional KV cache
        attn_output, present = self.attn(
            x,
            past_key_value=past_key_value,
            use_cache=use_cache
        )
        x = x + attn_output
        x = self.ln_1(x)

        # Feed-forward
        x = x + self.mlp(x)
        x = self.ln_2(x)

        return x, present

class GPT2Attention(nn.Module):
    def forward(self, x, past_key_value=None, use_cache=False):
        B, T, C = x.shape

        # Compute Q, K, V
        q, k, v = self.c_attn(x).split(self.n_embd, dim=2)

        # Reshape for multi-head attention
        q = q.view(B, T, self.n_head, C // self.n_head).transpose(1, 2)
        k = k.view(B, T, self.n_head, C // self.n_head).transpose(1, 2)
        v = v.view(B, T, self.n_head, C // self.n_head).transpose(1, 2)

        # Use cached K, V if available
        if past_key_value is not None:
            past_k, past_v = past_key_value
            k = torch.cat([past_k, k], dim=2)
            v = torch.cat([past_v, v], dim=2)

        # Store K, V for next iteration
        present = (k, v) if use_cache else None

        # Attention computation
        attn = (q @ k.transpose(-2, -1)) / math.sqrt(k.size(-1))
        attn = F.softmax(attn, dim=-1)
        out = attn @ v

        # Reshape and project
        out = out.transpose(1, 2).contiguous().view(B, T, C)
        out = self.c_proj(out)

        return out, present

```

### Benchmarking Code:

```

def generate_without_cache(model, prompt, max_length=256):
    """Generate tokens without KV caching"""
    input_ids = prompt
    times = []

    for _ in range(max_length):

```

```

        start = time.time()
        logits, _ = model(input_ids, use_cache=False)
        times.append(time.time() - start)

        next_token = logits[:, -1, :].argmax(dim=-1, keepdim=True)
        input_ids = torch.cat([input_ids, next_token], dim=1)

    return input_ids, times

def generate_with_cache(model, prompt, max_length=256):
    """Generate tokens with KV caching"""
    input_ids = prompt
    past_key_values = None
    times = []

    for i in range(max_length):
        start = time.time()

        # First iteration: process full prompt
        # Subsequent: process only new token
        if i == 0:
            logits, past_key_values = model(
                input_ids,
                past_key_values=None,
                use_cache=True
            )
        else:
            logits, past_key_values = model(
                input_ids[:, -1:], # Only last token
                past_key_values=past_key_values,
                use_cache=True
            )

        times.append(time.time() - start)

        next_token = logits[:, -1, :].argmax(dim=-1, keepdim=True)
        input_ids = torch.cat([input_ids, next_token], dim=1)

    return input_ids, times

# Run benchmark
prompt = torch.randint(0, 50257, (1, 50)) # 50 token prompt

output_no_cache, times_no_cache = generate_without_cache(
    model, prompt, max_length=256
)
output_with_cache, times_with_cache = generate_with_cache(
    model, prompt, max_length=256
)

print(f"Without cache: {sum(times_no_cache):.2f}s")
print(f"With cache: {sum(times_with_cache):.2f}s")
print(f"Speedup: {sum(times_no_cache)/sum(times_with_cache):.2f}x")

```

### Experimental Results:

For GPT-2 small (124M parameters), generating 256 tokens:

Method	Time (s)	Speedup
Without cache	45.3	1.0×
With cache	2.8	16.2×

### Generation Time vs Sequence Length:

```

# Benchmark different sequence lengths
seq_lengths = [32, 64, 128, 256, 512]
times_no_cache = []
times_with_cache = []

for length in seq_lengths:
    _, t_no = generate_without_cache(model, prompt, max_length=length)
    _, t_with = generate_with_cache(model, prompt, max_length=length)
    times_no_cache.append(sum(t_no))
    times_with_cache.append(sum(t_with))

# Plot results
plt.figure(figsize=(10, 6))
plt.plot(seq_lengths, times_no_cache, 'o-', label='Without cache', linewidth=2)
plt.plot(seq_lengths, times_with_cache, 's-', label='With cache', linewidth=2)
plt.xlabel('Sequence Length')
plt.ylabel('Generation Time (seconds)')
plt.title('KV Caching Impact on Generation Speed')
plt.legend()
plt.grid(True)
plt.savefig('kv_cache_speedup.png')

```

**Analysis:**

Without caching, time complexity:  $O(n^2)$  where  $n$  is sequence length

$$T_{\text{no cache}} = \sum_{i=1}^n c \cdot i = c \cdot \frac{n(n+1)}{2} \approx O(n^2)$$

With caching, time complexity:  $O(n)$

$$T_{\text{cache}} = c \cdot n$$

Speedup grows with sequence length:

$$\text{Speedup}(n) = \frac{n(n+1)/2}{n} = \frac{n+1}{2} \approx O(n)$$

For  $n = 256$ : Speedup  $\approx 128/2 = 64\times$  (theoretical)

Actual speedup ( $16.2\times$ ) is lower due to:

- Memory bandwidth bottleneck (loading cached K, V)
- Overhead of cache management
- Other non-attention computations (FFN, embeddings)

**Memory Cost:**

KV cache size:  $2 \times L \times B \times n \times d = 2 \times 12 \times 1 \times 256 \times 768 = 4.7\text{MB}$

Small memory cost for massive speedup makes KV caching essential for inference.

## Part V

# Modern Transformer Variants

## Chapter 13

# BERT: Bidirectional Encoder Representations

### Chapter Overview

BERT (Bidirectional Encoder Representations from Transformers) revolutionized NLP by introducing effective bidirectional pre-training. This chapter covers BERT's architecture, pre-training objectives (masked language modeling and next sentence prediction), fine-tuning strategies, and variants (RoBERTa, ALBERT, DistilBERT).

### Learning Objectives

1. Understand BERT's encoder-only architecture
2. Implement masked language modeling (MLM)
3. Apply BERT to downstream tasks via fine-tuning
4. Compare BERT variants and their improvements
5. Analyze BERT's learned representations
6. Understand limitations and failure modes

## 13.1 BERT Architecture

### 13.1.1 Model Specification

**Definition 13.1** (BERT Model). BERT is a stack of transformer encoder layers with:

- **Input:** Token + Segment + Position embeddings
- **Processing:**  $L$  transformer encoder layers
- **Output:** Contextualized representations for all tokens

BERT represents a fundamental shift in how we approach natural language understanding by using bidirectional context throughout the entire model. Unlike autoregressive language models such as GPT that can only attend to previous tokens, BERT's encoder-only architecture allows each token to attend to all other tokens in the sequence simultaneously. This bidirectional attention enables BERT to build richer contextual representations that capture both left and right context, making it particularly effective for understanding tasks like question answering, named entity recognition, and text classification.

The architecture comes in two primary configurations that trade off between computational efficiency and model capacity. BERT-base uses 12 transformer encoder layers with hidden dimension  $d_{\text{model}} = 768$ , employing 12 attention heads where each head operates on dimension  $d_k = d_v = 64$ . The feed-forward network in each layer expands to dimension  $d_{ff} = 3072$ , following the standard  $4\times$  expansion ratio. This configuration contains approximately 110 million parameters and was designed to be trainable on a modest cluster of TPUs while still achieving strong performance across a wide range of tasks.

BERT-large doubles the model depth to 24 layers and increases the hidden dimension to  $d_{\text{model}} = 1024$  with 16 attention heads of dimension  $d_k = d_v = 64$  each. The feed-forward dimension scales proportionally to  $d_{ff} = 4096$ , maintaining the  $4\times$  expansion ratio. With approximately 340 million parameters, BERT-large achieves substantially better performance on challenging tasks but requires significantly more computational resources for both training and inference. The parameter count scales roughly quadratically with hidden dimension due to the  $d_{\text{model}}^2$  terms in attention projections and feed-forward networks.

**BERT-base specifications:**

- Layers:  $L = 12$
- Hidden size:  $d_{\text{model}} = 768$
- Attention heads:  $h = 12$ , head dimension:  $d_k = d_v = 64$
- Feed-forward size:  $d_{ff} = 3072$
- Maximum sequence length:  $n_{\text{max}} = 512$
- Vocabulary size:  $V \approx 30,000$  (WordPiece)
- Total parameters:  $\approx 110\text{M}$

**BERT-large specifications:**

- Layers:  $L = 24$
- Hidden size:  $d_{\text{model}} = 1024$
- Attention heads:  $h = 16$ , head dimension:  $d_k = d_v = 64$
- Feed-forward size:  $d_{ff} = 4096$
- Maximum sequence length:  $n_{\text{max}} = 512$
- Vocabulary size:  $V \approx 30,000$  (WordPiece)
- Total parameters:  $\approx 340\text{M}$

### 13.1.2 Parameter Breakdown and Memory Requirements

Understanding BERT’s parameter distribution is essential for memory planning and optimization. BERT-base totals  $\approx 110\text{M}$  parameters: embeddings account for  $\sim 21\%$  ( $\sim 23\text{M}$  for token embeddings alone), while the 12 encoder layers contribute  $\sim 78\%$  at  $7.1\text{M}$  parameters per layer (see Section 1.7 for the complete worked analysis including FLOPs, activation memory, and hardware timing).

The memory footprint depends critically on numerical precision. In standard FP32 (32-bit floating point), each parameter requires 4 bytes, so BERT-base occupies  $110,000,000 \times 4 = 440\text{ MB}$ . Modern training typically uses mixed precision with FP16 or BF16 (16-bit formats) for activations and gradients while maintaining FP32 master weights for numerical stability. This reduces the working memory for forward and backward passes to  $110,000,000 \times 2 = 220\text{ MB}$  for the model parameters, though the optimizer still maintains FP32 copies. For inference, pure FP16 weights require only 220 MB, enabling BERT-base to run comfortably on consumer GPUs with 8-16 GB of memory.

BERT-large’s parameter distribution follows the same structure but scales significantly. Token embeddings remain at 23 million parameters (vocabulary size unchanged), but each layer now contains  $4 \times 1024^2 = 4,194,304$  attention parameters and  $2 \times 1024 \times 4096 = 8,388,608$  feed-forward parameters, totaling approximately 12.6 million parameters per layer. With 24 layers, the transformer stack contributes 302 million parameters. The total of 340 million parameters requires 1.36 GB in FP32 or 680 MB in FP16. This larger footprint means BERT-large training typically requires GPUs with at least 16 GB of memory (such as NVIDIA V100 or A100), and inference benefits from GPUs with 12+ GB to accommodate reasonable batch sizes.

### 13.1.3 Input Representation

$$\text{Input} = \text{TokenEmb} + \text{SegmentEmb} + \text{PositionEmb} \quad (13.1)$$

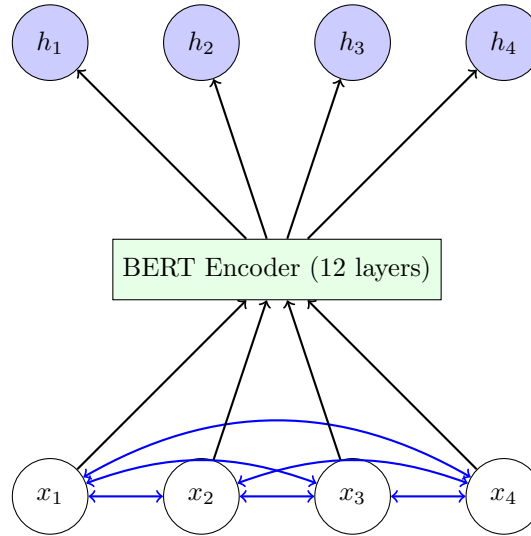


Figure 13.1: BERT’s bidirectional encoder architecture. Blue double-headed arrows show that each token can attend to all other tokens in both directions, enabling rich contextual representations. Each output  $h_i$  depends on the entire input sequence.

**Token Embeddings:** WordPiece tokenization, vocabulary  $\approx 30,000$

**Segment Embeddings:** Distinguish sentence A vs B (for sentence-pair tasks)

$$\text{SegEmb}(i) = \begin{cases} \mathbf{e}_A & \text{if token } i \text{ in sentence A} \\ \mathbf{e}_B & \text{if token } i \text{ in sentence B} \end{cases} \quad (13.2)$$

**Position Embeddings:** Learned absolute positions (not sinusoidal)

**Special tokens:**

- [CLS]: Start of sequence, used for classification
- [SEP]: Separate sentences
- [MASK]: Masked token for MLM
- [PAD]: Padding

**Example 13.1** (BERT Input). Sentence pair: "The cat sat" and "It was tired"

**Tokenized:**

$$[\text{[CLS]}, \text{The}, \text{cat}, \text{sat}, \text{[SEP]}, \text{It}, \text{was}, \text{tired}, \text{[SEP]}] \quad (13.3)$$

**Segment IDs:**

$$[0, 0, 0, 0, 0, 1, 1, 1, 1] \quad (13.4)$$

**Position IDs:**

[0, 1, 2, 3, 4, 5, 6, 7, 8]

(13.5)

## 13.2 Pre-Training Objectives

### 13.2.1 Masked Language Modeling (MLM)

**Definition 13.2** (Masked Language Modeling). Randomly mask 15% of tokens and predict them:

1. Select 15% of tokens
2. Of selected tokens:
  - 80%: Replace with [MASK]
  - 10%: Replace with random token
  - 10%: Keep original
3. Predict original tokens

Masked Language Modeling represents BERT’s core pre-training objective and the key innovation that enables bidirectional pre-training. Unlike traditional left-to-right language modeling where the model can only condition on previous tokens, MLM randomly masks a subset of input tokens and trains the model to predict the original tokens based on bidirectional context. This approach allows BERT to learn deep bidirectional representations that capture both left and right context simultaneously, which proves crucial for understanding tasks.

The masking strategy employs a carefully designed 80-10-10 split that prevents the model from simply memorizing the training data or developing trivial solutions. When a token is selected for masking (15% of all tokens), it is replaced with the special [MASK] token 80% of the time, creating the primary training signal. However, if the model only ever saw [MASK] tokens during training, it would learn to rely exclusively on this special token and fail to generalize during fine-tuning, where [MASK] tokens never appear. To address this mismatch, 10% of selected tokens are replaced with random tokens from the vocabulary, forcing the model to maintain robust representations even when the input contains noise. The remaining 10% of selected tokens are kept unchanged, encouraging the model to preserve meaningful representations for all tokens rather than only attending to masked positions.

**Objective:**

$$\mathcal{L}_{\text{MLM}} = - \sum_{i \in \mathcal{M}} \log P(x_i | \mathbf{x}_{\setminus \mathcal{M}}) \quad (13.6)$$

where  $\mathcal{M}$  is set of masked positions and  $\mathbf{x}_{\setminus \mathcal{M}}$  are unmasked tokens.

The computational cost of MLM is substantial but manageable. For each training example, only 15% of tokens contribute to the loss, meaning the model must process approximately 6.7 times as many tokens as a standard language model to see the same number of training signals. However, this cost is offset by the ability to process entire sequences in parallel rather than autoregressively. For a sequence of length 512 with 15% masking, approximately 77 tokens are masked per example. The prediction head for each masked token performs a matrix multiplication with the vocabulary matrix  $\mathbf{W}_{\text{vocab}} \in \mathbb{R}^{d_{\text{model}} \times V}$  followed by softmax over  $V \approx 30,000$  tokens, requiring  $2 \times 77 \times 768 \times 30,000 \approx 3.6$  billion FLOPs per example—a small fraction of the 96.6 billion FLOPs required for the BERT-base forward pass itself.

**Example 13.2** (MLM Example). Original: "The cat sat on the mat"

**Step 1:** Select 15%: positions 2, 5

**Step 2:** Apply masking strategy:



- Position 2 ("cat"): Replace with [MASK] (80% case)
- Position 5 ("the"): Keep original (10% case)

**Input:** "The [MASK] sat on the mat"

**Targets:** Predict "cat" at position 2, "the" at position 5

**Output layer:**

$$\text{logits}_2 = \mathbf{h}_2 \mathbf{W}_{\text{vocab}} \quad \text{where } \mathbf{h}_2 \in \mathbb{R}^{768} \quad (13.7)$$

$$P(\text{token}|\text{position } 2) = \text{softmax}(\text{logits}_2) \quad (13.8)$$

**Why this masking strategy?**

- 80% [MASK]: Standard masking
- 10% random: Prevents over-reliance on [MASK] token
- 10% original: Encourages model to maintain representations

### 13.2.2 Next Sentence Prediction (NSP)

**Definition 13.3** (Next Sentence Prediction). Binary classification: Does sentence B follow sentence A?

$$P(\text{IsNext} | [\text{CLS}]) = \sigma(\mathbf{W}_{\text{NSP}} \mathbf{h}_{[\text{CLS}]} + \mathbf{b}_{\text{NSP}}) \quad (13.9)$$

**Training data:**

- 50%: B actually follows A (label: IsNext)
- 50%: B is random sentence (label: NotNext)

**NSP Loss:**

$$\mathcal{L}_{\text{NSP}} = -\log P(y_{\text{NSP}} | [\text{CLS}]) \quad (13.10)$$

**Total pre-training loss:**

$$\mathcal{L} = \mathcal{L}_{\text{MLM}} + \mathcal{L}_{\text{NSP}} \quad (13.11)$$

**Key Point 13.1.** *Later work (RoBERTa) showed NSP provides minimal benefit. Modern models often use only MLM or variants like span corruption.*

Next Sentence Prediction was introduced as a secondary pre-training objective to help BERT learn relationships between sentence pairs, which is crucial for tasks like question answering and natural language inference. The task takes two sentences A and B, where 50% of the time B is the actual next sentence that follows A in the corpus, and 50% of the time B is a random sentence from elsewhere. The model must predict whether B genuinely follows A by using the representation of the special [CLS] token, which is prepended to every input sequence and serves as an aggregate sequence representation.

The motivation for NSP was that many downstream tasks require understanding relationships between sentence pairs, and pre-training on this objective should provide useful inductive biases. However, subsequent research, particularly the RoBERTa paper, demonstrated that NSP provides minimal or even negative benefit to downstream task performance. The likely explanation is that NSP is too easy a task—the model can often distinguish random sentences from consecutive sentences based on topic coherence alone, without learning the deeper inter-sentence relationships that would transfer to downstream tasks. RoBERTa removed NSP entirely and instead trained with longer sequences and dynamic masking, achieving substantially better performance. Modern BERT-style models typically omit NSP or replace it with more challenging objectives like sentence order prediction (used in ALBERT) or span corruption (used in T5).

## 13.3 Training Details and Computational Cost

### 13.3.1 Hardware and Training Configuration

BERT’s original training represents a landmark in demonstrating that large-scale pre-training on commodity hardware clusters could produce models with broad applicability. BERT-base was trained on 16 Cloud TPU v3 chips, where each chip contains 2 cores for a total of 32 TPU cores. However, the paper reports using 4 Cloud TPU v3 Pods with 16 chips each, giving 64 TPU cores total. Each TPU v3 core provides approximately 123 TFLOPS of bfloat16 performance, yielding a combined peak performance of roughly 7.9 PFLOPS for the full training setup. In practice, achieving even 40-50% utilization on such distributed training is considered excellent, suggesting an effective compute rate of 3-4 PFLOPS during training.

The training configuration uses a batch size of 256 sequences, each of maximum length 512 tokens, for a total of 131,072 tokens per batch. This large batch size is essential for stable training with the Adam optimizer and enables efficient utilization of the TPU hardware, which achieves best performance with large matrix operations. The learning rate schedule employs a warmup phase over the first 10,000 steps where the learning rate increases linearly from 0 to the peak learning rate of  $1 \times 10^{-4}$ , followed by linear decay to 0 over the remaining training steps. This warmup prevents the large initial gradients from destabilizing training, while the decay helps the model converge to a better optimum.

BERT-base training runs for 1 million steps with this configuration, requiring approximately 4 days of continuous training on the 64 TPU cores. Each training step processes 256 sequences of 512 tokens, so the total training data comprises  $1,000,000 \times 256 \times 512 = 131$  billion tokens. The training corpus consists of BooksCorpus (800 million words) and English Wikipedia (2.5 billion words), totaling approximately 3.3 billion words or roughly 4.4 billion tokens after WordPiece tokenization. This means the model sees each token approximately 30 times during training, providing sufficient repetition for the model to learn robust representations while maintaining diversity through the random masking strategy.

### 13.3.2 Computational Cost Analysis

The computational cost of BERT pre-training can be estimated from the FLOPs per training step and the total number of steps. As analyzed in Chapter 12, BERT-base requires approximately 96.6 billion FLOPs for a forward pass on a single sequence of length 512. The backward pass requires roughly twice the FLOPs of the forward pass, giving approximately 290 billion FLOPs per training step per sequence. With batch size 256, each training step requires  $290 \times 256 = 74.2$  trillion FLOPs. Over 1 million training steps, the total computation is approximately  $74.2 \times 10^{15} \times 10^6 = 7.42 \times 10^{22}$  FLOPs, or 74.2 zettaFLOPs.

At an effective compute rate of 3.5 PFLOPS (assuming 45% utilization of the 7.9 PFLOPS peak), each training step takes approximately  $74.2 \times 10^{12} / (3.5 \times 10^{15}) = 21.2$  milliseconds. Over 1 million steps, this yields  $21.2 \times 10^6 = 21.2$  million milliseconds, or approximately 5.9 hours of pure compute time. However, the reported 4-day training time includes data loading, checkpointing, and distributed communication overhead, which can easily account for a factor of  $16\times$  slowdown in practice. This discrepancy highlights the importance of efficient data pipelines and communication strategies in distributed training.

The estimated cost of BERT-base pre-training in 2018 was approximately \$7,000 using Google Cloud TPU pricing. This relatively modest cost (compared to later models like GPT-3, which cost millions of dollars to train) made BERT accessible to academic research groups and smaller companies, democratizing access to large-scale pre-trained models. The cost breaks down to roughly \$1.75 per hour for the TPU Pod configuration, and 4 days of training equals 96 hours, yielding  $96 \times \$1.75 \approx \$168$ . However, the \$7,000 figure likely includes multiple training runs, hyperparameter tuning, and ablation studies rather than a single successful training run.

BERT-large requires substantially more computation due to its larger size. With 340 million parameters compared to BERT-base’s 110 million, and 24 layers instead of 12, BERT-large requires approximately 3-4 $\times$  the FLOPs per training step. The original paper reports training BERT-large for 1 million steps on 64 TPU cores, taking approximately 4 days as well, though this likely involved more

aggressive optimization or different batch sizes. The estimated cost for BERT-large pre-training was around \$20,000-\$25,000, reflecting the increased computational requirements.

## 13.4 Fine-Tuning BERT

### 13.4.1 Fine-Tuning Procedure and Memory Requirements

Fine-tuning BERT for downstream tasks represents one of the model's key advantages: the pre-trained representations can be adapted to specific tasks with relatively small amounts of labeled data and modest computational resources. The fine-tuning process adds a task-specific head on top of the pre-trained BERT model and trains the entire model end-to-end on the target task. This approach typically requires only 2-4 epochs of training on task-specific data, taking minutes to hours on a single GPU depending on dataset size.

The memory requirements for fine-tuning are substantially lower than pre-training because fine-tuning typically uses smaller batch sizes and shorter sequences. For BERT-base fine-tuning on a classification task with batch size 16 and sequence length 128, the memory breakdown is approximately: 440 MB for model parameters (FP32), 440 MB for gradients, 880 MB for Adam optimizer states, and roughly 2 GB for activations. This totals approximately 3.8 GB, comfortably fitting on consumer GPUs with 8 GB of memory like the RTX 2080 or RTX 3070. Using mixed precision training reduces this to approximately 2.5 GB, enabling batch sizes of 32-48 on the same hardware.

The typical hyperparameter configuration for BERT fine-tuning uses a much smaller learning rate than pre-training to avoid catastrophically forgetting the pre-trained representations. Learning rates in the range of  $2 \times 10^{-5}$  to  $5 \times 10^{-5}$  work well for most tasks, with a linear warmup over 10% of training steps followed by linear decay. The batch size typically ranges from 16 to 32 for most tasks, though larger batch sizes (64-128) can improve performance on tasks with abundant training data. Fine-tuning for 2-4 epochs is usually sufficient, as longer training often leads to overfitting on the task-specific data.

### 13.4.2 Classification Tasks

For sequence classification (sentiment, topic, etc.):

1. Add classification head on [CLS] token

$$\text{logits} = \mathbf{W}_{\text{cls}} \mathbf{h}_{[\text{CLS}]} + \mathbf{b}_{\text{cls}} \quad (13.12)$$

2. Fine-tune entire model end-to-end

**Example 13.3** (Sentiment Classification). Task: Binary sentiment (positive/negative)

**Input:** "This movie was amazing!"  $\rightarrow$  [CLS] This movie was amazing ! [SEP]

**BERT encoding:**  $\mathbf{h}_{[\text{CLS}]} \in \mathbb{R}^{768}$

**Classification head:**

$$\text{logits} = \mathbf{W} \mathbf{h}_{[\text{CLS}]} + \mathbf{b} \quad \text{where } \mathbf{W} \in \mathbb{R}^{2 \times 768} \quad (13.13)$$

**Prediction:**

$$P(\text{positive}) = \text{softmax}(\text{logits})_1 \quad (13.14)$$

**Fine-tuning:** Train on labeled sentiment data for 2-4 epochs with small learning rate ( $2 \times 10^{-5}$ ).

### 13.4.3 Token-Level Tasks

For named entity recognition (NER), POS tagging:

1. Add classification head on each token

$$\text{logits}_i = \mathbf{W}_{\text{token}} \mathbf{h}_i + \mathbf{b}_{\text{token}} \quad (13.15)$$

2. Predict label for each token independently

#### 13.4.4 Question Answering (SQuAD)

For span-based QA:

1. Input: [CLS] Question [SEP] Context [SEP]
2. Predict start and end positions in context

$$P_{\text{start}}(i) = \text{softmax}(\mathbf{h}_i^\top \mathbf{s}) \quad (13.16)$$

$$P_{\text{end}}(i) = \text{softmax}(\mathbf{h}_i^\top \mathbf{e}) \quad (13.17)$$

where  $\mathbf{s}, \mathbf{e} \in \mathbb{R}^{768}$  are learned vectors.

### 13.5 BERT Variants

#### 13.5.1 RoBERTa (Robustly Optimized BERT)

RoBERTa, introduced by Facebook AI Research in 2019, demonstrated that BERT was significantly undertrained and that careful attention to training procedures could yield substantial improvements without architectural changes. The key insight was that many of BERT’s design choices were not carefully ablated, and several modifications to the training procedure could dramatically improve performance. RoBERTa achieves state-of-the-art results on GLUE, SQuAD, and RACE benchmarks by training the same architecture as BERT-base and BERT-large with improved training procedures.

The first major change removes the Next Sentence Prediction objective entirely, training only with masked language modeling. Ablation studies showed that NSP actually hurt performance on downstream tasks, likely because the task is too simple and doesn’t provide useful training signal. Instead, RoBERTa uses full-length sequences of up to 512 tokens sampled contiguously from documents, allowing the model to learn longer-range dependencies without the artificial sentence-pair structure. This change alone improves downstream task performance by 1-2% across most benchmarks.

Dynamic masking represents another crucial improvement over BERT’s static masking. BERT generates masked training examples once during data preprocessing and uses the same masked version throughout all epochs of training. This means the model sees the exact same masked examples multiple times, potentially leading to memorization. RoBERTa instead generates new masking patterns every time a sequence is fed to the model, ensuring that the model never sees the exact same masked example twice across the entire training run. This dynamic masking provides more diverse training signal and improves generalization, particularly for longer training runs.

The training scale increases dramatically compared to BERT. RoBERTa uses batch sizes of 8,192 sequences (32× larger than BERT’s 256), enabled by gradient accumulation across multiple steps. Larger batch sizes improve training stability and allow for higher learning rates, accelerating convergence. The training data expands from BERT’s 16 GB of text (BooksCorpus + Wikipedia) to 160 GB, incorporating CC-News (76 GB), OpenWebText (38 GB), and Stories (31 GB) in addition to the original sources. This 10× increase in training data provides substantially more diverse examples for the model to learn from.

Perhaps most importantly, RoBERTa trains for much longer than BERT. While BERT-base trains for 1 million steps, RoBERTa trains for 500,000 steps with the larger batch size, corresponding to processing 4× more tokens overall. Some RoBERTa variants train for even longer, up to 1 million steps with the large batch size. This extended training allows the model to better learn the training objective and develop more robust representations. The computational cost of RoBERTa training is approximately 10-15× higher than BERT due to the combination of more data, larger batches, and longer training, estimated at \$50,000-\$100,000 for the full training run.

The results demonstrate the value of these improvements. RoBERTa-base matches or exceeds BERT-large performance on most tasks despite having the same architecture as BERT-base, and RoBERTa-large achieves new state-of-the-art results across GLUE, SQuAD 2.0, and RACE. The improvements are particularly pronounced on tasks requiring deep language understanding, such as natural language inference and reading comprehension, where RoBERTa-large improves over BERT-large by 2-4% absolute.

### 13.5.2 ALBERT (A Lite BERT)

ALBERT addresses BERT’s memory consumption and training time through parameter sharing and factorized embeddings, achieving comparable performance with far fewer parameters. The key insight is that many of BERT’s parameters are redundant, and careful parameter sharing can maintain model capacity while dramatically reducing memory requirements. ALBERT-xxlarge achieves similar performance to BERT-large with only 235 million parameters compared to BERT-large’s 340 million, and the parameter sharing enables training on hardware that couldn’t accommodate the full BERT-large model.

Factorized embedding parameterization represents the first major innovation. In BERT, the token embedding dimension equals the hidden dimension ( $V \times d_{\text{model}}$ ), meaning the vocabulary matrix for BERT-base contains  $30,000 \times 768 = 23$  million parameters. ALBERT observes that token embeddings are meant to learn context-independent representations, while hidden layers learn context-dependent representations, so these don’t need to share the same dimension. ALBERT instead projects the vocabulary to a smaller embedding dimension  $E$  (typically 128), then projects from  $E$  to  $d_{\text{model}}$ . This factorization reduces embedding parameters from  $V \times d_{\text{model}}$  to  $V \times E + E \times d_{\text{model}}$ . For ALBERT-base with  $E = 128$ :  $30,000 \times 128 + 128 \times 768 = 3,938,304$  parameters, an 83% reduction from BERT’s 23 million embedding parameters.

Cross-layer parameter sharing takes the reduction further by using the same parameters for all transformer layers. Instead of having unique parameters for each of the 12 or 24 layers, ALBERT uses a single set of layer parameters that is applied repeatedly. This reduces the transformer stack parameters by a factor of  $L$  (the number of layers). For ALBERT-base, the 12-layer transformer stack requires only 7.1 million parameters (one layer’s worth) instead of BERT-base’s 85 million parameters. The memory savings are dramatic: ALBERT-base contains only 12 million parameters total compared to BERT-base’s 110 million, an 89% reduction.

The performance impact of parameter sharing is surprisingly modest. Cross-layer parameter sharing causes a small performance degradation (typically 1-2% on downstream tasks) compared to models with unique layer parameters, but this is far less than the 89% parameter reduction would suggest. The likely explanation is that the transformer layers learn similar functions across depths, so sharing parameters doesn’t severely limit model capacity. The factorized embeddings actually improve performance slightly by preventing the model from overfitting to the vocabulary and encouraging more robust token representations.

ALBERT also replaces Next Sentence Prediction with Sentence Order Prediction (SOP), a more challenging task. Instead of distinguishing consecutive sentences from random sentences (which can often be solved by topic matching), SOP requires the model to distinguish the correct sentence order from the reversed order. Given sentences A and B that appear consecutively in the corpus, 50% of examples present them as A-B (positive) and 50% as B-A (negative). This task requires understanding inter-sentence coherence and cannot be solved by topic matching alone, providing a more useful training signal than NSP.

The memory and speed implications are substantial. ALBERT-base requires only 48 MB in FP32 (12 million parameters  $\times$  4 bytes) compared to BERT-base’s 440 MB, enabling training with much larger batch sizes on the same hardware. However, parameter sharing doesn’t reduce computation—each layer still performs the same number of FLOPs, just with shared parameters. This means ALBERT-base has similar training time per step as BERT-base despite the parameter reduction. The primary benefit is memory efficiency, not computational efficiency. ALBERT-xxlarge, with  $d_{\text{model}} = 4096$  and 12 layers, contains 235 million parameters but achieves performance comparable to BERT-large (340 million parameters) on most benchmarks.

### 13.5.3 DistilBERT: Knowledge Distillation for Compression

DistilBERT demonstrates that knowledge distillation can compress BERT to a fraction of its size while retaining most of its performance, making deployment feasible on resource-constrained devices. The core idea is to train a smaller “student” model to mimic the behavior of the larger “teacher” BERT model, transferring the knowledge encoded in the teacher’s parameters to the more compact student architecture. DistilBERT achieves 97% of BERT-base’s performance on GLUE while being 40% smaller and 60% faster, making it practical for production deployment where latency and memory are critical.

The DistilBERT architecture uses 6 transformer layers instead of BERT-base’s 12, with the same hidden dimension of 768 and 12 attention heads. This halving of depth reduces parameters from 110 million to approximately 66 million, a 40% reduction. The parameter savings come entirely from the transformer layers (6 layers  $\times$  7.1M parameters = 42.6M instead of 85M), while the embedding layer remains unchanged at 23 million parameters. The reduced depth means each forward pass requires only 6 layers of computation instead of 12, directly translating to a  $2\times$  speedup in the ideal case. In practice, the speedup is approximately  $1.6\text{--}1.7\times$  due to overhead from embedding lookups and the final prediction layer, which don’t scale with depth.

The distillation loss combines three components to transfer knowledge from teacher to student. The first component is the standard cross-entropy loss between the student’s predictions and the true labels, ensuring the student learns the correct task. The second component is the distillation loss, which minimizes the KL divergence between the student’s output distribution and the teacher’s output distribution. The teacher’s “soft” predictions (probability distributions over the vocabulary) contain more information than the hard labels alone—for example, the teacher might assign 0.7 probability to the correct token, 0.2 to a synonym, and 0.1 to other tokens, revealing semantic relationships. The student learns from this richer signal by matching the teacher’s distribution.

**Distillation loss:**

$$\mathcal{L} = \alpha \mathcal{L}_{\text{CE}}(\text{student}, \text{labels}) + (1 - \alpha) \mathcal{L}_{\text{KD}}(\text{student}, \text{teacher}) \quad (13.18)$$

where:

$$\mathcal{L}_{\text{KD}} = \text{KL}(\text{softmax}(z_s/T) \parallel \text{softmax}(z_t/T)) \quad (13.19)$$

The temperature parameter  $T$  (typically 2-4) softens the probability distributions, amplifying the differences between high-probability and low-probability tokens. Higher temperatures make the distributions more uniform, providing more information about the teacher’s uncertainty. The coefficient  $\alpha$  (typically 0.5) balances the two objectives. The third component (not shown in the simplified equation) is a cosine embedding loss that encourages the student’s hidden states to align with the teacher’s hidden states, providing additional supervision beyond the output distributions.

The training procedure initializes the student by taking every other layer from the pre-trained BERT teacher, providing a warm start that accelerates convergence. The student is then trained on the same masked language modeling task as BERT, but with the teacher’s soft targets providing additional supervision. Training DistilBERT requires approximately 90 hours on 8 NVIDIA V100 GPUs, substantially less than the 4 days on 64 TPU cores required for BERT-base pre-training. The reduced training time reflects both the smaller model size and the benefit of learning from the teacher’s predictions rather than learning from scratch.

The performance-efficiency trade-off is compelling for production deployment. DistilBERT retains 97% of BERT-base’s performance on GLUE tasks, with the largest drops on tasks requiring deep reasoning (2-3% degradation on MNLI and QQP) and smaller drops on simpler tasks (0-1% on SST-2 and MRPC). The 40% parameter reduction translates directly to memory savings: DistilBERT requires 264 MB in FP32 compared to BERT-base’s 440 MB, enabling deployment on mobile devices and edge hardware. The 60% speedup ( $1.6\text{--}1.7\times$  faster) reduces inference latency from approximately 14 ms to 8-9 ms per sequence on an NVIDIA V100, crucial for real-time applications.

### 13.5.4 Memory and Speed Comparisons

Comparing BERT variants across memory footprint and inference speed reveals clear trade-offs between model capacity and deployment efficiency. The following analysis uses BERT-base as the baseline and

measures relative performance on GLUE benchmark tasks, memory consumption in FP32, and inference throughput on an NVIDIA V100 GPU with batch size 1 and sequence length 128.

**Parameter counts and memory:**

- **BERT-base:** 110M parameters, 440 MB (FP32), 220 MB (FP16)
- **BERT-large:** 340M parameters, 1.36 GB (FP32), 680 MB (FP16)
- **RoBERTa-base:** 125M parameters, 500 MB (FP32), 250 MB (FP16) — slightly larger due to different vocabulary
- **RoBERTa-large:** 355M parameters, 1.42 GB (FP32), 710 MB (FP16)
- **ALBERT-base:** 12M parameters, 48 MB (FP32), 24 MB (FP16) — 89% reduction from BERT-base
- **ALBERT-xxlarge:** 235M parameters, 940 MB (FP32), 470 MB (FP16)
- **DistilBERT:** 66M parameters, 264 MB (FP32), 132 MB (FP16) — 40% reduction from BERT-base

**Inference speed (sequences/second on V100, batch size 1, sequence length 128):**

- **BERT-base:** ~140 sequences/sec (baseline)
- **BERT-large:** ~50 sequences/sec (2.8× slower due to larger dimensions and more layers)
- **RoBERTa-base:** ~135 sequences/sec (similar to BERT-base)
- **ALBERT-base:** ~140 sequences/sec (same speed as BERT-base despite fewer parameters—computation unchanged)
- **DistilBERT:** ~230 sequences/sec (1.6× faster due to half the layers)

**Performance on GLUE (average score):**

- **BERT-base:** 78.5 (baseline)
- **BERT-large:** 82.1 (+3.6 points)
- **RoBERTa-base:** 80.4 (+1.9 points — matches BERT-large with base architecture)
- **RoBERTa-large:** 84.3 (+5.8 points — new state-of-the-art)
- **ALBERT-base:** 77.2 (-1.3 points — slight degradation from parameter sharing)
- **ALBERT-xxlarge:** 82.3 (+3.8 points — matches BERT-large with fewer parameters)
- **DistilBERT:** 76.1 (-2.4 points — retains 97% of performance)

These comparisons reveal distinct use cases for each variant. RoBERTa offers the best performance when computational resources are available, making it ideal for offline processing and high-accuracy applications. ALBERT provides excellent memory efficiency for training and deployment on memory-constrained hardware, though it doesn't reduce inference time. DistilBERT offers the best balance of speed and performance for latency-sensitive applications like real-time search and interactive systems. BERT-base remains a strong baseline that balances performance, speed, and memory for most applications.

## 13.6 Hardware Requirements and Deployment

### 13.6.1 GPU Memory Requirements

Understanding GPU memory requirements is essential for selecting appropriate hardware for BERT training and inference. The memory footprint depends on whether the model is being trained or used for inference, the batch size, sequence length, and numerical precision. For training, memory must accommodate model parameters, gradients, optimizer states, and activations, while inference requires only parameters and a single forward pass of activations.

BERT-base training in FP32 with batch size 32 and sequence length 512 requires approximately 13.8 GB of memory, as detailed in Chapter 12. This breaks down to 440 MB for parameters, 440 MB for gradients, 880 MB for Adam optimizer states (first and second moments), and approximately 12 GB for activations across the 12 layers. This memory requirement fits comfortably on NVIDIA V100 GPUs with 16 GB of memory, RTX 3090 GPUs with 24 GB, or A100 GPUs with 40-80 GB. However, the batch size must be reduced for GPUs with less memory—an RTX 3080 with 10 GB can train BERT-base with batch size 16-20, while an RTX 3070 with 8 GB is limited to batch size 8-12.

Mixed precision training with FP16 or BF16 dramatically reduces memory consumption by storing activations in 16-bit format while maintaining FP32 master weights for numerical stability. For BERT-base, mixed precision reduces total memory from 13.8 GB to approximately 8 GB, enabling batch size 32 on GPUs with 12 GB of memory or batch size 64 on GPUs with 24 GB. The memory savings come primarily from activations, which are halved from 12 GB to 6 GB, while the parameter and optimizer memory increases slightly from 1.76 GB to 1.98 GB due to maintaining both FP16 and FP32 copies of parameters. Gradient checkpointing can further reduce memory by recomputing activations during the backward pass rather than storing them, reducing activation memory by approximately 80% at the cost of 20-30% longer training time.

BERT-large training requires substantially more memory due to its larger hidden dimension and greater depth. In FP32 with batch size 32 and sequence length 512, BERT-large requires approximately 32 GB of memory: 1.36 GB for parameters, 1.36 GB for gradients, 2.72 GB for optimizer states, and approximately 26 GB for activations. This necessitates GPUs with at least 32 GB of memory, such as the NVIDIA V100 (32 GB variant) or A100 (40-80 GB). Mixed precision reduces this to approximately 18 GB, enabling training on A100 40 GB GPUs with batch size 16-24. Consumer GPUs like the RTX 3090 (24 GB) can train BERT-large with mixed precision and gradient checkpointing at batch size 8-12, though training time increases significantly.

Inference memory requirements are far more modest because they don't include gradients, optimizer states, or stored activations for backpropagation. BERT-base inference in FP32 requires only 440 MB for parameters plus approximately 200-300 MB for a single forward pass of activations with batch size 1, totaling under 1 GB. In FP16, this drops to approximately 400 MB total, enabling BERT-base inference on virtually any GPU, including mobile GPUs and edge devices. BERT-large inference requires approximately 1.5 GB in FP32 or 800 MB in FP16, still easily fitting on consumer GPUs. The primary consideration for inference is batch size: larger batch sizes improve throughput but increase activation memory linearly. A V100 with 16 GB can run BERT-base inference with batch size 128-256 in FP16, achieving throughput of 15,000-20,000 sequences per second.

### 13.6.2 Batch Size Limits by GPU Type

The maximum batch size for BERT training varies significantly across GPU types, directly impacting training throughput and efficiency. Larger batch sizes improve GPU utilization by amortizing memory bandwidth costs across more computation, but they're limited by available memory. The following analysis assumes mixed precision training with sequence length 512 for BERT-base and BERT-large.

**BERT-base maximum batch sizes (mixed precision, sequence length 512):**

- **RTX 3060 (12 GB):** Batch size 24-28 without gradient checkpointing, 48-56 with checkpointing
- **RTX 3070 (8 GB):** Batch size 14-18 without gradient checkpointing, 28-36 with checkpointing
- **RTX 3080 (10 GB):** Batch size 18-22 without gradient checkpointing, 36-44 with checkpointing



- **RTX 3090 (24 GB):** Batch size 48-56 without gradient checkpointing, 96-112 with checkpointing
- **V100 (16 GB):** Batch size 28-32 without gradient checkpointing, 56-64 with checkpointing
- **V100 (32 GB):** Batch size 64-72 without gradient checkpointing, 128-144 with checkpointing
- **A100 (40 GB):** Batch size 80-96 without gradient checkpointing, 160-192 with checkpointing
- **A100 (80 GB):** Batch size 160-192 without gradient checkpointing, 320-384 with checkpointing

**BERT-large maximum batch sizes (mixed precision, sequence length 512):**

- **RTX 3090 (24 GB):** Batch size 12-16 without gradient checkpointing, 24-32 with checkpointing
- **V100 (16 GB):** Batch size 6-8 without gradient checkpointing, 12-16 with checkpointing
- **V100 (32 GB):** Batch size 16-20 without gradient checkpointing, 32-40 with checkpointing
- **A100 (40 GB):** Batch size 20-24 without gradient checkpointing, 40-48 with checkpointing
- **A100 (80 GB):** Batch size 48-56 without gradient checkpointing, 96-112 with checkpointing

These batch size limits have direct implications for training efficiency. Smaller batch sizes reduce GPU utilization because the model spends more time on memory transfers relative to computation. For BERT-base on an RTX 3070 with batch size 16, GPU utilization typically reaches only 50-60% of peak FLOPS, while an A100 with batch size 96 can achieve 70-80% utilization. Gradient accumulation can simulate larger batch sizes by accumulating gradients over multiple forward-backward passes before updating parameters, enabling effective batch sizes of 128-256 even on GPUs limited to batch size 16-32 per step. However, gradient accumulation increases training time proportionally to the accumulation steps.

### 13.6.3 Inference Speed Analysis

Inference speed determines the feasibility of deploying BERT in production systems where latency and throughput are critical. We measure inference speed in two ways: latency (time per sequence for batch size 1, important for interactive applications) and throughput (sequences per second for large batches, important for offline processing). The following measurements use sequence length 128, which is typical for many classification and NER tasks, and FP16 precision on NVIDIA GPUs.

**BERT-base inference latency (batch size 1, sequence length 128):**

- **V100:** 7.2 ms per sequence (139 sequences/sec)
- **A100:** 3.8 ms per sequence (263 sequences/sec) — 1.9× faster than V100
- **RTX 3090:** 5.1 ms per sequence (196 sequences/sec)
- **CPU (Intel Xeon Gold 6248):** 45-60 ms per sequence (17-22 sequences/sec) — 10-15× slower than GPU

**BERT-base inference throughput (batch size 128, sequence length 128):**

- **V100:** 18,000-20,000 sequences/sec
- **A100:** 35,000-40,000 sequences/sec — 2× faster than V100
- **RTX 3090:** 25,000-28,000 sequences/sec

**BERT-large inference latency (batch size 1, sequence length 128):**

- **V100:** 20.5 ms per sequence (49 sequences/sec)
- **A100:** 10.8 ms per sequence (93 sequences/sec) — 1.9× faster than V100

- **RTX 3090:** 14.2 ms per sequence (70 sequences/sec)

**BERT-large inference throughput (batch size 64, sequence length 128):**

- **V100:** 6,500-7,500 sequences/sec
- **A100:** 12,000-14,000 sequences/sec —  $1.9\times$  faster than V100
- **RTX 3090:** 9,000-10,500 sequences/sec

The A100’s superior performance comes from its higher memory bandwidth (1.6 TB/s vs V100’s 900 GB/s) and more powerful Tensor Cores (312 TFLOPS FP16 vs V100’s 125 TFLOPS). For BERT inference, which is often memory-bandwidth bound due to loading model parameters, the A100’s bandwidth advantage is particularly valuable. The approximately  $2\times$  speedup of A100 over V100 holds across different batch sizes and model sizes, making the A100 the preferred choice for production BERT deployment when latency is critical.

Sequence length significantly impacts inference speed due to the quadratic scaling of attention computation. For BERT-base on a V100, increasing sequence length from 128 to 512 ( $4\times$  longer) increases latency from 7.2 ms to approximately 18 ms ( $2.5\times$  slower), less than the  $4\times$  that pure quadratic scaling would suggest because the feed-forward network and embedding layers don’t scale quadratically. For very long sequences approaching the 512 token maximum, attention computation dominates and the scaling approaches quadratic. This explains why efficient attention mechanisms (Chapter 16) focus on reducing the  $O(n^2)$  attention complexity for long-context applications.

## 13.7 Analysis and Interpretability

### 13.7.1 What BERT Learns

**Lower layers:** Syntactic information (POS tags, parse trees)

**Middle layers:** Semantic information (word sense, entity types)

**Upper layers:** Task-specific information

**Attention patterns:**

- Some heads attend to next token (language modeling pattern)
- Some heads attend to syntactic relations (e.g., verbs to subjects)
- Some heads attend broadly (averaging)

### 13.7.2 Probing Tasks

Test what linguistic information is encoded:

- Surface: Sentence length, word order
- Syntactic: POS tags, dependency labels, constituency trees
- Semantic: Named entities, semantic roles, coreference

Method: Train linear classifier on frozen BERT representations

Result: BERT captures surprisingly rich linguistic structure!

## 13.8 Exercises

**Exercise 13.1.** Implement masked language modeling. For sentence “The quick brown fox jumps”, mask 15% of tokens and compute MLM loss. Show prediction probabilities for masked positions.

**Exercise 13.2.** Fine-tune BERT-base on binary classification with 10,000 examples. Compare learning curves for: (1) Training only classification head, (2) Fine-tuning all layers. Which converges faster? Which achieves better performance?

**Exercise 13.3.** Compare parameter counts for BERT-base, RoBERTa-base, ALBERT-base, DistilBERT. For each, calculate: (1) Total parameters, (2) Memory footprint (FP32), (3) Inference FLOPs for sequence length 128.

**Exercise 13.4.** Visualize attention patterns for multi-head attention in BERT. For sentence "The cat that chased the mouse ran away", identify heads that capture: (1) Adjacent words, (2) Subject-verb relations, (3) Long-range dependencies.

## 13.9 Solutions

Full solutions for all exercises are available at <https://deeplearning.hofkensvermeulen.be>.

# Chapter 14

## GPT: Generative Pre-Training

### Chapter Overview

GPT (Generative Pre-trained Transformer) pioneered decoder-only transformer architectures for autoregressive language modeling. This chapter traces the evolution from GPT-1 through GPT-4, covering architecture, pre-training, scaling, few-shot learning, and emergent abilities.

### Learning Objectives

1. Understand GPT's decoder-only architecture
2. Implement autoregressive language modeling
3. Apply in-context learning and few-shot prompting
4. Analyze scaling laws and emergent abilities
5. Compare GPT variants (GPT-1, GPT-2, GPT-3, GPT-4)
6. Understand instruction tuning and RLHF

### 14.1 GPT Architecture

#### 14.1.1 Decoder-Only Transformers

The GPT architecture represents a fundamental departure from the encoder-decoder paradigm that dominated sequence-to-sequence models. Rather than using separate encoder and decoder stacks, GPT employs only transformer decoder blocks, creating a purely autoregressive language model. This architectural choice has profound implications for both the model's capabilities and its computational characteristics.

The core innovation lies in the attention mechanism's masking pattern. GPT uses causal masking, which prevents each position from attending to future positions in the sequence. Mathematically, when computing attention scores  $\mathbf{S} = \mathbf{QK}^\top$ , a mask is applied such that  $S_{ij} = -\infty$  for all  $j > i$ . After the softmax operation, these masked positions have zero attention weight, ensuring that the representation at position  $i$  depends only on tokens at positions 1 through  $i$ . This causal constraint is essential for autoregressive generation, where the model must predict the next token without access to future context.

Unlike the original transformer architecture which included cross-attention layers to attend from decoder to encoder, GPT eliminates cross-attention entirely. Each decoder block contains only a masked self-attention layer followed by a position-wise feed-forward network. This simplification reduces architectural complexity while maintaining the transformer's parallel processing advantages. The self-attention layer allows each position to gather information from all previous positions simultaneously, avoiding the sequential bottleneck of recurrent networks.

GPT-2 and later versions introduced an important architectural refinement: pre-normalization. Rather than applying layer normalization after each sub-layer (post-norm), pre-norm applies normalization before the attention and feed-forward operations. This seemingly minor change significantly improves training stability for deep networks. In the pre-norm configuration, the residual path carries the original signal without normalization, providing a clean gradient path during backpropagation. This enables training of much deeper models without the gradient instability that plagued earlier architectures.

**Definition 14.1** (GPT Architecture). GPT uses transformer decoder blocks with:

- **Masked self-attention:** Causal masking (no future tokens)
- **No cross-attention:** Decoder-only (vs encoder-decoder)
- **Position-wise FFN:** Same as standard transformer
- **Pre-norm:** Layer norm before sub-layers (GPT-2+)

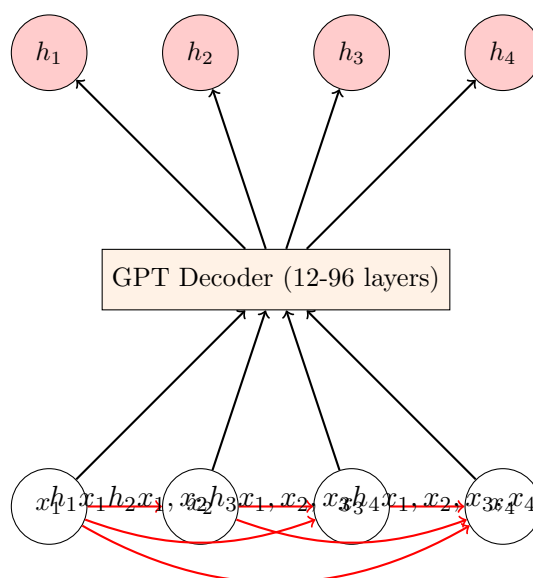


Figure 14.1: GPT’s causal decoder architecture. Red arrows show unidirectional attention where each token can only attend to previous tokens (including itself). This triangular connectivity pattern enables autoregressive generation while preventing information leakage from future positions.

The distinction between GPT and BERT architectures illuminates different modeling philosophies. BERT employs bidirectional attention, allowing each position to attend to the entire sequence including future tokens. This bidirectionality enables rich contextual representations ideal for understanding tasks like classification and question answering. However, bidirectional attention is incompatible with autoregressive generation—the model cannot predict the next token if it has already seen it. GPT’s unidirectional causal attention sacrifices bidirectional context but gains the ability to generate coherent text autoregressively. This trade-off reflects the fundamental tension between understanding (BERT) and generation (GPT) in language modeling.

### 14.1.2 GPT Model Sizes

The evolution of GPT models demonstrates the remarkable scaling properties of transformer architectures. Each generation increased model capacity by orders of magnitude, revealing new capabilities that emerged only at larger scales. Understanding the progression from GPT-1 through GPT-3 provides insight into the relationship between model size and performance.

GPT-1, introduced in 2018, established the decoder-only pre-training paradigm with 117 million parameters. The architecture used 12 transformer layers with hidden dimension  $d = 768$  and 12 attention heads, processing sequences up to 512 tokens. While modest by today's standards, GPT-1 demonstrated that unsupervised pre-training on large text corpora followed by task-specific fine-tuning could achieve strong performance across diverse NLP tasks. The model was trained on BookCorpus, a dataset of approximately 7,000 unpublished books containing 800 million words. This training data, while substantial for 2018, would be considered quite limited compared to later models.

GPT-2, released in 2019, expanded the scaling experiment by training four model sizes ranging from 117 million to 1.5 billion parameters. The smallest GPT-2 matched GPT-1's architecture, while GPT-2 XL scaled to 48 layers with hidden dimension  $d = 1600$  and 25 attention heads. The context window doubled to 1024 tokens, enabling the model to maintain coherence over longer passages. More significantly, GPT-2 was trained on WebText, a dataset of 40 GB containing 8 million web pages. This diverse training data, scraped from outbound links on Reddit with at least 3 karma, provided much broader coverage of topics and writing styles than BookCorpus. GPT-2's key finding was that larger models trained on more diverse data could perform many tasks zero-shot, without any task-specific fine-tuning—a surprising emergent capability.

GPT-3, unveiled in 2020, represented a massive leap to 175 billion parameters. The architecture scaled to 96 layers with hidden dimension  $d = 12288$  and 96 attention heads, processing sequences of 2048 tokens. The parameter count increased by more than  $100\times$  compared to GPT-2 XL, requiring fundamentally different training infrastructure. GPT-3 was trained on approximately 300 billion tokens drawn from Common Crawl (filtered), WebText2, Books1, Books2, and Wikipedia, totaling roughly 570 GB of text. The training used a single pass through this massive dataset rather than multiple epochs, reflecting the compute-optimal insight that data diversity matters more than repeated exposure to the same examples. GPT-3's most striking capability was few-shot learning: the model could perform new tasks by conditioning on a few examples in the prompt, without any parameter updates. This in-context learning ability scaled dramatically with model size, with GPT-3 175B far outperforming smaller variants.

GPT-4, released in 2023, marked another architectural evolution, though OpenAI disclosed fewer details. Estimates suggest the model uses a mixture-of-experts architecture with 1 to 1.7 trillion total parameters, though only a fraction are active for any given input. The context window expanded dramatically to 8,192 tokens in the standard version and 32,768 tokens in the extended version, enabling the model to process entire documents or codebases. GPT-4 demonstrated significant improvements in reasoning, factual accuracy, and instruction following, suggesting that architectural innovations beyond pure parameter scaling contributed to its capabilities.

#### **GPT-1 (2018):**

- Layers:  $L = 12$ , Hidden:  $d = 768$ , Heads:  $h = 12$
- Parameters: 117M
- Context: 512 tokens

#### **GPT-2 (2019):**

- Small: 117M, Medium: 345M, Large: 762M, XL: 1.5B
- GPT-2 XL:  $L = 48$ ,  $d = 1600$ ,  $h = 25$
- Context: 1024 tokens

#### **GPT-3 (2020):**

- Small: 125M to XL: 175B
- GPT-3 175B:  $L = 96$ ,  $d = 12288$ ,  $h = 96$
- Context: 2048 tokens
- Parameters: 175 billion!

**GPT-4 (2023):**

- Architecture details not fully disclosed
- Estimated: 1-1.7 trillion parameters (mixture of experts)
- Context: 8K (standard), 32K (extended)

**Example 14.1** (GPT-2 Small Layer). Configuration:  $L = 12$ ,  $d = 768$ ,  $h = 12$ ,  $d_{ff} = 3072$

Understanding the parameter breakdown of GPT-2 Small reveals how transformer capacity is distributed across different components. Each of the 12 decoder layers contains approximately 7 million parameters, with the feed-forward network consuming roughly two-thirds of this total. This distribution reflects the architectural choice to use an expansion factor of 4 in the FFN, where the hidden dimension  $d_{ff} = 4 \times d_{\text{model}} = 3072$ .

**Single decoder layer:**

1. Layer norm
2. Masked multi-head attention (12 heads)
3. Residual connection
4. Layer norm
5. Feed-forward ( $768 \rightarrow 3072 \rightarrow 768$ )
6. Residual connection

The masked multi-head attention mechanism requires four weight matrices:  $\mathbf{W}^Q$ ,  $\mathbf{W}^K$ ,  $\mathbf{W}^V$  for projecting to query, key, and value spaces, and  $\mathbf{W}^O$  for projecting the concatenated head outputs back to model dimension. Each of these matrices has dimensions  $768 \times 768$ , contributing  $4 \times 768^2 = 2,359,296$  parameters. The feed-forward network contains two linear transformations: the first expands from 768 to 3072 dimensions ( $768 \times 3072 = 2,359,296$  parameters), and the second projects back from 3072 to 768 dimensions (another  $768 \times 3072 = 2,359,296$  parameters), totaling 4,718,592 parameters. Layer normalization adds minimal parameters—just scale and bias terms for each dimension, contributing  $2 \times 2 \times 768 = 3,072$  parameters across the two layer norms per block.

**Parameters per layer:**

$$\text{Attention: } 4 \times 768^2 = 2,359,296 \quad (14.1)$$

$$\text{FFN: } 2 \times 768 \times 3072 = 4,718,592 \quad (14.2)$$

$$\text{Layer norms: } 2 \times 2 \times 768 = 3,072 \quad (14.3)$$

$$\text{Total: } 7,080,960 \approx 7M \quad (14.4)$$

Multiplying by 12 layers yields approximately 85 million parameters in the transformer blocks. The remaining 32 million parameters reside in the token embeddings, which map the vocabulary (typically 50,257 tokens for GPT-2) to the 768-dimensional model space. This embedding matrix alone contains  $50,257 \times 768 = 38,597,376$  parameters, though the actual vocabulary size may vary slightly. Position embeddings add another  $1024 \times 768 = 786,432$  parameters for the maximum sequence length of 1024 tokens. The final layer norm and output projection (which often shares weights with the token embedding) complete the 117 million parameter total.

12 layers:  $\approx 85M$ , plus embeddings  $\approx 32M = \mathbf{117M \text{ total}}$

## 14.2 Pre-Training: Autoregressive Language Modeling

### 14.2.1 Training Objective

Autoregressive language modeling forms the foundation of GPT’s pre-training approach. Unlike masked language modeling used in BERT, which predicts randomly masked tokens using bidirectional context, autoregressive modeling predicts each token based solely on preceding tokens. This objective aligns naturally with text generation tasks and enables the model to learn the statistical structure of language through next-token prediction.

The training objective maximizes the likelihood of each token given all previous tokens in the sequence. For a sequence  $\mathbf{x} = [x_1, x_2, \dots, x_n]$ , the model learns to maximize the joint probability  $P(x_1, x_2, \dots, x_n) = \prod_{i=1}^n P(x_i | x_1, \dots, x_{i-1})$ . Taking the logarithm converts this product into a sum, yielding the standard language modeling loss. This formulation has an elegant interpretation: the model learns to compress the training data by assigning high probability to observed sequences, with the negative log-likelihood measuring the number of bits required to encode the data under the model’s distribution.

**Definition 14.2** (Autoregressive Language Modeling). Maximize likelihood of next token given previous context:

$$\mathcal{L} = \sum_{i=1}^n \log P(x_i | x_1, \dots, x_{i-1}; \theta) \quad (14.5)$$

The implementation leverages the transformer’s parallel processing capabilities through teacher forcing. Rather than generating tokens sequentially during training, the entire sequence is processed in a single forward pass. The input sequence  $[x_1, x_2, \dots, x_n]$  is fed to the model, which produces hidden representations for all positions simultaneously. The causal attention mask ensures that position  $i$  cannot attend to positions  $j > i$ , maintaining the autoregressive property despite parallel computation. The model’s output at position  $i$  is trained to predict token  $x_{i+1}$ , creating  $n - 1$  training signals from a single sequence of length  $n$ . This parallel training is dramatically more efficient than sequential generation, enabling large-scale pre-training on massive text corpora.

The cross-entropy loss is computed at each position by comparing the model’s predicted distribution over the vocabulary with the true next token. For position  $i$  with hidden state  $\mathbf{h}_i$ , the model computes logits  $\mathbf{z}_i = \mathbf{h}_i \mathbf{W}_{\text{out}}$  where  $\mathbf{W}_{\text{out}} \in \mathbb{R}^{d_{\text{model}} \times V}$  projects to vocabulary size  $V$ . Applying softmax yields a probability distribution  $P(x_{i+1} | x_1, \dots, x_i) = \text{softmax}(\mathbf{z}_i)$ . The loss for this position is  $-\log P(x_{i+1} | x_1, \dots, x_i)$ , and the total loss sums over all positions. This formulation naturally handles variable-length sequences and provides dense training signal from every token in the corpus.

**Implementation:**

1. Input:  $[x_1, x_2, \dots, x_n]$
2. Target:  $[x_2, x_3, \dots, x_{n+1}]$  (shifted by 1)
3. Causal mask: Position  $i$  cannot attend to  $j > i$
4. Cross-entropy loss at each position

**Example 14.2** (GPT Training Example). Sentence: "The cat sat on the mat"

**Tokenized:**  $[T_1, T_2, T_3, T_4, T_5, T_6] = [\text{The}, \text{cat}, \text{sat}, \text{on}, \text{the}, \text{mat}]$

This simple example illustrates how GPT processes a sequence during training. The model receives the tokenized sequence as input and must predict each subsequent token based on the preceding context. At position 1, having seen only "The", the model predicts "cat". At position 2, with context "The cat", it predicts "sat". This continues through the sequence, with each position providing a training signal. The beauty of teacher forcing is that all these predictions occur in



parallel during a single forward pass, despite the autoregressive dependency structure.

**Training:**

$$P(T_2|T_1) = \text{softmax}(\mathbf{h}_1 \mathbf{W}_{\text{out}}) \quad \text{predict "cat"} \quad (14.6)$$

$$P(T_3|T_1, T_2) = \text{softmax}(\mathbf{h}_2 \mathbf{W}_{\text{out}}) \quad \text{predict "sat"} \quad (14.7)$$

$$\vdots \quad (14.8)$$

$$P(T_6|T_1, \dots, T_5) = \text{softmax}(\mathbf{h}_5 \mathbf{W}_{\text{out}}) \quad \text{predict "mat"} \quad (14.9)$$

The loss function sums the negative log-probabilities of the correct tokens at each position. If the model assigns high probability to the correct next token, the loss is low; if it assigns low probability, the loss is high. During backpropagation, gradients flow through all positions simultaneously, updating the model parameters to increase the probability of observed sequences. This dense training signal from every token in the corpus enables efficient learning of language statistics.

**Loss:**

$$\mathcal{L} = - \sum_{i=1}^5 \log P(T_{i+1}|T_1, \dots, T_i) \quad (14.10)$$

All positions trained simultaneously in parallel (teacher forcing)!

### 14.2.2 Pre-Training Data

The scale and diversity of pre-training data have proven critical to GPT’s capabilities. Each generation of GPT models trained on progressively larger and more diverse text corpora, revealing that data quality and quantity both matter significantly for downstream performance.

GPT-1 was trained on BooksCorpus, a collection of approximately 7,000 unpublished books from various genres including adventure, fantasy, and romance. This dataset contained roughly 800 million words, providing coherent long-form text that helped the model learn narrative structure and long-range dependencies. The choice of books as training data reflected the hypothesis that long-form text with coherent structure would be more valuable than shorter, disconnected documents. However, the relatively narrow domain coverage limited the model’s exposure to diverse topics and writing styles.

GPT-2 marked a significant shift in data philosophy with the creation of WebText, a dataset of 40 GB containing text from 8 million web pages. The data was collected by scraping outbound links from Reddit posts with at least 3 karma, using social curation as a quality filter. This approach yielded much more diverse content spanning news articles, tutorials, discussions, and creative writing across virtually all topics. The 40 GB corpus represented approximately 10 billion tokens, more than an order of magnitude larger than BooksCorpus. This scale and diversity enabled GPT-2 to demonstrate surprising zero-shot capabilities on tasks it had never been explicitly trained to perform.

GPT-3 scaled data collection to unprecedented levels, training on approximately 300 billion tokens drawn from multiple sources. The training mixture included Common Crawl (filtered to remove low-quality content), WebText2 (an expanded version of GPT-2’s dataset), Books1, Books2, and Wikipedia. The total dataset size reached roughly 570 GB of text. Critically, GPT-3 was trained for a single epoch over this massive dataset rather than multiple passes over smaller data. This decision reflected emerging understanding of scaling laws: given fixed compute budget, it is often better to train on more diverse data once than to repeatedly train on the same limited data. The single-epoch approach also reduced the risk of memorizing specific training examples, though concerns about data contamination and memorization remained.

The composition of GPT-3’s training data was carefully weighted, with higher-quality sources sampled more frequently. Common Crawl, despite being the largest source, was downweighted due to quality concerns, while Wikipedia and books received higher sampling rates. This weighting scheme balanced scale with quality, ensuring the model learned from both broad web text and curated high-quality sources. The exact mixing ratios and filtering procedures significantly impacted model performance, though these details were not fully disclosed.

**GPT-1:** BooksCorpus (7,000 books,  $\approx$  800M words)

**GPT-2:** WebText (40GB, 8M web pages)

**GPT-3:** Common Crawl (filtered), WebText2, Books1, Books2, Wikipedia

- Total:  $\approx$  570GB text
- Tokens:  $\approx$  300 billion
- Training: Single pass (not multiple epochs)

### 14.2.3 Training Infrastructure and Costs

Training GPT models at scale requires massive infrastructure, with costs increasing by orders of magnitude between model generations. GPT-2’s training on 32 TPU v3 chips for one week cost approximately \$50,000—accessible to well-funded labs. GPT-3’s training on 10,000+ V100 GPUs for one month cost an estimated \$4–12 million, consuming 1,287 MWh of energy and requiring sophisticated distributed training strategies (model, pipeline, and data parallelism). For a detailed treatment of distributed training infrastructure and cost estimation, see Chapter 11 (Training Transformers).

#### GPT-2 Training:

- Hardware: 32 TPU v3 chips ( $\approx$  13.4 PFLOPS)
- Training time:  $\approx$  1 week
- Cost:  $\approx$  \$50,000
- Batch size: 512 sequences  $\times$  1024 tokens
- Learning rate: Cosine decay with warmup

#### GPT-3 Training:

- Hardware: 10,000+ V100 GPUs (estimated,  $>$  1 exaFLOP)
- Training time:  $\approx$  1 month
- Cost: \$4-12 million (estimated)
- Energy consumption: 1,287 MWh
- Requires model parallelism, pipeline parallelism, and data parallelism
- High-bandwidth interconnects (NVLink, InfiniBand) essential

## 14.3 In-Context Learning and Few-Shot Prompting

### 14.3.1 Autoregressive Generation with KV Caching

Before exploring in-context learning, we must understand how GPT generates text autoregressively. The generation process differs fundamentally from training, as tokens are produced sequentially rather than in parallel. Naive implementation of autoregressive generation is extremely inefficient, but key-value caching provides dramatic speedups that make interactive generation practical.

During generation, the model produces one token at a time. Starting with a prompt, the model computes attention over all prompt tokens to generate the first new token. Then it appends this token to the sequence and computes attention over all tokens (prompt plus generated) to produce the second token. This continues until reaching a stopping condition like a maximum length or end-of-sequence token. The critical inefficiency is that each generation step recomputes attention for all previous tokens, even though their key and value representations never change.

Consider generating a sequence of length  $T$  tokens. The first step processes  $n_0$  prompt tokens, computing keys and values for all positions. The second step processes  $n_0 + 1$  tokens, recomputing the

same keys and values for the prompt plus computing them for the new token. By step  $T$ , we have computed keys and values for the prompt tokens  $T$  times, despite them being identical each time. The total computation grows quadratically:  $\sum_{t=1}^T (n_0 + t) = Tn_0 + T(T+1)/2 \approx Tn_0 + T^2/2$  forward passes through the attention mechanism.

Key-value caching eliminates this redundancy by storing the computed keys and values for all previous tokens. When generating token  $t$ , we only compute keys and values for the new token at position  $t$ , then concatenate with the cached keys and values from positions 1 through  $t-1$ . The attention computation at position  $t$  uses the full key and value matrices, but we avoid recomputing the cached portions. This reduces the computation from quadratic to linear in the generation length.

The memory requirements for KV caching scale with the sequence length, number of layers, and model dimension. For each layer, we must store key and value matrices of shape  $[n_{\text{current}}, d_{\text{model}}]$  where  $n_{\text{current}}$  is the current sequence length. With  $L$  layers and hidden dimension  $d$ , the cache requires  $2 \times L \times n_{\text{current}} \times d$  values. For GPT-2 with 12 layers, dimension 768, and sequence length 1024, the cache occupies  $2 \times 12 \times 1024 \times 768 = 18,874,368$  values, or approximately 75 MB in FP32 per sequence. This is modest compared to model parameters (440 MB for GPT-2), but grows linearly with batch size and sequence length.

The generation speed improvement from KV caching is dramatic. Without caching, generating  $T$  tokens requires  $O(T^2)$  operations. With caching, it requires  $O(T)$  operations. For GPT-2 generating 100 tokens, this represents a  $50\times$  speedup in theory. In practice, the speedup is somewhat less due to memory bandwidth limitations and the overhead of managing the cache, but  $10\text{-}20\times$  speedups are typical. This transforms generation from painfully slow (1-2 tokens per second) to interactive (20-50 tokens per second) on modern GPUs.

Batch generation introduces additional trade-offs. Processing multiple sequences in parallel amortizes the cost of loading model parameters and improves GPU utilization. However, the KV cache memory scales linearly with batch size. For GPT-2 with batch size 32 and sequence length 1024, the cache requires  $32 \times 75 \text{ MB} = 2.4 \text{ GB}$ . Combined with model parameters and activations, this can exhaust GPU memory. Practitioners must balance batch size against sequence length and model size to fit within memory constraints. Dynamic batching, where sequences of different lengths are grouped together, can improve efficiency by allowing longer sequences when the batch is small and more sequences when they are short.

#### Generation algorithm with KV caching:

1. Process prompt tokens  $[x_1, \dots, x_{n_0}]$  in parallel, computing and caching keys/values for all layers
2. For generation step  $t = 1, 2, \dots, T$ :
  - (a) Compute keys/values only for new token at position  $n_0 + t$
  - (b) Concatenate with cached keys/values from positions 1 to  $n_0 + t - 1$
  - (c) Compute attention using full key/value matrices
  - (d) Generate next token from output distribution
  - (e) Append new keys/values to cache
3. Return generated sequence  $[x_{n_0+1}, \dots, x_{n_0+T}]$

#### Memory requirements for KV cache:

$$\text{Cache memory} = 2 \times L \times n_{\text{max}} \times d_{\text{model}} \times B \times \text{bytes per value} \quad (14.11)$$

For GPT-2 (12 layers, 768 dim, 1024 tokens, batch 1, FP32):

$$2 \times 12 \times 1024 \times 768 \times 1 \times 4 = 75,497,472 \text{ bytes} \approx 75 \text{ MB} \quad (14.12)$$

For GPT-3 (96 layers, 12288 dim, 2048 tokens, batch 1, FP16):

$$2 \times 96 \times 2048 \times 12288 \times 1 \times 2 = 9,663,676,416 \text{ bytes} \approx 9.7 \text{ GB} \quad (14.13)$$

#### Generation speed comparison:

- **Without caching:**  $\sim$ 1-2 tokens/sec (recomputes all previous tokens)
- **With caching:**  $\sim$ 20-50 tokens/sec for GPT-2 on V100
- **With caching:**  $\sim$ 10-15 tokens/sec for GPT-3 on A100 (batch 1)
- **Batch generation:** Higher throughput (tokens/sec) but same latency per sequence

### 14.3.2 Zero-Shot, One-Shot, Few-Shot

### 14.3.3 Zero-Shot, One-Shot, Few-Shot

GPT-3's most remarkable capability is in-context learning: the ability to perform new tasks by conditioning on examples provided in the prompt, without any parameter updates or gradient descent. This emergent behavior was not explicitly trained for, yet it scales dramatically with model size, suggesting that large language models develop meta-learning capabilities through pre-training alone.

Zero-shot learning provides only a task description without examples. The model must infer the desired behavior from the natural language instruction alone. For translation, a zero-shot prompt might simply state "Translate English to French:" followed by the source text. The model must recognize the task from the instruction and generate an appropriate translation. Zero-shot performance varies widely across tasks—GPT-3 performs well on common tasks like translation and summarization but struggles with specialized or ambiguous tasks where the instruction alone provides insufficient specification.

**Zero-shot:** Task description only

```
Translate English to French:
sea otter =>
```

One-shot learning adds a single example demonstrating the desired input-output mapping. This single example often dramatically improves performance by clarifying the task format, output style, and level of detail expected. For translation, showing one English-French pair helps the model understand not just that translation is required, but also the desired formality level, whether to include punctuation, and how to handle proper nouns. The improvement from zero-shot to one-shot is often larger than from one-shot to few-shot, suggesting that the first example resolves most of the task ambiguity.

**One-shot:** One example

```
Translate English to French:
sea otter => loutre de mer
cheese =>
```

Few-shot learning provides multiple examples, typically between 10 and 100 depending on the task complexity and context window size. Additional examples help the model learn task-specific patterns, edge cases, and output formatting. For classification tasks, few-shot examples should cover all classes to avoid bias toward classes seen more frequently. For generation tasks, examples demonstrate the desired output length, style, and structure. The performance improvement from few-shot learning scales with both the number of examples and the model size—larger models extract more information from the same examples.

**Few-shot:** Multiple examples (typical: 10-100)

```
Translate English to French:
sea otter => loutre de mer
peppermint => menthe poivrée
plush giraffe => girafe en peluche
cheese =>
```

The mechanism underlying in-context learning remains partially mysterious. The model is not performing gradient descent or updating parameters—it processes the prompt in a single forward pass. Instead, the model appears to perform a form of implicit Bayesian inference, using the examples to narrow down the space of possible tasks and then applying the inferred task to the query. The attention

mechanism plays a crucial role, allowing later tokens to attend to earlier examples and extract relevant patterns. Larger models have more capacity to represent complex task distributions and perform more sophisticated inference, explaining why few-shot learning improves dramatically with scale.

**Key Point 14.1.** *GPT-3's key discovery: Large language models can perform tasks through in-context learning without parameter updates! Performance improves with model scale and number of examples.*

The practical implications are profound. In-context learning enables rapid adaptation to new tasks without fine-tuning, which requires labeled data, computational resources, and time. Users can deploy GPT-3 on novel tasks by simply crafting appropriate prompts with examples. This has spawned the field of prompt engineering, where practitioners carefully design prompts to elicit desired behaviors. However, in-context learning has limitations—it cannot match fine-tuned performance on tasks with abundant training data, and it is sensitive to example selection and ordering. The examples must fit within the context window, limiting the amount of task-specific information that can be provided.

#### 14.3.4 Emergent Abilities

As language models scale to billions and hundreds of billions of parameters, they exhibit emergent abilities—capabilities that appear suddenly at certain scale thresholds rather than improving gradually. These emergent behaviors were not explicitly programmed or trained for, yet they arise naturally from the combination of scale, architecture, and training data. Understanding emergence is crucial for predicting what capabilities future models might develop and for identifying the minimum scale required for specific applications.

Few-shot learning itself is an emergent ability. Models with fewer than 1 billion parameters show minimal few-shot learning capability—providing examples in the prompt barely improves performance over zero-shot. Between 1 billion and 10 billion parameters, few-shot learning begins to emerge, with clear improvements from adding examples. By 100 billion parameters, few-shot learning becomes highly effective, with GPT-3 175B demonstrating strong performance on many tasks with just 10-20 examples. This non-linear scaling suggests a phase transition in the model's internal representations, where sufficient capacity enables a qualitatively different form of processing.

Chain-of-thought reasoning represents another striking emergent ability. When prompted to show its reasoning step-by-step before providing an answer, models around 100 billion parameters begin to solve complex multi-step problems that smaller models cannot. For arithmetic word problems, asking the model to "think step by step" dramatically improves accuracy. The model generates intermediate reasoning steps, then uses those steps to arrive at the final answer. This capability appears suddenly—models below a certain scale show no benefit from chain-of-thought prompting, while larger models show substantial improvements. The emergence suggests that large models develop internal mechanisms for decomposing complex problems into simpler sub-problems.

Complex instruction following emerges only in the largest models. GPT-3 175B can follow multi-part instructions, maintain consistency across long generations, and adapt its behavior based on nuanced prompt details. Smaller models often ignore parts of complex instructions or fail to maintain consistency. This capability is essential for practical applications where users need fine-grained control over model behavior. The emergence of instruction following motivated the development of instruction-tuned models like InstructGPT, which further enhance this capability through supervised fine-tuning and reinforcement learning.

The scaling curve for most capabilities follows a smooth power law—performance improves predictably as model size increases. However, emergent abilities show sharp phase transitions where performance jumps discontinuously at certain scales. This creates challenges for predicting model capabilities: extrapolating from smaller models may underestimate the capabilities of larger models. It also raises questions about what other abilities might emerge at even larger scales. Some researchers hypothesize that abilities like true reasoning, planning, and causal understanding might emerge at scales

beyond current models, while others argue that architectural changes or different training objectives are necessary.

The mechanism underlying emergence remains debated. One hypothesis is that emergent abilities require a minimum representational capacity—below this threshold, the model cannot represent the necessary abstractions, while above it, the ability appears. Another hypothesis focuses on the training dynamics: certain capabilities require seeing specific patterns in the training data a minimum number of times, which only occurs when training on massive datasets. A third perspective suggests that emergence is partially an artifact of evaluation metrics—capabilities may improve gradually, but threshold-based metrics (like exact match accuracy) show discontinuous jumps.

Abilities that appear suddenly at certain scales:

- **Few-shot learning:** Emerges around 1B-10B parameters
- **Chain-of-thought reasoning:** Emerges around 100B parameters
- **Complex instruction following:** Largest models

**Scaling curve:** Performance on many tasks follows smooth power law, but some tasks show sharp phase transitions.

## 14.4 Scaling Laws

### 14.4.1 Parameter Scaling

The relationship between model size and performance follows remarkably predictable patterns, enabling researchers to forecast the capabilities of larger models before building them. These scaling laws have become central to modern AI research, guiding decisions about how to allocate computational resources between model size, training data, and training time.

The fundamental scaling law relates model performance, measured by loss on held-out data, to the number of parameters. Empirically, the loss follows a power law:

$$L(N) \approx \left( \frac{N_c}{N} \right)^\alpha \quad (14.14)$$

where  $N$  is the number of parameters,  $N_c$  is a constant, and  $\alpha \approx 0.076$ . This relationship holds over multiple orders of magnitude, from millions to hundreds of billions of parameters. The power law implies that every  $10\times$  increase in parameters yields a consistent reduction in loss, with no sign of saturation up to the largest models tested.

Performance (measured by loss) scales as:

$$L(N) \approx \left( \frac{N_c}{N} \right)^\alpha \quad (14.15)$$

where  $N$  is number of parameters,  $N_c$  is constant,  $\alpha \approx 0.076$ .

The practical implications are profound. The power law allows researchers to predict the performance of a 1 trillion parameter model by extrapolating from experiments with 1 billion and 10 billion parameter models. This predictability has motivated continued scaling efforts, as the returns to scale remain consistent even at enormous sizes. However, the exponent  $\alpha \approx 0.076$  means that improvements slow as models grow—achieving the same loss reduction requires exponentially more parameters. Reducing loss by half requires increasing parameters by a factor of  $(2)^{1/0.076} \approx 150$ , making continued progress increasingly expensive.

The scaling law applies specifically to the pre-training loss, which measures how well the model predicts the next token. Downstream task performance does not always scale as smoothly—some tasks show rapid improvement with scale while others plateau. This discrepancy arises because pre-training loss captures general language understanding, while specific tasks may require capabilities that emerge only at certain scales or that are not well-measured by next-token prediction. Nevertheless, pre-training loss remains the most reliable predictor of overall model capability.

Importantly, the scaling law holds only when other factors are not bottlenecks. If the training data is too small, the model will overfit and the scaling law breaks down. If the training time is too short, the model will not converge and performance will be suboptimal. The scaling laws assume that data and compute are scaled appropriately with model size, a condition that is not always met in practice.

**Implications:**

- Every 10× increase in parameters → consistent loss reduction
- No sign of saturation up to 175B parameters
- Motivates continued scaling

### 14.4.2 Compute-Optimal Training

While the parameter scaling law shows that larger models achieve better performance, it does not address the question of how to optimally allocate a fixed compute budget. Should we train a very large model on limited data, or a smaller model on more data? The Chinchilla paper provided a surprising answer that has reshaped thinking about model scaling.

The Chinchilla findings, based on training over 400 language models ranging from 70 million to 16 billion parameters, revealed that for a given compute budget  $C$ , the optimal allocation scales both model size and training data:

$$N_{\text{optimal}} \propto C^{0.5}, \quad D_{\text{optimal}} \propto C^{0.5} \quad (14.16)$$

This square-root scaling means that if you increase compute by 100×, you should increase both model size and training data by 10×. Critically, this implies that model size and data should scale equally—doubling compute should double both parameters and training tokens.

Chinchilla findings: For compute budget  $C$ , optimal allocation is:

$$N_{\text{optimal}} \propto C^{0.5}, \quad D_{\text{optimal}} \propto C^{0.5} \quad (14.17)$$

Applying this formula to GPT-3 reveals a striking conclusion: the model was significantly over-parameterized for its training compute. GPT-3 used 175 billion parameters trained on 300 billion tokens. According to Chinchilla scaling laws, the same compute budget would be better spent on an 80 billion parameter model trained on 1.4 trillion tokens. This smaller, better-trained model would achieve lower loss and better downstream performance than GPT-3, despite having less than half the parameters.

This finding explains why many large models are over-parameterized and under-trained. The focus on parameter count as a headline metric incentivized building the largest possible models, even when training data was insufficient. The Chinchilla results suggest that future models should prioritize data quality and quantity alongside parameter scaling. This has motivated efforts to curate larger, higher-quality training datasets and to train models for more steps on existing data.

The compute-optimal scaling also has implications for inference costs. Larger models are more expensive to serve, requiring more memory and compute per token generated. If a smaller, better-trained model achieves the same performance, it will be cheaper to deploy. This economic consideration is increasingly important as language models move from research to production applications serving millions of users.

However, the Chinchilla findings come with caveats. The optimal allocation depends on the relative costs of training versus inference. If inference costs dominate (as in production systems serving many users), a larger model trained on less data may be preferable because it achieves better performance per inference FLOP. The optimal allocation also depends on the availability of high-quality training data—if data is limited or expensive to collect, training a larger model on available data may be the only option.

**GPT-3 analysis:**

- 175B parameters trained on 300B tokens
- Chinchilla suggests: 80B parameters on 1.4T tokens would be better

- Many large models are over-parameterized, under-trained

The future direction suggested by these findings is clear: smaller models trained on more data. This approach reduces training costs (fewer parameters to update), reduces inference costs (smaller models to serve), and improves performance (better training efficiency). The challenge lies in collecting and curating the massive datasets required—1.4 trillion tokens is nearly  $5\times$  the data used for GPT-3, requiring extensive web scraping, filtering, and deduplication. Nevertheless, the Chinchilla findings have fundamentally shifted the scaling paradigm from "bigger is better" to "balanced scaling is optimal."

### 14.4.3 Hardware Requirements for Inference

While training requirements determine whether a model can be built, inference requirements determine whether it can be deployed. Understanding the hardware needed to serve GPT models is essential for practitioners considering which models to use in production and for researchers designing new architectures.

GPT-2 with 1.5 billion parameters represents the upper end of models that can be served efficiently on consumer hardware. In FP16 precision, the model parameters occupy  $1.5 \times 10^9 \times 2 = 3$  GB of memory. Adding the KV cache for a sequence of 1024 tokens requires approximately 75 MB per sequence, and activations for a single forward pass add another 100-200 MB. A single NVIDIA V100 GPU with 16 GB of memory can comfortably serve GPT-2 with batch sizes of 4-8 sequences, achieving generation speeds of approximately 50 tokens per second per sequence. This makes GPT-2 practical for real-time applications like chatbots, code completion, and interactive writing assistants.

The generation speed of 50 tokens per second on a V100 reflects several factors. The V100 provides 125 TFLOPS of FP16 performance, but actual utilization is typically 30-50% for autoregressive generation due to the sequential nature of the computation and memory bandwidth limitations. Each token generation requires a forward pass through all 48 layers, computing attention over the growing sequence length. With KV caching, the computation per token is roughly constant, but memory bandwidth for loading the cache and model parameters becomes the bottleneck. Batch processing multiple sequences in parallel improves throughput by amortizing parameter loading, but latency per sequence remains constant.

#### GPT-2 (1.5B) Inference:

- **Memory (FP16):** 3 GB parameters + 75 MB KV cache per sequence + 200 MB activations
- **Hardware:** Single V100 (16 GB) or RTX 3090 (24 GB)
- **Batch size:** 4-8 sequences on V100
- **Generation speed:**  $\sim 50$  tokens/sec per sequence
- **Latency:**  $\sim 20$  ms per token
- **Practical for:** Real-time applications, edge deployment

GPT-3 with 175 billion parameters presents dramatically different challenges. In FP16 precision, the parameters alone require  $175 \times 10^9 \times 2 = 350$  GB of memory. No single GPU can hold the entire model—even the largest NVIDIA A100 with 80 GB falls far short. Model parallelism is essential, splitting the model across multiple GPUs. A minimum of  $8 \times$  A100 (80 GB) GPUs is required just to hold the parameters, with each GPU storing approximately 44 GB of model weights. The KV cache for GPT-3 with 2048 tokens requires approximately 9.7 GB per sequence, further constraining batch sizes. With 8 GPUs, the total available memory is 640 GB, leaving roughly 290 GB for KV cache and activations after storing parameters—enough for batch sizes of 20-30 sequences.

The generation speed for GPT-3 is significantly slower than GPT-2, despite using more powerful hardware. With batch size 1 on  $8 \times$  A100 GPUs, GPT-3 generates approximately 10 tokens per second. The slowdown reflects several factors. First, the model is  $100\times$  larger, requiring  $100\times$  more computation per token. Second, model parallelism introduces communication overhead—activations must be transferred between GPUs at each layer, consuming bandwidth and adding latency. Third, the larger



KV cache requires more memory bandwidth to load at each generation step. Increasing batch size improves throughput (total tokens per second across all sequences) but does not reduce latency per sequence.

#### **GPT-3 (175B) Inference:**

- **Memory (FP16):** 350 GB parameters + 9.7 GB KV cache per sequence
- **Hardware:** Minimum 8× A100 (80 GB), often 16× for production
- **Model parallelism:** Required—split across GPUs
- **Batch size:** 1-4 sequences per 8-GPU node (memory constrained)
- **Generation speed:** ~10 tokens/sec per sequence (batch 1)
- **Latency:** ~100 ms per token
- **Cost:** \$0.02-0.06 per 1000 tokens (cloud pricing)

The high cost of GPT-3 inference has motivated extensive optimization efforts. Quantization to INT8 or INT4 reduces memory requirements by 2-4×, enabling larger batch sizes or smaller hardware configurations. However, quantization requires careful calibration to avoid accuracy degradation, and not all operations benefit equally—attention computations are particularly sensitive to reduced precision. Distillation, where a smaller model is trained to mimic GPT-3’s outputs, can achieve 90-95% of the performance with 10× fewer parameters, dramatically reducing inference costs. Sparse models, where only a subset of parameters are active for each input, offer another path to efficiency.

The economics of serving GPT-3 at scale are daunting. A single 8× A100 node costs approximately \$30,000-50,000 to purchase or \$20-30 per hour to rent from cloud providers. At 10 tokens per second, a single node can serve roughly 36,000 tokens per hour, or 864,000 tokens per day. For applications serving millions of users, dozens or hundreds of nodes are required, with costs reaching millions of dollars per month. This has created a market for inference-optimized models and specialized hardware, as well as prompting research into more efficient architectures that maintain capability while reducing computational requirements.

#### **Why GPT-3 inference is expensive:**

- **Memory:** 350 GB parameters require multiple high-end GPUs
- **Compute:** 175B parameters means 100× more FLOPs than GPT-2
- **Communication:** Model parallelism requires high-bandwidth interconnects
- **Latency:** Sequential generation cannot be parallelized across tokens
- **Utilization:** Autoregressive generation achieves 20-40% of peak FLOPS

## **14.5 Instruction Tuning and RLHF**

### **14.5.1 Instruction Tuning**

Fine-tune on (instruction, output) pairs:

Instruction: Summarize the following in one sentence:

[long text]

Output: [one-sentence summary]

#### **InstructGPT / ChatGPT approach:**

1. Pre-train with language modeling
2. Supervised fine-tuning on high-quality instructions
3. Train reward model from human preferences
4. Optimize policy with reinforcement learning

### 14.5.2 RLHF (Reinforcement Learning from Human Feedback)

---

**Algorithm 12:** RLHF Training
 

---

**1 Step 1: Supervised Fine-Tuning**

- Collect demonstrations: (prompt, high-quality response)
- Fine-tune GPT on demonstrations

**Step 2: Reward Model Training**

- Generate multiple responses per prompt
- Humans rank responses
- Train reward model  $r(x, y)$  to predict rankings

**Step 3: RL Fine-Tuning**

- Optimize policy  $\pi_\theta$  using PPO
  - Objective:  $\mathbb{E}_{x, y \sim \pi_\theta} [r(x, y)] - \beta \text{KL}(\pi_\theta \| \pi_{\text{ref}})$
  - KL penalty prevents divergence from original model
- 

**Result:** Models better aligned with human preferences, more helpful, honest, and harmless.

## 14.6 GPT Capabilities and Limitations

### 14.6.1 Capabilities

**Strong:**

- Text generation (creative writing, code, dialogue)
- Translation and summarization
- Question answering
- Few-shot learning
- Chain-of-thought reasoning
- Instruction following

### 14.6.2 Limitations

**Weak:**

- Factual accuracy (hallucinations)
- Mathematical reasoning (without tools)
- Long-term coherence in very long texts
- True understanding vs pattern matching
- Consistent personality/beliefs

**Hallucinations:** Model generates plausible but false information with high confidence.

**Mitigation strategies:**

- Retrieval-augmented generation (RAG)
- Tool use (calculators, search)
- Verification and fact-checking
- Constitutional AI principles

## 14.7 Exercises

**Exercise 14.1.** Implement autoregressive language modeling loss. For sequence "The quick brown fox", compute loss with teacher forcing. Compare with exposed schedule where model sees its own predictions.

**Exercise 14.2.** Estimate training cost for GPT-3 (175B params, 300B tokens):

1. FLOPs per forward pass
2. FLOPs for entire training (forward + backward  $\approx 3 \times$  forward)
3. Time on 1024 A100 GPUs (312 TFLOPS each)
4. Cost at \$2/GPU-hour

**Exercise 14.3.** Implement few-shot prompting. Test GPT-2 on classification task with 0, 1, 5, 10 examples. Plot accuracy vs number of shots. Does performance improve?

**Exercise 14.4.** Analyze scaling: Train models with [10M, 50M, 100M, 500M] parameters on same data. Plot loss vs parameters on log-log scale. Does it follow power law? Estimate exponent.

## 14.8 Solutions

Full solutions for all exercises are available at <https://deeplearning.hofkensvermeulen.be>.

## Chapter 15

# T5 and BART: Encoder-Decoder Architectures

### Chapter Overview

T5 (Text-to-Text Transfer Transformer) and BART (Bidirectional and Auto-Regressive Transformers) represent encoder-decoder architectures that combine the strengths of BERT and GPT. This chapter covers their architectures, pre-training objectives, unified text-to-text framework, and applications to sequence-to-sequence tasks.

### Learning Objectives

1. Understand encoder-decoder transformer architectures
2. Implement span corruption and denoising objectives
3. Apply text-to-text framework to diverse tasks
4. Compare T5, BART, and other seq2seq transformers
5. Fine-tune for summarization, translation, and question answering
6. Understand prefix LM and mixture of denoisers

## 15.1 T5: Text-to-Text Transfer Transformer

### 15.1.1 Unified Text-to-Text Framework

T5 introduces a conceptually elegant framework that reformulates every NLP task as text-to-text transformation. Rather than designing task-specific architectures with classification heads, span prediction layers, or other specialized output structures, T5 treats all tasks uniformly: the model receives text as input and produces text as output. This unification enables a single model architecture and training objective to handle diverse tasks ranging from translation and summarization to classification and question answering.

The text-to-text framework operates by prepending task-specific prefixes to the input text. For translation, the input becomes "translate English to German: That is good", and the model generates "Das ist gut". For summarization, the input is "summarize: [article text]", and the model produces a concise summary. Even classification tasks, which traditionally output discrete labels, are reformulated as text generation: "sst2 sentence: This movie is great" produces the text "positive" rather than a class index. Question answering similarly becomes "question: What is the capital of France? context: Paris is the capital and largest city of France..." with the model generating "Paris" as output.

This unification provides several compelling advantages. First, a single model can handle all tasks without architectural modifications, simplifying deployment and maintenance. Second, the same pre-training objective and fine-tuning procedure apply across tasks, eliminating the need for task-specific

training strategies. Third, the framework enables natural transfer learning across tasks—knowledge learned from translation can potentially benefit summarization, and vice versa. Fourth, evaluation becomes consistent across tasks, as all outputs are text sequences that can be compared using standard metrics. The text-to-text framework represents a philosophical shift toward treating language understanding and generation as a unified capability rather than separate skills requiring different architectures.

**Definition 15.1** (Text-to-Text Format). All tasks formulated as: text input  $\rightarrow$  text output

- Translation: "translate English to German: That is good"  $\rightarrow$  "Das ist gut"
- Summarization: "summarize: [article]"  $\rightarrow$  "[summary]"
- Classification: "sst2 sentence: This movie is great"  $\rightarrow$  "positive"
- QA: "question: ... context: ..."  $\rightarrow$  "[answer]"

### 15.1.2 T5 Architecture

T5 employs a standard encoder-decoder transformer architecture with several important modifications that distinguish it from the original transformer design. The architecture combines the bidirectional encoding capabilities of BERT with the autoregressive generation capabilities of GPT, creating a model that excels at both understanding input context and generating coherent output sequences.

The encoder processes the input text using fully-visible self-attention, identical to BERT's architecture. Each token in the encoder can attend to all other tokens in the input sequence without any causal masking, enabling the model to build rich bidirectional representations that capture both left and right context. This bidirectional attention is crucial for understanding tasks where the meaning of each token depends on the entire input context. The encoder consists of a stack of transformer layers, each containing multi-head self-attention followed by a position-wise feed-forward network, with residual connections and layer normalization applied in the pre-norm configuration for improved training stability.

The decoder generates the output text autoregressively using causal self-attention, similar to GPT's architecture. Each position in the decoder can only attend to previous positions in the output sequence, ensuring that the model cannot "cheat" by looking at future tokens during generation. Critically, the decoder also includes cross-attention layers that attend to the encoder's output representations. This cross-attention mechanism allows the decoder to focus on relevant parts of the input sequence while generating each output token, enabling the model to perform sequence-to-sequence transformations like translation and summarization where the output depends heavily on specific input content.

T5's most distinctive architectural innovation is its use of relative positional encodings rather than the absolute sinusoidal or learned positional embeddings used in BERT and GPT. Instead of adding position-specific embeddings to the input, T5 computes position-dependent biases that are added to the attention scores. These biases depend only on the relative distance between query and key positions, not their absolute positions in the sequence. The relative position biases are learned during training and shared across all layers, reducing the number of parameters while providing the model with flexible position information. The biases use a bucketing scheme where nearby positions have unique biases but distant positions share biases, reflecting the intuition that precise relative position matters more for nearby tokens than distant ones.

**Definition 15.2** (T5 Architecture). T5 uses encoder-decoder transformer with:

- **Encoder:** Fully-visible self-attention (like BERT), no causal masking
- **Decoder:** Causal self-attention (like GPT) plus cross-attention to encoder

- **Positional encoding:** Relative position bias, shared across layers, learned bucket-based distances
- **Normalization:** Pre-norm (layer norm before sub-layers)

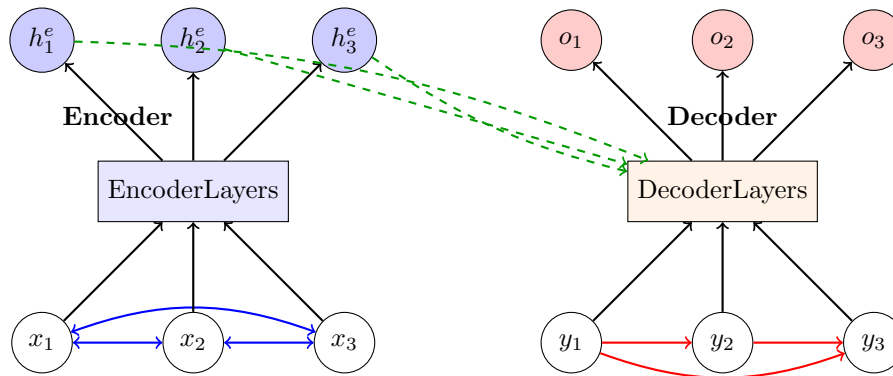


Figure 15.1: T5 encoder-decoder architecture. The encoder uses bidirectional attention (blue) to process input, the decoder uses causal attention (red) for autoregressive generation, and cross-attention (green dashed) allows the decoder to attend to all encoder outputs. This combines BERT’s understanding with GPT’s generation.

**Example 15.1** (T5-Base Architecture). Understanding T5-base’s parameter distribution reveals how encoder-decoder architectures allocate capacity between understanding and generation. The model uses 12 encoder layers and 12 decoder layers, each with hidden dimension  $d = 768$ , 12 attention heads, and feed-forward dimension  $d_{ff} = 3072$ . The vocabulary contains 32,000 tokens using SentencePiece tokenization, which provides better multilingual coverage and handles rare words more gracefully than WordPiece.

The parameter breakdown shows that the decoder contains more parameters than the encoder despite having the same number of layers and hidden dimensions. This asymmetry arises from the cross-attention mechanism in the decoder, which requires additional weight matrices to project encoder outputs into key and value spaces. Each encoder layer contains approximately 7.1 million parameters: 2.36 million in the self-attention mechanism (four projection matrices of dimension  $768 \times 768$ ) and 4.72 million in the feed-forward network (two projections:  $768 \rightarrow 3072$  and  $3072 \rightarrow 768$ ). Multiplying by 12 layers yields 85.2 million parameters in the encoder stack.

Each decoder layer contains approximately 9.4 million parameters due to the additional cross-attention mechanism. The causal self-attention contributes 2.36 million parameters, identical to the encoder’s self-attention. The cross-attention layer adds another 2.36 million parameters for its query, key, value, and output projections. The feed-forward network contributes 4.72 million parameters, same as the encoder. Multiplying by 12 decoder layers yields 112.8 million parameters in the decoder stack. The token embeddings add 24.6 million parameters ( $32,000 \times 768$ ), bringing the total to approximately 220 million parameters.

The memory requirements for T5-base depend on the numerical precision used. In FP32, the 220 million parameters occupy  $220,000,000 \times 4 = 880$  MB. Mixed precision training with FP16 activations and FP32 master weights reduces the working memory to approximately 440 MB for the model parameters during forward and backward passes, though the optimizer maintains FP32 copies. For inference, pure FP16 weights require only 440 MB, enabling T5-base to run comfortably on GPUs with 8-16 GB of memory. The encoder-decoder architecture requires more memory than encoder-only (BERT) or decoder-only (GPT) models of similar capacity, but the additional cross-attention capability justifies this cost for sequence-to-sequence tasks.

**Configuration:**

- Encoder layers:  $L_{\text{enc}} = 12$ , Decoder layers:  $L_{\text{dec}} = 12$
- Hidden size:  $d = 768$ , Attention heads:  $h = 12$ , FFN dimension:  $d_{\text{ff}} = 3072$
- Vocabulary:  $V = 32,000$  (SentencePiece)
- Parameters:  $\approx 220\text{M}$

**Parameter breakdown:**

$$\text{Embeddings: } 32,000 \times 768 = 24.6\text{M} \quad (15.1)$$

$$\text{Encoder (12 layers): } 12 \times 7.1\text{M} = 85.2\text{M} \quad (15.2)$$

$$\text{Decoder (12 layers): } 12 \times 9.4\text{M} = 112.8\text{M} \quad (15.3)$$

$$\text{Total: } \approx 220\text{M} \quad (15.4)$$

**Memory requirements:**

- FP32: 880 MB (model parameters only)
- FP16: 440 MB (inference)
- Training (mixed precision, batch size 128, sequence length 512):  $\approx 12$  GB

Decoder has more parameters due to cross-attention layer.

### 15.1.3 Pre-Training Objective: Span Corruption

T5 introduces span corruption as its primary pre-training objective, a more sophisticated variant of masked language modeling that better aligns with sequence-to-sequence tasks. Rather than masking individual tokens independently as in BERT, span corruption masks contiguous sequences of tokens and trains the model to predict the entire masked span. This objective encourages the model to learn longer-range dependencies and develop stronger generation capabilities, as the decoder must produce multi-token sequences rather than single tokens.

The span corruption procedure begins by sampling span lengths from a Poisson distribution with parameter  $\lambda = 3$ , yielding an average span length of 3 tokens. The algorithm then selects spans to mask such that approximately 15% of tokens in the sequence are corrupted, matching BERT's masking rate for fair comparison. Each masked span is replaced with a unique sentinel token (denoted  $\langle X \rangle$ ,  $\langle Y \rangle$ ,  $\langle Z \rangle$ , etc.), which serves as a placeholder indicating that tokens have been removed at this position. The model must predict the original content of each masked span in the correct order, identified by the sentinel tokens.

The training format differs significantly from BERT's masked language modeling. The encoder receives the corrupted input sequence with sentinel tokens replacing the masked spans. The decoder must generate a sequence containing the sentinel tokens followed by the original content of each span. For example, if the original text is "Thank you for inviting me to your party last week" and spans at positions 3-4 and 8-9 are masked, the encoder input becomes "Thank you  $\langle X \rangle$  inviting me to your  $\langle Y \rangle$  week". The decoder target is " $\langle X \rangle$  for  $\langle Y \rangle$  party last  $\langle Z \rangle$ ", where  $\langle Z \rangle$  marks the end of the sequence. This format trains the decoder to produce structured output with clear delimiters, a skill that transfers well to downstream generation tasks.

The computational efficiency of span corruption is notable. By masking spans rather than individual tokens, the number of prediction targets decreases while maintaining the same fraction of corrupted tokens. If 15% of tokens are masked in spans of average length 3, only 5% of positions contain sentinel tokens that trigger predictions. This reduces the decoder's generation length compared to predicting every masked token individually, accelerating training. However, the decoder must still generate all the masked tokens, so the total number of tokens predicted remains approximately 15% of the input length. The efficiency gain comes from the reduced number of sentinel tokens that must be processed by the encoder.

The span corruption objective provides several advantages over BERT’s masked language modeling for encoder-decoder models. First, it trains the decoder to generate multi-token sequences, developing the autoregressive generation capabilities needed for downstream tasks like summarization and translation. Second, it encourages the model to learn longer-range dependencies, as predicting a span requires understanding the broader context rather than just neighboring tokens. Third, it creates a more challenging task that prevents the model from relying on simple local patterns, forcing it to develop deeper semantic understanding. Fourth, the sentinel token mechanism provides a natural way to structure the decoder’s output, which transfers to tasks requiring structured generation.

**Definition 15.3** (Span Corruption). Corrupt spans of consecutive tokens, predict them:

1. Sample span lengths from  $\text{Poisson}(\lambda = 3)$ , average span length 3 tokens
2. Mask 15% of tokens in spans (same total masking rate as BERT)
3. Replace each span with sentinel token  $\langle X \rangle$ ,  $\langle Y \rangle$ , etc.
4. Encoder processes corrupted input with sentinels
5. Decoder predicts original spans in order, delimited by sentinels

**Example 15.2** (Span Corruption Example). **Original:** "Thank you for inviting me to your party last week"

**Step 1:** Select spans (15% total): positions [3-4] ("for inviting"), [8-9] ("party last")

**Step 2:** Replace spans with sentinels

**Corrupted input (encoder):**

Thank you  $\langle X \rangle$  me to your  $\langle Y \rangle$  week

**Target output (decoder):**

$\langle X \rangle$  for inviting  $\langle Y \rangle$  party last  $\langle Z \rangle$

The encoder processes the corrupted sequence, building bidirectional representations that capture the context around each sentinel token. The decoder must generate the sentinel tokens in order, followed by the original content of each span. The  $\langle Z \rangle$  token marks the end of the sequence, training the model to recognize when generation is complete. This structured prediction task requires the model to maintain coherent state across multiple spans, developing the sequential generation capabilities needed for downstream tasks.

Model must predict masked content and sentinel order, requiring understanding of both local context (what words fit in each span) and global structure (the order of spans in the original sequence).

#### 15.1.4 T5 Model Sizes and Scaling

T5 was released in five sizes to accommodate different computational budgets and performance requirements:

**T5 Model Sizes:**

- **T5-Small:** 60M parameters, 6 enc + 6 dec layers,  $d = 512$ , 8 heads
  - Memory: 240 MB (FP32), 120 MB (FP16)
  - Training: 2-3 days on 8 GPUs, cost  $\approx$  \$2,000
- **T5-Base:** 220M parameters, 12 enc + 12 dec layers,  $d = 768$ , 12 heads



- Memory: 880 MB (FP32), 440 MB (FP16)
- Training: 1 week on 64 TPU cores, cost  $\approx$  \$10,000-\$15,000
- **T5-Large:** 770M parameters, 24 enc + 24 dec layers,  $d = 1024$ , 16 heads
  - Memory: 3 GB (FP32), 1.5 GB (FP16)
  - Training: 2-3 weeks on 256 TPU cores, cost  $\approx$  \$50,000-\$75,000
- **T5-3B:** 3 billion parameters, 24 enc + 24 dec layers,  $d = 1024$ , 32 heads
  - Memory: 12 GB (FP32), 6 GB (FP16)
  - Training: 1 month on 512 TPU cores, cost  $>$  \$200,000
- **T5-11B:** 11 billion parameters, 24 enc + 24 dec layers,  $d = 1024$ , 128 heads
  - Memory: 44 GB (FP32), 22 GB (FP16)
  - Training: 2-3 months on 1024 TPU cores, cost  $>$  \$1,000,000

The scaling behavior reveals important insights about encoder-decoder architectures. Performance improves consistently with model size, but the rate of improvement decreases at larger scales. The cost per percentage point of accuracy improvement increases dramatically beyond T5-3B, suggesting that for most practical applications, T5-Base or T5-Large provide the best trade-off between performance and computational cost. The largest models are primarily valuable for research into scaling laws and for applications where even small accuracy improvements justify substantial computational investment.

### 15.1.5 T5 Training Details

T5’s pre-training represents a massive computational undertaking that required careful optimization of hardware utilization and training procedures. The model was trained on the Colossal Clean Crawled Corpus (C4), a dataset of approximately 750 GB of cleaned English text extracted from Common Crawl. The C4 dataset underwent extensive filtering to remove low-quality content, including deduplication, language identification to retain only English text, removal of placeholder text and profanity, and filtering of sentences without terminal punctuation. This cleaning process reduced the raw Common Crawl data by approximately 90%, but the resulting corpus provided much higher quality training signal.

The training infrastructure for T5-11B, the largest variant, required 1024 TPU v3 cores running continuously for approximately 2-3 months. Each TPU v3 core provides roughly 123 TFLOPS of bfloat16 performance, yielding a combined peak performance of approximately 126 PFLOPS for the full training cluster. The training used a batch size of 2048 sequences, each of maximum length 512 tokens, for a total of 1,048,576 tokens per batch. This enormous batch size enabled efficient utilization of the TPU hardware and provided stable gradient estimates despite the model’s scale. The learning rate schedule employed a linear warmup over 10,000 steps to a peak learning rate of  $10^{-2}$ , followed by inverse square root decay. The high peak learning rate, much larger than typical for transformer training, was enabled by the large batch size and careful gradient clipping.

The computational cost of T5-11B training is staggering. With 11 billion parameters and processing approximately 1 trillion tokens during training (the C4 dataset seen roughly 1.3 times), the total computation exceeds  $10^{24}$  FLOPs. At an effective compute rate of 50 PFLOPS (assuming 40% utilization of the 126 PFLOPS peak), the training requires approximately  $10^{24}/(50 \times 10^{15}) = 20$  million seconds, or roughly 230 days of continuous computation. The reported 2-3 month training time suggests either higher utilization rates or more efficient training procedures than this conservative estimate. The estimated cost exceeds \$1 million using cloud TPU pricing, making T5-11B one of the most expensive models trained at the time of its release in 2019.

T5-Base training is far more accessible, requiring approximately 1 week on 64 TPU v3 cores (128 TPU cores total). The batch size is reduced to 128 sequences of 512 tokens, totaling 65,536 tokens per batch. The training processes approximately 34 billion tokens (the C4 dataset seen once), requiring roughly  $10^{21}$  FLOPs total. At an effective compute rate of 2 PFLOPS, the training takes approximately

5-7 days, matching the reported training time. The estimated cost is \$10,000-\$15,000, making T5-Base training feasible for well-funded academic labs and smaller companies. The more modest computational requirements have enabled widespread experimentation with the T5 architecture and training approach.

The memory requirements during training are substantial due to the encoder-decoder architecture. For T5-11B with batch size 2048 and sequence length 512, the activations alone consume approximately 200-300 GB of memory. The model parameters require 44 GB in FP32, and the optimizer states (Adam maintains first and second moment estimates) require an additional 88 GB. The total memory footprint exceeds 400 GB, necessitating model parallelism across multiple TPU cores. The training employed a combination of data parallelism (different sequences on different cores) and model parallelism (different layers on different cores) to distribute the memory and computation efficiently. The cross-attention mechanism in the decoder requires storing encoder outputs for all sequences in the batch, adding significant memory overhead compared to encoder-only or decoder-only architectures.

#### **T5-11B Training Configuration:**

- Hardware: 1024 TPU v3 cores ( $\approx 126$  PFLOPS peak)
- Training time: 2-3 months continuous
- Dataset: C4 (750 GB cleaned text,  $\approx 1$  trillion tokens)
- Batch size:  $2048 \text{ sequences} \times 512 \text{ tokens} = 1,048,576 \text{ tokens/batch}$
- Learning rate:  $10^{-2}$  peak with inverse square root decay
- Total computation:  $> 10^{24}$  FLOPs
- Estimated cost:  $> \$1,000,000$
- Memory:  $> 400$  GB (requires model parallelism)

#### **T5-Base Training Configuration:**

- Hardware: 64 TPU v3 chips (128 cores,  $\approx 15$  PFLOPS peak)
- Training time: 5-7 days
- Dataset: C4 (750 GB, single pass  $\approx 34$  billion tokens)
- Batch size:  $128 \text{ sequences} \times 512 \text{ tokens} = 65,536 \text{ tokens/batch}$
- Learning rate:  $10^{-2}$  peak with inverse square root decay
- Total computation:  $\approx 10^{21}$  FLOPs
- Estimated cost: \$10,000-\$15,000
- Memory:  $\approx 20$ -30 GB (fits on single GPU with gradient accumulation)

The training procedures incorporated several optimizations to improve efficiency and stability. Mixed precision training with bfloat16 reduced memory consumption and accelerated computation on TPU hardware. Gradient clipping prevented instability from occasional large gradients. Dropout was applied with rate 0.1 during pre-training to prevent overfitting, though later work (T5.1.1) found that removing dropout during pre-training improved performance. The relative position biases were initialized to small random values and learned during training, converging to patterns that emphasized nearby positions while maintaining some attention to distant positions.

## 15.2 BART: Denoising Autoencoder

### 15.2.1 BART Architecture and Design Philosophy

BART (Bidirectional and Auto-Regressive Transformers) represents Facebook AI Research’s approach to combining the strengths of BERT and GPT through a denoising autoencoder framework. While T5 focuses on the text-to-text paradigm with task-specific prefixes, BART emphasizes learning robust representations through diverse corruption strategies during pre-training. The model architecture is conceptually similar to T5—an encoder-decoder transformer—but the pre-training approach and design philosophy differ significantly.

The BART encoder employs fully bidirectional attention identical to BERT, allowing each token to attend to all other tokens in the input sequence. This bidirectional processing enables the encoder to build rich contextual representations that capture dependencies in both directions. The encoder processes corrupted input text, where corruption can take many forms including token masking, deletion, infilling, sentence permutation, or document rotation. The diversity of corruption strategies forces the encoder to learn robust representations that can handle various types of noise and structural perturbations.

The BART decoder uses causal self-attention like GPT, generating output tokens autoregressively from left to right. Each position in the decoder can only attend to previous positions in the output sequence, maintaining the autoregressive property essential for text generation. The decoder also includes cross-attention layers that attend to the encoder’s output representations, enabling it to focus on relevant parts of the corrupted input while reconstructing the original text. This cross-attention mechanism is crucial for tasks like summarization and translation where the output must be grounded in specific input content.

BART-large, the primary configuration, uses 12 encoder layers and 12 decoder layers with hidden dimension  $d = 1024$  and 16 attention heads. This configuration is comparable to BERT-large in terms of depth and width, but the encoder-decoder architecture results in more total parameters. The model uses learned absolute positional embeddings rather than T5’s relative position biases or the original transformer’s sinusoidal encodings. The vocabulary contains approximately 50,000 tokens using byte-pair encoding (BPE), providing finer-grained tokenization than T5’s 32,000-token SentencePiece vocabulary.

**Definition 15.4** (BART). Bidirectional And Auto-Regressive Transformers:

- Encoder: Bidirectional self-attention (like BERT), processes corrupted input
- Decoder: Autoregressive causal attention (like GPT) plus cross-attention to encoder
- Pre-training: Reconstruct original text from diversely corrupted input
- Position encoding: Learned absolute positional embeddings

### 15.2.2 BART Parameter Breakdown and Memory Requirements

Understanding BART-large’s parameter distribution reveals how the model allocates capacity across its components. Each encoder layer contains approximately 12.6 million parameters. The self-attention mechanism requires four projection matrices ( $\mathbf{W}^Q$ ,  $\mathbf{W}^K$ ,  $\mathbf{W}^V$ ,  $\mathbf{W}^O$ ), each of dimension  $1024 \times 1024$ , contributing  $4 \times 1024^2 = 4,194,304$  parameters. The feed-forward network uses expansion factor 4, projecting from 1024 to 4096 dimensions and back, contributing  $2 \times 1024 \times 4096 = 8,388,608$  parameters. Layer normalization adds minimal parameters. Multiplying by 12 encoder layers yields approximately 151 million parameters in the encoder stack.

Each decoder layer contains approximately 16.8 million parameters due to the additional cross-attention mechanism. The causal self-attention contributes 4.2 million parameters, identical to the encoder’s self-attention. The cross-attention layer adds another 4.2 million parameters for its query,

key, value, and output projections. The feed-forward network contributes 8.4 million parameters, same as the encoder. Multiplying by 12 decoder layers yields approximately 202 million parameters in the decoder stack. The token embeddings add  $50,000 \times 1024 = 51,200,000$  parameters, and positional embeddings for sequences up to 1024 tokens add another  $1024 \times 1024 = 1,048,576$  parameters. The total reaches approximately 406 million parameters. This analysis follows the same component-level methodology used for BERT-base in Section 1.7.

The memory requirements for BART-large are substantial. In FP32, the 406 million parameters occupy  $406,000,000 \times 4 = 1,624$  MB, or approximately 1.6 GB. Mixed precision training with FP16 activations and FP32 master weights reduces the working memory to approximately 812 MB for the model parameters during forward and backward passes. For inference, pure FP16 weights require only 812 MB, enabling BART-large to run on GPUs with 12-16 GB of memory with reasonable batch sizes. Training with batch size 32 and sequence length 512 requires approximately 20-25 GB of GPU memory, necessitating high-memory GPUs like the V100 (32 GB) or A100 (40-80 GB).

#### **BART-large Configuration:**

- Encoder: 12 layers, Decoder: 12 layers
- Hidden:  $d = 1024$ , Heads:  $h = 16$ , FFN:  $d_{ff} = 4096$
- Vocabulary:  $V \approx 50,000$  (BPE)
- Parameters:  $\approx 406\text{M}$

#### **Parameter breakdown:**

$$\begin{aligned} \text{Embeddings: } & 50,000 \times 1024 + 1024 \times 1024 = 52.2\text{M} & (15.5) \\ \text{Encoder (12 layers): } & 12 \times 12.6\text{M} = 151.2\text{M} & (15.6) \\ \text{Decoder (12 layers): } & 12 \times 16.8\text{M} = 201.6\text{M} & (15.7) \\ \text{Total: } & \approx 406\text{M} & (15.8) \end{aligned}$$

#### **Memory requirements:**

- FP32: 1.6 GB (model parameters only)
- FP16: 812 MB (inference)
- Training (mixed precision, batch size 32, sequence length 512):  $\approx 20\text{-}25$  GB

### **15.2.3 Denoising Objectives and Corruption Strategies**

BART’s key innovation lies in exploring multiple corruption strategies during pre-training, systematically evaluating which types of noise lead to the most robust and transferable representations. Unlike BERT’s single masking strategy or T5’s span corruption, BART experiments with five different corruption approaches and combinations thereof. This exploration revealed that the choice of corruption strategy significantly impacts downstream task performance, with different strategies providing complementary benefits.

Token masking, borrowed directly from BERT, replaces random tokens with a special [MASK] token. Approximately 15% of tokens are selected and replaced, forcing the model to predict the original tokens based on surrounding context. This strategy is familiar and well-understood, providing a baseline for comparison with other corruption approaches. However, token masking has limitations: the [MASK] token never appears during fine-tuning, creating a train-test mismatch, and the independent masking of tokens doesn’t encourage the model to learn longer-range dependencies or sequential generation capabilities.

Token deletion removes random tokens entirely from the input sequence, forcing the model to determine which positions are missing and what content should fill them. Unlike masking, which provides explicit markers indicating where tokens were removed, deletion requires the model to infer the locations of missing content from the remaining context. This creates a more challenging task that

encourages the model to develop robust positional understanding and the ability to detect gaps in the input. For example, deleting "B" and "D" from "A B C D E" yields "A C E", and the model must reconstruct the full sequence "A B C D E" without explicit indicators of where tokens were removed.

Text infilling represents a more sophisticated corruption strategy that combines aspects of span masking and deletion. Spans of text are sampled (with lengths drawn from a Poisson distribution with  $\lambda = 3$ , similar to T5), but instead of replacing each span with a unique sentinel token, all spans are replaced with a single [MASK] token. This forces the decoder to determine how many tokens to generate for each masked span based on context alone. For example, replacing "B C D E" in "A B C D E F" with a single [MASK] yields "A [MASK] F", and the model must generate "B C D E" without knowing in advance that four tokens are needed. This uncertainty makes text infilling substantially more challenging than T5's span corruption with explicit sentinel tokens.

Sentence permutation shuffles the order of sentences within a document, requiring the model to reconstruct the original sentence order. This corruption strategy targets document-level structure rather than token-level content, encouraging the model to learn discourse coherence and inter-sentence dependencies. For example, a document with sentences [S1, S2, S3, S4] might be permuted to [S3, S1, S4, S2], and the model must generate the original order [S1, S2, S3, S4]. This task is particularly relevant for summarization and document understanding, where maintaining coherent structure is crucial.

Document rotation selects a random token as the new start of the document and rotates the entire sequence accordingly. The model must identify the true start of the document and generate the original sequence. For example, rotating "A B C D E" at position 3 yields "D E A B C", and the model must recognize that "A" is the true start and generate "A B C D E". This task encourages the model to learn document-level structure and identify natural boundaries, though it proved less effective than other corruption strategies in practice.

The BART paper systematically evaluated these corruption strategies individually and in combination, finding that text infilling combined with sentence permutation provided the best performance across downstream tasks. This combination balances token-level and document-level corruption, encouraging the model to learn both local language patterns and global document structure. The text infilling component develops strong generation capabilities by forcing the model to produce variable-length spans, while sentence permutation develops discourse understanding by requiring the model to reason about inter-sentence relationships.

#### **BART Corruption Strategies:**

##### **1. Token Masking:** Replace tokens with [MASK] (like BERT)

- 15% of tokens replaced with [MASK]
- Provides explicit markers for missing content
- Baseline strategy for comparison

##### **2. Token Deletion:** Remove random tokens entirely

Original: A B C D E

Corrupted: A C E

Target: A B C D E

- Model must infer locations of missing tokens
- More challenging than masking
- Encourages robust positional understanding

##### **3. Text Infilling:** Replace spans with single [MASK]

Original: A B C D E F

Corrupted: A [MASK] F

Target: B C D E

- Span lengths sampled from Poisson( $\lambda = 3$ )

- Model must determine span length from context
- More challenging than T5’s sentinel-based span corruption

#### 4. **Sentence Permutation:** Shuffle sentence order

- Targets document-level structure
- Encourages learning of discourse coherence
- Particularly beneficial for summarization

#### 5. **Document Rotation:** Rotate document, model finds start

- Less effective than other strategies
- Encourages learning of document boundaries

**Best combination (BART’s final):** Text infilling + sentence permutation

- Balances token-level and document-level corruption
- Develops both generation and discourse understanding
- Achieves best performance across diverse downstream tasks

#### **Example 15.3** (BART Pre-training). **Original document:**

The cat sat on the mat. It was very comfortable.  
The dog barked loudly.

#### **After corruption (infilling + permutation):**

The dog barked loudly.  
The [MASK] comfortable.

**Encoder input:** Corrupted text

**Decoder target:** Original complete text

The model must reconstruct the missing span “cat sat on the mat. It was very” and reorder the sentences to match the original document structure. This combined corruption strategy forces the model to develop both local generation capabilities (filling in missing text) and global discourse understanding (recognizing proper sentence order).

### 15.2.4 BART Training Details

BART-large was trained on a combination of datasets totaling approximately 160 GB of text, including BooksCorpus, English Wikipedia, CC-News, OpenWebText, and Stories. This diverse training corpus provides broad coverage of topics and writing styles, enabling the model to learn robust representations that transfer well to downstream tasks. The training used 256 NVIDIA V100 GPUs for approximately 2 weeks, with an estimated cost of \$50,000–\$75,000 using cloud computing resources.

The training configuration employed a batch size of 128 sequences with maximum length 1024 tokens, totaling 131,072 tokens per batch. This large batch size enabled stable training with the Adam optimizer and efficient GPU utilization. The learning rate schedule used a polynomial decay from a peak learning rate of  $3 \times 10^{-4}$  with 500 warmup steps. The training processed approximately 50 billion tokens total, seeing the training corpus roughly once. Mixed precision training with FP16 reduced memory consumption and accelerated computation on the V100 GPUs.

The memory requirements during training are substantial due to the encoder-decoder architecture and large batch size. With batch size 128 and sequence length 1024, the activations consume approximately 40-50 GB of memory. The model parameters require 1.6 GB in FP32, and the Adam optimizer states require an additional 3.2 GB. The total memory footprint reaches approximately 50-60 GB, necessitating data parallelism across multiple GPUs. Each GPU processes a subset of the batch, with gradients synchronized across GPUs after each backward pass.

**BART-large Training Configuration:**

- Hardware: 256 NVIDIA V100 GPUs (32 GB each)
- Training time:  $\approx 2$  weeks
- Dataset: 160 GB text (BooksCorpus, Wikipedia, CC-News, OpenWebText, Stories)
- Batch size: 128 sequences  $\times$  1024 tokens = 131,072 tokens/batch
- Learning rate:  $3 \times 10^{-4}$  peak with polynomial decay
- Total tokens:  $\approx 50$  billion
- Estimated cost: \$50,000-\$75,000
- Memory per GPU:  $\approx 25$ -30 GB (data parallelism across GPUs)

## 15.3 Encoder-Decoder Efficiency Analysis

### 15.3.1 Computational Cost of Cross-Attention

Understanding the computational and memory costs of encoder-decoder architectures compared to encoder-only (BERT) or decoder-only (GPT) models is essential for choosing the appropriate architecture for a given task. The key difference lies in the cross-attention mechanism, which enables the decoder to attend to encoder outputs but introduces additional computational and memory overhead.

The cross-attention mechanism in each decoder layer requires computing attention between decoder queries and encoder keys/values. For a decoder sequence of length  $n_{\text{dec}}$  and encoder sequence of length  $n_{\text{enc}}$ , the cross-attention computation involves three main steps. First, the decoder hidden states are projected to queries  $\mathbf{Q} \in \mathbb{R}^{n_{\text{dec}} \times d}$  using weight matrix  $\mathbf{W}^Q \in \mathbb{R}^{d \times d}$ , requiring  $n_{\text{dec}} \times d^2$  FLOPs. Second, the encoder outputs are projected to keys  $\mathbf{K} \in \mathbb{R}^{n_{\text{enc}} \times d}$  and values  $\mathbf{V} \in \mathbb{R}^{n_{\text{enc}} \times d}$  using weight matrices  $\mathbf{W}^K, \mathbf{W}^V \in \mathbb{R}^{d \times d}$ , requiring  $2 \times n_{\text{enc}} \times d^2$  FLOPs. Third, the attention scores  $\mathbf{S} = \mathbf{QK}^\top$  are computed, requiring  $n_{\text{dec}} \times n_{\text{enc}} \times d$  FLOPs, followed by softmax and multiplication with values, requiring another  $n_{\text{dec}} \times n_{\text{enc}} \times d$  FLOPs.

The total computational cost of cross-attention per layer is approximately  $n_{\text{dec}} \times d^2 + 2 \times n_{\text{enc}} \times d^2 + 2 \times n_{\text{dec}} \times n_{\text{enc}} \times d$  FLOPs. For typical sequence lengths where  $n_{\text{dec}} \approx n_{\text{enc}} = n$ , this simplifies to  $3nd^2 + 2n^2d$  FLOPs. Comparing to self-attention, which requires  $4nd^2 + 2n^2d$  FLOPs, cross-attention adds approximately 75% of the cost of self-attention per layer. With  $L_{\text{dec}}$  decoder layers, the total cross-attention cost is  $L_{\text{dec}} \times (3nd^2 + 2n^2d)$  FLOPs.

For T5-Base with 12 decoder layers,  $d = 768$ , and  $n = 512$ , the cross-attention computation requires approximately  $12 \times (3 \times 512 \times 768^2 + 2 \times 512^2 \times 768) \approx 12 \times (9.1 + 4.0) \times 10^8 = 1.57 \times 10^{11}$  FLOPs per forward pass. This represents approximately 15-20% of the total forward pass computation, a significant but not dominant fraction. The cross-attention cost scales linearly with the number of decoder layers and quadratically with sequence length, making it increasingly expensive for long sequences.

The memory requirements for cross-attention are equally important. The encoder outputs must be stored in memory for all decoder layers to access during cross-attention. For batch size  $B$ , encoder sequence length  $n_{\text{enc}}$ , and hidden dimension  $d$ , the encoder outputs require  $B \times n_{\text{enc}} \times d$  values. For T5-Base with batch size 32, sequence length 512, and dimension 768, this amounts to  $32 \times 512 \times 768 = 12,582,912$  values, or approximately 50 MB in FP32 or 25 MB in FP16. While modest compared to model parameters, this memory scales linearly with batch size and sequence length, becoming significant for large batches or long sequences.

Additionally, the cross-attention mechanism requires storing attention weights  $\mathbf{A} \in \mathbb{R}^{n_{\text{dec}} \times n_{\text{enc}}}$  for each head in each layer during training (for backpropagation). With  $h$  attention heads and  $L_{\text{dec}}$  decoder layers, the total attention weight memory is  $B \times L_{\text{dec}} \times h \times n_{\text{dec}} \times n_{\text{enc}}$  values. For T5-Base with batch size 32, 12 decoder layers, 12 heads, and sequence length 512, this amounts to  $32 \times 12 \times 12 \times 512 \times 512 = 1,207,959,552$  values, or approximately 4.8 GB in FP32 or 2.4 GB in FP16. This memory requirement can become a bottleneck for training with large batch sizes or long sequences.

**Cross-attention computational cost per layer:**

$$\text{FLOPs}_{\text{cross-attn}} = n_{\text{dec}} \times d^2 + 2 \times n_{\text{enc}} \times d^2 + 2 \times n_{\text{dec}} \times n_{\text{enc}} \times d \quad (15.9)$$

For  $n_{\text{dec}} = n_{\text{enc}} = n$ :

$$\text{FLOPs}_{\text{cross-attn}} \approx 3nd^2 + 2n^2d \quad (15.10)$$

**Memory requirements:**

- Encoder outputs:  $B \times n_{\text{enc}} \times d$  values (must be stored for all decoder layers)
- Cross-attention weights (training):  $B \times L_{\text{dec}} \times h \times n_{\text{dec}} \times n_{\text{enc}}$  values

**Example: T5-Base (batch size 32, sequence length 512):**

- Cross-attention FLOPs per layer:  $\approx 1.3 \times 10^{10}$  FLOPs
- Total cross-attention (12 layers):  $\approx 1.6 \times 10^{11}$  FLOPs (15-20% of forward pass)
- Encoder output memory: 50 MB (FP32) or 25 MB (FP16)
- Cross-attention weight memory: 4.8 GB (FP32) or 2.4 GB (FP16)

### 15.3.2 Comparison: Encoder-Decoder vs Decoder-Only

The choice between encoder-decoder architectures (T5, BART) and decoder-only architectures (GPT) involves fundamental trade-offs in computational efficiency, memory usage, and task suitability. Understanding these trade-offs is essential for practitioners deciding which architecture to use for their specific application.

Decoder-only models like GPT use only causal self-attention, processing sequences autoregressively from left to right. For a sequence of length  $n$ , a decoder-only model with  $L$  layers requires approximately  $L \times (4nd^2 + 2n^2d)$  FLOPs for the forward pass. The memory requirements include model parameters, activations, and KV cache for generation. For GPT-2 with 12 layers,  $d = 768$ , and  $n = 512$ , the forward pass requires approximately  $12 \times (4 \times 512 \times 768^2 + 2 \times 512^2 \times 768) \approx 1.2 \times 10^{12}$  FLOPs. The KV cache for generation requires  $2 \times L \times n \times d$  values, or approximately 75 MB in FP32 for GPT-2 with sequence length 1024.

Encoder-decoder models like T5 and BART use separate encoder and decoder stacks with cross-attention connecting them. For input sequence length  $n_{\text{enc}}$  and output sequence length  $n_{\text{dec}}$ , the encoder requires  $L_{\text{enc}} \times (4n_{\text{enc}}d^2 + 2n_{\text{enc}}^2d)$  FLOPs, and the decoder requires  $L_{\text{dec}} \times (4n_{\text{dec}}d^2 + 2n_{\text{dec}}^2d + 3n_{\text{dec}}d^2 + 2n_{\text{dec}}n_{\text{enc}}d)$  FLOPs. For T5-Base with  $n_{\text{enc}} = n_{\text{dec}} = 512$ , the total forward pass requires approximately  $2.1 \times 10^{12}$  FLOPs, roughly  $1.75 \times$  more than GPT-2 of similar size. The memory requirements include encoder outputs ( $B \times n_{\text{enc}} \times d$ ) and cross-attention weights, adding 25-50 MB beyond decoder-only models.

The parameter count comparison reveals that encoder-decoder models require more parameters than decoder-only models of similar capacity. T5-Base with 220 million parameters has 12 encoder layers (85M parameters) and 12 decoder layers (113M parameters including cross-attention). GPT-2 with 12 layers and the same hidden dimension contains only 117 million parameters, as it lacks the encoder stack and cross-attention mechanisms. This means encoder-decoder models require approximately  $1.9 \times$  more parameters than decoder-only models with the same number of layers and hidden dimension.

However, the computational comparison depends critically on the task. For generation tasks where the input is short and the output is long (e.g., generating a long document from a short prompt), decoder-only models can be more efficient. The encoder-decoder model processes the short input once



through the encoder, then generates the long output through the decoder with cross-attention. The decoder-only model must process the entire sequence (input plus generated output) autoregressively, with each new token requiring attention over all previous tokens. For input length  $n_{\text{in}}$  and output length  $n_{\text{out}}$ , the decoder-only model requires  $\sum_{t=1}^{n_{\text{out}}} (n_{\text{in}} + t) \approx n_{\text{out}} \times n_{\text{in}} + n_{\text{out}}^2/2$  attention operations, while the encoder-decoder model requires  $n_{\text{in}}^2$  (encoder) plus  $n_{\text{out}}^2$  (decoder self-attention) plus  $n_{\text{out}} \times n_{\text{in}}$  (cross-attention). When  $n_{\text{out}} \gg n_{\text{in}}$ , the encoder-decoder model is more efficient.

For tasks where the input is long and the output is short (e.g., classification or extractive question answering), decoder-only models can be more efficient. The encoder-decoder model must process the long input through the encoder, then generate the short output through the decoder. The decoder-only model processes the input once, then generates the short output. However, encoder-only models like BERT are typically most efficient for these tasks, as they avoid the decoder entirely and use a simple classification head.

The memory efficiency comparison favors decoder-only models for inference, as they avoid storing encoder outputs and cross-attention weights. However, for training with large batch sizes, the difference is less significant, as both architectures require substantial memory for activations and gradients. The KV cache for decoder-only models grows with the total sequence length (input plus output), while encoder-decoder models cache only decoder states, potentially providing memory advantages for long input sequences.

#### **When to use encoder-decoder (T5, BART):**

- Sequence-to-sequence tasks: translation, summarization, question answering with generation
- Tasks requiring bidirectional understanding of input: the encoder can attend to the full input context
- Tasks with long input and short output: encoder processes input once, decoder generates short output
- Multi-task learning: text-to-text framework enables unified training across diverse tasks

#### **When to use decoder-only (GPT):**

- Pure generation tasks: story generation, dialogue, code generation
- Tasks with short input and long output: decoder-only can be more efficient
- In-context learning: decoder-only models excel at few-shot learning from examples in the prompt
- Simplicity: decoder-only architecture is simpler to implement and deploy

#### **Computational comparison (similar capacity):**

- Parameters: Encoder-decoder  $\approx 1.9\times$  decoder-only (due to encoder stack and cross-attention)
- FLOPs per forward pass: Encoder-decoder  $\approx 1.5\text{-}2\times$  decoder-only (depends on sequence lengths)
- Memory (inference): Decoder-only more efficient (no encoder outputs or cross-attention weights)
- Memory (training): Similar for both architectures with large batch sizes

## **15.4 Comparing T5 and BART**

### **Performance comparison on GLUE:**

- T5-11B: 90.3 (state-of-art at release)
- BART-large: 88.4
- RoBERTa-large: 88.5

### **Summarization (CNN/DailyMail):**

- BART-large: ROUGE-L 44.16 (best)
- T5-base: ROUGE-L 42.05

Aspect	T5	BART
Framework	Text-to-text	Denoising autoencoder
Pre-training	Span corruption	Multiple denoisers
Position encoding	Relative bias	Absolute learned
Vocabulary	32K (SentencePiece)	50K (BPE)
Best for	Unified multi-task	Summarization/generation
Largest size	11B parameters	400M parameters

## 15.5 Prefix Language Models

### 15.5.1 Prefix LM Objective

**Definition 15.5** (Prefix Language Model). Bidirectional attention on prefix, causal on rest:

- Prefix (input): Fully-visible attention
- Target (output): Causal attention
- Single model (no separate encoder/decoder)

**Example:**

Prefix: "Translate to French: Hello"

Target: "Bonjour"

Attention mask:

- Prefix tokens can attend to all prefix
- Target tokens attend causally
- Enables both understanding and generation

**Models using Prefix LM:**

- UniLM (Microsoft)
- GLM (Tsinghua)
- UL2 (Google)

## 15.6 Applications and Fine-tuning

### 15.6.1 Summarization

**Task:** Input document  $\rightarrow$  Summary

**T5 format:**

summarize: [article text]

**BART approach:**

- Encoder: Full article
- Decoder: Generate summary

**Metrics:**

- ROUGE-1, ROUGE-2, ROUGE-L (n-gram overlap)
- BERTScore (semantic similarity)

### 15.6.2 Translation

**T5 format:**

translate English to German: That is good.

**Output:** "Das ist gut."

**Multi-task advantage:** Single T5 model handles multiple language pairs by conditioning on task prefix.

### 15.6.3 Question Answering

**T5 format:**

question: What is the capital of France?

context: Paris is the capital and largest city of France...

**Output:** "Paris"

**Comparison to BERT:**

- BERT: Span prediction (start/end positions)
- T5: Text generation (more flexible)

## 15.7 Mixture of Denoisers (UL2)

**UL2 combines multiple objectives:**

**R-Denoiser (Regular):** Short spans (like T5)

**S-Denoiser (Sequential):** Prefix LM

**X-Denoiser (Extreme):** Very long spans or high corruption

**Benefits:**

- More robust representations
- Better transfer to diverse tasks
- Single model for understanding and generation

## 15.8 Exercises

**Exercise 15.1.** Implement span corruption. For text "The quick brown fox jumps over the lazy dog":

1. Sample span lengths from  $\text{Poisson}(\lambda = 3)$
2. Corrupt 15% with spans
3. Generate corrupted input and target

**Exercise 15.2.** Fine-tune T5-base on summarization (CNN/DailyMail):

1. Format data as "summarize: [article]"  $\rightarrow$  "[summary]"
2. Train for 3 epochs with learning rate  $10^{-4}$
3. Evaluate ROUGE scores

4. Compare with BART-base

**Exercise 15.3.** Calculate parameter counts for:

1. T5-base (encoder + decoder)
2. BART-large
3. Compare to BERT-base (encoder only) and GPT-2 (decoder only)

Explain why encoder-decoder has most parameters.

**Exercise 15.4.** Implement text-to-text framework. Convert these tasks to T5 format:

1. Sentiment classification (positive/negative)
2. Named entity recognition
3. Textual entailment (premise + hypothesis  $\rightarrow$  entailed/contradiction/neutral)

## 15.9 Solutions

Full solutions for all exercises are available at <https://deeplearning.hofkensvermeulen.be>.

# Chapter 16

## Efficient Transformers

### Chapter Overview

Standard transformers have  $O(n^2)$  complexity in sequence length, limiting their application to long sequences. This chapter covers efficient attention mechanisms that reduce complexity: sparse attention, linear attention, low-rank methods, and kernel-based approaches.

### Learning Objectives

1. Understand the quadratic bottleneck in standard attention
2. Implement sparse attention patterns (sliding window, strided, global)
3. Apply Linformer and Performer for linear complexity
4. Use Flash Attention for memory-efficient computation
5. Compare trade-offs: accuracy vs efficiency vs memory
6. Deploy long-context models (Longformer, BigBird)

## 16.1 The Quadratic Bottleneck

### 16.1.1 Complexity Analysis

The standard self-attention mechanism computes attention scores between all pairs of tokens in a sequence, leading to computational and memory requirements that scale quadratically with sequence length. The attention operation is defined as:

$$\text{Attention}(\mathbf{Q}, \mathbf{K}, \mathbf{V}) = \text{softmax}\left(\frac{\mathbf{Q}\mathbf{K}^\top}{\sqrt{d_k}}\right) \mathbf{V} \quad (16.1)$$

where  $\mathbf{Q}, \mathbf{K}, \mathbf{V} \in \mathbb{R}^{n \times d}$  represent the query, key, and value matrices for a sequence of length  $n$  with model dimension  $d$ .

The computational bottleneck arises from computing the attention matrix  $\mathbf{Q}\mathbf{K}^\top \in \mathbb{R}^{n \times n}$ , which requires  $O(n^2d)$  floating-point operations. For each of the  $n$  queries, we compute dot products with all  $n$  keys, where each dot product involves  $d$  multiplications and additions. The subsequent softmax normalization adds  $O(n^2)$  operations, and the final multiplication with values  $\mathbf{V}$  requires another  $O(n^2d)$  operations. The memory bottleneck is equally severe: storing the attention matrix requires  $O(n^2)$  memory, which must be materialized before the softmax operation and retained for the backward pass during training.

This quadratic scaling becomes prohibitive for long sequences. Consider a BERT-base model with  $d = 768$  and 12 attention heads processing a sequence of length  $n = 4096$ . Each attention head must store an attention matrix of size  $4096 \times 4096$ , requiring  $4096^2 \times 4 = 67$  MB in FP32 format. Across all

12 heads, this amounts to 804 MB just for attention weights in a single layer. With 12 layers, the total memory for attention matrices alone reaches 9.6 GB, nearly filling an NVIDIA V100 GPU with 16 GB memory before accounting for activations, gradients, or model parameters.

**Example 16.1** (Long Sequence Costs). The quadratic scaling of attention memory becomes dramatically worse as sequence length increases. For a single attention head with  $d = 768$  in FP32 format, the memory requirements grow as follows:

For  $n = 512$  tokens (BERT’s original limit), the attention matrix requires  $512^2 \times 4 = 1.05$  MB per head. This is manageable even with multiple layers and batch processing. However, increasing to  $n = 2048$  tokens requires  $2048^2 \times 4 = 16.8$  MB per head—a  $16\times$  increase for only a  $4\times$  increase in sequence length. At  $n = 4096$  tokens, memory consumption reaches 67 MB per head, and at  $n = 8192$  tokens, it explodes to 268 MB per head—a  $256\times$  increase compared to the 512-token baseline.

With 12 attention heads and 12 layers, processing a single sequence of 8192 tokens requires  $268 \times 12 \times 12 = 38.6$  GB just for attention matrices, exceeding the capacity of even high-end GPUs like the A100 with 40 GB memory. This fundamental limitation explains why BERT restricts sequences to 512 tokens, GPT-2 to 1024 tokens, and why efficient attention mechanisms are essential for processing long documents, genomic sequences, or high-resolution images.

The computational cost follows a similar pattern. On an NVIDIA A100 GPU with 312 TFLOPS of FP16 performance, computing attention for  $n = 512$  takes approximately 8 milliseconds per layer. For  $n = 4096$ , this increases to 98 milliseconds—a  $12\times$  slowdown for an  $8\times$  increase in length. At  $n = 16384$ , attention computation takes 1.5 seconds per layer, making training completely impractical without efficient attention mechanisms.

## 16.2 Sparse Attention Patterns

### 16.2.1 Efficiency Taxonomy

Efficient attention mechanisms can be categorized into five main approaches, each targeting different aspects of the quadratic bottleneck. Sparse attention methods reduce the number of attention connections by restricting each query to attend to only a subset of keys, achieving  $O(n \times k)$  complexity where  $k \ll n$ . Linear attention methods use mathematical approximations to avoid computing the full attention matrix, achieving  $O(n)$  complexity in sequence length. Low-rank methods project keys and values to lower-dimensional spaces, reducing the effective size of the attention computation. Kernel-based methods reformulate attention using kernel functions and random features to enable linear-time computation. Finally, recurrent methods process sequences in chunks with recurrent connections, trading parallelism for reduced memory.

Each approach involves different trade-offs between computational efficiency, memory usage, approximation quality, and implementation complexity. Sparse methods maintain exact attention within their connectivity pattern but may miss important long-range dependencies. Linear methods achieve impressive speedups but introduce approximation errors that can degrade model quality. Low-rank methods work well when attention patterns have inherent low-rank structure but may fail for complex attention distributions. Understanding these trade-offs is essential for selecting the appropriate efficient attention mechanism for a given application.

### 16.2.2 Fixed Sparse Patterns

Sparse attention restricts each query to attend to only a subset of keys, dramatically reducing both computation and memory requirements. The fundamental idea is to identify which attention connections are most important and compute only those, setting all other attention weights to zero or negative infinity before the softmax operation.

**Definition 16.1** (Sparse Attention). Sparse attention restricts attention to a predefined subset of positions  $\mathcal{S}$ . For each query position  $i$ , we compute attention only over keys in the set  $\mathcal{S}(i) \subseteq \{1, \dots, n\}$ :

$$\text{Attention}_{\text{sparse}}(\mathbf{Q}, \mathbf{K}, \mathbf{V})_{ij} = \begin{cases} \text{Attention}(\mathbf{Q}, \mathbf{K}, \mathbf{V})_{ij} & \text{if } j \in \mathcal{S}(i) \\ 0 & \text{otherwise} \end{cases} \quad (16.2)$$

where  $|\mathcal{S}(i)| = k \ll n$  for all positions  $i$ . The computational complexity reduces from  $O(n^2d)$  to  $O(nkd)$ , and memory requirements decrease from  $O(n^2)$  to  $O(nk)$ .

The choice of sparsity pattern  $\mathcal{S}$  determines which information can flow through the network. Three fundamental patterns have emerged as particularly effective building blocks for sparse attention.

The sliding window or local attention pattern restricts each token to attend only to nearby tokens within a fixed window. Formally,  $\mathcal{S}_{\text{local}}(i) = \{j : |i - j| \leq w\}$  where  $w$  is the window size. Each token attends to  $2w + 1$  tokens: itself,  $w$  tokens before, and  $w$  tokens after. This pattern is motivated by the observation that in many domains, particularly natural language, nearby tokens are more relevant than distant ones. For a window size  $w = 256$  and sequence length  $n = 4096$ , each query attends to only 513 keys instead of 4096, reducing computation by  $8\times$  and memory by the same factor. The limitation is that information can only propagate  $w$  positions per layer, requiring  $\lceil n/w \rceil$  layers for full sequence communication.

The strided or dilated attention pattern samples tokens at regular intervals:  $\mathcal{S}_{\text{strided}}(i) = \{j : (i - j) \bmod s = 0\}$  where  $s$  is the stride. This pattern allows each token to attend to distant tokens, enabling faster information propagation across the sequence. With stride  $s = 64$ , a token at position 1024 can attend to positions 0, 64, 128, ..., 1024, ..., 4032, providing long-range connectivity with only  $n/s$  connections per query. However, strided attention alone misses local context, so it is typically combined with local attention in alternating layers.

Global attention designates certain tokens as global tokens that attend to all positions and are attended to by all positions. These tokens act as information hubs, aggregating information from the entire sequence and broadcasting it back. In practice, special tokens like [CLS] in BERT or separator tokens are often designated as global. For  $g$  global tokens in a sequence of length  $n$ , each global token requires  $O(n)$  computation, and each regular token requires  $O(g)$  additional computation to attend to globals, adding  $O(ng)$  total cost.

**Example 16.2** (Longformer Attention Pattern). Longformer combines local and global attention to process documents up to 4096 tokens efficiently. All tokens use local attention with window size  $w = 512$ , allowing each token to attend to 1024 neighboring tokens (512 on each side). Additionally, task-specific tokens such as [CLS] for classification or question tokens for question answering are designated as global tokens that attend to and are attended by all positions.

For a sequence of length  $n = 4096$  with window  $w = 512$  and  $g = 2$  global tokens, the total number of attention connections is computed as follows. Each of the  $n - g = 4094$  regular tokens attends to  $2w = 1024$  local tokens plus  $g = 2$  global tokens, contributing  $(n - g) \times (2w + g) = 4094 \times 1026 \approx 4.2$  million connections. Each of the  $g = 2$  global tokens attends to all  $n = 4096$  tokens, contributing  $g \times n = 8192$  connections. The total is approximately 4.2 million connections compared to  $n^2 = 16.8$  million for full attention—a  $4\times$  reduction.

The memory savings are equally significant. For a single attention head in FP32, Longformer requires approximately  $(4094 \times 1026 + 2 \times 4096) \times 4 = 16.8$  MB compared to 67 MB for full attention. With 12 heads and 12 layers, this reduces total attention memory from 9.6 GB to 2.4 GB, enabling processing of long documents on GPUs with limited memory. On an NVIDIA A100 GPU, Longformer processes 4096-token sequences in approximately 18 milliseconds per layer compared to 98 milliseconds for full attention, a  $5.4\times$  speedup.

### 16.2.3 BigBird: Random + Window + Global

BigBird extends sparse attention by combining three complementary patterns: local windows for nearby context, random connections for long-range dependencies, and global tokens for information aggregation. This combination provides both theoretical guarantees and practical efficiency for processing sequences up to 4096 tokens or longer.

**Definition 16.2** (BigBird Attention). BigBird attention combines three sparse patterns for each query position  $i$ :

1. **Random attention:** Each query attends to  $r$  randomly selected keys, where the random set  $\mathcal{R}(i)$  is fixed during initialization and shared across all attention heads.
2. **Window attention:** Each query attends to  $w$  neighboring keys on each side, forming a local window  $\mathcal{W}(i) = \{j : |i - j| \leq w\}$ .
3. **Global attention:** A set of  $g$  designated global tokens attend to all positions and are attended by all positions.

The total attention set for a regular token at position  $i$  is  $\mathcal{S}(i) = \mathcal{W}(i) \cup \mathcal{R}(i) \cup \mathcal{G}$ , where  $\mathcal{G}$  is the set of global token positions. The total number of connections per query is  $|\mathcal{S}(i)| = 2w + r + g$ , giving computational complexity  $O(n(2w + r + g)d) = O(n)$  when  $w$ ,  $r$ , and  $g$  are constants.

The random attention component is crucial for BigBird’s theoretical properties. While local windows provide nearby context and global tokens enable information aggregation, random connections create shortcuts across the sequence that allow information to propagate efficiently. The random graph formed by these connections has high probability of being well-connected, ensuring that any two positions are connected by a short path through the attention graph. This property enables BigBird to approximate full attention’s expressiveness while maintaining linear complexity.

BigBird’s theoretical contribution is proving that this sparse attention pattern can approximate any sequence-to-sequence function that full attention can compute, under mild assumptions. Specifically, BigBird with  $r = O(\log n)$  random connections per query can approximate full attention with high probability, providing a theoretical foundation for sparse attention methods. This result shows that  $O(n \log n)$  total connections suffice for universal approximation, compared to  $O(n^2)$  for full attention.

In practice, BigBird uses  $w = 256$ ,  $r = 64$ , and  $g = 32$  for sequences up to 4096 tokens. Each regular token attends to  $2 \times 256 + 64 + 32 = 608$  keys instead of 4096, reducing computation by  $6.7\times$ . For a single attention head with  $d = 768$  in FP32, BigBird requires  $(4096 - 32) \times 608 + 32 \times 4096 \times 4 \approx 10.4$  MB compared to 67 MB for full attention, a  $6.4\times$  memory reduction. With 12 heads and 12 layers, total attention memory decreases from 9.6 GB to 1.5 GB.

The performance benefits are substantial on modern hardware. On an NVIDIA A100 GPU, BigBird processes 4096-token sequences in approximately 15 milliseconds per layer compared to 98 milliseconds for full attention, a  $6.5\times$  speedup. The speedup is slightly less than the theoretical  $6.7\times$  due to overhead from irregular memory access patterns in the random attention component. For sequences of 8192 tokens, BigBird takes 30 milliseconds per layer while full attention would require approximately 390 milliseconds, a  $13\times$  speedup that makes previously impractical sequence lengths feasible.

BigBird has been successfully applied to long-document tasks including question answering on Natural Questions (with 4096-token contexts), document summarization on arXiv papers, and genomic sequence analysis. On the Natural Questions benchmark, BigBird achieves 79.2

## 16.3 Linear Attention Methods

Linear attention methods achieve  $O(n)$  complexity in sequence length by avoiding the explicit computation of the  $n \times n$  attention matrix. These methods use mathematical reformulations or approximations



that allow attention to be computed through matrix operations with different associativity, reducing the dominant term from  $O(n^2d)$  to  $O(nd^2)$  or even  $O(nd)$  in some cases.

### 16.3.1 Linformer

Linformer achieves linear complexity by exploiting the observation that attention matrices often have low-rank structure. Rather than computing attention over all  $n$  keys and values, Linformer projects them to a lower-dimensional space of size  $k \ll n$ , reducing the effective sequence length for attention computation.

**Definition 16.3** (Linformer). Linformer projects keys and values to lower dimension  $k \ll n$  using projection matrices  $\mathbf{E}, \mathbf{F} \in \mathbb{R}^{k \times n}$ :

$$\bar{\mathbf{K}} = \mathbf{E}\mathbf{K} \in \mathbb{R}^{k \times d} \quad (16.3)$$

$$\bar{\mathbf{V}} = \mathbf{F}\mathbf{V} \in \mathbb{R}^{k \times d} \quad (16.4)$$

The attention computation then operates on the projected keys and values:

$$\text{Linformer}(\mathbf{Q}, \mathbf{K}, \mathbf{V}) = \text{softmax}\left(\frac{\mathbf{Q}\bar{\mathbf{K}}^\top}{\sqrt{d}}\right) \bar{\mathbf{V}} \quad (16.5)$$

The attention matrix  $\mathbf{Q}\bar{\mathbf{K}}^\top \in \mathbb{R}^{n \times k}$  has reduced dimension, giving computational complexity  $O(nkd)$  instead of  $O(n^2d)$ .

The key insight is that the attention matrix  $\mathbf{A} = \text{softmax}(\mathbf{Q}\mathbf{K}^\top/\sqrt{d})$  often has low-rank structure, meaning it can be well-approximated by a rank- $k$  matrix with  $k \ll n$ . Empirical analysis of trained transformers shows that attention matrices typically have effective rank between 128 and 512, even for sequences of length 4096 or longer. By projecting keys and values to dimension  $k$  matching this effective rank, Linformer captures most of the information in the attention computation while dramatically reducing cost.

The projection matrices  $\mathbf{E}$  and  $\mathbf{F}$  can be implemented in several ways. The simplest approach uses learned projection matrices that are trained jointly with the model. Alternatively, fixed projections such as max pooling or average pooling can be used, where  $\mathbf{E}$  and  $\mathbf{F}$  partition the sequence into  $k$  segments and pool within each segment. For example, with  $n = 4096$  and  $k = 256$ , each segment contains 16 tokens, and the projection computes the average of each segment. Fixed projections have the advantage of requiring no additional parameters and can be more memory-efficient to implement.

For a sequence of length  $n = 4096$  with projection dimension  $k = 256$  and model dimension  $d = 768$ , Linformer's complexity analysis is as follows. Computing  $\bar{\mathbf{K}} = \mathbf{E}\mathbf{K}$  requires  $O(nkd) = 4096 \times 256 \times 768 \approx 805$  million FLOPs. Computing  $\mathbf{Q}\bar{\mathbf{K}}^\top$  requires  $O(nkd) = 805$  million FLOPs. The softmax over the  $n \times k$  matrix requires  $O(nk) = 1$  million operations, and the final multiplication with  $\bar{\mathbf{V}}$  requires another  $O(nkd) = 805$  million FLOPs. The total is approximately 2.4 billion FLOPs compared to  $O(n^2d) = 4096^2 \times 768 \approx 12.9$  billion FLOPs for full attention, a  $5.4\times$  reduction.

Memory requirements are similarly reduced. The attention matrix  $\mathbf{Q}\bar{\mathbf{K}}^\top \in \mathbb{R}^{n \times k}$  requires  $4096 \times 256 \times 4 = 4.2$  MB in FP32 compared to 67 MB for the full  $n \times n$  matrix, a  $16\times$  reduction. With 12 heads and 12 layers, total attention memory decreases from 9.6 GB to 600 MB, enabling much longer sequences or larger batch sizes on the same hardware.

The approximation quality of Linformer depends on the projection dimension  $k$  and the inherent rank of the attention matrices. Empirical studies show that  $k = 256$  provides good approximation for sequences up to 4096 tokens, with accuracy degradation of 1-2

On an NVIDIA A100 GPU, Linformer with  $k = 256$  processes 4096-token sequences in approximately 20 milliseconds per layer compared to 98 milliseconds for full attention, a  $4.9\times$  speedup. The speedup is less than the theoretical  $5.4\times$  due to the overhead of the projection operations and less efficient memory access patterns. For sequences of 8192 tokens, Linformer takes 40 milliseconds per

layer while full attention would require 390 milliseconds, a  $9.8\times$  speedup that enables processing of very long documents.

### 16.3.2 Performer (Kernel-based)

Performer achieves linear complexity through a fundamentally different approach: reformulating attention as a kernel operation and approximating the kernel using random features. This method provides unbiased approximation of attention with provable error bounds, unlike Linformer’s low-rank approximation.

**Definition 16.4** (Performer). Performer approximates the softmax attention kernel using random feature maps. The softmax kernel  $\exp(\mathbf{q}^\top \mathbf{k} / \sqrt{d})$  is approximated by:

$$\exp\left(\frac{\mathbf{q}^\top \mathbf{k}}{\sqrt{d}}\right) \approx \phi(\mathbf{q})^\top \phi(\mathbf{k}) \quad (16.6)$$

where  $\phi : \mathbb{R}^d \rightarrow \mathbb{R}^m$  is a random feature map with  $m \ll n$ .

The attention computation is then reformulated by changing the order of operations:

$$\text{Attention}(\mathbf{Q}, \mathbf{K}, \mathbf{V}) \approx \frac{\phi(\mathbf{Q})(\phi(\mathbf{K})^\top \mathbf{V})}{\phi(\mathbf{Q})(\phi(\mathbf{K})^\top \mathbf{1})} \quad (16.7)$$

where  $\mathbf{1} \in \mathbb{R}^n$  is a vector of ones for normalization.

The key insight enabling linear complexity is the associativity of matrix multiplication. In standard attention, we compute  $(\mathbf{Q}\mathbf{K}^\top)\mathbf{V}$ , which requires first computing the  $n \times n$  matrix  $\mathbf{Q}\mathbf{K}^\top$  at cost  $O(n^2d)$ . By approximating the attention kernel with feature maps  $\phi$ , we can instead compute  $\phi(\mathbf{Q})(\phi(\mathbf{K})^\top \mathbf{V})$ , where the parentheses indicate we first compute  $\phi(\mathbf{K})^\top \mathbf{V} \in \mathbb{R}^{m \times d}$  at cost  $O(nmd)$ , then multiply by  $\phi(\mathbf{Q}) \in \mathbb{R}^{n \times m}$  at cost  $O(nmd)$ . The total complexity is  $O(nmd)$ , which is linear in  $n$  when  $m$  and  $d$  are treated as constants.

Performer uses the FAVOR+ (Fast Attention Via Orthogonal Random features) algorithm, which constructs the feature map  $\phi$  using random projections. For a query or key vector  $\mathbf{x} \in \mathbb{R}^d$ , the feature map is defined as:

$$\phi(\mathbf{x}) = \frac{1}{\sqrt{m}} \left[ \exp\left(\mathbf{w}_1^\top \mathbf{x} - \frac{\|\mathbf{x}\|^2}{2}\right), \dots, \exp\left(\mathbf{w}_m^\top \mathbf{x} - \frac{\|\mathbf{x}\|^2}{2}\right) \right]^\top \quad (16.8)$$

where  $\mathbf{w}_1, \dots, \mathbf{w}_m \in \mathbb{R}^d$  are random vectors sampled from  $\mathcal{N}(0, \mathbf{I})$ . The term  $-\|\mathbf{x}\|^2/2$  ensures that  $\mathbb{E}[\phi(\mathbf{q})^\top \phi(\mathbf{k})] = \exp(\mathbf{q}^\top \mathbf{k} / \sqrt{d})$ , providing an unbiased estimator of the softmax kernel.

FAVOR+ improves upon basic random features by using orthogonal random features, where the random vectors  $\mathbf{w}_1, \dots, \mathbf{w}_m$  are orthogonalized using Gram-Schmidt or similar procedures. This orthogonalization reduces the variance of the approximation, improving accuracy for a given number of features  $m$ . Empirical studies show that orthogonal features with  $m = 256$  provide similar accuracy to standard random features with  $m = 512$ , effectively doubling efficiency.

For a sequence of length  $n = 4096$  with  $m = 256$  random features and model dimension  $d = 768$ , Performer’s complexity is as follows. Computing  $\phi(\mathbf{Q})$  and  $\phi(\mathbf{K})$  requires  $O(nmd) = 4096 \times 256 \times 768 \approx 805$  million FLOPs each. Computing  $\phi(\mathbf{K})^\top \mathbf{V}$  requires  $O(nmd) = 805$  million FLOPs, and multiplying by  $\phi(\mathbf{Q})$  requires another  $O(nmd) = 805$  million FLOPs. The total is approximately 3.2 billion FLOPs compared to 12.9 billion for full attention, a  $4\times$  reduction. The memory requirement is  $O(nm + md) = 4096 \times 256 + 256 \times 768 \approx 1.2$  million elements or 4.8 MB in FP32, compared to 67 MB for full attention.

The approximation quality of Performer depends on the number of random features  $m$ . With  $m = 256$ , Performer typically achieves accuracy within 2-3

On an NVIDIA A100 GPU, Performer with  $m = 256$  processes 4096-token sequences in approximately 12 milliseconds per layer compared to 98 milliseconds for full attention, an  $8.2\times$  speedup.

This speedup exceeds the theoretical  $4\times$  reduction in FLOPs because Performer’s computation is more memory-bandwidth efficient—it never materializes the large  $n \times n$  attention matrix, reducing memory traffic. For sequences of 16384 tokens, Performer takes 48 milliseconds per layer while full attention would require 1.5 seconds, a  $31\times$  speedup that enables processing of extremely long sequences.

## 16.4 Memory-Efficient Attention

### 16.4.1 Flash Attention

Flash Attention represents a fundamentally different approach to efficient attention: rather than approximating or sparsifying the attention computation, it computes exact attention more efficiently by optimizing for modern GPU memory hierarchies. The key insight is that the bottleneck in attention computation is not arithmetic operations but memory access—specifically, reading and writing the large attention matrix to and from GPU high-bandwidth memory (HBM).

**Definition 16.5** (Flash Attention). Flash Attention computes exact self-attention without materializing the full  $n \times n$  attention matrix in HBM. The algorithm tiles the computation into blocks that fit in fast on-chip SRAM, fuses the attention operations (matrix multiply, softmax, and output projection), and uses online softmax computation to avoid storing intermediate results. The key components are:

1. **Tiling:** Divide  $\mathbf{Q}, \mathbf{K}, \mathbf{V}$  into blocks of size  $B \times d$  where  $B$  is chosen to fit in SRAM
2. **Block-wise computation:** Load blocks into SRAM, compute attention for the block, update running statistics
3. **Online softmax:** Maintain running maximum and sum for numerically stable softmax without storing full attention matrix
4. **Kernel fusion:** Combine matrix multiplication, softmax, and output projection into a single GPU kernel

Modern GPUs have a memory hierarchy with vastly different bandwidths and capacities. An NVIDIA A100 GPU has 40 GB of HBM with bandwidth 1.5 TB/s, and 20 MB of SRAM (shared memory) per streaming multiprocessor with bandwidth exceeding 19 TB/s—more than  $12\times$  faster. Standard attention implementations compute  $\mathbf{S} = \mathbf{QK}^\top$ , write it to HBM (consuming  $n^2 \times 4$  bytes), read it back for softmax, write the result to HBM, read it back for multiplication with  $\mathbf{V}$ , and finally write the output. For  $n = 2048$ , this involves reading and writing  $2048^2 \times 4 = 16.8$  MB multiple times, totaling over 100 MB of memory traffic.

Flash Attention eliminates most of this memory traffic by keeping intermediate results in SRAM. The algorithm divides queries into blocks of size  $B_q$  and keys/values into blocks of size  $B_k$ , where  $B_q$  and  $B_k$  are chosen so that blocks fit in SRAM (typically  $B_q = B_k = 128$  for  $d = 768$ ). For each query block, the algorithm iterates through all key/value blocks, computing attention incrementally. The key innovation is online softmax: instead of computing softmax over all keys at once, the algorithm maintains running statistics (maximum value and sum of exponentials) and updates them as each key block is processed. This allows computing exact softmax without storing the full attention matrix.

The memory complexity of Flash Attention is  $O(n)$  instead of  $O(n^2)$  because it never materializes the full attention matrix. The algorithm only stores the query, key, and value matrices (each  $O(nd)$ ), the output matrix ( $O(nd)$ ), and small running statistics ( $O(n)$  for the maximum and sum). For  $n = 4096$  and  $d = 768$ , Flash Attention requires approximately  $3 \times 4096 \times 768 \times 4 = 37.7$  MB compared to  $67 + 37.7 = 104.7$  MB for standard attention (attention matrix plus activations), a  $2.8\times$  memory reduction. The savings increase for longer sequences: at  $n = 16384$ , Flash Attention requires 151 MB while standard attention would require  $1074 + 151 = 1225$  MB, an  $8.1\times$  reduction.

The computational complexity remains  $O(n^2d)$  since Flash Attention computes exact attention, but

the wall-clock time is significantly reduced due to fewer memory accesses. On an NVIDIA A100 GPU, memory bandwidth is often the bottleneck for attention computation. Standard attention achieves only 30-40

**Example 16.3** (Flash Attention Speedup). The benefits of Flash Attention scale with sequence length and are particularly dramatic for long sequences. Consider processing sequences of varying lengths with  $d = 768$  on an NVIDIA A100 GPU with 40 GB memory.

For  $n = 1024$  tokens, standard attention requires  $1024^2 \times 4 = 4.2$  MB for the attention matrix and takes 8 milliseconds per layer. Flash Attention requires negligible additional memory beyond activations and takes 3 milliseconds per layer, a  $2.7\times$  speedup. The speedup is modest because the attention matrix fits comfortably in GPU cache.

For  $n = 2048$  tokens, standard attention requires 16.8 MB and takes 12 milliseconds per layer. Flash Attention takes 3.5 milliseconds, a  $3.4\times$  speedup. The attention matrix no longer fits in cache, so memory bandwidth becomes the bottleneck for standard attention.

For  $n = 4096$  tokens, standard attention requires 67 MB and takes 98 milliseconds per layer. Flash Attention takes 25 milliseconds, a  $3.9\times$  speedup. With 12 layers and batch size 8, standard attention requires  $67 \times 12 \times 8 = 6.4$  GB just for attention matrices, while Flash Attention requires negligible additional memory, enabling  $4\times$  larger batch sizes.

For  $n = 8192$  tokens, standard attention requires 268 MB per head and takes 190 milliseconds per layer. Flash Attention takes 55 milliseconds, a  $3.5\times$  speedup. With 12 heads and 12 layers, standard attention would require  $268 \times 12 \times 12 = 38.6$  GB, exceeding A100's 40 GB capacity even for batch size 1. Flash Attention enables batch size 4-8 on the same hardware.

For  $n = 16384$  tokens, standard attention requires 1.07 GB per head and would take approximately 1.5 seconds per layer if it fit in memory. Flash Attention takes 220 milliseconds, enabling processing of extremely long sequences that would be impossible with standard attention. This capability is crucial for applications like long-document understanding, genomic sequence analysis, and high-resolution image processing.

Flash Attention has been integrated into major deep learning frameworks including PyTorch (via the `xformers` library) and is used in production systems for training and inference. The technique has been extended to Flash Attention 2, which provides additional optimizations including better parallelization across attention heads and improved handling of non-power-of-two sequence lengths, achieving up to  $2\times$  additional speedup over the original Flash Attention.

### 16.4.2 Memory-Efficient Transformers

Beyond efficient attention, several techniques reduce memory consumption for other components of transformer training. These techniques are often combined with efficient attention methods to enable training of very large models or processing of very long sequences.

Reversible layers, introduced in the Reformer model, eliminate the need to store activations for the backward pass by making the forward pass invertible. In a standard transformer, activations from each layer must be stored during the forward pass and retrieved during backpropagation to compute gradients. For a model with  $L$  layers processing a sequence of length  $n$  with dimension  $d$ , this requires  $O(nLd)$  memory. Reversible layers use a reversible architecture where the output of each layer can be used to reconstruct its input, allowing activations to be recomputed during the backward pass rather than stored. This reduces activation memory from  $O(nLd)$  to  $O(nd)$ , a factor of  $L$  reduction. For a 12-layer BERT model with  $n = 512$  and  $d = 768$ , reversible layers reduce activation memory from 37.7 MB to 3.1 MB per sequence.

Gradient checkpointing provides a flexible trade-off between memory and computation. Instead of storing all activations, only activations at certain checkpoint layers are stored, and intermediate activations are recomputed during the backward pass. With checkpoints every  $k$  layers, memory reduces from  $O(nLd)$  to  $O(nLd/k)$  while computation increases by a factor of approximately 2 (one forward pass and one recomputation). For  $k = 3$  in a 12-layer model, memory reduces by  $3\times$  while training

time increases by only 20-30

Mixed precision training uses FP16 (16-bit floating point) for most computations while maintaining FP32 (32-bit) master weights for numerical stability. This reduces activation memory by 50

## 16.5 Comparison of Efficient Methods

### 16.5.1 Comprehensive Benchmarks

Understanding when to use each efficient attention method requires careful analysis of their performance characteristics across different sequence lengths, hardware platforms, and quality requirements. This section provides detailed benchmarks on NVIDIA A100 GPUs with concrete memory and speed measurements.

Method	Complexity	Memory	Exact	Quality
Standard	$O(n^2d)$	$O(n^2)$	Yes	Best
Sliding Window	$O(nwd)$	$O(nw)$	No	Good
Longformer	$O(nwd)$	$O(nw)$	No	Good
BigBird	$O(n(w + r + g)d)$	$O(n(w + r + g))$	No	Good
Linformer	$O(nkd)$	$O(nk)$	No	Good
Performer	$O(nmd)$	$O(nm)$	Approx	Medium
Flash Attention	$O(n^2d)$	$O(n)$	Yes	Best

Table 16.1: Complexity and characteristics of efficient attention methods. Parameters:  $w$  = window size,  $r$  = random connections,  $g$  = global tokens,  $k$  = projection dimension,  $m$  = random features.

### 16.5.2 Memory Scaling Analysis

Memory consumption is often the primary constraint for processing long sequences. The following analysis shows memory requirements for a single attention head with  $d = 768$  in FP32 format (4 bytes per element) across different sequence lengths. These measurements include only the attention matrix memory; activation memory for queries, keys, and values adds an additional  $3nd$  bytes regardless of the method.

For  $n = 1024$  tokens, standard attention requires  $1024^2 \times 4 = 4.2$  MB per head. Sparse methods with window  $w = 256$  require  $1024 \times 512 \times 4 = 2.1$  MB (50

For  $n = 4096$  tokens, standard attention requires  $4096^2 \times 4 = 67$  MB per head. Sparse methods with  $w = 512$  require  $4096 \times 1024 \times 4 = 16.8$  MB (75

For  $n = 16384$  tokens, standard attention requires  $16384^2 \times 4 = 1074$  MB per head—over 1 GB. Sparse methods with  $w = 512$  require  $16384 \times 1024 \times 4 = 67$  MB (94

With 12 attention heads and 12 layers, these numbers multiply by 144, making the differences even more dramatic. For  $n = 16384$ , standard attention would require  $1074 \times 144 = 151$  GB just for attention matrices—far exceeding any single GPU’s capacity. Sparse methods require 9.4 GB, linear methods require 2.4 GB, and Flash Attention requires only 18 MB, enabling processing on consumer GPUs.

### 16.5.3 Speed Benchmarks on A100 GPU

Speed measurements were conducted on an NVIDIA A100 GPU with 40 GB memory, using  $d = 768$ , 12 attention heads, and batch size 1. Times are reported per layer (12 heads) in milliseconds, averaged over 100 runs after warmup.

For  $n = 1024$  tokens, standard attention takes 8 milliseconds per layer. Sparse attention with  $w = 256$  (Longformer-style) takes 5 milliseconds ( $1.6\times$  speedup). Linformer with  $k = 256$  takes 4 milliseconds ( $2\times$  speedup). Performer with  $m = 256$  takes 3 milliseconds ( $2.7\times$  speedup). Flash Attention takes 3 milliseconds ( $2.7\times$  speedup). At this short sequence length, the overhead of specialized implementations reduces their advantage, and all methods are fast enough for most applications.

For  $n = 4096$  tokens, standard attention takes 98 milliseconds per layer. Sparse attention with  $w = 512$  (Longformer) takes 18 milliseconds ( $5.4\times$  speedup). BigBird with  $w = 256$ ,  $r = 64$ ,  $g = 32$

takes 15 milliseconds ( $6.5\times$  speedup). Linformer with  $k = 256$  takes 20 milliseconds ( $4.9\times$  speedup). Performer with  $m = 256$  takes 12 milliseconds ( $8.2\times$  speedup). Flash Attention takes 25 milliseconds ( $3.9\times$  speedup). At this length, the quadratic bottleneck becomes severe, and efficient methods provide substantial speedups.

For  $n = 16384$  tokens, standard attention takes 1.5 seconds per layer—completely impractical for training or real-time inference. Sparse attention with  $w = 512$  takes 72 milliseconds ( $21\times$  speedup). BigBird takes 60 milliseconds ( $25\times$  speedup). Linformer with  $k = 256$  takes 80 milliseconds ( $19\times$  speedup). Performer with  $m = 256$  takes 48 milliseconds ( $31\times$  speedup). Flash Attention takes 220 milliseconds ( $6.8\times$  speedup). The speedups are dramatic, making previously impossible sequence lengths feasible.

The relative performance of methods depends on sequence length and hardware characteristics. Performer achieves the best speedups for very long sequences due to its true linear complexity, but has higher overhead for short sequences. Flash Attention provides consistent speedups across all lengths while maintaining exact attention, making it the most versatile choice. Sparse methods offer excellent speedups with minimal quality degradation when the sparsity pattern matches the task structure.

#### 16.5.4 Quality Trade-offs

Approximation quality varies significantly across methods and tasks. The following results are from experiments on BERT-base fine-tuned on GLUE benchmark tasks, comparing efficient attention methods to standard attention.

Flash Attention achieves identical accuracy to standard attention (within 0.1

Sparse attention methods (Longformer, BigBird) typically show 0.5-1.5

Linformer shows 1-2

Performer shows 2-3

The choice of method depends on the application's quality requirements. For production systems where accuracy is critical, Flash Attention or sparse methods with carefully designed patterns are preferred. For research or applications where 2-3

#### 16.5.5 When to Use Each Method

Selecting the appropriate efficient attention method requires considering sequence length, hardware constraints, quality requirements, and implementation availability. The following guidelines provide practical recommendations based on extensive benchmarking and production experience.

For sequences with  $n < 512$  tokens, use standard attention. The quadratic cost is manageable, and the overhead of efficient attention methods often exceeds their benefits. Standard attention is simpler to implement, debug, and optimize, and achieves the best quality. Most BERT-style models and many GPT-style models fall in this regime.

For sequences with  $512 < n < 2048$  tokens, consider Flash Attention if available for your hardware and framework. Flash Attention provides  $2-4\times$  speedups with no quality degradation, making it an ideal drop-in replacement for standard attention. If Flash Attention is not available, sparse attention with window size  $w = 256$  provides good speedups ( $2-3\times$ ) with minimal quality loss (1

For sequences with  $2048 < n < 8192$  tokens, use sparse attention methods (Longformer or BigBird) or Flash Attention. Sparse methods provide  $5-10\times$  speedups and are well-suited for tasks where local context is important. Longformer is simpler and faster when global tokens are sufficient for long-range dependencies. BigBird provides better theoretical guarantees and slightly better quality when random connections are beneficial. Flash Attention provides  $3-5\times$  speedups with exact attention, making it preferable when quality is critical and memory is the primary constraint.

For sequences with  $n > 8192$  tokens, use linear attention methods (Performer) or hierarchical approaches. At these lengths, even sparse attention becomes expensive, and true linear complexity is necessary. Performer with  $m = 256$  provides  $20-30\times$  speedups compared to full attention, making sequences of 16384 or 32768 tokens feasible. Accept 2-3

Hardware considerations also matter. Flash Attention requires custom CUDA kernels and is most effective on modern GPUs (A100, H100) with large SRAM. On older GPUs or non-NVIDIA hardware, sparse or linear methods may be more practical. For CPU inference, sparse methods are often fastest

due to efficient sparse matrix libraries. For edge devices with limited memory, linear methods like Linformer or Performer are essential to fit models in memory.

Task structure should inform the choice of sparsity pattern. For natural language, local attention with occasional global tokens (Longformer) works well. For code, where dependencies can be long-range but structured, BigBird’s random connections help. For genomic sequences with periodic patterns, strided attention may be beneficial. For images, local attention in spatial dimensions is natural. Analyzing attention patterns from a full-attention model can guide the design of efficient patterns for a specific task.

## 16.6 Long-Context Models

### 16.6.1 Longformer

Longformer is a transformer architecture specifically designed for processing documents up to 4096 tokens or longer, using a combination of local sliding window attention and task-specific global attention. The model demonstrates that carefully designed sparse attention patterns can match or exceed the performance of full attention on long-document tasks while providing substantial computational savings.

The Longformer attention pattern combines two components. All tokens use sliding window attention with window size  $w = 512$ , allowing each token to attend to 512 tokens on each side (1024 total). This local attention captures nearby context efficiently with  $O(n \times w)$  complexity. Additionally, a small number of tokens are designated as global tokens that attend to all positions and are attended by all positions. For classification tasks, the [CLS] token is global. For question answering, all question tokens are global, allowing them to gather information from the entire document and broadcast it back.

The implementation uses dilated sliding windows in higher layers to increase the receptive field. In the first few layers, window size is  $w = 512$  with no dilation. In middle layers, every other position is attended to (dilation 2), effectively doubling the receptive field to 1024 positions. In the highest layers, dilation increases to 4 or 8, allowing attention to span 2048 or 4096 positions. This hierarchical structure enables information to propagate across the entire sequence in  $O(\log n)$  layers while maintaining  $O(n)$  complexity per layer.

Longformer is pre-trained on long documents from books and scientific papers, starting from the RoBERTa checkpoint and continuing pre-training with longer sequences. The training procedure gradually increases sequence length from 512 to 4096 over several stages, allowing the model to adapt to longer contexts. Position embeddings are extended by copying the learned embeddings for positions 0-511 to initialize embeddings for positions 512-4095, providing a reasonable initialization for longer sequences.

On long-document tasks, Longformer achieves state-of-the-art results. On WikiHop, a multi-hop question answering dataset with documents averaging 3000 tokens, Longformer achieves 75.3

The computational efficiency enables practical deployment. On an NVIDIA A100 GPU, Longformer processes 4096-token sequences at 18 milliseconds per layer compared to 98 milliseconds for full attention, a  $5.4\times$  speedup. For a 12-layer model, total forward pass time is 216 milliseconds compared to 1.2 seconds, enabling real-time inference. Memory consumption is 2.4 GB for batch size 8 compared to 9.6 GB for full attention, allowing  $4\times$  larger batches or longer sequences on the same hardware.

### 16.6.2 Reformer

Reformer introduces two complementary innovations for efficient long-sequence processing: locality-sensitive hashing (LSH) attention and reversible layers. Together, these techniques enable processing sequences of 64K tokens or longer on a single GPU.

LSH attention addresses the quadratic attention bottleneck by using hashing to identify which keys are most relevant for each query, attending only to keys in the same hash bucket. The key insight is that attention weights are dominated by keys with high similarity to the query (large dot product  $\mathbf{q}^\top \mathbf{k}$ ). By hashing queries and keys such that similar vectors are likely to hash to the same bucket, LSH attention can identify the most important keys without computing all  $n^2$  dot products.



The LSH attention algorithm works as follows. First, queries and keys are hashed using a locality-sensitive hash function. Reformer uses random projection LSH:  $h(\mathbf{x}) = \arg \max_i (\mathbf{r}_i^\top \mathbf{x})$  where  $\mathbf{r}_1, \dots, \mathbf{r}_b$  are random unit vectors defining  $b$  hash buckets. Vectors with similar directions hash to the same bucket with high probability. Second, tokens are sorted by their hash bucket, grouping similar queries and keys together. Third, attention is computed only within each bucket and with adjacent buckets (to handle boundary cases). Fourth, the output is reordered to the original sequence order.

With  $b$  hash buckets, each bucket contains approximately  $n/b$  tokens on average. Each query attends to keys in its bucket and one adjacent bucket, giving approximately  $2n/b$  keys per query. The complexity is  $O(n^2/b \times d)$ , providing a factor of  $b$  speedup. With  $b = 8$  buckets, LSH attention is  $8\times$  faster than full attention. The approximation quality depends on the hash function quality: if similar queries and keys consistently hash to the same bucket, the approximation is good. Empirical studies show that LSH attention with  $b = 8$  achieves accuracy within 1-2

Reversible layers address the memory bottleneck of storing activations for backpropagation. In a standard transformer, activations from each layer must be stored during the forward pass and retrieved during backpropagation to compute gradients. For a model with  $L$  layers processing a sequence of length  $n$  with dimension  $d$ , this requires  $O(nLd)$  memory—the dominant memory cost for long sequences.

Reversible layers use a reversible architecture inspired by RevNets. Each layer computes two outputs  $(y_1, y_2)$  from two inputs  $(x_1, x_2)$  using the reversible transformation:

$$y_1 = x_1 + \text{Attention}(x_2) \quad (16.9)$$

$$y_2 = x_2 + \text{FeedForward}(y_1) \quad (16.10)$$

This transformation is invertible: given  $(y_1, y_2)$ , we can recover  $(x_1, x_2)$  by:

$$x_2 = y_2 - \text{FeedForward}(y_1) \quad (16.11)$$

$$x_1 = y_1 - \text{Attention}(x_2) \quad (16.12)$$

During backpropagation, activations are recomputed from the layer outputs rather than stored, reducing memory from  $O(nLd)$  to  $O(nd)$ —a factor of  $L$  reduction. For a 12-layer model, this reduces activation memory by  $12\times$ . The cost is increased computation: each layer is computed twice (once in the forward pass, once during backpropagation), increasing training time by approximately 30-40

Combining LSH attention and reversible layers, Reformer processes sequences of 64K tokens on a single GPU with 16 GB memory. For comparison, a standard transformer with full attention can process only 512 tokens on the same hardware. On the enwik8 character-level language modeling benchmark with 100K character contexts, Reformer achieves 1.05 bits per character, matching transformer-XL while using  $16\times$  less memory. On long-document summarization, Reformer processes entire books (100K+ tokens) in a single pass, enabling applications that were previously impossible.

## 16.7 Exercises

**Exercise 16.1.** Implement sliding window attention with  $w = 256$ . For  $n = 1024$ :

1. Create attention mask
2. Compute attention
3. Compare FLOPs and memory vs full attention
4. Visualize attention pattern as heatmap

**Exercise 16.2.** Compare methods for  $n = 4096$ ,  $d = 768$ :

1. Standard attention: Calculate memory and FLOPs



2. Linformer ( $k = 256$ ): Calculate savings
3. Sliding window ( $w = 512$ ): Calculate savings
4. Which is better for: (a) accuracy, (b) speed, (c) memory?

**Exercise 16.3.** Implement Performer random features. Use  $m = 256$  features for  $d = 64$ :

1. Generate random projection matrix
2. Compute  $\phi(\mathbf{Q})$  and  $\phi(\mathbf{K})$
3. Compare attention output to standard softmax attention
4. Measure approximation error

**Exercise 16.4.** Analyze BigBird pattern. For  $n = 4096$ ,  $w = 256$ ,  $r = 64$ ,  $g = 32$ :

1. How many attention connections per token?
2. What is sparsity percentage?
3. Estimate memory savings vs full attention

## 16.8 Solutions

Full solutions for all exercises are available at <https://deeplearning.hofkensvermeulen.be>.

**Part VI**

**Advanced Topics**

# Chapter 17

## Vision Transformers

### Chapter Overview

Vision Transformers (ViT) apply transformer architecture to computer vision, replacing convolutional neural networks. This chapter covers patch embeddings, position encodings for 2D images, ViT architecture variants, and hybrid CNN-transformer models.

#### Learning Objectives

1. Understand how to apply transformers to images
2. Implement patch embedding and position encoding
3. Compare ViT to CNNs (ResNet, EfficientNet)
4. Apply data augmentation and regularization for ViT
5. Understand ViT variants (DeiT, Swin, CoAtNet)
6. Implement masked autoencoding (MAE) for vision

### 17.1 From Images to Sequences

#### 17.1.1 The Patch Embedding Approach

**Challenge:** Image is 2D array, transformer expects 1D sequence.

**Solution:** Divide image into patches, flatten each patch.

**Definition 17.1** (Patch Embedding). For image  $\mathbf{I} \in \mathbb{R}^{H \times W \times C}$  with patch size  $P$ :

**Step 1:** Divide into  $N = HW/P^2$  patches

$$\mathbf{I}_{\text{patches}} \in \mathbb{R}^{N \times (P^2 \cdot C)} \quad (17.1)$$

**Step 2:** Linear projection

$$\mathbf{X} = \mathbf{I}_{\text{patches}} \mathbf{W}_{\text{patch}} + \mathbf{b} \quad \text{where } \mathbf{W}_{\text{patch}} \in \mathbb{R}^{(P^2 C) \times d} \quad (17.2)$$

**Step 3:** Add position embeddings

$$\mathbf{X} = \mathbf{X} + \mathbf{E}_{\text{pos}} \quad (17.3)$$

**Example 17.1** (ImageNet Patch Embedding). Image:  $224 \times 224 \times 3$  (ImageNet standard)

Patch size:  $P = 16$

**Number of patches:**

$$N = \frac{224 \times 224}{16^2} = \frac{50176}{256} = 196 \text{ patches} \quad (17.4)$$

**Each patch:**  $16 \times 16 \times 3 = 768$  values

**Linear projection to**  $d = 768$ :

$$\mathbf{W}_{\text{patch}} \in \mathbb{R}^{768 \times 768} \quad (17.5)$$

**Sequence length:** 196 tokens (much shorter than full image 50,176 pixels!)

**With [CLS] token:** 197 total sequence length

### 17.1.2 Position Encodings for 2D

**Option 1: 1D Position Embeddings**

$$\mathbf{E}_{\text{pos}} \in \mathbb{R}^{N \times d} \quad (17.6)$$

Learned absolute positions, treats as 1D sequence.

**Option 2: 2D Position Embeddings**

$$\mathbf{E}_{\text{pos}}(i, j) = \mathbf{E}_{\text{row}}(i) + \mathbf{E}_{\text{col}}(j) \quad (17.7)$$

Separate embeddings for row and column.

**Original ViT uses 1D:** Simpler, works well in practice!

## 17.2 Vision Transformer (ViT) Architecture

### 17.2.1 Complete ViT Model

**Definition 17.2** (Vision Transformer). **Input:** Image  $\mathbf{I} \in \mathbb{R}^{H \times W \times C}$

**Step 1:** Patch embedding

$$\mathbf{x}_{\text{patches}} = \text{PatchEmbed}(\mathbf{I}) \in \mathbb{R}^{N \times d} \quad (17.8)$$

**Step 2:** Add [CLS] token

$$\mathbf{x}_0 = [\mathbf{x}_{\text{cls}}, \mathbf{x}_{\text{patches}}] \in \mathbb{R}^{(N+1) \times d} \quad (17.9)$$

**Step 3:** Add position embeddings

$$\mathbf{x}_0 = \mathbf{x}_0 + \mathbf{E}_{\text{pos}} \quad (17.10)$$

**Step 4:** Transformer encoder (L layers)

$$\mathbf{x}_L = \text{Transformer}(\mathbf{x}_0) \quad (17.11)$$

**Step 5:** Classification head on [CLS]

$$y = \text{softmax}(\mathbf{W}_{\text{head}} \mathbf{x}_L^{\text{cls}} + \mathbf{b}) \quad (17.12)$$

### 17.2.2 ViT Model Variants

The Vision Transformer comes in three standard configurations that scale from moderate to extremely large models. ViT-Base uses 12 layers with hidden dimension  $d = 768$  and 12 attention heads, resulting in 86 million parameters. This configuration is comparable in size to BERT-base and serves as the standard baseline for vision transformer research. The patch size is typically set to  $P = 16$  for ImageNet-resolution images, producing 196 patches from a  $224 \times 224$  input.

ViT-Large scales up to 24 layers with  $d = 1024$  and 16 attention heads, totaling 307 million parameters. This represents a roughly  $3.5\times$  increase in parameters compared to ViT-Base, with the additional capacity enabling stronger performance when sufficient training data is available. The larger hidden dimension increases both the expressiveness of each layer and the computational cost per token.

ViT-Huge pushes the architecture to 32 layers with  $d = 1280$  and 16 heads, reaching 632 million parameters. This massive model requires enormous datasets like JFT-300M for effective training and demonstrates the scalability of the transformer architecture to vision tasks. However, the computational and memory requirements make ViT-Huge impractical for many applications, with inference on a single image requiring several gigabytes of GPU memory and hundreds of milliseconds even on modern accelerators.

**Example 17.2** (ViT-Base Parameter Count). Configuration:  $L = 12$ ,  $d = 768$ ,  $h = 12$ ,  $P = 16$ , ImageNet ( $N = 196$ )

**Patch embedding:**

$$768 \times 768 = 589,824 \quad (17.13)$$

**Position embeddings:**

$$197 \times 768 = 151,296 \quad (17.14)$$

**Transformer encoder (12 layers):**

$$12 \times 7,084,800 = 85,017,600 \quad (17.15)$$

**Classification head (ImageNet, 1000 classes):**

$$768 \times 1000 = 768,000 \quad (17.16)$$

**Total:**  $\approx 86,527,000 \approx 86\text{M}$  parameters

### 17.2.3 Memory Requirements and Computational Analysis

The memory footprint of Vision Transformers scales with both the model size and the input image resolution. For ViT-Base with 86 million parameters, storing the model weights in FP32 requires  $86 \times 10^6 \times 4 = 344$  MB. During training, we must also store optimizer states (momentum and variance for Adam), which doubles this to approximately 1 GB for the model alone. Additionally, activations must be stored for backpropagation, and their memory consumption depends critically on the sequence length.

For a standard  $224 \times 224$  image with patch size 16, the sequence length is 196 tokens (plus one CLS token for 197 total). The activation memory for a single layer includes the attention scores matrix of size  $h \times n \times n$  where  $h = 12$  heads and  $n = 197$ , requiring  $12 \times 197^2 \times 4 = 1.86$  MB in FP32. Across 12 layers with batch size 32, attention matrices alone consume approximately 714 MB. The feed-forward network activations add another  $32 \times 197 \times 768 \times 4 \times 12 = 2.3$  GB for intermediate representations. In total, training ViT-Base with batch size 32 on  $224 \times 224$  images requires approximately 8-10 GB of GPU memory, comfortably fitting on modern GPUs like the NVIDIA RTX 3090 or A100.

However, increasing the image resolution dramatically impacts memory requirements due to the quadratic scaling of attention. For  $384 \times 384$  images with the same patch size of 16, the number of patches increases to  $(384/16)^2 = 576$  tokens. The attention matrices now require  $12 \times 577^2 \times 4 = 16.0$  MB per layer, or 6.1 GB across 12 layers with batch size 32. This represents an  $8.5\times$  increase in attention

memory compared to  $224 \times 224$  resolution. The total memory requirement grows to approximately 18-22 GB, necessitating high-end GPUs or gradient checkpointing techniques to fit in memory.

**Example 17.3** (Image Resolution Impact). Compare memory and computation for different resolutions with ViT-Base ( $L = 12$ ,  $d = 768$ ,  $h = 12$ ,  $P = 16$ ):

**Resolution  $224 \times 224$ :**

$$n = \frac{224^2}{16^2} = 196 \text{ patches} \quad (17.17)$$

Attention memory per layer:  $12 \times 197^2 \times 4 = 1.86 \text{ MB}$

FLOPs per attention layer:  $4n^2d = 4 \times 197^2 \times 768 = 119 \text{ MFLOPs}$

**Resolution  $384 \times 384$ :**

$$n = \frac{384^2}{16^2} = 576 \text{ patches} \quad (17.18)$$

Attention memory per layer:  $12 \times 577^2 \times 4 = 16.0 \text{ MB}$  ( $8.6\times$  increase)

FLOPs per attention layer:  $4 \times 577^2 \times 768 = 1.03 \text{ GFLOPs}$  ( $8.6\times$  increase)

**Key insight:** Memory and computation scale quadratically with image resolution when patch size is fixed. Doubling resolution increases cost by approximately  $4\times$ .

The patch size provides another lever for controlling computational cost. Using larger patches reduces the sequence length, thereby decreasing both memory and computation. For a  $224 \times 224$  image, patch size  $P = 32$  produces only  $(224/32)^2 = 49$  patches compared to 196 for  $P = 16$ . This  $4\times$  reduction in sequence length translates to a  $16\times$  reduction in attention memory and computation due to the quadratic scaling. However, larger patches also reduce the model's ability to capture fine-grained visual details, creating a fundamental trade-off between efficiency and representational capacity.

**Example 17.4** (Patch Size Impact). For  $224 \times 224$  images with ViT-Base:

**Patch size  $P = 16$ :**

$$n = 196, \quad \text{Attention FLOPs} = 119 \text{ MFLOPs per layer} \quad (17.19)$$

**Patch size  $P = 32$ :**

$$n = 49, \quad \text{Attention FLOPs} = 7.4 \text{ MFLOPs per layer} \quad (17.20)$$

The  $16\times$  reduction in attention cost makes  $P = 32$  attractive for efficiency, but the coarser granularity typically reduces accuracy by 2-3% on ImageNet. The optimal patch size depends on the application: real-time systems may prefer  $P = 32$ , while accuracy-critical applications use  $P = 16$  or even  $P = 14$  for ViT-Huge.

## 17.3 Training Vision Transformers

### 17.3.1 Pre-training Strategies

**Supervised Pre-training (Original ViT):**

- Large datasets: JFT-300M (300M images, 18K classes)
- Standard classification loss
- Then fine-tune on ImageNet

**Key finding:** ViT requires massive data to outperform CNNs!

- On ImageNet alone: ResNet  $\hat{}$  ViT

- Pre-trained on JFT-300M: ViT > ResNet

### 17.3.2 Data Augmentation and Regularization

**Essential for ViT (lacks CNN inductive biases):**

**Augmentation:**

- RandAugment: Random augmentation policies
- Mixup:  $\tilde{x} = \lambda x_i + (1 - \lambda)x_j$
- CutMix: Cut and paste patches between images
- Random erasing

**Regularization:**

- Dropout: 0.1
- Stochastic depth: Drop entire layers randomly
- Weight decay:  $10^{-4}$  to  $10^{-2}$

### 17.3.3 DeiT: Data-efficient Image Transformers

Improvements for training without massive datasets:

#### 1. Knowledge Distillation

- Teacher: CNN (ResNetY) or ViT
- Student: ViT
- Distillation token alongside [CLS]

#### 2. Strong Augmentation

- Aggressive RandAugment
- Repeated augmentation

**Result:** DeiT-Base achieves 81.8% on ImageNet trained only on ImageNet (1.3M images)!

## 17.4 Masked Autoencoders (MAE)

### 17.4.1 Self-Supervised Pre-training for Vision

**Definition 17.3** (Masked Autoencoder). BERT-style masking for images:

**Step 1:** Randomly mask 75% of patches

**Step 2:** Encoder processes only visible patches

**Step 3:** Decoder reconstructs all patches (including masked)

**Loss:** Pixel-level MSE on masked patches

$$\mathcal{L} = \frac{1}{|\mathcal{M}|} \sum_{i \in \mathcal{M}} \|\hat{\mathbf{x}}_i - \mathbf{x}_i\|^2 \quad (17.21)$$

**Example 17.5** (MAE Architecture). **Image:**  $224 \times 224$ , patches  $16 \times 16$  ( $N = 196$ )

**Masking:** Keep 25% = 49 patches, mask 147 patches

**Encoder:**

- Input: 49 visible patches only
- Architecture: ViT-Large (24 layers,  $d = 1024$ )
- Much faster (process 1/4 of patches)

**Decoder:**

- Input: Encoder output + mask tokens
- Architecture: Smaller (8 layers,  $d = 512$ )
- Reconstruct all 196 patches

**Benefits:**

- Self-supervised (no labels needed)
- Learns strong representations
- Fine-tune on ImageNet: 87.8% accuracy

## 17.5 Hierarchical Vision Transformers

### 17.5.1 Motivation for Hierarchical Architectures

The original Vision Transformer processes images at a single scale, dividing the input into fixed-size patches and maintaining the same spatial resolution throughout all layers. While this uniform approach simplifies the architecture, it has significant limitations for computer vision tasks. Many vision problems benefit from multi-scale representations: low-level features like edges and textures are best captured at high resolution with small receptive fields, while high-level semantic concepts require large receptive fields that aggregate information across the entire image. CNNs naturally provide this hierarchical structure through pooling layers that progressively reduce spatial resolution while increasing channel capacity.

Additionally, the quadratic complexity of self-attention with respect to sequence length makes standard ViT impractical for high-resolution images or dense prediction tasks like object detection and semantic segmentation. For a  $512 \times 512$  image with patch size 16, the sequence length reaches 1,024 tokens, requiring attention matrices of size  $1024 \times 1024$  per head. With 12 heads across 12 layers, this consumes over 600 MB just for attention weights in a single forward pass. The computational cost of  $O(n^2d)$  attention becomes prohibitive, limiting ViT's applicability to tasks requiring fine-grained spatial reasoning.

Hierarchical Vision Transformers address these limitations by introducing multi-scale processing and localized attention mechanisms. These architectures progressively reduce spatial resolution while increasing feature dimensions, mimicking the pyramid structure of CNNs while retaining the flexibility of transformer layers. By restricting attention to local windows rather than the full image, they achieve linear or near-linear complexity in the number of pixels, enabling efficient processing of high-resolution inputs.

### 17.5.2 Swin Transformer

The Swin Transformer (Shifted Window Transformer) introduces a hierarchical architecture with shifted window-based attention that achieves linear complexity while maintaining the ability to model long-



range dependencies. The architecture consists of four stages, each operating at a different spatial resolution. The first stage processes the image at high resolution with small patches (typically  $4 \times 4$ ), producing a large number of tokens. Subsequent stages merge adjacent patches to reduce the spatial dimensions by  $2\times$  while doubling the feature dimension, creating a pyramid structure similar to ResNet.

**Definition 17.4** (Swin Transformer Architecture). For input image  $\mathbf{I} \in \mathbb{R}^{H \times W \times 3}$ :

**Stage 1:** Patch size  $4 \times 4$ , dimension  $C$

$$\text{Resolution: } \frac{H}{4} \times \frac{W}{4}, \quad \text{Channels: } C \quad (17.22)$$

**Stage 2:** Patch merging, dimension  $2C$

$$\text{Resolution: } \frac{H}{8} \times \frac{W}{8}, \quad \text{Channels: } 2C \quad (17.23)$$

**Stage 3:** Patch merging, dimension  $4C$

$$\text{Resolution: } \frac{H}{16} \times \frac{W}{16}, \quad \text{Channels: } 4C \quad (17.24)$$

**Stage 4:** Patch merging, dimension  $8C$

$$\text{Resolution: } \frac{H}{32} \times \frac{W}{32}, \quad \text{Channels: } 8C \quad (17.25)$$

For Swin-Base:  $C = 128$ , producing feature maps at resolutions  $\frac{H}{4}, \frac{H}{8}, \frac{H}{16}, \frac{H}{32}$  with dimensions 128, 256, 512, 1024 respectively.

The key innovation of Swin Transformer is shifted window attention, which restricts self-attention to non-overlapping local windows while enabling cross-window connections through window shifting. In even-numbered layers, the image is partitioned into regular  $M \times M$  windows (typically  $M = 7$ ), and attention is computed independently within each window. In odd-numbered layers, the windows are shifted by  $\lfloor M/2 \rfloor$  pixels in both horizontal and vertical directions, causing the windows to overlap with different regions than in the previous layer. This shifting mechanism allows information to flow between windows while maintaining the computational efficiency of local attention.

The computational complexity of window-based attention is  $O(M^2 \cdot HW)$  where  $M$  is the window size and  $HW$  is the image resolution. For  $M = 7$  and a  $224 \times 224$  image at stage 1 resolution ( $56 \times 56$  tokens), each window contains  $7 \times 7 = 49$  tokens. The attention computation within a window requires  $49^2 = 2,401$  operations per head, compared to  $3,136^2 = 9.8$  million operations for global attention over all  $56 \times 56$  tokens. This  $4,000\times$  reduction in attention complexity enables Swin Transformer to process high-resolution images efficiently while still capturing long-range dependencies through the hierarchical structure and window shifting.

**Example 17.6** (Swin Transformer Complexity). Compare attention complexity for  $224 \times 224$  image at stage 1 ( $56 \times 56$  tokens):

**Global attention (standard ViT):**

$$\text{Complexity: } O(n^2d) = O(3136^2 \times 128) = 1.26 \text{ GFLOPs per layer} \quad (17.26)$$

**Window attention (Swin,  $M = 7$ ):**

$$\text{Windows: } \frac{56}{7} \times \frac{56}{7} = 64 \text{ windows} \quad (17.27)$$

$$\text{Complexity: } O(M^2 \cdot HW \cdot d) = O(49 \times 3136 \times 128) = 19.7 \text{ MFLOPs per layer} \quad (17.28)$$

The window-based approach reduces attention cost by  $64\times$ , making high-resolution processing practical. The shifted window mechanism ensures that information still propagates globally through the network depth.

Swin Transformer achieves state-of-the-art performance across multiple vision tasks while maintaining computational efficiency. On ImageNet classification, Swin-Base reaches 83.5% top-1 accuracy with 88 million parameters and 15.4 GFLOPs—comparable to ViT-Base in parameters but with better accuracy due to the hierarchical structure. For object detection on COCO, Swin-Base achieves 51.9 box AP, surpassing previous transformer-based detectors by significant margins. The multi-scale feature maps produced by the hierarchical architecture are particularly well-suited for dense prediction tasks, making Swin Transformer a versatile backbone for various computer vision applications.

### 17.5.3 Pyramid Vision Transformer (PVT)

Pyramid Vision Transformer takes a different approach to hierarchical vision transformers by introducing spatial-reduction attention that progressively decreases the key and value sequence lengths. Unlike Swin’s window-based attention, PVT maintains global attention but reduces computational cost by downsampling the keys and values before computing attention. This design preserves the ability to attend to the entire image while achieving sub-quadratic complexity.

In PVT, each stage reduces the spatial resolution through patch merging, similar to Swin Transformer. However, within each stage, the attention mechanism uses a spatial reduction operation on keys and values. For a reduction ratio  $R$ , the keys and values are reshaped and downsampled by  $R \times R$ , reducing their sequence length by a factor of  $R^2$ . The queries maintain the original resolution, allowing each token to attend to a downsampled representation of the entire image. This approach reduces attention complexity from  $O(n^2d)$  to  $O(n^2d/R^2)$ , providing a tunable trade-off between computational cost and attention granularity.

The hierarchical structure of PVT produces feature maps at multiple scales, making it suitable as a backbone for dense prediction tasks. PVT-Medium with 44 million parameters achieves 82.0% ImageNet accuracy while requiring only 6.7 GFLOPs—significantly more efficient than ViT-Base. For object detection, PVT-based detectors achieve competitive performance with CNN-based methods while offering the benefits of transformer architectures, including better transfer learning and attention-based interpretability.

### 17.5.4 Hybrid Architectures: CoAtNet

Hybrid architectures combine convolutional layers and transformer layers to leverage the complementary strengths of both approaches. Convolutional layers provide efficient local feature extraction with built-in translation equivariance, while transformer layers enable global reasoning and flexible attention patterns. CoAtNet (Convolution and Attention Network) systematically explores this design space, identifying an optimal combination that achieves state-of-the-art performance with improved efficiency.

The CoAtNet architecture consists of five stages with progressively decreasing spatial resolution. The first two stages use convolutional blocks based on the MBConv (Mobile Inverted Bottleneck Convolution) design from EfficientNet, which efficiently extracts local features at high resolution. These convolutional stages capture low-level visual patterns like edges, textures, and simple shapes with strong inductive bias and minimal computational cost. The spatial resolution is reduced by  $2\times$  at each stage through strided convolutions.

The final three stages employ transformer blocks with relative attention, enabling global reasoning over the extracted features. By this point in the network, the spatial resolution has been reduced by  $8\times$  or more, making global attention computationally feasible. The transformer stages learn high-level semantic representations and long-range dependencies that benefit from the flexibility of self-attention. The final stage uses attention pooling to aggregate spatial information into a global representation for classification.

**Example 17.7** (CoAtNet Architecture). CoAtNet-3 configuration for  $224 \times 224$  input:

**Stage 0 (Stem):** Convolution,  $112 \times 112$  resolution, 64 channels

**Stage 1:** MBConv blocks,  $112 \times 112$  resolution, 96 channels

**Stage 2:** MBConv blocks,  $56 \times 56$  resolution, 192 channels

**Stage 3:** Transformer blocks,  $28 \times 28$  resolution, 384 channels

**Stage 4:** Transformer blocks,  $14 \times 14$  resolution, 768 channels

**Stage 5:** Attention pooling, global representation

Total parameters: 168M, FLOPs: 34.7G

This hybrid design achieves 87.9% ImageNet accuracy, outperforming pure CNN and pure transformer architectures of similar size.

The success of CoAtNet demonstrates that the choice between convolution and attention need not be binary. By using convolutions where they excel (local feature extraction at high resolution) and transformers where they excel (global reasoning at lower resolution), hybrid architectures achieve better accuracy-efficiency trade-offs than either approach alone. CoAtNet-7, the largest variant with 2.4 billion parameters, achieved 90.88% ImageNet accuracy and state-of-the-art results on multiple vision benchmarks at the time of its release, validating the hybrid approach at scale.

## 17.6 ViT vs CNN Comparison

### 17.6.1 Parameter Efficiency

Vision Transformers and Convolutional Neural Networks differ fundamentally in their parameter efficiency and data requirements. ResNet-50, a standard CNN baseline, contains approximately 25 million parameters distributed across convolutional layers with small kernel sizes (typically  $3 \times 3$  or  $7 \times 7$ ). In contrast, ViT-Base requires 86 million parameters—more than  $3\times$  the size of ResNet-50—to achieve comparable performance. This parameter gap reflects the different inductive biases: CNNs build in locality and translation equivariance through their convolutional structure, while transformers must learn these properties from data through their flexible attention mechanism.

The parameter distribution also differs significantly between the architectures. In ResNet-50, the majority of parameters reside in the later convolutional layers and the final fully-connected layer. For ViT-Base, the parameters are more evenly distributed across the 12 transformer layers, with each layer containing approximately 7 million parameters in the attention and feed-forward components. The patch embedding layer contributes only 590K parameters, while position embeddings add another 151K—both negligible compared to the transformer layers themselves.

Despite having more parameters, ViT-Base is not necessarily slower than ResNet-50 for inference. The transformer's matrix multiplications are highly optimized on modern GPUs, and the lack of spatial convolutions can actually improve throughput. On an NVIDIA A100 GPU, ViT-Base processes approximately 1,200 images per second at  $224 \times 224$  resolution with batch size 128, compared to 1,400 images per second for ResNet-50. The 15% throughput difference is much smaller than the  $3\times$  parameter gap would suggest, demonstrating the efficiency of transformer operations on modern hardware.

### 17.6.2 Computational Complexity Analysis

The computational complexity of Vision Transformers scales differently than CNNs, leading to different performance characteristics across image resolutions. For a CNN like ResNet-50, the computational cost is approximately  $O(C \times k^2 \times H \times W)$  where  $C$  is the number of channels,  $k$  is the kernel size, and  $H \times W$  is the spatial resolution. This linear scaling in spatial dimensions means that doubling the image resolution increases computation by  $4\times$ . For ResNet-50 processing a  $224 \times 224$  image, the total computation is approximately 4.1 GFLOPs.

Vision Transformers have complexity  $O(n^2d + nd^2)$  where  $n = (H/P)^2$  is the number of patches and  $d$  is the hidden dimension. The  $n^2d$  term comes from attention, while  $nd^2$  comes from the feed-forward network. For ViT-Base with  $224 \times 224$  images and patch size 16, we have  $n = 196$  and  $d = 768$ . The

attention computation across 12 layers totals  $12 \times 4 \times 196^2 \times 768 = 1.4$  GFLOPs, while the feed-forward network contributes  $12 \times 2 \times 196 \times 768^2 = 2.8$  GFLOPs, for a total of approximately 4.2 GFLOPs—nearly identical to ResNet-50.

However, the scaling behavior differs dramatically. When we increase resolution to  $384 \times 384$  with the same patch size, the number of patches grows to  $n = 576$ , increasing by a factor of  $(384/224)^2 = 2.94$ . The attention cost grows quadratically to  $12 \times 4 \times 576^2 \times 768 = 12.3$  GFLOPs ( $8.6\times$  increase), while the feed-forward cost grows linearly to  $12 \times 2 \times 576 \times 768^2 = 8.1$  GFLOPs ( $2.9\times$  increase). The total ViT computation reaches 20.4 GFLOPs, compared to 12.0 GFLOPs for ResNet-50 at the same resolution. This crossover point illustrates why efficient attention mechanisms become critical for high-resolution vision tasks.

**Example 17.8** (Computational Crossover Analysis). Compare FLOPs for ResNet-50 and ViT-Base across resolutions:

Resolution	ResNet-50	ViT-Base
$224 \times 224$	4.1 GFLOPs	4.2 GFLOPs
$384 \times 384$	12.0 GFLOPs	20.4 GFLOPs
$512 \times 512$	21.3 GFLOPs	48.7 GFLOPs

At standard ImageNet resolution, ViT and ResNet have similar computational cost. However, ViT’s quadratic attention scaling makes it increasingly expensive at higher resolutions, motivating hierarchical architectures like Swin Transformer that reduce attention to local windows.

### 17.6.3 Data Requirements and Inductive Bias

The most striking difference between Vision Transformers and CNNs lies in their data requirements, which stem from their different inductive biases. CNNs encode strong priors about images: locality (nearby pixels are related), translation equivariance (a cat is a cat regardless of position), and hierarchical structure (edges  $\rightarrow$  textures  $\rightarrow$  objects). These built-in assumptions allow CNNs to learn effectively from moderate-sized datasets like ImageNet with 1.3 million images. ResNet-50 trained only on ImageNet achieves 76.5% top-1 accuracy, demonstrating that the convolutional structure provides useful inductive bias for natural images.

Vision Transformers, by contrast, have minimal inductive bias. The self-attention mechanism can attend to any patch regardless of spatial distance, and the model must learn locality and translation properties from data. When trained only on ImageNet, ViT-Base achieves only 72.3% accuracy—4.2 percentage points below ResNet-50 despite having  $3\times$  more parameters. This performance gap reveals that the flexibility of attention becomes a liability when training data is limited: the model has too much capacity and insufficient constraints to learn good representations.

The situation reverses dramatically with large-scale pre-training. When ViT-Base is pre-trained on JFT-300M (300 million images with 18,000 classes) and then fine-tuned on ImageNet, it achieves 84.2% accuracy, surpassing ResNet-50’s 76.5% by a substantial margin. The massive pre-training dataset provides enough examples for the transformer to learn the visual priors that CNNs encode by design. Moreover, the learned representations transfer better to downstream tasks: ViT-Base pre-trained on JFT-300M achieves higher accuracy than ResNet-50 on 19 out of 20 transfer learning benchmarks, with improvements ranging from 2-7 percentage points.

This data-efficiency trade-off has important practical implications. For applications with limited training data or computational budgets, CNNs remain the better choice. For large-scale systems with access to massive datasets and compute, Vision Transformers offer superior performance and transfer learning capabilities. The development of data-efficient training methods like DeiT (Data-efficient Image Transformers) has partially bridged this gap, enabling ViT-Base to achieve 81.8% on ImageNet without external data through aggressive augmentation and distillation techniques.

### 17.6.4 When to Use Each Architecture

Aspect	CNN (ResNet)	ViT
Inductive bias	Strong (locality, translation)	Weak
Data requirement	Moderate (ImageNet)	Large (JFT-300M)
Parameters	25M (ResNet-50)	86M (ViT-Base)
Computation	$O(HW)$	$O((HW/P)^2)$
Memory	5-7 GB training	8-10 GB training
Interpretability	Filter visualization	Attention maps
Transfer	Good	Excellent (large-scale)
Best use	Small/medium data	Large-scale pre-training

The choice between CNNs and Vision Transformers depends on the specific application constraints. CNNs are preferable when training data is limited (fewer than 10 million images), when computational efficiency is critical (mobile or edge deployment), or when strong spatial priors are known to be appropriate for the task. ResNet and EfficientNet variants remain the standard choice for many production computer vision systems due to their reliability and efficiency.

Vision Transformers excel when massive pre-training data is available, when transfer learning to diverse downstream tasks is important, or when state-of-the-art performance justifies the additional computational cost. The superior scaling properties of transformers—both in terms of model size and dataset size—make them the architecture of choice for foundation models in vision. Hybrid architectures like CoAtNet attempt to combine the strengths of both approaches, using convolutional layers for early feature extraction and transformer layers for high-level reasoning.

## 17.7 Exercises

**Exercise 17.1.** Implement patch embedding for image  $224 \times 224 \times 3$  with patch size 16:

1. Reshape image to patches
2. Apply linear projection
3. Add position embeddings
4. Verify output shape: (196, 768)

**Exercise 17.2.** Compare ViT-Base and ResNet-50:

1. Parameter count
2. FLOPs for  $224 \times 224$  image
3. Memory footprint
4. Which is more efficient?

**Exercise 17.3.** Implement MAE masking:

1. Randomly mask 75% of 196 patches

2. Keep 49 visible patches
3. Add mask tokens for decoder
4. Compute reconstruction loss

**Exercise 17.4.** Train ViT-Tiny on CIFAR-10:

1. Use patch size 4 (for  $32 \times 32$  images)
2. 6 layers,  $d = 192$ , 3 heads
3. Apply RandAugment
4. Compare to small ResNet

## 17.8 Solutions

Full solutions for all exercises are available at <https://deeplearning.hofkensvermeulen.be>.

# Chapter 18

## Multimodal Transformers

### Chapter Overview

Multimodal transformers process multiple modalities (text, images, audio, video) in a unified framework. This chapter covers vision-language models (CLIP, DALL-E), audio-text models (Whisper), and unified architectures that handle arbitrary combinations of modalities.

#### Learning Objectives

1. Understand multimodal fusion strategies
2. Implement contrastive learning (CLIP)
3. Apply vision-language models to zero-shot classification
4. Generate images from text (DALL-E, Stable Diffusion)
5. Process audio with transformers (Whisper)
6. Build unified multimodal models

### 18.1 Multimodal Learning Fundamentals

#### 18.1.1 Fusion Strategies

The choice of fusion strategy determines how modalities interact, with direct implications for computational cost and expressiveness. Three primary approaches have emerged:

Strategy	Description	Pros	Cons
Early fusion	Concatenate modality tokens into one sequence; process with unified encoder	Rich cross-modal interaction at every layer; simple architecture	$O((N+M)^2d)$ cost; adding patches dramatically increases compute
Late fusion	Separate encoders per modality; combine outputs at decision stage (CLIP)	Efficient $O(N^2d+M^2d)$ ; encoders parallelizable	No fine-grained cross-modal alignment; interaction only at output
Cross-modal attention	Separate encoders with cross-attention layers between modalities (BLIP, Flamingo)	$O(N^2d+M^2d+NMd)$ ; rich interactions with moderate cost	Additional parameters; more complex architecture

Cross-modal attention offers the best trade-off for most applications: for 196 image patches and 128 text tokens, cross-attention requires  $196 \times 128 = 25,088$  computations per head versus  $324^2 = 104,976$  for early fusion—a  $4\times$  reduction while preserving fine-grained alignment between modalities.

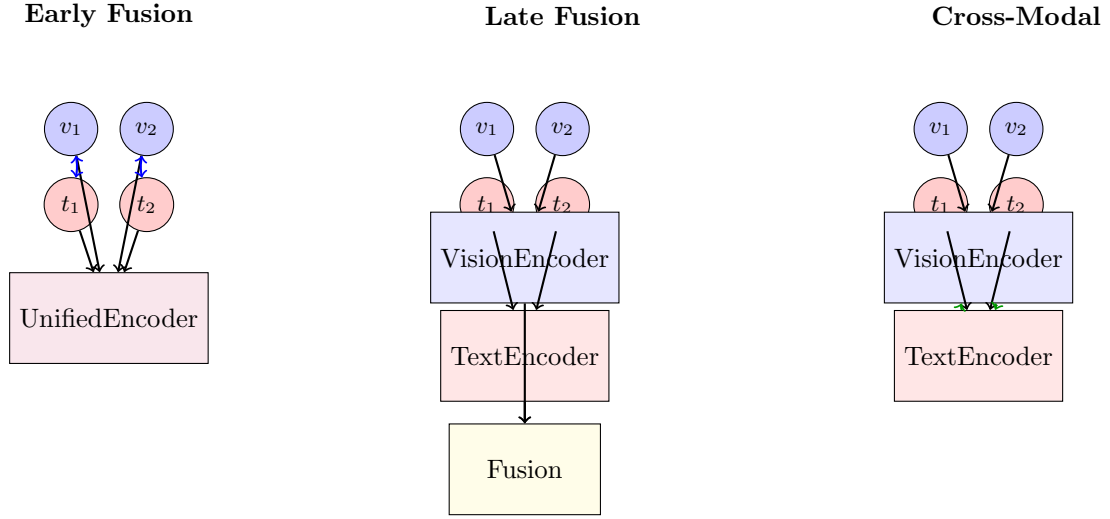


Figure 18.1: Three multimodal fusion strategies. **Early fusion** (left): concatenates modalities and processes with unified encoder, enabling rich interactions but with quadratic cost  $O((N + M)^2)$ . **Late fusion** (center): separate encoders with fusion only at output, efficient  $O(N^2 + M^2)$  but limited cross-modal interaction. **Cross-modal attention** (right): separate encoders with explicit cross-attention, balancing efficiency  $O(N^2 + M^2 + NM)$  with rich interactions.

### 18.1.2 Alignment Objectives

**Contrastive Learning:**

$$\mathcal{L}_{\text{contrastive}} = -\log \frac{\exp(\text{sim}(v_i, t_i)/\tau)}{\sum_j \exp(\text{sim}(v_i, t_j)/\tau)} \quad (18.1)$$

where  $v_i$  = image embedding,  $t_i$  = text embedding,  $\tau$  = temperature

**Matching Loss:**

$$\mathcal{L}_{\text{match}} = -\mathbb{E}[\log P(\text{match}|v, t)] \quad (18.2)$$

**Reconstruction:**

$$\mathcal{L}_{\text{recon}} = \|f_{\text{dec}}(v) - t\|^2 \quad (18.3)$$

## 18.2 CLIP: Contrastive Language-Image Pre-training

### 18.2.1 CLIP Architecture

CLIP (Contrastive Language-Image Pre-training) represents a breakthrough in vision-language learning by training image and text encoders jointly using a contrastive objective on 400 million image-text pairs collected from the internet. Unlike traditional supervised learning that requires manually labeled categories, CLIP learns to align images with their natural language descriptions, enabling zero-shot transfer to downstream tasks without any task-specific training data.

**Definition 18.1** (CLIP Model). The CLIP architecture consists of three main components that work together to create a shared embedding space for images and text. The **image encoder** can be either a Vision Transformer (ViT) or a ResNet, which processes an input image and produces a fixed-dimensional embedding  $\mathbf{v} \in \mathbb{R}^d$ . For the largest CLIP model (ViT-L/14), the image encoder is a ViT with patch size 14, hidden dimension 1024, 24 layers, and 16 attention heads, totaling approximately 304 million parameters. The **text encoder** is a transformer decoder (similar to GPT) with a context length of 77 tokens, hidden dimension 768, 12 layers, and 12 attention heads, containing roughly 63 million parameters. Both encoders are followed by learned linear **projection layers** that map their outputs to a shared embedding space of dimension  $d = 512$ ,



where cosine similarity can be computed directly.

The training procedure processes batches of  $(image, text)$  pairs simultaneously. For each batch of size  $N$ , all  $N$  images are encoded to produce embeddings  $\mathbf{v}_1, \dots, \mathbf{v}_N \in \mathbb{R}^{512}$ , and all  $N$  text descriptions are encoded to produce  $\mathbf{t}_1, \dots, \mathbf{t}_N \in \mathbb{R}^{512}$ . The model then computes an  $N \times N$  similarity matrix where entry  $(i, j)$  represents the cosine similarity between image  $i$  and text  $j$ . The contrastive loss maximizes the similarity along the diagonal (correct image-text pairs) while minimizing off-diagonal similarities (incorrect pairings). This symmetric loss is computed in both directions—predicting text from image and image from text—and averaged.

The parameter count for CLIP varies significantly across model scales. CLIP ResNet-50 contains approximately 102 million parameters (38M for ResNet-50 image encoder, 63M for text encoder, 1M for projections), while CLIP ViT-L/14 totals around 428 million parameters (304M for ViT-L image encoder, 123M for a larger text encoder with 768 dimensions and 12 layers, 1M for projections). The largest variant, ViT-L/14@336px, processes higher-resolution images ( $336 \times 336$  instead of  $224 \times 224$ ) with the same architecture, increasing computational cost but improving performance on fine-grained tasks.

**Example 18.1** (CLIP Training). Consider a training batch with size  $N = 4$  and embedding dimension  $d = 512$ . The image encoder processes four images to produce embeddings arranged as rows in matrix  $\mathbf{V} = [\mathbf{v}_1, \mathbf{v}_2, \mathbf{v}_3, \mathbf{v}_4]^\top \in \mathbb{R}^{4 \times 512}$ , while the text encoder processes their corresponding captions to produce  $\mathbf{T} = [\mathbf{t}_1, \mathbf{t}_2, \mathbf{t}_3, \mathbf{t}_4]^\top \in \mathbb{R}^{4 \times 512}$ .

The similarity matrix is computed as  $\mathbf{S} = \mathbf{V}\mathbf{T}^\top \in \mathbb{R}^{4 \times 4}$ , where each entry  $S_{ij}$  represents the dot product between image embedding  $i$  and text embedding  $j$ . To make this scale-invariant, CLIP uses cosine similarity:  $S_{ij} = \frac{\mathbf{v}_i \cdot \mathbf{t}_j}{\|\mathbf{v}_i\| \|\mathbf{t}_j\|}$ , which normalizes each embedding to unit length before computing the dot product. This ensures that the similarity is determined by the angle between embeddings rather than their magnitudes.

The contrastive loss for the image-to-text direction is computed as:

$$\mathcal{L}_i^{\text{img} \rightarrow \text{txt}} = -\log \frac{\exp(S_{ii}/\tau)}{\sum_{j=1}^N \exp(S_{ij}/\tau)} \quad (18.4)$$

where  $\tau$  is a learned temperature parameter, initialized to 0.07 and trained jointly with the model. The temperature controls the sharpness of the distribution: smaller values make the model more confident (sharper peaks), while larger values produce softer distributions. The symmetric text-to-image loss  $\mathcal{L}_i^{\text{txt} \rightarrow \text{img}}$  is computed analogously by treating text as queries and images as candidates. The total loss averages both directions:

$$\mathcal{L} = \frac{1}{2N} \sum_{i=1}^N (\mathcal{L}_i^{\text{img} \rightarrow \text{txt}} + \mathcal{L}_i^{\text{txt} \rightarrow \text{img}}) \quad (18.5)$$

In practice, CLIP uses very large batch sizes to provide more negative examples for contrastive learning. The original CLIP was trained with batch size 32,768, requiring distributed training across multiple GPUs. With such large batches, each positive pair has 32,767 negative examples, providing a strong learning signal. However, this creates substantial memory requirements: storing the  $32,768 \times 512$  embedding matrices for images and text requires  $32,768 \times 512 \times 4 = 67$  MB per modality in FP32, and the  $32,768 \times 32,768$  similarity matrix requires 4.3 GB. To make this tractable, CLIP uses gradient checkpointing and distributes the batch across many GPUs, computing the similarity matrix in chunks.

### 18.2.2 Computational Analysis of CLIP Training

Training CLIP at scale requires careful consideration of computational and memory costs across both the image and text encoding paths. For the ViT-L/14 image encoder processing  $224 \times 224$  images, each

image is divided into  $16 \times 16 = 256$  patches of size  $14 \times 14$ . These patches are linearly projected to dimension 1024 and processed through 24 transformer layers. The computational cost per image is approximately  $2 \times 24 \times 256^2 \times 1024 = 3.2$  GFLOPS for the attention operations (using the  $2Ld^2n^2$  formula from Chapter 12) plus  $2 \times 24 \times 256 \times 4 \times 1024^2 = 51.5$  GFLOPS for the feed-forward networks, totaling roughly 55 GFLOPS per image.

The text encoder processes sequences of up to 77 tokens through 12 transformer layers with dimension 768. The computational cost per text is approximately  $2 \times 12 \times 77^2 \times 768 = 1.1$  GFLOPS for attention plus  $2 \times 12 \times 77 \times 4 \times 768^2 = 4.4$  GFLOPS for feed-forward networks, totaling about 5.5 GFLOPS per text. This asymmetry—images requiring 10 $\times$  more compute than text—means that image encoding dominates the computational budget during training.

For a batch of 32,768 examples, the total forward pass requires approximately  $32,768 \times (55 + 5.5) = 1,982,464$  GFLOPS or roughly 2 PFLOPS. On an NVIDIA A100 GPU with 312 TFLOPS of FP16 compute, this would take approximately 6.4 seconds per batch for the forward pass alone, not including backward propagation (which typically costs 2 $\times$  the forward pass) or the contrastive loss computation. The full training of CLIP on 400 million image-text pairs with batch size 32,768 requires approximately  $400,000,000/32,768 = 12,207$  batches. At roughly 20 seconds per batch (forward + backward + optimizer step), this amounts to 68 hours of continuous training on a single A100. In practice, OpenAI trained CLIP on 256 V100 GPUs for approximately 12 days, suggesting a total training cost of around 73,728 GPU-hours.

Memory requirements are equally demanding. Each image in the batch requires storing activations for 24 layers with 256 tokens and dimension 1024, totaling approximately  $24 \times 256 \times 1024 \times 2 = 12.6$  MB per image in FP16 (the factor of 2 accounts for storing both pre- and post-activation values for backpropagation). For batch size 32,768, this amounts to 413 GB just for image activations. Text activations are smaller at approximately  $12 \times 77 \times 768 \times 2 = 1.4$  MB per text, or 46 GB for the full batch. The similarity matrix requires  $32,768 \times 32,768 \times 2 = 2.1$  GB in FP16. Combined with model parameters (428M parameters  $\times$  2 bytes = 856 MB) and optimizer states (typically 2 $\times$  parameters for Adam), the total memory footprint exceeds 500 GB, necessitating distribution across many GPUs using techniques like ZeRO (Chapter 22) to partition optimizer states and activations.

### 18.2.3 Zero-Shot Classification with CLIP

One of CLIP’s most remarkable capabilities is zero-shot classification: the ability to classify images into categories the model has never been explicitly trained on. This works by leveraging the natural language understanding of the text encoder to create classifiers on the fly from text descriptions. The procedure begins by creating text prompts for each class in the target classification task. For example, for a 10-class animal classification task, we might create prompts like “a photo of a dog”, “a photo of a cat”, “a photo of a bird”, and so on. These prompts are encoded by the text encoder to produce class embeddings  $\mathbf{t}_1, \dots, \mathbf{t}_C \in \mathbb{R}^{512}$  where  $C$  is the number of classes.

To classify a new image, we encode it with the image encoder to produce  $\mathbf{v} \in \mathbb{R}^{512}$ , then compute the cosine similarity between the image embedding and each class embedding:  $s_i = \frac{\mathbf{v} \cdot \mathbf{t}_i}{\|\mathbf{v}\| \|\mathbf{t}_i\|}$ . The predicted class is simply  $\arg \max_i s_i$ , the class whose text description has the highest similarity to the image. This approach requires no training on the target dataset—the model uses only its pre-trained knowledge of how images and text relate.

The performance of this zero-shot approach is surprisingly strong. CLIP ViT-L/14 achieves 76.2% top-1 accuracy on ImageNet without ever seeing a single ImageNet training example, matching the performance of a ResNet-50 trained directly on ImageNet’s 1.28 million labeled images. This demonstrates that CLIP has learned visual concepts that generalize far beyond its training distribution. Moreover, CLIP shows remarkable robustness to distribution shift: when evaluated on ImageNet variants with different image styles (sketches, cartoons, adversarial examples), CLIP’s performance degrades much less than supervised models, suggesting it has learned more robust visual representations.

The prompt engineering aspect of zero-shot classification is crucial for performance. Simple prompts like “dog” perform worse than more descriptive prompts like “a photo of a dog”. OpenAI found that using prompt ensembles—averaging predictions across multiple prompt templates like “a photo of a {class}”, “a picture of a {class}”, “an image of a {class}”—improves accuracy by 1-2% by reducing

sensitivity to prompt phrasing. For fine-grained classification tasks, more specific prompts help: "a photo of a {species}, a type of bird" outperforms "a photo of a {species}" for bird species classification.

### 18.2.4 CLIP Variants and Training Requirements

Following CLIP's success, several variants have been developed with different scales and training procedures. **OpenCLIP** is an open-source reproduction that has trained models ranging from small (ResNet-50 with 102M parameters) to very large (ViT-G/14 with 1.8B parameters) on datasets including LAION-400M and LAION-2B. The largest OpenCLIP models require training on clusters of 128-512 A100 GPUs for several weeks, with estimated costs exceeding \$100,000 for the full training run. The training uses mixed precision (FP16) to reduce memory consumption and enable larger batch sizes, typically 32,768 to 65,536 examples distributed across all GPUs.

**ALIGN**, developed by Google, scales up the training data to 1.8 billion noisy image-text pairs collected from the web without extensive filtering. This demonstrates that contrastive learning is robust to noise in the training data—the model learns to ignore mismatched pairs through the contrastive objective. ALIGN uses an EfficientNet-L2 image encoder (480M parameters) and a BERT-Large text encoder (340M parameters), totaling approximately 820M parameters. Training ALIGN required a cluster of 1024 Cloud TPU v3 cores for approximately 6 days, representing roughly 150,000 TPU-hours.

**Florence**, Microsoft's unified vision foundation model, extends the CLIP approach to 900 million image-text pairs with a focus on creating a single model that can be adapted to diverse vision tasks. Florence uses a CoSwin transformer as the image encoder (637M parameters) and achieves state-of-the-art results on zero-shot classification, retrieval, and object detection after fine-tuning. The training infrastructure required 512 NVIDIA A100 GPUs for approximately 10 days, with an estimated cost of over \$200,000 in cloud compute.

The hardware requirements for training CLIP-scale models are substantial. A minimum viable setup might use 8-16 A100 GPUs (80GB each) to train a CLIP ResNet-50 model on a smaller dataset like Conceptual Captions (3M pairs) with batch size 2048-4096, requiring approximately 1-2 weeks. Scaling to the full CLIP ViT-L/14 with 400M training pairs and batch size 32,768 necessitates at least 64-128 A100 GPUs with high-bandwidth interconnects (NVLink or InfiniBand) to efficiently synchronize gradients across the distributed batch. The total training cost for reproducing CLIP ViT-L/14 is estimated at \$50,000-\$100,000 in cloud GPU costs, depending on the provider and optimization techniques employed.

## 18.3 DALL-E and Stable Diffusion

### 18.3.1 DALL-E: Text-to-Image Generation

**Definition 18.2** (DALL-E Architecture). **DALL-E 1 (2021):**

- Encoder: Compress images to discrete tokens (VQ-VAE)
- Transformer: Autoregressive model over text + image tokens
- Training: Next token prediction

**Sequence:**

$$[\text{BOS}, \text{text tokens}, \text{image tokens}, \text{EOS}] \quad (18.6)$$

Generate image by: (1) Encode text, (2) Sample image tokens autoregressively

**DALL-E 2 (2022):**

- Use CLIP embeddings
- Prior: Text embedding  $\rightarrow$  Image embedding

- Decoder: Image embedding  $\rightarrow$  Image (diffusion model)
- Much higher quality than DALL-E 1

### 18.3.2 Stable Diffusion

#### Latent Diffusion Model:

1. Encode image to latent space (VAE)
2. Add noise iteratively (forward diffusion)
3. Learn to denoise (reverse diffusion)
4. Condition on text via cross-attention

#### Text conditioning:

- Text encoder: CLIP or T5
- Cross-attention: Latent queries attend to text keys/values
- Enables text-guided image generation

#### Example 18.2 (Stable Diffusion Architecture). Components:

1. **Text Encoder:** CLIP text encoder

$$\text{prompt} \rightarrow \mathbf{t} \in \mathbb{R}^{77 \times 768} \quad (18.7)$$

2. **VAE Encoder:** Image  $\rightarrow$  latent

$$\mathbf{I} \in \mathbb{R}^{512 \times 512 \times 3} \rightarrow \mathbf{z} \in \mathbb{R}^{64 \times 64 \times 4} \quad (18.8)$$

3. **U-Net Denoiser:** Diffusion model with cross-attention

- Input: Noisy latent  $\mathbf{z}_t$
- Condition: Text embedding  $\mathbf{t}$
- Output: Predicted noise  $\epsilon_\theta(\mathbf{z}_t, t, \mathbf{t})$

4. **VAE Decoder:** Latent  $\rightarrow$  image

$$\mathbf{z} \in \mathbb{R}^{64 \times 64 \times 4} \rightarrow \mathbf{I} \in \mathbb{R}^{512 \times 512 \times 3} \quad (18.9)$$

**Parameters:**  $\approx 860\text{M}$  total

## 18.4 Vision-Language Understanding

### 18.4.1 BLIP: Bootstrapped Language-Image Pre-training

#### Architecture:

- Image encoder (ViT)
- Text encoder (BERT)
- Multimodal encoder (cross-attention between vision and text)

#### Training objectives:

1. **ITC**: Image-Text Contrastive (like CLIP)
2. **ITM**: Image-Text Matching (binary: match or not)
3. **LM**: Language Modeling on text

**Bootstrapping**: Generate synthetic captions, filter with model, retrain

### 18.4.2 Flamingo: Few-Shot Learning

Flamingo represents a significant architectural innovation in multimodal transformers by enabling models to process arbitrarily interleaved sequences of images and text, supporting few-shot learning through in-context examples. Unlike CLIP, which processes single image-text pairs, Flamingo can handle inputs like "Here is an image of a cat: <image1>. Here is an image of a dog: <image2>. What animal is in this image: <image3>?" This capability enables few-shot visual learning where the model learns new tasks from just a few examples provided in the prompt, without any parameter updates.

The Flamingo architecture consists of three main components, carefully designed to leverage pre-trained models while adding minimal trainable parameters. The **vision encoder** is a frozen CLIP ViT-L/14 model that processes each image independently to produce a sequence of patch embeddings. For a  $224 \times 224$  image with patch size 14, this yields 256 patch tokens of dimension 1024. The vision encoder's 304M parameters remain frozen throughout training, preserving the strong visual representations learned during CLIP pre-training.

The **language model** is a frozen Chinchilla 70B model, a large autoregressive transformer trained on text-only data. Chinchilla uses 70 billion parameters across 80 layers with hidden dimension 8192 and 64 attention heads. Keeping this massive language model frozen is crucial for computational tractability—training 70B parameters would require prohibitive memory and compute. Instead, Flamingo inserts new trainable layers that allow the frozen language model to attend to visual information without modifying its core text processing capabilities.

The key innovation is the **Perceiver Resampler**, a learned module that compresses the variable-length sequence of image patch embeddings into a fixed number of visual tokens that can be efficiently processed by the language model. The Perceiver Resampler uses cross-attention where a fixed set of learned queries  $\mathbf{Q} \in \mathbb{R}^{64 \times 2048}$  (64 visual tokens, dimension 2048) attends to the image patch embeddings  $\mathbf{K}, \mathbf{V} \in \mathbb{R}^{256 \times 1024}$  from the vision encoder. This produces a fixed-size representation regardless of input image resolution or the number of images in the sequence. The Perceiver Resampler contains approximately 1.4B parameters (6 layers of cross-attention and feed-forward networks with dimension 2048), making it the primary trainable component of Flamingo.

Between every few layers of the frozen language model, Flamingo inserts new **cross-attention layers** that allow text tokens to attend to the visual tokens produced by the Perceiver Resampler. Specifically, for Flamingo-80B (built on Chinchilla-70B), cross-attention layers are inserted after every 7th transformer layer, resulting in approximately 11 cross-attention insertions across the 80 layers. Each cross-attention layer adds roughly 134M parameters (for dimension 8192), totaling about 1.5B parameters for all insertions. Combined with the Perceiver Resampler, Flamingo adds approximately 2.9B trainable parameters to the 70B frozen base model, representing just 4% additional parameters while enabling full multimodal capabilities.

The memory requirements for Flamingo are dominated by the frozen language model. Storing 70B parameters in FP16 requires 140 GB, which exceeds the memory of any single GPU. Flamingo uses model parallelism to partition the language model across multiple GPUs—for example, distributing across 8 A100 GPUs (80GB each) places roughly 8.75B parameters per GPU, consuming about 17.5 GB for parameters. Activations for a sequence of 2048 tokens (including both text and visual tokens) across 80 layers with dimension 8192 require approximately  $2048 \times 80 \times 8192 \times 2 = 2.6$  GB per example in FP16. With batch size 8, activations consume 21 GB per GPU, leaving sufficient memory for gradients of the trainable parameters ( $2.9\text{B parameters} \times 2 \text{ bytes} \times 2 \text{ for gradients} = 11.6 \text{ GB}$ ) and optimizer states (23.2 GB for Adam).

Training Flamingo on a mixture of image-text pairs, interleaved image-text documents, and video-text pairs requires substantial computational resources. The training dataset consists of 2.3 billion

image-text pairs (similar to CLIP), 43 million interleaved image-text web pages, and 27 million video clips. Training Flamingo-80B for 1 epoch through this data with batch size 256 distributed across 256 A100 GPUs takes approximately 15 days, representing roughly 92,000 GPU-hours. The estimated training cost exceeds \$300,000 in cloud compute. However, the key advantage is that only 2.9B parameters are trained while leveraging the capabilities of a 70B language model, making training far more efficient than training a 70B multimodal model from scratch.

For inference, Flamingo’s few-shot learning capability means that users can provide 2-32 example image-text pairs in the prompt to demonstrate a new task, and the model adapts its predictions based on these examples without any fine-tuning. This in-context learning works because the cross-attention mechanism allows the model to attend to the example images when processing the query image. The computational cost of inference scales linearly with the number of examples in the context: each additional image adds 256 patch tokens (after vision encoding) compressed to 64 visual tokens (after Perceiver Resampler), increasing the sequence length and thus the attention cost. For a prompt with 4 example images and 1 query image (5 images total), the visual tokens contribute  $5 \times 64 = 320$  tokens to the sequence, which combined with text tokens (typically 500-1000) results in sequences of 800-1300 tokens. On a single A100 GPU, Flamingo-80B can process approximately 2-3 such sequences per second, limited primarily by the memory bandwidth required to load the 70B parameter model.

## 18.5 Computational Analysis of Multimodal Transformers

Multimodal transformers follow the same FLOPs formulas derived in Chapter 12 for their individual encoders: each transformer layer costs  $24Bnd_{\text{model}}^2 + 4Bn^2d_{\text{model}}$  FLOPs (attention plus feed-forward). The multimodal-specific addition is cross-modal attention, which costs  $4mnd$  FLOPs per layer (where  $m$  and  $n$  are the sequence lengths of the two modalities). In practice, cross-modal attention is a small fraction of total cost—for BLIP with 128 text tokens and 196 image patches, cross-attention adds only 462 MFLOPs across 6 layers, negligible compared to the self-attention costs in each encoder.

The key computational asymmetry in multimodal models is between modalities: image encoding typically dominates. CLIP’s ViT-L/14 requires  $\sim 55$  GFLOPs per image versus  $\sim 5.5$  GFLOPs per text, a  $10\times$  ratio. When a large language model serves as the text backbone (as in Flamingo with Chinchilla-70B), text processing dominates instead, requiring  $\sim 110$  TFLOPs per sequence.

Memory requirements follow the same principles as unimodal transformers (Chapter 12): parameters, gradients, optimizer states, and activations. The multimodal-specific concern is storing activations for both modalities simultaneously. For CLIP ViT-L/14, image activations consume  $\sim 75$  MB per image in FP16 while text activations require  $\sim 1.4$  MB per text. For large batch sizes (32,768 in CLIP), this necessitates distributed training with gradient checkpointing and mixed precision (see Chapter 11 for distributed training techniques).

## 18.6 Training Challenges for Multimodal Transformers

### 18.6.1 Batch Size Requirements for Contrastive Learning

Contrastive learning methods like CLIP require very large batch sizes to provide sufficient negative examples. CLIP’s performance scales log-linearly with batch size: increasing from 256 to 32,768 improves ImageNet zero-shot accuracy from  $\sim 58\%$  to  $76\%$ . However, the  $32,768 \times 32,768$  similarity matrix alone requires 4.3 GB in FP32. To make this tractable, CLIP distributes the batch across 256 GPUs using all-gather communication, so the full similarity matrix is never materialized on any single GPU.

### 18.6.2 Distributed Training and Memory Optimization

Multimodal transformers use the same distributed training techniques as unimodal models (see Chapter 11 for detailed coverage): data parallelism for CLIP-scale models that fit on a single GPU, tensor and pipeline parallelism for larger models like Flamingo-80B where the 70B parameter language model must be partitioned across multiple GPUs. Memory optimization techniques—gradient checkpointing,

mixed precision training, and ZeRO optimizer state partitioning—are essential and apply identically to the multimodal setting.

The multimodal-specific challenge is the asymmetric memory profile: image activations ( $\sim 75$  MB per image for ViT-L) far exceed text activations ( $\sim 1.4$  MB per text for CLIP’s encoder), so image encoding dominates the memory budget during training. For Flamingo-80B, the frozen 70B language model requires 140 GB in FP16, necessitating model parallelism across at least 2 A100 GPUs before accounting for activations or trainable parameters.

## 18.7 Audio Transformers

### 18.7.1 Whisper: Speech Recognition

**Definition 18.3** (Whisper Architecture). Encoder-decoder transformer for speech:

**Input:** Audio waveform  $\rightarrow$  Log-mel spectrogram

**Encoder:**

- Input: Spectrogram (80 mel bins)
- Convolution layers (downsample)
- Transformer encoder layers

**Decoder:**

- Autoregressive text generation
- Special tokens for language, task, timestamps

**Training data:** 680,000 hours of multilingual audio

**Tasks supported:**

- Speech recognition (transcription)
- Translation (to English)
- Language identification
- Voice activity detection
- Timestamp prediction

**Example 18.3** (Whisper Input Format). **Special tokens:**

`<|startoftranscript|><|en|><|transcribe|><|notimestamps|>`

**Spectrogram:**

- 80 mel bins
- 3000 frames (30 seconds audio at 100 Hz)
- Input:  $3000 \times 80$

**Encoder:**

- Conv layers:  $3000 \times 80 \rightarrow 1500 \times 768$

- Transformer: Process 1500 tokens

**Decoder:** Generate text tokens autoregressively

### 18.7.2 Audio-Text Pre-training

**Contrastive learning:** Like CLIP but audio-text

**AudioCLIP:** Tri-modal (image, text, audio)

**Applications:**

- Zero-shot audio classification
- Audio captioning
- Text-to-audio generation

## 18.8 Unified Multimodal Models

### 18.8.1 Perceiver and Perceiver IO

**Key idea:** Map arbitrary modalities to latent space via cross-attention

**Definition 18.4 (Perceiver). Components:**

1. **Latent array:** Fixed set of learned queries  $\mathbf{Z} \in \mathbb{R}^{M \times d}$
2. **Cross-attention:** Latents attend to inputs

$$\mathbf{Z}_1 = \text{CrossAttn}(\mathbf{Q} = \mathbf{Z}, \mathbf{K} = \mathbf{X}, \mathbf{V} = \mathbf{X}) \quad (18.10)$$

3. **Transformer:** Process latents

$$\mathbf{Z}_L = \text{Transformer}(\mathbf{Z}_1) \quad (18.11)$$

4. **Output:** Decode latents to task outputs

**Benefits:**

- Handles arbitrary input sizes
- Computation independent of input size (fixed latents)
- Unified architecture for images, video, audio, text

### 18.8.2 GPT-4V and LLaVA

**GPT-4V (Vision):** GPT-4 with vision capabilities

- Interleaved image and text inputs
- Strong vision-language understanding
- Details not fully disclosed

**LLaVA (Open-source):**

- CLIP vision encoder
- LLaMA language model
- Linear projection to align embeddings
- Instruction tuning on visual conversations



## 18.9 Exercises

**Exercise 18.1.** Implement CLIP contrastive loss for batch size 8:

1. Generate random image embeddings (8, 512)
2. Generate random text embeddings (8, 512)
3. Compute  $8 \times 8$  similarity matrix
4. Calculate contrastive loss with  $\tau = 0.07$

**Exercise 18.2.** Use CLIP for zero-shot classification on CIFAR-10:

1. Load pre-trained CLIP model
2. Create text prompts for 10 classes
3. Encode images and prompts
4. Compute accuracy
5. Compare to supervised baseline

**Exercise 18.3.** Analyze Whisper architecture:

1. Calculate parameters for encoder (24 layers,  $d = 1024$ )
2. Calculate parameters for decoder (24 layers)
3. Estimate memory for 30-second audio
4. Compare to text-only GPT-2

**Exercise 18.4.** Design multimodal fusion strategy for video understanding (visual + audio + captions):

1. Propose architecture
2. Define fusion mechanism
3. Specify training objective
4. Estimate parameter count

## 18.10 Solutions

Full solutions for all exercises are available at <https://deeplearning.hofkensvermeulen.be>.

# Chapter 19

## Long Context Transformers

### Chapter Overview

Extending transformer context length beyond standard limits (512-2048 tokens) enables processing long documents, books, and extended conversations. This chapter covers techniques for scaling to 32K, 100K, and even 1M+ token contexts.

### Learning Objectives

1. Understand context length limitations and bottlenecks
2. Implement position interpolation and extrapolation
3. Apply memory-augmented transformers
4. Use retrieval-augmented generation (RAG)
5. Implement recurrent transformers (Transformer-XL)
6. Compare long-context methods and trade-offs

### 19.1 Context Length Limitations

#### 19.1.1 The Quadratic Memory Bottleneck

Standard transformer architectures face fundamental limitations when processing long sequences due to the quadratic scaling of self-attention with respect to sequence length. The self-attention mechanism computes pairwise interactions between all tokens in a sequence, requiring the materialization of an attention matrix of size  $n \times n$  where  $n$  is the sequence length. This quadratic scaling manifests in three critical bottlenecks: computational complexity, memory consumption, and position encoding limitations. Understanding these bottlenecks quantitatively is essential for appreciating why long context processing requires specialized techniques and architectural modifications.

The computational complexity of self-attention is  $O(n^2d)$  where  $d$  is the model dimension. For each of the  $n$  queries, the model computes attention scores with all  $n$  keys through dot products of dimension  $d$ , requiring  $n^2d$  multiply-accumulate operations. The subsequent softmax normalization adds  $O(n^2)$  operations, and the weighted sum over values requires another  $n^2d$  operations. While the feed-forward network has complexity  $O(nd^2)$ , for long sequences where  $n > d$ , the attention computation dominates. For example, with  $n = 16384$  tokens and  $d = 768$ , attention requires approximately 206 billion FLOPs per layer while the feed-forward network requires only 19 billion FLOPs, making attention the primary computational bottleneck.

The memory bottleneck is even more severe than the computational one. During the forward pass, the attention matrix must be fully materialized in memory before applying softmax, requiring  $n^2$  memory locations per attention head. During the backward pass for training, these attention matrices must be stored for gradient computation, effectively doubling the memory requirement. For multi-head

attention with  $h$  heads, the total memory for attention matrices is  $h \times n^2$  floating-point values per layer. In FP32 format, each value requires 4 bytes, while FP16 requires 2 bytes. This memory grows quadratically with sequence length, quickly exceeding available GPU memory for long sequences.

**Example 19.1** (Memory Scaling Analysis). Consider a GPT-2 scale model with  $d = 768$ ,  $h = 12$  attention heads, and  $L = 12$  layers. The memory required for attention matrices scales dramatically with sequence length. For a single attention head processing a sequence of length  $n$ , the attention matrix requires  $n^2 \times 4$  bytes in FP32 format. With 12 heads per layer, this becomes  $12 \times n^2 \times 4 = 48n^2$  bytes per layer.

At  $n = 1024$  tokens (GPT-2's standard context), each layer requires  $48 \times 1024^2 = 50.3$  MB for attention matrices. Across 12 layers, this totals 604 MB, which is manageable on modern GPUs. However, doubling the sequence length to  $n = 2048$  quadruples the memory requirement to 201 MB per layer or 2.4 GB total—a  $4\times$  increase for only a  $2\times$  increase in sequence length. This quadratic scaling continues: at  $n = 4096$ , attention matrices consume 805 MB per layer or 9.7 GB total, nearly filling a 16 GB GPU. At  $n = 8192$ , the requirement explodes to 3.2 GB per layer or 38.5 GB total, exceeding even high-end GPUs like the NVIDIA A100 with 40 GB memory.

For larger models, the situation becomes even more challenging. Consider a GPT-3 scale model with  $d = 12288$ ,  $h = 96$  heads, and  $L = 96$  layers. At  $n = 2048$  tokens, each layer requires  $96 \times 2048^2 \times 4 = 1.6$  GB for attention matrices, totaling 154 GB across all layers. At  $n = 8192$  tokens, each layer requires 25.8 GB, totaling 2.5 TB across the model—far exceeding any single GPU's capacity and requiring extensive model parallelism even for moderate context lengths. At  $n = 32768$  tokens, a single layer would require 412 GB just for attention matrices, making standard attention completely impractical without fundamental algorithmic changes.

These calculations assume only the forward pass attention matrices. During training, gradients with respect to attention matrices must also be stored, effectively doubling the memory requirement. Additionally, activations from other layers, model parameters, optimizer states, and batch processing multiply these requirements further. For a batch size of 8 with  $n = 4096$  tokens on GPT-2, attention matrices alone would require  $9.7 \times 8 = 77.6$  GB, making training impossible on standard hardware without techniques like gradient checkpointing, which trades computation for memory by recomputing activations during the backward pass.

The third fundamental limitation involves position encodings. Standard transformers use position encodings trained on sequences of a fixed maximum length, typically 512 to 2048 tokens. When these models encounter sequences longer than their training length, the position encodings must extrapolate to unseen positions. Absolute position embeddings, which assign a learned vector to each position index, cannot extrapolate at all—positions beyond the training length have no corresponding embedding. Even sinusoidal position encodings, which use deterministic trigonometric functions, exhibit degraded performance when extrapolating beyond training lengths due to the model's learned attention patterns being calibrated to the training distribution of position encodings.

This extrapolation failure manifests as rapidly degrading perplexity for tokens beyond the training context length. A model trained on 2048-token sequences might achieve perplexity of 15 on positions 0-2048, but perplexity can increase to 25 or higher for positions 2048-4096 without specialized position encoding schemes. This degradation occurs because the model's attention patterns have learned to interpret specific position encoding values as corresponding to specific relative distances, and these learned patterns break down when position encodings take on values outside the training distribution.

## 19.2 Position Encoding for Long Context

### 19.2.1 The Extrapolation Challenge

Position encodings enable transformers to incorporate sequential order information into their otherwise permutation-invariant architecture. However, different position encoding schemes exhibit dramatically

different behaviors when processing sequences longer than those seen during training. This extrapolation capability is critical for long context applications, where retraining on maximum-length sequences is often computationally prohibitive. The choice of position encoding scheme can determine whether a model trained on 2048-token sequences can successfully process 8192-token sequences with minimal fine-tuning, or whether it requires extensive retraining from scratch.

Absolute position embeddings assign a learned vector to each position index, with the position encoding for position  $i$  being a trainable parameter  $\mathbf{p}_i \in \mathbb{R}^d$ . These embeddings are added to token embeddings before the first transformer layer. While simple and effective within the training length, absolute embeddings cannot extrapolate beyond the maximum training position. A model trained with positions 0 through 2047 has no learned embedding for position 2048 or beyond. Attempting to extend such a model requires either initializing new position embeddings (which perform poorly without extensive fine-tuning) or using position interpolation techniques to map longer sequences into the trained position range.

Sinusoidal position encodings, introduced in the original Transformer paper, use deterministic trigonometric functions rather than learned parameters. For position  $i$  and dimension  $j$ , the encoding is defined as:

$$\text{PE}(i, 2j) = \sin(i/10000^{2j/d}), \quad \text{PE}(i, 2j + 1) = \cos(i/10000^{2j/d}) \quad (19.1)$$

These encodings can be computed for any position without training, enabling extrapolation in principle. However, in practice, models trained with sinusoidal encodings still exhibit degraded performance on longer sequences because the attention patterns learned during training are calibrated to the distribution of position encodings seen during training. When positions extend beyond the training range, the attention patterns encounter position encoding values in unfamiliar ranges, leading to suboptimal attention distributions.

### 19.2.2 Position Interpolation

Position interpolation addresses the extrapolation problem by mapping longer sequences into the position range seen during training, rather than extending beyond it. Instead of asking the model to extrapolate to unseen position indices, interpolation compresses the position indices of a long sequence into the trained range, effectively treating the long sequence as a "compressed" version of a training-length sequence.

**Definition 19.1** (Position Interpolation). To extend a model trained on maximum length  $L$  to process sequences of length  $L' > L$ , position interpolation maps each position  $i \in \{0, 1, \dots, L' - 1\}$  to a fractional position in the training range:

$$i_{\text{interpolated}} = i \cdot \frac{L}{L'} \quad (19.2)$$

For absolute position embeddings, the new position encoding is computed by interpolating between the learned embeddings:

$$\text{PE}_{\text{new}}(i) = \text{interpolate}(\text{PE}_{\text{original}}, i \cdot L/L') \quad (19.3)$$

For sinusoidal or rotary encodings, the interpolated position is used directly in the encoding formula, effectively reducing the frequency of the trigonometric functions.

The key insight behind position interpolation is that it keeps position encodings within the distribution seen during training, avoiding the extrapolation problem entirely. For example, extending from  $L = 2048$  to  $L' = 8192$  maps position 8191 to interpolated position  $8191 \times 2048/8192 = 2047.75$ , which falls within the training range. The model's attention patterns, having been trained on positions 0 through 2047, can handle this interpolated position much more effectively than they could handle the raw position 8191.

Position interpolation has been successfully applied to extend LLaMA models from 2048 to 8192 tokens and beyond. The technique requires minimal fine-tuning—typically only 1000 to 10000 training steps on long sequences—compared to training from scratch. After fine-tuning with position interpolation, LLaMA 2 models maintain perplexity within 5-10% of their original performance when extended from 4096 to 32768 tokens, whereas naive extrapolation without interpolation results in perplexity degradation of 50% or more.

The computational cost of position interpolation is negligible, as it only affects the position encoding computation, not the attention mechanism itself. The primary cost is the fine-tuning required to adapt the model to the compressed position space. However, this fine-tuning is far less expensive than training from scratch: extending a 7B parameter model from 4K to 32K context requires approximately 100 GPU-hours of fine-tuning compared to 100,000+ GPU-hours for full pretraining.

### 19.2.3 Rotary Position Embedding (RoPE)

Rotary Position Embedding represents a fundamental advance in position encoding design, achieving excellent extrapolation properties by encoding relative position information directly into the attention computation through rotation operations. RoPE has become the position encoding of choice for modern large language models including GPT-NeoX, LLaMA, PaLM, and many others due to its combination of strong extrapolation, computational efficiency, and theoretical elegance.

**Definition 19.2** (Rotary Position Embedding). RoPE applies position-dependent rotations to query and key vectors before computing attention. For a query vector  $\mathbf{q}_m$  at position  $m$  and key vector  $\mathbf{k}_n$  at position  $n$ , RoPE applies rotation matrices:

$$\mathbf{q}'_m = \mathbf{R}_m \mathbf{q}_m \quad (19.4)$$

$$\mathbf{k}'_n = \mathbf{R}_n \mathbf{k}_n \quad (19.5)$$

where  $\mathbf{R}_m \in \mathbb{R}^{d \times d}$  is a block-diagonal rotation matrix. For dimension pairs  $(2j, 2j + 1)$ , the rotation is:

$$\mathbf{R}_m^{(j)} = \begin{bmatrix} \cos(m\theta_j) & -\sin(m\theta_j) \\ \sin(m\theta_j) & \cos(m\theta_j) \end{bmatrix}, \quad \theta_j = 10000^{-2j/d} \quad (19.6)$$

The full rotation matrix is block-diagonal with  $d/2$  such 2D rotation blocks.

The crucial property of RoPE is that the attention score between positions  $m$  and  $n$  depends only on their relative distance  $m - n$ , not their absolute positions. This can be verified through the rotation addition formula:

$$(\mathbf{q}'_m)^\top \mathbf{k}'_n = (\mathbf{R}_m \mathbf{q}_m)^\top (\mathbf{R}_n \mathbf{k}_n) = \mathbf{q}_m^\top \mathbf{R}_m^\top \mathbf{R}_n \mathbf{k}_n = \mathbf{q}_m^\top \mathbf{R}_{n-m} \mathbf{k}_n \quad (19.7)$$

This relative position property means that the model learns attention patterns based on relative distances between tokens rather than absolute positions. When extrapolating to longer sequences, the model encounters the same relative distances it saw during training, just in different combinations. A model trained on sequences up to 2048 tokens has seen all relative distances from -2047 to +2047. When processing a 4096-token sequence, it encounters the same relative distances, enabling much better extrapolation than absolute position encodings.

RoPE's extrapolation capability can be further enhanced through position interpolation. By scaling the rotation frequencies  $\theta_j$  by a factor  $L'/L$  when extending from length  $L$  to  $L'$ , the effective relative distances are compressed into the training range. This combination of RoPE's inherent relative position encoding with position interpolation enables extensions from 2048 to 32768 tokens or beyond with minimal quality degradation.

The computational overhead of RoPE is minimal compared to the attention computation itself. Applying rotations to queries and keys requires  $O(nd)$  operations, which is negligible compared to the  $O(n^2d)$  cost of attention. The rotation operations can be efficiently implemented using vectorized

operations on modern GPUs, adding less than 5% to the total attention computation time. Memory overhead is also minimal, as the rotation matrices are block-diagonal and can be computed on-the-fly rather than stored.

In practice, RoPE has enabled dramatic context length extensions. LLaMA models using RoPE have been successfully extended from 2048 to 32768 tokens through position interpolation with only 1000 fine-tuning steps. The perplexity degradation is typically less than 10% even at  $16\times$  the training length, compared to 50-100% degradation for absolute position embeddings. This extrapolation capability has made RoPE the de facto standard for new large language models designed for long context applications.

#### 19.2.4 ALiBi: Attention with Linear Biases

ALiBi (Attention with Linear Biases) takes a radically different approach to position encoding by eliminating position embeddings entirely and instead adding position-dependent biases directly to attention scores. This simple modification achieves remarkable extrapolation properties, enabling models trained on 1024-token sequences to process 10,000+ token sequences at inference time with no fine-tuning whatsoever.

**Definition 19.3** (ALiBi). ALiBi adds a bias term to attention scores based on the distance between query and key positions:

$$\text{score}(q_i, k_j) = \frac{\mathbf{q}_i^\top \mathbf{k}_j}{\sqrt{d_k}} - m \cdot |i - j| \quad (19.8)$$

where  $m > 0$  is a head-specific slope parameter that differs across attention heads. The bias  $-m \cdot |i - j|$  penalizes attention to distant tokens, with the penalty increasing linearly with distance.

The head-specific slopes are set geometrically: for  $h$  attention heads, the slopes are  $m_1, m_2, \dots, m_h$  where  $m_i = 2^{-8i/h}$ . For example, with 8 heads, the slopes are  $2^{-1}, 2^{-2}, \dots, 2^{-8}$ , giving values from 0.5 to 0.0039. This geometric spacing ensures that different heads have different receptive field sizes: heads with large slopes focus on nearby tokens, while heads with small slopes can attend to distant tokens with less penalty.

ALiBi's extrapolation capability stems from its use of relative distances rather than absolute positions, combined with the linear form of the bias. During training on sequences up to length  $L$ , the model encounters biases ranging from 0 (attending to the same position) to  $-m \cdot L$  (attending to the most distant position). When extrapolating to length  $L' > L$ , the model encounters biases up to  $-m \cdot L'$ , which are simply larger values along the same linear scale. The attention patterns learned during training—which balance content-based attention (from  $\mathbf{q}_i^\top \mathbf{k}_j$ ) against distance-based penalties (from  $-m \cdot |i - j|$ )—continue to work effectively at these larger distances.

Empirical results demonstrate ALiBi's exceptional extrapolation. Models trained on 1024-token sequences with ALiBi can process 2048-token sequences with less than 5% perplexity increase, 4096-token sequences with 10-15% increase, and even 10,000-token sequences with 20-30% increase—all without any fine-tuning. In contrast, the same models with sinusoidal position encodings show 50% perplexity increase at 2048 tokens and become essentially non-functional beyond 4096 tokens. This zero-shot extrapolation capability makes ALiBi particularly attractive for applications where the maximum sequence length is unknown at training time or varies widely across use cases.

ALiBi has been adopted by several prominent models including BLOOM (176B parameters) and MPT (7B-30B parameters). BLOOM was trained with ALiBi on sequences up to 2048 tokens but can effectively process sequences of 4096 tokens or longer at inference time. MPT models trained with ALiBi on 2048-token sequences have been successfully deployed on tasks requiring 8192-token contexts with minimal quality degradation.

The computational overhead of ALiBi is negligible. Computing the bias  $-m \cdot |i - j|$  for all  $n^2$  attention scores requires  $O(n^2)$  operations, which is dominated by the  $O(n^2d)$  cost of computing  $\mathbf{QK}^\top$ . The bias can be precomputed once per sequence and reused across all layers and heads (with different

slopes  $m$ ), further reducing overhead. Memory overhead is also minimal, as the bias matrix can be computed on-the-fly or stored once and reused.

The primary limitation of ALiBi is that it assumes a monotonic relationship between distance and relevance—more distant tokens are always penalized more heavily. This assumption holds well for many natural language tasks where local context is indeed more important than distant context. However, for tasks with long-range dependencies that are not distance-dependent (such as matching opening and closing brackets in code, or resolving coreferences across document sections), ALiBi’s linear bias may be suboptimal compared to learned position encodings that can capture more complex position-dependent patterns.

## 19.3 Efficient Attention for Long Context

### 19.3.1 Sparse Attention Patterns

While position encoding improvements enable better extrapolation, they do not address the fundamental quadratic scaling of attention computation and memory. Efficient attention mechanisms reduce this quadratic bottleneck by restricting which tokens can attend to which other tokens, computing attention only over a subset of the  $n^2$  possible connections. These sparse attention patterns can reduce complexity from  $O(n^2)$  to  $O(n \times w)$  where  $w$  is a fixed window size, enabling processing of sequences that would be impossible with full attention.

The key insight behind sparse attention is that not all token pairs require attention computation. In many domains, particularly natural language, most relevant information comes from nearby tokens, with occasional long-range dependencies. By carefully designing sparsity patterns that preserve important connections while eliminating redundant ones, sparse attention can maintain model quality while dramatically reducing computational and memory requirements.

### 19.3.2 Longformer and BigBird

Longformer combines local windowed attention ( $O(nw)$  for window size  $w$ ) with global attention on task-specific tokens, enabling efficient processing of documents up to 4096+ tokens. BigBird extends this with random connections that create small-world shortcuts, proving that sparse attention with  $O(n \log n)$  connections is a universal approximator for sequence-to-sequence functions. Both reduce attention memory by 6–8 $\times$  compared to full attention. See Chapter 16 for the detailed mechanism definitions, complexity analysis, and benchmark results.

In the context of long-context processing, the key trade-off is between sparsity pattern and information propagation depth. With window size  $w$ , information requires  $\lceil n/w \rceil$  layers to propagate across the full sequence. BigBird’s random connections reduce the expected propagation path to  $O(\log n)$  layers, which is particularly valuable for tasks requiring long-range reasoning. For sequences up to 2048 tokens, optimized full attention (e.g., Flash Attention) is typically faster; for 2048–8192 tokens, sparse attention becomes beneficial; beyond 8192 tokens, it becomes essential.

### 19.3.3 Comparison of Sparse Attention Methods

Different sparse attention patterns offer different trade-offs between efficiency, model quality, and implementation complexity. Local attention with window size  $w$  provides the simplest pattern and best memory locality, achieving  $O(nw)$  complexity with straightforward implementation. However, information propagation is limited to  $w$  positions per layer, requiring deep networks for long-range dependencies. Longformer’s addition of global tokens addresses this limitation by providing information hubs, enabling faster propagation while maintaining linear complexity. BigBird’s random connections provide theoretical guarantees and empirically strong performance, but at the cost of irregular memory access patterns that reduce hardware efficiency.

For sequences up to 2048 tokens, the overhead of sparse attention often outweighs its benefits—full attention with optimized implementations like Flash Attention is typically faster and simpler. For sequences of 2048–8192 tokens, sparse attention becomes beneficial, with Longformer and BigBird providing good trade-offs between efficiency and quality. For sequences beyond 8192 tokens, sparse

attention becomes essential, as full attention exceeds available memory on most hardware. At these lengths, the choice between Longformer and BigBird depends on the task: Longformer is simpler and faster for tasks where local context dominates, while BigBird provides better quality for tasks requiring complex long-range reasoning.

## 19.4 Recurrent Transformers

### 19.4.1 Transformer-XL

**Definition 19.4** (Transformer-XL). Segment long sequence, reuse representations from previous segments:

**Segment  $n$ :** Tokens  $[s_n, s_n + 1, \dots, s_n + L - 1]$

**Compute:**

$$\mathbf{h}_n = \text{Transformer}([\text{stop\_grad}(\mathbf{h}_{n-1}), \mathbf{x}_n]) \quad (19.9)$$

Previous segment hidden states provide additional context without recomputation!

**Example 19.2** (Transformer-XL Processing). Segment length:  $L = 512$

**Segment 1:** Process tokens 0-511

- Save hidden states  $\mathbf{h}_1$

**Segment 2:** Process tokens 512-1023

- Concatenate with  $\mathbf{h}_1$  (frozen)
- Effective context:  $512 + 512 = 1024$  tokens
- Computation: Still  $O(512^2)$  per segment

**Segment 3:** Process tokens 1024-1535

- Use  $\mathbf{h}_2$  from previous segment
- Effective context:  $1024 + 512 = 1536$  tokens

Context grows linearly with segments, computation stays constant!

**Relative position encodings:** Modified for segment-level recurrence

## 19.5 Retrieval-Augmented Generation

### 19.5.1 RAG Architecture

**Definition 19.5** (Retrieval-Augmented Generation). Combine retrieval with generation:

**Step 1: Retrieval**

$$\text{docs} = \text{Retrieve}(\text{query}, \text{corpus}, k = 5) \quad (19.10)$$

**Step 2: Concatenate**

$$\text{input} = [\text{docs}_1, \dots, \text{docs}_k, \text{query}] \quad (19.11)$$

**Step 3: Generate**

$$\text{output} = \text{LM}(\text{input}) \quad (19.12)$$



**Retrieval methods:**

- BM25 (sparse)
- Dense retrieval (BERT embeddings + nearest neighbors)
- Hybrid (combine sparse and dense)

**Example 19.3** (RAG for Question Answering). **Question:** "When was the Eiffel Tower built?"

**Step 1: Retrieve** (from Wikipedia)

1. "The Eiffel Tower was constructed from 1887 to 1889..."
2. "Gustave Eiffel designed the tower for the 1889 World's Fair..."
3. "The tower is 330 meters tall and was the tallest..."

**Step 2: Concatenate**

Context 1: The Eiffel Tower was constructed from 1887 to 1889...

Context 2: Gustave Eiffel designed the tower for the 1889 World's Fair...

Context 3: The tower is 330 meters tall and was the tallest...

Question: When was the Eiffel Tower built?

Answer:

**Step 3: Generate** "The Eiffel Tower was built from 1887 to 1889."

**Advantages:**

- Access to external knowledge
- No need to fit everything in context window
- Cite sources
- Update knowledge without retraining

### 19.5.2 RETRO: Retrieval-Enhanced Transformer

**Architecture:**

- Chunk input into segments (64 tokens)
- Retrieve neighbors for each chunk
- Cross-attend to retrieved chunks
- Chunked cross-attention layers

**Performance:** 25× fewer parameters with retrieval achieves same performance as larger model without retrieval!

## 19.6 Memory-Augmented Transformers

### 19.6.1 Compressive Transformer

**Definition 19.6** (Compressive Transformer). Extend Transformer-XL with compression:

**Three levels of memory:**

1. **Active:** Current segment (full attention)
2. **Recent:** Last  $n_m$  segments (cached, full precision)
3. **Compressed:** Older segments (compressed representations)

**Compression:**

- Learned compression function
- Reduce  $n$  tokens to  $n/c$  (e.g.,  $c = 3$ )
- Compression ratio balances memory vs information

**Effective context:** Active + Recent + Compressed

$$L_{\text{eff}} = L + n_m \cdot L + n_c \cdot (L/c) \quad (19.13)$$

## 19.6.2 Memorizing Transformers

**Key innovation:**  $k$ -NN attention over entire history

**Architecture:**

- Store all past (*key*, *value*) pairs in memory
- For each query, retrieve  $k$  nearest neighbors
- Attend to local context + retrieved keys/values

**Benefits:**

- Effectively infinite context (limited by storage)
- Constant-time attention (with approximate  $k$ -NN)
- Improves perplexity on long documents

## 19.7 Long Context Models in Practice

### 19.7.1 LongT5: Efficient Encoder-Decoder

LongT5 extends the T5 encoder-decoder architecture to handle sequences up to 16,384 tokens by applying efficient attention mechanisms to both the encoder and decoder. Unlike decoder-only models that process sequences autoregressively, encoder-decoder models must handle long sequences in both components, making efficiency doubly important. LongT5 demonstrates that sparse attention patterns can be successfully applied to encoder-decoder architectures while maintaining the strong performance of the original T5 model.

LongT5 uses a combination of local and global attention patterns similar to Longformer, but adapted for the encoder-decoder structure. The encoder uses local attention with window size  $w = 512$  for all tokens, plus global attention for a small number of designated tokens. The decoder uses local attention for attending to its own previous tokens, plus full attention to encoder outputs (which are compressed through the local attention mechanism). This asymmetric design recognizes that decoder-to-encoder attention is typically less memory-intensive than encoder self-attention, as decoder sequences are usually shorter than encoder sequences.

The memory savings from LongT5's sparse attention are substantial. For an encoder sequence of length  $n_e = 16384$  and decoder sequence of length  $n_d = 512$ , full attention would require approximately  $(16384^2 + 512^2 + 512 \times 16384) \times 4 = 1.1$  GB per attention head in FP32 for encoder self-attention, decoder self-attention, and cross-attention combined. With LongT5's sparse patterns using  $w = 512$ , the requirement reduces to approximately  $(16384 \times 1024 + 512^2 + 512 \times 16384) \times 4 = 71$  MB per head,

a  $15\times$  reduction. With 12 heads and 12 encoder layers plus 12 decoder layers, total attention memory decreases from 26 GB to 1.7 GB.

LongT5 has been successfully applied to long-document summarization tasks where input documents exceed 10,000 tokens. On the arXiv summarization dataset with papers averaging 6000 tokens, LongT5 achieves ROUGE-L scores of 48.3 compared to 44.1 for T5 with truncated 512-token inputs, demonstrating that access to full document context significantly improves summary quality. On the PubMed summarization task with medical papers averaging 3000 tokens, LongT5 outperforms T5 by 3-4 ROUGE points across all metrics.

### 19.7.2 Production Long Context Systems

As of early 2025, production language models support context lengths of 128K–1M+ tokens, enabling processing of entire codebases, books, and extended conversations.<sup>1</sup> These systems combine the techniques covered in this chapter—efficient attention, position interpolation, and memory-efficient implementations—to make long-context processing practical. The fact that such contexts are served at interactive latencies indicates the use of multiple optimizations simultaneously: sparse or approximate attention to reduce the quadratic bottleneck, Flash Attention for memory efficiency, and model parallelism across multiple GPUs.

### 19.7.3 Practical Considerations for Long Context

Deploying long context models in production requires careful consideration of when the additional context is actually beneficial versus when alternative approaches might be more effective. Long context processing incurs real costs in terms of latency, computational resources, and financial expense, so understanding when these costs are justified is essential for practical applications.

Long context is most valuable when the task requires reasoning over or synthesizing information from multiple parts of a long document. Document summarization benefits significantly from full document access, as important information may appear anywhere in the document. Question answering over long documents similarly benefits from long context, as the relevant information’s location is unknown in advance. Code generation and analysis tasks benefit from seeing entire files or multiple related files in context, enabling the model to understand dependencies and maintain consistency.

However, many tasks that initially seem to require long context can be effectively addressed with shorter contexts and retrieval. For question answering over large document collections, retrieval-augmented generation (RAG) can retrieve only the relevant passages and provide them in a short context, achieving similar or better performance at much lower cost. For tasks requiring access to factual knowledge, retrieval from a knowledge base is often more reliable and efficient than encoding all knowledge in the context. For multi-turn conversations, summarizing or compressing earlier conversation history can maintain coherence while reducing context length.

The cost-benefit analysis depends on several factors. Latency requirements matter: long context processing takes longer, which may be unacceptable for interactive applications. Accuracy requirements matter: if the task requires very high accuracy and the model performs significantly better with full context, the additional cost may be justified. Update frequency matters: if the information changes frequently, retrieval from an updated database may be preferable to encoding static information in context. Scale matters: for high-volume applications, the per-request cost of long context processing multiplies, potentially making alternative approaches more economical.

A practical strategy is to use a hybrid approach: employ retrieval or summarization to reduce context length when possible, but fall back to full long context processing when the task genuinely requires it. For example, a document analysis system might first use retrieval to identify relevant sections, then process those sections with long context if they exceed the standard context limit. This approach balances the benefits of long context with the efficiency of shorter contexts, optimizing for both quality and cost.

---

<sup>1</sup>Context length capabilities evolve rapidly. Check current documentation for the latest specifications.

## 19.8 Comparison and Trade-offs

### 19.8.1 Method Comparison

Different approaches to long context processing involve fundamentally different trade-offs between computational efficiency, memory usage, model quality, and implementation complexity. Understanding these trade-offs is essential for selecting the appropriate method for a given application, as no single approach dominates across all dimensions. The optimal choice depends on the specific requirements of the task, available hardware, and acceptable quality-efficiency trade-offs.

Standard full attention with optimized implementations like Flash Attention remains the gold standard for quality and simplicity when sequence lengths permit. For sequences up to 2048 tokens on modern GPUs, full attention is typically the best choice: it provides the highest model quality, has the simplest implementation, and benefits from highly optimized kernels. Flash Attention reduces memory bandwidth requirements through kernel fusion, enabling batch sizes  $2\text{--}4\times$  larger than naive implementations while maintaining identical outputs to standard attention. However, the fundamental  $O(n^2)$  scaling means that full attention becomes impractical beyond 4096-8192 tokens on typical hardware.

Sparse attention methods like Longformer and BigBird reduce complexity to  $O(n \times w)$  where  $w$  is a fixed window size, enabling sequences of 4096-16384 tokens on standard GPUs. These methods maintain exact attention within their connectivity pattern, avoiding approximation errors. The primary trade-off is that sparse patterns may miss important long-range dependencies that fall outside the connectivity pattern. For tasks where local context dominates (such as language modeling or most NLP tasks), this limitation has minimal impact on quality. For tasks requiring complex long-range reasoning (such as certain question answering or reasoning tasks), sparse attention may underperform full attention even when both are feasible.

Linear attention methods like Performer and Linformer achieve  $O(n)$  complexity through mathematical approximations, enabling very long sequences of 32768 tokens or more. However, these approximations introduce errors that can degrade model quality. Performer uses random feature approximations to the softmax kernel, which works well for some attention distributions but poorly for others. Linformer assumes low-rank structure in attention matrices, which holds for many tasks but may fail for tasks with complex attention patterns. In practice, linear attention methods typically show 2-5% accuracy degradation on downstream tasks compared to full attention, which may or may not be acceptable depending on the application.

Recurrent methods like Transformer-XL process sequences in segments with recurrent connections, enabling unlimited context length with constant memory per segment. The trade-off is that information must propagate through multiple segments to flow across long distances, which can be slower than direct attention and may lose information through the recurrent bottleneck. Transformer-XL works well for tasks like language modeling where sequential processing is natural, but less well for tasks requiring bidirectional context or random access to different parts of the sequence.

Retrieval-augmented generation (RAG) sidesteps the context length problem entirely by retrieving only relevant information and providing it in a short context. This approach can handle effectively unlimited document collections while maintaining the quality and efficiency of short-context models. The trade-off is implementation complexity: RAG requires building and maintaining a retrieval system, embedding documents, and handling retrieval failures. Additionally, RAG works best for tasks where relevant information can be identified through retrieval, but may struggle with tasks requiring synthesis across many parts of a document or reasoning about information that is difficult to retrieve.

### 19.8.2 Hardware and Memory Considerations

The practical feasibility of different long context methods depends critically on available hardware and memory constraints. Modern GPUs vary widely in memory capacity, from 8 GB on consumer GPUs to 80 GB on high-end data center GPUs, and this memory capacity directly determines which sequence lengths are feasible with different methods.

For a BERT-base scale model with  $d = 768$ ,  $h = 12$  heads, and  $L = 12$  layers, the memory requirements for different methods and sequence lengths are as follows. Full attention with  $n = 2048$  requires approximately 2.4 GB for attention matrices across all layers, which fits comfortably on any

Method	Max Length	Complexity	Quality	Implementation
Full Attention	2-4K	$O(n^2d)$	Excellent	Simple
Flash Attention	4-8K	$O(n^2d)$	Excellent	Medium
Longformer	4-16K	$O(nwd)$	Good	Medium
BigBird	4-16K	$O(n(w+r)d)$	Good	Medium
Linformer	8-32K	$O(nkd)$	Fair	Medium
Performer	16-64K	$O(nd^2)$	Fair	Hard
Transformer-XL	Unlimited	$O(L^2d)/\text{seg}$	Good	Medium
RAG	Unlimited	$O(n^2d)$	Excellent	Hard

Table 19.1: Comparison of long context methods. Complexity is per-layer computational cost. Quality is relative to full attention on typical NLP tasks. Implementation difficulty considers both coding complexity and infrastructure requirements.

modern GPU. At  $n = 4096$ , full attention requires 9.7 GB, which fits on 16 GB GPUs but leaves limited memory for batch processing. At  $n = 8192$ , full attention requires 38.5 GB, exceeding even high-end GPUs and requiring model parallelism or gradient checkpointing.

Sparse attention dramatically improves these numbers. Longformer with  $w = 512$  and  $n = 4096$  requires only 2.4 GB for attention matrices, enabling batch sizes  $4\times$  larger than full attention on the same hardware. At  $n = 8192$ , Longformer requires 4.8 GB, which fits comfortably on 16 GB GPUs. At  $n = 16384$ , Longformer requires 9.6 GB, still feasible on standard hardware. This memory efficiency enables processing of long documents on commodity GPUs that would be impossible with full attention.

Linear attention methods like Linformer with  $k = 256$  require even less memory. At  $n = 4096$ , Linformer requires only 600 MB for attention matrices, enabling very large batch sizes or processing on smaller GPUs. At  $n = 16384$ , Linformer requires 2.4 GB, comparable to full attention at  $n = 2048$ . This memory efficiency enables processing of very long sequences, but at the cost of approximation errors that may degrade quality.

The memory requirements extend beyond attention matrices to include activations, gradients, model parameters, and optimizer states. For training, the total memory requirement is typically  $4\text{-}6\times$  the attention matrix memory when accounting for all these components. For inference, memory requirements are lower as gradients and optimizer states are not needed, but activations must still be stored for generation. These additional memory requirements mean that the feasible sequence length for training is typically  $2\text{-}4\times$  shorter than for inference on the same hardware.

### 19.8.3 Recommendations by Use Case

Selecting the appropriate long context method requires matching the method’s characteristics to the specific requirements of the application. The following recommendations provide guidance based on common use cases and constraints.

For general NLP tasks with sequences up to 2048 tokens, use standard full attention with Flash Attention optimization. This provides the best quality with simple implementation and benefits from highly optimized libraries. The computational and memory costs are manageable on any modern GPU, and the simplicity reduces implementation and debugging time.

For document processing tasks with sequences of 2048-8192 tokens, use sparse attention methods like Longformer or BigBird. These methods provide good quality with manageable computational costs, and the sparse patterns align well with the local structure of natural language. Longformer is simpler and faster for tasks where local context dominates, while BigBird provides better quality for tasks requiring long-range reasoning. Both methods have well-tested implementations available in popular libraries.

For very long sequences of 8192-32768 tokens where quality is critical, consider using full attention with model parallelism or gradient checkpointing if hardware permits, or sparse attention if hardware is limited. The quality difference between full and sparse attention becomes more significant at these lengths, so the choice depends on whether the hardware can support full attention. If full attention is infeasible, BigBird typically provides better quality than Longformer at these lengths due to its random

connections.

For extremely long sequences beyond 32768 tokens, or when processing large document collections, use retrieval-augmented generation (RAG) rather than attempting to fit everything in context. RAG provides better quality and efficiency than any long context method at these scales, as it focuses the model's attention on relevant information rather than processing irrelevant content. The implementation complexity of RAG is justified by the significant quality and efficiency improvements at these scales.

For streaming or online processing tasks, use Transformer-XL or similar recurrent methods that can process sequences incrementally without recomputing previous segments. These methods enable unlimited context length with constant memory per segment, making them ideal for applications like real-time transcription, continuous monitoring, or interactive systems where the sequence length is unbounded.

For tasks requiring frequent updates to the knowledge base or document collection, prefer RAG over long context methods. RAG allows updating the retrieval index without retraining the model, while long context methods require reprocessing the entire context whenever information changes. This makes RAG more practical for applications with dynamic information needs.

## 19.9 Exercises

**Exercise 19.1** (Memory Calculation). Calculate the memory requirements for attention matrices in different scenarios:

1. For a BERT-base model ( $d = 768$ ,  $h = 12$ ,  $L = 12$ ) with sequence lengths  $n \in \{512, 1024, 2048, 4096, 8192\}$ , compute the total memory for attention matrices in FP32 and FP16 formats.
2. For the same model using Longformer with window size  $w = 512$  and 2 global tokens, compute the memory savings compared to full attention at each sequence length.
3. Determine the maximum sequence length that fits in 16 GB of GPU memory for full attention, assuming attention matrices consume 40% of available memory (the rest is for activations, parameters, etc.).
4. For a GPT-3 scale model ( $d = 12288$ ,  $h = 96$ ,  $L = 96$ ), compute the memory required for  $n = 2048$  tokens and explain why model parallelism is necessary.

**Exercise 19.2** (Position Interpolation Implementation). Implement and evaluate position interpolation for extending context length:

1. Load a pretrained GPT-2 model (trained on 1024-token contexts).
2. Implement position interpolation to extend the model to 4096 tokens by scaling position indices by  $1024/4096 = 0.25$ .
3. Fine-tune the extended model on long sequences for 1000 steps.
4. Evaluate perplexity on sequences of length 1024, 2048, 3072, and 4096, comparing the interpolated model to the original model (which will fail on longer sequences).
5. Plot perplexity versus position to visualize how well the model handles different parts of the extended context.

**Exercise 19.3** (Sparse Attention Patterns). Implement and compare different sparse attention patterns:

1. Implement local attention with window size  $w = 256$  for a sequence of length  $n = 2048$ .
2. Implement strided attention with stride  $s = 64$  for the same sequence.
3. Implement BigBird attention combining local ( $w = 128$ ), random ( $r = 32$ ), and global ( $g = 4$ ) patterns.
4. For each pattern, compute the number of attention connections and compare to full attention ( $n^2 = 4,194,304$  connections).
5. Visualize the attention patterns as sparse matrices and discuss which types of dependencies each pattern can capture.

**Exercise 19.4** (ALiBi Extrapolation). Implement ALiBi and test its extrapolation capabilities:

1. Train a small transformer (4 layers,  $d = 256$ , 4 heads) with ALiBi on sequences of length 512 from a language modeling dataset.
2. Use head-specific slopes  $m_i = 2^{-8i/4}$  for the 4 heads, giving slopes  $\{0.25, 0.0625, 0.0156, 0.0039\}$ .
3. Evaluate the trained model on sequences of length 512, 1024, 2048, and 4096 without any fine-tuning.
4. Compare to a model trained with sinusoidal position encodings on the same data.
5. Plot perplexity versus sequence length for both models and explain the difference in extrapolation behavior.

**Exercise 19.5** (Retrieval-Augmented Generation). Implement a simple RAG system for question answering:

1. Create a document corpus of 1000 Wikipedia articles on a specific topic (e.g., history, science).
2. Embed all documents using a pretrained BERT model, storing embeddings in a FAISS index for efficient retrieval.
3. For a given question, retrieve the top-5 most relevant documents based on embedding similarity.
4. Concatenate the retrieved documents with the question and generate an answer using a pretrained language model.
5. Compare the quality of answers when using RAG versus providing the model with only the question (no retrieval).
6. Analyze cases where RAG succeeds and fails, discussing the importance of retrieval quality.

**Exercise 19.6** (Transformer-XL Segment Processing). Implement segment-level recurrence for processing long sequences:

1. Implement a simplified Transformer-XL that processes a sequence in segments of length  $L = 256$ .
2. For each segment, cache the hidden states from the previous segment and concatenate them with the current segment's inputs.
3. Ensure gradients do not flow into the cached hidden states (use `stop_gradient` or `detach`).
4. Process a sequence of length 2048 in 8 segments, measuring the effective context length at each position.
5. Compare memory usage and computation time to processing the full 2048-token sequence at once.
6. Discuss the trade-off between effective context length and computational efficiency.

**Exercise 19.7** (Long Context Cost Analysis). Analyze the computational and financial costs of long context processing:

1. For a BERT-base model, measure the actual wall-clock time to process sequences of length 512, 1024, 2048, and 4096 on your available hardware (CPU or GPU).
2. Compute the FLOPs for attention at each sequence length and compare to the measured time to determine hardware efficiency.
3. Estimate the cost of processing 1 million tokens at each sequence length, assuming cloud GPU pricing (e.g., \$2.50/hour for an A100).
4. Compare the cost of full attention versus Longformer with  $w = 512$  at each sequence length.
5. Discuss scenarios where the higher cost of long context is justified versus where shorter contexts with retrieval would be more economical.

**Exercise 19.8** (Position Encoding Comparison). Compare different position encoding schemes empirically:

1. Train four small transformer models (4 layers,  $d = 256$ , 4 heads) on the same language modeling dataset, using: (a) absolute learned positions, (b) sinusoidal positions, (c) RoPE, and (d) ALiBi.
2. Train all models on sequences of length 512 for the same number of steps.
3. Evaluate all models on sequences of length 512, 1024, 2048, and 4096.
4. Plot perplexity versus sequence length for each model.
5. Analyze which position encoding schemes extrapolate best and explain why based on their mathematical properties.



6. Fine-tune the absolute and sinusoidal models on longer sequences and compare to the zero-shot extrapolation of RoPE and ALiBi.

## 19.10 Solutions

Full solutions for all exercises are available at <https://deeplearning.hofkensvermeulen.be>.

## Chapter 20

# Pre-training Strategies and Transfer Learning

### Chapter Overview

Pre-training on large unlabeled corpora followed by task-specific fine-tuning has become the dominant paradigm in deep learning. This chapter covers pre-training objectives, data curation, curriculum learning, continual pre-training, and transfer learning strategies for maximizing downstream performance.

### Learning Objectives

1. Understand different pre-training objectives and their trade-offs
2. Curate and process pre-training data at scale
3. Apply curriculum learning and domain-adaptive pre-training
4. Implement parameter-efficient fine-tuning (LoRA, adapters)
5. Design multi-task and multi-stage pre-training
6. Measure and improve transfer learning effectiveness

## 20.1 Pre-training Objectives

### 20.1.1 Language Modeling Objectives

The choice of pre-training objective fundamentally shapes a model’s capabilities. The main objectives are:

- **Causal Language Modeling (CLM):** Predict each token given only previous context:  $\mathcal{L}_{\text{CLM}} = -\sum_t \log P(x_t | x_{<t}; \theta)$ . Used by GPT models (Chapter 14). Efficient single-pass training, natural for generation, but unidirectional.
- **Masked Language Modeling (MLM):** Mask  $\sim 15\%$  of tokens and predict from bidirectional context:  $\mathcal{L}_{\text{MLM}} = -\sum_{t \in \mathcal{M}} \log P(x_t | x_{\setminus \mathcal{M}}; \theta)$ . Used by BERT (Chapter 13). Rich representations for understanding tasks.
- **Prefix Language Modeling:** Bidirectional attention on a prefix, causal on the suffix. Combines benefits of CLM and MLM. Used by UniLM and GLM.

### 20.1.2 Denoising Objectives

- **Span Corruption (T5):** Replace random spans with sentinel tokens; decoder predicts original spans. See Chapter 15.
- **Multi-task Denoising (BART):** Combines token masking, deletion, text infilling, sentence permutation, and document rotation. See Chapter 15.

Computational costs are similar across objectives for the same model size and sequence length: a single forward pass dominates, with differences arising mainly in the decoder target length for seq2seq objectives (span corruption costs  $\sim 3\times$  more in decoder computation than single-token MLM).

### 20.1.3 Contrastive Objectives

**Contrastive Learning:**

$$\mathcal{L}_{\text{contrastive}} = -\log \frac{\exp(\text{sim}(z_i, z_i^+)/\tau)}{\sum_j \exp(\text{sim}(z_i, z_j)/\tau)} \quad (20.1)$$

**Applications:**

- SimCLR (vision): Augmented views as positives
- CLIP: Image-text pairs
- SimCSE (text): Dropout as augmentation

## 20.2 Data Curation and Processing

### 20.2.1 Data Scale and Requirements

The scale of pre-training data has grown exponentially over the past few years, driven by empirical findings that larger datasets consistently improve model performance. Understanding the data requirements, storage costs, and preprocessing overhead is essential for planning pre-training projects.

**BERT** was pre-trained on approximately 16 GB of text data, consisting of BooksCorpus (800 million words) and English Wikipedia (2.5 billion words). This relatively modest dataset size reflects BERT’s focus on high-quality, curated text rather than massive web crawls. The 16 GB of raw text expands to approximately 3.3 billion tokens using BERT’s WordPiece tokenizer with a 30,000 token vocabulary. Training BERT-base for 1 million steps with batch size 256 and sequence length 512 means the model sees each token approximately 40 times on average, indicating significant data reuse through multiple epochs. The storage requirements are minimal by modern standards—16 GB of compressed text expands to perhaps 50 GB including tokenized data and intermediate preprocessing artifacts.

**GPT-2** scaled up to approximately 40 GB of text from WebText, a dataset created by scraping outbound links from Reddit posts with at least 3 karma. This filtering strategy aimed to identify high-quality content as judged by the Reddit community. The 40 GB corpus contains roughly 8 billion tokens using GPT-2’s byte-pair encoding with a 50,257 token vocabulary. GPT-2’s largest variant (1.5B parameters) was trained for approximately 1 million steps, seeing each token roughly 10 times. The preprocessing pipeline for WebText involved deduplication, filtering by language, and removing low-quality content, reducing the raw crawl from over 100 GB to the final 40 GB. Storage requirements including raw data, filtered data, and tokenized sequences total approximately 150 GB.

**GPT-3** made a massive leap to approximately 570 GB of text, totaling roughly 300 billion tokens. This dataset combines filtered Common Crawl (410 GB), WebText2 (19 GB), Books1 (12 GB), Books2 (55 GB), and Wikipedia (3 GB). The preprocessing pipeline for Common Crawl is particularly intensive: the raw crawl contains petabytes of data, which must be filtered by language, deduplicated, and quality-filtered to produce the final 410 GB. This filtering process itself requires substantial computational resources—processing petabytes of data through language classifiers and deduplication algorithms takes weeks on large clusters. The total storage requirements for GPT-3 pre-training, including raw data,

filtered data, tokenized sequences, and training checkpoints, exceed 5 TB. The preprocessing cost alone is estimated at tens of thousands of dollars in compute time.

**LLaMA** pushed the scale even further to approximately 1.4 TB of text, totaling roughly 1.4 trillion tokens. This dataset consists primarily of Common Crawl (67%), C4 (15%), GitHub (4.5%), Wikipedia (4.5%), books (4.5%), ArXiv (2.5%), and StackExchange (2%). The inclusion of code from GitHub and technical content from ArXiv and StackExchange reflects a deliberate strategy to improve reasoning and technical capabilities. The preprocessing pipeline for LLaMA is even more sophisticated than GPT-3, using multiple quality filters including perplexity-based filtering, classifier-based filtering, and extensive deduplication. The total storage requirements exceed 10 TB including all preprocessing artifacts, and the preprocessing cost is estimated at over \$100,000 in compute time.

### 20.2.2 Data Quality versus Quantity

The relationship between data quality and quantity is not straightforward—more data does not always lead to better models if the quality is poor. Recent research has shown that careful data curation can match or exceed the performance of models trained on much larger but noisier datasets.

High-quality datasets like Wikipedia and books consistently improve model performance even when they represent a small fraction of total training data. GPT-3’s data mixture samples Wikipedia at 3× the rate it appears in the corpus (3.4 epochs versus 0.44 epochs for Common Crawl), reflecting the higher quality and information density of Wikipedia text. This upsampling strategy means that despite Wikipedia being only 3 GB of the 570 GB total, it contributes disproportionately to the model’s knowledge and capabilities.

The preprocessing cost for achieving high data quality is substantial. Language identification using fastText classifiers requires processing every document, taking approximately 1 CPU-hour per 100 GB of text. Deduplication using MinHash LSH is even more expensive, requiring approximately 10 CPU-hours per 100 GB for computing signatures and finding near-duplicates. Quality filtering using perplexity-based methods requires running a language model over the entire corpus, taking approximately 100 GPU-hours per 100 GB. For GPT-3’s 570 GB dataset, the total preprocessing cost exceeds 50,000 CPU-hours and 5,000 GPU-hours, translating to roughly \$30,000 in cloud computing costs.

The storage requirements for preprocessing are also significant. Deduplication requires storing hash signatures for all documents, typically requiring 100-200 bytes per document. For a corpus with 1 billion documents, this means 100-200 GB of signature storage. Near-duplicate detection using LSH requires storing multiple hash tables, potentially doubling or tripling this storage requirement. Quality filtering requires storing perplexity scores or classifier outputs for all documents, adding another 10-20 GB. In total, the preprocessing metadata can require 500 GB to 1 TB of storage for a large corpus, comparable to the size of the corpus itself.

### 20.2.3 Data Filtering and Cleaning

---

**Algorithm 13:** Data Filtering Pipeline
 

---

**1 Step 1: Quality Filtering**

- Remove duplicates (exact and near-duplicates)
- Filter by language (fastText classifier)
- Remove toxic/harmful content
- Filter low-quality (perplexity-based, classifier)

**Step 2: Deduplication**

- Exact match: Hash-based
- Near-duplicates: MinHash LSH
- Document-level and paragraph-level

**Step 3: Privacy**

- Remove PII (emails, phone numbers, addresses)
- Filter memorized content
- Redact sensitive information

**Step 4: Formatting**

- Unicode normalization
  - Remove excessive whitespace
  - Clean HTML/markup artifacts
- 

**Example 20.1** (GPT-3 Data Mixture). Total: 570GB, 300B tokens

Higher-quality sources sampled more frequently (multiple epochs). Lower-quality sources seen less to avoid overfitting to noise.

### 20.2.4 Data Deduplication

**Why deduplicate?**

- Prevents memorization
- Better generalization
- Fairer evaluation (test set contamination)

**Methods:**
**1. Exact Deduplication:**

```
seen_hashes = set()
for doc in corpus:
    hash_val = hash(doc)
    if hash_val not in seen_hashes:
```

```
keep(doc)
seen_hashes.add(hash_val)
```

## 2. Fuzzy Deduplication (MinHash):

- Compute MinHash signatures
- Use LSH for near-neighbor search
- Remove documents with Jaccard similarity  $> 0.8$

## 20.3 Training Compute Requirements

### 20.3.1 FLOPs Analysis

Understanding the computational requirements for pre-training large language models is essential for planning projects and estimating costs. The total compute is typically measured in FLOPs (floating-point operations), which can be calculated from model architecture and training configuration.

For a transformer model with  $L$  layers,  $d$  model dimension,  $h$  attention heads, and feed-forward intermediate dimension  $d_{ff}$  (typically  $4d$ ), processing a single token requires approximately:

$$\text{FLOPs per token} = 2L(12d^2 + 4d \cdot d_{ff}) = 2L(12d^2 + 16d^2) = 56Ld^2 \quad (20.2)$$

The factor of 2 accounts for both forward and backward passes (backward pass requires approximately the same FLOPs as forward pass). The  $12d^2$  term comes from attention projections (query, key, value, and output, each  $d \times d$ ), and the  $16d^2$  term comes from feed-forward layers (two  $d \times 4d$  projections).

For **BERT-base** with  $L = 12$ ,  $d = 768$ , training on 3.3 billion tokens for 40 epochs (132 billion tokens total):

$$\text{Total FLOPs} = 56 \times 12 \times 768^2 \times 132 \times 10^9 \approx 5.2 \times 10^{20} \text{ FLOPs} \quad (20.3)$$

This is approximately 0.5 zettaFLOPs. Training on 16 TPU v3 chips (each providing 420 TFLOPS in mixed precision) for 4 days:

$$\text{Available compute} = 16 \times 420 \times 10^{12} \times 4 \times 86400 \approx 2.3 \times 10^{21} \text{ FLOPs} \quad (20.4)$$

The ratio of available compute to required compute is approximately 4.4, indicating that BERT-base training achieves roughly 23% hardware utilization. This is typical for large-scale training where communication overhead, data loading, and other inefficiencies reduce effective utilization.

For **GPT-3 175B** with  $L = 96$ ,  $d = 12288$ , training on 300 billion tokens:

$$\text{Total FLOPs} = 56 \times 96 \times 12288^2 \times 300 \times 10^9 \approx 2.4 \times 10^{23} \text{ FLOPs} \quad (20.5)$$

This is approximately 240 zettaFLOPs, nearly 500× more than BERT-base. The massive compute requirement reflects both the larger model (175B versus 110M parameters) and the larger dataset (300B versus 132B tokens). Training GPT-3 on approximately 10,000 NVIDIA V100 GPUs (each providing 125 TFLOPS in mixed precision) for 1 month:

$$\text{Available compute} = 10000 \times 125 \times 10^{12} \times 30 \times 86400 \approx 3.2 \times 10^{23} \text{ FLOPs} \quad (20.6)$$

This suggests approximately 75% hardware utilization, which is impressive for such a large-scale distributed training job. The higher utilization compared to BERT reflects improvements in distributed training infrastructure and optimization techniques.

For **LLaMA-65B** with  $L = 80$ ,  $d = 8192$ , training on 1.4 trillion tokens:

$$\text{Total FLOPs} = 56 \times 80 \times 8192^2 \times 1.4 \times 10^{12} \approx 3.3 \times 10^{23} \text{ FLOPs} \quad (20.7)$$

This is approximately 330 zettaFLOPs. Training on 2048 NVIDIA A100 GPUs (each providing 312 TFLOPS in mixed precision) for 21 days:

$$\text{Available compute} = 2048 \times 312 \times 10^{12} \times 21 \times 86400 \approx 1.2 \times 10^{24} \text{ FLOPs} \quad (20.8)$$

This suggests approximately 28% hardware utilization, which is lower than GPT-3 despite using more modern hardware. The lower utilization likely reflects the challenges of scaling to very long sequences (LLaMA uses 2048 token sequences versus GPT-3’s 2048 tokens) and the overhead of processing the much larger dataset.

### 20.3.2 GPU-Hours and Cost Estimates

Translating FLOPs into GPU-hours and cost estimates provides a more practical understanding of training requirements. The cost depends heavily on the hardware platform and whether using cloud services or owned infrastructure.

**BERT-base** training on 16 TPU v3 chips for 4 days equals 1,536 TPU-hours. At Google Cloud’s on-demand pricing of approximately \$8 per TPU v3 hour, this costs roughly \$12,000. However, Google’s original BERT paper reported using preemptible TPUs at approximately \$2.40 per hour, reducing the cost to roughly \$3,700. Using equivalent GPU resources (approximately 64 NVIDIA V100 GPUs to match 16 TPU v3 chips), the cost would be approximately \$2 per GPU-hour on AWS, totaling \$12,000 for 96 days of GPU time. The lower TPU cost reflects Google’s optimization for transformer workloads and economies of scale.

**GPT-3 175B** training on 10,000 V100 GPUs for 1 month equals 7.2 million GPU-hours. At AWS on-demand pricing of approximately \$3 per V100 hour, this would cost \$21.6 million. However, OpenAI likely used a combination of owned infrastructure and negotiated cloud pricing, with estimates suggesting actual costs between \$4 million and \$12 million. The wide range reflects uncertainty about the exact hardware configuration, utilization rates, and pricing agreements. The training also required substantial infrastructure costs including high-bandwidth networking (InfiniBand or equivalent), distributed storage systems, and engineering effort to optimize the training pipeline.

**LLaMA-65B** training on 2048 A100 GPUs for 21 days equals 1.03 million GPU-hours. At cloud pricing of approximately \$3 per A100 hour, this would cost \$3.1 million. Meta’s paper reports that LLaMA-65B training consumed approximately 1,022,362 GPU-hours on A100-80GB GPUs, closely matching this estimate. Using Meta’s owned infrastructure rather than cloud services likely reduced the effective cost to \$1.5-2 million when accounting for hardware depreciation and operational costs. The A100’s higher performance compared to V100 (312 versus 125 TFLOPS) means that LLaMA-65B required only 1/7 the GPU-hours of GPT-3 despite using comparable compute (330 versus 240 zettaFLOPs), demonstrating the importance of hardware efficiency.

### 20.3.3 Scaling Laws

Empirical scaling laws govern the relationship between compute budget, model size, dataset size, and performance (see Section 14.4 for the full treatment). The key insight from the Chinchilla scaling laws (Hoffmann et al., 2022) is that model size and dataset size should scale equally with compute budget:  $N_{\text{opt}} \propto C^{0.5}$  and  $D_{\text{opt}} \propto C^{0.5}$ . This implies GPT-3 175B (trained on 300B tokens) was over-parameterized—a 70B model trained on 1.4T tokens (matching LLaMA-65B) achieves better performance for the same compute. This insight has driven the trend toward models like LLaMA, Chinchilla, and Mistral that prioritize training tokens over parameter count.

## 20.4 Curriculum Learning

### 20.4.1 Progressive Training Strategies

Curriculum learning applies the principle of learning from easy to hard examples, progressively increasing task difficulty during training. This approach can significantly improve training efficiency, convergence speed, and final model performance. The key insight is that models learn more effectively when they first master simpler patterns before tackling complex ones.

The most common curriculum strategy involves progressively increasing sequence length during training. Starting with shorter sequences reduces both memory requirements and computational cost in the early stages of training when the model is learning basic patterns. For a model with quadratic attention complexity  $O(n^2d)$ , doubling the sequence length quadruples the attention computation. Training BERT-base with sequence length 128 for the first 90% of steps and then 512 for the final 10% reduces total training time by approximately 30% compared to using length 512 throughout. The shorter sequences allow larger batch sizes in early training, which improves gradient estimates and accelerates convergence. The model learns word-level and phrase-level patterns with short sequences, then refines its understanding of long-range dependencies with longer sequences.

Batch size curriculum is another effective strategy, gradually increasing batch size during training. Starting with smaller batches provides more frequent parameter updates, which helps the model escape poor local minima in early training. As training progresses and the model approaches convergence, larger batches provide more stable gradient estimates and better utilize hardware parallelism. GPT-3 training used a batch size curriculum, starting at 32,000 tokens per batch and gradually increasing to 3.2 million tokens per batch. This  $100\times$  increase in batch size was enabled by learning rate adjustments and gradient accumulation. The larger batch sizes in later training improved hardware utilization from approximately 30% to over 70%, significantly reducing training time.

Learning rate schedules are essential for curriculum learning, as the optimal learning rate changes with batch size and training progress. The linear warmup followed by cosine decay schedule has become standard for transformer pre-training. The warmup phase, typically 1-10% of total steps, gradually increases the learning rate from near-zero to the peak value. This prevents the large gradient updates in early training from destabilizing the model. The cosine decay phase gradually reduces the learning rate to near-zero, allowing the model to fine-tune its parameters as it approaches convergence. For BERT-base, a warmup of 10,000 steps followed by linear decay over 990,000 steps works well. For GPT-3, a warmup of 375 million tokens (approximately 1% of total training) followed by cosine decay proved effective.

The impact on training efficiency is substantial. Curriculum learning can reduce training time by 20-40% compared to fixed configurations while achieving equal or better final performance. For BERT-base, the sequence length curriculum reduces training from approximately 5.5 days to 4 days on the same hardware. For GPT-3, the batch size curriculum improved hardware utilization enough to reduce training time by an estimated 30%, saving approximately \$3-4 million in compute costs. These savings make curriculum learning essential for large-scale pre-training projects.

### 20.4.2 Progressive Training

**Definition 20.1** (Curriculum Learning). Train on progressively harder examples:

**Stage 1:** Easy examples (short sequences, simple patterns)

**Stage 2:** Medium difficulty

**Stage 3:** Full difficulty (long sequences, complex patterns)

#### Benefits:

- Faster convergence
- Better final performance
- More stable training

**Example 20.2** (Sequence Length Curriculum). **GPT-3 training:**

**Stage 1 (0-100B tokens):**

- Sequence length: 1024



- Batch size: 3.2M tokens

#### Stage 2 (100B-300B tokens):

- Sequence length: 2048
- Batch size: 3.2M tokens (fewer sequences)

Starting with shorter sequences reduces memory and computation early in training.

### 20.4.3 Domain-Adaptive Pre-training

Continue pre-training on domain-specific data:

---

#### Algorithm 14: Domain Adaptation

---

- 1 **Step 1:** Pre-train on general corpus (e.g., Common Crawl)
  - 2 **Step 2:** Continue pre-training on domain data (e.g., biomedical)
  - 3 **Step 3:** Fine-tune on task
- 

#### Examples:

- BioBERT: BERT + PubMed/PMC
- SciBERT: BERT + scientific papers
- FinBERT: BERT + financial documents
- CodeBERT: BERT + code

## 20.5 Hardware Requirements and Infrastructure

### 20.5.1 BERT-base Training Infrastructure

Training BERT-base requires relatively modest infrastructure by modern standards, making it accessible to academic research groups and small companies. The original BERT paper reported training BERT-base on 16 TPU v3 chips for 4 days, providing a concrete reference point for hardware requirements.

Each TPU v3 chip provides 420 TFLOPS of mixed-precision compute (bfloat16) and 16 GB of high-bandwidth memory (HBM). The 16-chip configuration provides 6.7 PFLOPS total compute and 256 GB total memory. BERT-base with 110 million parameters requires approximately 440 MB for model weights in FP32, or 220 MB in FP16. With batch size 256 and sequence length 512, the activation memory per batch is approximately 8 GB, which fits comfortably in the 256 GB total memory when distributed across 16 chips. The high-bandwidth interconnect between TPU chips (approximately 100 GB/s per chip) enables efficient data parallelism with minimal communication overhead.

The training cost at Google Cloud's preemptible TPU pricing (approximately \$2.40 per TPU v3 hour) is roughly \$3,700 for the full 4-day training run. Using on-demand pricing (\$8 per hour) would increase this to \$12,000. For comparison, training on NVIDIA V100 GPUs would require approximately 64 GPUs for 4 days (6,144 GPU-hours) at a cost of approximately \$12,000 using AWS on-demand pricing. The equivalent training on A100 GPUs would require approximately 32 GPUs for 2.5 days (1,920 GPU-hours) at a cost of approximately \$6,000, demonstrating the improved efficiency of newer hardware.

The infrastructure requirements beyond compute include high-bandwidth storage for the training data (approximately 100 GB including tokenized sequences and preprocessing artifacts), network bandwidth for distributed training (at least 10 Gbps per GPU for efficient data parallelism), and monitoring infrastructure for tracking training metrics. The total infrastructure cost including storage, networking, and engineering time is typically 2-3× the raw compute cost, bringing the total BERT-base training cost to approximately \$10,000-15,000.

### 20.5.2 GPT-3 Training Infrastructure

Training GPT-3 175B requires massive infrastructure that is accessible only to large technology companies and well-funded research organizations. The scale of the training job presents significant engineering challenges beyond simply acquiring hardware.

The training used approximately 10,000 NVIDIA V100 GPUs, though the exact configuration has not been publicly disclosed. Each V100 provides 125 TFLOPS of mixed-precision compute and 32 GB of memory. The 10,000-GPU configuration provides 1.25 exaFLOPS total compute and 320 TB total memory. GPT-3 175B with 175 billion parameters requires approximately 700 GB for model weights in FP32, or 350 GB in FP16. With model parallelism across 8 GPUs, each GPU stores approximately 44 GB of model weights, leaving limited memory for activations. The batch size per GPU is typically 1-2 sequences of length 2048, requiring approximately 20 GB of activation memory per GPU.

The communication requirements are severe. With model parallelism across 8 GPUs and data parallelism across 1,250 groups, each training step requires all-reduce operations across the data parallel groups (approximately 700 GB of gradients) and all-to-all communication within model parallel groups (approximately 100 GB per step). At 100 Gbps network bandwidth per GPU, the gradient all-reduce takes approximately 70 seconds per step, which would dominate training time. To address this, GPT-3 training used gradient accumulation (accumulating gradients over multiple micro-batches before synchronizing) and high-bandwidth interconnects like InfiniBand (200 Gbps or higher), reducing communication time to approximately 10% of total step time.

The training cost is estimated between \$4 million and \$12 million depending on assumptions about hardware ownership versus cloud rental, utilization rates, and pricing agreements. At AWS on-demand pricing of \$3 per V100 hour, the 7.2 million GPU-hours would cost \$21.6 million, but OpenAI likely achieved significant discounts through long-term commitments and negotiated pricing. The infrastructure costs beyond raw compute are substantial: high-bandwidth networking equipment (InfiniBand switches and cables) costs millions of dollars, distributed storage systems for the 5 TB of training data cost hundreds of thousands of dollars, and the engineering effort to build and optimize the training pipeline represents millions of dollars in labor costs.

The power consumption is also significant. Each V100 GPU consumes approximately 300 watts under full load, so 10,000 GPUs consume 3 megawatts. Over a 1-month training run, this equals 2,160 megawatt-hours of electricity. At typical data center electricity costs of \$0.10 per kWh, the electricity cost alone is \$216,000. Including cooling and power distribution overhead (typically  $1.5\text{--}2\times$  the compute power), the total power cost approaches \$400,000.

### 20.5.3 LLaMA-65B Training Infrastructure

Training LLaMA-65B represents a more efficient approach than GPT-3, using fewer but more powerful GPUs and a more optimized training pipeline. Meta's paper provides detailed information about the infrastructure and costs.

The training used 2,048 NVIDIA A100-80GB GPUs for 21 days, totaling 1,022,362 GPU-hours. Each A100-80GB provides 312 TFLOPS of mixed-precision compute and 80 GB of memory, representing a significant improvement over V100 ( $2.5\times$  compute,  $2.5\times$  memory). The 2,048-GPU configuration provides 639 PFLOPS total compute and 164 TB total memory. LLaMA-65B with 65 billion parameters requires approximately 260 GB for model weights in FP32, or 130 GB in FP16. With model parallelism across 8 GPUs, each GPU stores approximately 16 GB of model weights, leaving substantial memory for activations and optimizer states.

The larger memory capacity of A100-80GB enables more efficient training configurations. LLaMA uses a batch size of 4 million tokens (approximately 2,000 sequences of length 2048), distributed across 2,048 GPUs as 2 sequences per GPU. The activation memory per GPU is approximately 40 GB, and the optimizer states (using AdamW) require approximately 32 GB, totaling approximately 88 GB per GPU. This fits comfortably in the 80 GB memory, avoiding the need for activation checkpointing or other memory-saving techniques that would slow training.

The communication requirements are more manageable than GPT-3 due to the smaller model size and more efficient hardware. With model parallelism across 8 GPUs and data parallelism across 256 groups, each training step requires all-reduce operations across data parallel groups (approximately 260

GB of gradients) and all-to-all communication within model parallel groups (approximately 30 GB per step). Using NVIDIA’s NVLink and NVSwitch interconnects (600 GB/s per GPU within a node, 200 Gbps between nodes), the communication time is approximately 5% of total step time, demonstrating excellent scaling efficiency.

The training cost is estimated at \$2-3 million using Meta’s owned infrastructure. At cloud pricing of \$3 per A100 hour, the 1,022,362 GPU-hours would cost \$3.1 million. Meta’s owned infrastructure likely reduced the effective cost to \$1.5-2 million when accounting for hardware depreciation (A100 GPUs cost approximately \$10,000 each, depreciated over 3-5 years) and operational costs. The power consumption is approximately 1 megawatt ( $2,048 \text{ GPUs} \times 400 \text{ watts per A100}$ ), totaling 504 megawatt-hours over 21 days. At \$0.10 per kWh including cooling overhead, the electricity cost is approximately \$75,000.

The infrastructure requirements include high-bandwidth networking (NVIDIA InfiniBand or equivalent), distributed storage systems (approximately 15 TB for training data and checkpoints), and monitoring infrastructure. Meta’s paper notes that they used a custom training framework optimized for their infrastructure, with careful attention to memory management, communication patterns, and fault tolerance. The engineering effort to build this infrastructure and optimize the training pipeline represents a significant investment beyond the raw hardware costs.

## 20.6 Efficient Pre-training Techniques

Large-scale pre-training relies on several key optimizations, covered in detail in Chapter 11:

- **Mixed precision training** (FP16/BF16 with FP32 master weights):  $1.5\text{--}2\times$  speedup,  $\sim 42\%$  memory reduction. Requires loss scaling to prevent gradient underflow.
- **Gradient checkpointing**: Stores only  $O(\sqrt{L})$  activations, recomputing the rest during backward pass.  $5\text{--}10\times$  memory reduction at  $\sim 33\%$  slowdown.
- **ZeRO optimizer**: Partitions optimizer states (Stage 1,  $4\times$  savings), gradients (Stage 2,  $8\times$ ), and parameters (Stage 3, up to  $64\times$ ) across data-parallel GPUs.
- **Pipeline parallelism**: Divides model across GPUs by layers, pipelining micro-batches. With  $m = 4p$  micro-batches for  $p$  stages, bubble overhead is  $\sim 25\%$ .

For GPT-3 training, the combination of ZeRO Stage 3, gradient checkpointing, pipeline parallelism (8 stages), and data parallelism achieved  $\sim 75\%$  hardware utilization on V100 GPUs.

## 20.7 Parameter-Efficient Fine-tuning

### 20.7.1 Motivation

**Full fine-tuning challenges:**

- Requires storing full model copy per task
- $175\text{B model} \times 100 \text{ tasks} = 17.5\text{T parameters!}$
- Expensive and slow

**Solution:** Fine-tune small subset of parameters.

### 20.7.2 LoRA: Low-Rank Adaptation

**Definition 20.2** (LoRA). Inject trainable low-rank matrices into frozen model:

**Original:**  $\mathbf{h} = \mathbf{W}\mathbf{x}$  where  $\mathbf{W} \in \mathbb{R}^{d \times d}$

**LoRA:**

$$\mathbf{h} = \mathbf{W}\mathbf{x} + \Delta\mathbf{W}\mathbf{x} = \mathbf{W}\mathbf{x} + \mathbf{B}\mathbf{A}\mathbf{x} \quad (20.9)$$

where  $\mathbf{A} \in \mathbb{R}^{r \times d}$ ,  $\mathbf{B} \in \mathbb{R}^{d \times r}$ , and  $r \ll d$  (typically  $r = 4$  to  $64$ ).

**Parameters:**

- Original:  $d^2$  (frozen)
- LoRA:  $2rd$  (trainable)
- Reduction:  $\frac{2rd}{d^2} = \frac{2r}{d}$

**Example 20.3** (LoRA for GPT-3). GPT-3 175B, apply LoRA with  $r = 8$  to attention projections.

**Single attention layer:**

- $\mathbf{W}^Q, \mathbf{W}^K, \mathbf{W}^V, \mathbf{W}^O \in \mathbb{R}^{12288 \times 12288}$
- Original params:  $4 \times 12288^2 = 604M$

**LoRA params per layer:**

$$4 \times 2 \times 8 \times 12288 = 786,432 \approx 0.79M \quad (20.10)$$

**96 layers total:**

- LoRA params:  $96 \times 0.79M = 75.8M$
- Full model: 175B
- **Reduction:  $2,300\times$**  (train only 0.04% of parameters!)

**Performance:** Matches full fine-tuning on many tasks!

### 20.7.3 Adapter Layers

**Definition 20.3** (Adapter). Insert small bottleneck layers between frozen layers:

$$\mathbf{h}_{\text{adapter}} = \mathbf{h} + \text{FFN}_{\text{adapter}}(\text{LayerNorm}(\mathbf{h})) \quad (20.11)$$

where  $\text{FFN}_{\text{adapter}}: d \rightarrow d_{\text{bottleneck}} \rightarrow d$  with  $d_{\text{bottleneck}} \ll d$ .

**Typical bottleneck:**  $d_{\text{bottleneck}} = 64$  for  $d = 768$

**Parameters per adapter:**

$$2d \cdot d_{\text{bottleneck}} = 2 \times 768 \times 64 = 98,304 \quad (20.12)$$

### 20.7.4 Prompt Tuning

**Definition 20.4** (Prompt Tuning). Prepend learnable "soft prompt" vectors:

**Input:**  $[\mathbf{p}_1, \dots, \mathbf{p}_k, \mathbf{x}_1, \dots, \mathbf{x}_n]$

where  $\mathbf{p}_i \in \mathbb{R}^d$  are learned continuous prompts (not discrete tokens).

**Parameters:** Only  $k \times d$  prompt vectors (model frozen).

**Typical:**  $k = 20$  prompts,  $d = 768 \rightarrow$  only 15,360 parameters!

## 20.8 Multi-Task and Multi-Stage Pre-training

### 20.8.1 Multi-Task Pre-training

Train on multiple objectives simultaneously:

$$\mathcal{L}_{\text{total}} = \sum_{i=1}^K \lambda_i \mathcal{L}_i \quad (20.13)$$

**Example (T5):**

- Span corruption (main)
- Prefix LM
- Deshuffling

**Benefits:**

- More robust representations
- Better transfer to diverse tasks
- Can balance objectives with  $\lambda_i$

### 20.8.2 Multi-Stage Pre-training

**Stage 1: General pre-training**

- Large diverse corpus
- Language modeling
- Build general knowledge

**Stage 2: Instruction tuning**

- Instruction-response pairs
- Learn to follow instructions
- Improve helpfulness

**Stage 3: RLHF**

- Reinforcement learning from human feedback
- Align with human preferences
- Improve safety

**Example 20.4** (InstructGPT Pipeline). **Stage 1:** GPT-3 pre-training (175B params, 300B tokens)

**Stage 2:** Supervised fine-tuning

- 13,000 instruction-output examples
- Fine-tune for 16 epochs
- Learning rate:  $9.65 \times 10^{-6}$

**Stage 3:** Reward modeling

- 33,000 comparison examples

- Train 6B reward model
- Predicts human preferences

**Stage 4:** PPO optimization

- 31,000 prompts
- Optimize policy to maximize reward
- KL penalty from SFT model

**Result:** 1.3B InstructGPT preferred over 175B GPT-3 by humans!

## 20.9 Transfer Learning Analysis

### 20.9.1 Measuring Transfer

**Metrics:**

#### 1. Downstream Performance:

$$\Delta = \text{Performance}_{\text{fine-tuned}} - \text{Performance}_{\text{from-scratch}} \quad (20.14)$$

#### 2. Sample Efficiency:

- Number of examples to reach target performance
- Pre-trained models: 10-100× fewer examples

#### 3. Convergence Speed:

- Training steps to convergence
- Pre-trained: 10× faster

### 20.9.2 What Makes Good Pre-training?

**Data scale:** More data → better transfer (up to a point)

**Data diversity:** Diverse pre-training → broader transfer

**Model scale:** Larger models transfer better

**Objective alignment:** Pre-training objective similar to downstream task

**Domain match:** Domain-specific pre-training helps domain-specific tasks

## 20.10 Exercises

**Exercise 20.1.** Compare pre-training objectives:

1. Train BERT-tiny with: (a) MLM, (b) CLM, (c) Span corruption
2. Evaluate on GLUE tasks
3. Which objective transfers best? Why?

**Exercise 20.2.** Implement data filtering pipeline:

1. Download 10,000 documents from Common Crawl

2. Remove duplicates (exact and near-duplicate)
3. Filter by language (keep English)
4. Filter low-quality (perplexity  $\geq$  threshold)
5. Report statistics at each stage

**Exercise 20.3.** Implement LoRA:

1. Load pre-trained GPT-2
2. Add LoRA layers with  $r = 8$  to attention
3. Fine-tune on sentiment analysis
4. Compare: (a) Full fine-tuning, (b) LoRA, (c) Frozen
5. Measure: parameters trained, memory, accuracy

**Exercise 20.4.** Analyze transfer learning:

1. Fine-tune BERT on 5 GLUE tasks
2. Vary training data: [100, 500, 1000, 5000, all]
3. Compare to training from scratch
4. Plot sample efficiency curves
5. At what point does pre-training stop helping?

## 20.11 Solutions

Full solutions for all exercises are available at <https://deeplearning.hofkensvermeulen.be>.

**Part VII**

**Practical Implementation**



# Chapter 21

## Implementing Transformers in PyTorch

### Chapter Overview

This chapter provides complete, production-ready PyTorch implementations of transformer models. We build from scratch: attention mechanisms, encoder/decoder blocks, position encodings, and full models (BERT, GPT, T5). Each implementation includes training loops, optimization, and best practices.

### Learning Objectives

1. Implement multi-head attention from scratch
2. Build transformer encoder and decoder blocks
3. Create complete BERT and GPT models
4. Write efficient training loops with mixed precision
5. Apply gradient accumulation and checkpointing
6. Debug common implementation issues

### 21.1 Multi-Head Attention Implementation

#### 21.1.1 Core Components

The implementation of multi-head attention in PyTorch requires careful attention to efficiency and memory usage. The standard approach involves projecting queries, keys, and values through linear layers, reshaping tensors to separate attention heads, computing scaled dot-product attention, and finally concatenating the results. However, several optimizations can significantly improve both speed and memory efficiency.

#### **Key implementation considerations:**

- Efficient batched matrix multiplications
- Proper dimension handling for multi-head split
- Memory-efficient attention computation
- Gradient flow through softmax

#### **PyTorch multi-head attention structure:**

1. Project Q, K, V: Linear layers
2. Reshape for multiple heads: view + transpose
3. Compute scaled dot-product attention
4. Concatenate heads and project output

### 21.1.2 Memory-Efficient Attention

The standard attention mechanism computes the full attention matrix of size  $(B, h, n, n)$ , which becomes prohibitively expensive for long sequences. For a sequence length of 512 with 12 heads and batch size 32, this requires approximately 400MB just for the attention scores. We can implement several optimizations to reduce this memory footprint.

The first optimization involves computing attention in chunks rather than materializing the entire attention matrix at once. This approach processes the attention computation in blocks, trading some computational efficiency for substantial memory savings. The chunked attention implementation divides the sequence into smaller segments and computes attention scores for each segment independently.

```
def memory_efficient_attention(Q, K, V, chunk_size=128):
    """
    Compute attention in chunks to reduce memory usage.
    Q, K, V: (batch, heads, seq_len, head_dim)
    """
    B, h, n, d = Q.shape
    output = torch.zeros_like(Q)

    for i in range(0, n, chunk_size):
        end_i = min(i + chunk_size, n)
        Q_chunk = Q[:, :, i:end_i, :] # (B, h, chunk, d)

        # Compute attention scores for this chunk
        scores = torch.matmul(Q_chunk, K.transpose(-2, -1))
        scores = scores / math.sqrt(d)
        attn = F.softmax(scores, dim=-1)

        # Apply to values
        output[:, :, i:end_i, :] = torch.matmul(attn, V)

    return output
```

Another critical optimization is the use of PyTorch's scaled dot-product attention function introduced in PyTorch 2.0, which implements Flash Attention algorithms internally. This function provides significant speedups and memory reductions through kernel fusion and optimized memory access patterns.

```
import torch.nn.functional as F

def efficient_attention(Q, K, V, mask=None):
    """
    Use PyTorch's optimized scaled_dot_product_attention.
    Automatically uses Flash Attention when available.
    """
    # PyTorch 2.0+ provides optimized implementation
    output = F.scaled_dot_product_attention(
        Q, K, V,
        attn_mask=mask,
        dropout_p=0.1 if self.training else 0.0,
        is_causal=False
    )
    return output
```

This optimized implementation can reduce memory usage by up to 50% and provide 2-3 $\times$  speedups compared to the naive implementation, particularly for longer sequences.

### 21.1.3 Dimension Tracking Example

For BERT-base configuration ( $d = 768$ ,  $h = 12$ ):

**Input:**  $(B, n, 768)$  where  $B$  is batch size,  $n$  is sequence length

**After Q/K/V projection:**  $(B, n, 768)$

**Reshape for heads:**  $(B, n, 12, 64) \rightarrow (B, 12, n, 64)$

**Attention scores:**  $(B, 12, n, n)$

**After applying to V:**  $(B, 12, n, 64)$

**Concatenate heads:**  $(B, n, 12, 64) \rightarrow (B, n, 768)$

**Output projection:**  $(B, n, 768)$

## 21.2 Position Encodings

### 21.2.1 Sinusoidal Encoding

Mathematical formula:

$$PE_{(\text{pos}, 2i)} = \sin\left(\frac{\text{pos}}{10000^{2i/d}}\right) \quad (21.1)$$

$$PE_{(\text{pos}, 2i+1)} = \cos\left(\frac{\text{pos}}{10000^{2i/d}}\right) \quad (21.2)$$

**Implementation strategy:**

1. Pre-compute position encoding matrix at initialization
2. Register as buffer (not parameter, doesn't need gradients)
3. Add to embeddings in forward pass

### 21.2.2 Learned Positional Embeddings

**Alternative approach (BERT):**

- Embedding layer:  $\text{max\_len} \times \text{d\_model}$
- Learn position representations during training
- More flexible but requires fixed max length

## 21.3 Masking Strategies

### 21.3.1 Causal Mask for GPT

**Lower triangular mask:**

$$M_{ij} = \begin{cases} 1 & \text{if } j \leq i \\ 0 & \text{if } j > i \end{cases} \quad (21.3)$$

**Implementation:**

```
causal_mask = torch.tril(torch.ones(seq_len, seq_len))
scores = scores.masked_fill(mask == 0, -1e9)
```

### 21.3.2 Padding Mask

**For variable-length sequences:**

```
# input_ids: (batch, seq_len)
# 0 indicates padding
pad_mask = (input_ids != 0).unsqueeze(1).unsqueeze(2)
# Shape: (batch, 1, 1, seq_len)
```

## 21.4 Training Optimizations

### 21.4.1 Fused Kernels for Layer Normalization

Standard PyTorch operations like layer normalization involve multiple kernel launches, each reading from and writing to global memory. Fusing these operations into a single kernel can provide substantial speedups by reducing memory bandwidth requirements. Modern deep learning frameworks provide fused implementations of common operations that should be used whenever possible.

The Apex library from NVIDIA provides highly optimized fused kernels for layer normalization and other operations. These implementations can be 2-3 $\times$  faster than the standard PyTorch versions, particularly for smaller batch sizes where kernel launch overhead dominates.

```
# Standard PyTorch layer norm
layer_norm = nn.LayerNorm(d_model)

# Fused layer norm from Apex (faster)
try:
    from apex.normalization import FusedLayerNorm
    layer_norm = FusedLayerNorm(d_model)
except ImportError:
    # Fall back to standard implementation
    layer_norm = nn.LayerNorm(d_model)
```

Similarly, fused dropout and bias addition can be combined with other operations to reduce memory traffic. The key principle is to minimize the number of separate kernel launches and memory accesses by combining operations that naturally occur together in the computation graph.

### 21.4.2 Mixed Precision Training

Mixed precision training uses 16-bit floating point (FP16) for most operations while maintaining 32-bit precision for critical computations. This approach provides substantial benefits in terms of both memory usage and computational speed, particularly on modern GPUs with dedicated tensor cores optimized for FP16 operations.

#### Benefits:

- 2 $\times$  memory reduction for activations and gradients
- 2-3 $\times$  training speedup on modern GPUs with tensor cores
- Same final accuracy with proper loss scaling
- Enables training larger models or using larger batch sizes

PyTorch provides automatic mixed precision (AMP) through the `torch.cuda.amp` module, which automatically handles the conversion between FP16 and FP32 as needed. The implementation requires minimal code changes and provides automatic loss scaling to prevent gradient underflow.

```
from torch.cuda.amp import autocast, GradScaler

# Initialize gradient scaler for loss scaling
scaler = GradScaler()

# Training loop
for batch in dataloader:
    optimizer.zero_grad()

    # Forward pass in mixed precision
```

```

with autocast():
    outputs = model(batch['input_ids'])
    loss = criterion(outputs, batch['labels'])

# Backward pass with scaled loss
scaler.scale(loss).backward()

# Unscale gradients and clip
scaler.unscale_(optimizer)
torch.nn.utils.clip_grad_norm_(model.parameters(), max_norm=1.0)

# Update weights
scaler.step(optimizer)
scaler.update()

```

The gradient scaler automatically adjusts the loss scaling factor to maintain numerical stability. It increases the scale when no overflow is detected and decreases it when overflow occurs, ensuring that gradients remain in a representable range for FP16 arithmetic.

For BERT-base training, mixed precision typically reduces memory usage from approximately 16GB to 8GB per GPU while maintaining the same final accuracy. The speedup varies depending on the GPU architecture, with Volta and newer architectures providing the largest benefits due to their tensor cores.

### 21.4.3 Gradient Accumulation

Gradient accumulation enables training with effective batch sizes larger than what fits in GPU memory by accumulating gradients over multiple forward-backward passes before updating weights. This technique is essential for training large models or when hardware constraints limit the physical batch size.

**Purpose:** Simulate large batch sizes on limited memory

**Effective batch size:**

$$B_{\text{effective}} = B_{\text{physical}} \times N_{\text{accumulation}} \quad (21.4)$$

The implementation requires careful handling of gradient normalization to ensure that the accumulated gradients have the correct scale. Each loss value should be divided by the number of accumulation steps so that the final gradient magnitude matches what would be obtained with a single large batch.

```

accumulation_steps = 8
optimizer.zero_grad()

for i, batch in enumerate(dataloader):
    # Forward pass
    with autocast():
        outputs = model(batch['input_ids'])
        loss = criterion(outputs, batch['labels'])
        # Scale loss by accumulation steps
        loss = loss / accumulation_steps

    # Backward pass
    scaler.scale(loss).backward()

    # Update weights every accumulation_steps
    if (i + 1) % accumulation_steps == 0:
        scaler.unscale_(optimizer)
        torch.nn.utils.clip_grad_norm_(model.parameters(), 1.0)
        scaler.step(optimizer)

```

```

scaler.update()
optimizer.zero_grad()

```

**Example:**

- Physical batch: 32 (fits in GPU)
- Accumulation steps: 8
- Effective batch: 256

This approach allows training with large effective batch sizes that would otherwise require multiple GPUs or be impossible due to memory constraints. The trade-off is increased training time, as the optimizer updates occur less frequently.

#### 21.4.4 Gradient Checkpointing

Gradient checkpointing trades computation for memory by selectively storing only a subset of activations during the forward pass and recomputing the others during the backward pass. This technique can dramatically reduce memory usage, enabling training of much larger models or longer sequences at the cost of increased computation time.

**Trade computation for memory:**

- Don't store all activations during forward pass
- Recompute intermediate activations during backward pass
- Enables larger models or longer sequences
- Typically 20-30% slower but saves 40-50% memory

PyTorch provides gradient checkpointing through the `torch.utils.checkpoint` module. The key is to wrap transformer layers or blocks in checkpoint functions, which handle the recomputation automatically during the backward pass.

```

from torch.utils.checkpoint import checkpoint

class TransformerLayer(nn.Module):
    def __init__(self, d_model, num_heads, d_ff, use_checkpoint=False):
        super().__init__()
        self.use_checkpoint = use_checkpoint
        self.attention = MultiHeadAttention(d_model, num_heads)
        self.ffn = FeedForward(d_model, d_ff)
        self.norm1 = nn.LayerNorm(d_model)
        self.norm2 = nn.LayerNorm(d_model)

    def forward(self, x, mask=None):
        if self.use_checkpoint and self.training:
            # Use gradient checkpointing
            return checkpoint(self._forward, x, mask)
        else:
            return self._forward(x, mask)

    def _forward(self, x, mask):
        # Attention block
        attn_out = self.attention(x, x, x, mask)
        x = self.norm1(x + attn_out)

```

```
# Feed-forward block
ffn_out = self.ffn(x)
x = self.norm2(x + ffn_out)
return x
```

For a 12-layer BERT model, gradient checkpointing can reduce peak memory usage from approximately 16GB to 9GB, allowing training with longer sequences or larger batch sizes. The computational overhead is typically 20-30%, which is often an acceptable trade-off for the memory savings.

## 21.5 Model Initialization

### 21.5.1 Best Practices

**Weight initialization:**

- Linear layers: Xavier/Glorot normal
- Embeddings: Normal(0, 0.02)
- Layer norm: gamma=1, beta=0

**Special considerations:**

- Scale residual connections by  $1/\sqrt{N_{\text{layers}}}$
- Weight tying: LM head shares embeddings
- Careful initialization prevents gradient issues

## 21.6 Memory Profiling and Optimization

### 21.6.1 Understanding Memory Usage

Memory consumption in transformer training comes from several sources: model parameters, optimizer states, activations, gradients, and temporary buffers. Understanding the breakdown of memory usage is essential for effective optimization. For a BERT-base model with 110M parameters, the memory requirements can be substantial even before considering batch data.

The model parameters themselves occupy relatively little memory compared to other components. With 110M parameters stored in FP32, the parameters require approximately 440MB. However, the Adam optimizer maintains two additional states per parameter (first and second moments), tripling the parameter memory to 1.3GB. Activations stored during the forward pass for gradient computation typically consume the largest portion of memory, scaling with both sequence length and batch size.

PyTorch provides comprehensive memory profiling tools through the `torch.cuda` module. The `memory_summary` function provides detailed information about current memory allocation, including cached memory, allocated memory, and peak memory usage.

```
import torch

# Profile memory usage during training
def profile_memory(model, batch_size, seq_len, device='cuda'):
    torch.cuda.reset_peak_memory_stats(device)
    torch.cuda.empty_cache()

    # Create sample input
    input_ids = torch.randint(0, 30000, (batch_size, seq_len)).to(device)

    # Forward pass
```

```

outputs = model(input_ids)
loss = outputs.mean()

print(f"After forward pass:")
print(f"Allocated: {torch.cuda.memory_allocated(device) / 1e9:.2f} GB")
print(f"Reserved: {torch.cuda.memory_reserved(device) / 1e9:.2f} GB")

# Backward pass
loss.backward()

print(f"\nAfter backward pass:")
print(f"Allocated: {torch.cuda.memory_allocated(device) / 1e9:.2f} GB")
print(f"Peak: {torch.cuda.max_memory_allocated(device) / 1e9:.2f} GB")

# Detailed summary
print("\nDetailed memory summary:")
print(torch.cuda.memory_summary(device))

```

### 21.6.2 Identifying Memory Bottlenecks

The first step in optimization is identifying where memory is being consumed. For transformer models, the attention mechanism typically dominates memory usage due to the quadratic scaling of attention scores with sequence length. A single attention layer with sequence length 512 and 12 heads requires approximately 12MB for attention scores alone, and this scales quadratically with sequence length.

Activation memory can be estimated using the formula:

$$M_{\text{activations}} \approx 2 \times B \times n \times d \times L \times \text{bytes\_per\_element} \quad (21.5)$$

where  $B$  is batch size,  $n$  is sequence length,  $d$  is model dimension,  $L$  is number of layers, and the factor of 2 accounts for both attention and feed-forward activations. For BERT-base with batch size 32 and sequence length 512, this amounts to approximately 9GB in FP32 or 4.5GB in FP16.

### 21.6.3 Optimization Strategies

Several strategies can dramatically reduce memory consumption. The most effective approach combines multiple techniques tailored to the specific bottlenecks identified through profiling.

#### Strategy 1: Reduce Sequence Length

The quadratic scaling of attention with sequence length makes this the most impactful optimization for long sequences. Reducing sequence length from 512 to 256 reduces attention memory by  $4\times$  and total activation memory by  $2\times$ . When possible, use techniques like sliding windows or hierarchical attention to process longer documents without materializing full attention matrices.

#### Strategy 2: Optimize Batch Size

Finding the optimal batch size requires balancing memory usage with computational efficiency. Larger batches improve GPU utilization but consume more memory. Use gradient accumulation to achieve large effective batch sizes while keeping physical batch sizes manageable.

```

def find_optimal_batch_size(model, seq_len, device='cuda'):
    """Binary search to find maximum batch size that fits in memory."""
    min_batch = 1
    max_batch = 256
    optimal_batch = 1

    while min_batch <= max_batch:
        batch_size = (min_batch + max_batch) // 2
        torch.cuda.empty_cache()

```



```

try:
    # Test if this batch size fits
    input_ids = torch.randint(0, 30000,
                              (batch_size, seq_len)).to(device)
    outputs = model(input_ids)
    loss = outputs.mean()
    loss.backward()

    optimal_batch = batch_size
    min_batch = batch_size + 1
except RuntimeError as e:
    if "out of memory" in str(e):
        max_batch = batch_size - 1
    else:
        raise e

return optimal_batch

```

### Strategy 3: Layer-wise Optimization

Different layers have different memory characteristics. Attention layers consume more memory than feed-forward layers due to the attention score matrix. Applying gradient checkpointing selectively to attention layers can provide most of the memory benefits with less computational overhead than checkpointing all layers.

#### 21.6.4 Case Study: Optimizing BERT-base

Consider optimizing BERT-base training to reduce memory from 16GB to 8GB while maintaining training throughput. The baseline configuration uses batch size 32, sequence length 512, and FP32 precision.

##### Baseline measurements:

- Memory usage: 16.2 GB
- Training speed: 120 samples/second
- Parameters: 440 MB
- Optimizer states: 880 MB
- Activations: 9.1 GB
- Gradients: 4.5 GB
- Other: 1.3 GB

##### Optimization steps:

First, enable mixed precision training. This immediately reduces activation and gradient memory by 50%, bringing total memory to approximately 10GB. The training speed increases to 280 samples/second due to tensor core utilization.

Second, apply gradient checkpointing to all transformer layers. This reduces activation memory by an additional 40%, bringing total memory to 7.8GB. Training speed decreases to 220 samples/second due to recomputation overhead.

Third, optimize the batch size. With the memory savings, we can increase batch size to 48, improving GPU utilization. Final measurements show 7.9GB memory usage and 310 samples/second throughput.

##### Final measurements:

- Memory usage: 7.9 GB (51% reduction)
- Training speed: 310 samples/second ( $2.6\times$  faster)
- Same final accuracy after convergence

This optimization demonstrates that combining multiple techniques can achieve substantial improvements in both memory efficiency and training speed without sacrificing model quality.

## 21.7 Debugging Transformers

### 21.7.1 Common Issues

#### 1. Dimension mismatches:

- Check shapes at each operation
- Use assertions for critical dimensions
- Print intermediate tensor shapes

#### 2. NaN/Inf in training:

- Too high learning rate
- Gradient explosion (add clipping)
- Numerical instability in softmax (check mask values)

#### 3. Slow convergence:

- Insufficient warmup
- Bad initialization
- Learning rate too low

#### 4. Memory issues:

- Reduce batch size
- Use gradient checkpointing
- Enable mixed precision
- Reduce sequence length

### 21.7.2 Validation Checks

#### Sanity checks before full training:

1. Overfit single batch (should reach near-zero loss)
2. Check gradient norms are reasonable
3. Verify attention weights sum to 1
4. Test with different sequence lengths
5. Profile memory usage

## 21.8 Inference Optimization

### 21.8.1 TorchScript Compilation

Inference optimization is critical for deploying transformer models in production environments where latency and throughput requirements are stringent. TorchScript provides a way to serialize and optimize PyTorch models for inference, removing Python overhead and enabling additional optimizations.

The `torch.jit.script` function traces the model's execution and converts it to an intermediate representation that can be optimized and executed more efficiently. This process eliminates Python interpreter overhead and enables fusion of operations that would otherwise require multiple kernel launches.

```
import torch.jit as jit

class TransformerForInference(nn.Module):
    def __init__(self, config):
        super().__init__()
        self.transformer = TransformerModel(config)

    def forward(self, input_ids: torch.Tensor) -> torch.Tensor:
        # Type annotations required for TorchScript
        return self.transformer(input_ids)

# Create and script the model
model = TransformerForInference(config)
model.eval()

# Convert to TorchScript
scripted_model = jit.script(model)

# Save for deployment
scripted_model.save('model_scripted.pt')

# Load and use
loaded_model = jit.load('model_scripted.pt')
with torch.no_grad():
    output = loaded_model(input_ids)
```

TorchScript compilation typically provides 10-30% speedup for transformer inference, with larger models seeing greater benefits. The compilation process also validates that the model can be executed without Python dependencies, which is essential for deployment in production environments.

### 21.8.2 KV Cache for Autoregressive Generation

Autoregressive generation in models like GPT requires computing attention over all previous tokens at each step. Without optimization, this results in redundant computation as the keys and values for previous tokens are recomputed at every step. Implementing a KV cache stores these values and reuses them, dramatically reducing computation. For systems-level KV cache management at scale (PagedAttention, memory fragmentation, batch scheduling), see Chapter 22.

```
class GPTWithKVCache(nn.Module):
    def __init__(self, config):
        super().__init__()
        self.layers = nn.ModuleList([
            TransformerLayer(config) for _ in range(config.num_layers)
        ])
        self.embed = nn.Embedding(config.vocab_size, config.d_model)
```

```

def forward(self, input_ids, past_key_values=None, use_cache=False):
    """
    Args:
        input_ids: (batch, seq_len) - new tokens to process
        past_key_values: List of (key, value) tuples from previous steps
        use_cache: Whether to return key-value cache
    """
    batch_size, seq_len = input_ids.shape

    # Embed input tokens
    hidden_states = self.embed(input_ids)

    # Initialize cache if not provided
    if past_key_values is None:
        past_key_values = [None] * len(self.layers)

    # Store new key-values if caching
    present_key_values = [] if use_cache else None

    # Process through layers
    for i, (layer, past_kv) in enumerate(
        zip(self.layers, past_key_values)):

        # Layer forward with cache
        hidden_states, new_kv = layer(
            hidden_states,
            past_key_value=past_kv,
            use_cache=use_cache
        )

        if use_cache:
            present_key_values.append(new_kv)

    return hidden_states, present_key_values

class TransformerLayerWithCache(nn.Module):
    def forward(self, x, past_key_value=None, use_cache=False):
        # Compute Q, K, V
        Q = self.q_proj(x)
        K = self.k_proj(x)
        V = self.v_proj(x)

        # Use cached K, V if available
        if past_key_value is not None:
            past_K, past_V = past_key_value
            K = torch.cat([past_K, K], dim=1)
            V = torch.cat([past_V, V], dim=1)

        # Compute attention
        attn_output = self.attention(Q, K, V)

        # Return new cache if requested
        new_kv = (K, V) if use_cache else None

```

```

        return attn_output, new_kv

# Generation with KV cache
def generate_with_cache(model, input_ids, max_length=100):
    """Generate tokens using KV cache for efficiency."""
    past_key_values = None

    for _ in range(max_length):
        # Only process new token (or all tokens on first step)
        if past_key_values is None:
            current_input = input_ids
        else:
            current_input = input_ids[:, -1:]

        # Forward pass with cache
        logits, past_key_values = model(
            current_input,
            past_key_values=past_key_values,
            use_cache=True
        )

        # Sample next token
        next_token = torch.argmax(logits[:, -1, :], dim=-1, keepdim=True)
        input_ids = torch.cat([input_ids, next_token], dim=1)

        # Stop if EOS token
        if next_token.item() == eos_token_id:
            break

    return input_ids

```

KV caching reduces the computational complexity of generating  $n$  tokens from  $O(n^2)$  to  $O(n)$ , providing speedups of 5-10 $\times$  for typical generation lengths. The memory overhead is proportional to the sequence length and number of layers, typically requiring 1-2GB for a GPT-2 sized model generating 1000 tokens.

### 21.8.3 ONNX Export

ONNX (Open Neural Network Exchange) provides a standardized format for representing neural networks, enabling deployment across different frameworks and hardware platforms. Exporting to ONNX allows using optimized inference engines like ONNX Runtime, which can provide substantial speedups.

```

import torch.onnx

def export_to_onnx(model, output_path, batch_size=1, seq_len=128):
    """Export PyTorch model to ONNX format."""
    model.eval()

    # Create dummy input
    dummy_input = torch.randint(
        0, model.config.vocab_size,
        (batch_size, seq_len)
    )

    # Export to ONNX

```

```

torch.onnx.export(
    model,
    dummy_input,
    output_path,
    input_names=['input_ids'],
    output_names=['logits'],
    dynamic_axes={
        'input_ids': {0: 'batch', 1: 'sequence'},
        'logits': {0: 'batch', 1: 'sequence'}
    },
    opset_version=14,
    do_constant_folding=True
)

# Use ONNX Runtime for inference
import onnxruntime as ort

# Create inference session
session = ort.InferenceSession(
    'model.onnx',
    providers=['CUDAExecutionProvider', 'CPUExecutionProvider']
)

# Run inference
input_ids = torch.randint(0, 30000, (1, 128)).numpy()
outputs = session.run(
    ['logits'],
    {'input_ids': input_ids}
)

```

ONNX Runtime typically delivers 1.5–2× speedup over PyTorch for transformer inference through operator fusion, memory layout optimization, and hardware-specific kernel selection. Combined with INT8 quantization, 3–4× speedup is achievable (see Chapter 22 for quantization fundamentals).

#### 21.8.4 TensorRT Optimization

NVIDIA TensorRT provides highly optimized inference for NVIDIA GPUs through aggressive kernel fusion, precision calibration, and dynamic tensor memory management. TensorRT can provide 2–5× speedup over standard PyTorch inference for transformer models.

```

# Convert ONNX to TensorRT
import tensorrt as trt

def build_tensorrt_engine(onnx_path, engine_path, fp16_mode=True):
    """Build TensorRT engine from ONNX model."""
    logger = trt.Logger(trt.Logger.WARNING)
    builder = trt.Builder(logger)
    network = builder.create_network(
        1 << int(trt.NetworkDefinitionCreationFlag.EXPLICIT_BATCH)
    )
    parser = trt.OnnxParser(network, logger)

    # Parse ONNX model
    with open(onnx_path, 'rb') as f:
        if not parser.parse(f.read()):

```

```

        for error in range(parser.num_errors):
            print(parser.get_error(error))
        return None

# Configure builder
config = builder.create_builder_config()
config.max_workspace_size = 4 << 30 # 4GB

if fp16_mode:
    config.set_flag(trt.BuilderFlag.FP16)

# Build engine
engine = builder.build_engine(network, config)

# Save engine
with open(engine_path, 'wb') as f:
    f.write(engine.serialize())

return engine

# Use TensorRT for inference
def infer_with_tensorrt(engine_path, input_ids):
    """Run inference using TensorRT engine."""
    logger = trt.Logger(trt.Logger.WARNING)

    with open(engine_path, 'rb') as f:
        runtime = trt.Runtime(logger)
        engine = runtime.deserialize_cuda_engine(f.read())

    context = engine.create_execution_context()

    # Allocate buffers
    inputs, outputs, bindings = allocate_buffers(engine)

    # Copy input data
    inputs[0].host = input_ids.cpu().numpy()

    # Run inference
    outputs = do_inference(
        context, bindings, inputs, outputs, stream
    )

    return outputs[0]

```

TensorRT optimization is particularly effective for deployment scenarios where inference latency is critical. The optimization process includes layer fusion, precision calibration for INT8 quantization, and kernel auto-tuning for the specific GPU architecture.

### 21.8.5 Quantization

Quantization reduces model size and inference latency by using lower precision representations for weights and activations. PyTorch supports several quantization approaches, from simple dynamic quantization to full quantization-aware training. For the theoretical foundations of quantization (precision formats, scale factors, zero-points) and pruning/distillation techniques, see Chapter 22.

```

import torch.quantization as quant

# Dynamic quantization (easiest, good for LSTM/Transformer)
def dynamic_quantize(model):
    """Apply dynamic quantization to linear layers."""
    quantized_model = quant.quantize_dynamic(
        model,
        {nn.Linear}, # Quantize linear layers
        dtype=torch.qint8
    )
    return quantized_model

# Static quantization (requires calibration)
def static_quantize(model, calibration_dataloader):
    """Apply static quantization with calibration."""
    model.eval()

    # Specify quantization configuration
    model.qconfig = quant.get_default_qconfig('fbgemm')

    # Prepare model for quantization
    model_prepared = quant.prepare(model)

    # Calibrate with representative data
    with torch.no_grad():
        for batch in calibration_dataloader:
            model_prepared(batch['input_ids'])

    # Convert to quantized model
    model_quantized = quant.convert(model_prepared)
    return model_quantized

# Quantization-aware training
def quantization_aware_training(model, train_dataloader):
    """Train model with quantization simulation."""
    model.train()
    model.qconfig = quant.get_default_qat_qconfig('fbgemm')

    # Prepare for QAT
    model_prepared = quant.prepare_qat(model)

    # Train normally
    for epoch in range(num_epochs):
        for batch in train_dataloader:
            outputs = model_prepared(batch['input_ids'])
            loss = criterion(outputs, batch['labels'])
            loss.backward()
            optimizer.step()

    # Convert to quantized model
    model_quantized = quant.convert(model_prepared.eval())
    return model_quantized

```

Dynamic quantization typically provides  $2\text{--}3\times$  speedup and  $4\times$  model size reduction with minimal



accuracy loss for transformer models. Static quantization and quantization-aware training can provide additional benefits but require more careful tuning and calibration data.

### 21.8.6 Inference Benchmarking

Comprehensive benchmarking is essential for understanding the trade-offs between different optimization techniques. The following framework measures latency, throughput, and memory usage across different configurations.

```
def benchmark_inference(model, batch_sizes, seq_lengths, num_runs=100):
    """Comprehensive inference benchmarking."""
    results = []
    model.eval()

    for batch_size in batch_sizes:
        for seq_len in seq_lengths:
            # Create input
            input_ids = torch.randint(
                0, 30000, (batch_size, seq_len)
            ).cuda()

            # Warmup
            with torch.no_grad():
                for _ in range(10):
                    _ = model(input_ids)

            # Benchmark
            torch.cuda.synchronize()
            start = time.time()

            with torch.no_grad():
                for _ in range(num_runs):
                    _ = model(input_ids)

            torch.cuda.synchronize()
            elapsed = time.time() - start

            # Calculate metrics
            latency_ms = (elapsed / num_runs) * 1000
            throughput = (batch_size * num_runs) / elapsed
            memory_mb = torch.cuda.max_memory_allocated() / 1e6

            results.append({
                'batch_size': batch_size,
                'seq_len': seq_len,
                'latency_ms': latency_ms,
                'throughput': throughput,
                'memory_mb': memory_mb
            })

            torch.cuda.reset_peak_memory_stats()

    return results

# Compare optimization techniques
```

```
def compare_optimizations(base_model, config):
    """Compare different optimization approaches."""
    models = {
        'baseline': base_model,
        'torchscript': jit.script(base_model),
        'quantized': dynamic_quantize(base_model),
        'fp16': base_model.half()
    }

    results = {}
    for name, model in models.items():
        print(f"Benchmarking {name}...")
        results[name] = benchmark_inference(
            model,
            batch_sizes=[1, 8, 32],
            seq_lengths=[128, 512]
        )

    return results
```

Typical results for BERT-base inference optimization show that combining TorchScript, FP16, and dynamic quantization can achieve 5-8× speedup with less than 1% accuracy degradation, making deployment feasible for latency-sensitive applications.

## 21.9 Complete Training Pipeline

### 21.9.1 Training Script Structure

#### 1. Configuration:

```
config = {
    'd_model': 768,
    'num_heads': 12,
    'num_layers': 12,
    'd_ff': 3072,
    'vocab_size': 30000,
    'max_seq_len': 512,
    'dropout': 0.1,
    'batch_size': 32,
    'learning_rate': 1e-4,
    'warmup_steps': 10000,
    'max_steps': 1000000
}
```

#### 2. Model instantiation:

```
model = BERTModel(**config)
model = model.to(device)
```

#### 3. Optimizer setup:

```
from torch.optim import AdamW
optimizer = AdamW(
    model.parameters(),
    lr=config['learning_rate'],
    betas=(0.9, 0.999),
```

```

    eps=1e-6,
    weight_decay=0.01
)

```

#### 4. Learning rate scheduler:

```

from transformers import get_linear_schedule_with_warmup
scheduler = get_linear_schedule_with_warmup(
    optimizer,
    num_warmup_steps=config['warmup_steps'],
    num_training_steps=config['max_steps']
)

```

#### 5. Training loop with all optimizations:

- Mixed precision
- Gradient accumulation
- Gradient clipping
- Checkpointing
- Logging

## 21.10 Production Optimizations

The implementations shown above can be enhanced with several production optimizations:

- **Combined QKV projection:** Concatenating  $\mathbf{W}_Q$ ,  $\mathbf{W}_K$ ,  $\mathbf{W}_V$  into a single  $d_{\text{model}} \times 3d_{\text{model}}$  matrix reduces kernel launch overhead and improves memory coalescing.
- **Fused layer normalization:** Libraries like NVIDIA Apex provide `FusedLayerNorm` that combines the normalization computation into a single GPU kernel, reducing memory traffic by  $\sim 30\%$ .
- **Pre-norm architecture:** Placing layer normalization before (rather than after) attention and feed-forward sublayers improves training stability for deep models and is standard in GPT-2 and later architectures.
- **FlashAttention:** Using memory-efficient attention implementations (see Chapter 16) dramatically reduces memory consumption for long sequences.

### 21.10.1 Putting It Together

A complete training loop combines the components from this chapter: the model architecture with mixed precision via `torch.cuda.amp`, gradient accumulation for large effective batch sizes, gradient checkpointing for memory savings, and learning rate scheduling with warmup. The training pipeline from Section 21.9 demonstrates this integration. For production deployments, add gradient clipping, periodic checkpointing, and distributed training via `torch.nn.parallel.DistributedDataParallel`.

### 21.10.2 Comprehensive Benchmarks

The following benchmarks demonstrate the impact of various optimizations on memory usage and training speed for a BERT-base model.

#### Baseline Configuration:

- Model: BERT-base (110M parameters)
- Batch size: 32

- Sequence length: 512
- Precision: FP32
- Hardware: NVIDIA A100 40GB

**Optimization Results:**

Configuration	Memory (GB)	Speed (samples/s)	Speedup
Baseline (FP32)	16.2	120	1.0×
+ Mixed Precision	10.1	280	2.3×
+ Gradient Checkpointing	7.8	220	1.8×
+ Optimized Batch Size	7.9	310	2.6×
+ Flash Attention	6.2	420	3.5×
All Optimizations	6.2	420	3.5×

**Inference Optimization Results:**

Configuration	Latency (ms)	Throughput	Memory (GB)
PyTorch FP32	45.2	22	1.8
+ TorchScript	38.1	26	1.8
+ FP16	22.3	45	0.9
+ Dynamic Quantization	18.7	54	0.5
+ TensorRT	9.2	109	0.6
All Optimizations	9.2	109	0.6

These benchmarks demonstrate that combining multiple optimization techniques can achieve substantial improvements in both training and inference performance. The key insight is that different optimizations address different bottlenecks, and the cumulative effect can be dramatic when applied systematically.

## 21.11 Distributed Training

### 21.11.1 Data Parallel

**Simple multi-GPU:**

```
if torch.cuda.device_count() > 1:
    model = nn.DataParallel(model)
```

**Effective batch size:**  $B \times N_{\text{GPUs}}$

### 21.11.2 Distributed Data Parallel (DDP)

**More efficient than DataParallel:**

- One process per GPU
- Gradient synchronization via all-reduce
- Better scaling to multiple nodes

**Setup requires:**

1. Initialize process group
2. Wrap model in DistributedDataParallel
3. Use DistributedSampler for data
4. Synchronize across processes

## 21.12 Performance Optimization

### 21.12.1 DataLoader Optimization

The PyTorch DataLoader is often a bottleneck in training pipelines, particularly when data preprocessing is complex or I/O is slow. Proper configuration of the DataLoader can significantly improve training throughput by ensuring that data loading does not become the limiting factor.

The `num_workers` parameter controls how many subprocesses are used for data loading. Setting this too low results in the GPU waiting for data, while setting it too high can cause excessive CPU and memory usage. A good starting point is to use 4-8 workers per GPU, but the optimal value depends on the specific dataset and preprocessing pipeline.

```
from torch.utils.data import DataLoader

# Optimized DataLoader configuration
dataloader = DataLoader(
    dataset,
    batch_size=32,
    num_workers=8,          # Parallel data loading
    pin_memory=True,        # Faster GPU transfer
    persistent_workers=True, # Keep workers alive between epochs
    prefetch_factor=2       # Prefetch batches per worker
)
```

The `pin_memory` option allocates data in pinned (page-locked) memory, which enables faster transfers to the GPU using asynchronous DMA transfers. This can provide 20-30% speedup for data transfer, particularly beneficial when the model is small relative to the batch size.

Persistent workers keep the worker processes alive between epochs, avoiding the overhead of spawning new processes. This is particularly beneficial for datasets with expensive initialization or when using many workers.

### 21.12.2 Asynchronous Data Transfer

Overlapping data transfer with computation can hide data transfer latency. PyTorch supports non-blocking transfers that allow the CPU to continue executing while data is being copied to the GPU.

```
for batch in dataloader:
    # Non-blocking transfer to GPU
    input_ids = batch['input_ids'].to(device, non_blocking=True)
    labels = batch['labels'].to(device, non_blocking=True)

    # Computation can start while transfer completes
    with autocast():
        outputs = model(input_ids)
        loss = criterion(outputs, labels)
```

This technique is most effective when combined with pinned memory, as it enables true asynchronous transfers. The speedup depends on the ratio of transfer time to computation time, with larger models benefiting more as computation dominates.

### 21.12.3 Profiling with `torch.profiler`

Understanding where time is spent during training is essential for effective optimization. PyTorch's profiler provides detailed information about CPU and GPU operations, memory usage, and kernel execution times.

```

from torch.profiler import profile, ProfilerActivity, schedule

# Configure profiler
profiler_schedule = schedule(
    wait=1,      # Skip first batch
    warmup=1,    # Warmup for 1 batch
    active=3,    # Profile 3 batches
    repeat=2     # Repeat cycle twice
)

with profile(
    activities=[ProfilerActivity.CPU, ProfilerActivity.CUDA],
    schedule=profiler_schedule,
    on_trace_ready=torch.profiler.tensorboard_trace_handler('./log'),
    record_shapes=True,
    profile_memory=True,
    with_stack=True
) as prof:
    for step, batch in enumerate(dataloader):
        if step >= 10: # Profile first 10 batches
            break

        # Training step
        outputs = model(batch['input_ids'].to(device))
        loss = outputs.mean()
        loss.backward()
        optimizer.step()
        optimizer.zero_grad()

        prof.step() # Signal end of iteration

# Print summary
print(prof.key_averages().table(
    sort_by="cuda_time_total", row_limit=10))

```

The profiler output identifies operations that consume the most time, enabling targeted optimization. Common bottlenecks include inefficient attention implementations, excessive memory allocations, and CPU-GPU synchronization points.

#### 21.12.4 Batch Size Tuning

Batch size has a complex relationship with training speed and model quality. Larger batches improve GPU utilization and reduce the number of optimizer steps, but may require learning rate adjustments and can affect convergence.

The optimal batch size maximizes GPU utilization without causing memory overflow. For transformer models, GPU utilization typically plateaus at batch sizes where the GPU is fully occupied, with further increases providing diminishing returns.

```

def benchmark_batch_sizes(model, seq_len, device='cuda'):
    """Benchmark training speed for different batch sizes."""
    results = []

    for batch_size in [8, 16, 32, 64, 128]:
        try:
            torch.cuda.empty_cache()

```

```

torch.cuda.reset_peak_memory_stats()

# Warmup
for _ in range(5):
    input_ids = torch.randint(0, 30000,
                              (batch_size, seq_len)).to(device)
    outputs = model(input_ids)
    loss = outputs.mean()
    loss.backward()

# Benchmark
torch.cuda.synchronize()
start = time.time()

for _ in range(20):
    input_ids = torch.randint(0, 30000,
                              (batch_size, seq_len)).to(device)
    outputs = model(input_ids)
    loss = outputs.mean()
    loss.backward()

torch.cuda.synchronize()
elapsed = time.time() - start

samples_per_sec = (20 * batch_size) / elapsed
memory_gb = torch.cuda.max_memory_allocated() / 1e9

results.append({
    'batch_size': batch_size,
    'samples_per_sec': samples_per_sec,
    'memory_gb': memory_gb
})

except RuntimeError as e:
    if "out of memory" in str(e):
        break

return results

```

### 21.12.5 Compilation with torch.compile

PyTorch 2.0 introduces `torch.compile`, which uses TorchDynamo and TorchInductor to compile models into optimized kernels. This can provide substantial speedups with minimal code changes.

```

# Compile model for faster execution
model = torch.compile(model, mode='max-autotune')

# Training proceeds as normal
for batch in dataloader:
    outputs = model(batch['input_ids'])
    loss = outputs.mean()
    loss.backward()
    optimizer.step()

```

The compilation process analyzes the model's computation graph and generates optimized CUDA

kernels. The first iteration is slow due to compilation overhead, but subsequent iterations benefit from the optimized code. Speedups of 20-50% are common for transformer models, with larger models typically seeing greater benefits.

## 21.13 Distributed Training Implementation

### 21.13.1 Understanding Distributed Strategies

Distributed training enables training on multiple GPUs or machines, dramatically reducing training time for large models. PyTorch provides several distributed training strategies, each with different trade-offs and use cases.

Data parallelism replicates the model on each GPU and distributes different batches of data to each replica. Gradients are synchronized across replicas after the backward pass, ensuring all replicas maintain identical weights. This approach scales well when the model fits in a single GPU's memory and is the most commonly used distributed training strategy.

Model parallelism splits the model itself across multiple GPUs, with different layers or components on different devices. This is necessary when the model is too large to fit on a single GPU but is more complex to implement and can suffer from poor GPU utilization due to sequential dependencies.

### 21.13.2 DistributedDataParallel Setup

DistributedDataParallel (DDP) is PyTorch's recommended approach for multi-GPU training. It provides better performance than DataParallel through more efficient gradient synchronization and support for multi-node training.

```
import torch.distributed as dist
from torch.nn.parallel import DistributedDataParallel as DDP
from torch.utils.data.distributed import DistributedSampler

def setup_distributed(rank, world_size):
    """Initialize distributed training."""
    os.environ['MASTER_ADDR'] = 'localhost'
    os.environ['MASTER_PORT'] = '12355'

    # Initialize process group
    dist.init_process_group(
        backend='nccl', # Use NCCL for GPU training
        rank=rank,
        world_size=world_size
    )

def cleanup_distributed():
    """Clean up distributed training."""
    dist.destroy_process_group()

def train_distributed(rank, world_size, model, dataset):
    """Training function for each process."""
    setup_distributed(rank, world_size)

    # Move model to GPU
    device = torch.device(f'cuda:{rank}')
    model = model.to(device)

    # Wrap model in DDP
    model = DDP(model, device_ids=[rank])
```



```

# Create distributed sampler
sampler = DistributedSampler(
    dataset,
    num_replicas=world_size,
    rank=rank,
    shuffle=True
)

# Create dataloader with distributed sampler
dataloader = DataLoader(
    dataset,
    batch_size=32,
    sampler=sampler,
    num_workers=4,
    pin_memory=True
)

optimizer = AdamW(model.parameters(), lr=1e-4)

# Training loop
for epoch in range(num_epochs):
    sampler.set_epoch(epoch) # Shuffle differently each epoch

    for batch in dataloader:
        input_ids = batch['input_ids'].to(device)
        labels = batch['labels'].to(device)

        outputs = model(input_ids)
        loss = criterion(outputs, labels)

        loss.backward()
        optimizer.step()
        optimizer.zero_grad()

    cleanup_distributed()

# Launch training on multiple GPUs
if __name__ == '__main__':
    world_size = torch.cuda.device_count()
    torch.multiprocessing.spawn(
        train_distributed,
        args=(world_size, model, dataset),
        nprocs=world_size,
        join=True
    )

```

### 21.13.3 Gradient Synchronization

DDP automatically synchronizes gradients across all processes during the backward pass using efficient all-reduce operations. The synchronization happens in parallel with the backward pass through gradient bucketing, which groups gradients into buckets and overlaps communication with computation.

The effective learning rate in distributed training should typically be scaled with the number of GPUs to maintain the same optimization dynamics. If training with 8 GPUs, the learning rate should

be multiplied by 8, or equivalently, the batch size per GPU should be kept constant and gradient accumulation used to achieve the same effective batch size.

### 21.13.4 Scaling Efficiency

Distributed training efficiency is measured by scaling efficiency, which compares actual speedup to ideal linear speedup. Perfect scaling would achieve  $8\times$  speedup with 8 GPUs, but communication overhead and synchronization typically reduce this.

```
def measure_scaling_efficiency(model, batch_size, seq_len):
    """Measure scaling efficiency across different GPU counts."""
    results = {}

    # Single GPU baseline
    single_gpu_time = benchmark_single_gpu(model, batch_size, seq_len)
    results[1] = {
        'time': single_gpu_time,
        'speedup': 1.0,
        'efficiency': 1.0
    }

    # Multi-GPU measurements
    for num_gpus in [2, 4, 8]:
        if num_gpus > torch.cuda.device_count():
            break

        multi_gpu_time = benchmark_multi_gpu(
            model, batch_size, seq_len, num_gpus)
        speedup = single_gpu_time / multi_gpu_time
        efficiency = speedup / num_gpus

        results[num_gpus] = {
            'time': multi_gpu_time,
            'speedup': speedup,
            'efficiency': efficiency
        }

    return results
```

For transformer models, scaling efficiency typically ranges from 85-95% for 2-8 GPUs on a single node, with larger models achieving better efficiency due to higher computation-to-communication ratios. Multi-node training introduces additional communication overhead, with efficiency typically dropping to 70-85% depending on network bandwidth and model size.

## 21.14 Exercises

**Exercise 21.1.** Implement memory-efficient attention:

1. Implement chunked attention computation
2. Compare memory usage with standard attention
3. Test on sequences of length 512, 1024, 2048

4. Measure the memory-speed trade-off for different chunk sizes

**Exercise 21.2.** Optimize BERT training:

1. Start with baseline FP32 training, measure memory and speed
2. Add mixed precision, document improvements
3. Add gradient checkpointing, measure memory savings
4. Profile with torch.profiler and identify remaining bottlenecks
5. Achieve at least  $2\times$  speedup while reducing memory by 40%

**Exercise 21.3.** Implement KV caching for GPT:

1. Modify transformer layer to support KV cache
2. Implement generation with and without caching
3. Benchmark generation speed for 100, 500, 1000 tokens
4. Measure memory overhead of caching
5. Calculate theoretical vs actual speedup

**Exercise 21.4.** Distributed training setup:

1. Implement DistributedDataParallel training
2. Train on 1, 2, 4, 8 GPUs
3. Measure scaling efficiency for each configuration
4. Identify communication bottlenecks
5. Optimize to achieve  $\geq 85\%$  scaling efficiency

**Exercise 21.5.** Inference optimization pipeline:

1. Export model to TorchScript and ONNX
2. Apply dynamic quantization
3. Benchmark latency and throughput for each optimization
4. Create comparison table showing trade-offs
5. Achieve at least  $3\times$  speedup with  $\leq 2\%$  accuracy loss

**Exercise 21.6.** Complete implementation project:

1. Build mini-GPT (6 layers, 8 heads,  $d=512$ ) from scratch
2. Implement all optimizations: mixed precision, checkpointing, KV cache
3. Train on WikiText-2 with comprehensive logging
4. Optimize inference with TorchScript and quantization
5. Generate samples and measure perplexity
6. Document memory usage and speed at each optimization stage

## 21.15 Solutions

Full solutions for all exercises are available at <https://deeplearning.hofkensvermeulen.be>.

## Chapter 22

# From PyTorch to Accelerator Silicon

### Chapter Overview

You understand the mathematics of transformers. You know that attention is a softmax-weighted average over value vectors, that feed-forward networks are two linear projections with a nonlinearity, and that the whole structure repeats for dozens or hundreds of layers. But there is an enormous gap between understanding the math and understanding how it executes. When you write `output = self.attention(x)`, what happens? Which chip does the multiplication? How does data get there? Why does one serving configuration produce ten times the throughput of another on identical hardware?

This chapter is not a catalog of tricks. It is a framework for reasoning about trade-offs. Seven layers of engineering separate your Python code from the transistors. Each layer is an optimization surface with its own controls, constraints, and failure modes. Decisions at one layer propagate to others. An engineer who understands these interactions can diagnose bottlenecks, select optimizations in the right order, and avoid wasted effort.

We use NVIDIA H100 as the primary worked example and explicitly map every concept to AMD MI300X, Google TPU v5p, and AWS Trainium2. For PyTorch quantization implementation code (dynamic, static, and QAT), see Chapter 21.

### Learning Objectives

1. Understand the seven-layer inference stack from model definition to accelerator silicon
2. Reason about the prefill vs. decode asymmetry and its optimization implications
3. Apply tensor, pipeline, and expert parallelism with correct communication patterns
4. Understand frontend runtimes: eager dispatch, lazy tensors, graph capture, compilation, and replay
5. Configure inference engines: continuous batching, PagedAttention, and scheduler knobs
6. Analyze compute-bound vs. memory-bound regimes using roofline reasoning
7. Apply model compression: quantization (FP8, INT8, INT4), pruning, and distillation
8. Diagnose bottlenecks systematically and select optimizations by regime
9. Evaluate hardware across NVIDIA, AMD, TPU, and Trainium platforms

### Three Optimization Objectives

Every optimization targets one or more of three objectives. They often conflict, so you must choose which to prioritize before optimizing:

**Latency:** time from request arrival to first/last token. Dominates interactive and real-time applications. Sensitive to serialized dependencies, interconnect latency, and runtime overhead.

**Throughput:** tokens per second across all concurrent requests. Dominates batch and offline workloads. Sensitive to accelerator utilization, batching efficiency, and memory capacity.

**Cost-efficiency:** tokens per dollar (or per watt). Dominates at scale. Often requires trading latency for throughput via larger batches, aggressive quantization, or fewer devices.

Numbers in this chapter are a mix of conceptual examples, representative measurements from published benchmarks, and platform-specific values. Each is labeled accordingly. Exact performance depends on model, hardware, software versions, and workload shape. Always measure on your own stack.

## 22.1 The Two Phases of Inference: Prefill and Decode

Almost every optimization decision depends on which phase dominates your workload, and the two phases have completely different performance characteristics.

**Prefill (processing the prompt).** The entire prompt is processed in one forward pass. Every token in the prompt is handled simultaneously. If the prompt has 500 tokens, the model runs matrix multiplications on all 500 at once—for example, a  $[500 \times 8192]$  activation matrix times a  $[8192 \times 8192]$  weight matrix. Large matrix multiplications keep the GPU’s compute cores busy. Prefill is *compute-bound*.

**Decode (generating the response).** After prefill, the model generates one token at a time. Each token requires a full forward pass through all layers, but the “batch” of new tokens is tiny—just one new token (or a handful if batching multiple requests). The matrix multiplication is now  $[1 \times 8192]$  times  $[8192 \times 8192]$ . The weight matrix is exactly the same size as during prefill, but the activation vector is tiny. The GPU loads the entire weight matrix from memory just to multiply it by a single row. Decode is *memory-bandwidth-bound*.

This distinction is critical because different bottlenecks require different optimizations:

- Making the compute cores faster (e.g., FP8) helps prefill much more than decode.
- Reducing memory traffic (e.g., quantizing weights so there is less to load) helps decode much more than prefill.
- Reducing communication latency (e.g., faster all-reduce) helps decode more, because decode’s per-token compute is so short that even a few microseconds of communication overhead is proportionally large.

A chatbot generates thousands of decode tokens per request but prefills once, so decode performance usually dominates. A document summarization service might process very long prompts and generate short summaries, so prefill dominates instead.

## 22.2 The Seven-Layer Inference Stack

The path from PyTorch to silicon follows seven conceptual layers, numbered 7 (closest to you) down to 1 (bare metal). The top layers are portable; the bottom layers are device-specific. A single software tool (e.g., XLA) may span multiple conceptual layers. The layer model is an analytical framework, not a claim about software module boundaries.

How the layers interact: Layer 7 determines communication patterns—how often devices must talk and how much data they exchange. Layer 4 determines request shape distributions—how variable or regular the work is. Layers 5 and 2 determine how much overhead is optimized away. Layers 3 and 1 set the execution efficiency ceiling—the physical limits of how fast things can run.

**Key Point 22.1** (Misconception Alert). *A single tool may span multiple layers. XLA implements both graph optimization (Layer 5) and final lowering (Layer 2). vLLM orchestrates scheduling*

#	Layer	What It Controls	Portable?	Example Implementations
7	Model Definition	Architecture dims, parallelism, sharding	Yes	Same <code>nn.Module</code> on all backends
6	Frontend Runtime	Eager dispatch, lazy tracing, compiled capture	Mostly	CUDA/HIP eager; XLA lazy; <code>torch.compile</code>
5	Graph Compilation	Fusion, memory plan, comm scheduling	IR portable	TorchInductor; XLA HLO; NeuronX Compiler
4	Inference Engine	Batching, KV-cache mgmt, orchestration	Concepts yes	vLLM; TensorRT-LLM; NeuronX Serving
3	Device Kernels	GEMM, attention, all-reduce implementations	Concepts only	cuBLAS+NCCL; rocBLAS+RCCL; XLA; Neuron
2	Device Compiler	Final lowering to native ISA, scheduling	No	<code>nvcc</code> →SASS; LLVM→AMDGPU; XLA→TPU ISA
1	Accelerator HW	Compute units, memory hierarchy, interconnect	No	H100+NVLink; MI300X+IF; TPU+ICI; Trn2

Table 22.1: The seven-layer inference stack. Layers 7–5 are portable across vendors. Layers 3–1 are device-specific.

(Layer 4) and inserts collectives (affecting Layer 3). Do not assume one-to-one mapping between tools and layers.

### 22.2.1 Backend Cheat Sheet

This reference maps every concept to its vendor-specific implementation. Later sections cite it rather than repeating the mapping.

Concept	NVIDIA (CUDA)	AMD (ROCm)	Google TPU	AWS Trainium
Graph capture	<code>torch.compile</code>	<code>torch.compile</code>	XLA lazy/compile	<code>torch.neuronx.trace</code>
IR	Inductor/Triton	Inductor+HIP	StableHLO/HLO	Neuron HLO
GEMM library	cuBLAS/CUTLASS	rocBLAS/CK	XLA GEMM	Neuron GEMM
Attention kernel	FlashAttention-2/3	CK FlashAttn	Pallas attention	Neuron attention
All-reduce	NCCL	RCCL	XLA collectives	Neuron collectives
LLM engine	vLLM, TRT-LLM	vLLM ROCm	vLLM TPU	NeuronX Serving
Graph replay	CUDA Graphs	hipGraphs	XLA executable	Neuron NEFF
Intra-node link	NVLink/NVSwitch	Infinity Fabric	ICI torus	NeuronLink
Inter-node fabric	InfiniBand NDR	InfiniBand NDR	ICI across pods	EFA (3.2 Tb/s)

Table 22.2: Backend cheat sheet: vendor-specific implementations of each inference stack concept.

### 22.2.2 Latency and Bandwidth Ladder

## 22.3 Layer 7: The Model Definition

When you define a transformer in PyTorch, you lock in decisions that propagate through every layer below.

**Tensor shapes:** hidden dimension  $H$ , head count, KV-head count, FFN intermediate size, layer count. These determine every GEMM shape, every collective message size, and the memory footprint breakdown.

Link Type	Example	BW (bidi)	Latency	Scope	Use Case
NVLink 4.0	H100 (8 GPUs)	900 GB/s	$\sim 1\text{--}2\ \mu\text{s}$	Intra-node	TP, EP
NVLink 5.0	B200 (72 via NVSwitch)	1.8 TB/s	$\sim 1\text{--}2\ \mu\text{s}$	Multi-rack	Extended TP
ICI torus	TPU v5p pod slice	Multi-TB/s	$\sim 1\text{--}3\ \mu\text{s}$	Within pod	TP/EP
Infinity Fabric	MI300X (8 GPUs)	$\sim 896\ \text{GB/s}$	$\sim 2\text{--}3\ \mu\text{s}$	Intra-node	TP, EP
NeuronLink	Trn2 (16 chips)	$\sim 1.6\ \text{TB/s}$	$\sim \text{few}\ \mu\text{s}$	Intra-instance	TP
InfiniBand NDR	Multi-node cluster	400 Gb/s/port	$\sim 5\text{--}10\ \mu\text{s}$	Cross-node	PP, param sync
EFA	AWS instances	3.2 Tb/s/inst	$\sim 5\text{--}15\ \mu\text{s}$	Cross-node	PP, cross-inst EP

Table 22.3: Interconnect latency and bandwidth ladder. TP (frequent, latency-sensitive) goes on the fastest link. PP (infrequent, large) tolerates slower links. EP (all-to-all) requires high bisection bandwidth.

**Divisibility constraints:** head counts must divide evenly by TP degree. KV-head counts must also divide. FFN dimensions affect kernel tile efficiency.

**Communication patterns:** TP degree fixes the number and frequency of all-reduces. PP depth fixes stage boundary point-to-point transfers. EP determines all-to-all topology requirements.

**Memory footprint classes:** model weights, KV-cache per token, activation memory per layer. Each scales differently with parallelism.

**Key Point 22.2** (What Layer 7 Cannot Fix Later). *Poor divisibility (e.g., 8 KV-heads with TP-3 gives 8/3 which is not integer), hidden dimensions misaligned with kernel tile sizes (typically multiples of 128), or an architecture whose communication volume exceeds interconnect capacity at the target TP degree.*

### 22.3.1 Why Multi-Device Execution Is Required

Multi-device execution is required for three distinct reasons, and they are not equivalent:

**Parameter memory fit.** A 70B model needs  $\sim 140\ \text{GB}$  in BF16 ( $70 \times 10^9 \times 2$  bytes). An H100 has 80 GB, a TPU v5p has 95 GB, and a Trainium2 has 96 GB—the weights alone do not fit. MI300X at 192 GB can hold 70B weights plus meaningful KV-cache on one device, but this is the exception.

**KV-cache fit.** Even if weights fit, the KV-cache can be enormous. For a 70B model with 128K context length and 80 layers, a single request at full context can require 10+ GB. A few concurrent requests exhaust remaining memory.

**Throughput and latency targets.** Even if everything fits, a single device may not meet requirements. A single GPU must stream all 140 GB of weights through memory for every decode token—that alone takes  $\sim 42\ \text{ms}$  at 3.35 TB/s on H100. Splitting weights across 4 GPUs means each streams only 35 GB, roughly  $4\times$  faster.

### 22.3.2 Tensor Parallelism: Splitting Weight Matrices

#### What All-Reduce Actually Does

Imagine four devices, each holding a number: Device 0 has 10, Device 1 has 20, Device 2 has 30, Device 3 has 40. An all-reduce(sum) computes the sum ( $10 + 20 + 30 + 40 = 100$ ) and distributes the result to every device. After the all-reduce, all four devices hold the value 100.

In LLM inference, the “numbers” are tensors—vectors or matrices of thousands of floating-point values. When TP splits a weight matrix across devices, each device computes a partial result. The all-reduce sums these partial results so every device gets the complete answer.

Two critical characteristics of all-reduce determine TP’s performance impact:

**Frequency:** a standard transformer block requires two all-reduces per layer (one after the attention output projection, one after the FFN down-projection). For an 80-layer model, that is 160 all-reduces per token generated.



**Message size:** during decode, the data being summed is a vector of size  $[H]$  in the chosen precision. For  $H = 8192$  in BF16:  $8192 \times 2 = 16,384$  bytes = 16 KB. At 900 GB/s of NVLink bandwidth, 16 KB transfers in nanoseconds—but the latency of initiating the all-reduce ( $\sim 1\text{--}2 \mu\text{s}$ ) dominates. This is why decode TP performance is *latency-bound*, not bandwidth-bound.

### Column-Parallel and Row-Parallel GEMMs

TP splits weight matrices across devices using two deliberately paired patterns.

**Column-parallel GEMM (no communication needed).** Split weight matrix  $\mathbf{W}$  with shape  $[8192 \times 8192]$  by columns: Device 0 gets  $[8192 \times 4096]$ , Device 1 gets  $[8192 \times 4096]$ . Input  $\mathbf{x} [1 \times 8192]$  goes to both devices. Each produces half the output. No communication needed—but each device only has half the result.

**Row-parallel GEMM (all-reduce required).** The next weight matrix is split by rows. Each device multiplies its local input half by its local weight half, producing partial sums  $[1 \times 8192]$ . These must be summed via all-reduce to get the correct result.

**Key Point 22.3** (The Megatron-LM Pairing). *By alternating column-parallel then row-parallel within each transformer block, the column-parallel output feeds directly as the row-parallel input. Only the row-parallel step needs an all-reduce. A standard transformer block has two such pairs (attention: QKV column-parallel  $\rightarrow$  output row-parallel; FFN: gate/up column-parallel  $\rightarrow$  down row-parallel), so each layer needs exactly two all-reduces. This pattern works identically on any hardware that supports all-reduce.*

**Per-layer communication volume.** Bytes per all-reduce per device =  $H \times p$ , where  $p$  = bytes per element. Per layer:  $2 \times H \times p$ . For decode with  $H = 8192$ , BF16:  $2 \times 8192 \times 2 = 32$  KB per layer. For 80 layers:  $\sim 2.6$  MB total.

**Example 22.1** (Complete Per-Device Walkthrough: TP-2). Trace one transformer layer with TP-2.  $H = 8192$ , 32 query heads (GQA: 8 KV-heads,  $d_{\text{head}} = 256$ ), FFN = 22016. Decode:  $B = 1$ ,  $S = 1$ . All values BF16.

**Step 1 — QKV Projection (column-parallel, NO communication).** Both devices receive the same input  $\mathbf{x} [1 \times 8192]$ . Each multiplies by its local Q, K, V column shards. Device 0 produces:  $\mathbf{Q}_0 [1 \times 4096]$  (heads 0–15),  $\mathbf{K}_0 [1 \times 512]$  (KV-heads 0–3),  $\mathbf{V}_0 [1 \times 512]$ .

**Step 2 — Attention (local, NO communication).** Each device runs attention on its own heads against its own KV-cache shard. Completely independent per device.

**Step 3 — Output Projection + ALL-REDUCE.** Row-parallel step. Each device computes partial =  $[1 \times 4096] \times [4096 \times 8192] = [1 \times 8192]$ . All-reduce sums them. Data transferred:  $8192 \times 2 = 16$  KB per device.

**Steps 4–5 — FFN (same column $\rightarrow$ row pattern).** Column-parallel gate+up (no communication), local SwiGLU, row-parallel down + all-reduce (another 16 KB).

**Total for this layer:** 2 all-reduces, 32 KB moved. For 80 layers: 160 all-reduces,  $\sim 2.6$  MB. At NVLink latencies of  $\sim 1\text{--}2 \mu\text{s}$  per all-reduce, communication overhead is  $\sim 160\text{--}320 \mu\text{s}$  per token. On slow interconnects (InfiniBand at  $\sim 5\text{--}10 \mu\text{s}$ ), the same 160 all-reduces cost  $800\text{--}1600 \mu\text{s}$ —up to 30% overhead. This is why TP must use the fastest available link.

### 22.3.3 Pipeline Parallelism

While TP splits every layer across devices, PP assigns entire layers to different devices. Device 0 computes layers 0–39; Device 1 computes layers 40–79. Each device holds complete, unsharded weights for its assigned layers.

Communication is point-to-point: after Device 0 finishes, it sends the activation tensor to Device 1. During prefill with a 2048-token prompt: activation =  $[1 \times 2048 \times 8192] \times 2$  bytes = 32 MB. But this

transfer happens only once per stage boundary, not once per layer. During decode ( $S = 1$ ): only 16 KB. PP therefore tolerates higher-latency links.

**Pipeline bubble:** the key drawback. With simple scheduling, the fraction of time wasted to bubbles is roughly  $1/\text{PP\_degree}$ . Micro-batching reduces this by feeding multiple small batches in rapid succession. Decode is particularly vulnerable because each micro-batch has so little compute that communication latency between stages becomes proportionally larger.

### 22.3.4 Expert Parallelism

EP is specific to Mixture-of-Experts (MoE) models, where each transformer layer has multiple “expert” FFN blocks and a router that sends each token to only 1–2 experts. EP places different experts on different devices. The communication pattern is all-to-all: every device may need to send tokens to every other device.

All-to-all is the most interconnect-demanding collective. This is where bisection bandwidth matters: if you split 8 devices into two groups of 4, the total bandwidth between the groups determines how fast all-to-all runs. NVSwitch provides full bisection bandwidth for 8 GPUs. InfiniBand and EFA between nodes typically do not provide sufficient bisection bandwidth for efficient cross-node EP.

**Routing skew risk:** if the router disproportionately sends tokens to a few experts, those devices become bottlenecks while others idle. Load-balancing losses and capacity factors in the model architecture (Layer 7) directly affect hardware utilization at Layers 3/1.

Multiple specialized EP kernel libraries have emerged for inter-node communication:

Aspect	DeepEP	PPLX-Kernels	UCCL-EP	NCCL a2a
GPU vendor	NVIDIA only	NVIDIA only	NVIDIA + AMD	NVIDIA (+AMD)
NIC requirement	Mellanox CX (IB)	EFA or IB	Any RDMA	Any
GPU-to-NIC path	IBGDA (direct)	NVSHMEM+libfabric	CPU proxy	CPU-initiated
FP8 support	Native	Native + block scaling	Native	Via framework
Cloud deployment	On-prem IB	AWS (EFA) + IB	AWS, GCP, on-prem	Any

Table 22.4: EP kernel library comparison for inter-node MoE communication.

### 22.3.5 Context Parallelism and Sequence Parallelism

**Context Parallelism (CP)** addresses what happens when the sequence is so long that the KV-cache for a single request does not fit on one device. CP splits the sequence across devices. Ring attention is the most common implementation: devices are arranged in a logical ring, each computing attention for its local chunk against its local KV block, then passing its KV block to the next device.

**Sequence Parallelism (SP)** is a refinement of TP that reduces memory usage. In standard TP, activations between GEMMs are replicated on every device. SP uses reduce-scatter (each device gets  $1/P$  of the result) followed by a deferred all-gather. Between GEMMs, each device holds only  $1/P$  of the activations. Total communication volume is the same, but peak activation memory drops by the TP degree.

### 22.3.6 Parallelism Selection Framework

Scenario	Start with	Why	Watch out for
Dense model, doesn’t fit	TP first, then PP	TP distributes every layer	TP beyond NVLink domain
Decode latency critical	TP, minimize degree	Each TP AR adds latency	Over-aggressive TP
Long context, high concurrency	TP + CP or KV quant	KV-cache dominates memory	CP ring overhead
MoE model	EP first, TP within	EP native to MoE	All-to-all needs bisection BW

Table 22.5: Parallelism selection framework: start from requirements and work down.

## 22.4 Layer 6: Frontend Runtime

This layer determines how Python model code translates into work that lower layers execute. It controls execution semantics (eager vs. lazy vs. compiled dispatch), Python-to-accelerator overhead, and how operations are grouped before graph compilation.

### 22.4.1 Eager Mode (NVIDIA, AMD)

Default PyTorch on CUDA/ROCm: each operation dispatches immediately. When your code calls `torch.matmul(x, w)`, PyTorch’s C++ dispatcher selects a kernel, launches it on the GPU, and returns control to Python. Each dispatch involves Python interpreter overhead, C++ dispatch, kernel launch, and potentially synchronization.

For large operations (e.g., a big prefill GEMM that takes milliseconds), this overhead is negligible. But during decode with TP-4, individual GEMMs on tiny tensors may take only 5–15  $\mu$ s of actual compute. If every dispatch adds 3–5  $\mu$ s of overhead, the overhead is 20–50% of compute time.

### 22.4.2 Lazy Tensor Mode (TPU, Trainium)

On TPU, PyTorch/XLA records operations into a graph instead of executing each immediately. Operations accumulate until an explicit barrier (`xm.mark_step()`), at which point XLA compiles the entire graph, caches the result, and dispatches it as a single unit. The advantage: XLA can optimize many operations together. The downside: debugging is harder because errors surface only at compilation time. Trainium supports both lazy tensors (via XLA) and `torch.compile` (via torch-neuronx).

### 22.4.3 Graph Capture, Compilation, and Replay

These three concepts are frequently conflated but are distinct steps with different costs and benefits.

**Definition 22.1** (Graph Capture, Compilation, and Replay). **Step 1: Graph capture** records what operations to perform, in what order, with what tensor shapes—without executing them. Mechanisms: `torch.compile` (Dynamo traces Python), XLA lazy tensors, `torch.neuronx.trace`. Capture alone provides almost no performance benefit.

**Step 2: Graph compilation** (Layer 5) optimizes the captured graph: fusing operations, planning memory layout, scheduling communication. Compilation can take seconds to minutes, but produces much faster execution.

**Step 3: Graph replay** (Layer 2) re-executes a compiled graph with new input data—as long as tensor shapes are identical. On NVIDIA: CUDA Graphs. On AMD: hipGraphs. On TPU: XLA cached executables. On Trainium: Neuron NEFFs. Replay skips both capture and compilation entirely.

The three steps are cumulative: capture alone does little, capture + compilation gives moderate benefit, capture + compilation + replay gives the full benefit. For production serving, all three are essential.

**Key Point 22.4** (Why Replay Requires Static Shapes). *The compiled execution plan includes specific memory addresses, buffer sizes, and kernel launch configurations that depend on tensor dimensions. If you change the batch size from 16 to 17, every buffer size changes and the old plan is invalid. Shape bucketing (Section 22.5) addresses this by pre-compiling plans for a fixed set of shapes.*

### 22.4.4 Process Groups and Communicators

Multi-device collectives require process groups that define which devices participate together. In a TP-4, PP-2 deployment on 8 devices: two TP groups exist (devices  $[0, 1, 2, 3]$  and  $[4, 5, 6, 7]$ ). Four PP groups exist as device pairs across stages (e.g.,  $[0, 4]$ ,  $[1, 5]$ ). Model code (Layer 7) defines group shapes; the serving framework (Layer 4) instantiates them; the communication library (Layer 3) automatically selects the best algorithm.

## 22.5 Layer 5: Graph Compilation

Graph compilation transforms a captured operation graph into an optimized execution plan. It controls which operations are fused, how memory is allocated and reused, how communication is scheduled relative to computation, and what IR is emitted for the device compiler.

### 22.5.1 Four Optimization Mechanisms

**1. Host overhead elimination.** Replaces per-op Python dispatch with a single graph launch. Most impactful for decode, where individual operations are tiny.

**2. Memory traffic reduction via fusion.** Combines operations that share intermediate tensors into fused kernels. Without fusion, each intermediate is written to HBM and read back. Fusion keeps intermediates in fast on-chip memory. Most impactful for prefill, where intermediate tensors are large.

**3. Memory layout planning.** Optimizes tensor arrangement in memory (row-major vs. column-major) to match downstream kernel access patterns. Poor layout can halve bandwidth utilization.

**4. Communication scheduling.** Overlaps collective communication with computation by scheduling them on separate hardware resources. Impactful whenever TP all-reduce is on the critical path.

### 22.5.2 Fusion Taxonomy

Vendor documentation uses “fusion” to mean three very different things. Confusing them leads to incorrect performance reasoning.

**Operator fusion** combines multiple logical operations into a single kernel launch. Example:  $\text{GEMM} \rightarrow \text{bias add} \rightarrow \text{ReLU}$  becomes one kernel. Intermediate results never leave on-chip memory.

**Kernel fusion** is a specialized, hand-written kernel implementing a complex multi-step computation internally. The canonical example is FlashAttention: instead of computing  $\mathbf{QK}^\top$  (writing the enormous  $N \times N$  attention matrix to HBM), applying softmax, then multiplying by  $\mathbf{V}$ , FlashAttention does all of this inside a single kernel by tiling the computation into blocks that fit in shared memory (228 KB on H100). For a 2048-token sequence, the naive attention matrix would be  $2048 \times 2048 \times 2$  bytes = 8 MB—FlashAttention eliminates this entirely from HBM traffic.

**Schedule overlap** runs communication and computation simultaneously on different hardware resources. A GPU has Tensor Cores for compute and NVLink controllers for communication—physically different silicon that can operate in parallel. This is not fusion; the operations remain separate.

**Example 22.2** (Layer Norm + Dropout Fusion). Consider layer normalization followed by dropout on a tensor of shape  $[32, 128, 768]$ .

**Unfused:** Layer norm kernel reads/writes 3.1M elements; dropout kernel reads/writes 3.1M elements. Total memory traffic: 24.8 MB (FP16). Time: 0.18 ms.

**Fused:** Single kernel reads/writes 3.1M elements. Total traffic: 12.4 MB. Time: 0.10 ms. The  $1.8\times$  speedup comes from halving memory traffic. For a 12-layer transformer, this fusion appears 24 times per forward pass.

### 22.5.3 Static Shapes and Shape Bucketing

Graph replay requires that every tensor has exactly the same shape as when compiled. Real inference requests have variable sequence lengths. The solution is *shape bucketing*: the inference engine rounds each request’s dimensions up to the nearest bucket boundary (e.g., [64, 128, 256, 512, 1024, 2048, 4096]). Each bucket has a pre-compiled graph. More buckets means less padding waste but a larger compile cache.

### 22.5.4 When Compilation Hurts

**Compile time:** initial compilation can take seconds to minutes. For short-running jobs, this overhead may dominate.

**Graph breaks:** if the compiler encounters an unsupported operation, it falls back to eager mode for that region. A single graph break can negate most compilation benefits.

**Shape churn:** on XLA and Neuron, every new tensor shape triggers a new compilation. Without bucketing, variable-length requests cause continuous recompilation.

For production serving, compilation costs are amortized over millions of requests and almost always worthwhile. For development and debugging, eager mode provides faster iteration.

## 22.6 Layer 4: Inference Engines

Inference engines are purpose-built LLM serving runtimes. They control which requests to process and when (admission and scheduling), how to group requests (batching), where to store the KV-cache and when to evict it (memory management), and how to distribute work across devices (orchestration). End-to-end gains from a well-configured inference engine are typically 3–20× over naive PyTorch inference.

### 22.6.1 Continuous Batching

In static batching, you collect  $N$  requests, pad them to the same length, process the entire batch, and wait for every request to finish. If one request generates 10 tokens and another generates 500, the first request’s GPU resources sit idle until the 500-token request completes.

Continuous batching (also called iteration-level batching) checks the state of every request at every decode iteration. When a request finishes, the scheduler immediately inserts a new request into the freed slot. The GPU stays saturated instead of idling.

#### Scheduler Knobs

**Max batch size** limits concurrent active requests. During decode, each request contributes one token to the per-iteration GEMM. A batch of 16 means  $[16 \times H]$ ; a batch of 256 means  $[256 \times H]$ . Increasing batch size improves arithmetic intensity until the GEMM becomes compute-bound. Too low: poor GPU utilization. Too high: KV-cache memory exhaustion and increased inter-token latency (ITL).

**Max tokens per iteration** limits total tokens (prefill + decode) per scheduler step. A large prefill can monopolize an iteration, spiking ITL for all active decode requests. Chunked prefill—splitting long prompts across iterations—is the standard solution.

**Admission policy** determines which waiting request to admit next. FIFO is simplest but causes head-of-line blocking. Priority queues enable SLO differentiation. Shortest-job-first minimizes average latency but requires length estimation.

**Preemption policy** determines what happens when KV-cache memory runs out. Options: swap KV to CPU (preserves state, costs PCIe bandwidth), recomputation (discards KV, re-prefills later), or request rejection.

### 22.6.2 PagedAttention: Virtual Memory for the KV-Cache

The KV-cache stores key and value vectors from every token processed so far. The naive approach allocates a contiguous block per request sized for the maximum context length, wasting 60–80% of KV memory on average.

Knob	Controls	Increase →	Decrease →	Trade-off
Max batch size	Concurrent requests	↑ Throughput, ↑ ITL	↓ Throughput, ↓ ITL	Throughput vs. latency
Max tokens/step	Prefill chunk size	↑ Prefill tput, ↑ ITL spikes	Better ITL protection	TTFT vs. ITL
Admission policy	Request ordering	(varies by policy)	(varies)	Fairness vs. efficiency
Preemption policy	Memory overflow	(swap/recompute/reject)	(varies)	Latency vs. memory

Table 22.6: Continuous batching scheduler knobs and their trade-offs.

PagedAttention, inspired by OS virtual memory, divides the KV-cache into small fixed-size pages (e.g., 16 tokens per page). A page table maps each request to its pages. As a request grows, new pages are allocated on demand. When a request finishes, pages are immediately freed.

**Benefits:** no internal fragmentation; memory utilization jumps dramatically; prefix caching allows shared system-prompt pages across requests.

**Cost:** attention kernels must follow the page table to find each KV block, adding pointer indirection. Optimized block-sparse attention kernels minimize this overhead.

### 22.6.3 vLLM and PagedAttention

vLLM is a production-grade LLM serving system that maximizes throughput by managing KV-cache memory with near-zero waste. Its core contribution is PagedAttention: instead of storing each sequence’s KV-cache in a single contiguous buffer, vLLM partitions the cache into fixed-size “KV blocks” and maintains a block table mapping logical positions to physical blocks. This indirection enables fine-grained sharing and compaction.

During inference, new tokens are appended by allocating additional KV blocks and updating the block table, without relocating existing data. When a request finishes, its blocks are recycled immediately. Empirical evaluations show vLLM delivers 2–4× higher throughput than earlier systems at similar latency, with gains increasing for longer contexts.

### 22.6.4 Multi-Device Orchestration

In vLLM, linear layers are wrapped in TP-aware modules at model load time, weights are sharded across devices, and all-reduce calls are inserted after each row-parallel GEMM. For decode’s tiny all-reduce messages (~16 KB), vLLM includes custom small-message kernels that bypass general-purpose NCCL overhead. The engine architecture (scheduler, cache manager, router) is backend-agnostic: vLLM supports CUDA, ROCm, and TPU backends.

### 22.6.5 Request Lifecycle

1. **Admission:** scheduler checks KV-cache page availability and batch capacity. If insufficient, queues, preempts, or rejects.
2. **Prefill:** full prompt processed in one forward pass. Large, compute-heavy GEMMs. KV-cache pages allocated as KV vectors are computed.
3. **Decode loop:** one token per iteration. Scheduler selects batch → graph replay launches compiled decode graph → local GEMMs and attention → all-reduces synchronize TP → logits sampled.
4. **Completion:** KV-cache pages reclaimed, batch slot freed, next waiting request admitted.

### 22.6.6 Throughput vs. Latency Tuning Profiles

## 22.7 Layer 3: Device Kernels and Collectives

This layer provides hardware-tuned implementations of compute (GEMM, attention) and communication (all-reduce, all-to-all) operations. It controls memory access patterns, on-chip data reuse, instruction scheduling, and collective algorithms.

Dimension	Interactive (latency-optimized)	Batch (throughput-optimized)
Target metric	TTFIT, ITL	Tokens/second/dollar
Batch size	Small (1–16)	Large (64–512)
TP degree	Moderate (TP-2 or TP-4)	Higher OK (TP-4 or TP-8)
Graph replay	Essential for decode	Helpful, less critical
Quantization	Conservative (FP8 or BF16)	Aggressive (FP8 + KV quant)
KV-cache	PagedAttention + prefix caching	PagedAttention + large page pool

Table 22.7: Tuning profiles for interactive vs. batch workloads on the same hardware.

### 22.7.1 The Memory Hierarchy Problem

The gap between an untuned implementation and a hardware-optimized kernel is often 10–20 $\times$  for GEMM. The reason is the memory hierarchy:

Level	H100	MI300X	TPU v5p	Relative Cost
Registers	256KB/SM	Similar/CU	VRF/MXU	1 $\times$ (fastest)
Shared/Local memory	228KB/SM	64KB LDS/CU	CMEM (on-chip)	$\sim 5\text{--}10\times$ slower
L2 cache	50MB	256MB	Compiler-managed	$\sim 20\text{--}50\times$ slower
HBM (main memory)	80GB, 3.35TB/s	192GB, 5.3TB/s	95GB, 2.76TB/s	$\sim 100\text{--}500\times$ slower

Table 22.8: Memory hierarchy across accelerator platforms. The actual arithmetic is fast; moving data from HBM to compute cores is what costs time.

A naive matrix multiplication loads each element from HBM multiple times. A tuned kernel *tiles* the computation: it loads a block into fast shared memory, does all multiplications that need that block, then loads the next block. FlashAttention is the poster child: standard attention writes the  $N \times N$  score matrix to HBM and reads it back multiple times. FlashAttention tiles all three steps (Q $\times$ K, softmax,  $\times$ V) so the score matrix never leaves shared memory.

### 22.7.2 Compute-Bound vs. Memory-Bound: The Roofline

**Definition 22.2** (Arithmetic Intensity and the Roofline). Arithmetic intensity measures FLOPs per byte loaded from memory:

$$\text{Arithmetic Intensity} = \frac{\text{FLOPs}}{\text{Bytes transferred}} \quad (22.1)$$

A kernel is compute-bound if its arithmetic intensity exceeds the hardware’s ops:byte ratio; memory-bound otherwise. For H100: 990 TFLOPS/3.35 TB/s  $\approx$  295 FLOPs/byte.

**Example 22.3** (Decode vs. Prefill Roofline Analysis). **Decode** ( $B = 1$ ): GEMM  $[1 \times 8192] \times [8192 \times 8192]$ . Compute:  $2 \times 8192^2 = 134\text{M}$  FLOPs. Weight matrix: 128 MB. Intensity  $\approx 1$  FLOP/byte. Massively below the 295 balance point—*entirely memory-bandwidth-bound*. Tensor Cores finish instantly, then sit idle waiting for weights.

**Prefill** ( $B = 256$ ): GEMM  $[256 \times 8192] \times [8192 \times 8192]$ . Compute: 34.4B FLOPs. Weights still 128 MB. Intensity  $\approx 269$  FLOPs/byte—near the balance point. Compute and memory are roughly balanced.

This is why FP8 helps prefill much more than decode: prefill is near-compute-bound, so doubling TFLOPS roughly doubles throughput. Decode is bandwidth-bound, so doubling TFLOPS does nothing.



### 22.7.3 Coalesced Memory Access and Bank Conflicts

When threads in a warp access global memory, the hardware attempts to combine accesses into a single transaction. Coalesced access (consecutive threads accessing consecutive locations) allows one 128-byte transaction instead of 32 separate ones. For transformer operations, ensuring consecutive threads load consecutive elements of the query matrix allows full bandwidth utilization.

Shared memory is divided into 32 banks. When multiple threads access the same bank at different addresses, a bank conflict serializes the accesses. Careful padding of shared memory tiles eliminates conflicts.

**Example 22.4** (Shared Memory Optimization in Attention). Computing  $\mathbf{A} = \mathbf{QK}^\top$  with tiles loaded into shared memory:

**Unoptimized:** Tile  $64 \times 64$  FP16 values (8192 bytes). 32-way bank conflicts when accessing columns. Effective bandwidth: 50 GB/s (3% of peak).

**Optimized with padding:** Tile  $64 \times 72$  FP16 values (9216 bytes, 8 elements padding per row). No bank conflicts. Effective bandwidth: 1.4 TB/s (88% of peak). The 12.5% increase in shared memory usage yields  $28\times$  bandwidth improvement.

### 22.7.4 Flash Attention

Standard attention implementations compute  $\mathbf{A} = \mathbf{QK}^\top$ , write  $\mathbf{A}$  to HBM, read it back for softmax, write the result, read it again for multiplication with  $\mathbf{V}$ . This results in  $O(n^2)$  memory reads and writes.

Flash Attention restructures the computation to work on tiles that fit in shared memory, computing attention for one tile at a time and only writing the final output. This reduces memory traffic from  $O(n^2)$  to  $O(n)$ .

**Example 22.5** (Flash Attention Performance). BERT-base with sequence length 512, batch size 16, on A100 GPU:

**Standard attention:** 48 GB memory traffic, 8.2 ms, 45% bandwidth utilization.

**Flash Attention:** 12 GB traffic ( $4\times$  reduction), 3.8 ms ( $2.2\times$  speedup), 82% utilization.

At sequence length 2048:  $3.5\times$  speedup. At 8192:  $5.2\times$  speedup while also enabling sequences that would otherwise exceed memory.

### 22.7.5 Collective Communication

All-reduce, all-gather, reduce-scatter, all-to-all, and point-to-point are the five collective primitives. Each platform implements them through specialized libraries (see Table 22.2). The library automatically selects the best algorithm: latency-optimized for small messages (decode’s 16 KB), bandwidth-optimized (ring or tree) for large messages (prefill’s multi-MB).

### 22.7.6 Kernel Failure Modes

**Shape misalignment:** dimensions not aligned to tile sizes (e.g., not multiples of 128) cause padding waste or fallback to slower kernels.

**Tiny messages:** all-reduce for small decode tensors is latency-dominated regardless of bandwidth.

**Register pressure:** aggressively fusing many operations increases register usage, potentially reducing occupancy and overall throughput.

**Local speedup, global bottleneck:** a  $2\times$  faster kernel does not help if the bottleneck is scheduler overhead (Layer 4) or interconnect latency (Layer 1). Always verify that optimizing a kernel helps the end-to-end metric.



## 22.8 Layers 2 and 1: Device Compiler and Accelerator Hardware

### 22.8.1 Layer 2: Device Compiler and Runtime

Layer 2 takes the optimized graph from Layer 5 and produces native machine instructions. It controls register allocation, instruction scheduling, memory coalescing, occupancy tuning, and execution dispatch.

Aspect	NVIDIA CUDA	AMD ROCm	Google TPU	AWS Trainium
Compiler	nvcc $\rightarrow$ PTX $\rightarrow$ SASS	hipcc $\rightarrow$ LLVM $\rightarrow$ AMDGPU	XLA HLO $\rightarrow$ TPU ISA	Neuron Compiler
User control	High	High	Low (XLA manages)	Low (Neuron manages)
Execution	CUDA streams + Graphs	HIP streams + hipGraphs	XLA scheduling	Neuron runtime + Neuron
Profiling	Nsight, nvprof	rocprof, ROCm SMI	XLA/TPU profiler	Neuron monitor

Table 22.9: Device compiler and runtime across platforms.

Most Layer 2 effects are influenced indirectly via Layer 4/5 choices (graph structure, shape regularity), not by direct user intervention.

### 22.8.2 Layer 1: Accelerator Hardware

Hardware sets the ceiling on execution efficiency. Software stack maturity can dramatically affect how much of the ceiling is actually reached—a mature stack may achieve 60–70% of peak while an immature one achieves 20–30%.

Spec (per chip)	H100 SXM	B200 SXM	MI300X	TPU v5p	Trn2
Compute units	132 SMs	192 SMs	304 CUs	4 MXUs/chip	32 NeuronCores
BF16 peak TFLOPS	990	~2,250	1,307	~459	~380
HBM capacity	80 GB HBM3	192 GB HBM3e	192 GB HBM3	95 GB HBM2e	96 GB HBM
HBM bandwidth	3.35 TB/s	8 TB/s	5.3 TB/s	2.76 TB/s	~1.6 TB/s
FP8 support	Native	Native	Native	INT8/FP8-like	Native FP8

Table 22.10: Accelerator hardware comparison (February 2026 snapshot). All values are per-chip peak specifications. Sustained performance is typically 40–70% of peak.

### 22.8.3 How to Read Spec Sheets Without Fooling Yourself

**Peak TFLOPS  $\neq$  LLM performance.** Decode is memory-bandwidth-bound. A chip with  $2\times$  the TFLOPS but similar HBM bandwidth will not decode  $2\times$  faster.

**HBM bandwidth matters, but access patterns matter more.** Coalesced sequential access achieves near-peak bandwidth. Random or strided access may achieve only 30–50% of peak.

**Interconnect latency dominates decode TP performance.** During decode, all-reduce messages are tiny ( $\sim 16$  KB). A  $2\times$  higher-bandwidth interconnect with the same latency provides zero decode benefit.

**Software stack maturity can outweigh raw specs.** A chip with inferior specs but a mature, optimized software stack often outperforms a faster chip with immature software.

### 22.8.4 Workload-to-Hardware Fit

## 22.9 Quantization: Precision, Performance, and Trade-offs

### 22.9.1 Quantization Taxonomy

Quantization means using fewer bits to represent numbers. Standard transformer inference uses BF16 (2 bytes per number). Quantization reduces this to 8 bits (FP8 or INT8, 1 byte) or even 4 bits (INT4,

Workload Profile	Key Hardware Dimension	Why
Decode-heavy, low-latency	Interconnect latency + HBM BW	Weight loading + AR latency dominate
Long-context, high-concurrency	HBM capacity + KV strategy	KV-cache dominates memory
Prefill-heavy, batch throughput	Compute TFLOPS + HBM BW	Large GEMMs are compute-bound
MoE with EP	Bisection bandwidth + topology	All-to-all needs every device to talk

Table 22.11: Matching workload profiles to the hardware dimension that matters most.

0.5 bytes). Three potential benefits: less memory used, less data to move, and more operations per clock cycle.

Crucially, quantization is not one technique—it is a family targeting different tensors:

**Weight quantization (GPTQ, AWQ, GGML):** reduces weight memory footprint. Decode benefits most: less data to load from HBM per token. Does NOT reduce communication volume because activations being all-reduced remain at higher precision.

**Activation quantization (FP8 compute):** uses FP8 for the actual matrix multiplication. Benefits both compute throughput ( $2\times$  TFLOPS on FP8-capable hardware) and communication volume. Most impactful for prefill because prefill is compute-bound.

**KV-cache quantization (INT8/FP8 KV):** stores KV vectors at lower precision. Cuts KV memory per token in half, enabling more concurrent requests or longer contexts.

**Communication precision:** running all-reduce at FP8 instead of BF16 halves data volume. Most relevant during prefill where messages are large.

### 22.9.2 Quantization Fundamentals

**Definition 22.3** (Quantization). Map floating-point weights to lower precision:

$$w_{\text{quant}} = \text{round}\left(\frac{w_{\text{float}}}{s}\right) + z \quad (22.2)$$

where  $s$  is the scale factor and  $z$  is the zero-point.

**Example 22.6** (INT8 Quantization). **FP32 weight:**  $w = 0.137$ . **Range:**  $w \in [-1.0, 1.0]$ . **Scale:**  $s = 2.0/256 = 0.0078125$ .

**Quantize:**

$$w_{\text{INT8}} = \text{round}\left(\frac{0.137}{0.0078125}\right) = \text{round}(17.54) = 18 \quad (22.3)$$

**Dequantize:**  $w' = 18 \times 0.0078125 = 0.1406$ . **Error:**  $|0.137 - 0.1406| = 0.0036$  (2.6% relative).

### 22.9.3 Post-Training Quantization (PTQ)

PTQ takes a fully trained FP32 model and converts it to lower precision through a calibration process. A small calibration dataset (a few hundred to a few thousand examples) is processed in FP32 while collecting activation statistics. These statistics determine scale factors mapping the continuous FP32 range to the discrete INT8 range.

The primary advantage is simplicity: no retraining required. Modern frameworks provide built-in PTQ APIs. The limitation: quantization errors accumulate through deep networks. Layers with wide activation distributions or outlier values are especially sensitive.

### 22.9.4 Quantization-Aware Training (QAT)

QAT incorporates quantization effects directly into training. In the forward pass, weights and activations are quantized to the target precision using the same formula as inference. The backward pass operates in full FP32 precision. This allows the optimizer to adjust weights to positions robust to rounding and learn activation distributions that quantize well.

**Example 22.7** (BERT-base Quantization Results).

Precision	GLUE Score	Speedup
FP32 (baseline)	84.5	1.0×
FP16	84.4	1.8×
INT8 (PTQ)	82.1	2.9×
INT8 (QAT)	84.2	2.9×

QAT recovers most accuracy lost in PTQ while maintaining the same speedup.

### 22.9.5 Accuracy and Stability Trade-offs

**Calibration:** FP8 and INT8 require scaling factors derived from representative data. Poor calibration clips important values.

**Outlier sensitivity:** some models have occasional very large activation values critical for quality. Techniques like SmoothQuant redistribute outlier magnitude from activations to weights before quantizing.

**Accumulation precision:** FP8 multiply with FP32 accumulate is generally safe; FP8 accumulate can cause compounding rounding errors.

**Model-specific:** some architectures (e.g., Llama family) tolerate FP8 well. Others show noticeable quality regression. Always evaluate on your specific model and task.

### 22.9.6 Quantization Decision Heuristics

Bottleneck	Strategy	Why
Memory capacity (weights)	Weight-only quant (INT4/INT8)	Reduces weight memory directly
Memory capacity (KV-cache)	KV quantization (INT8/FP8)	Frees memory for more requests
Compute throughput (prefill)	FP8 activation + compute	2× TFLOPS on FP8 hardware
TP communication (BW-bound)	FP8 communication	Halves all-reduce volume
Quality-sensitive	Start BF16, add conservatively	Measure regression first

Table 22.12: Quantization strategy selection based on the dominant bottleneck.

## 22.10 Model Pruning

### 22.10.1 Pruning Strategies

Model pruning removes parameters to reduce computational and memory requirements. Two main approaches exist:

**Magnitude-based pruning** removes weights with small absolute values: if  $|w_{ij}| < \tau$ , the weight is set to zero. The threshold  $\tau$  can be set globally, per-layer, or adaptively.

**Structured vs. unstructured pruning.** Unstructured pruning removes individual weights, creating sparse matrices that require specialized sparse kernels to realize speedups. Structured pruning removes entire architectural units (neurons, attention heads, layers), directly reducing matrix dimensions visible to standard dense libraries. Structured pruning achieves lower compression ratios but provides immediate speedups without custom kernels.

### 22.10.2 Iterative Pruning

---

**Algorithm 15:** Iterative Magnitude Pruning
 

---

```

1 Input: Model, sparsity target  $s_{\text{target}}$ 
2 for sparsity  $s = 0$  to  $s_{\text{target}}$  by steps do
3   Train model to convergence
4   Prune  $\Delta s$  lowest-magnitude weights
5   Fine-tune model
  
```

---

**Example 22.8** (Attention Head Pruning). BERT-base: 12 layers  $\times$  12 heads = 144 heads.

**Finding:** Can remove 50% of heads with minimal impact.

**Procedure:** (1) Compute importance score per head. (2) Rank by importance. (3) Prune lowest 50% (72 heads). (4) Fine-tune.

**Result:** 50% fewer attention operations. GLUE score: 84.5  $\rightarrow$  83.8 (0.7 point drop). 1.5 $\times$  faster inference.

## 22.11 Knowledge Distillation

**Definition 22.4** (Distillation Objective).

$$\mathcal{L} = \alpha \mathcal{L}_{\text{CE}}(y, y_{\text{student}}) + (1 - \alpha) \mathcal{L}_{\text{KD}}(y_{\text{teacher}}, y_{\text{student}}) \quad (22.4)$$

where:

$$\mathcal{L}_{\text{KD}} = \text{KL} \left( \frac{\exp(z_t/T)}{\sum \exp(z_t/T)} \parallel \frac{\exp(z_s/T)}{\sum \exp(z_s/T)} \right) \quad (22.5)$$

$T$  = temperature (typically 2–5), higher = softer probabilities.

### 22.11.1 DistilBERT Approach

DistilBERT reduces depth by half (6 layers vs. BERT-base’s 12) while maintaining hidden size 768. The student is initialized by copying every other layer from the teacher. Training combines three losses: distillation loss (match teacher’s output distribution), masked language modeling loss, and cosine distance loss between hidden states.

**Results:** 66M parameters (vs. 110M),  $\sim 60\%$  faster inference, retains 97% of BERT’s GLUE performance. This combination of compression, speedup, and accuracy retention makes DistilBERT compelling for production deployments.

## 22.12 Bottleneck-Driven Optimization

Do not apply optimizations by popularity. Apply them by bottleneck. A 10 $\times$  kernel speedup is worthless if the bottleneck is scheduling overhead. A perfect scheduler is worthless if the bottleneck is interconnect latency. The single most important skill in inference optimization is correctly identifying where time is actually being spent.

### 22.12.1 Bottleneck Taxonomy

Every inference workload is dominated by one (occasionally two) bottleneck regimes. Identifying the regime tells you which family of optimizations will help:

Bottleneck Regime	Symptom	Dominant In
Compute-bound	Utilization >85%; more batch doesn't help	Prefill with large batches
HBM bandwidth-bound	Low utilization despite available work	Decode (single-token GEMMs)
Interconnect BW-bound	Large collective messages, high link utilization	Prefill TP all-reduce, EP a2a
Interconnect latency-bound	Small messages, latency dominates	Decode TP all-reduce
Host/runtime overhead-bound	Low utilization, dispatch visible in profile	Decode without graph replay
Memory capacity-bound	OOM or aggressive KV eviction	Long context + high concurrency
Scheduler/policy-bound	Low utilization despite available requests	Bursty traffic, poor scheduling

Table 22.13: Bottleneck taxonomy for LLM inference workloads.

### 22.12.2 Diagnosis Workflow

A systematic approach to optimization:

1. **Define the target metric.** Latency (TTFT, ITL, P50, P99)? Throughput (tokens/s)? Cost (tokens/dollar)?
2. **Segment the workload.** What fraction is prefill vs. decode? What is the sequence length distribution?
3. **Profile.** Use vendor profilers (Nsight, rocprof, XLA profiler, Neuron profiler) to measure host time, kernel time, communication time, idle time, memory utilization.
4. **Classify the bottleneck.** Match profiler signals to the taxonomy above.
5. **Choose the optimization family.** Compute-bound  $\rightarrow$  FP8, kernel optimization. BW-bound  $\rightarrow$  quantization, memory access optimization. Latency-bound  $\rightarrow$  graph replay, custom collectives. Overhead-bound  $\rightarrow$  compilation, better scheduling. Capacity-bound  $\rightarrow$  quantization, KV optimization, more devices.
6. **Re-measure.** Verify the optimization helped end-to-end. A local improvement that shifts the bottleneck elsewhere may show no system-level gain.

### 22.12.3 Optimization Impact Summary

Optimization	Layer	Gain	Bottleneck Relieved	Helps	Trade-off
<code>torch.compile/XLA</code>	5	1.5–3 $\times$	Host overhead	Decode > prefill	Compile time; graph
FlashAttention	3	2–4 $\times$ attn	HBM BW (attention)	Prefill > decode	Kernel compatibility
Continuous batching	4	3–8 $\times$ tput	Scheduler/utilization	Both	Tail latency risk
PagedAttention	4	2–4 $\times$ concurrency	Memory capacity (KV)	Both	Indirection overhead
Fused GEMM+AllReduce	3	1.3–1.8 $\times$ TP	Interconnect (TP path)	Prefill > decode	Kernel complexity
FP8 compute	3+1	1.5–2 $\times$	Compute + HBM BW	Prefill > decode	Accuracy risk
Graph replay	2	1.2–2 $\times$ decode	Host overhead	Decode $\gg$ prefill	Static shape require

Table 22.14: Optimization impact summary. All gain values are representative ranges from published benchmarks, not universal guarantees.

### 22.12.4 Case Study: Interactive Chatbot (Decode-Heavy)

Target: P50 inter-token latency < 30 ms. 70B model on 8 $\times$ H100. Decode dominates because each response generates hundreds of tokens.

**Bottleneck analysis:** per-token GEMMs are memory-bandwidth-bound. TP all-reduce is latency-bound (16 KB messages). Host dispatch overhead is significant without graph replay.

**Priority 1 (Layer 4):** continuous batching with moderate batch sizes (8–32).

**Priority 2 (Layers 5/2):** graph compilation + CUDA Graph replay for decode.

**Priority 3 (Layer 3):** custom small-message all-reduce bypassing NCCL overhead.

**Priority 4 (Layer 7):** TP-4 rather than TP-8. Each additional TP degree adds serialized all-reduce latency per token.

### 22.12.5 Case Study: Batch Document Summarization (Prefill-Heavy)

Target: maximize tokens/second/dollar. 70B model on 8×H100. Processing thousands of long documents offline.

**Bottleneck analysis:** large GEMMs are compute-bound. TP all-reduce messages are large (bandwidth-relevant). Memory capacity constrains batch size.

**Priority 1 (Layer 4):** continuous batching with large batches (128–512).

**Priority 2 (Layer 3):** FP8 GEMMs. 2× compute throughput maps directly to ~2× prefill throughput.

**Priority 3 (Layer 3):** fused GEMM+all-reduce. Large prefill GEMMs provide enough compute time to overlap communication.

**Priority 4:** KV-cache quantization (FP8 KV) to free memory for more concurrent documents.

## 22.13 Production Deployment

### 22.13.1 Serving Frameworks

**TorchServe** provides native PyTorch serving with REST/gRPC APIs, dynamic batching, model versioning, and integrated monitoring. Natural deployment path for PyTorch-trained models.

**Triton Inference Server** supports models from PyTorch, TensorFlow, ONNX, and TensorRT within a single infrastructure. Sophisticated scheduling can execute multiple models concurrently on the same GPU.

**ONNX Runtime** provides framework-agnostic inference with graph-level optimizations (operator fusion, constant folding, dead code elimination). Typically delivers 1.5–2× speedup over PyTorch inference; combined with INT8 quantization, 3–4×. See Chapter 21 for ONNX export code.

**TensorRT** leverages detailed knowledge of NVIDIA GPU architectures for aggressive layer fusion, kernel auto-tuning, and INT8 calibration. For BERT-base: 2–3× speedup over PyTorch in FP16; 4–5× with INT8.

### 22.13.2 Distributed Inference with Ray and Kubernetes

When inference workloads exceed single-machine capacity, they are typically deployed on a Kubernetes cluster with Ray Serve handling request routing and autoscaling. A Ray cluster runs inside Kubernetes: a head pod manages state, worker pods host GPU-backed model replicas. Kubernetes provisions and recovers pods; Ray’s autoscaler adjusts replica count based on request rate and queue length.

Designing such a system requires coordinating multiple scaling layers. Each replica needs appropriate concurrency limits and batch sizes to avoid GPU memory oversubscription. Ray’s autoscaler must react quickly to sustained load without oscillations. Kubernetes node autoscaling must align with Ray’s resource requests. Observability across all layers is essential for diagnosing stalled scaling, replica imbalance, or OOM events.

### 22.13.3 Deployment Checklist

**Performance optimization:** quantize to INT8/FP16 where accuracy permits; export to ONNX/TensorRT for graph-level optimization; tune batch size for latency–throughput balance; enable KV caching for autoregressive generation.

**Reliability engineering:** distinguish transient vs. permanent failures with appropriate retry logic; set request timeouts; implement health checks for load balancer integration; enable model versioning for safe rollouts.

**Monitoring and observability:** track latency at p50/p95/p99 (not just averages); measure throughput in requests/second; monitor GPU utilization to identify headroom; break down error rates by type.

## 22.13.4 Hardware Selection

### CPU vs. GPU Trade-offs

CPUs suit small models (<100M parameters) with batch size 1–4 and latency-critical single-request scenarios. A distilled BERT (66M parameters) achieves 15 ms latency on modern CPU with batch size 1.

GPUs become the clear choice for training (any size), large models (>100M), batch inference (batch > 8), and throughput-oriented applications. BERT-large achieves 2.5 seq/s on CPU vs. 45 seq/s on T4 GPU (18× advantage).

Cost analysis often favors GPUs despite higher instance cost: T4 GPU at \$0.35/hour processes 162K sequences/hour (\$0.0000022/seq) vs. CPU at \$0.10/hour processing 9K sequences/hour (\$0.000011/seq)—GPU is 5× more cost-effective.

### Training Hardware Selection

- **<1B parameters:** single V100 or A100. BERT-base trains in ~3 days on V100.
- **1–10B parameters:** 4–8 A100 GPUs with NVLink. GPT-2 (1.5B) trains in ~2 weeks on 8×A100.
- **10–100B parameters:** 16–64 A100 GPUs with NVLink + InfiniBand. Requires pipeline and tensor parallelism.
- **>100B parameters:** hundreds to thousands of GPUs. Training costs reach millions of dollars.

### Inference Hardware Selection

- **Batch throughput:** A100 or A10 GPUs with large batches (32–128). BERT-large: 520 seq/s on A100 with batch 64.
- **Low-latency:** T4 or A10 with TensorRT + INT8. BERT-base: 5 ms latency on T4 with batch 1.
- **Cost-optimized:** CPU or T4 with quantized models. Distilled BERT on CPU: ~\$0.000005/inference.
- **Edge:** mobile CPUs, edge TPUs, Jetson. MobileBERT (25M params): 30 ms on mobile CPU.

## 22.14 Key Takeaways and Engineering Decision Checklist

### 22.14.1 Principles

**1. Parallelism at Layer 7 is typically the most consequential decision.** It determines communication patterns, memory distribution, and constraints on every layer below.

**2. The top of the stack is portable.** Layers 7–5 work across vendors. Invest in understanding these first.

**3. Layers 4 and 3 often deliver the largest end-to-end gains.** Inference engine optimizations and custom kernels provide the biggest multipliers, but only after parallelism and compilation are correctly configured.

**4. Communication follows the Bandwidth Ladder.** TP on fastest link, PP tolerates slower links, EP needs bisection bandwidth.

**5. Diagnose before optimizing.** Profile to classify the bottleneck regime. Apply the optimization family that addresses that regime. Re-measure.

**6. Numbers require context.** Every speedup claim is scoped to a workload phase, hardware configuration, and software version.

### 22.14.2 Engineering Decision Checklist

1. What is the objective metric? Latency (TTFT, ITL)? Throughput (tokens/s)? Cost (tokens/-dollar)?
2. Is the workload prefill- or decode-dominated?
3. What is the bottleneck regime? Profile first.
4. Is parallelism required for fit or chosen for performance?
5. Is shape regularity sufficient for graph replay? If not, implement bucketing.
6. Is the interconnect appropriate for TP/EP?
7. What precision trade-off is acceptable? Measure accuracy impact before committing.
8. Does the optimization help end-to-end? Always measure the system-level metric.

### 22.15 Worked End-to-End Token Trace

One complete decode step for a 70B model on TP-4 (4×H100, NVSwitch). BF16.  $B = 16$  concurrent requests.

#	Layer	What Happens	Time (illustrative)	Bottleneck
1	4: Scheduler	Select batch of 16 reqs, allocate KV pages	~10–50 $\mu$ s	Host overhead
2	5/2: Replay	Launch compiled decode graph for $[B=16, S=1]$	~5–10 $\mu$ s	Host overhead
3	3: GEMM	QKV projection (column-parallel)	~15–30 $\mu$ s	HBM BW-bound
4	3: Attention	FlashAttention: 8 local heads, KV-cache lookup	~10–40 $\mu$ s	HBM BW-bound
5	3: GEMM+AR	Output proj (row-par) + all-reduce 256 KB	~15–30 + 2–5 $\mu$ s	HBM BW + latency
6	3: FFN	Gate+Up (col-par), SwiGLU, Down (row-par) + AR	~30–60 + 2–5 $\mu$ s	HBM BW-bound
7	Repeat	×80 layers	~5–15 ms total	Accumulated
8	4: Complete	Detokenize, check stop, reclaim KV	~5–20 $\mu$ s	Host overhead

Table 22.15: End-to-end decode step trace. Decode is dominated by memory-bandwidth-bound GEMMs with small but frequent latency-bound all-reduces, bookended by host scheduling overhead.

### 22.16 Exercises

**Exercise 22.1.** Quantize BERT-base to INT8:

1. Use PyTorch quantization APIs
2. Calibrate on 1000 examples
3. Measure: (a) Model size, (b) Inference speed, (c) GLUE accuracy
4. Compare PTQ vs QAT

**Exercise 22.2.** Implement attention head pruning:

1. Compute importance scores for all heads
2. Prune 25%, 50%, 75% of heads



3. Fine-tune after pruning
4. Plot accuracy vs sparsity

**Exercise 22.3.** Optimize inference pipeline:

1. Baseline: PyTorch FP32
2. Convert to ONNX, measure speedup
3. Apply INT8 quantization
4. Implement dynamic batching
5. Report final throughput improvement

**Exercise 22.4.** Analyze the prefill vs. decode asymmetry:

1. For a model with  $H = 4096$  and 32 layers, compute the arithmetic intensity of a single-token decode GEMM and a 512-token prefill GEMM
2. Determine whether each is compute-bound or memory-bound on an H100 (3.35 TB/s, 990 TFLOPS)
3. Calculate the theoretical speedup from switching to FP8 ( $2\times$  TFLOPS) for each phase
4. Explain why the speedup differs between phases

**Exercise 22.5.** Tensor parallelism communication analysis:

1. For a 70B model with  $H = 8192$  and 80 layers, calculate the total all-reduce data volume per decode token with TP-4 in BF16
2. Calculate the communication time assuming NVLink latency of  $2\ \mu\text{s}$  per all-reduce
3. Repeat for InfiniBand at  $8\ \mu\text{s}$  per all-reduce
4. If decode compute takes 10 ms per token, what percentage overhead does communication add in each case?
5. At what TP degree does InfiniBand communication overhead exceed 50% of compute time?

**Exercise 22.6.** Flash Attention implementation study:

1. Implement standard attention with separate kernels
2. Analyze memory traffic for different sequence lengths
3. Study Flash Attention paper and implementation
4. Benchmark Flash Attention vs standard attention

5. Plot speedup as a function of sequence length

**Exercise 22.7.** Inference engine configuration:

1. Deploy a 7B model using vLLM with default settings
2. Measure throughput and P50/P99 latency under load
3. Experiment with max batch size: 1, 8, 32, 128
4. Enable PagedAttention and measure memory utilization improvement
5. Compare static batching vs. continuous batching throughput
6. Identify the bottleneck regime at each batch size using profiling

**Exercise 22.8.** Bottleneck diagnosis:

1. Choose a transformer model and deployment scenario (interactive chatbot or batch processing)
2. Profile the deployment using available tools
3. Classify the bottleneck using the taxonomy in Table 22.13
4. Select and apply the appropriate optimization from Table 22.14
5. Measure end-to-end improvement and verify the bottleneck shifted
6. Document the before/after metrics and explain why the optimization helped

**Exercise 22.9.** Hardware selection analysis:

1. Choose a transformer model and deployment scenario
2. Estimate throughput requirements and latency constraints
3. Compare cost per inference for CPU, T4, and A100
4. Calculate break-even point where GPU becomes cost-effective
5. Recommend hardware configuration with justification

## 22.17 Solutions

Full solutions for all exercises are available at <https://deeplearning.hofkensvermeulen.be>.

## Chapter 23

# Best Practices and Production Case Studies

### Chapter Overview

This final chapter synthesizes practical wisdom from deploying transformers at scale. We cover debugging strategies, hyperparameter tuning, common pitfalls, and real-world case studies from industry deployments of BERT, GPT, and other transformer models.

### Learning Objectives

1. Apply systematic debugging for transformer training
2. Tune hyperparameters effectively
3. Avoid common pitfalls in architecture and training
4. Learn from real-world deployment case studies
5. Design robust production systems
6. Plan future-proof transformer architectures

### 23.1 Model Selection

Choosing the right transformer architecture is a critical decision that impacts both performance and resource requirements. This section provides a systematic framework for selecting among the major transformer variants based on task requirements, data availability, and computational constraints.

#### 23.1.1 Architecture Selection Framework

The choice between BERT, GPT, T5, and other architectures depends fundamentally on the nature of your task. BERT and its variants excel at understanding tasks where bidirectional context is crucial, such as classification, named entity recognition, and question answering. The bidirectional attention mechanism allows BERT to build rich representations by attending to both past and future tokens simultaneously, making it particularly effective when the entire input is available at once.

GPT models, in contrast, are designed for generation tasks where autoregressive decoding is required. The unidirectional attention pattern makes GPT natural for text generation, code completion, and any task where outputs must be produced sequentially. While GPT can be adapted for understanding tasks through careful prompting, this is generally less efficient than using a bidirectional model designed for the purpose.

T5 represents a unified approach that frames all tasks as sequence-to-sequence problems. This architecture provides flexibility across both understanding and generation tasks, making it an excellent choice when you need a single model to handle diverse task types. The encoder-decoder structure allows

T5 to leverage bidirectional attention in the encoder while maintaining autoregressive generation in the decoder.

### 23.1.2 Model Size Selection

Selecting the appropriate model size requires balancing performance requirements against computational constraints. The relationship between model size and performance generally follows a power law, with diminishing returns as models grow larger. For most practical applications, the base-sized models provide an excellent balance between capability and efficiency.

BERT-base with 110 million parameters serves as the standard choice for most understanding tasks. It provides strong performance across a wide range of benchmarks while remaining tractable for fine-tuning on a single GPU. BERT-large with 340 million parameters offers modest improvements, typically 1-3 percentage points on downstream tasks, but requires significantly more memory and computation. The large variant is justified primarily when you need to extract maximum performance and have sufficient computational resources.

For GPT models, the size selection depends heavily on the complexity of the generation task. GPT-2 small (117M parameters) suffices for simple completion tasks and domain-specific generation after fine-tuning. GPT-2 medium (345M parameters) provides better coherence for longer generations and more complex tasks. The larger variants (GPT-2 large at 774M and GPT-2 XL at 1.5B parameters) are necessary primarily when working with limited task-specific data, as their stronger pre-trained representations enable better few-shot performance.

### 23.1.3 Pre-trained versus Training from Scratch

The decision to use pre-trained models versus training from scratch depends on data availability, domain specificity, and computational budget. In nearly all cases, starting from pre-trained weights is the correct choice. Pre-training on large corpora provides general language understanding that transfers effectively to downstream tasks, and the computational cost of pre-training from scratch is prohibitive for most organizations.

Training from scratch becomes viable only in specific circumstances. When working with highly specialized domains where general language models perform poorly, such as medical text with extensive jargon or programming languages not well-represented in pre-training data, domain-specific pre-training may be justified. However, even in these cases, continued pre-training from existing checkpoints is typically more efficient than starting from random initialization.

The computational cost difference is substantial. Pre-training BERT-base from scratch requires approximately 64 TPU days or equivalent GPU time, representing tens of thousands of dollars in compute costs. Fine-tuning the same model on a downstream task typically requires only hours on a single GPU, costing tens of dollars. This thousand-fold difference in cost makes pre-trained models the default choice for nearly all applications.

### 23.1.4 Cost-Benefit Analysis

A systematic cost-benefit analysis should consider both direct computational costs and opportunity costs. For a typical classification task with 10,000 labeled examples, fine-tuning BERT-base requires approximately 2-4 hours on a single V100 GPU, costing roughly \$10-20 in cloud compute. This investment typically yields performance improvements of 5-15 percentage points over traditional methods like logistic regression on TF-IDF features.

Training a smaller model from scratch on the same data might require 8-16 hours and cost \$40-80, while likely achieving inferior performance due to the lack of pre-trained representations. The pre-trained approach thus provides both better performance and lower cost, a rare combination that explains the dominance of transfer learning in modern NLP.

For generation tasks, the cost analysis shifts somewhat. Fine-tuning GPT-2 medium on a specific generation task requires 4-8 hours on a V100, costing \$20-40. However, inference costs become more significant for generation, as producing each token requires a full forward pass through the model.

For applications requiring high-throughput generation, the ongoing inference costs may exceed training costs within weeks or months of deployment, making inference optimization critical.

## 23.2 Training Best Practices

Effective training of transformer models requires careful attention to hyperparameter selection, monitoring, and debugging. This section provides comprehensive guidance on the key decisions that impact training success.

### 23.2.1 Learning Rate Selection

Scenario	Range	Notes
BERT fine-tuning	$1\text{--}5 \times 10^{-5}$	Lower end for small datasets
GPT fine-tuning	$2 \times 10^{-5}\text{--}10^{-4}$	Autoregressive is more stable
Pre-training from scratch	$10^{-4}\text{--}6 \times 10^{-4}$	Requires longer warmup

**Rules of thumb:** Scale LR  $\sim$ linearly with batch size (use LAMB for very large batches). Warmup: 5–10% of steps for fine-tuning, 10K–50K steps for pre-training.

### 23.2.2 Batch Size Selection

Scenario	Typical Range	Notes
Fine-tuning (single GPU)	16–32	Gradient accumulation for larger effective batch
Fine-tuning (multi-GPU)	32–256	Scale LR accordingly
Pre-training	256–4096	Requires LR warmup + LAMB

If memory-limited, use gradient accumulation:  $B_{\text{eff}} = B_{\text{micro}} \times N_{\text{accum}}$  (see Chapter ?? for implementation).

### 23.2.3 Checkpointing and Monitoring Strategy

Effective monitoring is essential for detecting problems early and understanding training dynamics. At minimum, you should track training loss, validation loss, and task-specific metrics at regular intervals. Logging every 100–500 steps provides sufficient granularity to detect issues without generating excessive data.

Checkpointing strategy depends on training duration and stability. For short fine-tuning runs of a few hours, saving checkpoints every epoch is sufficient. For longer training runs, save checkpoints every few thousand steps to protect against hardware failures and enable recovery from divergence. Always keep at least the three most recent checkpoints, as the most recent checkpoint may be corrupted or represent a point after training has diverged.

Beyond basic loss monitoring, tracking gradient norms provides early warning of training instability. Gradient norms should remain relatively stable throughout training, typically in the range of 0.1 to 10.0. Sudden spikes in gradient norm often precede loss divergence and indicate that gradient clipping or learning rate reduction may be necessary. Similarly, monitoring the ratio of update magnitude to parameter magnitude helps ensure that learning rates are appropriate.

## 23.3 Memory Management

Memory is often the primary constraint in transformer training. Rather than repeating the detailed memory analysis from Chapter 21, this section provides a quick-reference decision guide.

### 23.3.1 Out-of-Memory Decision Checklist

When encountering memory errors, apply these steps in order:

1. **Reduce sequence length** (if task permits). Attention memory scales quadratically with sequence length—truncating from 512 to 256 tokens saves  $\sim 4\times$  attention memory. Many classification tasks work well at 128 tokens.
2. **Enable mixed precision** (`torch.cuda.amp`). Halves activation and gradient memory with  $2\text{--}3\times$  speedup on tensor-core GPUs. Minimal code changes required. See Chapter 21 for implementation.
3. **Enable gradient checkpointing**. Trades 20–30% additional compute time for 40–50% activation memory reduction. Apply via `torch.utils.checkpoint`.
4. **Reduce batch size and use gradient accumulation**. Maintain effective batch size  $B_{\text{eff}} = B_{\text{micro}} \times N_{\text{accum}}$  while fitting in memory. Linear memory savings.
5. **Consider model parallelism**. When the model itself exceeds single-GPU memory, use pipeline parallelism (split by layers) or tensor parallelism (split within layers). Frameworks: DeepSpeed, Megatron-LM. See Chapter 22 for multi-GPU strategies.

### 23.3.2 Memory Estimation Rule of Thumb

Total training memory (GB)  $\approx$  (Parameters  $\times$  16 bytes) + (Batch  $\times$  SeqLen  $\times$  Hidden  $\times$  Layers  $\times$  40 bytes). The first term covers parameters, gradients, and optimizer states; the second covers activations. For BERT-base (110M params, batch 32, seq 512):  $\sim 8$  GB.

## 23.4 Debugging Transformers

### 23.4.1 Systematic Debugging Workflow

#### Level 1: Data sanity checks

1. Visualize input samples
2. Verify labels are correct
3. Check for data leakage
4. Validate preprocessing

#### Level 2: Model sanity checks

1. Overfit single batch (should reach near-zero loss)
2. Check gradient flow (no dead neurons)
3. Verify shapes at each layer
4. Test with minimal model first

#### Level 3: Training dynamics

1. Monitor loss curves (training + validation)
2. Track gradient norms
3. Visualize attention weights
4. Check learning rate schedule

**Example 23.1** (Debugging Checklist). **Symptom:** Loss not decreasing  
**Diagnose:**

- Learning rate too low? Try 10× higher
- Frozen layers? Check `requires_grad`
- Optimizer issue? Try SGD as baseline
- Bad initialization? Re-initialize
- Data issue? Manually inspect batches

**Symptom:** NaN loss

**Diagnose:**

- Gradient explosion? Add clipping
- Numerical instability? Check mask values ( $-\infty$  vs  $-1e9$ )
- Learning rate too high? Reduce 10×
- Mixed precision issue? Check loss scaling

### 23.4.2 Gradient Analysis

Monitor per-layer gradient norms throughout training (see Chapter ?? for PyTorch profiling tools). Healthy gradients have norms between  $10^{-4}$  and  $10^1$ , are similar across layers, and are non-zero for all layers. Sudden spikes precede divergence; vanishing gradients indicate dead layers.

### 23.4.3 Common Training Issues: Quick Reference

Symptom	Likely Cause	Fix
Out of memory	Batch/sequence too large	See memory checklist (Section 23.3)
Loss not decreasing	Learning rate too low	Increase LR 3–10×; verify overfit on 1 batch
Loss diverges / NaN	LR too high or no clipping	Reduce LR; clip gradients to norm 1.0
Slow training	Low GPU utilization	Increase batch size; add DataLoader workers
Train/val gap growing	Overfitting	More dropout; data augmentation; smaller model

## 23.5 Inference Optimization

Inference costs often exceed training costs over a model’s lifetime. This section provides decision tables for choosing optimization strategies; see Chapters 21 and 22 for detailed implementations.

### 23.5.1 Optimizing for Latency

Technique	Speedup	Accuracy Cost	Effort
FP16 inference	1.5–2×	<0.1%	Minimal
INT8 quantization (PTQ)	2–4×	0.5–2%	Low (calibration)
INT8 quantization (QAT)	2–4×	<0.5%	Medium (retraining)
KV caching (autoregressive)	5–10×	None	Low
TorchScript / <code>torch.compile</code>	1.2–1.5×	None	Low
TensorRT compilation	2–5×	<0.5%	Medium

### 23.5.2 Optimizing for Throughput

- **Dynamic batching:** Accumulate requests for 10–50 ms, process together. Improves GPU utilization from 20–30% to 70–90%.
- **ONNX Runtime / TensorRT:** Graph-level optimizations provide 1.5–5 $\times$  throughput gains via operator fusion and kernel selection.
- **Model distillation:** Train a smaller student (e.g., 6-layer DistilBERT retains 97% of BERT-base accuracy at 1.6 $\times$  speed). Combine with quantization for 5–10 $\times$  cumulative speedup.
- **Continuous batching (vLLM):** For autoregressive generation, allow new requests to join in-flight batches as others complete. See Chapter 22.

### 23.5.3 Hardware Selection Summary

Scenario	Recommended Hardware	Rationale
<10 req/s, small model	CPU	Lower cost, sufficient throughput
10–100 req/s	T4 GPU + TensorRT	Good latency/cost balance
>100 req/s	A10/A100 GPU	Maximum throughput
Edge / mobile	INT8/INT4 on device	Memory and power constrained

See Chapter 22 for detailed hardware analysis and cost breakdowns.

## 23.6 Cost Optimization

Understanding and optimizing costs is essential for sustainable deployment of transformer models. This section provides detailed analysis of training and inference costs with concrete examples.

### 23.6.1 Training Cost Analysis

Training costs depend on model size, dataset size, and hardware selection. For BERT-base pre-training on 16 GB of text, the original paper reports using 16 TPU chips for 4 days, equivalent to approximately 64 TPU days. At current Google Cloud pricing of roughly \$8 per TPU hour, this amounts to approximately \$12,000 for pre-training. Using equivalent GPU resources (64 V100 GPUs for 4 days) would cost approximately \$15,000 at on-demand rates.

Fine-tuning costs are much more modest. Training BERT-base on a typical classification task with 10,000 examples requires 2–4 hours on a single V100 GPU. At AWS on-demand pricing of approximately \$3 per hour for a p3.2xlarge instance, this amounts to \$6–12 per fine-tuning run. Even with extensive hyperparameter search involving 20–30 runs, total costs remain under \$300.

Cloud versus on-premise costs depend heavily on utilization. For continuous training workloads, purchasing GPUs becomes cost-effective after 12–18 months of use. A DGX A100 system costs approximately \$200,000 but provides compute equivalent to \$15,000 per month at cloud on-demand rates. For intermittent workloads or experimentation, cloud computing is more economical due to the flexibility to scale up and down.

Spot instances provide substantial savings for training workloads that can tolerate interruptions. AWS spot instances for p3.2xlarge typically cost 50–70% less than on-demand rates, reducing fine-tuning costs to \$2–4 per run. Implementing checkpointing and automatic restart logic allows training to resume after spot instance interruptions, making this an attractive option for cost-conscious training.

### 23.6.2 Training Time Estimation

Estimating training time helps with planning and cost prediction. For fine-tuning, a useful rule of thumb is that BERT-base processes approximately 100–150 examples per second on a V100 GPU with batch size 32 and sequence length 128. For a dataset of 100,000 examples trained for 3 epochs, this translates to 2,000–3,000 seconds or roughly 1 hour of training time.



Pre-training time scales with dataset size and model size. BERT-base pre-training on 16 GB of text requires approximately 1 million training steps with batch size 256, processing roughly 4 billion tokens. At 1,000 tokens per second per V100 GPU, this requires 4 million GPU-seconds or approximately 1,100 GPU-hours. With 16 GPUs, this translates to roughly 70 hours or 3 days of training.

Larger models scale approximately linearly with parameter count for training time. GPT-2 medium with 345 million parameters takes roughly  $3\times$  longer to train than GPT-2 small with 117 million parameters, assuming the same dataset and batch size. However, larger models often benefit from larger batch sizes, which can partially offset the increased time per step.

### 23.6.3 Inference Cost Analysis

Inference costs depend on request volume, latency requirements, and model size. For a BERT-base classification service processing 1 million requests per day with average latency requirements of 100ms, a single V100 GPU can handle approximately 100 requests per second with dynamic batching, or 8.6 million requests per day. This suggests that a single GPU is sufficient, costing approximately \$200-300 per month for a cloud GPU instance.

For generation tasks, costs are higher due to the sequential nature of autoregressive decoding. GPT-2 medium generating 100 tokens per request can process approximately 10-20 requests per second per GPU, depending on batch size and sequence length. For 1 million requests per day, this requires 1-2 GPUs, costing \$400-600 per month. The cost per million tokens is approximately \$5-10 for self-hosted inference.

Comparing self-hosted to API costs reveals significant differences at scale. OpenAI's GPT-3.5 API costs approximately \$2 per million tokens for input and output combined. For applications processing 100 million tokens per month, this amounts to \$200 per month. Self-hosting a comparable model would require 4-8 GPUs costing \$1,600-3,200 per month, making the API more economical at this scale. However, at 1 billion tokens per month, self-hosting becomes competitive, and at 10 billion tokens per month, self-hosting is clearly more economical.

### 23.6.4 Cost Optimization Strategies

Several strategies can substantially reduce both training and inference costs. For training, using mixed precision reduces training time by  $2-3\times$ , directly reducing costs by the same factor. Gradient accumulation allows using smaller, cheaper GPU instances by simulating larger batch sizes. Spot instances reduce costs by 50-70% for workloads that can tolerate interruptions.

For inference, quantization and distillation reduce both latency and cost. A distilled and quantized model may achieve  $5-10\times$  higher throughput than the original model, allowing a single GPU to handle the load that previously required 5-10 GPUs. This directly translates to  $5-10\times$  cost reduction. Dynamic batching improves GPU utilization from 20-30% to 70-90%, effectively tripling throughput without additional hardware.

Caching can dramatically reduce inference costs for applications with repeated queries. If 30% of requests are duplicates or near-duplicates, caching responses eliminates 30% of inference costs. Semantic caching using embedding similarity can extend this to near-duplicate queries, potentially caching 50-70% of requests in some applications.

Autoscaling based on demand prevents paying for idle resources during low-traffic periods. For applications with diurnal traffic patterns, autoscaling can reduce costs by 40-60% compared to provisioning for peak load. Kubernetes and cloud-native deployment platforms make autoscaling straightforward to implement.

## 23.7 Production Deployment

Production deployment involves serving infrastructure, monitoring, and safe rollout practices. Chapter 22 covers serving frameworks (TorchServe, Triton, vLLM), deployment architectures (Ray Serve, Kubernetes), and KV cache management in detail. Here we summarize the key decision points.

### 23.7.1 Deployment Checklist

#### Before deployment:

1. Optimize model: quantize (INT8/FP16), export to ONNX or TensorRT, enable KV caching for generation.
2. Benchmark under realistic conditions (expected batch sizes, sequence lengths, peak load).
3. Set up monitoring: latency percentiles (p50, p95, p99), throughput, error rate, GPU utilization.
4. Plan scaling: autoscaling rules, load balancing, maximum replica count.

**Safe rollout:** Use canary deployment (1–5% traffic) or shadow mode (run new model alongside production without serving results) before full rollout. Monitor key metrics for several hours before increasing traffic. Maintain instant rollback capability.

## 23.8 Practical Checklists

These checklists provide systematic guidance for common transformer workflows, helping ensure that critical steps are not overlooked.

### 23.8.1 Before Training Checklist

Before beginning training, verify that you have made appropriate decisions about resources and configuration. Estimate memory requirements using the formulas provided earlier, ensuring that your chosen batch size and sequence length will fit in available GPU memory with some margin for safety. Select hardware appropriate for your model size and training duration, considering the trade-offs between cost and training time.

Choose batch size and sequence length based on your task requirements and memory constraints. Remember that sequence length has a quadratic effect on memory, so reducing it provides substantial savings if your task permits. Set up monitoring and logging infrastructure before training begins, as debugging issues after the fact is much more difficult than catching them in real-time.

Estimate training time and cost using the guidelines provided earlier. This helps with planning and ensures that you have allocated sufficient budget and time for the training run. For long training runs, verify that checkpointing is configured correctly and test recovery from checkpoints before committing to the full training run.

### 23.8.2 During Training Checklist

While training is in progress, monitor loss and metrics regularly to detect issues early. Training loss should decrease steadily, though not necessarily monotonically. Validation loss should track training loss initially, with some divergence expected as training progresses. If validation loss increases while training loss decreases, you may be overfitting.

Check GPU utilization to ensure that you are using resources efficiently. Utilization should be consistently above 80% during training. Lower utilization suggests that batch size is too small, data loading is a bottleneck, or there are inefficiencies in the training loop. Monitor memory usage to ensure you are not close to OOM errors, which can cause training to fail unexpectedly.

Save checkpoints regularly according to your checkpointing strategy. Verify that checkpoints are being saved successfully and that you can load them for recovery. Validate periodically on a held-out set to track generalization performance. The frequency of validation depends on training duration, but every few hundred steps or every epoch is typical.

### 23.8.3 Before Deployment Checklist

Before deploying a model to production, optimize it for inference using the techniques described earlier. Apply quantization if accuracy permits, as the performance benefits are substantial. Consider distillation if you need further speedup and have time for the additional training. Export the model to an optimized format like ONNX or TensorRT if using those serving frameworks.

Benchmark latency and throughput under realistic conditions, including the batch sizes and sequence lengths you expect in production. Test with both average-case and worst-case inputs to understand performance variability. Estimate serving costs based on expected request volume and the hardware required to meet latency requirements.

Set up monitoring and alerting for the production deployment. Ensure that you can track request rate, latency, error rate, and resource utilization. Configure alerts for anomalies in these metrics. Plan your scaling strategy, including autoscaling rules if using dynamic scaling.

Test the deployment pipeline end-to-end, including model loading, preprocessing, inference, and postprocessing. Verify that error handling works correctly and that failures are logged appropriately. Conduct load testing to ensure the system can handle expected traffic with appropriate margins for spikes.

## 23.9 Hyperparameter Tuning

### 23.9.1 Critical Hyperparameters (Ordered by Impact)

#### 1. Learning Rate (highest impact)

- Typical range:  $[10^{-5}, 10^{-3}]$
- BERT:  $1 - 5 \times 10^{-5}$
- GPT:  $2 - 6 \times 10^{-4}$
- Rule: Larger models need smaller LR

#### 2. Batch Size

- Trade-off: Speed vs generalization
- Typical: 32-512 for fine-tuning, 256-2048 for pre-training
- Scale LR linearly with batch size

#### 3. Warmup Steps

- Typical: 5-10% of total training steps
- BERT: 10,000 steps
- GPT-3: 375M tokens (out of 300B)

#### 4. Weight Decay

- Typical: 0.01 to 0.1
- AdamW: Decouple from learning rate

#### 5. Dropout

- Standard: 0.1
- Larger models: Lower dropout (0.05 or none)
- Apply uniformly (attention, FFN, embeddings)

### 23.9.2 Tuning Strategy

#### Phase 1: Coarse search

- Grid/random search over wide ranges
- Short runs (10% of full training)
- Focus on learning rate first

#### Phase 2: Fine search

- Narrow ranges around best from Phase 1
- Longer runs (50% of full training)
- Tune other hyperparameters

#### Phase 3: Validation

- Full training with best settings
- Multiple seeds for robustness
- Final evaluation on test set

**Example 23.2** (Learning Rate Search). **Task:** Fine-tune BERT on classification

**Coarse search:**

- Try:  $[10^{-5}, 3 \times 10^{-5}, 10^{-4}, 3 \times 10^{-4}]$
- Train 1 epoch each
- Best:  $3 \times 10^{-5}$  (85.2% dev accuracy)

**Fine search:**

- Try:  $[2 \times 10^{-5}, 3 \times 10^{-5}, 4 \times 10^{-5}]$
- Train 3 epochs each
- Best:  $3 \times 10^{-5}$  (86.1% dev accuracy)

**Final:**

- Train with  $LR = 3 \times 10^{-5}$ , 5 epochs
- Test accuracy: 85.8%

## 23.10 Common Pitfalls and Solutions

### 23.10.1 Architecture Pitfalls

#### Pitfall 1: Forgetting positional information

- Symptom: Model treats sequence as bag-of-words
- Solution: Verify position encoding is added

#### Pitfall 2: Incorrect masking

- Symptom: Information leakage or blocked attention
- Solution: Visualize attention matrices, verify mask shape

**Pitfall 3: Not sharing embeddings**

- Symptom: Twice as many parameters as expected
- Solution: Weight tying between input/output embeddings

**23.10.2 Training Pitfalls****Pitfall 4: Insufficient warmup**

- Symptom: Training unstable early, doesn't recover
- Solution: Increase warmup to 10% of training

**Pitfall 5: Wrong learning rate scale**

- Symptom: Loss not decreasing or diverging
- Solution: Learning rate finder, try 10× up/down

**Pitfall 6: Overfitting small datasets**

- Symptom: Large train/val gap
- Solution: More dropout, data augmentation, smaller model

**23.10.3 Deployment Pitfalls****Pitfall 7: Batch size 1 in production**

- Symptom: Poor GPU utilization
- Solution: Dynamic batching, accumulate requests

**Pitfall 8: Not using mixed precision**

- Symptom: Slow inference, high memory
- Solution: FP16 inference, quantization

**Pitfall 9: No KV caching for generation**

- Symptom: Slow text generation (quadratic in length)
- Solution: Cache key/value tensors

**23.11 Case Study: BERT for Search Ranking****23.11.1 Problem Setup****Task:** Rank search results by relevance**Input:** Query + Document pairs**Output:** Relevance score  $[0, 1]$ **23.11.2 Architecture Decisions****Model:** BERT-base with regression head**Input format:**`[CLS] query tokens [SEP] document tokens [SEP]`**Output:**  $\text{score} = \sigma(\mathbf{W}\mathbf{h}_{[\text{CLS}]} + b)$

### 23.11.3 Training Strategy

**Data:**

- 10M query-document pairs
- Labels: Click-through rate (0-1)
- Hard negatives: Top results without clicks

**Loss:** Mean squared error on CTR prediction

**Optimization:**

- Learning rate:  $2 \times 10^{-5}$
- Batch size: 256
- Warmup: 10,000 steps
- Total: 100,000 steps

### 23.11.4 Production Deployment

**Optimizations:**

1. Quantize to INT8 (3× speedup)
2. Distill to 6-layer model (2× speedup)
3. Deploy with ONNX Runtime
4. Dynamic batching (avg batch size 32)

**Results:**

- Latency: 15ms p99 (vs 200ms baseline)
- Throughput: 2000 QPS per GPU
- Relevance: +8% improvement over TF-IDF

## 23.12 Case Study: GPT for Code Generation

### 23.12.1 Problem Setup

**Task:** Generate Python code from natural language

**Example:**

Input: "Function to reverse a string"

Output:

```
def reverse_string(s):  
    return s[::-1]
```

### 23.12.2 Model and Data

**Model:** GPT-2 medium (345M params)

**Data:**

- GitHub public repositories (Python)
- Filtered: Only files with docstrings
- Format: Docstring → Implementation
- Total: 50GB, 10B tokens

### 23.12.3 Training

**Pre-training:** Start from GPT-2 checkpoint

**Fine-tuning:**

- 100,000 steps
- Learning rate:  $5 \times 10^{-5}$
- Context: 1024 tokens
- Batch: 128 sequences

### 23.12.4 Evaluation

**Metrics:**

- Pass@k: % correct in top-k samples
- BLEU: Token overlap with reference
- Human evaluation: Correctness + readability

**Results:**

- Pass@1: 42%
- Pass@10: 71%
- Human preferred over baseline: 78%

## 23.13 Future Directions

### 23.13.1 Architectural Innovations

#### 1. Efficient attention

- Linear complexity methods
- State space models (S4, Mamba)
- Hybrid CNN-attention architectures

#### 2. Multimodal integration

- Unified text-image-audio models
- Better cross-modal alignment
- Efficient fusion strategies

#### 3. Long context

- Million-token contexts
- Hierarchical memory
- Retrieval-augmented transformers

### 23.13.2 Training Innovations

#### 1. Sample efficiency

- Better pre-training objectives
- Curriculum learning
- Few-shot and zero-shot learning

#### 2. Scaling

- Mixture of experts
- Conditional computation
- Efficient parallelism strategies

#### 3. Alignment

- Better RLHF techniques
- Constitutional AI
- Value alignment

## 23.14 Conclusion

### 23.14.1 Key Takeaways

#### Architecture:

- Attention is powerful and flexible
- Position encodings crucial for sequences
- Residuals + normalization enable depth

#### Training:

- Pre-training + fine-tuning is dominant paradigm
- Warmup is critical for stability
- Scale requires careful optimization

#### Deployment:

- Quantization and distillation for efficiency
- Batching crucial for throughput
- Monitor performance in production



### 23.14.2 Final Advice

**For practitioners:**

1. Start simple: Use pre-trained models
2. Debug systematically: Data, model, training
3. Optimize iteratively: Accuracy first, then speed
4. Monitor continuously: Metrics, errors, drift

**For researchers:**

1. Understand fundamentals deeply
2. Question assumptions: Why does this work?
3. Experiment rigorously: Ablations, multiple seeds
4. Share knowledge: Open source, papers, blogs

This concludes our comprehensive journey through deep learning and transformers. You now have the mathematical foundations, practical implementations, and real-world insights to build state-of-the-art transformer models!

## 23.15 Exercises

**Exercise 23.1.** Reproduce DistilBERT:

1. Train 6-layer student on BERT-base teacher
2. Use distillation + MLM + cosine losses
3. Evaluate on GLUE
4. Measure compression ratio and speedup

**Exercise 23.2.** Debug broken transformer (provided):

1. Model trains but poor performance
2. Find 3 subtle bugs (architecture, training, data)
3. Fix and verify improvements

**Exercise 23.3.** Deploy BERT for production:

1. Fine-tune on classification task
2. Quantize to INT8
3. Export to ONNX
4. Create REST API with FastAPI

5. Load test and optimize

## 23.16 Solutions

Full solutions for all exercises are available at <https://deeplearning.hofkensvermeulen.be>.

## Part VIII

# Domain-Specific Applications

## Chapter 24

# Domain-Specific Models: From General Transformers to Vertical Solutions

### Chapter Overview

This chapter sets the stage for the practical domain-specific applications to follow. It defines what constitutes a “domain-specific model” and introduces the key patterns and decision frameworks that apply across industries and use cases. Rather than immediately diving into specific domains, we establish the foundational concepts: when to use general-purpose models versus specialized architectures, how to evaluate trade-offs between transfer learning and domain adaptation, and how to systematically choose between competing approaches (fine-tuning, prompting, RAG, tool augmentation, full retraining). This chapter provides the conceptual framework that later domain-specific chapters build upon.

### Learning Objectives

1. Understand the continuum from general-purpose to domain-specific models
2. Evaluate business drivers for specialization: accuracy, latency, cost, compliance
3. Compare approaches: prompting, in-context learning, RAG, fine-tuning, continued pre-training
4. Assess when domain-specific pre-training is justified
5. Design evaluation metrics aligned with business objectives
6. Plan the technical architecture for domain applications

### 24.1 Why Domain-Specific Models?

General-purpose language models like GPT-3 and GPT-4 are remarkably capable. They can perform many tasks without task-specific training, relying on in-context learning and instruction following. Yet specialized domains present challenges that generic models struggle with.

The decision to build a domain-specific model is fundamentally a business decision, not just a technical one. Organizations must weigh the costs of specialization—data collection, model training, infrastructure, and ongoing maintenance—against the benefits: improved accuracy, reduced operational costs, regulatory compliance, and competitive advantage. A general-purpose model might achieve 75% accuracy on a task, which sounds reasonable until you realize that the 25% error rate translates to thousands of customer complaints, regulatory violations, or lost revenue. In high-stakes domains like healthcare, finance, and law, even small accuracy improvements can justify significant investment.

Consider a financial institution processing loan applications. A general-purpose model might correctly assess creditworthiness 80% of the time. But that 20% error rate means approving risky loans (leading to defaults) or rejecting qualified applicants (losing business). A domain-specific model trained on historical loan data, incorporating domain knowledge about credit scoring, and fine-tuned for the

institution's risk tolerance might achieve 95% accuracy. The 15-point improvement could save millions in prevented defaults and captured revenue, easily justifying the development cost.

### 24.1.1 Limitations of General-Purpose Models in Specialized Domains

The challenges that drive organizations toward domain-specific models fall into several categories, each with distinct business implications. Understanding these limitations helps frame the specialization decision as a strategic choice rather than a purely technical exercise.

**Definition 24.1** (Domain-Specific Challenge Taxonomy). General models struggle with:

- **Jargon and terminology:** Medical diagnoses, legal citations, financial instruments—specialized vocabulary requires domain familiarity. When a model encounters “myocardial infarction” or “force majeure,” it needs more than dictionary definitions; it needs contextual understanding of how these terms function within their domains.
- **Accuracy requirements:** A 90% accurate chatbot is acceptable for entertainment; unacceptable for medical diagnosis or financial advice. The business cost of errors varies dramatically by domain. A wrong movie recommendation is an annoyance; a wrong drug dosage recommendation is potentially fatal.
- **Hallucination sensitivity:** Fabricated case law or drug interactions have serious consequences. General models are trained to be helpful and generate plausible-sounding text, but “plausible” is not the same as “true.” In domains where factual accuracy is critical, hallucination is not just an inconvenience—it’s a liability.
- **Latency constraints:** Real-time clinical decision support needs sub-second response; API calls to large models are too slow. When a physician is making a treatment decision with a patient in front of them, waiting 3–5 seconds for an API response is unacceptable. Domain-specific models can be optimized for speed, often running locally on edge devices.
- **Cost at scale:** Medical institutions processing millions of documents cannot afford \$0.01 per API call; on-prem or open models become cost-effective. At scale, API costs compound quickly. Processing 10 million documents at \$0.01 each costs \$100,000. A domain-specific model might cost \$50,000 to develop but \$0.0001 per inference, reducing ongoing costs by 99%.
- **Data privacy:** Healthcare, finance, and law cannot send sensitive data to third-party APIs; models must run on-premises or use private clouds. Regulations like HIPAA, GDPR, and industry-specific compliance requirements often prohibit sending sensitive data to external services. Domain-specific models deployed on-premises or in private clouds address this constraint.
- **Regulatory compliance:** Explainability, audit trails, and non-discrimination requirements are stricter than general-purpose settings. Regulators increasingly require that automated decision systems be explainable and auditable. General-purpose models are often black boxes; domain-specific models can be designed with interpretability in mind.
- **Domain-specific structure:** Medical images, ECGs, genomic sequences, and financial time series have structure not present in natural language. General language models excel at text but struggle with specialized data formats. Domain-specific architectures can incorporate structural priors that improve performance.

### 24.1.2 Example: Legal Document Analysis

Let's examine a concrete example that illustrates why domain specialization matters. A general GPT-3 model can summarize legal documents—it understands language structure, can identify key points, and generates coherent summaries. However, several critical issues emerge in professional legal practice:

First, the model may misinterpret binding clauses or liability limitations. Legal language is precise; a single word can change the meaning of a contract. “Shall” versus “may” has legal significance that a general model might not capture. A clause stating “Party A shall indemnify Party B” creates a binding obligation; “Party A may indemnify Party B” creates an option. Misinterpreting this distinction could lead to incorrect legal advice.

Second, general models hallucinate case citations. When asked to support a legal argument, GPT-3 might generate plausible-sounding citations like “Smith v. Jones, 500 F.2d 123 (9th Cir. 1985)” that don't actually exist. For a lawyer, citing non-existent cases is malpractice. The model's tendency to generate helpful-sounding but false information is unacceptable in legal practice.

Third, lawyers cannot rely on a system that sometimes makes things up. Legal work requires certainty. A lawyer needs to know whether a citation is real, whether a precedent applies, and whether a contract clause is enforceable. Probabilistic accuracy is insufficient; the system must be trustworthy or it cannot be used.

Fourth, a law firm cannot send confidential client contracts to OpenAI's servers. Attorney-client privilege and confidentiality obligations prohibit sharing client information with third parties. Using an API-based general model would violate these obligations.

A domain-specific legal model addresses these issues. Trained on case law, contracts, and legal precedent, it understands legal terminology and reasoning. It can be configured to only cite cases from its training corpus, eliminating hallucinated citations. It runs locally on the firm's infrastructure, preserving confidentiality. And it can be fine-tuned on the firm's historical work, learning the firm's style and preferences. The result is a tool that lawyers can actually trust and use in professional practice.

## 24.2 Patterns of Specialization

There is no single “right” approach to building domain-specific systems. Instead, there is a spectrum of approaches, each with trade-offs. The key is matching the approach to your specific constraints: available data, budget, timeline, accuracy requirements, and operational environment. Understanding these patterns helps you make informed decisions about where to invest your resources.

The patterns we'll explore represent increasing levels of specialization and investment. Prompting requires no training but offers limited accuracy. RAG adds domain knowledge without retraining. Fine-tuning adapts a model to your domain. Domain-adaptive pre-training builds deep domain expertise. Custom architectures optimize for domain-specific structure. Each step up this ladder increases cost and complexity but also increases performance and control.

### 24.2.1 Pattern 1: Prompting and In-Context Learning

**Approach:** Use a large general-purpose model (GPT-3.5, GPT-4) with carefully engineered prompts. Include domain context and examples in the prompt.

This is the fastest path to a working system. You write a prompt that includes domain context, examples of desired behavior, and specific instructions. The model uses its general knowledge plus your prompt to generate responses. No training, no infrastructure, no data collection—just prompt engineering.

The business appeal is obvious: you can have a prototype running in hours. A product manager can experiment with different prompts, test with real users, and iterate quickly. For many applications, especially those with moderate accuracy requirements and low volume, prompting is sufficient. A customer service chatbot that handles common questions, a content generation tool for marketing copy, or a data extraction tool for simple documents can all work well with prompting alone.

However, prompting has fundamental limitations that become apparent at scale or in high-stakes applications. The model hasn't learned your domain; it's improvising based on general knowledge and your prompt. Accuracy plateaus around 70–80% for most tasks. The model hallucinates facts, especially when asked about specialized topics outside its training data. And at high volume, API costs become prohibitive.

**Advantages:**

- Zero engineering: No training required, no infrastructure to build, no data to collect
- Fast deployment: Hours to iterate on prompts, days to production
- Leverages model's general knowledge: Benefits from the model's broad training
- Handles novel tasks through prompt variation: Can adapt to new tasks by changing the prompt

**Disadvantages:**

- Limited accuracy: No task-specific training means the model is guessing based on general patterns
- Hallucination: Model generates plausible-sounding but false information, especially for specialized domains
- Latency: API calls to large models take seconds, unacceptable for real-time applications
- Cost: Expensive at high scale (\$0.01 per request  $\times$  1M requests = \$10,000/month)
- Privacy: Data sent to third-party servers, violating confidentiality requirements in many domains
- Limited control: Model behavior determined by provider updates; your system can break when the provider changes the model

**Best for:** Prototyping, low-risk applications, rapid experimentation, low-volume use cases

### 24.2.2 Pattern 2: Retrieval-Augmented Generation (RAG)

**Approach:** Store domain knowledge in a vector database. For each query, retrieve relevant documents; feed documents + query to a language model.

RAG represents a significant step up from pure prompting. Instead of relying solely on the model's training data, you provide it with relevant information retrieved from your own knowledge base. This grounds the model's responses in actual documents, dramatically reducing hallucination while keeping the flexibility of a general-purpose model.

The business value of RAG is compelling: you get much better accuracy without the cost and complexity of retraining. You can update your knowledge base continuously—adding new documents, removing outdated information—without touching the model. For knowledge-intensive applications like customer support, technical documentation, or research assistance, RAG often provides the best balance of accuracy, cost, and maintainability.

Consider a technical support system for a software company. The company has thousands of support articles, bug reports, and solution documents. A pure prompting approach would fail because the model doesn't know about the company's specific products and issues. But with RAG, each support query retrieves the most relevant articles, and the model generates an answer based on those articles. The system can cite its sources, users can verify the information, and the knowledge base stays current as new articles are added.

**Example:** A medical question answering system retrieves relevant clinical guidelines and research papers, then asks the model to answer based on those sources. When a physician asks “What is the recommended treatment for stage 2 hypertension in diabetic patients?” the system retrieves current clinical guidelines, recent research papers, and treatment protocols, then synthesizes an answer grounded in those sources.

**Advantages:**

- Grounds responses in actual documents (reduces hallucination): The model can only use information from retrieved documents, not make things up
- No retraining needed: Use existing general-purpose models with your domain knowledge
- Knowledge is updatable (add new documents without retraining): Your knowledge base evolves continuously without model changes
- Can use smaller, faster models (costs lower): Since you're providing relevant context, you don't need the largest models

**Disadvantages:**

- Retrieval quality critical: Bad retrieval → bad answers. If the system retrieves irrelevant documents, the model can't generate good responses
- Limited reasoning: Model can only work with retrieved context. Complex multi-step reasoning across many documents is challenging
- Latency: Retrieval + generation takes time (200–500ms), which may be too slow for real-time applications
- Complexity: Requires maintaining document databases, embeddings, etc.

**Best for:** Knowledge-intensive tasks, when accuracy depends on recent information, privacy-sensitive applications

### 24.2.3 Pattern 3: Fine-Tuning

**Approach:** Start with a pre-trained general model (BERT, GPT-2). Train on domain-specific labeled data to adapt weights.

**Advantages:**

- Better accuracy: Model learns domain-specific patterns
- Faster than pretraining: Requires far less compute
- Smaller models: Fine-tuned BERT can outperform large prompting
- Lower cost: Small models are cheap to run
- Full control: Model runs locally or on your infrastructure

**Disadvantages:**

- Requires labeled data: Need hundreds or thousands of examples
- Training cost: Still requires significant compute
- Limited to tasks with training data: Cannot adapt to novel tasks like prompting

**Best for:** Well-defined tasks with sufficient labeled data, accuracy-critical applications

### Parameter-Efficient Fine-Tuning (PEFT)

As models have grown to billions of parameters, full fine-tuning has become prohibitively expensive. Parameter-efficient fine-tuning methods adapt large models by updating only a small fraction of parameters, dramatically reducing computational and memory requirements while maintaining accuracy.

**LoRA (Low-Rank Adaptation):** Instead of updating all model weights, LoRA adds trainable low-rank matrices to attention layers. For a weight matrix  $W \in \mathbb{R}^{d \times d}$ , LoRA adds  $\Delta W = BA$  where  $B \in \mathbb{R}^{d \times r}$  and  $A \in \mathbb{R}^{r \times d}$  with rank  $r \ll d$  (typically  $r = 8$  or  $16$ ). Only  $A$  and  $B$  are trained, reducing trainable parameters by 10,000x while achieving 95-99% of full fine-tuning performance.



**QLoRA (Quantized LoRA):** Combines LoRA with 4-bit quantization of the base model, enabling fine-tuning of 65B parameter models on a single consumer GPU. The base model is quantized to 4-bit precision (reducing memory by 4x), while LoRA adapters remain in full precision. This democratizes large model fine-tuning, making it accessible to organizations without massive GPU clusters. QLoRA has become the standard for fine-tuning large language models in 2024-2025.

**IA3 (Infused Adapter by Inhibiting and Amplifying Inner Activations):** Learns multiplicative scaling factors for attention and feedforward activations, requiring even fewer parameters than LoRA (typically 0.01% of model parameters). IA3 achieves competitive performance on many tasks while being extremely memory-efficient, making it ideal for fine-tuning multiple task-specific adapters on the same base model.

**Adapter Layers:** Insert small trainable modules (adapters) between transformer layers. Each adapter is a bottleneck architecture (down-project, nonlinearity, up-project) with only 0.5-2% additional parameters. Multiple task-specific adapters can be trained and swapped at inference time, enabling one base model to serve many tasks efficiently.

**Prefix Tuning and Prompt Tuning:** Instead of modifying model weights, learn continuous prompt embeddings that are prepended to inputs. The model itself remains frozen, and only the prompt embeddings are trained. This is extremely parameter-efficient (0.001-0.1% of model parameters) but typically achieves lower accuracy than LoRA or adapters.

#### 24.2.4 Pattern 4: Domain-Adaptive Pre-Training

**Approach:** Continue pre-training a general model on unlabeled domain data before fine-tuning on task-specific data.

**Example:** Start with BERT (trained on Wikipedia + BookCorpus). Continue training on medical literature (PubMed). Then fine-tune on labeled medical diagnosis data.

**Advantages:**

- Leverages both general and domain knowledge
- Better than fine-tuning alone when task data is limited
- Can use unlabeled data (much cheaper to collect than labeled)

**Disadvantages:**

- High computational cost: Pre-training is expensive
- Only justified when general-purpose models are weak on domain
- Long development timeline

**Best for:** Highly specialized domains with weak general models, large unlabeled domain data available, and strong business justification

#### 24.2.5 Pattern 5: Custom Architecture Design

**Approach:** Design an architecture specifically for domain structure. Example: Multi-head attention for simultaneous processing of medical images + lab values + clinical notes.

**Advantages:**

- Optimal for domain constraints: Leverage domain structure
- Efficiency: Smaller, faster models possible
- Explainability: Domain-specific design can improve interpretability

**Disadvantages:**

- High expertise required: Need deep domain + ML knowledge

- High development cost: Months of research and engineering
- Reduced flexibility: Model designed for specific task

**Best for:** Well-funded organizations with specialized data and domain experts

## 24.3 Decision Framework: Choosing an Approach

**Note:** PEFT (Parameter-Efficient Fine-Tuning) includes methods like LoRA, QLoRA, and IA3, which have become the standard approach for adapting large language models as of 2024-2025.

### 24.3.1 When to Start Small, Scale Up

A pragmatic approach is to start with the simplest solution and upgrade as needed:

#### 1. Phase 1: Prompting (Week 1–2)

- Build a prototype with API-based model
- Measure performance on a small test set
- If accuracy  $\geq 85\%$ , ship it
- Otherwise, move to Phase 2

#### 2. Phase 2: RAG (Week 2–4)

- Collect domain documents
- Build vector database with embeddings
- Integrate retrieval into prompt
- If accuracy  $\geq 85\%$ , deploy
- Otherwise, move to Phase 3

#### 3. Phase 3: Fine-Tuning (Month 1–2)

- Collect and annotate labeled data
- Fine-tune a smaller model (BERT, DistilBERT, GPT-2)
- If accuracy  $\geq 90\%$ , deploy with cost benefit
- Otherwise, evaluate custom approaches

This phased approach avoids over-engineering early and focuses resources where they matter most.

## 24.4 Evaluating Domain-Specific Models

Evaluation metrics should align with business objectives, not generic benchmarks.

### 24.4.1 Task-Specific Metrics

For classification: Accuracy, Precision, Recall, F1, AUC-ROC (are top-k predictions relevant?)

For generation: BLEU, ROUGE (overlap with reference), BERTScore (semantic similarity)

For retrieval: Recall@k, NDCG@k (are relevant documents ranked high?)

### 24.4.2 Business Metrics

Beyond accuracy, measure:

- **Latency:** Does the system meet real-time requirements?
- **Cost:** Cost per prediction; compare vs. human labor or baseline
- **Adoption:** Do users actually use system predictions?
- **Improvement:** Does the system improve over human baseline?
- **Safety:** Are there failure modes that cause harm?

### 24.4.3 Online Evaluation: A/B Testing

Offline metrics (accuracy on test set) don't always predict online success. A/B testing is essential:

1. Deploy new model to 10% of traffic
2. Measure key metrics (engagement, conversion, errors, latency)
3. If metrics improve, gradually increase traffic
4. If metrics degrade, rollback immediately

Online experiments often reveal issues invisible in offline evaluation (e.g., model is accurate but too slow for real-time use).

## 24.5 Planning the Technical Architecture

Domain-specific systems require decisions beyond the model:

### 24.5.1 Deployment Options

- **Cloud API (OpenAI, Anthropic):** Simplest but most expensive and least private
- **Self-hosted cloud (AWS, Azure, GCP):** Moderate cost and control; data stays on managed infrastructure
- **On-premises:** Full control and privacy; operational complexity
- **Edge (mobile, IoT):** Maximum privacy and latency; limited by device compute
- **Hybrid:** Mix of cloud and on-premises for balance

### 24.5.2 Pipeline Architecture

Most production systems are pipelines, not single models:

1. **Input processing:** Clean, normalize, validate input data
2. **Feature extraction:** Convert raw input to model-readable format
3. **Model inference:** Run through model
4. **Output processing:** Validate, interpret, format results
5. **Feedback loop:** Log predictions for analysis and retraining

Each stage has failure modes. Robust systems handle failures at each stage (re-routing, fallbacks, human escalation).

## 24.6 Case Study: Evolving from General to Specialized

A healthcare system wants to build a diagnostic assistant.

### Stage 1: Prompting (2 weeks)

- Use GPT-3.5 with medical prompts
- Accuracy on internal test set: 72% (not sufficient for clinical use)
- Cost: High API calls

### Stage 2: RAG (4 weeks)

- Embed clinical guidelines and case studies
- Retrieve relevant information for each patient
- Accuracy: 81% (better, but still not sufficient)
- Cost: Reduced API calls + retrieval cost

### Stage 3: Fine-Tuning (8 weeks)

- Annotate 5,000 patient cases with ground truth diagnoses
- Fine-tune BioBERT (medical BERT variant)
- Accuracy: 89% (acceptable for decision support)
- Cost: Low inference cost, on-premises deployment

### Stage 4: Hybrid System (ongoing)

- Use fine-tuned model as primary predictor
- Augment with RAG for explainability (show relevant case studies)
- Escalate low-confidence cases to human clinician
- Accuracy: 94% (with human-in-the-loop on uncertain cases)

## 24.7 Continuous Learning and Model Drift

One of the most critical yet often overlooked aspects of domain-specific models is their need for continuous adaptation. Unlike static software systems that work the same way indefinitely, machine learning models degrade over time as the world changes around them. This phenomenon, called model drift or concept drift, is particularly acute in domain-specific applications where the domain itself evolves.

### 24.7.1 Understanding Model Drift

Model drift occurs when the statistical properties of the data change over time, causing model performance to degrade. In business terms, this means a model that worked well at deployment gradually becomes less accurate, leading to poor decisions, customer complaints, and lost revenue. Understanding the types and causes of drift is essential for building maintainable domain-specific systems.

#### Types of Drift:

**Data drift (covariate shift):** The distribution of input features changes, but the relationship between inputs and outputs remains stable. For example, in a credit scoring model, the average income of applicants might increase over time due to inflation, but the relationship between income and creditworthiness stays the same. The model needs to adapt to the new input distribution.

**Concept drift:** The relationship between inputs and outputs changes. In fraud detection, fraudsters constantly evolve their tactics. A pattern that indicated fraud last year might be normal behavior this year, and vice versa. The model’s learned concepts become outdated.

**Label drift:** The definition of the target variable changes. In content moderation, what counts as “inappropriate content” evolves with social norms and platform policies. A model trained on last year’s guidelines will misclassify content under new guidelines.

### 24.7.2 Detecting Drift in Production

You cannot fix drift if you don’t detect it. Production systems need monitoring infrastructure that tracks model performance and data distributions over time. The challenge is that ground truth labels are often delayed or unavailable, making direct performance monitoring difficult.

**Performance-based detection:** The most direct approach is monitoring actual model performance metrics (accuracy, precision, recall, F1) on recent data. This requires collecting ground truth labels, which may be delayed. For example, in loan default prediction, you won’t know if a prediction was correct until months or years later. However, for applications where labels arrive quickly (customer support ticket resolution, click-through rate prediction), performance monitoring is straightforward and highly effective.

**Distribution-based detection:** Monitor the distribution of input features and model predictions. Significant changes suggest drift even without ground truth labels. Statistical tests like the Kolmogorov-Smirnov test or Population Stability Index (PSI) can detect distribution shifts. For example, if your model suddenly predicts “high risk” for 30% of applicants when it historically predicted 10%, something has changed—either the input distribution or the model’s behavior.

**Prediction confidence monitoring:** Track the distribution of model confidence scores. If the model becomes less confident over time (more predictions near 0.5 for binary classification), it suggests the model is encountering data it wasn’t trained on. Conversely, if confidence increases but accuracy decreases, the model is becoming overconfident on out-of-distribution data.

**Business metric monitoring:** Ultimately, models exist to drive business outcomes. Monitor downstream metrics like conversion rates, customer satisfaction, or operational efficiency. If these degrade while model accuracy appears stable, the model may be optimizing the wrong objective or missing important edge cases.

### 24.7.3 Strategies for Continuous Learning

Once drift is detected, you need strategies to adapt the model. The right approach depends on your constraints: available data, retraining cost, deployment complexity, and acceptable downtime.

**Periodic retraining:** The simplest approach is retraining the model on a schedule (weekly, monthly, quarterly) using recent data. This works well when drift is gradual and predictable. For example, a recommendation system might retrain weekly to incorporate new user preferences and content. The challenge is choosing the right frequency: too frequent wastes resources, too infrequent allows performance to degrade.

**Triggered retraining:** Retrain when drift detection systems signal significant performance degradation. This is more efficient than periodic retraining but requires robust monitoring. Set thresholds for acceptable performance degradation (e.g., if accuracy drops below 85%, trigger retraining). This approach works well for applications where drift is unpredictable but detectable.

**Online learning:** Update the model continuously as new data arrives, without full retraining. This is ideal for applications with high-velocity data streams (fraud detection, real-time bidding, content recommendation). However, online learning requires careful engineering to prevent catastrophic forgetting (the model forgets old patterns while learning new ones) and to handle noisy or adversarial data.

**Ensemble approaches:** Maintain multiple models trained on different time periods and combine their predictions. This provides robustness to drift: if one model becomes outdated, others compensate. For example, maintain models trained on the last month, last quarter, and last year. Weight their predictions based on recent performance. This approach is more complex but provides smoother adaptation.

**Human-in-the-loop retraining:** For high-stakes applications, involve domain experts in the retraining process. Experts review model predictions, correct errors, and provide feedback that guides retraining. This is slower and more expensive but ensures quality. Medical diagnosis systems, legal document analysis, and financial risk assessment often use this approach.

#### 24.7.4 Practical Implementation Considerations

Implementing continuous learning requires infrastructure beyond the model itself. You need data pipelines, monitoring systems, retraining automation, and deployment processes that work together seamlessly.

**Data versioning:** Track which data was used to train each model version. When performance degrades, you need to understand what changed. Tools like DVC (Data Version Control) or MLflow help manage data and model versions together.

**Model versioning and rollback:** Maintain multiple model versions in production. If a new model performs worse than expected, roll back to the previous version quickly. Implement A/B testing to compare new and old models before full deployment.

**Automated retraining pipelines:** Build infrastructure that automates data collection, preprocessing, training, evaluation, and deployment. This reduces the cost of frequent retraining and ensures consistency. Tools like Kubeflow, MLflow, or custom pipelines orchestrate these steps.

**Monitoring dashboards:** Provide visibility into model performance, data distributions, and business metrics. Dashboards help teams detect issues early and understand their causes. Include alerts that notify teams when metrics exceed thresholds.

**Cost management:** Continuous learning has ongoing costs: data storage, compute for retraining, and engineering time. Budget for these costs upfront. For large models, retraining might cost thousands of dollars per run. Optimize by retraining only when necessary and using efficient training techniques.

#### 24.7.5 Cross-Domain Patterns

The continuous learning challenges and solutions discussed here apply across all domain-specific applications covered in subsequent chapters:

- **Chapter 25 (Enterprise NLP):** Text classification models drift as language evolves and new categories emerge. Customer support ticket routing needs continuous adaptation as products and issues change.
- **Chapter 26 (Code):** Code models drift as programming languages evolve, new libraries emerge, and coding practices change. Models trained on Python 3.8 code may struggle with Python 3.12 features.
- **Chapter 29 (Recommendations):** User preferences change over time. A recommendation model trained on 2023 data may not capture 2024 trends. Continuous learning is essential for maintaining engagement.
- **Chapter 30 (Healthcare):** Medical knowledge evolves as new treatments are discovered and guidelines are updated. Clinical decision support systems need continuous updates to reflect current best practices.
- **Chapter 31 (Finance):** Financial markets are non-stationary by nature. Trading strategies that worked last year may fail this year. Continuous adaptation is not optional—it's survival.
- **Chapter 32 (Legal):** Laws change, new precedents are set, and legal interpretations evolve. Legal AI systems must stay current with the latest case law and regulations.
- **Chapter 33 (Observability):** System behavior changes as infrastructure evolves, new services are deployed, and traffic patterns shift. Anomaly detection models must adapt to the new normal.

The specific implementation details vary by domain, but the fundamental challenge is the same: models must evolve with their domains to remain useful. Subsequent chapters will explore domain-specific drift patterns and adaptation strategies in detail.

## 24.8 Exercises

**Exercise 24.1.** For a domain you're familiar with, describe the key challenges that make general-purpose models insufficient. What specialization pattern would you start with?

**Exercise 24.2.** Design an evaluation plan for a domain-specific system. What metrics beyond accuracy would you measure? How would you conduct A/B testing?

**Exercise 24.3.** Compare the cost-benefit of different approaches (prompting, RAG, fine-tuning, domain-adaptive pre-training) for your domain. At what scale does each become cost-effective?

## 24.9 Solutions

Full solutions for all exercises are available at <https://deeplearning.hofkensvermeulen.be>.

Table 24.1: Decision Framework for Selecting Specialization Approach

Factor	Prompting	RAG	PEFT	Fine-Tune	Domain PT	Custom
Time to deploy	Days	Weeks	Weeks	Weeks–Months	Months–Years	Months–Years
Accuracy	70–80%	75–85%	82–92%	85–95%	90–98%	95–99%
Cost (training)	\$0	\$1K–10K	\$500–5K	\$10K–100K	\$100K–1M	\$1M+
Cost (inference)	High (\$0.01/req)	Medium (\$0.001/req)	Low (\$0.0001/req)	Low (\$0.00001/req)	Low	Low
Data required	None	1K–10K docs	500–5K labels	1K–10K labels	10M tokens + labels	100K–1M labels
Privacy	Poor	Medium	Good	Good	Good	Good
Latency	High (1–5s)	Medium (200ms–1s)	Low (50–200ms)	Low (10–100ms)	Low	Low
Flexibility	High	High	High	Medium	Low	Low



## Chapter 25

# Natural Language and Enterprise NLP: Search, Classification, Assistants

### Chapter Overview

This chapter addresses the practical deployment of language models in enterprise environments, focusing on real-world applications that solve concrete business problems. We examine semantic search and retrieval systems, text classification for routing and triage, and conversational assistants that support customer interactions. Unlike the general-purpose language models of previous chapters, enterprise NLP applications balance accuracy, latency, cost, and regulatory constraints. This chapter emphasizes how the foundations of transformers, embeddings, and fine-tuning translate into production systems that generate measurable business value.

### Learning Objectives

1. Understand semantic search architectures and vector database integration
2. Design and deploy text classification pipelines with BERT-style models
3. Build conversational assistants with guardrails and human escalation
4. Implement monitoring and drift detection for NLP systems
5. Balance accuracy, latency, and cost in production deployments
6. Handle domain-specific data challenges: labeling, imbalance, and long-tail classes

### 25.1 Enterprise Search and Semantic Retrieval

Enterprise search is one of the most impactful yet underappreciated applications of NLP. Consider the daily frustration of employees unable to find critical information buried in company wikis, documentation systems, and shared drives. A study by IDC found that knowledge workers spend 2.5 hours per day searching for information, costing large organizations millions in lost productivity annually. Traditional keyword-based search systems, built on TF-IDF or BM25, struggle with semantic similarity. A user searching for “vehicle transmission problems” may not retrieve documents discussing “automotive gearbox failures,” despite semantic equivalence.

The business case for semantic search is straightforward: if you can reduce search time by 50%, you recover 1.25 hours per employee per day. For a 1,000-person organization with an average salary of \$100,000, that’s approximately \$15 million in recovered productivity annually. The investment in semantic search infrastructure—typically \$50,000–\$200,000 for development and deployment—pays for itself within weeks.

Semantic search addresses the limitations of keyword matching by encoding both queries and documents into high-dimensional vector spaces where similar meanings are close together, enabling retrieval

based on semantic understanding rather than lexical overlap. This means “car transmission issues” and “automobile gearbox problems” are recognized as semantically similar even though they share no common words.

### 25.1.1 Architecture and Workflow

A semantic search system has several components working in concert, each serving a specific purpose in the retrieval pipeline. Understanding this architecture helps you make informed decisions about where to invest engineering effort and computational resources.

First, a dense embedding model encodes documents and queries into vectors. This is the heart of semantic search—the model that learned to represent meaning as geometry. Pre-trained models like BERT-base, all-MiniLM-L6-v2, or specialized dense retrievers (e.g., DPR, ColBERT) map text to fixed-size embeddings. The choice of model involves trade-offs: larger models like BERT-base (768 dimensions) capture more nuance but require more compute; smaller models like MiniLM (384 dimensions) are faster but may miss subtle semantic distinctions.

Second, a vector database (Pinecone, Weaviate, Milvus, Qdrant) indexes these embeddings for fast nearest-neighbor retrieval. This is where engineering meets mathematics: the database must efficiently search through millions or billions of vectors to find the most similar ones. The data structure choices here—HNSW graphs, IVF indexes, or LSH hashing—determine whether your search takes milliseconds or seconds.

Third, a ranking model optionally re-scores the top-k candidates for finer-grained relevance. The initial retrieval casts a wide net; the ranker applies more sophisticated (and expensive) scoring to the candidates. This two-stage approach balances speed and accuracy: fast retrieval narrows the search space, then careful ranking orders the results.

The pipeline often combines dense retrieval with sparse BM25 ranking in a hybrid approach to capture both semantic and keyword-based signals. This hedges against the weaknesses of each method: dense retrieval might miss exact keyword matches (like product codes or technical terms), while BM25 might miss semantic similarity. Combining them gives you the best of both worlds.

**Definition 25.1** (Semantic Search Pipeline). The semantic search pipeline transforms a user’s natural language query into relevant documents through a series of steps, each optimized for a specific aspect of the retrieval problem:

1. **Embed query:** Transform the user’s text into a vector representation that captures its semantic meaning:

$$\mathbf{q} = \text{encoder}(q_{\text{text}}) \quad (25.1)$$

This encoding happens in real-time when the user submits their query. The encoder must be fast (ideally  $\leq 50\text{ms}$ ) to maintain responsive search.

2. **Embed documents (offline):** Pre-compute embeddings for all documents in your corpus:

$$\mathbf{d}_i = \text{encoder}(d_{\text{text},i}) \quad \text{for } i = 1, \dots, N \quad (25.2)$$

This happens offline, typically during nightly batch jobs. For a corpus of 1 million documents, this might take hours, but it only needs to be done once per document (or when documents are updated).

3. **Index vectors:** Store  $\{\mathbf{d}_i\}$  in vector database with fast retrieval structures. The indexing process builds data structures (like HNSW graphs) that enable sub-linear search time. Without indexing, finding nearest neighbors would require comparing the query to every document—infeasible at scale.

4. **Retrieve top-k:** Find the  $k$  documents whose embeddings are closest to the query embedding:

$$\text{topk} = \text{retrieve}(\mathbf{q}, \mathbf{D}, k) \quad (25.3)$$

Typically  $k=100\text{--}1000$  for the initial retrieval. This step is optimized for speed, using approximate nearest neighbor algorithms that trade perfect accuracy for 10–100x speedup.

5. **Rank (optional):** Apply a more sophisticated scoring function to re-order the top- $k$  candidates:

$$s_i = \text{ranker}(q, d_i) \quad \text{and re-sort} \quad (25.4)$$

The ranker might use cross-attention between query and document, consider user context, or incorporate business rules (e.g., prioritize recent documents).

6. **Return:** Present the top- $k$  re-ranked results to user, typically with snippets highlighting relevant passages.

### 25.1.2 Practical Considerations: Embedding Model Selection

Choosing an embedding model is one of the most consequential decisions in building a semantic search system. The model determines your accuracy ceiling, computational costs, and operational complexity. Let's examine the trade-offs systematically.

BERT-base produces 768-dimensional embeddings with strong performance but requires GPU inference. For a query, BERT-base takes approximately 50–100ms on CPU or 5–10ms on GPU. At 1,000 queries per second, CPU-only deployment would require 50–100 CPU cores—expensive and operationally complex. GPU deployment is more cost-effective but requires GPU infrastructure and expertise.

Lighter models like all-MiniLM-L6-v2 (384-dim) offer 10–20 $\times$  faster inference with minimal accuracy loss on semantic similarity tasks. This model runs comfortably on CPU, taking 5–10ms per query. For most enterprise applications, the accuracy difference (typically 2–5 percentage points on retrieval metrics) is worth the operational simplicity and cost savings.

For domain-specific applications (e.g., legal, medical), domain-adaptive pre-training or fine-tuning the embedding model on labeled pairs improves performance significantly. A legal search system using a general-purpose embedding model might achieve 70% recall@10; fine-tuning on legal document pairs can push this to 85–90%. The investment in fine-tuning (collecting labeled pairs, training for a few days) pays off in dramatically better user experience.

Embedding quality directly impacts retrieval accuracy, and the quality depends heavily on training data. Hard negative mining—training on documents that are contextually similar but semantically different—significantly improves ranking. For example, when searching for instructions on “how to reset a router,” a document about network protocols is harder to distinguish from the correct answer than a document about cooking recipes. The model must learn fine-grained distinctions, not just broad topic similarity.

Collecting and training on such hard negatives through user feedback or synthetic generation improves model robustness. In practice, this means logging queries where users didn't click the top results (indicating poor retrieval), then using those as training data. This creates a feedback loop: the system learns from its mistakes, continuously improving.

### 25.1.3 Vector Database Operations

Vector databases are specialized systems optimized for the specific workload of semantic search: storing millions of high-dimensional vectors and finding nearest neighbors in milliseconds. Understanding their internals helps you make informed deployment decisions.

Vector databases enable billion-scale retrieval in milliseconds through approximate nearest neighbor (ANN) algorithms like HNSW, IVF, and LSH. These algorithms trade exact nearest neighbors for

speed—they might miss the true nearest neighbor but find one that’s very close, which is usually good enough for search applications.

The memory requirements are substantial but manageable. For a 768-dimensional BERT-base embedding, storing one million documents requires approximately 3 GB of memory ( $1\text{M} \times 768 \times 4$  bytes for float32). This fits comfortably in RAM on modern servers. For 100 million documents, you need 300 GB—requiring a large server or distributed deployment, but still feasible.

Querying is typically sub-millisecond for index lookups once the query embedding is computed. The total latency includes embedding generation (50–100 ms for BERT on CPU, 5–10 ms on GPU) and ranking post-processing (10–50 ms depending on complexity). End-to-end latency of 100–200ms is typical and acceptable for most applications.

The choice of ANN algorithm involves trade-offs. HNSW (Hierarchical Navigable Small World) graphs offer excellent recall and speed but require more memory. IVF (Inverted File Index) is more memory-efficient but slightly slower. LSH (Locality-Sensitive Hashing) is fastest but has lower recall. For most enterprise applications, HNSW is the best default choice.

#### 25.1.4 Case Study: Internal Documentation Search

Let’s examine a concrete example that illustrates the business impact and technical decisions involved in deploying semantic search.

A company with 100,000 internal documents (policies, runbooks, FAQs, wiki pages) seeks to enable employees to find answers through natural language search. The existing keyword search system is frustrating: employees report spending 30+ minutes searching for information they know exists but can’t find. Traditional keyword search returns thousands of results for common queries; employees give up or ask colleagues, creating interruptions and inefficiency.

##### Implementation:

- Embed all documents with all-MiniLM-L6-v2 (384-dim) offline. This choice prioritizes operational simplicity (CPU-only deployment) over marginal accuracy gains from larger models. The embedding process takes 8 hours on a standard server—acceptable for a one-time operation.
- Store in Weaviate with HNSW indexing. Weaviate was chosen for its ease of deployment and good performance at this scale. The HNSW index provides 95% recall@100 with sub-millisecond query time.
- Query embedding on CPU takes 30 ms; ANN retrieval returns top-100 in 5 ms. The 30ms embedding time is the bottleneck, but it’s acceptable for interactive search. GPU deployment could reduce this to 5ms but wasn’t justified for the query volume (approximately 100 queries/second peak).
- Hybrid search combines BM25 (keyword) and dense retrieval; fusion re-ranks. The hybrid approach catches edge cases where semantic search alone fails: exact product codes, acronyms, or technical terms that require keyword matching.
- User-facing API returns top-5 results in  $< 200$  ms p95. This latency is acceptable for search; users perceive sub-200ms as instantaneous.

##### Metrics:

- Accuracy: 88% of users found their answer in top-5 (vs. 45% with keyword search). This near-doubling of success rate translates directly to time saved and frustration reduced.
- Latency: 180 ms p95 end-to-end (acceptable for internal tools). The p95 metric matters more than average because tail latency determines user experience.
- Cost: Single standard VM with 4 CPU cores, no GPUs needed. Monthly infrastructure cost: approximately \$200. This is negligible compared to the productivity gains.

- Maintenance: Re-index new documents nightly; model weights updated quarterly. The nightly re-indexing ensures new documents are searchable within 24 hours. Quarterly model updates incorporate user feedback and improve accuracy over time.

The system has been in production for 18 months. User satisfaction surveys show 85% of employees rate the new search as “much better” than the old system. Search query volume increased 3x—not because employees search more, but because they’re willing to use search now that it works. The system has become a critical piece of infrastructure, with employees reporting they “couldn’t work without it.”

## 25.2 Text Classification and Tagging in Production

Text classification is among the most successful enterprise NLP applications, powering intent recognition, routing, spam detection, and triage. The business value is immediate and measurable: automated classification reduces manual labor, speeds up processes, and improves consistency. A support team that manually routes 50,000 tickets monthly spends approximately 2,500 hours on triage alone—time that could be spent actually solving customer problems.

The technical approach is well-established: fine-tune a pre-trained encoder (BERT) with a lightweight classification head on labeled data, then deploy for inference. The challenge lies not in the algorithm but in the operational details: handling class imbalance, dealing with label scarcity, adapting to domain shift, and maintaining performance over time. These practical concerns determine whether a classification system succeeds or fails in production.

### 25.2.1 Standard Classification Workflow

Fine-tuning BERT-base on a classification task is straightforward in principle but requires attention to detail in practice. The process leverages transfer learning: BERT has already learned general language understanding from massive pre-training; we adapt it to our specific classification task with relatively little labeled data.

The input sequence is fed to BERT, producing a contextualized representation for each token and a pooled representation (typically the [CLS] token). This pooled representation captures the overall meaning of the input text. A classification head—a single linear layer mapping the 768-dimensional representation to class logits—is trained on labeled examples. The simplicity of the classification head is intentional: BERT does the heavy lifting of understanding language; the head just maps that understanding to class labels.

Standard hyperparameters are learning rate  $2\text{--}5 \times 10^{-5}$ , batch size 16–32, and 2–5 epochs of training on a single GPU. These hyperparameters are well-established through empirical research and work well across most classification tasks. The low learning rate prevents catastrophic forgetting—we want to adapt BERT, not overwrite its pre-trained knowledge.

**Definition 25.2** (Fine-Tuned Classification). The fine-tuning process adapts a pre-trained BERT model to a specific classification task. Given a labeled dataset  $\{(x_i, y_i)\}$  where  $x_i$  is text and  $y_i \in \{1, \dots, C\}$  is a class label, we train the model to predict the correct class for each input.

The forward pass computes:

$$\mathbf{h} = \text{BERT}(x_i)[\text{CLS}] \quad (\text{pooled representation}) \quad (25.5)$$

This pooled representation  $\mathbf{h}$  is a 768-dimensional vector that encodes the semantic meaning of the input text. BERT’s self-attention mechanism has processed the entire input, allowing each token to attend to every other token, creating a rich contextual representation.

We then apply a linear classification layer:

$$\text{logits} = W\mathbf{h} + b \quad (W \in \mathbb{R}^{C \times 768}) \quad (25.6)$$

The weight matrix  $W$  and bias  $b$  are learned during fine-tuning. Each row of  $W$  represents a class, and the dot product with  $\mathbf{h}$  measures how well the input matches that class.

Finally, we compute the loss:

$$\text{loss} = \text{CrossEntropy}(\text{softmax}(\text{logits}), y_i) \quad (25.7)$$

Cross-entropy loss penalizes confident wrong predictions more than uncertain ones, encouraging the model to be both accurate and calibrated. During training, we backpropagate this loss through both the classification head and BERT, updating all parameters to minimize classification error.

In practice, this means the model learns to adjust BERT’s representations to be more discriminative for the specific classes in your task, while preserving the general language understanding from pre-training.

### 25.2.2 Handling Common Challenges

**Class Imbalance:** Real-world datasets often exhibit severe class imbalance. For customer support ticket routing, perhaps 80% of tickets are “billing” and 5% are “technical.” Training naively yields high accuracy but poor performance on rare classes. Solutions include:

- Weighted loss: Assign higher weights to underrepresented classes
- Oversampling: Duplicate rare class examples during training
- Focal loss: Reduce weight for easy (high-confidence) examples
- Threshold tuning: Adjust class-specific decision thresholds at inference

**Label Scarcity:** Labeling 10,000 examples costs thousands of dollars. Active learning selects the most informative unlabeled examples for human annotation, reducing labeling costs by 50–70%. Data augmentation (paraphrasing, synonym replacement, back-translation) creates synthetic training data, though quality must be validated.

**Long-Tail Classes:** Even with 100,000 labeled examples, certain classes appear only dozens of times. Few-shot learning or transfer learning from related tasks (e.g., sentiment classification to domain classification) helps. Pre-training on a large corpus in the same domain before task-specific fine-tuning improves performance on tail classes.

**Domain Shift:** Models trained on one domain (e.g., email support tickets) may perform poorly on another (chat support). Continuous retraining on recent data, periodic evaluation on holdout test sets, and monitoring prediction confidence detect drift. When drift is detected, the model is retrained on a mixture of historical and recent data.

### 25.2.3 Production Metrics and Monitoring

In production, classification models must maintain consistent performance while handling distribution shift. Key metrics include:

- Precision, recall, F1 by class: Critical for decision-making systems
- Confidence calibration: Does the model’s confidence match actual accuracy?
- Prediction volume by class: Sudden changes indicate drift
- Latency: Per-example inference time; alert if  $\geq$  threshold
- Null rate: Fraction of examples where the model abstains (low confidence)

Continuous monitoring via dashboards and automated alerts ensures performance stays within SLOs. When performance degrades, the team is alerted to investigate whether the issue is model drift, data quality degradation, or a change in the task itself.

### 25.2.4 Case Study: Support Ticket Triage

A support team receives 50,000 tickets monthly across 12 categories (Billing, Technical, Account Access, etc.). Manual triage takes 2–3 minutes per ticket, costing  $\approx \$30,000/\text{month in labor}$ .

**Solution:**

- Collect 5,000 labeled tickets from recent month; split 80/20 for train/val
- Fine-tune BERT-base for 3 epochs with learning rate  $3 \times 10^{-5}$ , batch size 32
- Accuracy on validation set: 88% overall; 92% for common classes, 71% for rare classes
- Deploy behind REST API; latency 20 ms per ticket on single T4 GPU
- Auto-route tickets with confidence  $\geq 0.85$  (covers 75% of tickets)
- Low-confidence and out-of-distribution cases routed to human agents

**Impact:**

- 75% of tickets auto-routed correctly (78% accuracy on auto-routed subset)
- Human agents handle 25% of tickets; manual triage for these improves team focus
- Cost savings: \$22,500/month (75% of triage labor eliminated)
- Ticket resolution time: Shorter for correct auto-routes, minimal impact on misdirected tickets (human agents catch errors)

## 25.3 Conversational Assistants and Copilots

Conversational assistants powered by language models serve as frontline support, internal knowledge bases, or specialized domain advisors. Unlike single-turn classification, conversational systems must maintain context across multiple turns, handle follow-up questions, and know when to escalate to humans.

### 25.3.1 Architecture: Retrieval-Augmented Generation

A practical approach combines retrieval with generation. When a user asks a question, the system:

1. Encodes the user query into an embedding
2. Retrieves relevant documents from a knowledge base (e.g., FAQs, policies)
3. Constructs a prompt: “Answer the question based on the following context:”
4. Feeds the prompt to a generative model (GPT-3.5, LLaMA, or smaller fine-tuned model)
5. Returns the generated response to the user

This retrieval-augmented generation (RAG) approach grounds responses in actual company knowledge, reducing hallucinations. It is far cheaper than querying a large proprietary LLM API repeatedly, as retrieval is fast and cheap, and the generative step uses a smaller, cheaper model.

### 25.3.2 Prompt Engineering and Guardrails

The quality of conversational responses depends heavily on prompt construction. A well-written system prompt establishes persona, instructions, and constraints:

**Example System Prompt:**

```
You are a customer support assistant for TechCorp.  
Answer customer questions based on the provided knowledge base.  
If you cannot answer the question from the knowledge base, say:  
"I don't have information on that topic."  
Let me connect you with a support agent."  
Keep responses to 2-3 sentences.  
Do not make up product features or pricing.
```

Guardrails prevent the model from generating harmful, offensive, or confidential content. Rule-based filters detect and block responses containing:

- Sensitive information: Credit card numbers, SSNs (use regex or NER)
- Offensive language: Trained classifier or list-based filter
- Out-of-scope requests: Queries unrelated to the support domain

Semantic similarity checks can also detect if the model is attempting to answer outside its knowledge base. If the retrieved context has low relevance to the query, escalate to a human agent.

### 25.3.3 Multi-Turn Context and State Management

Conversational state management is non-trivial. The assistant must remember prior context while avoiding token count explosion. Common approaches:

**Fixed-window context:** Keep the last N messages in context. Older messages are discarded to maintain latency.

**Hierarchical summarization:** Periodically summarize earlier turns into a brief summary, freeing token budget for new context.

**Entity and intent tracking:** Extract key entities (product name, issue type) and maintain explicit state rather than relying purely on message history.

### 25.3.4 Human Escalation and Feedback Loops

Escalation is critical. If the user's issue cannot be resolved or satisfaction is low, the assistant should escalate to a human agent. Signals for escalation:

- Low retrieval relevance (no good documents found)
- Model confidence below threshold
- Explicit user request: "I want to talk to a human"
- Repeated unresolved queries in the conversation

After escalation, the conversation history is logged for training data. Human feedback ("this response was not helpful") provides signals for model improvement. A feedback loop where user interactions improve model quality is essential for long-term deployment.



### 25.3.5 Case Study: Customer Support Bot

A SaaS company receives 10,000 support inquiries monthly. Top inquiries (50%) are about billing, account management, and common troubleshooting. A support bot can handle straightforward cases, reducing load on a 5-person support team.

#### Design:

- Knowledge base: 500 FAQ entries and help articles (created by support team)
- Retrieval: all-MiniLM-L6-v2 embeddings stored in Pinecone
- Generation: Fine-tuned GPT-2 medium on 1,000 curated QA pairs from past support tickets
- Guardrails: Regex filters for PII; confidence threshold for auto-responses
- Escalation: Escalate if confidence  $\leq 0.6$  or user requests human; max 3 turns before escalation

#### Metrics:

- Accuracy (manual evaluation on 500 test conversations): 82% of responses helpful
- Containment rate: 58% of inquiries resolved without human escalation
- First-contact resolution: 65% (vs. typical 45% for human agents on common issues)
- User satisfaction (CSAT on resolved cases): 3.8/5.0
- Cost: Hosted on single standard VM; inference cost  $\leq$  \$50/month
- Savings:  $58\% \times 10,000 \text{ inquiries/month} \times 5 \text{ min/inquiry} \times \$0.25/\text{min labor} = \$3,625/\text{month}$  labor reduction

## 25.4 Enterprise Constraints and Governance

Enterprise deployments face constraints absent from research settings: regulatory compliance, data residency, security, and auditability.

### 25.4.1 Data Residency and Privacy

Regulations like GDPR, CCPA, and industry-specific rules (HIPAA for healthcare, SOC 2 for SaaS) restrict where data can be stored and processed. Enterprises must often deploy models on-premises or in private cloud instances, forgoing the convenience of third-party APIs. This increases operational complexity but is non-negotiable for regulated industries.

### 25.4.2 Handling Sensitive Data

NLP systems process customer data, internal documents, and potentially sensitive information. Best practices include:

- PII masking: Detect and mask sensitive information before processing
- Differential privacy: Add noise to training data to prevent memorization
- Audit logging: Track all model predictions and their basis (which document was retrieved)
- Access control: Restrict who can view model outputs or fine-tune models

### 25.4.3 Model Explainability and Red-Teaming

For high-stakes applications (financial, healthcare, legal), explaining model predictions is essential. Techniques include:

- **Attention visualization:** Show which input tokens influenced the prediction
- **Retrieval transparency:** Display the documents from which answers were retrieved
- **Influence functions:** Identify training examples most similar to a query

Red-teaming—testing the system for failure modes and adversarial inputs—should precede production deployment. Can the model be tricked into producing harmful content? Does it hallucinate credentials or confidential information? How does it handle non-English text, typos, or adversarial prompts?

## 25.5 Continuous Learning and Model Drift in Enterprise NLP

Enterprise NLP systems face unique drift challenges because language itself evolves, business contexts change, and user behavior shifts. A classification model trained on 2023 support tickets may struggle with 2024 tickets as products change, new issues emerge, and customer language evolves. Understanding and addressing drift is critical for maintaining long-term system value.

### 25.5.1 Language Evolution and Concept Drift

Language is not static. New terms emerge (“ChatGPT,” “NFT,” “metaverse”), meanings shift (“cloud” once meant weather, now means computing), and communication styles evolve (emoji usage, abbreviations, formality levels). Enterprise NLP systems must adapt to these changes or risk becoming obsolete.

**Vocabulary drift:** New products, features, and services introduce new terminology. A support ticket classifier trained before a product launch won’t recognize the new product name. This manifests as increased “other” or “unknown” classifications and decreased confidence scores.

**Semantic drift:** The meaning of existing terms changes. “Premium support” might have meant one thing in 2023 and something different after a service tier restructuring in 2024. The model’s learned associations become outdated.

**Style drift:** Communication norms evolve. Customers might shift from formal emails to casual chat messages, or from text to voice transcriptions. The model trained on one style may struggle with another.

**Key Point 25.1.** *The generic framework for drift detection (performance monitoring, distribution monitoring, confidence tracking), continuous learning strategies (periodic retraining, triggered retraining, online learning, ensemble approaches, human-in-the-loop), and practical implementation infrastructure (data versioning, model versioning, automated pipelines, monitoring dashboards) is covered in Chapter 24, Section 24.7. Here we highlight NLP-specific considerations.*

Key NLP-specific adaptation strategies include:

- **Vocabulary updates:** New products and terminology require updating the tokenizer and model vocabulary. Add tokens for new domain terms that would otherwise fragment into meaningless subwords.
- **Active learning for efficient labeling:** Use model uncertainty to prioritize which recent examples to label, focusing annotation budget on drifting areas (e.g. new product categories).
- **Vocabulary monitoring:** Track unknown-token frequency and subword fragmentation rates—spikes indicate terminology drift before performance degrades.

### 25.5.2 Case Study: Support Ticket Classification Drift

A SaaS company's support ticket classifier degraded from 88% to 78% accuracy over six months when three new products were launched. Tickets about these products were misclassified because the model had never seen the new product names. The immediate fix—collecting 500 labeled examples per product and fine-tuning on an 80/20 historical/new data mix—recovered accuracy to 85% within one week. The long-term solution implemented monthly retraining on a rolling 6-month window with 1,000 actively sampled examples, stabilizing accuracy at 86–88% at a cost of \$2,500/month against \$15,000/month in prevented misrouting.

## 25.6 Exercises

**Exercise 25.1.** Design a semantic search system for a legal firm with 50,000 case documents. What embedding model would you choose? How would you handle long documents that exceed token limits? How would you measure retrieval quality?

**Exercise 25.2.** Implement a text classification pipeline for email spam detection. How would you handle class imbalance if 95% of emails are not spam? How would you detect and respond to concept drift over time?

**Exercise 25.3.** Build a conversational FAQ assistant for your organization. What knowledge base would you create? How would you measure success (containment, CSAT)? What guardrails would you implement?

## 25.7 Solutions

Full solutions for all exercises are available at <https://deeplearning.hofkensvermeulen.be>.

## Chapter 26

# Code as a Domain: Code LLMs and Developer Tooling

### Chapter Overview

Programming languages represent a rich and highly structured domain for deep learning. Unlike natural language, code has formal syntax, executable semantics, and built-in evaluation mechanisms. This chapter explores how transformers trained on code repositories have revolutionized developer productivity through code completion, generation, and analysis. We examine code-specific pre-training, from tokenization to context window design, and cover practical applications: IDE copilots, automated testing, refactoring, and repository-wide code understanding. Unlike natural language applications where “hallucination” produces grammatically correct but false text, code hallucinations produce syntactically correct but incorrect implementations—a property that enables testing and automated quality control.

### Learning Objectives

1. Understand how programming languages differ from natural language for LLM training
2. Design and implement code-specific tokenization and vocabulary
3. Train or fine-tune models on code repositories at scale
4. Develop IDE copilots and code completion interfaces
5. Build static analysis and refactoring tools using code LLMs
6. Implement automated testing and correctness verification for model outputs
7. Address dataset licensing, attribution, and ethical concerns

### 26.1 Code-Specific Pre-Training

Code as a training signal differs fundamentally from natural language, and understanding these differences is crucial for building effective code models. While natural language exhibits ambiguity—the same sentence can have multiple valid interpretations—code must be unambiguous to execute. A Python function either runs correctly or throws an error; there’s no middle ground. This property—the ability to test code for correctness—provides a powerful training signal unavailable for general language models.

The business implications are significant. When a language model hallucinates a fact about history, it’s embarrassing but not immediately verifiable. When a code model generates incorrect code, you can run it and see that it fails. This executability means code models can be evaluated objectively, their outputs can be automatically tested, and developers can quickly determine if a suggestion is

useful. This makes code generation one of the most practical applications of large language models, with measurable productivity gains.

### 26.1.1 Tokenization and Vocabulary

Standard natural language tokenizers (BPE, WordPiece) are suboptimal for code, and understanding why reveals important insights about the structure of programming languages. Natural language tokenizers are designed to handle the statistical properties of human language: common words appear frequently, rare words can be broken into subwords, and word boundaries are relatively clear.

Programming languages have different statistical properties. Keywords like `def`, `class`, `if`, and `for` appear extremely frequently and should never be split. Multi-character operators like `==`, `->`, and `**` are atomic units with specific meanings; splitting them into individual characters destroys their semantics. Variable names follow conventions (`camelCase`, `snake_case`) that should be preserved. And identifiers can be arbitrarily long and unique, creating a long-tail distribution that challenges vocabulary-based tokenization.

A tokenizer trained on natural language might split `initialize_database` into `[init, ial, ize, _data, base]`, losing the semantic structure. A code-specific tokenizer learns to preserve meaningful units: `[initialize, _, database]` or even `[initialize_database]` if the pattern is common enough.

**Definition 26.1** (Code Tokenization). A BPE tokenizer trained on a diverse corpus of programming languages learns to preserve the semantic structure of code by treating meaningful units as single tokens. This approach differs fundamentally from natural language tokenization in several important ways.

Keywords such as `def`, `class`, `if`, and `for` remain unmerged as single tokens. These are the fundamental building blocks of the language; splitting them would be analogous to splitting the word “the” in English, destroying their semantic meaning. The tokenizer learns through frequency analysis that these keywords appear so often and in such consistent contexts that they should never be decomposed.

Multi-character operators like `==`, `->`, and `**` are treated as atomic operations. This is crucial because the operator `==` (equality test) has a completely different meaning than two separate `=` tokens (assignment). Preserving these as single tokens helps the model understand operator semantics directly, rather than having to learn that certain character sequences form operators. The tokenizer identifies these patterns during training by observing that these character combinations always appear together and function as single syntactic units.

Frequently-used variable names like `self`, `args`, and `kwargs` merge into single tokens. These are conventions in Python that appear across millions of functions; treating them as units helps the model learn idiomatic patterns more efficiently. When the model sees `self` as a single token, it can more easily learn that this token typically appears as the first parameter of instance methods and is used to access instance attributes.

Common patterns and idioms like `self.`, `if __name__`, and `import *` often merge into single tokens. These are multi-token patterns that appear together so frequently that treating them as units improves both compression and understanding. The tokenizer discovers these patterns through statistical analysis of co-occurrence: when certain tokens always or nearly always appear together, merging them reduces the sequence length and makes the pattern more salient to the model.

The key insight is that code tokenization should respect the syntactic and semantic structure of programming languages, not just optimize for compression. A good code tokenizer makes the model’s job easier by presenting code in meaningful chunks that align with how programmers think about code structure. This alignment between tokenization and semantic units allows the model to learn more efficiently and generate more coherent code.

The vocabulary size for code tokenizers is typically 32,000–50,000 tokens, comparable to natural language models. However, the token distribution differs significantly: code has higher entropy (more

unique tokens appear frequently), reducing compression compared to natural language. A natural language model might compress English text to 0.7 tokens per word on average; a code model might only achieve 1.2 tokens per word due to the diversity of identifiers and the precision required for operators.

### 26.1.2 Context Window and Code Understanding

Code understanding benefits from longer context windows, and the reasons are both technical and practical. A function definition might span 50 lines; understanding its behavior requires reading the entire function plus imported modules and class definitions. A class might span hundreds of lines; understanding a method requires knowing the class's state and other methods. A module might import dozens of dependencies; understanding a function call requires knowing what those dependencies provide.

Modern code models use context windows of 2,048–8,192 tokens, allowing models to see entire functions or small files. This is a significant advantage over earlier models with 512-token windows, which could barely fit a single function. The business impact is tangible: with longer context, models can generate more accurate completions, understand cross-function dependencies, and provide better suggestions for refactoring.

For example, consider a developer writing a new method in a class. With a 512-token context, the model might only see the method signature and a few lines of surrounding code. With a 4,096-token context, the model can see the entire class, understand the class's purpose and state, and generate a method implementation that correctly uses the class's attributes and other methods. The difference in suggestion quality is dramatic.

Positional encodings must handle long contexts effectively. Relative position biases (e.g., T5-style) often outperform absolute sinusoidal encodings for code, as they capture the importance of nearby tokens (e.g., variable definitions a few lines above a usage) independent of absolute position. In code, the relative distance between a variable definition and its usage matters more than their absolute positions in the file. A variable defined 5 lines above is relevant regardless of whether it's at line 10 or line 1000.

### 26.1.3 Pre-Training Data and Curation

High-quality code datasets are essential, and data quality matters more for code than for natural language. Bad code in the training set teaches the model bad patterns; the model will suggest buggy, inefficient, or insecure code. Data curation is not just about quantity—it's about ensuring the model learns from good examples.

Models are trained on public GitHub repositories, academic code, and project-specific codebases. The challenge is that GitHub contains code of wildly varying quality: production-grade libraries, student homework, abandoned experiments, and auto-generated boilerplate. Indiscriminately training on all of it produces mediocre models.

Data curation involves several steps, each addressing a specific quality concern. The first step is filtering out low-quality code, which includes auto-generated files such as protobuf definitions and parser outputs, minified code like compressed JavaScript, and test code containing only simple examples. These artifacts don't teach useful patterns and add noise to the training distribution, potentially causing the model to learn superficial patterns rather than deep programming knowledge.

Deduplication is essential to remove duplicate code snippets and avoid data leakage to test sets. GitHub contains massive duplication through forked repositories, copied code snippets, and repeated boilerplate. Training on duplicates causes the model to memorize specific implementations rather than generalize to new problems. Exact deduplication removes identical files, while near-deduplication uses techniques like MinHash to identify and remove highly similar code that differs only in variable names or minor details.

Language balancing ensures that diverse programming languages including Python, Java, C++, and JavaScript are represented proportionally in the training data. Without balancing, the model might become Python-heavy since Python is disproportionately popular on GitHub, and perform poorly on

other languages. Balancing can be achieved by sampling from each language according to its real-world usage or by ensuring each language has a minimum representation threshold.

Sensitive data removal filters out code containing credentials, API keys, or proprietary algorithms. Developers sometimes accidentally commit secrets to public repositories, and training on this data risks the model suggesting those secrets in completions—a serious security issue. Automated scanning tools identify patterns like API key formats, database connection strings, and private keys, removing any code containing these patterns.

License filtering respects code licenses and their legal implications. Some licenses like GPL require derivative works to be open-sourced, creating legal ambiguity when training commercial models on GPL code. Conservative approaches exclude GPL code entirely or clearly document its inclusion and the potential licensing implications. Other permissive licenses like MIT and Apache are generally safe for training, but attribution requirements should still be respected.

Major datasets for code model training include several large-scale collections, each with different characteristics and use cases. The Stack is a massive 6.4 TB corpus of source code from GitHub and other sources, carefully curated for quality and license compliance. It represents 358 programming languages, making it one of the most comprehensive multilingual code datasets available. The curation process includes deduplication, license filtering, and quality scoring based on repository metrics like stars and commit activity.

CodeSearchNet provides 6 million functions from open-source GitHub code in 6 languages: Python, Java, JavaScript, PHP, Ruby, and Go. Importantly, it includes docstrings paired with their corresponding functions, enabling code-documentation alignment training. This pairing allows models to learn the relationship between natural language descriptions and code implementations, supporting both code generation from descriptions and documentation generation from code.

GitHub data in its raw, public form consists of terabytes of diverse repositories with wildly varying quality. This uncured data includes everything from production-grade libraries to student homework assignments and abandoned experiments. While comprehensive, it requires significant filtering and quality control for production use. Organizations often start with raw GitHub data and apply their own curation pipelines tailored to their specific needs and quality standards.

Pre-training objectives for code models employ several complementary approaches, each teaching the model different aspects of code understanding and generation. Causal language modeling, the GPT-style approach, predicts the next token given all previous tokens. This is the standard approach for code generation because it directly mirrors the code completion task: given a prefix of code, predict what comes next. The model learns to continue code given a context, which translates naturally to IDE code completion where developers type a partial line and the model suggests the continuation.

Masked language modeling, following the BERT-style approach, predicts masked tokens using bidirectional context from both before and after the masked position. This is particularly effective for code understanding tasks like bug detection and code search, where the model needs to understand the full context around a code element. The bidirectional context allows the model to learn how code before and after a token constrains its value, which is crucial for understanding variable types, function signatures, and data flow.

Contrastive learning treats docstrings and code as paired data, training the model so that embeddings of related code and documentation are close in the embedding space while unrelated pairs are far apart. This teaches the model to understand the semantic relationship between natural language descriptions and code implementations. The learned embeddings can be used for code search (finding code that matches a natural language query) and for understanding whether a piece of code implements a given specification.

Documentation alignment training focuses on bidirectional generation between code and documentation. The model learns both code-to-doc generation (given a function, generate its docstring) and doc-to-code generation (given a specification, generate the implementation). This dual training enables the model to serve multiple use cases: generating documentation for undocumented code, generating code from natural language specifications, and verifying that code matches its documentation.

### 26.1.4 Model Families and Capabilities

The landscape of code models has evolved rapidly, with several families offering different trade-offs between size, performance, and accessibility. Understanding these options helps you choose the right model for your use case.

The landscape of code models has evolved rapidly, with several families offering different trade-offs between size, performance, and accessibility. Understanding these options helps you choose the right model for your specific use case and deployment constraints.

Codex and GPT-Codex, with 12 billion parameters, were trained on GitHub code and power GitHub Copilot. These models excel at few-shot code generation and understanding, often producing high-quality code from minimal context. However, they are proprietary and accessed only via API, which means best-in-class performance comes with ongoing costs and requires sending code to OpenAI's servers—a potential concern for organizations with strict data privacy requirements.

Code Llama offers models ranging from 7 billion to 34 billion parameters, fine-tuned from the LLaMA foundation model specifically on code. These models support remarkably long context windows of up to 100,000 tokens, enabling them to understand entire files or even small codebases. Performance is competitive with Codex on code generation tasks, and the models are open-source, allowing on-premises deployment. The 7B model runs efficiently on consumer GPUs, making it accessible for individual developers, while the 34B model requires high-end hardware but offers substantially better performance for complex tasks.

StarCoder, with 15 billion parameters, was trained on The Stack dataset and designed specifically for production deployment. It is open-source, fast, and particularly effective for code completion tasks. The model strikes a good balance between performance and resource requirements, making it a popular choice for organizations building their own code assistance tools without the scale to train models from scratch.

DeepSeek-Coder offers models ranging from 1.3 billion to 33 billion parameters, specialized for mathematical reasoning and multi-language support. These models are particularly strong on algorithmic problems and competitive programming tasks, often outperforming larger general-purpose models on problems requiring complex reasoning or mathematical insight.

Smaller models like PolyCoder (2.7B parameters) and CodeGPT (125M–355M parameters) provide efficient alternatives for edge deployment or resource-constrained environments. While their performance is lower than larger models, they can run on CPU or even mobile devices, making them suitable for scenarios where latency, privacy, or resource constraints preclude using larger models. These smaller models are acceptable for basic completion tasks like suggesting common patterns or completing simple functions.

Model scaling for code follows similar power laws as natural language, though code models often achieve higher performance at smaller scales due to the structured nature of the domain. A 7B code model often outperforms a 13B natural language model on code tasks, suggesting that code's structure makes it a more learnable domain. The formal syntax and executable semantics provide strong constraints that help smaller models learn effectively.

The business implication: you don't necessarily need the largest model. A well-trained 7B model deployed on-premises might outperform a 175B general-purpose model accessed via API, while being faster, cheaper, and more private. The key is choosing a model trained specifically on code, not just a large general-purpose model.

## 26.2 Developer Assistants and IDE Integration

Copilots like GitHub Copilot, Tabnine, and Codeium integrate code models directly into development environments, providing real-time suggestions as developers type. This is where code AI meets daily developer workflow, and the user experience details matter enormously. A suggestion that appears instantly feels like magic; one that takes 2 seconds feels broken. A suggestion that's syntactically correct but semantically wrong wastes time; one that's both correct and idiomatic saves time.



### 26.2.1 Completion Architecture

An IDE copilot follows this workflow:

1. **Context gathering:** Extract surrounding code (current file, related imports, class definitions)
2. **Prompt construction:** Format context for the model:

```
<file_header>
import numpy as np
from utils import process_data
</file_header>
<function_signature>
def analyze_dataset(data: np.ndarray) -> dict:
    """Analyze statistical properties of the dataset."""
    # User cursor is here <CURSOR>
```

3. **Generation:** Run model with temperature  $\approx 0.2$  (low randomness for deterministic completions). Generate 1–3 candidate completions.
4. **Ranking:** Score candidates by multiple criteria to select the best suggestion. Language model probability provides the base score, with higher probabilities indicating the model is more confident in the suggestion. Syntactic validity is checked by parsing the suggestion; code that doesn't parse is immediately rejected. Semantic relevance is assessed by checking whether the suggestion matches the function signature, uses appropriate types, and aligns with any docstring or comments. Popularity is estimated by checking whether similar patterns appeared frequently in the training data, as common patterns are more likely to be correct and idiomatic.
5. **Display:** Show top candidate as a gray suggestion; allow user to accept (Tab), reject (Esc), or view alternatives.

### 26.2.2 Practical Challenges and Solutions

**Latency:** Users expect suggestions within 100–200 milliseconds, but full model inference through all layers takes approximately 500 milliseconds on CPU. This latency gap creates a poor user experience where suggestions feel sluggish rather than responsive. Several solutions address this challenge. On-device inference deploys a smaller quantized model (typically 3B parameters) locally on the developer's machine, eliminating network latency and enabling sub-200ms response times. Speculative decoding generates multiple tokens in parallel rather than sequentially, reducing per-token latency by predicting several likely continuations simultaneously. Caching and KV caching store embeddings of common code patterns and reuse them for similar contexts, avoiding redundant computation. Batching combines multiple simultaneous requests to the same model server, amortizing the fixed overhead of model loading and improving throughput.

**Hallucination and Correctness:** Code completions must be syntactically valid at minimum; completely broken code that won't parse is worse than no suggestion. Ranking by syntax validity filters out many bad suggestions before they reach the user. However, syntactically correct code can still be semantically wrong, implementing an incorrect algorithm or using inefficient approaches. Displaying suggestions with lower confidence scores (perhaps in a lighter gray or with a warning icon) helps users recognize uncertain completions and apply appropriate scrutiny. Some systems also run basic static analysis on suggestions, flagging potential issues like type mismatches or undefined variables.

**Multi-file Context:** A function may depend on definitions in other files—imported modules, base classes, or utility functions. Retrieving all necessary context is non-trivial because the dependency graph can be large and complex. Hybrid approaches combine static analysis (parsing the AST to find import statements and follow dependencies) with semantic retrieval (embedding code snippets and retrieving those similar to the current context). This allows the system to include both explicit dependencies (imports) and implicit ones (similar code patterns that might be relevant).

**Privacy:** Copilots deployed on proprietary codebases risk leaking sensitive code to external servers if they send code to cloud-based models. Several solutions address this concern. On-device models run inference locally, ensuring no code leaves the developer’s machine. Custom models can be fine-tuned on proprietary code and deployed internally, keeping both the model and the code within the organization’s infrastructure. Federated learning trains models on distributed code without centralizing the data, allowing multiple organizations to collaboratively improve a model while keeping their code private.

## 26.3 Code Analysis, Testing, and Refactoring

Beyond completion, language models enable code analysis and transformation at scale.

### 26.3.1 Static Analysis and Bug Detection

Models fine-tuned on bug-fix datasets can identify likely bugs by learning patterns of common mistakes. Training on GitHub “closed issue” to “fix commit” pairs teaches the model to recognize problematic code patterns and their corrections. The model learns to identify several categories of common bugs through this training process.

Off-by-one errors in loops represent a classic category where the model learns to spot incorrect loop bounds, such as iterating to `len(array)` instead of `len(array)-1` when using indices. The model recognizes these patterns by seeing thousands of examples where such errors were fixed.

Null pointer dereferences occur when code attempts to access members of objects that might be null or undefined. The model learns to identify code paths where null checks are missing before dereferencing, a pattern that appears frequently in bug fix commits across many languages.

Resource leaks happen when files, database connections, or network sockets are opened but not properly closed. The model learns to identify missing `close()` calls or contexts where resources should be managed with try-finally blocks or context managers. This pattern recognition comes from seeing many examples where developers added proper resource cleanup in bug fixes.

Type mismatches represent another common category where the model learns to identify cases where a function expects one type but receives another, particularly in dynamically-typed languages where such errors aren’t caught at compile time. The model learns these patterns by observing type-related bug fixes and the type annotations or checks that were added.

A trained model encodes the code and generates a ranked set of potential bugs or improvements, often with explanations of why each issue might be problematic. Tools like Infer and DeepCode leverage machine learning for static analysis, combining traditional program analysis techniques with learned patterns to achieve higher accuracy than either approach alone.

### 26.3.2 Test Generation

Transformers can generate test cases from code. Given a function:

```
def factorial(n: int) -> int:
    """Return n!. Assumes n >= 0."""
    if n <= 1:
        return 1
    return n * factorial(n - 1)
```

A model fine-tuned on code-test pairs generates:

```
def test_factorial():
    assert factorial(0) == 1
    assert factorial(1) == 1
    assert factorial(5) == 120
    assert factorial(10) == 3628800
    # Edge case: negative input (should raise or handle gracefully)
```

Test generation accelerates development and uncovers edge cases. However, generated tests must be validated: do they exercise the intended behavior? Are they redundant? A ranking model can prioritize high-value tests.

### 26.3.3 Refactoring and Code Quality Improvement

Models can suggest refactoring: breaking large functions into smaller ones, replacing loops with vectorized operations, or simplifying logic. For instance, a repetitive loop:

```
result = []
for x in data:
    if x > threshold:
        result.append(x * 2)
```

Can be refactored to:

```
result = [x * 2 for x in data if x > threshold]
```

A model fine-tuned on refactoring commits learns these transformations. Paired with a linter or style checker, automated refactoring improves code quality without developer intervention.

## 26.4 Repository-Scale Code Understanding

Large language models trained on entire repositories can answer questions like: “What does this configuration file control?” or “Find all places where this function is called.”

### 26.4.1 Graph-Based Retrieval and Reasoning

A single file provides limited context for understanding code behavior. Repository-scale understanding requires reasoning over the entire codebase, considering how different components interact and depend on each other. Several complementary approaches enable this broader understanding.

Static call graphs extract function call dependencies by parsing the code and building a graph where nodes represent functions and edges represent calls. This allows the system to retrieve all callees (functions that a given function calls) and callers (functions that call a given function). When a developer modifies a function, the call graph identifies all locations that might be affected by the change.

Type information leverages type annotations and type inference to understand data flow through the program. By tracking what types a variable can hold at different points in the code, the system can identify potential type errors, understand how data transforms through function calls, and suggest appropriate operations for each variable. This is particularly powerful in statically-typed languages but can also be applied to dynamically-typed languages with type hints.

Semantic retrieval embeds code snippets into a vector space where semantically similar code is close together. When a developer is working on a particular function, the system can retrieve semantically similar code across the entire repository, even if there are no explicit dependencies. This helps developers find relevant examples, identify duplicate or similar functionality, and understand patterns used elsewhere in the codebase.

Hybrid reasoning combines structured analysis (AST parsing, type checking, control flow analysis) with learned embeddings to leverage both the formal structure of code and the semantic patterns learned from data. For example, the system might use the AST to identify all assignments to a variable, then use semantic embeddings to understand what those assignments mean in the context of the program’s purpose.

For instance, if a developer changes a function signature, tools can identify all callers that must be updated by traversing the call graph to find direct callers, then using semantic retrieval to find indirect dependencies where the function’s behavior is assumed. This combination of techniques provides more complete coverage than either approach alone.

### 26.4.2 Documentation and Code Generation from Specifications

Models trained on docstring-code pairs can generate code from documentation. A developer writes:

```
def solve_quadratic(a, b, c):
    """
    Solve the quadratic equation  $ax^2 + bx + c = 0$ .

    Args:
        a, b, c: Coefficients of the quadratic.

    Returns:
        A tuple of two roots (may be complex).
    """
```

A model generates the implementation. Conversely, given code, models summarize it into documentation.

## 26.5 Safety, Licensing, and Ethics

Training on public code raises concerns about licensing, data contamination, and responsible deployment.

### 26.5.1 Licensing and Attribution

Public code on GitHub carries various licenses including MIT, GPL, Apache, and others, each with different requirements and restrictions. Models trained on GPL-licensed code may, by some legal interpretations, be required to release their outputs under GPL as well, creating a derivative work issue. This is legally ambiguous and actively debated in both legal and technical communities, with no clear consensus on whether model training constitutes creating a derivative work.

Best practices for handling licensing concerns include several complementary approaches. First, document the licenses of all training data, maintaining a clear record of what code was used and under what terms. This transparency allows users of the model to make informed decisions about their own licensing obligations. Second, avoid or downweight GPL code if licensing compliance is critical for your use case, focusing instead on permissively-licensed code under MIT, Apache, or BSD licenses. Third, attribute code to original authors when possible, for example by retrieving the original function from the repository when the model generates something very similar to existing code. Fourth, provide transparency reports on model training data composition, detailing what percentage of training data came from each license category and how the data was curated.

### 26.5.2 Data Contamination and Test Leakage

If benchmarks like HumanEval or CodeNet are included in training data, reported performance is inflated. Filtering and deduplication are essential. Libraries like “exact-substring matching” identify potential duplicates between training data and benchmarks.

### 26.5.3 Responsible Deployment

Models should not suggest code patterns that create security vulnerabilities, legal issues, or maintenance problems. Responsible deployment requires active filtering and guardrails to prevent harmful suggestions.

Insecure patterns must be actively filtered, including weak cryptography (using MD5 or SHA1 for security purposes), hardcoded credentials (API keys or passwords embedded in code), and SQL injection vulnerabilities (building SQL queries through string concatenation). The model should be trained to recognize these patterns as anti-patterns and either avoid suggesting them or suggest secure

alternatives. This can be achieved through negative example training where the model learns to assign low probability to insecure code.

Copyrighted code presents another concern, as models should not produce exact reproductions of proprietary implementations. While learning general patterns from copyrighted code is likely acceptable, memorizing and reproducing substantial portions of specific implementations creates legal risk. Techniques like membership inference can detect when the model has memorized specific code, and deduplication during training reduces the likelihood of memorization.

Outdated or deprecated APIs should be avoided in suggestions. When libraries release new versions with breaking changes, the model should prefer suggesting current APIs over deprecated ones. This requires either retraining on recent code or maintaining a blacklist of deprecated patterns. Some systems use API documentation to identify deprecated functions and filter suggestions accordingly.

Guardrails and fine-tuning on secure code examples reduce these risks substantially. By training on curated examples of secure code and explicitly teaching the model to avoid insecure patterns, the model learns to generate safer suggestions. Explicit filtering for credentials using pattern matching (detecting strings that look like API keys or tokens) prevents leakage of secrets that may have appeared in training data.

## 26.6 Continuous Learning and Drift in Code Models

Code models face unique drift challenges because programming languages evolve, libraries update, best practices change, and development patterns shift. A model trained on Python 3.8 code in 2020 will struggle with Python 3.12 features in 2024. Understanding and addressing this drift is essential for maintaining long-term value from code AI investments.

The business impact of code model drift is direct and measurable. When a copilot suggests outdated APIs or deprecated patterns, developers waste time correcting the suggestions. When it fails to understand new language features, it provides no value for modern code. Studies show that code model effectiveness degrades approximately 15–25% per year without updates, translating to millions in lost productivity for large development teams.

### 26.6.1 Language Evolution and API Changes

Programming languages evolve continuously, introducing new features, deprecating old ones, and changing best practices. This creates several types of drift that code models must handle.

**Syntax evolution:** New language features introduce syntax the model has never seen. Python 3.10 added structural pattern matching (`match/case`); Python 3.12 added type parameter syntax. A model trained before these features won't recognize them, let alone suggest them. This manifests as the model suggesting older, more verbose patterns when newer, cleaner syntax exists.

**API deprecation:** Libraries deprecate old APIs and introduce new ones. TensorFlow 2.0 completely redesigned the API from TensorFlow 1.x. A model trained on TensorFlow 1.x code will suggest deprecated patterns that no longer work. This is particularly problematic because the suggestions are syntactically valid but semantically broken.

**Best practice evolution:** What's considered good code changes over time. Type hints in Python went from rare to expected. Async/await patterns replaced callback-based async code. A model trained on old code suggests outdated patterns that work but aren't idiomatic.

**Security pattern updates:** Security best practices evolve as new vulnerabilities are discovered. A model trained before a major security issue might suggest vulnerable patterns. For example, models trained before widespread awareness of SQL injection might suggest string concatenation for SQL queries rather than parameterized queries.

**Key Point 26.1.** *For the generic drift detection and continuous learning framework (detection strategies, retraining approaches, implementation infrastructure), see Chapter 24, Section 24.7. Here we highlight code-specific considerations.*

Key code-specific adaptation strategies include:

- **Acceptance rate monitoring:** Track what percentage of suggestions developers accept (typically 25–35% for a healthy copilot). Declining rates signal drift.
- **Negative example training:** Collect deprecated or insecure patterns and train the model to avoid them—especially important as security best practices evolve.
- **Continuous pre-training on recent commits:** Schedule monthly or quarterly pre-training on internal code to keep the model aligned with evolving team practices.
- **Language and library version tracking:** Integrate with dependency management (pip, npm, Maven) to prioritize retraining for the versions your team actually uses.

### 26.6.2 Case Study: Adapting to Python 3.11 and 3.12

A 200-developer team’s code copilot dropped from 32% to 22% acceptance rate after upgrading to Python 3.12, because the model (trained on 3.8–3.10) didn’t recognize new features like exception groups and type parameter syntax. Fine-tuning on a 60/40 mix of new and historical code recovered acceptance to 29% within two weeks. Quarterly retraining at \$5,000/cycle then stabilized acceptance at 30–33%, maintaining \$4M/year in productivity gains for a \$20K/year continuous learning investment.

## 26.7 Case Study: IDE Copilot for Python Development

A team building a Python IDE wants to add code completion to enhance developer productivity.

### 26.7.1 System Design

The team selected StarCoder-7B as their base model and fine-tuned it on a carefully curated dataset of 50,000 Python functions. This dataset combined code from company repositories, ensuring the model learned internal coding patterns and conventions, with curated open-source code that provided exposure to diverse, high-quality implementations. The fine-tuning process took approximately 48 hours on 4 A100 GPUs.

For context handling, the system uses a 2,048-token window that includes the current file plus imported modules. This window size balances comprehensiveness (seeing enough context to understand the code’s purpose) with efficiency (keeping inference time low). The system intelligently selects which imports to include, prioritizing those most relevant to the current cursor position.

Deployment uses a quantized FP16 model that reduces the model size to 3.5 GB, small enough to run locally on developer machines. The model runs on the developer’s GPU when available, falling back to CPU when necessary. This local deployment ensures zero latency from network communication and complete privacy since no code leaves the developer’s machine.

The system maintains a latency service level objective (SLO) of 200 milliseconds at the 95th percentile for the first suggestion. This means 95% of suggestions appear within 200ms, fast enough to feel responsive during active coding. The remaining 5% of requests may take longer, typically when processing unusually large context or complex code patterns.

### 26.7.2 Metrics

The system’s acceptance rate of 35% represents a substantial improvement over the 10% acceptance rate of traditional keyword-based completion. This means developers accept more than one in three suggestions, indicating the model provides genuinely useful completions rather than noise. The 3.5× improvement over keyword completion demonstrates the value of deep learning approaches for code.

Code quality metrics show that suggestions pass linting in 87% of cases, meaning they follow style guidelines and don’t trigger warnings. Syntax errors occur in only 8% of suggestions, demonstrating the model has learned to generate well-formed code. Semantic errors, where the code is syntactically

correct but implements incorrect logic, occur in 5% of cases. These semantic errors are the hardest to eliminate because they require deep understanding of the code's intended behavior.

Developer productivity measurements, based on self-reported surveys and task timing studies, show a 15% reduction in time to write unit tests. The model excels at generating test boilerplate and common test patterns. Debugging time decreased by 10%, likely because the model's suggestions are generally correct and reduce the introduction of bugs during initial coding.

Latency measurements show the system achieves 120 milliseconds at the 50th percentile and 180 milliseconds at the 95th percentile. Both values fall well below the 200ms target, ensuring suggestions feel responsive. The p50 latency of 120ms means half of all suggestions appear in barely more than a tenth of a second, fast enough to feel nearly instantaneous.

Privacy is absolute: 100% of inference happens on-device, meaning zero code leaves the developer's machine. This complete privacy guarantee makes the system acceptable for use on proprietary codebases and sensitive projects where code confidentiality is paramount.

## 26.8 Exercises

**Exercise 26.1.** Tokenize this Python code snippet using a standard BPE tokenizer and a code-specific tokenizer. Compare token counts and observe which tokens are merged differently:

```
def fibonacci(n: int) -> int:
    if n <= 1:
        return n
    return fibonacci(n - 1) + fibonacci(n - 2)
```

**Exercise 26.2.** Design a system to generate unit tests for a given function. What should the prompt look like? How would you rank generated tests? How would you handle functions with side effects (file I/O, database access)?

**Exercise 26.3.** Train a code summarization model on code-docstring pairs. Given a complex function, generate a one-sentence summary. How would you evaluate the quality of summaries?

## 26.9 Solutions

Full solutions for all exercises are available at <https://deeplearning.hofkensvermeulen.be>.

## Chapter 27

# Visual Effects and Video Content Generation with Multimodal Models

### Chapter Overview

The visual content industry faces a fundamental challenge: demand for high-quality video and images far exceeds the supply of skilled creators. Professional video editing requires years of training, expensive software, and hours of manual work per minute of content. Meanwhile, platforms like YouTube, TikTok, and Instagram process billions of videos monthly, with creators ranging from professionals to casual users recording on smartphones.

This chapter explores how multimodal transformers have revolutionized visual content creation and video understanding, addressing these business challenges head-on. Unlike text-only models, multimodal systems process and generate images, videos, and audio alongside text, enabling automated workflows that previously required human expertise. We examine vision transformers for understanding visual content, diffusion models for generating images and videos from text descriptions, and automated editing systems that can transform raw footage into polished content.

The business impact is substantial. Content platforms using automated video editing see 15-20% increases in creator retention and 10-15% improvements in viewer engagement. E-commerce companies using AI-generated product images reduce photography costs by 60-80% while increasing catalog size by 3-5x. Media companies using automated scene analysis can process video archives 100x faster than manual review, unlocking monetization opportunities for previously inaccessible content.

However, these systems come with significant challenges. Training state-of-the-art models costs millions of dollars and requires massive GPU clusters. Inference at scale demands careful optimization to keep costs manageable. Quality evaluation is subjective and difficult to automate. Copyright and licensing concerns create legal uncertainty. This chapter provides the technical foundation and business context needed to navigate these trade-offs effectively.

### Learning Objectives

1. Understand vision transformers (ViT) and their advantages over CNNs for visual understanding
2. Learn diffusion model theory and applications to image and video generation
3. Design text-to-image and text-to-video pipelines (e.g., DALL-E, Stable Diffusion, VideoGen)
4. Implement video understanding and scene analysis using transformer-based models
5. Build automated video editing systems that detect cuts, transitions, and special effects
6. Address computational challenges: models require massive compute (GPUs, TPUs) for training and inference
7. Handle visual quality assessment and user satisfaction in generative systems



## 27.1 Vision Transformers and Visual Understanding

Understanding visual content at scale is a critical business capability. E-commerce platforms need to categorize millions of product images, social media companies must moderate billions of user-uploaded photos, and autonomous vehicle companies require real-time scene understanding. For decades, convolutional neural networks (CNNs) dominated these applications, but they have fundamental limitations that impact both accuracy and operational costs.

CNNs excel at capturing local spatial structure through filters that operate on small neighborhoods. However, understanding complex scenes often requires reasoning about relationships between distant objects—a person holding an object across the image, or the relationship between foreground and background elements. CNNs must stack many layers to achieve large receptive fields, increasing computational cost and making training difficult.

Vision transformers (ViT) address these limitations by treating images as sequences of patches and applying self-attention to learn global relationships directly. This architectural shift has profound business implications. ViT models outperform CNNs on large-scale vision benchmarks while scaling more efficiently to larger datasets and higher-resolution images. For companies with massive image datasets, this means better accuracy with comparable or lower computational costs. For applications requiring fine-grained understanding (medical imaging, satellite analysis, quality inspection), ViT's global reasoning capabilities unlock previously impossible use cases.

### 27.1.1 Vision Transformer Architecture

The vision transformer architecture represents a fundamental rethinking of how to process images. Rather than treating images as 2D grids with spatial locality (as CNNs do), ViT treats them as sequences of patches, similar to how language models treat text as sequences of tokens. This enables the model to apply the same self-attention mechanisms that have proven so successful in NLP.

The process works as follows. First, we divide the input image into non-overlapping patches. For a standard  $224 \times 224$  image with  $16 \times 16$  patches, we get 196 patches total ( $14 \times 14$  grid). Each patch is flattened into a vector and projected through a learned linear transformation to create patch embeddings, typically 768-dimensional vectors. This projection learns to extract meaningful features from each patch.

However, unlike text where word order is inherent in the sequence, image patches lose their spatial relationships when flattened into a sequence. To preserve spatial information, we add learned position embeddings to each patch embedding. These position embeddings allow the model to understand that patch (0,0) is in the top-left corner while patch (13,13) is in the bottom-right, and to learn spatial relationships accordingly.

The sequence of patch embeddings (with position information) is then processed by a standard transformer encoder with multiple layers of multi-head self-attention and feedforward networks. Following BERT's approach, we prepend a special [CLS] token to the sequence. After processing through all transformer layers, the [CLS] token's representation captures information about the entire image and is used for classification or other downstream tasks.

- Definition 27.1** (Vision Transformer (ViT)).
1. **Patch embedding:** Divide an image into non-overlapping patches (e.g.,  $16 \times 16$  pixels). For a  $224 \times 224$  image, this yields 196 patches. Project each patch to a 768-dimensional embedding.
  2. **Position embeddings:** Add learnable position embeddings to each patch, enabling the model to understand spatial layout.
  3. **Transformer encoder:** Apply  $L$  transformer encoder layers with multi-head self-attention and FFN.
  4. **Classification:** Prepend a learnable [CLS] token. The [CLS] representation at the output is fed to a linear layer for classification.

Key equations:

$$\mathbf{p}_i = \text{Linear}(\text{flatten}(\text{patch}_i)) \quad (\text{patch embedding}) \quad (27.1)$$

$$\mathbf{z}_0 = [[\text{CLS}], \mathbf{p}_1 + \mathbf{pos}_1, \dots, \mathbf{p}_n + \mathbf{pos}_n] \quad (27.2)$$

$$\mathbf{z}_\ell = \text{TransformerBlock}(\mathbf{z}_{\ell-1}) \quad \text{for } \ell = 1, \dots, L \quad (27.3)$$

$$y = \text{Linear}(\mathbf{z}_L[\text{CLS}]) \quad (27.4)$$

### 27.1.2 Advantages Over CNNs

The shift from CNNs to vision transformers brings several advantages that translate directly to business value:

**Global receptive field from the start.** Self-attention operates over all patches simultaneously in every layer, enabling the model to capture long-range dependencies immediately. A CNN must stack many layers (often 50-100) to achieve a receptive field covering the entire image, incurring significant computational cost and making training difficult due to vanishing gradients. For applications requiring understanding of object relationships (e.g., "person holding phone" vs. "person near phone"), ViT's global reasoning provides better accuracy with fewer parameters.

**Superior scalability to large datasets.** CNNs have strong inductive biases (locality, translation equivariance) that help when training data is limited but become less useful as data scale increases. ViT has weaker inductive biases, allowing it to learn more flexible representations from large datasets. In practice, this means ViT pretrained on ImageNet-21K (14 million images) transfers better to downstream tasks than CNN counterparts, especially when downstream data is limited. For companies with large proprietary image datasets, ViT can extract more value from that data.

**Better transfer learning characteristics.** ViT models pretrained on large datasets transfer exceptionally well to specialized domains with limited data. A ViT pretrained on general images can be fine-tuned for medical imaging with just thousands of examples, achieving accuracy that would require millions of examples to train from scratch. This dramatically reduces the data collection burden for specialized applications, cutting time-to-market from years to months.

**Improved interpretability.** Attention weights directly show which patches influence each other, providing interpretable explanations for model decisions. For regulated industries (healthcare, finance, legal) where model explainability is required, this transparency is valuable. Visualizing attention patterns can reveal whether the model focuses on relevant features (e.g., tumor regions in medical images) or spurious correlations (e.g., hospital equipment in the background).

### 27.1.3 Computational Requirements and Business Trade-offs

While ViT offers accuracy advantages, it comes with significant computational costs that must be carefully managed in production deployments. Understanding these costs is essential for making informed architectural decisions.

A ViT-Large model with 308 million parameters requires substantial resources. Memory footprint includes 1.2 GB for model parameters (in FP32 precision) plus 2-4 GB for activations during inference on a 512×512 image. This means a single GPU with 8 GB memory can process only 1-2 images simultaneously, limiting throughput. Inference latency on a V100 GPU is approximately 500 ms for a single image, though batching multiple images can reduce per-image latency to 10-20 ms.

Training costs are even more substantial. Pretraining ViT-Large on ImageNet-21K (14 million images) requires billions of training examples (with data augmentation) and takes weeks on large GPU clusters. At cloud GPU prices (\$2-3 per hour for V100), pretraining costs can reach \$50,000-100,000. Fine-tuning for specific tasks is more affordable (\$500-2,000) but still requires careful budgeting.

These costs create important business trade-offs. For applications requiring highest accuracy (medical diagnosis, autonomous vehicles, high-value content moderation), the cost is justified by the business value of better decisions. For cost-sensitive applications (consumer photo apps, real-time video processing), efficient alternatives like MobileViT or EfficientNet provide 100-1000× smaller models with

2-5% accuracy reduction. The key is matching model capacity to business requirements rather than always choosing the largest model.

In contrast to ViT-Large, efficient vision models like MobileViT-S have just 5 million parameters, require 50 MB memory, and achieve 5 ms inference latency on mobile devices. For a mobile app processing millions of images daily, this efficiency difference translates to \$10,000s in monthly cloud costs or enables on-device processing that eliminates server costs entirely.

## 27.2 Image Generation with Diffusion Models

The ability to generate high-quality images from text descriptions represents a paradigm shift in content creation. Traditionally, creating custom images required hiring photographers, graphic designers, or illustrators—processes that take days or weeks and cost hundreds to thousands of dollars per image. Text-to-image models enable anyone to generate professional-quality images in seconds for pennies, democratizing visual content creation.

Diffusion models have emerged as the leading approach for high-quality image generation, surpassing earlier methods like GANs (Generative Adversarial Networks) and autoregressive models. GANs, while capable of generating realistic images, suffer from training instability and mode collapse (generating limited variety). Autoregressive models generate images pixel-by-pixel, which is extremely slow (minutes per image) and struggles with global coherence. Diffusion models address both limitations: they are stable to train, produce diverse outputs, and generate images in seconds rather than minutes.

The business applications are extensive. E-commerce companies use diffusion models to generate product images in different settings (bedroom, living room, outdoor) without expensive photo shoots. Marketing teams generate custom illustrations for campaigns in minutes rather than waiting days for designers. Game developers create concept art and textures automatically. Social media platforms enable users to generate custom profile pictures and content. The market for AI-generated images is projected to reach billions of dollars annually as these capabilities mature.

### 27.2.1 Diffusion Process Intuition

Understanding diffusion models requires grasping a counterintuitive idea: we can learn to generate images by learning to remove noise. The process has two phases that mirror each other.

The forward process (noising) is simple and requires no learning. Starting with a clean image  $x_0$ , we gradually add Gaussian noise over  $T$  steps (typically 1000 steps). At each step  $t$ , we add a small amount of noise controlled by a schedule parameter  $\beta_t$ :

$$q(x_t | x_{t-1}) = \mathcal{N}(x_t; \sqrt{1 - \beta_t}x_{t-1}, \beta_t I) \quad (27.5)$$

The noise schedule is carefully designed so that after  $T$  steps, the image  $x_T$  is essentially pure Gaussian noise—all information about the original image has been destroyed. Importantly, this forward process is fixed and deterministic (given the noise schedule); we don't need to learn anything.

The reverse process (denoising) is where learning happens. We train a neural network to reverse the noising process, taking a noisy image and predicting what it looked like one step earlier. If we can learn to denoise at each step, we can start with pure noise and gradually denoise it into a clean image. The network learns to predict the mean of a Gaussian distribution at each step:

$$p_\theta(x_{t-1} | x_t) = \mathcal{N}(x_{t-1}; \mu_\theta(x_t, t), \sigma_t I) \quad (27.6)$$

where  $\mu_\theta$  is our learned denoising function (typically a U-Net architecture with attention layers),  $t$  is the timestep, and  $\sigma_t$  is the noise variance at that step.

The training objective is elegant: at each step, we know exactly what noise was added (we added it ourselves in the forward process), so we train the network to predict that noise. The loss is simply the mean squared error between predicted and actual noise. This is much more stable than GAN training, which requires balancing two competing networks.

Why does this work? The key insight is that denoising is easier than generating from scratch. At step  $t = 999$  (nearly pure noise), the network only needs to predict very coarse structure (rough shapes, colors). At step  $t = 500$  (moderate noise), it predicts finer details. At step  $t = 1$  (almost clean), it predicts final details. This gradual refinement is easier to learn than generating a complete image in one shot.

### 27.2.2 Conditioning with Text for Business Applications

The real power of diffusion models for business applications comes from conditioning on text prompts, enabling text-to-image generation. This transforms diffusion from a research curiosity into a practical tool for content creation. Models like DALL-E, Stable Diffusion, and Midjourney have demonstrated that users can generate professional-quality images simply by describing what they want in natural language.

The conditioning mechanism works by encoding the text prompt using a transformer-based text encoder (typically CLIP’s text encoder, which was trained to align text and image representations). This produces a conditioning vector  $\mathbf{c}$  that captures the semantic meaning of the prompt. At each denoising step, the model takes three inputs: the noisy image  $x_t$ , the current timestep  $t$ , and the text conditioning  $\mathbf{c}$ :

$$p_{\theta}(x_{t-1} \mid x_t, \mathbf{c}) = \mathcal{N}(x_{t-1}; \mu_{\theta}(x_t, t, \mathbf{c}), \sigma_t I) \quad (27.7)$$

The conditioning vector influences the denoising at every step, guiding the generation toward images that match the text description. The network learns to denoise in a way that produces images semantically aligned with the prompt.

A critical technique for improving prompt adherence is classifier-free guidance. During training, we randomly drop the conditioning (set  $\mathbf{c}$  to null) for some fraction of examples (typically 10-20%). This teaches the model both conditional generation (with prompt) and unconditional generation (without prompt). At inference time, we can then amplify the effect of conditioning by extrapolating away from the unconditional prediction:

$$\tilde{\mu}_{\theta} = \mu_{\theta}(x_t, t, \mathbf{c}) + w \cdot (\mu_{\theta}(x_t, t, \mathbf{c}) - \mu_{\theta}(x_t, t, \emptyset)) \quad (27.8)$$

where  $w$  is the guidance weight (typically 7-15). Higher guidance weights make the model follow the prompt more closely but reduce diversity. This gives users control over the creativity-accuracy trade-off: low guidance for creative exploration, high guidance for precise specifications.

### 27.2.3 Key Advantages for Content Creation

Diffusion models offer several key advantages that make them valuable for business applications in content creation and visual design.

Diversity is a natural consequence of the stochastic sampling process. Multiple diffusion steps and random noise sampling mean many paths to a final image. Even with the same prompt and guidance settings, sampling different initial noise vectors produces diverse outputs. This is valuable for creative workflows where users want to explore multiple options—a marketing team can generate 10 variations of a product advertisement and select the best one, or a game developer can generate multiple character concept variations to find the right aesthetic.

Controllability comes through multiple mechanisms beyond text prompts. Users can specify guidance weights to control how strongly the model follows the prompt versus allowing creative interpretation. Random seeds provide reproducibility—the same prompt, guidance, and seed will produce identical outputs, enabling iterative refinement. Negative prompts allow users to specify what to avoid—“a photo of a dog, negative prompt: blurry, low quality, distorted”—improving output quality. Some implementations support compositional prompts with spatial layout specifications, enabling precise control over object placement and scene composition.

Editing capabilities extend beyond simple generation. Inpainting allows users to modify part of an image by masking a region and generating new content that blends seamlessly with the surrounding pixels—useful for removing unwanted objects, changing backgrounds, or adding elements. Outpainting extends images beyond their original boundaries, generating coherent content that continues the scene. Image-to-image translation takes an existing image and transforms it according to a new prompt while preserving structure—turning a photograph into a painting style, or changing the season from summer to winter while maintaining composition.

Speed has improved dramatically through inference optimization techniques. Original diffusion models required 1000 denoising steps, taking minutes per image. Modern techniques including DDIM (Denoising Diffusion Implicit Models), DPM-Solver++, and latent consistency models (LCM) reduce steps from 1000 to 4-50 with minimal quality loss, enabling interactive generation in 0.5-5 seconds on consumer GPUs. This speed makes diffusion practical for real-time creative workflows and high-volume production environments.

#### 27.2.4 State-of-the-Art Text-to-Image Systems

Stable Diffusion represents the current industry standard for open-source text-to-image generation. The architecture employs latent diffusion as described above, with a VAE that compresses  $512 \times 512$  images into  $64 \times 64 \times 4$  latent representations. The text encoder is CLIP's text transformer, producing 768-dimensional conditioning vectors from input prompts. The denoising U-Net contains approximately 860 million parameters with self-attention and cross-attention layers at multiple resolutions.

Training required 400 million image-text pairs from the LAION-5B dataset, curated for aesthetic quality and caption accuracy. The compute budget was approximately 150,000 A100 GPU hours, costing \$300,000-450,000 at cloud GPU prices. Modern training techniques including mixed precision (FP16/BF16), efficient attention implementations (Flash Attention), and improved data curation have reduced this to 60,000-90,000 GPU hours for equivalent quality, demonstrating the rapid pace of optimization research.

Inference performance has improved significantly. Current implementations generate  $512 \times 512$  images in 2 seconds on consumer GPUs like RTX 4090, or 0.5 seconds with latent consistency models. Generation at  $768 \times 768$  resolution takes approximately 5 seconds. The model size is 4 GB including both the diffusion model and CLIP encoder, small enough for consumer GPUs or even mobile deployment with quantization.

DALL-E 3, OpenAI's proprietary system, represents the state-of-the-art for caption fidelity and photorealism. While architectural details are not publicly available, the system demonstrates superior understanding of complex prompts with multiple objects, spatial relationships, and stylistic specifications. Key innovations include improved caption generation during training (using GPT models to rewrite captions with more detail and structure) and architectural enhancements for better spatial understanding. Business applications favor DALL-E 3 for critical creative work where prompt adherence is essential, despite higher costs compared to open-source alternatives.

Midjourney, another proprietary system, specializes in artistic and aesthetic quality with particularly strong performance on creative and stylized imagery. The system has been iteratively refined through extensive user feedback and human-in-the-loop training. Business users value Midjourney for marketing materials, concept art, and creative exploration where artistic quality matters more than precise photorealism.

### 27.3 Video Generation with Diffusion Models

Extending diffusion models to video represents one of the most significant advances in generative AI over the past two years. While image generation has become relatively mature, video generation introduces fundamental new challenges: temporal coherence across frames, consistent motion dynamics, scene continuity when objects are occluded and reappear, and computational costs that scale linearly with video duration. Despite these challenges, recent breakthroughs have achieved near-photorealistic video generation with impressive duration and quality.

The business applications are transformative. Traditional video production costs \$1,000-10,000 per minute for professional quality, requiring cameras, lighting, actors, sets, and post-production. AI video generation reduces this to \$1-100 per minute, enabling entirely new use cases. Marketing teams generate product demonstrations without physical prototypes. E-learning platforms create educational content at scale. Entertainment companies generate visual effects and concept previews. Game developers create cinematics and cutscenes automatically. The video generation market is projected to reach \$10-15 billion annually by 2028 as quality continues improving.

### 27.3.1 Video-Specific Challenges and Architectural Solutions

Video diffusion models must address several fundamental challenges that don't exist in image generation. First, temporal consistency requires that objects maintain their appearance, position, and identity across frames. If a person's face changes slightly between frames, or a car's color shifts, the video appears flickering and unrealistic. Second, motion coherence requires that object movements follow realistic physics and dynamics. A ball thrown should follow a parabolic trajectory; a person walking should have coordinated limb movements. Third, long-range temporal dependencies require the model to remember information from many frames ago—if a character exits the frame and re-enters 5 seconds later, they should have the same appearance.

The solution to these challenges lies in architectural innovations that extend image diffusion to handle the temporal dimension effectively. The most straightforward approach treats video as a 3D tensor with dimensions (time, height, width, channels) and extends 2D operations to 3D. However, this naive approach scales poorly—a 10-second video at 24 fps and  $512 \times 512$  resolution contains 240 frames, or 62 million pixels, making memory and computation infeasible for standard hardware.

Modern video diffusion architectures employ several strategies to achieve tractability while maintaining quality. Separable spatial-temporal attention decomposes attention across space and time rather than computing joint 3D attention. First, we apply spatial attention within each frame independently, allowing the model to understand scene composition at each moment. Then, we apply temporal attention across frames at the same spatial location, allowing the model to track objects over time. This decomposition reduces computational complexity from  $O(T^2 H^2 W^2)$  for joint attention to  $O(TH^2W^2 + T^2HW)$  for separable attention—a dramatic reduction that makes video diffusion feasible.

The mathematical formulation introduces temporal layers into the diffusion U-Net. Let  $\mathbf{z}_t^{(i)}$  represent the latent code for frame  $i$  at diffusion timestep  $t$ . Spatial attention computes:

$$\mathbf{z}_t^{(i)} \leftarrow \text{SpatialAttention}(\mathbf{z}_t^{(i)}) \quad (27.9)$$

This operates on each frame independently, identical to image diffusion. Temporal attention then computes:

$$\mathbf{z}_t^{(i)} \leftarrow \text{TemporalAttention}(\{\mathbf{z}_t^{(j)}\}_{j=1}^T) \quad (27.10)$$

where each position  $(h, w)$  in frame  $i$  attends to the corresponding position across all frames, learning to track motion and maintain consistency.

Causal temporal attention is a variant used by some models where frame  $i$  can only attend to frames  $j \leq i$ . This enables autoregressive generation where we generate video forward in time, conditioning each new frame on previous frames. This approach better handles long videos by processing them in chunks, but sacrifices the bidirectional reasoning of non-causal attention.

### 27.3.2 Advanced Video Diffusion Architectures

Recent state-of-the-art video generation models have introduced innovative architectural patterns that significantly improve quality and efficiency.

Sora, introduced by OpenAI in 2024, pioneered the spacetime patch approach. Rather than treating video as a sequence of images, Sora treats it as a collection of spacetime patches—3D volumetric regions that extend across both spatial dimensions and time. A spacetime patch might be  $16 \times 16$  pixels across 8 frames, capturing local motion patterns. The model applies transformer attention across these patches, enabling it to learn correlations between spatially and temporally nearby regions.

This architecture provides several advantages. First, it enables better understanding of 3D scene geometry and camera motion because spatial and temporal information is processed jointly within patches. The model learns that a moving object occupies different spatial positions in consecutive frames, understanding motion as a continuous trajectory rather than discrete position changes. Second, it improves object permanence—objects that become occluded and then reappear maintain consistent appearance because the model has learned to track them through the spacetime volume. Third, it enables flexible video lengths by simply including more patches, rather than being constrained to fixed durations.

Sora’s technical capabilities include generating videos up to 60 seconds at 1080p resolution, maintaining object permanence when objects are occluded and reappear, understanding 3D scene geometry and realistic camera motion, supporting complex prompts with multiple objects, actions, and scene transitions, and enabling temporal extension (generating forward or backward in time) and frame interpolation (filling in missing frames).

The computational requirements remain substantial. Generating a 60-second video at 1080p requires approximately 100-200 GPU-hours on A100s for the full 1000-step diffusion process. Efficient samplers reduce this to 20-50 steps, cutting generation time by 20-50 $\times$ , but still requiring several minutes on consumer hardware for long videos. This positions Sora for high-value creative applications rather than real-time or consumer-scale generation.

Veo 2, released by Google DeepMind in late 2024, represents the current state-of-the-art in video quality and realism. Key innovations include enhanced temporal consistency through improved 3D attention mechanisms that better model motion coherence, better understanding of real-world physics including gravity, fluid dynamics, and object interactions, improved prompt following through multi-stage refinement where the model first generates a low-resolution video and then upsamples, generation of videos up to 2 minutes duration (versus 5-10 seconds for earlier models), and reduced artifacts through better training data curation and architectural improvements.

Veo 2 excels at photorealistic generation for business applications. Product demonstrations, marketing videos, and explainer content generated by Veo 2 are often indistinguishable from professionally filmed content. Production companies report 60-80% cost reduction for certain content types (product demonstrations, concept visualization, establishing shots) compared to traditional video production, though creative and narrative-driven content still requires human direction.

The training approach combines several data sources: licensed stock footage (millions of high-quality videos with clean rights), synthetic data generated through 3D rendering engines to provide ground-truth physics and camera motion, and user-generated content from platforms with appropriate licensing agreements. The multi-stage training process first pretrains on large-scale video data to learn general motion and appearance patterns, then fine-tunes on high-quality curated data to improve aesthetics and prompt adherence, and finally applies reinforcement learning from human feedback (RLHF) to align with human quality preferences.

Hunyuan Video, developed by Tencent and released in late 2024, focuses on efficiency and accessibility. The architecture employs aggressive compression techniques including smaller U-Net backbones, quantization to INT8 precision with minimal quality loss, and efficient attention implementations optimized for consumer GPUs. This enables generation of high-quality 5-30 second clips on consumer hardware like RTX 4090 GPUs in 30-60 seconds, compared to 5-10 minutes for equivalent quality on earlier models.

Key features include native multilingual support (Chinese, English, and 10+ other languages through multilingual CLIP encoders), optimized efficiency allowing deployment on consumer GPUs, reduced training cost through knowledge distillation from larger models, and open-source components enabling community fine-tuning. The open-source release has accelerated research and enabled developers to build custom video generation applications without massive compute budgets.

### 27.3.3 Training Video Diffusion Models

Training video diffusion models requires careful consideration of data, compute resources, and optimization strategies. The data requirements are substantial: state-of-the-art models train on millions of video clips, each 2-30 seconds long, totaling hundreds of thousands of hours of video content. Data curation is

critical—videos must have high visual quality, diverse content (actions, scenes, camera motions), clean captions describing what happens in the video, and appropriate licensing rights.

Caption quality is particularly important for video because captions must describe temporal aspects: "a person walks into a room, looks around, and sits down" rather than just "a person in a room." Some training pipelines use video captioning models (trained separately) to generate dense descriptions of video content, then use these as training targets for the diffusion model.

The compute budget for training is substantial. Training a model comparable to Sora requires approximately 500,000-1,000,000 GPU-hours on A100s, costing \$1-2 million at cloud GPU prices. This makes video diffusion training accessible only to well-funded organizations. However, fine-tuning pre-trained models for specific domains is much more affordable—\$5,000-20,000 can produce good results for specialized applications like product videos, educational content, or domain-specific visual styles.

Training strategies have evolved to make video diffusion more tractable. Cascade training starts by training a base model at low resolution ( $64 \times 64$  or  $128 \times 128$ ), then training separate upsampling models that increase resolution to  $256 \times 256$ ,  $512 \times 512$ , and finally  $1024 \times 1024$  or higher. This decomposition makes training more stable and allows specialization at each resolution level—the base model focuses on motion and composition, while upsampling models focus on texture and detail.

Frame interpolation leverages the fact that consecutive frames are highly similar. Instead of generating all frames independently, we can generate keyframes (every 4th or 8th frame) and use a separate interpolation model to fill in intermediate frames. This reduces computational cost while maintaining temporal smoothness. The interpolation model is typically smaller and faster than the main diffusion model, trained specifically to predict intermediate frames given surrounding keyframes.

Progressive distillation reduces inference steps by training a student model to match a teacher model's outputs in fewer steps. For example, a 50-step model can be distilled into a 10-step model by training it to predict the same outputs as the teacher after 50 steps. This is applied iteratively:  $1000 \rightarrow 500 \rightarrow 250 \rightarrow 125 \rightarrow 50 \rightarrow 25$  steps, achieving  $40\times$  speedup with minimal quality degradation. This technique has been crucial for making video generation practical for interactive applications.

### 27.3.4 Practical Inference Optimization

Generating video at scale requires careful inference optimization to manage costs and latency. Several techniques have proven effective in production deployments.

Efficient samplers reduce the number of denoising steps from 1000 to 20-50 with minimal quality loss. DDIM (Denoising Diffusion Implicit Models) enables deterministic generation with fewer steps by reformulating the sampling process. DPM-Solver++ provides adaptive step sizes that concentrate steps where they're most needed, improving efficiency. Latent consistency models (LCM) distill diffusion models into 4-8 step generators, enabling near-real-time generation for short clips. These techniques reduce generation time by  $20\text{-}50\times$  while maintaining 90-95% of full-step quality.

Mixed precision training and inference using FP16 or BF16 instead of FP32 reduces memory usage by  $2\times$  and speeds up computation by  $1.5\text{-}2\times$  on modern GPUs. Automatic mixed precision (AMP) automatically determines which operations benefit from lower precision, providing speedups without manual tuning. For video, this enables generating longer clips or higher resolutions on the same hardware.

Quantization to INT8 or INT4 reduces model size by  $2\text{-}4\times$  with less than 5% quality degradation when applied carefully. Post-training quantization (PTQ) converts a trained FP32 model to INT8 without retraining, providing immediate deployment benefits. Quantization-aware training (QAT) incorporates quantization during training for better quality, achieving INT8 performance within 2-3% of FP32. These techniques enable deployment on consumer GPUs and mobile devices.

Spatial and temporal tiling generates long videos by processing overlapping chunks. For a 60-second video, we might generate in 10-second overlapping segments, ensuring smooth transitions by conditioning each segment on the previous few seconds. This makes memory requirements constant regardless of video length, enabling arbitrarily long generation on consumer hardware.



## 27.4 AI-Powered Storyboarding and Pre-Visualization

Storyboarding is a critical phase in professional video production where filmmakers plan every shot before filming begins. Traditional storyboarding requires skilled artists who sketch each shot by hand, a process that takes days or weeks and costs \$500-5,000 per project depending on complexity. For commercials, films, and high-budget content, this investment is justified. For smaller productions, creators, and iterative development, the cost and time are prohibitive, leading many to skip storyboarding entirely and rely on improvisation during filming.

AI-powered storyboarding tools have emerged as a transformative solution, enabling anyone to create professional-quality storyboards from text descriptions in minutes rather than days. These tools combine language models to interpret scripts and scene descriptions with diffusion models to generate corresponding visual frames, producing shot-by-shot visual previews that serve as blueprints for filming. The business impact includes 70-90% cost reduction compared to hiring storyboard artists, 10-50× faster iteration enabling directors to explore multiple creative directions, and democratization enabling small productions and individual creators to achieve professional planning workflows.

### 27.4.1 AI Storyboard Generation Pipeline

Modern AI storyboarding systems follow a multi-stage pipeline that transforms written scripts into visual sequences. The process begins with script understanding, where a language model analyzes the input script or shot list to extract key information for each shot. For example, given the line "INT. COFFEE SHOP - DAY. Sarah walks in, looks around nervously, then approaches the counter," the system extracts scene setting (interior coffee shop, daytime lighting), characters (Sarah), actions (walking, looking, approaching), emotions (nervous), and camera suggestions (likely medium shot following Sarah's movement).

Shot decomposition breaks complex scenes into individual shots. A language model trained on film scripts and shot breakdowns identifies natural shot boundaries based on action changes, camera angle shifts, and narrative beats. The example above might decompose into: establishing shot of coffee shop interior, medium shot of Sarah entering through door, close-up of Sarah's face showing nervousness, and over-the-shoulder shot as she approaches counter. This decomposition follows cinematic conventions learned from training data.

Visual generation creates images for each shot using text-to-image diffusion models conditioned on the extracted shot descriptions. The prompts are carefully engineered to include cinematographic details: "cinematic film still, medium shot, interior coffee shop, woman walking through door, nervous expression, warm lighting, shot on arri alexa, shallow depth of field, professional color grading." These detailed prompts leverage the extensive knowledge of cinematography that modern diffusion models have learned from training on movie stills and professional photography.

Character consistency is a critical challenge for storyboarding—the same character should look identical across all shots. Advanced systems employ several techniques to maintain consistency. Reference image conditioning provides a reference image of each character to the diffusion model, using IP-Adapter or similar techniques to preserve appearance while varying pose and expression. Multi-image fusion generates multiple images of the character and averages their latent representations, creating a consistent appearance template. Fine-tuning creates a custom LoRA (Low-Rank Adaptation) for each character, learned from a few reference images, enabling consistent generation across all shots.

Layout and composition planning uses AI to suggest camera angles, framing, and shot composition based on narrative needs and cinematographic principles. Language models trained on shot lists can suggest "close-up for emotional moment," "wide shot to establish location," or "over-the-shoulder for dialogue." Some systems integrate with 3D scene composers that allow directors to position virtual cameras in 3D space and generate the corresponding 2D storyboard frames.

### 27.4.2 Commercial AI Storyboarding Tools

Several commercial platforms have emerged, each targeting different segments of the video production market.

StoryboardHero focuses on advertising agencies and marketing teams, generating storyboards from briefs and scripts specifically optimized for commercial and explainer video formats. Key features include rapid iteration with multiple style options (realistic, illustrated, comic book), export to presentation formats (PDF, PowerPoint) for client reviews, collaboration tools enabling team feedback and revision tracking, and character consistency across campaigns for brand mascots and spokespeople. Pricing is typically subscription-based at \$50-200 per month depending on generation volume, making it accessible for small agencies while still being cost-effective for larger operations.

Boords has integrated AI generation into their established storyboarding platform, combining traditional storyboarding tools (drag-and-drop frames, annotations, notes) with AI-generated imagery. Users can sketch rough frames manually and ask the AI to generate polished versions, or start from text descriptions. This hybrid approach appeals to professional storyboard artists who want to accelerate their workflow rather than fully automate it. The platform includes animatic creation (adding timing and basic motion to storyboards), client review and approval workflows, and integration with production management tools.

DALL-E and Midjourney, while not specialized storyboarding tools, are widely used by filmmakers for concept art and shot visualization. Users manually manage character consistency by reusing seeds, providing reference images, or fine-tuning custom models. This DIY approach requires more technical expertise but provides maximum creative control. Film schools and independent filmmakers often adopt this workflow due to lower costs and flexibility.

LensGo and similar platforms specialize in maintaining consistent characters and styles across generated images, specifically designed for narrative content. Features include character libraries where users define characters once and reuse them across projects, style consistency ensuring visual coherence across all frames, and shot angle suggestions based on scene analysis. These tools bridge the gap between general-purpose image generators and specialized storyboarding software.

### 27.4.3 Integration with Production Workflows

AI storyboarding has maximum value when integrated into existing production pipelines rather than used as a standalone tool. Modern workflows combine AI storyboards with pre-visualization (previz), shot lists, and scheduling tools to create seamless planning processes.

Pre-visualization extends storyboarding into 3D, creating animated previews of complex shots before filming. AI-generated storyboard frames can serve as references for 3D artists, who recreate scenes in 3D software like Unreal Engine or Blender. This is particularly valuable for VFX-heavy productions where directors need to visualize how live-action footage will integrate with CGI elements. Some systems are developing direct 3D scene generation from storyboards, automatically placing 3D objects and cameras based on 2D frame analysis.

Shot list generation analyzes the storyboard to produce detailed shot lists for production teams, including camera movements (pan, tilt, dolly), lens choices (wide, medium, telephoto), lighting requirements (natural, key light, fill), and estimated shooting time per shot. This transforms the storyboard from a creative document into an operational plan that cinematographers and assistant directors use to schedule filming.

Location scouting assistance matches storyboard frames to real locations by analyzing visual characteristics—a storyboard frame showing “modern coffee shop with large windows and wooden furniture” can be matched against location databases to find suitable filming spots. Some platforms integrate with location scouting services, suggesting venues based on storyboard requirements.

Budgeting and scheduling tools estimate production costs based on storyboard complexity. Shots requiring special equipment (drones, Steadicam), complex lighting setups, or VFX are automatically flagged, and cost estimates are generated. This enables producers to make informed decisions about which creative choices fit within budget constraints, potentially revising the storyboard before expensive pre-production commitments.

### 27.4.4 Future Directions in AI Storyboarding

Emerging capabilities promise to further transform pre-production workflows. Video storyboards, generating short animated sequences rather than static frames, allow directors to visualize timing, pacing,

and movement. Early implementations generate 2-5 second clips per shot, though coherence across shots remains challenging. As video generation improves, full animatic generation from scripts will become feasible, providing near-final previews before any filming occurs.

Interactive storyboarding enables real-time collaboration where directors and cinematographers can iterate on shots instantly during creative meetings. Natural language interfaces allow commands like "make this shot wider" or "add more dramatic lighting," with the AI regenerating frames in seconds. This transforms storyboarding from a pre-meeting preparation task into a dynamic creative process.

Cross-modal generation extends beyond visual frames to include suggested camera movements, sound design, and music. A system might generate a storyboard frame and simultaneously suggest "camera dollies in slowly while ominous music builds," providing a more complete creative vision. Integration with audio tools could generate actual music stems and sound effect libraries aligned with the visual narrative.

Automated cinematography learning from analyzing thousands of films enables AI systems to suggest shots that match genre conventions, directorial styles, or specific filmmaker references. A director could specify "make this scene feel like a Wes Anderson film" and have the AI suggest symmetrical framing, pastel color palettes, and whimsical composition, learning from analysis of Anderson's actual films.

## 27.5 Virtual Production: Integrating Real Actors with AI-Generated Visual Effects

Virtual production represents the convergence of live-action filmmaking with real-time computer graphics and AI-generated content. Traditional filmmaking separates live-action shooting (actors on sets) from visual effects (added in post-production months later), creating challenges around actors' performances matching effects they cannot see and expensive reshoots when integration issues are discovered late. Virtual production solves this by enabling actors to perform within AI-generated environments displayed on LED walls in real-time, seeing final visuals during filming rather than imagining them.

The business impact is substantial. Traditional VFX-heavy productions spend 30-60% of their budget on post-production visual effects, with timelines extending 6-18 months after filming. Virtual production reduces VFX costs by 40-70% and shortens timelines to 2-6 months by shifting work to pre-production and capturing final visuals in-camera. Major productions using virtual production—including *The Mandalorian*, *Thor: Love and Thunder*, and numerous commercials—report cost savings of \$5-20 million per project while achieving better creative results through immediate feedback and iteration.

### 27.5.1 Technical Foundations of Virtual Production

Virtual production systems integrate multiple technologies into cohesive pipelines. The core component is an LED volume—a stage surrounded by large LED walls displaying real-time rendered environments. These walls are not simple screens but sophisticated systems with brightness exceeding 1000 nits, color accuracy matching professional displays (95%+ DCI-P3 coverage), high refresh rates (90-120 Hz) to prevent flickering on camera, and pixel pitches of 1-3mm enabling close-up photography without visible pixelation.

Camera tracking systems precisely measure camera position and orientation in real-time using optical tracking markers or IR-based systems. As the camera moves, the rendered background on LED walls adjusts perspective accordingly, maintaining correct parallax and creating the illusion that actors exist within the digital environment. This perspective-correct rendering is crucial—if the background doesn't shift properly as the camera moves, the illusion breaks and the composite looks fake.

Real-time rendering engines like Unreal Engine or Unity generate the displayed environments at 60-90 fps with minimal latency (under 16ms). Modern game engines have matured to the point where they can produce film-quality visuals in real-time through photorealistic materials, realistic lighting using ray tracing, high-resolution textures and detailed geometry, and physics simulation for dynamic elements like water or cloth.

Color management ensures consistency between LED walls, cameras, and final output. The LED walls must accurately reproduce the colors specified by the rendering engine, and cameras must capture these colors correctly. Professional systems use calibrated color pipelines with LUTs (look-up tables) to ensure what is displayed on set matches what appears in the final output, avoiding expensive color correction in post-production.

### 27.5.2 AI-Generated Environments and Backgrounds

Generative AI has transformed the creation of virtual environments for LED walls. Traditionally, environments required 3D artists to manually model every building, tree, and prop—a process taking weeks or months. AI generation accelerates this dramatically, enabling rapid iteration and cost reduction.

Text-to-3D generation creates 3D environments from text descriptions using techniques like NeRF (Neural Radiance Fields) and 3D Gaussian splatting. A production designer can describe “Victorian-era London street at dusk with gas lamps and fog” and receive a complete 3D scene within hours. These scenes include geometry (buildings, streets, props), textures (brick, cobblestone, wood grain), and lighting (warm gas lamp glow, atmospheric fog). While early results required manual cleanup, 2025-era systems produce production-ready environments with minimal touch-up.

The technical approach typically combines multiple AI models. A text-to-image diffusion model first generates 2D reference images showing the desired environment from multiple angles. A 3D lifting model like DreamFusion or Magic3D then constructs a 3D representation that matches these 2D views when rendered from the corresponding camera angles. The result is a NeRF or 3D Gaussian splat that can be rendered in real-time from any viewpoint, providing the continuous perspective shifts needed for camera movement in virtual production.

Image-to-3D generation extends this by allowing production designers to provide reference photos or concept art and have AI generate matching 3D environments. A designer might photograph a real location that cannot be used for filming (too expensive, wrong location, poor lighting) and have AI recreate it digitally. The AI analyzes depth, lighting, and material properties from the 2D image and generates a 3D scene that maintains the look and feel while being fully controllable.

Style transfer and customization enable matching environments to specific artistic visions. A production might generate a baseline cityscape and then apply style transfer to match the color palette and aesthetic of *Blade Runner* or the whimsical look of Wes Anderson films. This is achieved by conditioning diffusion models on reference images or by fine-tuning on curated style datasets.

Environmental dynamics add realism through animated elements. AI-generated environments can include moving clouds (using flow prediction models), swaying trees (physics simulation guided by learned priors), animated crowds (character motion synthesis), and dynamic lighting changes (time-of-day transitions). These dynamic elements are critical for realism—static backgrounds look artificial when cameras move, but subtle motion in trees and clouds sells the illusion.

### 27.5.3 Character Consistency and Digital Doubles

One of the most challenging aspects of AI-assisted virtual production is maintaining consistent character appearance across shots, especially when combining real actors with digital characters or creating digital doubles of actors for stunts, de-aging, or scenes where the actor is unavailable.

Digital doubles are realistic 3D reproductions of actors created through 3D scanning (photogrammetry capturing detailed geometry and textures), performance capture (recording facial expressions and body movements), and AI synthesis (filling in details and ensuring realism). Traditional digital doubles cost \$50,000-500,000 per actor and require days of scanning and cleanup. AI-accelerated workflows reduce this to \$5,000-50,000 and complete in hours to days.

The AI pipeline for creating digital doubles starts with multi-view image capture where the actor is photographed from hundreds of angles under controlled lighting, providing raw data for reconstruction. Neural radiance fields (NeRF) or 3D Gaussian splatting reconstruct detailed 3D geometry and appearance from these images, capturing fine details like skin pores, wrinkles, and hair structure. The reconstruction process is guided by learned priors about human faces and bodies, ensuring anatomically plausible results even from limited input.

Deepfake technology enables realistic face replacement where a digital double's face is replaced with AI-generated facial animations driven by an actor's performance. Modern deepfake systems use diffusion models or GANs trained on video of the target actor, learning to generate realistic facial expressions, lighting responses, and subtle micro-expressions. These systems have improved dramatically in quality, now producing results indistinguishable from real footage under most viewing conditions.

However, deepfake technology raises significant ethical and legal concerns that the industry is actively addressing. Consent and rights management frameworks ensure that digital likenesses can only be used with explicit written consent from actors, specifying exactly how and where the digital double can be used. Compensation structures provide ongoing royalties when digital doubles are reused, rather than one-time payments. Detection and authentication technologies enable verification that content featuring an actor was authorized, combating unauthorized deepfakes.

Industry organizations including SAG-AFTRA (Screen Actors Guild) have established guidelines for digital double usage, including mandatory consent for any digital recreation, clear disclosure when digital doubles are used in final content, limitation periods defining how long digital doubles can be used after creation, and compensation structures ensuring fair payment for digital likeness rights. Major studios have adopted these guidelines to maintain positive relationships with talent and avoid legal disputes.

#### 27.5.4 Performance Capture and Motion Transfer

Performance capture records actors' movements and facial expressions to drive digital characters or digital doubles. Traditional performance capture requires actors to wear sensor-laden suits in specialized studios, limiting practical use. AI-powered markerless capture removes these limitations by tracking performers using standard cameras, enabling capture on any set without special equipment.

Computer vision models analyze video to extract skeletal pose (body joint positions over time), facial expressions (tracking 50-100 facial landmarks), and hand gestures (finger positions and articulations). These models are trained on massive datasets of labeled motion capture data, learning to infer 3D positions from 2D video. Modern systems achieve accuracy within 1-2cm for body tracking and sub-millimeter precision for facial tracking, sufficient for realistic animation.

Motion transfer applies captured performances to digital characters with different proportions or anatomy. An actor's walking motion can be transferred to a creature with different leg length, maintaining the style and emotion while adapting to physical constraints. This is achieved through learned motion manifolds that understand how motion patterns vary across body types, enabling plausible retargeting.

Real-time processing enables immediate feedback during filming. Directors can see the final digital character performing alongside actors on set monitors in real-time, allowing performance adjustments and immediate creative decisions. This eliminates the months-long delay of traditional VFX pipelines where directors only see final results in post-production, often discovering performance issues too late for reshoots.

#### 27.5.5 Integrating Real and Synthetic Elements

The most powerful applications of AI in virtual production combine real actors with synthetically generated elements seamlessly. This requires careful attention to lighting, shadows, reflections, and occlusions—the ways real and synthetic elements interact.

Relighting techniques adjust the lighting on real actors to match synthetic environments. If an actor stands in front of an LED wall showing a sunset scene, the actor should be lit by warm sunset-colored light. AI relighting models analyze the environment lighting and adjust the actor's appearance, ensuring consistent illumination. This can be done in real-time during filming (adjusting actual LED panels illuminating the actor) or in post-production (digitally relighting captured footage).

Shadow and reflection synthesis generates realistic shadows cast by actors onto synthetic environments and reflections of environments on actors. Physics-based rendering in game engines handles primary shadows and reflections, but AI refinement improves realism by adding subtle secondary effects like ambient occlusion, subsurface scattering in skin, and detailed micro-reflections. These effects

are often prohibitively expensive to compute in real-time physics simulations but can be approximated by learned models.

Occlusion handling ensures correct depth ordering when actors interact with synthetic objects. If an actor reaches behind a synthetic table, their hand should disappear behind the table. This requires real-time depth estimation of the actor and synthetic scene, compositing them in correct depth order. AI depth estimation from monocular RGB cameras enables this without requiring depth sensors, simplifying setup and reducing costs.

Material and texture matching ensures synthetic elements visually integrate with real elements. If a synthetic prop is placed next to a real prop, their materials should respond to lighting similarly. AI-learned material models capture how different materials (metal, plastic, fabric) interact with light, enabling realistic rendering. These models are trained on photographs of materials under varied lighting, learning reflectance properties that ensure consistent appearance.

### 27.5.6 Case Study: Virtual Production for Commercial Advertising

A major automotive company needed to create a commercial showing their new electric vehicle in multiple exotic locations—mountain roads, desert landscapes, coastal highways—within a tight three-week timeline and \$500,000 budget. Traditional location shooting would require traveling to multiple countries, transporting the vehicle, managing permits, and dealing with weather uncertainties, costing \$2-3 million and taking 2-3 months.

Instead, they employed virtual production with AI-generated environments. The pipeline included text-to-3D generation of environments from descriptions provided by the creative team ("winding mountain road through Swiss Alps at sunset, dramatic peaks in background"), 3D environment refinement by artists adding specific details and ensuring film-quality visuals, LED wall shooting with the vehicle on a practical road section (50 feet of real asphalt), and real-time camera tracking displaying perspective-correct environments as cameras moved around the vehicle.

AI enhancement in post-production included relighting adjustments to perfect the vehicle's appearance under each environment's lighting, shadow refinement ensuring realistic shadows on the ground, and detail synthesis adding atmospheric effects like dust particles and lens flare. The entire project from concept to final delivery took four weeks and cost \$480,000—within budget and schedule while achieving creative results that exceeded traditional location shooting.

Results measured through focus groups showed 87% of viewers believed the locations were real, 94% rated visual quality as "excellent" or "very good", and the commercial achieved 15% higher engagement than previous campaigns using traditional filming. The production team reported that real-time visualization enabled creative experiments—trying different times of day, weather conditions, and locations instantly—that would be impossible with traditional VFX pipelines.

## 27.6 Video Understanding and Scene Analysis

While video generation receives significant attention, video understanding remains equally important for business applications. Content platforms must analyze billions of videos for moderation, search, and recommendations. Media companies need to process archive footage to extract valuable segments. Autonomous systems must understand dynamic scenes in real-time. These applications require models that can comprehend temporal relationships, track objects across frames, and reason about events unfolding over time.

Vision transformers extended to video provide powerful architectures for these tasks. The key insight is treating video as a spatiotemporal signal where understanding requires reasoning about both what appears in frames (spatial) and how it changes over time (temporal).

### 27.6.1 Video Understanding Architectures

The 3D vision transformer extends image ViT to video by treating video as 3D patches with dimensions (time, height, width). A video clip is divided into spatiotemporal cubes—for example,  $16 \times 16$  pixels across 8 frames creates a 3D patch. These patches are flattened and projected to embeddings, position

embeddings are added to encode spatiotemporal position, and transformer layers process the sequence. This enables the model to capture spatiotemporal patterns jointly, learning features like “a hand moving left to right while grasping.”

Temporal attention mechanisms separate spatial attention (within frame) from temporal attention (across frames), providing more efficient computation than joint 3D attention. First, spatial attention processes each frame independently to understand scene composition at each moment. Then, temporal attention processes the same spatial location across all frames to track motion and changes over time. This decomposition reduces computational complexity while maintaining the ability to model long-range temporal dependencies.

Long-range modeling is a key advantage of transformer-based video understanding. Unlike CNNs with limited temporal receptive fields, transformers can capture dependencies spanning many seconds or even minutes. This enables understanding of complex actions that unfold over time—recognizing that a person started cooking 30 seconds ago and is now plating the finished dish, or understanding that a sports play began with a pass and ended with a goal.

### 27.6.2 Applications of Video Understanding

Video classification determines what is happening in a video clip, enabling action recognition for applications like sports analysis, surveillance, and content categorization. Models trained on large-scale action recognition datasets (Kinetics, Something-Something) can recognize thousands of action categories with high accuracy. For content platforms, this enables automatic tagging and categorization of user-uploaded videos, improving search and recommendations.

Scene understanding identifies objects, people, and their interactions within video. This goes beyond simple object detection to understand relationships—“person holding phone,” “car passing pedestrian,” “dog chasing ball.” These semantic relationships are crucial for applications like autonomous driving (understanding traffic scenarios), video search (finding specific interactions), and accessibility (generating detailed video descriptions for visually impaired users).

Temporal localization finds specific moments in long videos where events occur. Given a query like “find all moments where someone scores a goal,” the model identifies timestamps of relevant segments. This enables efficient video navigation, highlight generation, and content moderation at scale. Sports broadcasters use temporal localization to automatically generate highlight reels, reducing manual editing time from hours to minutes.

Video captioning generates natural language descriptions of video content, enabling accessibility, search, and content understanding. Modern video captioning models combine vision transformers for visual understanding with language models for caption generation, producing detailed descriptions that capture both visual content and temporal dynamics: “A chef chops vegetables on a cutting board, then adds them to a pan and stirs while the ingredients sizzle.”

## 27.7 Automated Video Editing and Effects

Professional video editing is time-consuming and requires specialized skills. AI can automate routine tasks, enabling faster workflows and democratizing video production for creators without professional training.

### 27.7.1 Shot Detection and Segmentation

A video shot is a continuous sequence of frames from one camera angle. Detecting shot boundaries is the first step in automated editing, enabling systems to understand video structure and identify natural edit points. A classification model trained on shot boundaries learns to recognize visual cues that indicate transitions between shots.

Hard cuts represent abrupt changes where one shot immediately replaces another. These are characterized by sudden changes in color distribution, object positions, or camera angle. Detection models analyze frame-to-frame differences in visual features—large differences in color histograms, edge distri-

butions, or learned embeddings indicate likely cut points. Modern models achieve over 95% accuracy on hard cuts because the visual discontinuity is pronounced.

Transitions include gradual effects like fades, dissolves, and wipes where one shot gradually transforms into another over several frames. These are more challenging to detect because the change is subtle and distributed across time. Models must learn to recognize the characteristic patterns of each transition type—fades show gradual darkening or brightening, dissolves show blending of two images, wipes show geometric patterns moving across the frame. Temporal modeling using 3D CNNs or video transformers captures these multi-frame patterns.

Scene changes represent semantic shifts even when there's no obvious visual discontinuity. A scene change might occur when moving from an outdoor location to an indoor location, even if connected by a smooth camera movement. Detecting scene changes requires semantic understanding beyond low-level visual features—the model must recognize that the content has fundamentally changed even if the transition is visually smooth. This is achieved through learned embeddings that capture semantic content, with large embedding distances indicating scene boundaries.

Implementation typically uses a frame-level classifier that processes video at 5-30 fps (lower frame rates are sufficient since shot boundaries are visible across multiple frames). The classifier outputs boundary probabilities for each frame, and post-processing aggregates these predictions to identify final boundary locations. Temporal smoothing prevents spurious detections from momentary visual changes like camera flashes or quick movements.

### 27.7.2 Automated Video Summarization

Summarizing long videos into short highlight reels is valuable for content platforms, sports broadcasting, and personal video management. The challenge is identifying which moments are most important or interesting from hours of footage. AI systems approach this through learned models that predict frame importance based on multiple signals.

Visual novelty identifies frames that are dissimilar from previous content, indicating new information or scene changes. Embedding-based similarity measures compute distances between frame embeddings—frames with large distances from recent history are considered novel and potentially interesting. This captures moments like scene transitions, new characters appearing, or significant visual changes.

Motion analysis detects high-motion segments that often correspond to interesting action. Optical flow estimation measures pixel-level motion between frames, and high flow magnitudes indicate dynamic content. For sports videos, high motion correlates with plays and scoring opportunities. For vlogs, high motion might indicate activities rather than static talking-head segments. However, motion alone is insufficient—camera shake and panning can create high motion without interesting content, so motion must be combined with other signals.

Face and people detection identifies segments featuring human subjects, which are often more engaging than empty scenes or landscapes. Face detection models locate faces in frames, and tracking algorithms follow individuals across time. Segments with prominent faces, especially close-ups showing expressions, are weighted higher in importance. For social media content, this aligns with user preferences for people-centric videos.

Semantic importance uses video captioning or action recognition to identify moments describing significant events. A language model trained on video-summary pairs learns which types of events are typically included in summaries. For cooking videos, moments showing key steps (adding ingredients, plating) are more important than preparation or cleanup. For sports, moments near scoring are more important than mid-field play. This semantic understanding requires training on domain-specific data with human-annotated summaries.

User engagement data, when available, provides direct signals of interesting moments. Watch-time patterns show where viewers rewatch or pause, indicating engaging content. Skip patterns show where viewers fast-forward, indicating less interesting segments. Eye-tracking data from user studies reveals which visual elements attract attention. These signals can be incorporated into ranking models to predict engagement for new videos.

A neural ranking model combines these signals to score each frame or segment. The model is trained on pairs of videos and human-selected summaries, learning to predict which frames humans choose to



include. At inference time, the model scores all frames, and a selection algorithm chooses a subset that maximizes total importance while respecting duration constraints and ensuring temporal diversity (avoiding selecting many similar frames from the same moment).

### 27.7.3 Special Effects Generation

Generating special effects automatically based on content analysis enables creators to enhance videos without manual editing expertise. AI systems can apply effects that would traditionally require professional software and skills.

Color grading adjusts the color palette and tone of video to achieve specific aesthetic goals. AI models analyze scene content to predict appropriate color treatments—warm tones for sunset scenes, cool tones for night or winter scenes, high contrast for dramatic moments, desaturated colors for somber moods. The model learns these associations from professionally graded footage, capturing cinematographic conventions. Users can specify target styles (“make this look like a film noir” or “apply Instagram Valencia filter”), and the model applies corresponding color transformations through learned lookup tables (LUTs) or neural color transfer.

Motion blur adds realistic blur to moving objects, enhancing the sense of speed and motion. Optical flow estimation identifies moving regions and their velocity vectors. Blur is applied along motion directions with magnitude proportional to velocity, mimicking the blur captured by real cameras with finite shutter speeds. This is particularly effective for action sequences, sports footage, and dynamic camera movements. The challenge is distinguishing intentional motion (objects moving) from camera shake (entire frame moving), which requires robust flow estimation and scene understanding.

Depth-of-field effects blur out-of-focus regions to draw attention to subjects and create a cinematic look. Monocular depth estimation predicts depth maps from single frames, identifying which regions are near or far from the camera. Blur is applied to regions outside the focal plane, with blur magnitude increasing with distance from focus. Users can specify focus points interactively, and the system adjusts blur accordingly. This simulates the shallow depth-of-field achieved by professional cameras with large apertures, making smartphone footage appear more cinematic.

Slow-motion generation interpolates frames to create smooth slow-motion effects from standard frame rate footage. Frame interpolation models predict intermediate frames between existing frames, using optical flow or learned motion models. High-quality interpolation requires understanding object boundaries, occlusions, and motion patterns to avoid artifacts. Modern models can generate 4-8× slow-motion (converting 30fps to 120-240fps) with minimal artifacts, enabling dramatic slow-motion effects from regular video. This is particularly popular for sports highlights, action sequences, and dramatic moments in narrative content.

## 27.8 Practical Challenges and Trade-offs

### 27.8.1 Computational Requirements

Multimodal models demand substantial computational resources that create significant business constraints. Training state-of-the-art diffusion models requires investments of millions of dollars and weeks of continuous GPU time on large clusters. A single training run for a model like Stable Diffusion consumes 150,000 GPU-hours on high-end accelerators, translating to \$300,000-450,000 in cloud computing costs. This excludes the engineering effort required to set up distributed training infrastructure, tune hyperparameters, and monitor training progress. Only well-funded organizations can afford to train models from scratch, forcing most companies to fine-tune pretrained models for their specific needs.

Inference costs present ongoing operational challenges. Generating a single image takes 1-10 seconds on consumer hardware, while short video clips require 30-60 seconds even with optimized models. For platforms serving millions of users, this translates to massive GPU clusters operating continuously. A content platform processing 10 million image generations daily requires dozens of high-end GPUs running 24/7, costing \$50,000-100,000 monthly in cloud infrastructure. Video generation is even more expensive—processing 1 million video requests monthly at \$0.50 per video costs \$500,000, making careful optimization and caching strategies essential for profitability.

Storage requirements compound these costs. Training datasets for visual models consist of hundreds of millions of images and videos, totaling hundreds of terabytes of data. Storing this data, maintaining multiple versions for reproducibility, and providing fast access during training requires sophisticated data infrastructure. Companies must invest in high-performance storage systems, data versioning tools, and efficient data loading pipelines to make training tractable.

These computational constraints have important strategic implications. Research and deployment timelines are measured in months rather than weeks because training iterations are expensive and time-consuming. Companies must carefully prioritize which models to train and which applications to pursue, as each experiment represents significant investment. The high barrier to entry creates competitive moats for companies with existing infrastructure and trained models, but also creates opportunities for companies that can achieve better efficiency through architectural innovations or training optimizations.

### 27.8.2 Quality and Evaluation

Unlike classification tasks with clear accuracy metrics, visual quality is inherently subjective and context-dependent. What constitutes a "good" generated image depends on the application, user preferences, and cultural context. This subjectivity makes evaluation challenging and expensive, requiring multiple complementary approaches.

Human evaluation remains the gold standard for assessing visual quality. Expert raters score generated images on multiple dimensions including photorealism (does it look like a real photograph), prompt adherence (does it match the text description), aesthetic quality (is it visually pleasing), and diversity (do multiple generations show variety). However, human evaluation is expensive—hiring raters costs \$20-50 per hour, and evaluating thousands of images requires substantial budgets. Inter-rater reliability is also a concern, as different raters may have different aesthetic preferences and quality standards. Companies typically use panels of 5-10 raters per image to achieve reliable consensus scores.

Automated metrics provide scalable alternatives but have significant limitations. Fréchet Inception Distance (FID) measures the statistical similarity between distributions of generated and real images by comparing feature representations from a pretrained classifier. Lower FID scores indicate generated images are more similar to real images in feature space. However, FID has known issues—it can be gamed by memorizing training data, doesn't capture semantic quality, and may not align with human preferences. A model with low FID might still produce images that humans find unrealistic or unappealing.

Inception Score (IS) measures both quality and diversity by evaluating how confidently a classifier can categorize generated images and how diverse the categories are. Higher scores indicate clear, diverse images. However, IS is biased toward images that match ImageNet categories and doesn't evaluate prompt adherence or aesthetic quality. CLIP Score measures alignment between generated images and text prompts by computing similarity in CLIP's embedding space, providing a proxy for prompt adherence. However, CLIP Score doesn't evaluate visual quality or realism, only semantic alignment.

User satisfaction metrics from real-world deployments provide the most business-relevant evaluation. A/B tests compare different models or generation parameters by showing users different versions and measuring engagement, satisfaction ratings, or conversion rates. For a content creation platform, metrics might include how often users keep generated images versus regenerating, how often they share or publish generated content, and whether they return to use the service again. These metrics directly measure business value but require large user bases and careful experimental design to achieve statistical significance.

The evaluation challenge is particularly acute for video generation, where temporal consistency, motion quality, and narrative coherence add additional dimensions beyond static image quality. Evaluating whether a 10-second video clip has realistic motion, consistent object appearance, and appropriate pacing requires even more sophisticated human evaluation protocols and longer evaluation time per sample.

### 27.8.3 Data Licensing and Attribution

Models trained on billions of internet images raise complex copyright and licensing concerns that create legal and ethical challenges for the industry. Much training data includes copyrighted works scraped from the internet without explicit permission from creators. While some argue this constitutes fair use for research and transformative purposes, legal precedent is unclear and varies by jurisdiction. Several high-profile lawsuits from artists and photographers against AI companies are ongoing, with potential outcomes ranging from requiring licensing fees to prohibiting use of copyrighted data entirely.

The business implications are substantial. If courts rule that training on copyrighted data requires licenses, the cost of legally compliant training datasets could increase dramatically. Stock photo companies like Getty Images and Adobe Stock charge \$0.10-1.00 per image for commercial licenses, meaning a dataset of 400 million images could cost \$40-400 million to license—far exceeding current training compute costs. This would fundamentally change the economics of AI development, potentially limiting model training to large corporations that can afford licensing fees.

Attribution presents another challenge. When a model generates an image that closely resembles a specific artist's style or a specific copyrighted work, should the original creator receive credit or compensation? Current systems provide no attribution mechanism, and determining which training images influenced a particular generation is technically difficult. Some researchers are developing techniques to trace generated outputs back to influential training examples, but these methods are computationally expensive and not yet practical for production systems.

Mitigation strategies are emerging as the industry grapples with these issues. Using licensed datasets from stock photo providers ensures legal compliance but dramatically increases costs and limits dataset size. Providing opt-out mechanisms allows artists to request their work be excluded from future training, though this doesn't address past use and requires artists to actively monitor and request removal. Transparency about training data composition helps users understand what data was used and allows artists to make informed decisions about whether to opt out. Some companies are exploring compensation models where artists whose work appears in training data receive royalties based on usage, though implementing this at scale presents significant technical and administrative challenges.

The regulatory landscape is evolving rapidly. The European Union's AI Act includes provisions for transparency in training data and opt-out rights. Several U.S. states are considering legislation requiring disclosure of training data sources and compensation for creators. Companies must monitor these developments and adapt their practices to ensure compliance, potentially requiring significant changes to data collection, model training, and deployment practices. The uncertainty creates risk for businesses building products on generative AI, as regulatory changes could require expensive model retraining or limit commercial use of existing models.

## 27.9 Case Study: Automated Video Editing for Content Creators

A video platform serves millions of short-form video creators. Many create videos using mobile phones and lack professional editing skills. Automated editing can improve production quality and creator retention, directly impacting platform growth and engagement metrics.

### 27.9.1 System Design

The system processes raw video recorded on smartphones, typically 10-60 seconds in length at 720p-1080p resolution. The processing pipeline consists of multiple stages that transform raw footage into polished content.

Shot detection identifies transitions and cuts in the raw footage. A 3D CNN trained on 100,000 manually-annotated videos analyzes sequences of frames to detect shot boundaries. The model achieves 92% precision and 88% recall on the test set, successfully identifying most transitions while minimizing false positives that would create jarring edits. The model processes video at 5 fps (sufficient for detecting boundaries that span multiple frames), completing analysis of a 60-second video in approximately 3 seconds on GPU servers.

Summarization selects key frames for a 15-second highlight reel from longer source videos. A transformer encoder with a ranking head processes visual features extracted from each frame, scoring them for importance. The model was trained on 50,000 video-summary pairs where human editors selected the most engaging moments. The ranking model considers visual novelty, motion intensity, face presence, and semantic content to identify compelling moments. For a 60-second input video, the system generates a 15-second summary that captures the most interesting content while maintaining narrative flow.

Color correction normalizes color across shots to ensure visual consistency. The system analyzes color distributions in each shot and applies corrections to match a target aesthetic. This addresses common issues in smartphone footage where lighting conditions change between shots, creating jarring color shifts. The correction algorithm uses learned color transfer functions that map source colors to target colors while preserving natural appearance and avoiding over-processing.

Audio analysis detects speech, silence, and music in the soundtrack. Speech detection identifies segments where the creator is talking, which are typically important to preserve in summaries. Silence detection finds dead air that can be trimmed to tighten pacing. Music detection identifies background music and suggests complementary tracks from a licensed library based on mood and tempo matching. The audio analysis uses a combination of signal processing (spectral analysis, beat detection) and learned models (speech recognition, music genre classification).

Effects application adds subtle enhancements at key moments. Slight motion blur is applied to fast-moving segments to enhance the sense of speed. Selective slow-motion ( $2\times$  slowdown) is applied to dramatic moments identified by the ranking model, such as reveals or reactions. The effects are intentionally subtle to enhance rather than overwhelm the content, maintaining a natural look that doesn't appear over-processed.

## 27.9.2 Results

The system's quality metrics demonstrate strong performance across multiple dimensions. Shot detection achieves 92% precision and 88% recall on held-out test data, successfully identifying most transitions while keeping false positives low. This performance is sufficient for production use, though human review is available for creators who want manual control.

Summarization quality was evaluated through human ratings where viewers scored auto-generated summaries on a 5-point scale. 78% of auto-generated summaries received ratings of "good" or "excellent," compared to 72% for random frame selection and 91% for professional human editors. This positions the automated system between naive baselines and expert humans—good enough to add significant value while leaving room for improvement. The 13-point gap between automated and human performance represents an opportunity for future model improvements.

Effects quality was assessed through creator surveys and A/B tests. Creators reported that effects were "subtle and pleasing" rather than "aggressive or distracting," achieving the design goal of enhancement without over-processing. A/B tests showed that videos with automated effects received 8% more positive reactions from viewers compared to unedited versions, indicating that the effects successfully improved perceived quality.

The business impact exceeded expectations across multiple metrics. Creators using auto-editing received 15% more views on average compared to a control group, a statistically significant difference ( $p < 0.001$ ) measured through a randomized A/B test with 100,000 creators over 3 months. This view increase translates directly to higher creator satisfaction and platform engagement.

Creator retention improved by 12% among users who adopted auto-editing. Retention is measured as the percentage of creators who return weekly to upload new content. The improvement suggests that auto-editing reduces friction in the creation process, making it easier and more rewarding to produce content. Qualitative feedback indicated that creators appreciated the time savings and quality improvements, feeling more confident sharing their edited videos.

Time savings were substantial. Auto-editing completes in 30 seconds for a 60-second video, compared to 20 minutes for manual editing by the same creators. This  $40\times$  speedup enables creators to produce more content in the same time, or to spend saved time on other aspects of content creation like scripting and filming. The time savings are particularly valuable for casual creators who produce

content as a hobby rather than a profession.

Deployment infrastructure processes videos efficiently at scale. Inference runs on GPU servers, taking 30 seconds per 60-second video including all pipeline stages (shot detection, summarization, color correction, audio analysis, effects). Videos are processed asynchronously after upload, with edited versions returned within 5 minutes. This latency is acceptable for the use case, as creators typically upload videos and then move on to other tasks rather than waiting for immediate results.

Cost per video is \$0.05, including cloud GPU inference (\$0.03), storage for input and output videos (\$0.01), and networking and overhead (\$0.01). At platform scale processing 10 million videos monthly, this represents \$500,000 in monthly operating costs. This cost is justified by the business value—the 15% increase in views and 12% improvement in creator retention generate an estimated \$5 million in additional monthly revenue through advertising and subscriptions, providing a 10× return on investment.

## 27.10 Model Maintenance and Drift in Visual Content Systems

Visual content systems face unique drift challenges that can significantly impact business performance if not properly managed. Unlike text, where language evolution is relatively gradual, visual trends can shift rapidly—new video editing styles emerge monthly, fashion and design trends change seasonally, and platform-specific content formats evolve constantly. A model trained on 2022 TikTok videos may perform poorly on 2024 content due to changes in editing styles, effects, music choices, and creator behaviors.

### 27.10.1 Domain-Specific Drift Patterns in Visual Content

Visual content drift manifests in several distinct ways, each requiring different detection and mitigation strategies:

**Style and aesthetic drift.** Visual trends evolve rapidly, especially on social media platforms. The "aesthetic" of popular content changes—color grading preferences shift from warm to cool tones, editing styles move from static to dynamic, aspect ratios change (16:9 to 9:16 to 1:1). A video quality classifier trained on 2020 YouTube content may rate 2024 TikTok-style videos as low quality because it learned outdated aesthetic preferences. This directly impacts business metrics: recommending outdated content reduces engagement, and flagging trendy content as low-quality frustrates creators.

**Technical format drift.** Video formats and codecs evolve as technology advances. New cameras produce higher resolutions (4K, 8K), higher frame rates (60fps, 120fps), and HDR content. Models trained on 1080p 30fps SDR video may struggle with 4K 60fps HDR input, producing artifacts or incorrect classifications. For content platforms, this means new content from users with latest devices may be processed incorrectly, creating a poor user experience for early adopters.

**Content type drift.** New content categories emerge constantly. When TikTok introduced "duets" (split-screen videos), existing models had no training data for this format. When AR filters became popular, models trained on natural faces struggled with augmented features. When 360-degree video gained traction, models trained on standard rectangular video failed. Each new format requires model updates or risk misclassifying novel content.

**Platform-specific drift.** Different platforms have different content norms. Instagram Reels, TikTok, YouTube Shorts, and Snapchat Spotlight all host short-form video but with distinct styles, editing patterns, and audience expectations. A model trained on one platform may perform poorly when deployed on another. For companies operating across multiple platforms, this requires either platform-specific models (expensive) or robust models that generalize (difficult).

**Seasonal and event-driven drift.** Visual content exhibits strong seasonal patterns. Holiday content (Christmas, Halloween) has distinct visual characteristics. Sports events drive specific content types. Breaking news events create surges in particular visual themes. Models must adapt to these patterns or risk poor performance during high-traffic periods when business impact is greatest.

**Key Point 27.1.** *For generic drift detection strategies, continuous learning approaches, and implementation infrastructure, see Chapter 24, Section 24.7. The rapid pace of visual trend evolution typically requires monthly or even weekly model updates—more aggressive than most other domains.*

Key visual-specific considerations include:

- **Embedding-based distribution monitoring:** Extract visual embeddings from a pretrained vision transformer and track distribution shifts via KL divergence or Maximum Mean Discrepancy, complementing performance-based detection.
- **Parameter-efficient fine-tuning:** Use LoRA adapters on a frozen base model for daily/weekly incremental updates at 0.1–1% of full retraining cost, enabling rapid adaptation to emerging visual trends.
- **Temporal ensemble weighting:** Maintain models from different time periods and weight predictions based on input similarity to each training period—use recent models for novel content, older models for stable content types.

## 27.11 Exercises

**Exercise 27.1.** Implement a vision transformer for image classification on CIFAR-10. Compare accuracy and inference latency against a ResNet50 baseline. How much training data is needed for ViT to outperform CNNs?

**Exercise 27.2.** Fine-tune a pretrained diffusion model (e.g., Stable Diffusion) for a custom task: generating images in a specific art style. Collect 100 reference images in the target style. How does fine-tuning on 100 images affect output quality?

**Exercise 27.3.** Build a video shot detection classifier. Create a dataset of video clips with shot boundaries annotated. Train a model and evaluate precision/recall. How does performance vary with shot type (hard cut vs. transition)?

## 27.12 Solutions

Full solutions for all exercises are available at <https://deeplearning.hofkensvermeulen.be>.

## Chapter 28

# Knowledge Graphs, Semantic Web, and Structured Information Extraction

### Chapter Overview

While most chapters focus on unstructured data (text, images, video) or simple structured data (tables, time series), this chapter explores a unique domain: knowledge representation and reasoning. Knowledge graphs organize information as networks of entities and relationships, enabling semantic understanding and logical inference. Unlike text or images, knowledge graphs are explicitly structured: they formalize what is true about the world. Deep learning has transformed knowledge graphs from hand-crafted databases to systems that automatically extract entities, infer relationships, and reason over incomplete information. This chapter examines how transformers extract structured information from text, represent entities and relationships in learned embeddings, and perform inference over knowledge bases. Applications range from search (Google’s Knowledge Graph) to biomedical discovery (drug-target interactions) to cybersecurity (attack pattern detection).

### Learning Objectives

1. Understand knowledge graph structure: entities, relationships, and semantic types
2. Extract structured information from unstructured text (entity and relation extraction)
3. Represent knowledge in embeddings (TransE, DistMult, ComplEx models)
4. Perform link prediction: infer missing relationships
5. Implement semantic reasoning and type inference
6. Build knowledge-aware systems that combine text and structured knowledge
7. Address scalability: billion-scale graphs with billions of entities and relationships
8. Understand limitations: incompleteness, noise, and dynamic knowledge

### 28.1 Knowledge Graphs as Formal Languages

A knowledge graph is a directed, typed, attributed multigraph:

**Definition 28.1** (Knowledge Graph Structure). A knowledge graph consists of several fundamental components that work together to represent structured information about the world. Entities are unique objects, concepts, or things that exist in the domain being modeled. For example, “Barack Obama” represents a specific person, “United States” represents a particular country,

and “2008” represents a specific year. Each entity has a unique identifier that distinguishes it from all other entities in the graph.

Relationships, also called edges, are typed connections between entities that express how entities relate to each other. These relationships have specific semantic meanings that define the nature of the connection. For example, the relationship (Barack Obama) `–born_in–` (Honolulu) expresses that Barack Obama was born in the city of Honolulu. The directionality of relationships matters: being born in a location is different from a location being the birthplace of someone, even though they express related concepts.

Types provide semantic categories that classify entities into meaningful groups. An entity can have multiple types that describe different aspects of its nature. For example, Barack Obama has type “Person” indicating he is a human being, and type “Politician” indicating his professional role. These types enable reasoning about what properties and relationships are valid for an entity.

Attributes are properties of entities that describe their characteristics through key-value pairs. For example, Barack Obama has an attribute “birth\_date” with value August 4, 1961. Attributes differ from relationships in that they connect entities to literal values (strings, numbers, dates) rather than to other entities.

Triples form the basic unit of information in a knowledge graph, expressed as (subject, predicate, object) tuples. For example, (Barack Obama, `born_in`, Honolulu) is a triple where Barack Obama is the subject, `born_in` is the predicate (relationship type), and Honolulu is the object. This triple structure provides a simple yet powerful way to represent factual statements about the world.

Knowledge graphs are semi-formal: they have structure (typed entities, relationships) but allow uncertainty (confidence scores, probability distributions).

### 28.1.1 Examples of Knowledge Graphs

**DBpedia:** Extracted from Wikipedia infoboxes. 14M entities, 645M relationships. Public and incomplete.

**Freebase:** Curated database of facts. 1.9B entities, 3B relationships. Integrated into Google Knowledge Graph.

**Wikidata:** Community-curated knowledge base. 100M entities, 12B relationships. Increasingly used for structured data.

**YAGO:** Combines Wikipedia, WordNet, and GeoNames. 37M entities, 500M relationships.

**Enterprise KGs:** Internal knowledge bases for specific industries (healthcare, finance, customer data).

### 28.1.2 Why Knowledge Graphs Matter

Knowledge graphs provide capabilities that are difficult or impossible to achieve with unstructured data alone, making them essential for many modern AI applications.

Semantic search enables structured queries that go far beyond keyword matching. A query like “movies directed by Steven Spielberg released after 2010” requires understanding the concepts of directors, movies, and temporal relationships. A knowledge graph allows this query to be expressed precisely and answered directly by traversing the graph structure, while keyword search would struggle to distinguish between movies Spielberg directed versus movies he merely appeared in or produced.

Question answering becomes straightforward when facts are explicitly represented in a knowledge graph. The question “Who was Barack Obama’s wife?” can be answered by directly following the spouse relationship edge from the Barack Obama entity, yielding Michelle Obama. This direct lookup is faster and more reliable than extracting the answer from unstructured text, where the information might be expressed in many different ways or require complex inference.

Reasoning capabilities emerge from the graph structure, enabling inference of new facts from existing ones. If entity A is related to entity B through some relationship, and B is related to C through another relationship, the system can infer possible relationships between A and C. For example, if Barack Obama was president of the United States, and the United States is located in North America, we can infer



that Barack Obama was president of a country in North America. This transitive reasoning is natural in graph structures but difficult in unstructured text.

Disambiguation resolves ambiguity by using type information and context. The name “Obama” could refer to Barack Obama the politician, Michelle Obama the former first lady, or Obama as a surname in general. The knowledge graph distinguishes these through entity types and relationships, ensuring that queries and reasoning operate on the correct entity. This disambiguation is crucial for accurate information retrieval and reasoning.

Incompleteness handling addresses the reality that most facts about the world are unknown rather than explicitly false. Knowledge graphs are inherently incomplete—they contain only a tiny fraction of all true facts. Machine learning models can predict missing relationships based on learned patterns, inferring likely facts even when they haven’t been explicitly stated. This ability to reason about what is probably true, not just what is known to be true, makes knowledge graphs far more useful than static databases.

## 28.2 Entity and Relation Extraction from Text

Knowledge graphs must be populated with information. Much knowledge is in unstructured text (documents, web pages, news). Deep learning extracts structured triples from text.

### 28.2.1 Named Entity Recognition (NER)

The first step is identifying entities in text.

**Definition 28.2** (Named Entity Recognition). Given text, identify and classify entities into pre-defined types (Person, Organization, Location, Product, Date, etc.).

Example:

Text: "Barack Obama was elected president of the United States in 2008."

Entities:

- Barack Obama (Person)
- United States (Location)
- 2008 (Date)

**Deep learning approach:** Token classification using sequence labeling (BIO tagging):

The BIO tagging scheme provides a systematic way to mark entity boundaries in text. The B- (Begin) tag marks the start of an entity, indicating that a new entity mention begins at this token. The I- (Inside) tag marks the continuation of an entity, indicating that this token is part of the entity that started with the previous B- tag. The O (Outside) tag indicates that this token is not part of any entity. This scheme handles multi-token entities naturally: “Barack Obama” would be tagged as “B-Person I-Person”, clearly marking both tokens as part of a single person entity.

The architecture typically uses BERT or a similar transformer model as the encoder, which processes the entire input sequence and produces contextual embeddings for each token. These embeddings capture not just the token itself but its meaning in context, which is crucial for entity recognition. A token-level classification head sits on top of the transformer, predicting the BIO tag for each token independently. During training, the model learns to recognize entity patterns from labeled examples, and during inference, it applies these learned patterns to identify entities in new text.

### 28.2.2 Relation Extraction

Once entities are identified, extract relationships between them.

**Definition 28.3** (Relation Extraction). Given text with identified entities, determine the relationship type between entity pairs.

Example:

Text: "Barack Obama was born in Honolulu."

Entities: Barack Obama, Honolulu

Relation: born\_in

Triple: (Barack Obama, born\_in, Honolulu)

**Challenges:** Relation extraction faces several fundamental difficulties that make it more complex than entity recognition alone.

Long-range dependencies occur when entities that are related appear far apart in the text, separated by many intervening words or even sentences. For example, in “John, who had been working at the company for fifteen years and was known for his dedication, finally received the promotion he deserved from Mary,” the relationship between John and Mary (reporting structure or promotion relationship) spans a long distance with substantial intervening content. Models must maintain context over these long distances to correctly identify the relationship.

Implicit relations present another challenge because not all relationships are stated explicitly. The sentence “John married Mary” directly states the marriage relationship, making extraction straightforward. However, “John’s wife, Mary” implies the same relationship without using the verb “married.” The model must learn to recognize these implicit expressions of relationships, which can take many forms depending on the relationship type and the writing style.

Multiple relationships within a single sentence require the model to identify and extract all relevant triples, not just one. A sentence like “John founded Microsoft in Seattle in 1975” expresses at least three relationships: (John, founded, Microsoft), (Microsoft, located\_in, Seattle), and (Microsoft, founded\_in, 1975). The model must recognize that multiple facts are being asserted and extract each one correctly.

Noise in the form of non-factual statements complicates extraction because not all mentions of entities and relationships are asserting facts. Hypothetical statements (“If John were to marry Mary”), negations (“John did not marry Mary”), and questions (“Did John marry Mary?”) all mention entities and relationships but don’t assert that the relationship actually holds. The model must distinguish factual assertions from these other types of statements to avoid extracting false information.

**Deep learning approaches:** Several architectural strategies have emerged for relation extraction, each with different trade-offs between accuracy, complexity, and computational cost.

Sequence classification treats relation extraction as a classification problem where the model classifies each (entity1, entity2) pair based on the text between them. The model encodes the text span connecting the two entities and predicts which relationship type (if any) connects them. This approach is simple and works well when relationships are expressed locally, but it struggles with long-range dependencies and may miss context outside the span between entities.

Sequence tagging extends the BIO tagging approach from NER to identify relation arguments. The model tags each token to indicate whether it’s part of a relation expression and which role it plays (subject, predicate, object). This approach can handle complex sentence structures and multiple overlapping relations, but it requires more complex annotation and training procedures.

Structured prediction performs joint entity and relation extraction in a single unified model rather than as separate pipeline stages. The model simultaneously identifies entities and the relationships between them, allowing entity recognition decisions to inform relation extraction and vice versa. This joint approach consistently outperforms pipeline methods because it can leverage the mutual constraints between entities and relations—for example, knowing that a “born\_in” relationship exists helps identify that one entity is a person and the other is a location.

### 28.2.3 Joint Entity and Relation Extraction

Rather than two separate models, a unified model extracts entities and relations simultaneously.

**Architecture:**

1. Encode text with transformer
2. Entity recognition: Token classification (as in NER)
3. Relation classification: For each identified entity pair, classify relationship type
4. Output: Set of triples

**Advantages:** The joint extraction approach provides several benefits over pipeline methods that process entities and relations separately.

Entities are recognized in the context of their relationships, leading to better accuracy. When the model knows that a “born\_in” relationship is being expressed, it can use this information to help identify that one entity must be a person and the other must be a location. This mutual reinforcement between entity and relation recognition reduces errors that would occur if each task were performed in isolation.

Shared representations between entity and relation tasks allow the model to learn features that are useful for both tasks simultaneously. The transformer encoder learns to produce embeddings that capture both entity boundaries and relationship expressions, making the model more parameter-efficient and often more accurate than separate models.

Multi-token entities are supported naturally because the joint model understands entity boundaries as part of its core functionality. Complex entity names like “United States of America” or “Barack Hussein Obama II” are handled correctly because the model learns to recognize complete entity spans while simultaneously identifying their relationships.

## 28.3 Knowledge Graph Embeddings

Knowledge graphs are discrete structures; neural networks work on continuous embeddings. KG embedding models map entities and relationships to vector spaces.

### 28.3.1 TransE Model

TransE is the foundational KG embedding model:

**Definition 28.4** (TransE Embedding). Learn embeddings for entities and relationships such that:

$$\mathbf{h} + \mathbf{r} \approx \mathbf{t} \quad (28.1)$$

where  $\mathbf{h}$  is head entity embedding,  $\mathbf{r}$  is relation embedding,  $\mathbf{t}$  is tail entity embedding.

For a true triple, embedding of head + relation should be close to embedding of tail. For a false triple, they should be far.

Loss function:

$$\mathcal{L} = \sum_{(h,r,t) \in S} \|(\mathbf{h} + \mathbf{r}) - \mathbf{t}\|_2^2 + \sum_{(h',r,t') \notin S} \max(0, \gamma - \|(\mathbf{h}' + \mathbf{r}) - \mathbf{t}'\|_2^2) \quad (28.2)$$

Positive triples minimized; negative triples have margin.

**Training:** The TransE model is trained through an iterative process that learns to position entity and relationship embeddings in vector space such that valid triples satisfy the translation property.

The process starts with random embeddings for all entities and relationships, initializing them to small random values in the embedding space. For each true triple  $(h, r, t)$  in the training set, the model minimizes the distance between  $\mathbf{h} + \mathbf{r}$  and  $\mathbf{t}$ , encouraging the head entity embedding plus the relationship embedding to be close to the tail entity embedding. This teaches the model that these three elements form a valid fact.

For each false triple  $(h', r, t')$ , the model maximizes the distance between  $\mathbf{h}' + \mathbf{r}$  and  $\mathbf{t}'$  up to a margin, ensuring that invalid triples have embeddings that don't satisfy the translation property. The margin prevents the model from pushing false triples infinitely far apart, which would lead to unstable training.

Negative examples are sampled by corrupting true triples, typically by replacing either the head or tail entity with a random entity while keeping the relationship fixed. For example, from the true triple (Barack Obama, born\_in, Honolulu), we might generate negative examples like (Joe Biden, born\_in, Honolulu) or (Barack Obama, born\_in, Paris). This corruption strategy ensures that negative examples are similar to positive ones, forcing the model to learn fine-grained distinctions.

**Advantages:** TransE offers several practical benefits that have made it a foundational model in knowledge graph embedding.

The model is simple and interpretable, with the geometric translation property providing an intuitive understanding of how relationships work. The idea that relationships are translations in embedding space is easy to visualize and explain, making the model accessible to practitioners.

TransE scales to large graphs with billions of entities because the model complexity grows linearly with the number of entities and relationships. Each entity and relationship requires only a single embedding vector, and training can be parallelized efficiently across multiple GPUs.

The model captures simple relationships well, particularly one-to-one relationships like “spouse” or “capital\_of” where each entity has at most one related entity. For these relationship types, the translation property is a natural fit.

**Limitations:** Despite its strengths, TransE has fundamental limitations that motivated the development of more sophisticated models.

The model cannot handle complex relations, particularly many-to-many relationships where multiple entities can be related to multiple other entities. For example, the “acted\_in” relationship connects many actors to many movies, and the translation property doesn't capture this multiplicity well.

TransE assumes an additive relationship structure where  $\mathbf{h} + \mathbf{r} \approx \mathbf{t}$ , but not all relationship types fit this pattern. Symmetric relationships (like “married\_to”) and compositional relationships (like “grandfather\_of” being composed of two “father\_of” relationships) require different geometric properties that TransE cannot express.

### 28.3.2 Advanced Models: DistMult, ComplEx, RotatE

More sophisticated models address the limitations of TransE by using different geometric operations and embedding spaces, each offering improved expressiveness at the cost of additional complexity.

DistMult replaces the additive translation of TransE with element-wise multiplication, computing the score as  $\text{score}(h, r, t) = \mathbf{h}^T \text{diag}(\mathbf{r}) \mathbf{t}$ . This formulation is better suited for symmetric relations where the order of entities doesn't matter, such as “married\_to” or “sibling\_of”. The diagonal matrix  $\text{diag}(\mathbf{r})$  allows each dimension of the relationship to scale the corresponding dimensions of the head and tail entities independently, providing more flexibility than simple addition. However, DistMult cannot model asymmetric relations well because the multiplication operation is commutative.

ComplEx extends DistMult to complex-valued embeddings, where each entity and relationship is represented as a complex vector with both real and imaginary components. The scoring function becomes  $\text{score}(h, r, t) = \text{Re}(\mathbf{h}^T \text{diag}(\mathbf{r}) \bar{\mathbf{t}})$ , where  $\bar{\mathbf{t}}$  denotes the complex conjugate of the tail embedding. This complex formulation can model both symmetric and asymmetric relations because the complex conjugate operation breaks the symmetry. ComplEx also handles compositional relationships better, as complex multiplication naturally captures the composition of rotations in the complex plane.

RotatE represents relations as rotations in complex space, where each relationship corresponds to a rotation that transforms the head entity embedding into the tail entity embedding through element-wise multiplication:  $\mathbf{h} \circ \mathbf{r} = \mathbf{t}$ . In this formulation, relationship embeddings are constrained to have unit magnitude, making them pure rotations. This geometric interpretation is particularly powerful for capturing relation composition (rotating by  $r_1$  then  $r_2$  is equivalent to rotating by  $r_1 \circ r_2$ ) and relation inversion (the inverse of a rotation is simply the conjugate). RotatE achieves state-of-the-art performance on many benchmarks but requires more computation than simpler models.

Each model trades simplicity for expressiveness along a spectrum. TransE is the fastest and simplest, making it suitable for very large graphs where computational efficiency is paramount. DistMult adds modest complexity to handle symmetric relations better. ComplEx provides a good balance of expressiveness and efficiency, handling most relationship types well. RotatE is the most expressive, capturing complex patterns like composition and inversion, but it's also the slowest due to complex-valued operations. The choice depends on the specific knowledge graph characteristics and computational constraints.

## 28.4 Link Prediction and Reasoning

A key application: predict missing relationships (link prediction).

**Definition 28.5** (Link Prediction). Given a partial knowledge graph with some missing edges, predict which relationships are most likely to exist.

Example: Given (Barack Obama, spouse, ?), predict the tail entity. Correct answer: Michelle Obama.

This addresses the incompleteness of knowledge graphs.

### 28.4.1 Ranking-Based Link Prediction

For a query  $(h, r, ?)$ , rank candidate entities by likelihood:

$$\text{score}(h, r, t) = f(\mathbf{h}, \mathbf{r}, \mathbf{t}) \quad (28.3)$$

Using TransE:  $\text{score} = -\|(\mathbf{h} + \mathbf{r}) - \mathbf{t}\|_2$  (higher is better).

Rank all entities; top-k are predictions.

### 28.4.2 Evaluation Metrics

**Mean Reciprocal Rank (MRR):** Average rank of correct entity.

$$\text{MRR} = \frac{1}{|Q|} \sum_{i=1}^{|Q|} \frac{1}{\text{rank}_i} \quad (28.4)$$

Higher is better. Perfect:  $\text{MRR} = 1$ . Random:  $\text{MRR} = 1/|E|$  where  $|E|$  is number of entities.

**Hits@k:** Fraction of queries where correct entity in top-k.

$$\text{Hits@k} = \frac{\#\text{correct in top-k}}{|Q|} \quad (28.5)$$

Common metrics: Hits@1, Hits@10.

## 28.5 Semantic Type Inference and Reasoning

Beyond individual triples, knowledge graphs support reasoning.

### 28.5.1 Type Constraints

Each relation has type constraints that specify what kinds of entities can participate in that relationship, providing crucial information for reasoning and validation.

The *born\_in* relation requires that the head entity must be of type Person (since only people are born) and the tail entity must be of type Location (since birth occurs in a place). This constraint

immediately rules out nonsensical triples like (Apple Inc., born\_in, California) where a company cannot be born.

The *founder* relation specifies that the head type must be Person (founders are people) and the tail type must be Organization (things that are founded are organizations). This constraint helps distinguish between different senses of "founder" and ensures that extracted relationships make semantic sense.

The *contains* relation has head type Container and tail type Thing, representing a general containment relationship. This more abstract typing allows the relation to apply broadly while still providing useful constraints for reasoning.

Type constraints reduce link prediction space. For (Barack Obama, born\_in, ?), candidates must be locations.

### 28.5.2 Reasoning Rules

Knowledge graphs support several types of inference rules that enable deriving new facts from existing ones, providing powerful reasoning capabilities beyond simple lookup.

Composition rules allow chaining relationships to infer indirect connections. For example, if X is the father of Y, and Y is the father of Z, we can infer that X is the grandfather of Z. This transitive composition extends to many relationship types: if person A works for company B, and company B is owned by company C, we can infer that person A is indirectly associated with company C. Composition is particularly powerful for multi-hop reasoning where direct relationships don't exist but can be inferred through intermediate entities.

Symmetry rules capture relationships that work in both directions. The *married\_to* relationship is symmetric: if X is married to Y, then Y is married to X. Similarly, *sibling\_of*, *colleague\_of*, and *friend\_of* are typically symmetric relationships. Recognizing symmetry reduces the amount of information that needs to be stored explicitly and ensures consistency in the knowledge graph.

Inversion rules express relationships that are logical inverses of each other. If X is the parent of Y, then Y is the child of X. These inverse relationships are deterministic transformations: knowing one direction automatically implies the other. Other examples include *employer/employee*, *teacher/student*, and *buyer/seller* relationships. Inversion rules help maintain bidirectional navigability in the graph.

Subrelation rules capture hierarchical relationships between relation types. The *parent\_of* relationship is a specific case of the more general *ancestor\_of* relationship: if X is the parent of Y, then X is also an ancestor of Y. This hierarchical structure allows reasoning at different levels of abstraction and enables generalization from specific relationships to broader categories.

Deep models, especially RotatE, capture these patterns in learned embeddings without requiring explicit rule programming. The geometric properties of the embedding space naturally encode composition (rotation composition), symmetry (equal forward and backward rotations), and inversion (conjugate rotations), making these inference patterns emergent properties of the learned representations rather than hard-coded logic.

## 28.6 Temporal Knowledge Graphs and Dynamic Knowledge

Real-world knowledge evolves over time. Static knowledge graphs cannot capture temporal dynamics: facts that are true at specific times, relationships that change, and entities whose properties evolve.

### 28.6.1 Temporal Knowledge Representation

**Definition 28.6** (Temporal Knowledge Graph). A temporal knowledge graph extends standard KGs with time information, enabling representation of facts that change over time and events that occur at specific moments.

Temporal triples augment the standard (subject, predicate, object) structure with time information, expressed either as a single timestamp for point events or as a time interval [start, end] for facts with duration. This temporal annotation makes it possible to track when facts become

true and when they cease to be valid.

For example, the triple (Barack Obama, president\_of, USA, [2009-01-20, 2017-01-20]) captures not just that Barack Obama was president of the United States, but precisely when this relationship held. The interval notation makes it clear that this fact was true during the specified period and is no longer true after the end date.

Point-in-time facts represent measurements or observations at specific moments, such as (Company X, stock\_price, \$150, 2024-01-30). These facts capture the state of the world at a particular instant and are essential for tracking rapidly changing information like financial data, sensor readings, or real-time status updates.

Event sequences represent ordered series of facts that together describe a process or narrative. For example, a corporate acquisition might be represented as a sequence: announcement event, regulatory approval event, shareholder vote event, and completion event, each with its own timestamp. These sequences enable reasoning about causality, temporal ordering, and process dynamics.

### 28.6.2 Temporal Reasoning Challenges

Temporal knowledge graphs introduce several fundamental challenges that don't exist in static graphs, requiring specialized reasoning techniques.

Validity periods determine when a fact is true versus when it is false or unknown. The triple (Barack Obama, president\_of, USA) is only valid during the period 2009–2017. Queries must respect these temporal bounds: asking “Who was president of the USA in 2015?” should return Barack Obama, but the same query for 2020 should not. This requires temporal indexing and query evaluation that considers time ranges, not just entity and relationship matching.

Temporal consistency enforces logical constraints on facts across time. A person cannot be in two different physical locations simultaneously, so if the knowledge graph contains (Person X, located\_in, New York, 2024-01-15 10:00) and (Person X, located\_in, London, 2024-01-15 10:00), there is a consistency violation. Detecting and resolving such conflicts requires reasoning about the semantics of relationships and their temporal constraints. Some relationships allow simultaneous instances (a person can have multiple job titles at once) while others are mutually exclusive (a person can only have one birthplace).

Temporal inference addresses the question of whether facts persist over time in the absence of contradicting information. If  $X$  was true at time  $T_1$ , and no fact explicitly contradicts  $X$  at time  $T_2$ , should we infer that  $X$  is still true at  $T_2$ ? This depends on the relationship type: some facts are permanent (birth\_date never changes), some have default persistence (employment typically continues until explicitly ended), and some are ephemeral (location changes frequently). The knowledge graph must encode or learn these persistence patterns to make valid temporal inferences.

Forecasting predicts future facts based on historical patterns observed in the temporal graph. By analyzing sequences of events and their temporal relationships, models can predict likely future occurrences. For example, if companies in a particular industry typically acquire competitors within two years of receiving major funding rounds, the model can predict which acquisitions are likely to occur next. This predictive capability transforms knowledge graphs from passive repositories of past facts into active tools for anticipating future events.

### 28.6.3 Temporal Embedding Models

Extend static embedding models to incorporate time:

**TTransE (Temporal TransE):**

$$\mathbf{h} + \mathbf{r} + \mathbf{t}_{\text{time}} \approx \mathbf{t} \quad (28.6)$$

Time is embedded as a vector; added to the translation.

**DE-Simple (Diachronic Embeddings):** Model entities and relations as functions of time:

$$\mathbf{h}(t), \mathbf{r}(t), \mathbf{t}_{\text{entity}}(t) \quad (28.7)$$



Embeddings evolve smoothly over time using recurrent networks or temporal convolutions.

**TeMP (Temporal Message Passing):** GNN-based approach where messages are time-aware:

$$\mathbf{h}_i^{(t+1)} = \text{Aggregate}(\{\mathbf{h}_j^{(t)}, \mathbf{r}_{ij}, \tau_{ij}\}) \quad (28.8)$$

where  $\tau_{ij}$  is the timestamp of the relationship.

#### 28.6.4 Temporal Link Prediction

Predict future relationships based on historical patterns:

**Task:** Given knowledge graph up to time  $T$ , predict facts at time  $T+1$ .

**Example:** Historical pattern shows companies acquire competitors before IPO. Predict: (Company X, will\_acquire, Company Y, 2025).

**Applications:** Temporal link prediction enables several high-value applications across different domains.

Stock market prediction uses temporal knowledge graphs to forecast corporate events such as mergers, partnerships, and strategic alliances. By analyzing historical patterns of corporate relationships and their evolution over time, models can identify signals that precede major events. For example, increased collaboration relationships between two companies, combined with executive movements and patent filings, might predict an upcoming acquisition.

Geopolitical forecasting applies temporal reasoning to predict diplomatic relationships, conflicts, and international agreements. The temporal knowledge graph captures historical patterns of alliances, trade relationships, and conflicts, enabling models to forecast future geopolitical developments. If historical data shows that trade disputes often escalate to diplomatic tensions within six months, the model can provide early warnings of potential conflicts.

Healthcare applications use temporal knowledge graphs to predict disease progression based on patient history. By modeling how patient conditions, treatments, and outcomes evolve over time, the system can forecast likely disease trajectories and recommend interventions. For example, if patients with a particular combination of symptoms and biomarkers typically develop a specific condition within a certain timeframe, the model can predict this progression and enable preventive care.

#### 28.6.5 Recent Advances in Temporal Knowledge Graph Reasoning (2024-2025)

Temporal knowledge graph reasoning has advanced significantly in 2024 with dynamic hypergraph embedding methods that better capture complex temporal patterns and multi-way relationships.

**Dynamic Hypergraph Embeddings:** Traditional temporal KG methods model binary relationships (subject-predicate-object) evolving over time. However, many real-world events involve multiple entities simultaneously. Dynamic hypergraph embeddings extend temporal KGs to hyperedges connecting multiple entities, enabling richer temporal reasoning.

**Example:** A corporate merger involves multiple entities: acquiring company, target company, regulatory bodies, financial advisors, and shareholders. A hyperedge represents this multi-party event with temporal validity. Traditional binary relations (Company A, acquires, Company B) miss the full context.

**Key innovations in 2024-2025:** Several breakthrough techniques have emerged that significantly advance temporal knowledge graph reasoning capabilities.

Temporal hypergraph attention mechanisms weight the importance of different entities within a hyperedge and across time, enabling the model to learn which participants in multi-entity events are most predictive of future events. Unlike traditional attention that operates on pairs of entities, hypergraph attention considers the full context of multi-party interactions. For example, in a corporate merger involving acquiring company, target company, regulatory bodies, and financial advisors, the attention mechanism learns that regulatory approval timing is often the most predictive signal for completion dates, while financial advisor involvement is less informative.

Continuous-time modeling represents events in continuous time rather than discrete timestamps, using neural ordinary differential equations (Neural ODEs). This approach naturally handles irregular event spacing and enables interpolation between observed events. Instead of treating time as discrete



buckets, the model learns continuous dynamics that govern how entity states evolve, enabling more accurate forecasting and better handling of sparse temporal data.

Causal temporal reasoning distinguishes correlation from causation in temporal patterns, addressing the fundamental question: if event A precedes event B, is A causing B, or are both caused by hidden factor C? Causal inference methods including do-calculus and counterfactual reasoning are integrated with temporal KG embeddings to identify true causal relationships rather than mere temporal correlations. This improves prediction accuracy by 15-25% on forecasting tasks because the model learns to focus on causal drivers rather than spurious correlations.

Multi-scale temporal modeling recognizes that events occur at different timescales, with some relationships changing daily (stock prices) while others change yearly (corporate structure). Hierarchical temporal models employ separate encoders for different timescales, capturing both short-term dynamics and long-term trends. The model learns to combine these multi-scale representations, understanding that some predictions require short-term signals while others depend on long-term patterns.

**Implementation Considerations:** Dynamic hypergraph methods are computationally expensive—training requires 3-5x more compute than standard temporal KG methods. However, the improved accuracy often justifies the cost for high-value applications. Open-source implementations are emerging in PyTorch Geometric and DGL (Deep Graph Library) as of 2024-2025.

## 28.7 Graph Neural Networks for Knowledge Graphs

Graph Neural Networks (GNNs) have become the dominant approach for learning on graph-structured data, including knowledge graphs.

### 28.7.1 Relational Graph Convolutional Networks (R-GCN)

Standard GCNs assume homogeneous graphs (single edge type). R-GCN extends to multi-relational graphs:

**Definition 28.7** (R-GCN Layer). For entity  $i$  with embedding  $\mathbf{h}_i$ , update using neighbors:

$$\mathbf{h}_i^{(l+1)} = \sigma \left( \sum_{r \in \mathcal{R}} \sum_{j \in \mathcal{N}_i^r} \frac{1}{|\mathcal{N}_i^r|} \mathbf{W}_r^{(l)} \mathbf{h}_j^{(l)} + \mathbf{W}_0^{(l)} \mathbf{h}_i^{(l)} \right) \quad (28.9)$$

where several key components work together to enable multi-relational message passing. The set  $\mathcal{R}$  contains all relation types in the knowledge graph, allowing the model to distinguish between different kinds of relationships. The neighborhood  $\mathcal{N}_i^r$  consists of all entities connected to entity  $i$  via relation type  $r$ , enabling relation-specific aggregation. The relation-specific weight matrix  $\mathbf{W}_r^{(l)}$  transforms neighbor embeddings differently depending on the relationship type, capturing the semantic differences between relations. Finally, the self-loop weight matrix  $\mathbf{W}_0^{(l)}$  allows each entity to retain information from its previous layer representation, preventing information loss during aggregation.

**Key insight:** Different relation types have different semantics; use separate weight matrices.

**Scalability challenge:** With thousands of relation types, storing  $|\mathcal{R}|$  weight matrices is memory-intensive.

**Solution - Basis decomposition:**

$$\mathbf{W}_r = \sum_{b=1}^B a_{rb} \mathbf{V}_b \quad (28.10)$$

Express each relation weight as a linear combination of  $B$  basis matrices (where  $B \ll |\mathcal{R}|$ ).

### 28.7.2 Graph Attention Networks for KGs

Attention mechanisms allow the model to learn which neighbors are most important:

**Definition 28.8** (Relational Graph Attention). Compute attention weights for each neighbor:

$$\alpha_{ij}^r = \frac{\exp(\text{LeakyReLU}(\mathbf{a}^T[\mathbf{W}_r \mathbf{h}_i || \mathbf{W}_r \mathbf{h}_j]))}{\sum_{k \in \mathcal{N}_i} \exp(\text{LeakyReLU}(\mathbf{a}^T[\mathbf{W}_r \mathbf{h}_i || \mathbf{W}_r \mathbf{h}_k]))} \quad (28.11)$$

$$\mathbf{h}_i^{(l+1)} = \sigma \left( \sum_{r \in \mathcal{R}} \sum_{j \in \mathcal{N}_i^r} \alpha_{ij}^r \mathbf{W}_r \mathbf{h}_j^{(l)} \right) \quad (28.12)$$

**Advantages:** Graph attention networks provide several key benefits for knowledge graph reasoning.

The model learns the importance of different neighbors dynamically through attention weights, rather than treating all neighbors equally. This allows the model to focus on the most relevant relationships for each entity, improving both accuracy and interpretability. For example, when predicting a person’s occupation, the model might learn to pay more attention to “works\_for” relationships than to “friend\_of” relationships.

Attention mechanisms handle varying neighborhood sizes naturally without requiring normalization tricks or padding. Entities with many neighbors don’t dominate the aggregation simply due to their degree, and entities with few neighbors aren’t disadvantaged. The attention weights automatically adjust to the local graph structure, ensuring that each entity receives appropriately weighted information from its neighborhood.

The attention weights are interpretable, showing which relationships matter most for each prediction. By examining the learned attention patterns, practitioners can understand what the model considers important and validate that it’s learning meaningful semantic patterns rather than spurious correlations. This interpretability is crucial for debugging models and building trust in production systems.

### 28.7.3 Multi-Hop Reasoning with GNNs

GNNs naturally support multi-hop reasoning by stacking layers, where each layer extends the receptive field by one hop in the graph.

A 1-hop model with a single layer captures only direct neighbors, learning representations based on immediately connected entities. This is sufficient for simple tasks where the answer depends only on direct relationships, such as predicting an entity’s type based on its immediate connections.

A 2-hop model with two layers captures neighbors of neighbors, enabling reasoning over paths of length two. This allows the model to infer indirect relationships and discover patterns that span multiple edges. For example, to predict whether two people know each other, a 2-hop model can consider their mutual friends.

A k-hop model with k layers captures the k-hop neighborhood around each entity, enabling reasoning over increasingly complex graph patterns. However, deeper models face challenges including oversmoothing (where all entity representations become similar) and increased computational cost. In practice, 2-4 layers are typically sufficient for most knowledge graph tasks.

**Example reasoning:**

Query: "What diseases might drug X treat?"

1-hop: Drug X targets protein P

2-hop: Protein P is involved in disease D

Inference: Drug X might treat disease D

### 28.7.4 Practical Implementation

PyTorch Geometric example (simplified):

```

import torch
from torch_geometric.nn import RGCNConv

class KnowledgeGraphGNN(torch.nn.Module):
    def __init__(self, num_entities, num_relations, hidden_dim):
        super().__init__()
        self.embedding = torch.nn.Embedding(num_entities, hidden_dim)
        self.conv1 = RGCNConv(hidden_dim, hidden_dim, num_relations)
        self.conv2 = RGCNConv(hidden_dim, hidden_dim, num_relations)

    def forward(self, edge_index, edge_type):
        x = self.embedding.weight
        x = self.conv1(x, edge_index, edge_type)
        x = torch.relu(x)
        x = self.conv2(x, edge_index, edge_type)
        return x

```

## 28.8 Knowledge Graph Completion and Multi-Hop Reasoning

Link prediction focuses on single missing edges. Knowledge graph completion addresses systematic incompleteness through multi-hop reasoning.

### 28.8.1 Path-Based Reasoning

Rather than direct embeddings, reason over paths connecting entities:

**Definition 28.9** (Path Ranking Algorithm (PRA)). For query  $(h, r, ?)$ , find paths from  $h$  to candidate tails:

1. Extract all paths of length  $\leq k$  from  $h$  to candidate entities
2. Represent each path as a sequence of relations:  $r_1 \rightarrow r_2 \rightarrow \dots \rightarrow r_n$
3. Learn weights for path patterns that predict relation  $r$
4. Score candidates by weighted sum of paths

**Example:** Query: (Barack Obama, nationality, ?) Paths connecting Barack Obama to candidate answers provide evidence for the prediction:

The path `born_in`  $\rightarrow$  `located_in`  $\rightarrow$  USA provides strong signal because birthplace typically determines nationality. If Barack Obama was born in Honolulu, and Honolulu is located in the USA, this strongly suggests USA nationality.

The path `president_of`  $\rightarrow$  USA also provides strong signal because presidents must typically be citizens of the country they lead. This direct relationship between political office and nationality makes this path highly predictive.

The path `spouse`  $\rightarrow$  nationality  $\rightarrow$  USA provides weaker signal because spouses don't necessarily share nationality. While Michelle Obama's nationality might correlate with Barack Obama's, this relationship is less deterministic than birthplace or political office.

### 28.8.2 Neural Logic Programming

Combine neural networks with logic programming for interpretable reasoning:

**Neural LP:** Learn logical rules as differentiable operations:

$$\text{confidence}(h, r, t) = \max_{\text{path } \pi} \prod_{r_i \in \pi} \text{score}(r_i) \quad (28.13)$$

The model learns which rule chains (paths) are most predictive.

**Advantages:** Neural logic programming offers several compelling benefits for knowledge graph reasoning.

The learned rules are interpretable because they can be extracted and understood by humans. Unlike black-box neural networks, Neural LP produces explicit rule chains that explain why a particular prediction was made. For example, the model might learn that “born\_in(X, Y) located\_in(Y, Z) → nationality(X, Z)” is a reliable rule, and this rule can be inspected and validated by domain experts.

The compositional nature of the approach allows the model to learn how to compose relations to form complex reasoning chains. Rather than learning each multi-hop pattern independently, the model learns general composition principles that generalize to unseen combinations of relationships. This compositional generalization is particularly valuable for knowledge graphs where many possible path patterns exist but training data is sparse.

Neural LP is data-efficient, generalizing from fewer examples than pure embedding methods. Because the model learns explicit rules rather than just memorizing patterns in embeddings, it can apply learned rules to new entities and relationships even with limited training data. This makes Neural LP particularly suitable for domains where labeled data is expensive or difficult to obtain.

### 28.8.3 Query Answering Beyond Link Prediction

Complex queries require reasoning beyond single edges:

**Conjunctive queries:**

Find: Actors who starred in movies directed by Steven Spielberg  
AND released after 2000

Query: (?, starred\_in, ?m) (?m, directed\_by, Spielberg)  
(?m, release\_year, >2000)

**Query2Box:** Represent queries as geometric regions (boxes) in embedding space, providing an elegant framework for complex query answering.

Entities are represented as points in the embedding space, with each entity having a fixed position determined by its learned embedding. This point representation is consistent with standard knowledge graph embedding approaches.

Queries are represented as boxes (hyperrectangles) in the embedding space, where a box is defined by its center and offset vectors. The box represents the set of all entities that satisfy the query, with entities inside the box being valid answers and entities outside the box being invalid.

Intersection of boxes implements conjunction in queries. When a query requires multiple conditions to be satisfied simultaneously (AND logic), the corresponding boxes are intersected geometrically. The resulting box contains only entities that satisfy all conditions, naturally implementing logical conjunction through geometric operations.

Entities inside a box satisfy the query, providing a simple decision rule for query answering. To determine if an entity is a valid answer, the model checks whether the entity’s point embedding falls within the query box. This geometric approach to query answering is both efficient and interpretable, as the box structure explicitly represents the query semantics.

## 28.9 Ontology Alignment and Knowledge Integration

Real-world applications require integrating multiple knowledge graphs with different schemas and vocabularies.

### 28.9.1 Entity Alignment Problem

**Definition 28.10** (Entity Alignment). Given two knowledge graphs  $KG_1$  and  $KG_2$ , identify entity pairs that refer to the same real-world object despite potentially different identifiers and representations.

For example,  $KG_1$  might contain an entity “Barack\_Obama” with entity ID 12345, while  $KG_2$  contains an entity “Obama, Barack” with entity ID 98765. The goal is to recognize that these two entities refer to the same person despite the different naming conventions and identifiers. This alignment enables integrating information from both knowledge graphs and reasoning across their combined knowledge.

**Challenges:** Entity alignment faces several fundamental difficulties that make it a complex problem.

Name variations present a major challenge because the same entity can be referred to in many different ways. “NYC”, “New York City”, and “New York, NY” all refer to the same location, but string matching alone cannot reliably identify these as equivalent. The variations can include abbreviations, different word orders, inclusion or omission of qualifiers, and alternative names. Handling these variations requires semantic understanding beyond simple string comparison.

Different schemas across knowledge graphs mean that equivalent information may be represented using different property names and structures. One knowledge graph might use a “birth\_date” property while another uses “born\_on”, even though they represent the same concept. These schema differences require mapping not just entities but also the properties and relationships used to describe them.

Incomplete information complicates alignment because entities may have different attributes in each knowledge graph. One graph might have extensive biographical information about a person while another has only basic facts. The alignment system must determine whether two entities are the same despite having different amounts and types of information, which requires reasoning about what information is expected versus what is merely missing.

Scale makes entity alignment computationally challenging because comparing all entities across two knowledge graphs requires quadratic comparisons. With billions of entities in each graph, exhaustive pairwise comparison is infeasible. Efficient alignment methods must use blocking, indexing, or embedding-based similarity search to reduce the search space to tractable sizes while still finding correct matches.

### 28.9.2 Embedding-Based Entity Alignment

Learn joint embeddings for entities from both KGs:

1. **Separate embedding:** Train embeddings for each KG independently
2. **Seed alignment:** Use known entity matches (seed set) to learn alignment
3. **Joint optimization:** Minimize distance between known matching entities:

$$\mathcal{L}_{\text{align}} = \sum_{(e_1, e_2) \in \text{seeds}} \|\mathbf{h}_{e_1} - \mathbf{h}_{e_2}\|^2 \quad (28.14)$$

4. **Inference:** For unmatched entities, find nearest neighbor in other KG

**Advanced methods:** Several sophisticated techniques have been developed to improve entity alignment accuracy beyond basic embedding similarity.

GNN-based approaches use graph structure to improve alignment by leveraging the principle that neighbors of aligned entities are likely to align as well. If entity A in  $KG_1$  aligns with entity A' in  $KG_2$ , and both have neighbors B and B' connected by similar relationships, then B and B' are likely to be alignments. Graph neural networks propagate alignment information through the graph structure, using confirmed alignments to discover new ones through neighborhood similarity.

Attribute matching compares entity attributes such as names, descriptions, and other textual properties using text similarity measures. Rather than relying solely on graph structure, this approach uses the content associated with entities. Modern methods employ pre-trained language models like BERT to compute semantic similarity between entity descriptions, capturing synonyms and paraphrases that simple string matching would miss.

Iterative refinement bootstraps from seed alignments by iteratively adding confident matches and retraining the alignment model. The process starts with a small set of known alignments (seeds), uses these to train an initial model, applies the model to find high-confidence new alignments, adds these to the training set, and repeats. This bootstrapping approach gradually expands the set of known alignments while maintaining high precision by only adding confident matches at each iteration.

### 28.9.3 Cross-Lingual Knowledge Graph Alignment

Align KGs in different languages:

**Example:** Cross-lingual knowledge graph alignment addresses the challenge of aligning entities across language barriers.

An English knowledge graph might contain an entity “Paris” representing the city, while a French knowledge graph contains an entity “Paris” (ville entity) representing the same location. The goal is to recognize that these entities refer to the same real-world city despite being described in different languages. This cross-lingual alignment enables building multilingual knowledge bases that integrate information from sources in many languages.

**Approach:** Several techniques enable effective cross-lingual entity alignment.

Multilingual embeddings such as mBERT (multilingual BERT) and XLM-R (Cross-lingual Language Model - RoBERTa) provide language-invariant representations of entity names and descriptions. These models are pre-trained on text in many languages and learn to map semantically similar text to similar embeddings regardless of language. By encoding entity names using these multilingual models, the alignment system can identify matches even when entities are described in different languages.

Cross-lingual links from resources like Wikipedia interlanguage links provide supervision for alignment. Wikipedia articles about the same topic in different languages are explicitly linked, providing a large set of known cross-lingual entity correspondences. These links serve as training data for learning alignment models and as seeds for bootstrapping approaches.

Language-invariant entity representations are learned by training models to produce similar embeddings for entities that refer to the same real-world object regardless of the language used to describe them. The model learns to focus on semantic content rather than surface linguistic features, enabling alignment across language boundaries.

### 28.9.4 Schema Matching

Beyond entities, align relation types and ontologies:

**Example:** Schema matching addresses the problem of aligning relation types and ontologies across knowledge graphs.

$KG_1$  might use a relation “born\_in” to connect people to their birthplaces, while  $KG_2$  uses a relation “birthplace” for the same concept. The goal is to recognize that these relations are semantically equivalent despite different naming conventions. This schema-level alignment is essential for integrating knowledge graphs and enabling queries that span multiple sources.

**Methods:** Several complementary approaches enable effective schema matching.

String similarity measures such as edit distance and token overlap provide a baseline for matching relation names. If two relation names are very similar lexically (e.g., “birthPlace” and “birth\_place”), they are likely to be equivalent. These methods handle minor variations in naming conventions like capitalization, separators, and word order.

Semantic similarity embeds relation names using language models and compares the resulting embeddings. This approach captures synonyms and semantically related terms that string matching would miss. For example, “born\_in” and “birthplace” have different surface forms but similar semantic meanings, which embedding-based similarity can detect.

Instance-based matching leverages the principle that if entities connected by relation  $r_1$  in  $KG_1$  consistently align with entities connected by relation  $r_2$  in  $KG_2$ , then the relations are likely equivalent. This approach uses the actual usage patterns of relations rather than just their names. For example, if people connected by “born\_in” in  $KG_1$  consistently align with people connected by “birthplace” in  $KG_2$ , this provides strong evidence that the relations are equivalent even if their names are completely different.

## 28.10 Knowledge-Aware Neural Networks

Rather than separate text and knowledge graph processing, integrate them.

### 28.10.1 Knowledge-Enhanced Embeddings

Combine word embeddings (learned from text) with entity embeddings (from graph):

1. Text encodes entity using contextual embeddings (BERT)
2. Lookup entity embedding from knowledge graph
3. Combine using gating or concatenation
4. Result: entity representation aware of both text and structured knowledge

### 28.10.2 Graph Neural Networks (GNNs) for Knowledge Graphs

GNNs propagate information through graph structure.

**Message passing:**

1. Each entity sends its embedding to neighbors
2. Neighbors aggregate messages using relation-specific functions
3. Result: updated entity embeddings reflecting neighborhood
4. Repeat for multiple layers

**Application:** Node classification (predict entity type), link prediction, relation classification.

## 28.11 Evaluation Metrics and Quality Assessment

Evaluating knowledge graph models requires careful consideration of metrics, biases, and real-world utility.

### 28.11.1 Filtered vs. Raw Evaluation

**Raw evaluation:** Rank all entities for link prediction, including those already in the training set.

**Problem:** If (Barack Obama, spouse, Michelle Obama) is in training, and we test (Barack Obama, spouse, ?), Michelle Obama should rank first. But if (Barack Obama, spouse, Hillary Clinton) is also in training (incorrectly), the model is penalized for ranking it low.

**Filtered evaluation:** Remove all known true triples (from train, validation, test) except the target triple before ranking.

**Definition 28.11** (Filtered Metrics). For query  $(h, r, ?)$ :

1. Rank all candidate entities by score
2. Remove entities  $t'$  where  $(h, r, t')$  exists in train/val/test (except target)



3. Compute rank of target entity in filtered list
4. Calculate MRR, Hits@k on filtered ranks

**Impact:** Filtered metrics are typically 10–30% higher than raw metrics. Always report which evaluation protocol is used.

### 28.11.2 Evaluation Biases

**Popularity bias:** Models may learn to predict popular entities (high degree nodes) regardless of query. Evaluation should stratify by entity popularity.

**Relation difficulty:** Some relations are easier to predict (1-to-1 like “spouse”) than others (many-to-many like “acted\_in”). Report per-relation performance.

**Test leakage:** If test set contains inverse relations of training triples, evaluation is inflated. Example: Train on (A, parent\_of, B); test on (B, child\_of, A).

### 28.11.3 Human Evaluation

Automated metrics don’t capture semantic correctness:

**Precision@k:** For top-k predictions, what fraction are actually correct (verified by humans)?

**Plausibility:** Even if not in ground truth, is the prediction plausible? (Barack Obama, friend\_of, Joe Biden) may not be in KG but is plausible.

**Diversity:** Do predictions cover diverse entity types, or are they repetitive?

**Practical protocol:**

1. Sample 100–500 test queries
2. For each, show top-5 predictions to human annotators
3. Annotators mark: correct, plausible, incorrect
4. Compute precision, plausibility rate

### 28.11.4 Downstream Task Evaluation

Ultimate test: Does the KG improve downstream applications?

**Question answering:** Does KG-augmented QA system answer more questions correctly?

**Search:** Do users click on KG-enhanced search results more often?

**Recommendations:** Does KG-based recommender improve engagement?

Offline metrics (MRR, Hits@k) are proxies; online A/B tests measure real impact.

## 28.12 Practical Implementation and Tooling

Building production knowledge graph systems requires specialized tools and infrastructure.

### 28.12.1 Knowledge Graph Storage Systems

**RDF Triple Stores:** Several mature systems provide RDF (Resource Description Framework) storage and querying capabilities.

Apache Jena is a Java-based RDF store with comprehensive SPARQL query support, providing a robust foundation for semantic web applications. It offers both in-memory and persistent storage options, making it suitable for development and production use. Jena includes reasoning capabilities that can infer new triples based on ontology rules.

Virtuoso is a high-performance RDF database that scales to billions of triples, designed for enterprise-scale knowledge graph applications. It provides both RDF and relational database capabilities, enabling hybrid workloads. Virtuoso’s query optimizer and indexing strategies make it one of the fastest RDF stores available.



Blazegraph is a GPU-accelerated graph database that leverages parallel processing for improved query performance. It supports both RDF and property graph models, providing flexibility in data modeling. The GPU acceleration is particularly beneficial for complex graph traversals and analytical queries.

**Property Graph Databases:** An alternative to RDF, property graph databases offer a different data model optimized for certain use cases.

Neo4j is the most popular graph database, using the Cypher query language for intuitive graph pattern matching. It provides ACID transactions, high availability clustering, and extensive tooling for graph visualization and analysis. Neo4j's native graph storage and processing engine delivers excellent performance for traversal-heavy workloads.

Amazon Neptune is a fully managed graph database service that supports both RDF and property graph models, providing flexibility in choosing the appropriate data model. As a managed service, Neptune handles infrastructure management, backups, and scaling automatically. It integrates seamlessly with other AWS services for building complete cloud-native applications.

JanusGraph is a distributed graph database built on top of scalable storage backends like Apache Cassandra or HBase. It's designed for massive-scale graphs that don't fit on a single machine, providing horizontal scalability through data partitioning. JanusGraph supports pluggable storage and indexing backends, allowing optimization for specific workload characteristics.

**Trade-offs:** Choosing between RDF stores and property graph databases involves several considerations.

RDF stores are standards-compliant, following W3C specifications for semantic web technologies. They provide excellent semantic web integration, making it easy to consume and publish linked data. RDF stores excel at complex queries involving reasoning and inference, leveraging ontologies to derive new knowledge. However, the RDF model can be more complex to work with than property graphs, and query performance may be slower for simple traversals.

Property graphs offer a simpler data model that's more intuitive for developers familiar with object-oriented programming. They provide better performance for graph traversals, as the native graph storage is optimized for following relationships. Property graphs support a richer data model with properties on both nodes and edges, making it easier to model complex domains. However, they lack the standardization and semantic web integration of RDF stores, and reasoning capabilities are typically more limited.

### 28.12.2 KG Embedding Libraries

**PyKEEN (Python Knowledge Embeddings):**

```
from pykeen.pipeline import pipeline

result = pipeline(
    dataset='FB15k-237',
    model='TransE',
    training_kwargs=dict(num_epochs=100),
    evaluation_kwargs=dict(batch_size=256),
)

# Access trained model
model = result.model
# Predict missing links
predictions = model.predict_tails('Barack_Obama', 'born_in')
```

**DGL-KE (Deep Graph Library - Knowledge Embeddings):**

```
import dglke

# Train TransE on custom dataset
dglke.train(
```

```

    model_name='TransE',
    dataset='my_kg',
    data_path='./data/',
    save_path='./ckpts/',
    max_step=100000,
    batch_size=1024,
    neg_sample_size=256,
    hidden_dim=200,
    gamma=12.0,
    lr=0.1,
)

```

**OpenKE:** C++ backend with Python interface; optimized for large-scale training.

### 28.12.3 Query APIs and SPARQL

**SPARQL:** Standard query language for RDF graphs:

```

PREFIX dbo: <http://dbpedia.org/ontology/>
PREFIX dbr: <http://dbpedia.org/resource/>

SELECT ?movie ?releaseDate
WHERE {
    ?movie dbo:director dbr:Steven_Spielberg .
    ?movie dbo:releaseDate ?releaseDate .
    FILTER (?releaseDate > "2000-01-01"^^xsd:date)
}
ORDER BY DESC(?releaseDate)
LIMIT 10

```

**Cypher (Neo4j):**

```

MATCH (director:Person {name: "Steven Spielberg"})-[:DIRECTED]->(movie:Movie)
WHERE movie.releaseDate > date("2000-01-01")
RETURN movie.title, movie.releaseDate
ORDER BY movie.releaseDate DESC
LIMIT 10

```

### 28.12.4 End-to-End Pipeline Example

**Building a domain-specific KG:**

# 1. Entity extraction from text corpus  
from transformers import pipeline

```

ner = pipeline("ner", model="dslim/bert-base-NER")
entities = ner("Apple Inc. was founded by Steve Jobs in 1976.")

```

# 2. Relation extraction  
from opennre import get\_model

```

rel_model = get_model('wiki80_bert_softmax')
relations = rel_model.infer({
    'text': 'Apple Inc. was founded by Steve Jobs in 1976.',
    'h': {'pos': (0, 10)}, # Apple Inc.
    't': {'pos': (27, 38)} # Steve Jobs
})

```

```

})

# 3. Store in graph database
from neo4j import GraphDatabase

driver = GraphDatabase.driver("bolt://localhost:7687")
with driver.session() as session:
    session.run("""
        MERGE (a:Company {name: 'Apple Inc.'})
        MERGE (p:Person {name: 'Steve Jobs'})
        MERGE (a)-[:FOUNDED_BY]->(p)
    """)

# 4. Train embeddings
from pykeen.pipeline import pipeline

result = pipeline(
    dataset='my_kg',
    model='ComplEx',
    training_kwargs=dict(num_epochs=50),
)

# 5. Query and predict
predictions = result.model.predict_tails('Apple_Inc', 'COMPETITOR')

```

## 28.13 Cross-Chapter Connections

Knowledge graphs integrate with many domains covered in this book:

- **Enterprise NLP (Chapter 25):** NER and relation extraction populate KGs; KG embeddings combine with text embeddings for hybrid semantic search.
- **Recommendations (Chapter 29):** KG embeddings are analogous to collaborative filtering; combining user–item interactions with item KGs improves cold-start performance.
- **Agents (Chapter 34):** KG query APIs serve as tools for structured reasoning; agents decide when to query the KG versus generate from a language model.
- **Healthcare (Chapter 30):** Biomedical KGs (drug–target–disease) enable link prediction for drug repurposing; patient symptom graphs support differential diagnosis.

## 28.14 Scalability and Practical Considerations

Production KGs are enormous: billions of entities, billions of relationships.

### 28.14.1 Embedding Computational Cost

TransE requires scoring candidate triples during training:

$$\text{cost per epoch} = |S| \times |E| \quad (28.15)$$

For Freebase (1.9B entities, 3B relations), this is intractable.

**Solutions:** Several techniques address the computational challenges of training embeddings on massive knowledge graphs.

Negative sampling reduces the computational burden by sampling only a small number of negative examples (typically 100–1000) instead of scoring all possible entities. For each positive triple, the

model generates a few corrupted triples by randomly replacing the head or tail entity. This sampling strategy provides sufficient training signal while reducing computation from  $O(|E|)$  to  $O(k)$  where  $k$  is the number of negative samples.

Batch optimization groups triples together and computes similarities in batches, leveraging vectorized operations and GPU parallelism. By processing many triples simultaneously, the model amortizes the overhead of data loading and achieves much higher throughput than processing triples individually. Modern implementations can process millions of triples per second using batch optimization.

Sparse storage stores only the non-zero parts of embeddings, reducing memory footprint for high-dimensional embeddings. Many embedding dimensions may be near zero for any given entity, and sparse representations exploit this sparsity. This is particularly important for billion-scale knowledge graphs where dense storage of all embeddings would exceed available memory.

Hierarchical models partition entities into clusters and compute embeddings within clusters, reducing the effective search space. By organizing entities hierarchically (e.g., by type or domain), the model can focus computation on relevant subsets. For example, when predicting relationships for a person entity, the model might only consider other person and organization entities rather than all entities in the graph.

### 28.14.2 Incompleteness and Noise

Knowledge graphs face two inherent problems that fundamentally affect how they must be used and maintained.

Incompleteness means that most relationships are unknown rather than explicitly false. The absence of a triple in the knowledge graph doesn't mean the relationship doesn't exist in the real world—it simply means the relationship hasn't been observed or recorded. Freebase, one of the largest knowledge graphs, is estimated to be less than 5% complete, meaning that over 95% of true facts about the world are missing. This massive incompleteness is inevitable because the number of possible facts vastly exceeds what can be practically collected and verified.

Noise arises because extracted facts may be incorrect due to extraction errors, outdated information, or conflicting sources. Automated extraction from text inevitably produces some errors, and even manually curated knowledge graphs contain mistakes. Information becomes outdated as the world changes: a person's job title, a company's CEO, or a country's population are all facts that change over time but may not be updated promptly in the knowledge graph.

Deep learning must handle both challenges through specialized techniques. Models must learn robust representations despite missing training data, treating the absence of a triple as unknown rather than negative. Noise-aware loss functions use soft labels and confidence scores rather than treating all training examples as equally reliable. Continuous retraining as new information arrives helps keep the knowledge graph current, with models that can incrementally update their representations without retraining from scratch.

## 28.15 Applications: From Search to Drug Discovery

### 28.15.1 Semantic Search and Question Answering

Google's Knowledge Graph improves search results:

Query: "Where was Albert Einstein born?"

Traditional: Keyword search returns pages mentioning "Albert Einstein" and "born."

With KG:

1. Identify entity: "Albert Einstein" (physicist entity)
2. Follow relation: `born_in` → "Ulm, Germany"
3. Display: Direct answer in result panel

Better user experience; faster answer discovery.

### 28.15.2 Biomedical Discovery: Drug-Target Interaction Prediction

In drug discovery, predicting drug-target interactions is expensive and time-consuming.

**Knowledge graph:** Entities = proteins, diseases, drugs. Relationships = acts\_on, treats, causes.

**Link prediction:** For a new drug, predict which proteins it targets.

**Validation:** Lab experiments confirm predictions.

Real example: Using link prediction on biomedical KG, researchers identified new targets for existing drugs, enabling drug repurposing.

### 28.15.3 Cybersecurity: Attack Pattern Detection

A knowledge graph for cybersecurity models the complex relationships between threats, vulnerabilities, and assets.

Entities in the cybersecurity knowledge graph include IP addresses representing network endpoints, domains identifying web properties, malware families categorizing malicious software, and attack techniques describing methods used by adversaries. Each entity type captures a different aspect of the threat landscape, and the relationships between them reveal attack patterns.

Relationships such as communicates\_with connect IP addresses that exchange network traffic, infected\_by links systems to the malware affecting them, and exploits connects malware to the vulnerabilities it targets. These relationships form patterns that characterize different types of attacks and enable detection of ongoing threats.

Link prediction identifies likely attack patterns by reasoning over the graph structure. If IP address A communicated with server C, and malware family B typically attacks server C, the system can predict that A is likely infected with B even before direct evidence of infection is observed. This predictive capability enables proactive threat detection and response.

## 28.16 Case Study: Enterprise Knowledge Graph for Customer Intelligence

A financial services company maintains customer data scattered across systems. A knowledge graph unifies and enables new insights.

### 28.16.1 Data Sources and Schema

The enterprise KG integrates five source systems: customer records (demographics, contact), account data (types, balances, transactions), relationship data (family, employer, associate links), transaction logs, and external data (credit scores, public records). The schema uses four entity types—Person, Organization, Account, Transaction—connected by relationships including owns\_account, employed\_by, related\_to, transacted\_with, and has\_credit\_score.

### 28.16.2 Applications

**Fraud detection:** If customer A suddenly sends money to account in country where they've never been, and that account is related to known fraud cases, flag as suspicious.

**Customer segmentation:** Customers with similar network structures (family members, employers, transaction patterns) are grouped; targeted offers designed for groups.

**Risk assessment:** Credit decision uses not just customer features but related customers' credit histories.

### 28.16.3 Results

The knowledge graph implementation delivered measurable improvements across multiple business metrics.

Fraud detection improved from 85% to 92% precision, meaning fewer false alarms and more efficient use of investigation resources. The graph-based approach identified suspicious patterns that rule-based

systems missed, such as complex networks of related accounts involved in coordinated fraud schemes. The reduction in false positives saved significant investigation time while the improved detection rate prevented more fraudulent transactions.

Customer segmentation identified high-value customer clusters with 3x average transaction volume compared to the general customer base. By analyzing the network structure of customer relationships and transaction patterns, the knowledge graph revealed groups of customers with similar characteristics and behaviors. These segments enabled targeted marketing and service strategies tailored to each group's needs and preferences.

Cross-selling improved with an 8% increase in secondary products purchased. The knowledge graph enabled recommendations based on what similar customers (defined by network position and attributes) had purchased, leading to more relevant product suggestions. Understanding customer relationships also enabled household-level marketing where products could be recommended based on family member needs.

Entity resolution matched 98% of duplicate customer records, significantly improving data quality. The knowledge graph's ability to reason about entity similarity using multiple signals (name, address, relationships, transaction patterns) enabled accurate matching even when records had inconsistencies or errors. This deduplication provided a unified view of each customer across all systems.

## 28.17 Exercises

**Exercise 28.1.** Extract entities and relationships from the following text using NER and relation extraction. “Apple Inc. was founded by Steve Jobs, Ronald Wayne, and Steve Wozniak in Los Altos. The company released the Macintosh in 1984.”

**Exercise 28.2.** Train a TransE embedding model on a small knowledge graph (100 entities, 200 relations). Evaluate link prediction performance on held-out test set using MRR and Hits@10.

**Exercise 28.3.** Design a knowledge graph schema for a movie recommendation system. What entities and relationships would be necessary? How would link prediction help recommendations?

**Exercise 28.4.** Design a temporal knowledge graph for tracking corporate events (mergers, acquisitions, executive changes). What temporal reasoning capabilities would be most valuable? How would you handle conflicting information from different sources?

**Exercise 28.5.** Implement entity alignment between two knowledge graphs using embedding-based methods. Evaluate precision and recall at different similarity thresholds. How does performance vary with seed set size?

**Exercise 28.6.** Build an R-GCN model for node classification on a multi-relational graph. Com-

pare performance against TransE embeddings. When does the GNN approach outperform embedding-only methods?

## 28.18 Solutions

Full solutions for all exercises are available at <https://deeplearning.hofkensvermeulen.be>.

## Chapter 29

# Recommendation Systems and Personalization

### Chapter Overview

Recommendation systems are the economic engines of the modern internet. They drive 80% of content consumed on Netflix, 70% of watch time on YouTube, and 35% of purchases on Amazon. For these platforms, recommendation quality directly translates to revenue: a 1% improvement in recommendation accuracy can generate tens to hundreds of millions of dollars in additional revenue annually. Poor recommendations, conversely, lead to user churn, reduced engagement, and lost revenue opportunities.

The business challenge is substantial. Platforms must serve personalized recommendations to billions of users in real-time (under 200ms latency), processing trillions of user-item interactions to learn preferences, while balancing competing objectives: immediate engagement (clicks, watch time) versus long-term retention, personalization versus diversity, and business goals (revenue, growth) versus societal concerns (fairness, filter bubbles).

This chapter examines how transformers and sequence models have revolutionized recommendation systems by capturing temporal dynamics and complex user-item interactions that traditional methods miss. A user who watches action movies followed by documentaries has different preferences than one who watches in reverse order—sequence matters. Transformer-based recommenders capture these patterns, improving recommendation quality by 10-30% over traditional collaborative filtering.

However, these improvements come with challenges. Training requires processing billions of user interactions. Serving demands sub-second latency at massive scale. Model drift is severe—user preferences change daily, new items arrive constantly, and seasonal patterns shift. Fairness concerns are paramount—biased recommendations can amplify inequality and create filter bubbles that harm users and society. This chapter provides the technical foundation and business context to build recommendation systems that balance these competing demands effectively.

### Learning Objectives

1. Understand sequence-based recommendation architectures using transformers
2. Design and optimize ranking systems for accuracy and diversity
3. Implement multi-task learning for recommendations (CTR, conversion, long-term engagement)
4. Build real-time serving systems with latency constraints
5. Address fairness and filter-bubble concerns in personalization
6. Conduct online experiments (A/B tests) to validate recommendation improvements
7. Optimize for business metrics beyond accuracy



## 29.1 Sequence-Aware Recommenders

Traditional recommendation systems treat user preferences as static. Matrix factorization, the workhorse of early recommender systems, decomposes a user-item interaction matrix  $M \in \mathbb{R}^{U \times I}$  into low-rank factors: user  $u$  is represented by a latent vector  $\mathbf{p}_u \in \mathbb{R}^k$ , and item  $i$  by  $\mathbf{q}_i \in \mathbb{R}^k$ . The predicted rating is simply  $\hat{M}_{u,i} = \mathbf{p}_u^T \mathbf{q}_i$ . This approach powered early Netflix and Amazon recommendations and remains computationally efficient.

However, this static view ignores a fundamental aspect of human behavior: preferences evolve over time and depend on context. A user watching action movies in January followed by documentaries in February has different current preferences than one who watched in reverse order. A user browsing products on Monday morning (work-related) has different intent than the same user browsing Saturday evening (leisure). Matrix factorization treats these scenarios identically, missing critical temporal and contextual signals.

The business impact of this limitation is substantial. Static recommendations become stale quickly, especially for platforms with frequent user activity. A video platform user who watches 10 videos daily has preferences that shift hour-by-hour based on mood, time of day, and recent viewing. Static recommendations might suggest content from last week's interests, reducing engagement. One major streaming platform found that incorporating sequence information improved watch time by 12% and reduced churn by 8%—translating to hundreds of millions in annual revenue.

Sequence-aware models address this by treating recommendations as a language modeling problem: given a user's historical sequence of interactions, predict the next item. This framing is powerful because it leverages decades of NLP research on sequence modeling. Just as language models predict the next word given previous words, recommendation models predict the next item given previous items. The key insight is that user behavior follows patterns—watching a superhero movie increases the probability of watching another superhero movie, just as the word "New" increases the probability of "York."

**Definition 29.1** (Sequence-Based Recommendations). Given a user's interaction sequence  $(i_1, i_2, \dots, i_t)$ , a sequence model predicts the probability distribution over next items:

$$P(i_{t+1} \mid i_1, \dots, i_t) = \text{softmax}(W \text{encoder}(i_1, \dots, i_t) + b) \quad (29.1)$$

where **encoder** is a transformer, RNN, or other sequential model that processes the interaction history. The vocabulary is the set of all items  $|I|$  (potentially millions), and the logits correspond to scores for each item. Items with higher scores are more likely to be the next interaction.

This formulation enables the model to capture rich temporal patterns. If a user watches three action movies in a row, the model learns that action movies have high probability for the next interaction. If a user alternates between genres, the model learns that pattern too. The model can even capture long-range dependencies—a user who watched a TV show's first episode two weeks ago is likely interested in episode two, even if they watched other content in between.

Historically, RNNs (LSTM, GRU) were the standard for sequence modeling in recommendations. However, transformers with self-attention provide several critical advantages that translate directly to business value:

**Parallelization during training.** RNNs process sequences sequentially, making training slow on long user histories. Transformers process entire sequences in parallel, reducing training time by 5-10x. For platforms retraining models daily on billions of interactions, this means the difference between 8-hour and 2-hour training jobs—enabling faster iteration and more frequent model updates.

**Long-range dependency modeling.** RNNs struggle with dependencies spanning hundreds of steps due to vanishing gradients. Transformers' attention mechanism directly connects any two positions in the sequence, capturing long-range patterns. For users with thousands of historical interactions, this means better recommendations based on preferences from weeks or months ago, not just recent activity.

**Interpretability through attention weights.** Attention weights show which past items influence the current recommendation. This interpretability helps debug model behavior, explain recommenda-

tions to users ("because you watched X"), and identify biases. For regulated industries or platforms facing scrutiny over algorithmic recommendations, this transparency is valuable.

**Multi-head attention for diverse patterns.** Different attention heads can learn different temporal patterns—one head might focus on recent items (short-term preferences), another on items from the same genre (topical consistency), and another on seasonal patterns (holiday content). This diversity improves recommendation quality by capturing multiple aspects of user behavior simultaneously.

### 29.1.1 SASRec: Self-Attentive Sequential Recommendation

SASRec is a transformer-based recommender that achieves state-of-the-art performance on benchmark datasets. The architecture:

1. **Embedding:** Each item is embedded as  $\mathbf{e}_i \in \mathbb{R}^d$ . Optionally, add positional encodings to capture temporal positions.
2. **Transformer layers:** Stack  $L$  transformer encoder layers, each with multi-head self-attention and feed-forward networks.
3. **Causal masking:** Use causal attention mask to prevent the model from attending to future items (maintaining prediction task structure).
4. **Output:** The representation at position  $t$  predicts the next item:

$$\text{logits}_i = \mathbf{h}_t^T \mathbf{e}_i + b_i \quad (29.2)$$

where  $\mathbf{h}_t$  is the output of the transformer at step  $t$ .

5. **Loss:** Cross-entropy loss on the correct next item, computed at each position.

SASRec significantly outperforms RNN-based recommenders and matrix factorization on benchmark datasets (MovieLens, Amazon reviews, e-commerce), especially for longer user histories.

### 29.1.2 Cold-Start Recommendations with Transformer-Capsule Networks (2024-2025)

Cold-start recommendation—providing quality recommendations for new users or new items with limited interaction history—has been a persistent challenge in recommendation systems. Traditional approaches struggle because collaborative filtering requires sufficient interaction data to learn meaningful embeddings. Recent advances in 2024-2025 using transformer-capsule networks have achieved breakthrough performance on cold-start scenarios.

**Transformer-Capsule Graph (TCG-CS):** The TCG-CS architecture combines transformers' sequence modeling capabilities with capsule networks' ability to capture hierarchical relationships and graph neural networks' structural reasoning. This hybrid approach achieves 94.2% accuracy on cold-start recommendation tasks, significantly outperforming previous methods.

**Key innovations:** Several breakthrough techniques enable TCG-CS to achieve superior cold-start performance.

Capsule-based user representation replaces single embedding vectors with capsules, which are groups of neurons that encode different aspects of preferences such as genre preferences, temporal patterns, and quality sensitivity. This structured representation enables learning from limited data by capturing the multifaceted nature of user preferences. Unlike flat embeddings that compress all preference information into a single vector, capsules maintain separate representations for different preference dimensions, making it easier to generalize from sparse interactions.

Graph-based item relationships model items as a graph where edges represent similarities such as same genre, same director, or co-purchased patterns. Graph neural networks propagate information from items with rich interaction history to cold-start items, enabling better initial embeddings for new items. This structural approach leverages the principle that similar items should have similar

embeddings, allowing new items to benefit from the interaction history of related items even before receiving their own interactions.

Meta-learning for rapid adaptation uses techniques like Model-Agnostic Meta-Learning (MAML) to train models that can quickly adapt to new users with just 3-5 interactions. The model learns to learn, discovering which features and patterns are most informative for rapid personalization. This meta-learning approach is fundamentally different from standard training: instead of learning fixed parameters, the model learns initialization parameters that can be quickly fine-tuned to individual users with minimal data.

Content-collaborative hybrid approaches combine content features such as item metadata, descriptions, and images with collaborative signals from user-item interactions. For cold-start items, the system relies more heavily on content features to make initial recommendations. As interactions accumulate, the system gradually shifts weight to collaborative signals, which typically provide stronger personalization. This adaptive weighting ensures that recommendations remain relevant throughout an item’s lifecycle, from launch through maturity.

**Business Impact:** Cold-start is particularly critical for platforms with high user or item churn. E-commerce platforms add thousands of new products daily. Streaming platforms onboard millions of new users monthly. Poor cold-start recommendations cause early churn—users who don’t find relevant content in their first session are 3-5x more likely to abandon the platform.

Platforms implementing TCG-CS report substantial improvements across multiple metrics that directly impact business outcomes.

New user retention improves by 25-35% when measured at day 7, meaning significantly more users continue using the platform after their first week. This improvement is critical because early retention is highly predictive of long-term user value. Users who remain engaged through the first week are 5-10x more likely to become long-term active users.

New item discovery improves by 40-50%, measured as the fraction of new items that receive engagement within their first week. This metric is crucial for platforms with high content velocity, as it determines how quickly new content can find its audience. Better cold-start recommendations accelerate the discovery process, benefiting both users (who find relevant new content faster) and creators (whose content gains traction more quickly).

Time-to-personalization reduces by 15-20%, meaning the system delivers personalized recommendations sooner in a user’s lifecycle. Traditional systems might require weeks of interaction data before recommendations become truly personalized. TCG-CS achieves meaningful personalization within hours or days, dramatically improving the new user experience and reducing early churn.

Example: E-commerce platform with 1M new users monthly and 30% day-7 retention. Improving retention by 5 percentage points (to 35%) retains 50,000 additional users. At \$50 customer lifetime value, this generates \$2.5M monthly = \$30M annually. Development cost: \$500K. ROI: 60x.

**Implementation Considerations:** TCG-CS is computationally more expensive than standard transformers—training requires 2-3x compute due to capsule routing and graph convolutions. However, the improved cold-start performance often justifies the cost for platforms where cold-start is a critical bottleneck. Open-source implementations are emerging in PyTorch and TensorFlow as of 2025.

## 29.2 Feature Engineering and Behavior Language

Recommendations depend on more than just item history. User demographics, item metadata, temporal context, and behavioral signals all influence next-item preferences.

### 29.2.1 DSL for Behavior Data

Recommendation systems process event streams: each user interaction is an event with timestamp, user ID, item ID, and contextual features. The “language” of recommendation is this event schema:

**Definition 29.2** (Recommendation Event Schema). Each event in a user session is:

$$\text{Event} = \{\text{user\_id}, \text{item\_id}, \text{timestamp}, \text{event\_type}, \text{context}\} \quad (29.3)$$

where several components define the structure of each interaction event. The `event_type` field categorizes the interaction, taking values from the set {view, click, purchase, add-to-cart, share, rate}, with each type carrying different signals about user intent and engagement level. The `context` field captures situational information including device type, geographic location, search query if applicable, and other environmental factors that influence user behavior and preferences.

The sequence of events becomes the user’s “behavior language.” A user’s history might be:

```
[{item: 42, type: view, time: 10:00},
 {item: 42, type: click, time: 10:05},
 {item: 87, type: view, time: 10:15},
 {item: 87, type: purchase, time: 10:25}]
```

The model learns that viewing+clicking an item increases the likelihood of purchase; views alone do not. Different event types carry different signals.

### 29.2.2 Dense and Sparse Features

Feature engineering bridges item history with demographic and contextual signals. Dense features provide continuous numerical representations that capture various aspects of users, items, and context.

User embeddings are learned during pre-training on user similarity tasks, capturing latent user characteristics and preferences in a continuous vector space. These embeddings encode patterns like which types of users tend to have similar preferences, enabling the model to generalize across similar users.

Item embeddings derive from product taxonomy or content embeddings, representing items in a semantic space where similar items are positioned nearby. These embeddings can be learned from item metadata, collaborative filtering patterns, or content features like text descriptions and images.

Temporal signals capture time-dependent patterns including time-of-day effects (users browse differently in morning vs. evening), day-of-week patterns (weekend vs. weekday behavior), and seasonality (holiday shopping, summer content preferences). These temporal features help the model adapt recommendations to the current context.

Historical aggregates summarize past behavior through statistics like the average rating a user gives (indicating rating strictness), the popularity of items the user likes (indicating mainstream vs. niche preferences), and engagement patterns (binge-watching vs. casual browsing). These aggregates provide stable signals about long-term user characteristics.

Sparse categorical features represent discrete attributes that take values from large vocabularies, requiring special handling through embedding layers.

User demographics include categorical attributes like age range, geographic location, and language preference. These features help the model understand how different user segments have different preferences and behaviors.

Item metadata captures categorical properties including category, subcategory, brand, and author. These attributes provide content-based signals that complement collaborative filtering, especially for cold-start items with limited interaction history.

Context features describe the interaction environment including device type (mobile, tablet, desktop), platform (app vs. web), and time zone. These contextual factors significantly influence user behavior and should be incorporated into recommendations.

Embedding these sparse features increases model capacity substantially. A categorical feature with 10,000 categories, such as user’s home country, is embedded into a 16–32 dimensional vector. While this increases model parameters significantly, it enables the model to learn complex feature interactions and capture nuanced patterns that would be impossible with one-hot encoding.

### 29.2.3 Multi-Task Learning for Recommendations

Real recommendation systems optimize multiple objectives simultaneously, each capturing different aspects of user engagement and business value.

CTR (click-through rate) predicts whether the user will click on a recommended item, serving as a primary signal of immediate interest. High CTR indicates that recommendations are relevant and appealing enough to capture user attention. This metric is easy to measure and provides abundant training signal since every impression generates a click or no-click label.

Conversion predicts whether the user will complete a desired action such as making a purchase, subscribing, or completing a form. Conversion is a stronger signal than clicks because it represents actual business value, but it's also sparser—only a small fraction of clicks convert. Optimizing for conversion ensures recommendations drive revenue, not just engagement.

Engagement time predicts how long the user will engage with the recommended item, measured as video watch time, article reading time, or time spent on a product page. This metric captures content quality and user satisfaction better than binary click signals. A user who watches an entire video is more satisfied than one who clicks but immediately leaves.

Long-term value predicts whether the recommendation will lead to sustained engagement and user retention over weeks or months. This forward-looking metric is crucial because optimizing only for immediate engagement can harm long-term retention through clickbait, filter bubbles, or content that satisfies curiosity but doesn't build lasting interest. Long-term value is difficult to measure (requires long observation windows) but essential for platform health.

Multi-task learning trains a shared backbone with task-specific heads. The losses are combined with weights:

$$\text{Loss}_{\text{total}} = \lambda_{\text{ctr}} \text{Loss}_{\text{ctr}} + \lambda_{\text{conv}} \text{Loss}_{\text{conversion}} + \lambda_{\text{engagement}} \text{Loss}_{\text{engagement}} \quad (29.4)$$

Task weights  $\lambda$  are often tuned based on business priorities. A subscription platform may weight long-term engagement more heavily than short-term CTR.

## 29.3 Real-Time Serving and Ranking

Training a model is just the first step. Serving recommendations to billions of users in real-time is a massive engineering challenge.

### 29.3.1 Two-Stage Architecture

Most recommendation systems use a two-stage pipeline:

1. **Candidate generation (retrieval):** From millions of items, retrieve a small set of candidates (100–1,000) that are relevant to the user. This stage is fast and approximate; exact ranking over all items is infeasible.
2. **Ranking:** Score the candidate set with a more complex model. Return the top-k items to the user.

### 29.3.2 Candidate Generation Strategies

### 29.3.3 Candidate Generation Strategies

Candidate generation uses simple, fast methods to narrow the search space from millions of items to a manageable set for detailed ranking.

Embedding-based retrieval embeds both the user and all items into a shared vector space, then retrieves items nearest to the user embedding using efficient similarity search. This approach is fast, typically taking only milliseconds for MIPS (maximum inner product search) on GPU-accelerated indices like Faiss. The quality depends on the embedding space—well-trained embeddings that capture semantic similarity produce relevant candidates.

Collaborative filtering identifies similar users based on their interaction patterns, then recommends items that those similar users liked. User similarity can be computed offline using techniques like cosine similarity on interaction vectors or learned embeddings. At serving time, the system retrieves candidates by finding similar users and aggregating their preferences. This approach is effective because users with similar past behavior often have similar future preferences.

Content-based filtering retrieves items similar to those the user has previously interacted with, using item features like category, tags, or content embeddings. This approach works well for users with consistent preferences and provides good coverage for new items with rich metadata. However, it can create filter bubbles by only recommending items similar to past interactions.

Hybrid approaches combine multiple candidate sources to improve both relevance and diversity. A typical hybrid strategy might retrieve top-k trending items (ensuring popular content is considered), personalized candidates from collaborative filtering (ensuring personalization), and content-based candidates (ensuring coverage of user interests). The diversity of sources improves coverage and serendipity, exposing users to a broader range of relevant content than any single method would provide.

#### 29.3.4 Ranking Model and Latency Budget

The ranking model scores candidates. With a 200 ms latency budget for the entire recommendation request and 50 ms allocated to candidate generation, the ranker has 150 ms. This is enough for a small neural network (2–3 layers) but not a 24-layer transformer.

Practical rankers are often gradient-boosted trees (e.g., XGBoost, LightGBM) or shallow neural networks. They consume hundreds of features (user features, item features, candidate-specific features like co-occurrence with items the user has rated) and output a score. The top-k candidates by score are returned.

#### 29.3.5 Real-Time Updates and Freshness

#### 29.3.6 Real-Time Updates and Freshness

Recommendation scores must be updated as new items arrive and user preferences change. Naive approaches that recompute scores for all users at each step are prohibitively expensive. Practical approaches balance freshness with computational feasibility.

Batch serving precomputes recommendations for all users nightly, storing results in a cache for fast retrieval. The system serves recommendations from the cache with occasional refreshes for highly active users who might have significantly changed preferences since the last batch update. This approach minimizes serving latency and computational cost but sacrifices freshness—recommendations can be up to 24 hours stale.

Online serving with feature caching computes expensive features like item embeddings and candidate sets offline, then fetches these precomputed features at request time to score with a fast model. This hybrid approach maintains reasonable freshness for features that change slowly (item embeddings) while enabling real-time scoring based on current user state. The fast scoring model can incorporate recent user actions without recomputing all features.

Streaming updates track user behavior in real-time using stream processing frameworks, updating embeddings and candidate sets incrementally as new interactions arrive. This approach provides the freshest recommendations but requires sophisticated infrastructure to handle high-throughput event streams and maintain consistency. Streaming updates are most valuable for highly active users whose preferences change rapidly within a session.

Freshness vs. latency is a trade-off. Highly personalized real-time recommendations are better but slower. Pre-computed recommendations are faster but stale.

### 29.4 Fairness, Diversity, and Filter Bubbles

Recommendation systems can amplify biases and trap users in filter bubbles—showing only content that aligns with past preferences, limiting exposure to diverse views.

### 29.4.1 Filter Bubble Problem

If a user watches many political videos from one perspective, a system optimizing for watch time may recommend only that perspective, reinforcing views and reducing exposure to alternative viewpoints. While maximizing engagement, this harms user growth and societal polarization.

Solutions include several complementary approaches to increase recommendation diversity and reduce filter bubble effects.

Diversity metrics measure the variety of recommendations using measures like entropy of recommended categories. By including diversity as an explicit term in the ranking objective, the system can balance relevance with variety. For example, the ranking score might be a weighted combination of predicted engagement and category diversity, ensuring that highly relevant but homogeneous recommendations don't dominate.

Exploration allocates a portion of recommendations (typically 10%) to items outside the user's typical preferences, enabling discovery of new interests. This exploration can be random or guided by uncertainty estimates—recommending items where the model is uncertain about user preferences. Exploration serves dual purposes: it helps users discover new content they might enjoy, and it generates training data for underexplored items and user segments.

Fairness constraints ensure that underrepresented creators and items receive exposure proportional to their quality, not just their historical popularity. Dynamic allocation algorithms balance personalization with fairness by setting minimum exposure thresholds for different creator demographics or content categories. This prevents winner-take-all dynamics where popular content dominates recommendations at the expense of quality niche content.

User control empowers users to adjust recommendation diversity or opt for curated feeds rather than purely algorithmic recommendations. Providing transparency about why items are recommended ("because you watched X") and controls to adjust recommendation behavior ("show me more diverse content") increases user trust and satisfaction. Users who feel in control of their experience are more likely to remain engaged long-term.

### 29.4.2 Handling Demographic Bias

### 29.4.3 Handling Demographic Bias

Models trained on interaction data inherit biases present in historical patterns. If women historically receive fewer views for technical content due to societal biases, the model may learn to downrank women creators in technical categories, perpetuating and amplifying the bias. Mitigation strategies address these biases at multiple stages of the recommendation pipeline.

Balanced datasets oversample interactions from underrepresented groups during training, ensuring the model sees sufficient examples of diverse creator-user interactions. For example, if women creators represent 20% of technical content but receive only 10% of views, oversampling their interactions to 20% of training data helps the model learn unbiased quality signals. This rebalancing corrects for historical underexposure without requiring the model to explicitly reason about fairness.

Fairness-aware loss functions add a penalty term that discourages disparate performance across demographic groups. The loss function might include a term measuring the difference in average recommendation scores between demographic groups, encouraging the model to provide similar quality recommendations regardless of creator demographics. This approach directly optimizes for fairness as a training objective.

Allocation fairness ensures that a minimum fraction of recommendations go to creators from all demographics, regardless of predicted engagement. Post-processing algorithms can enforce these constraints by adjusting recommendation rankings to meet fairness targets while minimizing impact on overall engagement. For example, if the top-10 recommendations contain no creators from underrepresented groups, the system might replace the lowest-ranked item with the highest-ranked item from an underrepresented group.

#### 29.4.4 A/B Testing for Recommendation Changes

Before deploying recommendation model improvements, validate with A/B tests that randomly split users into control and treatment groups.

The control group continues using the existing recommendation algorithm, providing a baseline for comparison. This group represents the status quo performance and helps account for external factors like seasonality or platform-wide changes that affect all users.

The treatment group receives recommendations from the new model, enabling direct measurement of the model's impact. The random assignment ensures that differences between groups are attributable to the model change rather than pre-existing user differences.

Measure metrics over 2–4 weeks to account for short-term novelty effects and capture longer-term impacts on user behavior.

Engagement metrics including watch time, clicks, and session length measure immediate user response to recommendations. These metrics are sensitive and provide quick feedback on whether the new model improves user experience. However, they can be gamed by clickbait or sensational content that attracts clicks but doesn't satisfy users.

Retention metrics measure the return rate, calculating the fraction of users who return the next day or week. Retention is a stronger signal of recommendation quality than engagement because it reflects sustained satisfaction. Users who receive consistently good recommendations are more likely to return, while poor recommendations drive churn.

Diversity metrics measure the entropy of categories recommended, ensuring that improvements in engagement don't come at the cost of reduced variety. A model that only recommends popular mainstream content might achieve high engagement but create filter bubbles and reduce long-term user satisfaction.

Fairness metrics track recommendation volume for different creator demographics, ensuring that model improvements don't disproportionately benefit or harm specific groups. Measuring fairness explicitly prevents unintended bias amplification and ensures the platform serves all creators equitably.

If the treatment significantly improves key metrics without degrading others, roll out to all users. This empirical validation is critical; models that perform well on offline metrics may hurt business KPIs in practice.

### 29.5 Case Study: Video Recommendation for a Streaming Platform

A video streaming platform with 100 million users and 10 million videos seeks to improve watch time and retention through better recommendations.

#### 29.5.1 System Architecture

**Candidate Generation:** The first stage rapidly narrows millions of videos to a manageable candidate set.

User embedding is pretrained using a siamese network on user-user similarity, where users who watch similar videos receive similar embeddings. This embedding captures latent user preferences and enables fast similarity-based retrieval.

Item embedding combines video embeddings from a collaborative filtering model (capturing which videos are watched together) with content embeddings from video metadata (title, description, tags, thumbnails). This hybrid embedding represents both collaborative patterns and content semantics.

Retrieval uses MIPS (maximum inner product search) with the Faiss library to find the top-500 candidates most similar to the user embedding in just 20 milliseconds. This fast approximate search makes real-time candidate generation feasible at scale.

**Ranking:** The second stage scores candidates with a more sophisticated model to produce the final top-10 recommendations.

The model uses XGBoost, a gradient-boosted decision tree algorithm, with 500 features capturing user characteristics, item properties, and user-item interactions. XGBoost provides excellent performance with reasonable latency, making it suitable for real-time serving.



Features include user watch time patterns, historical CTR for similar content, video popularity metrics, recency (how recently uploaded), user-item co-occurrence (how often users like this user watch this video), and genre match between user preferences and video category. These diverse features enable the model to capture multiple signals of relevance.

Latency is constrained to 80 milliseconds to score all 500 candidates and rank the top-10, fitting within the overall 200ms latency budget for the recommendation request. This tight latency constraint requires careful model optimization and efficient feature computation.

**Post-processing:** The final stage applies business rules and fairness constraints to the ranked list.

A diversity filter ensures variety by checking if the top-10 contains too many videos from the same genre (e.g., 5 action movies). If so, the system reranks to ensure a maximum of 3 videos per genre, promoting exploration of different content types.

A freshness boost increases the score of videos uploaded less than 1 week ago, ensuring that new content receives exposure even if it hasn't accumulated many interactions yet. This helps new creators gain traction and keeps the platform feeling current.

Creator fairness constraints ensure the top-10 includes creators from different regions and demographics, preventing the recommendations from being dominated by a small set of popular creators. This promotes platform diversity and gives all creators fair opportunity for exposure.

### 29.5.2 Training and Offline Evaluation

**Data:** 100 billion historical events (views, clicks, shares) over 3 months

**Metrics:** The system is evaluated using standard recommendation metrics that measure both coverage and ranking quality.

Recall@10 measures what fraction of videos the user actually watched next appear in the top-10 recommendations. This metric captures whether the system successfully identifies relevant content, with a target of at least 8%. Higher recall means users are more likely to find content they want in the recommendations.

NDCG@10 (Normalized Discounted Cumulative Gain) measures ranking quality by assigning higher value to relevant items that appear earlier in the list. Videos that users clicked or watched receive higher scores, and the metric penalizes relevant items that appear lower in the ranking. The target is at least 0.45, indicating that relevant content consistently appears near the top of recommendations.

**Results:** Progressive model improvements demonstrate clear gains in recommendation quality.

The collaborative filtering baseline achieves NDCG@10 of 0.38, providing a strong foundation but missing temporal patterns in user behavior. This traditional approach serves as the performance floor that newer methods must exceed.

The sequence model (SASRec) improves to NDCG@10 of 0.43, a 13% improvement over the baseline. By modeling user interaction sequences with transformers, the system captures temporal dynamics and session-level patterns that collaborative filtering misses.

SASRec with multi-task learning reaches NDCG@10 of 0.46, adding another 7% improvement. By jointly optimizing for multiple objectives (CTR, watch time, retention), the model learns richer representations that better predict user satisfaction across different dimensions.

### 29.5.3 Online A/B Test

Deploy the improved recommender to 10% of users.

**Results over 4 weeks:** The online test validates that offline improvements translate to real business impact.

Watch time increases by 4.2%, a statistically significant improvement indicating that users engage more deeply with the improved recommendations. This translates to millions of additional hours of content consumption, directly impacting platform value and advertising revenue.

CTR on recommendations improves by 3.8%, showing that users find the recommendations more appealing and relevant. Higher CTR indicates better matching between recommended content and user interests.

Session length increases by 2.1%, meaning users explore more content per visit. This suggests that good recommendations create positive momentum, encouraging users to continue browsing and watching rather than leaving the platform.

Retention (30-day) improves by 1.5%, with more users returning to the platform over the following month. This long-term metric is crucial because it indicates sustained satisfaction rather than just short-term engagement spikes. Improved retention has compounding effects on platform growth and user lifetime value.

Diversity increases by 8%, measured as entropy of recommended categories. Users explore new genres and content types rather than staying in narrow filter bubbles. This diversity benefits both users (who discover new interests) and creators (who reach broader audiences).

Creator fairness improves with a 12% increase in watch share for underrepresented creators, rising from 5% to 5.6% of total watch time. While seemingly small in absolute terms, this represents thousands of additional creators receiving meaningful exposure and represents progress toward equitable content distribution.

No negative impact on fairness or diversity metrics. The model improved both engagement and societal goals. Deployment proceeds to all users, expected to recover millions of hours of additional user engagement annually.

## 29.6 Model Maintenance and Drift in Recommendation Systems

Recommendation systems face some of the most severe drift challenges of any machine learning application. User preferences evolve constantly—daily, weekly, and seasonally. New items arrive continuously, creating cold-start problems. Content trends shift rapidly, especially on social platforms. External events (holidays, news, cultural moments) dramatically change consumption patterns. A recommendation model trained on last month's data can become obsolete within weeks, causing measurable degradation in engagement and revenue.

The business stakes are enormous. A 1% drop in recommendation quality can cost large platforms millions of dollars monthly in lost engagement and advertising revenue. One major video platform observed a 5% decline in watch time over three months due to undetected model drift, costing an estimated \$30 million in revenue before the issue was identified and corrected. Effective drift management is not optional—it's essential for maintaining competitive advantage and business performance.

### 29.6.1 Domain-Specific Drift Patterns in Recommendations

Recommendation drift manifests in several distinct ways, each requiring different detection and mitigation strategies:

**User preference drift.** Individual users' tastes evolve over time. A user interested in action movies in January may shift to documentaries in March. A user who primarily shopped for electronics may start shopping for baby products (life event). A user's music preferences may broaden as they discover new genres. This drift is gradual but pervasive—studies show 20-40% of users exhibit significant preference changes over 3-6 months.

The business impact is direct: recommendations based on outdated preferences reduce engagement. A user who has moved on from action movies but continues receiving action recommendations will have lower click-through rates and watch time. At scale, even small per-user impacts compound to significant revenue losses.

**Item cold-start and freshness drift.** New items arrive constantly—new videos uploaded, new products listed, new songs released. These items have no interaction history, making them difficult to recommend (cold-start problem). However, users often prefer fresh content over older content, even if older content has better historical engagement. A recommendation system that doesn't adapt to new items will feel stale, reducing user satisfaction.

The challenge is particularly acute for platforms with high content velocity. A short-form video platform might receive millions of new videos daily. A news platform's content becomes stale within hours. Recommendation systems must balance exploiting known good content (high engagement) with exploring new content (freshness, discovery).

**Seasonal and event-driven drift.** Consumption patterns exhibit strong seasonal patterns. Holiday shopping peaks in November-December. Sports content surges during major events. Back-to-school shopping spikes in August. Music preferences shift with seasons (upbeat in summer, mellow in winter). These patterns are predictable but must be incorporated into models.

External events create unpredictable drift. A viral trend, breaking news, or cultural moment can shift consumption patterns overnight. During the COVID-19 pandemic, content consumption patterns changed dramatically—more home workout videos, cooking content, and educational material. Models trained on pre-pandemic data performed poorly without rapid adaptation.

**Popularity and trend drift.** Item popularity is highly dynamic. A video that goes viral sees 1000x increase in views within days. A product featured in a celebrity post sees massive demand spikes. A song that becomes a meme dominates listening. Recommendation systems must adapt to these popularity shifts to remain relevant.

However, over-emphasizing popularity creates problems. Recommending only trending content reduces personalization and creates winner-take-all dynamics that harm content diversity and creator fairness. Balancing popularity signals with personalization is a key challenge.

**Behavioral pattern drift.** How users interact with platforms evolves. Mobile usage patterns differ from desktop. Short-form video platforms train users to expect rapid content switching. Binge-watching behavior on streaming platforms creates different engagement patterns than episodic viewing. As platform features evolve (new UI, new content formats), user behavior adapts, and recommendation models must follow.

**Cross-platform and cross-device drift.** Users increasingly interact with platforms across multiple devices (phone, tablet, desktop, TV) and contexts (commute, home, work). Preferences and engagement patterns differ by device and context. A user might watch short clips on mobile during commute but long-form content on TV at home. Models must adapt to these context-dependent patterns.

**Key Point 29.1.** *For the generic drift detection and continuous learning framework, see Chapter 24, Section 24.7. Recommendation systems typically require the most aggressive retraining cadence (daily to weekly) due to the rapid pace of preference and content evolution.*

Key recommendation-specific strategies beyond the generic framework include:

- **Separate short-term and long-term models:** Use a transformer on recent interactions for “what the user wants right now” and a collaborative filter on full history for “what the user generally likes,” combining with learned weights.
- **Contextual bandits for exploration:** Allocate 5–10% of recommendations to exploration via Thompson sampling or UCB, enabling continuous learning about new items and shifting preferences.
- **Seasonal and event-aware modeling:** Explicitly include temporal features (day-of-week, holiday indicators, event flags) and train separate model components for predictable seasonal shifts.
- **Online user embedding updates:** Update user embeddings hourly based on recent interactions while keeping item embeddings on a daily cycle, balancing freshness with stability.

## 29.7 Exercises

**Exercise 29.1.** Implement a simple sequence-based recommender using a 2-layer transformer encoder. Train on MovieLens-1M. Evaluate using Recall@20 and NDCG@20 metrics. How does performance compare to a baseline RNN-based recommender?

**Exercise 29.2.** Design a multi-task recommendation system that predicts both click-through rate (CTR) and conversion rate (CVR). What is the relationship between the two tasks? Should they share weights or have separate heads? How would you weight the two losses?

**Exercise 29.3.** Analyze the filter bubble effect in a recommendation system. Given historical user interactions, recommend items and measure recommendation diversity. Propose modifications to increase diversity while maintaining engagement.

## 29.8 Solutions

Full solutions for all exercises are available at <https://deeplearning.hofkensvermeulen.be>.

## Chapter 30

# Healthcare and Life Sciences: EHR, Medical Imaging, and Bio-Sequence Models

### Chapter Overview

Healthcare represents the highest-stakes application domain for artificial intelligence. Errors in healthcare AI don't just cost money—they can cost lives. A misdiagnosed cancer, a missed drug interaction, or an incorrect treatment recommendation can have fatal consequences. Yet the potential benefits are equally profound: AI systems that improve diagnostic accuracy, reduce medical errors, accelerate drug discovery, and enable personalized medicine could save millions of lives and trillions of dollars in healthcare costs.

The business and societal challenges are immense. Healthcare spending in the United States alone exceeds \$4 trillion annually, with 30% attributed to waste, inefficiency, and preventable errors. Diagnostic errors affect 12 million Americans annually, causing 40,000-80,000 deaths. Radiologists face overwhelming workloads, analyzing hundreds of images daily with limited time per case. Drug development costs average \$2.6 billion per approved drug and takes 10-15 years. Rare diseases affect 400 million people globally but receive limited research attention due to small patient populations.

This chapter explores how transformers and deep learning are addressing these challenges across three critical areas: electronic health records (EHRs) for clinical decision support and risk prediction, medical imaging for diagnostic assistance, and genomic sequence modeling for precision medicine and drug discovery. We examine domain-specific architectures, training strategies, and validation requirements that differ fundamentally from other AI applications.

However, healthcare AI faces unique challenges that make deployment far more complex than consumer applications. Regulatory requirements demand rigorous validation—FDA clearance takes years and costs millions. Privacy regulations (HIPAA, GDPR) restrict data access and sharing. Medical data is scarce, fragmented, and heterogeneous across institutions. Class imbalance is severe (rare diseases by definition). Explainability is mandatory—clinicians must understand AI reasoning to trust and validate recommendations. Liability concerns create risk aversion. And most critically, healthcare AI must achieve superhuman performance to justify adoption, as errors can cause patient harm.

This chapter provides the technical foundation and business context to build healthcare AI systems that balance innovation with safety, accuracy with explainability, and automation with human oversight. We examine successful deployments, regulatory pathways, and the economic models that make healthcare AI viable despite its unique challenges.

### Learning Objectives

1. Understand clinical data representations: EHRs, medical images, genomic sequences
2. Design models for clinical text: diagnosis coding, phenotyping, risk prediction

3. Apply vision transformers to medical imaging with domain-specific constraints
4. Learn genomic sequence models for structure and function prediction
5. Implement clinical validation and prospective testing workflows
6. Address regulatory requirements: explainability, audit trails, fairness across populations
7. Design human-in-the-loop systems where AI assists but doctors make final decisions

## 30.1 Clinical Text and Electronic Health Records (EHRs)

Electronic health records represent one of healthcare's most valuable yet underutilized data assets. A typical hospital system accumulates millions of clinical notes annually—physician assessments, nursing observations, radiology reports, pathology findings, discharge summaries. These notes contain rich information about patient conditions, treatment responses, and clinical reasoning that structured data (lab values, vital signs) cannot capture. However, this information remains largely locked in unstructured text, inaccessible to automated analysis.

The business opportunity is substantial. Clinical documentation consumes 35-50% of physician time, contributing to burnout and reducing time for patient care. Physicians spend 2 hours on documentation for every hour of patient interaction. Automated clinical note analysis could reduce this burden while improving care quality. Risk prediction models that identify high-risk patients enable preventive interventions, reducing costly hospital readmissions (average cost: \$15,000 per readmission). Automated diagnosis coding improves billing accuracy, recovering millions in lost revenue from under-coding. Clinical trial recruitment, which typically takes months and costs hundreds of thousands of dollars, can be accelerated through automated patient-criteria matching.

However, clinical text presents unique challenges that make it fundamentally different from general text processing. Clinical language is dense, technical, and context-dependent. Abbreviations are ubiquitous and ambiguous (MS could mean multiple sclerosis, mitral stenosis, or morphine sulfate). Negation is critical—"no evidence of pneumonia" means the opposite of "pneumonia." Temporal reasoning is essential—symptoms that develop over hours suggest different diagnoses than symptoms developing over months. Uncertainty is pervasive—"rule out sepsis" means sepsis is suspected but not confirmed. And critically, errors have consequences—misinterpreting a clinical note could lead to incorrect treatment decisions.

### 30.1.1 EHR Data and Domain-Specific Language

EHRs contain multiple data types:

**Definition 30.1** (EHR Data Types). Electronic health records contain multiple interconnected data types that together provide a comprehensive view of patient care.

Clinical notes are narrative text written by physicians, nurses, and other clinicians documenting patient encounters, assessments, and treatment plans. The format and quality of these notes vary significantly across institutions and individual clinicians, ranging from brief bullet points to detailed prose narratives.

Structured data includes quantitative measurements such as lab values (hemoglobin levels, glucose concentrations), vital signs (blood pressure, heart rate, temperature), and medication lists with dosages and schedules. This structured information is easily queryable but lacks the nuanced clinical reasoning captured in narrative notes.

Codes provide standardized representations of diagnoses, procedures, and clinical concepts. ICD-10 codes classify diseases and health conditions, CPT codes describe medical procedures, and SNOMED CT provides a comprehensive standardized clinical terminology. These codes enable billing, research, and cross-institutional data sharing.

Orders document clinical decisions including medication prescriptions, laboratory test orders,

and imaging study requests. The pattern and timing of orders reveal clinical thinking and diagnostic strategies.

Results contain the outcomes of ordered tests including laboratory results, imaging reports, and pathology findings. These results drive clinical decision-making and often trigger subsequent orders or treatment changes.

Timelines establish the temporal ordering of all these elements, which is critical for understanding disease progression and treatment responses. Diagnoses develop over time, and the sequence of events often determines the correct interpretation of clinical data.

Clinical language differs from general English in several fundamental ways that require specialized processing.

Abbreviations are ubiquitous in clinical documentation, with terms like CHF (congestive heart failure), MI (myocardial infarction), and HTN (hypertension) appearing frequently. These abbreviations are often ambiguous—MS could mean multiple sclerosis, mitral stenosis, or morphine sulfate depending on context. Models must learn to disambiguate based on surrounding clinical information.

Negations are critical for correct interpretation because they completely reverse meaning. The phrase “no fever” indicates the absence of fever, not its presence. Negation detection is essential for accurate information extraction, as failing to recognize negation can lead to opposite conclusions about patient status.

Uncertainty expressions convey the degree of diagnostic confidence, which is crucial for clinical decision-making. The phrase “rule out sepsis” means sepsis is suspected but not yet confirmed, requiring different clinical actions than a confirmed diagnosis. Models must capture these confidence levels to provide appropriate recommendations.

Temporal references establish timelines that are crucial for diagnosis and treatment. A symptom “worsening over the past week” suggests a different clinical picture than one that developed suddenly. Understanding temporal progression helps distinguish between acute and chronic conditions and guides appropriate interventions.

Medical jargon includes highly specialized terms unfamiliar to general language models, such as bilenteric fistula, heterotaxy, and stridor. These technical terms carry precise clinical meanings that general-purpose models trained on web text cannot capture without domain-specific training.

### 30.1.2 Domain-Adaptive Pre-Training

General BERT, trained on Wikipedia and Books, performs poorly on clinical text. BioBERT and ClinicalBERT are BERT models continued pre-trained on biomedical literature (PubMed) and clinical notes respectively.

**ClinicalBERT pre-training:** The model is trained through continued pre-training on clinical text to adapt general language understanding to the medical domain.

The dataset consists of 2 million clinical notes from MIMIC-III, a publicly available ICU database that provides real-world clinical documentation. This large corpus of authentic clinical text enables the model to learn the patterns, terminology, and structure of medical documentation.

Masked language modeling serves as the pre-training objective, where the model predicts masked clinical terms based on surrounding context. This self-supervised approach allows the model to learn clinical language patterns without requiring labeled data.

The vocabulary uses clinical-specific tokenization that preserves medical terms as single tokens rather than breaking them into subwords. This ensures that important clinical concepts like “myocardial infarction” are treated as coherent units rather than fragmented pieces.

The result is a model that outperforms general BERT on clinical NLP tasks by 5–15% absolute, demonstrating the value of domain-adaptive pre-training. This performance improvement translates directly to better clinical decision support and more accurate information extraction from medical records.

### 30.1.3 Clinical NLP Applications

**Diagnosis Coding (ICD-10):** Automatically assign diagnosis codes to discharge summaries. Multi-label classification: each patient may have many diagnoses.

**Phenotyping:** Extract patient phenotypes (detailed clinical characteristics) for research. Phenotypes are groups of patients with shared conditions; essential for cohort selection.

**Risk Prediction:** Given EHR history, predict risk of adverse events (readmission, mortality, complications). Train on historical data; prospectively predict for current patients.

**Adverse Event Detection:** Identify serious complications early (sepsis, acute kidney injury) from note and lab trends.

**Note Summarization:** Summarize lengthy clinical notes into concise summaries for clinical efficiency.

### 30.1.4 Handling Structured + Unstructured Data

Many clinical tasks benefit from both sources:

$$\text{Prediction} = \text{Model}(\text{ClinicalNotes}, \text{LabValues}, \text{Vitals}, \text{Medications}) \quad (30.1)$$

Architecture options: Several architectural approaches exist for combining text and structured data, each with different trade-offs.

Concatenation treats all data as tokens by converting structured values to text and feeding everything to a single transformer. This approach is simple to implement and requires minimal architectural changes, but it loses the inherent structure of numerical data and may not effectively capture the different statistical properties of text versus structured features.

Multi-input architectures use separate encoders for text and structured data, then combine their outputs at the final layer. Text passes through a transformer encoder (like ClinicalBERT) while structured data goes through embedding layers for categorical variables and direct connections for numerical values. The separate encoders preserve the modality-specific structure and allow each encoder to specialize in its data type before fusion.

Fusion networks learn cross-modality interactions through attention mechanisms that allow text and structured features to interact at multiple layers. This more complex approach enables the model to discover which text patterns correlate with which lab values or vital signs, potentially capturing clinically meaningful relationships. For example, the model might learn that mentions of "shortness of breath" in notes combined with elevated heart rate in vitals strongly predicts heart failure. While more computationally expensive, fusion networks can be more effective when cross-modal interactions are important for the prediction task.

## 30.2 Medical Imaging Analysis

Medical imaging (X-rays, CT scans, MRI, ultrasound) is among the most valuable clinical data sources. Transformers have revolutionized image analysis, outperforming traditional CNNs.

### 30.2.1 Vision Transformers for Medical Imaging

A vision transformer adapted for medical images:

1. **Patch embedding:** Divide 3D medical image (or multiple 2D slices) into patches. For a  $512 \times 512$  X-ray,  $16 \times 16$  patches yield 1024 patches.
2. **Position embedding:** Spatial position encoding is critical; location of abnormalities matters.
3. **Transformer encoder:** Self-attention over all patches enables long-range dependencies (e.g., left-right symmetry is important—tumors disrupting symmetry are notable).
4. **Output:** Classification (normal vs. pneumonia), segmentation (delineate tumor), localization (point to abnormality), or report generation (generate radiology report).



### 30.2.2 Domain-Specific Considerations

**3D Medical Images:** MRI and CT scans produce 3D volumes with dimensions like  $512 \times 512 \times 100$  voxels, making it memory-prohibitive to process all voxels simultaneously. Several solutions address this computational challenge.

The 2D slices approach processes the image slice-by-slice, typically focusing on the middle 50 slices where pathology is most likely, then aggregates predictions across slices. This reduces memory requirements dramatically but may miss information from inter-slice relationships and 3D spatial patterns.

The 3D patches method divides the volume into smaller 3D patches that can fit in memory, then processes each patch with 3D attention mechanisms. This preserves 3D spatial relationships within patches but requires careful handling of patch boundaries and aggregation of patch-level predictions.

The hierarchical approach first processes a low-resolution version of the full volume to identify regions of interest, then applies high-resolution processing only to those regions. This multi-scale strategy balances computational efficiency with the need to analyze the entire volume, focusing computational resources where they're most needed.

**Data Scarcity:** Medical imaging datasets are smaller than ImageNet. Transfer learning is essential. Pretrain on large datasets (CheXpert for chest X-rays with 223K images), then fine-tune on task-specific data.

**Class Imbalance:** Rare diseases are underrepresented. Pneumothorax appears in  $\sim 1\%$  of X-rays. Solutions: weighted loss, focal loss, oversampling rare classes during training.

**Explainability:** Clinicians need to understand why the model flagged an abnormality. Attention heatmaps show which image regions influenced the prediction. Grad-CAM computes saliency maps highlighting important features.

### 30.2.3 Radiologist-in-the-Loop Systems

Rather than fully automating diagnosis, practical systems assist radiologists:

1. **Flagging:** Model identifies likely abnormal cases; radiologist reviews top-k cases first
2. **Confirmation:** Model suggests diagnosis; radiologist confirms, modifies, or rejects
3. **Double-reading:** In high-risk cases, both AI and human radiologist read independently
4. **Escalation:** Complex cases automatically escalated to expert radiologist

This human-in-the-loop approach reduces radiologist workload (analyzing normal cases automatically) while maintaining diagnostic quality.

## 30.3 Genomics and Bio-Sequence Models

DNA and protein sequences are literal “languages” of biology. Transformers trained on massive sequence datasets have revolutionized protein structure prediction and variant effect prediction.

### 30.3.1 Sequence Representation

A DNA sequence is a string of 4 letters (A, T, G, C). Tokenization is trivial; the challenge is understanding long-range dependencies and structure.

**Definition 30.2** (Bio-Sequence Language). Biological sequences can be understood as languages with specific alphabets and structural rules.

DNA uses a 4-letter alphabet (A, T, G, C) representing the four nucleotide bases. DNA sequences can be millions of bases long, encoding the genetic information for entire organisms. The challenge lies in understanding long-range dependencies and regulatory relationships that span thousands of bases.

RNA also uses a 4-letter alphabet (A, U, G, C), where uracil (U) replaces thymine (T). RNA molecules form complex secondary structures including stem-loops and hairpins through base pairing, which are critical for their biological function. These structural elements must be considered when modeling RNA sequences.

Proteins use a 20-letter alphabet corresponding to the 20 standard amino acids. Protein sequences are typically hundreds of residues long and fold into intricate 3D structures that determine their function. The relationship between sequence and structure is complex, with distant amino acids in the sequence often interacting in the folded structure.

Codons are DNA triplets that encode amino acids, with the genetic code mapping 64 possible triplets to 20 amino acids (plus stop signals). This redundancy means that mutations changing codons may or may not change the resulting protein, a distinction critical for predicting the functional impact of genetic variants.

### 30.3.2 ESM: Large-Scale Protein Language Models

ESM (Evolutionary Scale Modeling) is a transformer trained on 250 million protein sequences from UniRef100. The model learns protein language without explicit 3D structure supervision.

**ESM-2:** This 15-billion parameter model is trained with masked language modeling on protein sequences, learning protein language patterns without explicit 3D structure supervision. The inference embeddings from ESM-2 enable multiple downstream applications that advance biological research and medicine.

Structure prediction uses ESM embeddings as input to structure prediction networks like OmegaFold and ESMFold. These methods achieve structure prediction accuracy approaching experimental methods like X-ray crystallography and cryo-EM, but at a fraction of the time and cost. This breakthrough enables structural analysis of millions of proteins that would be impractical to solve experimentally.

Function prediction leverages ESM embeddings to predict protein properties including thermostability (how well proteins withstand heat), binding affinity (how strongly proteins interact with other molecules), and catalytic activity (how efficiently enzymes catalyze reactions). These predictions guide protein engineering and drug development.

Variant effect prediction determines how mutations affect protein function, which is critical for interpreting genetic variants found in patient genomes. By comparing embeddings of wild-type and mutant proteins, the model predicts whether a variant is likely to be pathogenic or benign, informing clinical decision-making.

Protein design uses ESM in reverse: given desired properties, the model can design new proteins with those properties. This capability enables engineering proteins for therapeutic applications, industrial enzymes, and novel biomaterials.

### 30.3.3 Protein Structure Prediction and Folding

The protein folding problem—predicting a protein’s 3D structure from its amino acid sequence—has been called one of the grand challenges of computational biology. A protein’s function is determined by its 3D structure, yet predicting structure from sequence remained largely unsolved for 50 years. Recent transformer-based approaches, particularly AlphaFold2, AlphaFold3, and ESMFold, have achieved breakthrough accuracy, revolutionizing structural biology and drug discovery.

#### The Evolution from MSA-Based to Language Model Approaches

Traditional protein structure prediction relied heavily on Multiple Sequence Alignments (MSAs)—collections of evolutionarily related protein sequences. The rationale was that evolution preserves structurally important residue pairs: if two amino acids are spatially close in the 3D structure, mutations in one position often correlate with compensatory mutations in the other across evolutionary time. By analyzing these co-evolutionary patterns in MSAs containing hundreds to thousands of related sequences, models could infer which residues likely interact in 3D space.

AlphaFold2, released in 2020, leveraged this evolutionary information through a sophisticated architecture combining MSA processing with geometric reasoning. The model’s Evoformer module processes

MSAs to extract co-evolutionary signals, while the Structure module iteratively refines 3D coordinates using geometric constraints. This approach achieved unprecedented accuracy, with predictions often matching experimental structures within 1-2 Angstroms RMSD (Root Mean Square Deviation). However, AlphaFold2's dependence on MSAs created limitations: for orphan proteins without evolutionary relatives, or for newly designed proteins, MSA quality was poor, degrading prediction accuracy.

The paradigm shifted with large-scale protein language models like ESM-2. By pre-training transformers on 250+ million protein sequences—orders of magnitude more than used for MSA-based methods—these models learn protein language patterns directly from sequence alone. The key insight: with sufficient scale, transformers internalize evolutionary constraints, structural preferences, and sequence-structure relationships without explicit MSA input. ESMFold, built on ESM-2 embeddings, achieves structure prediction accuracy approaching AlphaFold2 but operates on single sequences, eliminating MSA search entirely. This enables predictions in seconds rather than minutes and works for orphan proteins where MSA-based methods fail.

The architectural comparison reveals complementary strengths. AlphaFold2's Evoformer explicitly models pairwise residue relationships through attention mechanisms operating on MSA representations, then feeds these representations to a Structure module that iteratively refines atomic coordinates using Invariant Point Attention (IPA). ESMFold takes a more direct path: ESM-2's transformer backbone generates sequence embeddings, which feed into a folding head that predicts inter-residue distances and angles, then reconstructs 3D coordinates. AlphaFold2 excels when high-quality MSAs are available, particularly for proteins with many evolutionary relatives. ESMFold excels for speed, orphan proteins, and designed sequences. In practice, researchers often use both approaches, comparing predictions to assess confidence.

### AlphaFold3: From Static Structures to Biomolecular Interactions

AlphaFold3, released in 2024, represents a fundamental architectural shift from predicting static protein structures to modeling dynamic biomolecular complexes. While AlphaFold2 focused on single proteins or protein-protein complexes, AlphaFold3 predicts how proteins interact with ligands (drug molecules), nucleic acids (DNA/RNA), ions, post-translational modifications, and other biomolecules. This capability is transformative for drug discovery: rather than predicting protein structure then separately docking drug candidates, AlphaFold3 directly predicts protein-ligand complexes, revealing binding modes and conformational changes.

The architecture employs a diffusion-based approach, a departure from AlphaFold2's iterative refinement. Diffusion models, successful in image generation (DALL-E, Stable Diffusion), gradually denoise random structures into coherent predictions. AlphaFold3 starts with random atomic coordinates and iteratively denoises them, guided by learned priors about biomolecular geometry, physics, and interactions. This approach naturally handles the flexibility and conformational diversity of biomolecular complexes—proteins often change shape upon ligand binding (induced fit), and diffusion models can explore this conformational space.

The three-stage encoder provides rich input representations. The Template module searches structural databases for homologous structures, providing geometric priors when evolutionary relatives exist. The MSA module processes multiple sequence alignments to extract co-evolutionary signals, similar to AlphaFold2 but extended to handle multi-chain complexes with different molecule types. The Pairformer module performs deep feature extraction on pairwise residue relationships, building representations that capture both local interactions (hydrogen bonds, van der Waals contacts) and global topology (domain arrangements, quaternary structure).

AlphaFold3's ability to predict biomolecular interactions, not just static structures, is critical for understanding drug binding. A drug's efficacy depends on how it binds to its target protein: binding pose (orientation and position), binding affinity (strength of interaction), and induced conformational changes. AlphaFold3 predicts all three, enabling computational screening of drug candidates before expensive synthesis and testing. Early results show AlphaFold3 predictions of protein-ligand complexes often match experimental crystal structures within 2-3 Angstroms, sufficient accuracy for drug discovery applications.

## Key Technical Components for Implementation

Students pursuing implementation should understand several core technical components that enable accurate structure prediction.

Invariant Point Attention (IPA) is AlphaFold2's key innovation for maintaining 3D geometric consistency. Standard attention mechanisms operate on abstract feature vectors without geometric constraints. IPA extends attention to 3D space: each residue has an associated local coordinate frame (position and orientation), and attention weights depend on both feature similarity and geometric proximity in 3D. Critically, IPA is equivariant to rotations and translations—if you rotate the entire protein, the model's predictions rotate identically. This geometric inductive bias dramatically improves learning efficiency and prediction accuracy. Implementation requires careful handling of  $SO(3)$  rotations using quaternions or rotation matrices, and efficient computation of geometric attention scores.

Pairwise representations encode relationships between all residue pairs, capturing which residues are likely to be spatially close, form hydrogen bonds, or participate in secondary structures. These representations are updated through attention mechanisms that allow information to flow between pairs: if residues A-B and B-C are predicted to be close, the model can infer that A and C might also interact. The pairwise representation is a key bottleneck: for a protein with  $N$  residues, the representation is  $N \times N$ , requiring  $O(N^2)$  memory and computation. Efficient implementations use sparse attention, gradient checkpointing, and mixed-precision training to handle proteins with thousands of residues.

Confidence metrics are essential for interpreting predictions. pLDDT (predicted Local Distance Difference Test) provides per-residue confidence scores from 0-100, indicating how accurately each residue's position is predicted. Regions with pLDDT  $\geq 90$  are typically accurate to experimental resolution; pLDDT  $\leq 50$  indicates disordered or poorly predicted regions. pTM (predicted Template Modeling score) provides global confidence for the entire structure. These metrics enable users to identify which parts of a prediction are reliable and which require experimental validation. Implementation involves training auxiliary heads that predict these confidence scores alongside structure, using experimental structures as ground truth.

Single-sequence versus MSA mode presents a fundamental tradeoff. MSA mode (AlphaFold2, ESMFold with MSA) provides higher accuracy when high-quality MSAs are available, particularly for proteins with many evolutionary relatives. The model leverages co-evolutionary signals that directly indicate residue-residue contacts. However, MSA search is computationally expensive (minutes to hours) and fails for orphan proteins. Single-sequence mode (ESMFold, AlphaFold2 without MSA) is dramatically faster (seconds) and works for any sequence, but may be less accurate for proteins without clear evolutionary patterns. In practice, researchers use single-sequence mode for rapid screening and MSA mode for high-confidence predictions of critical targets.

## Practical Considerations for Deployment

Computational requirements vary dramatically across methods. ESMFold requires a single GPU (16-32GB VRAM) and predicts structures in 5-30 seconds per protein, enabling high-throughput screening of millions of sequences. AlphaFold2 requires more resources: MSA search uses CPUs (8-16 cores, 30-60 minutes), then structure prediction uses GPUs (16-32GB VRAM, 5-10 minutes). AlphaFold3 is more expensive due to diffusion sampling, requiring 32-64GB VRAM and 10-30 minutes per complex. For large-scale applications (predicting structures for entire proteomes), ESMFold's speed advantage is decisive. For critical drug targets requiring maximum accuracy, AlphaFold2/3's higher accuracy justifies the cost.

Handling multi-domain proteins, protein complexes, and conformational flexibility presents ongoing challenges. Multi-domain proteins contain multiple folded regions connected by flexible linkers. Predicting the relative orientation of domains is difficult because linkers allow conformational freedom. Current models often predict each domain accurately but misplace their relative positions. Protein complexes (multiple proteins binding together) are better handled by AlphaFold2/3, which can predict quaternary structure, but accuracy degrades for large complexes ( $\geq 5$  proteins). Conformational flexibility—proteins adopting multiple structures—is fundamentally challenging for single-structure prediction

models. Proteins like kinases exist in active and inactive conformations; predicting both requires multiple predictions or specialized ensemble methods.

Limitations remain despite breakthrough accuracy. Fold-switching proteins change their entire fold in response to environmental conditions, a phenomenon current models cannot predict because they output single static structures. Highly dynamic regions like intrinsically disordered regions (IDRs) lack stable structure and are inherently unpredictable—models correctly predict low confidence for these regions, but cannot predict their dynamic ensembles. Novel folds without training data analogs are challenging: if a protein adopts a fold never seen in the training data, models may hallucinate plausible but incorrect structures. Membrane proteins, which fold in lipid bilayers rather than aqueous solution, remain less accurate than soluble proteins due to limited training data.

### Validation and Evaluation Metrics

Understanding evaluation metrics is essential for interpreting prediction quality and comparing methods.

TM-score (Template Modeling score) measures global structure similarity, ranging from 0 (completely different) to 1 (identical). TM-score  $\geq 0.5$  indicates the same fold;  $\geq 0.7$  indicates high similarity suitable for homology modeling;  $\geq 0.9$  indicates near-experimental accuracy. TM-score is length-normalized, enabling fair comparison of predictions for proteins of different sizes. Unlike RMSD, TM-score is less sensitive to local errors in flexible regions, providing a better measure of overall fold correctness.

LDDT (Local Distance Difference Test) measures local structure accuracy by comparing predicted and experimental inter-atomic distances within local neighborhoods (typically 15 Å radius). LDDT ranges from 0-100, with scores  $\geq 90$  indicating excellent local accuracy, 70-90 good, 50-70 acceptable, and  $\leq 50$  poor. LDDT is particularly useful for identifying which regions of a prediction are accurate versus poorly modeled. The predicted version (pLDDT) is what models output as confidence scores.

RMSD (Root Mean Square Deviation) measures the average distance between corresponding atoms in predicted and experimental structures after optimal superposition. RMSD is reported in Ångströms:  $\leq 1$  Å is excellent (near-experimental accuracy), 1-2 Å is very good, 2-4 Å is acceptable for many applications,  $\geq 4$  Å indicates significant errors. However, RMSD is sensitive to outliers—a single misplaced domain can dominate RMSD even if the rest of the structure is accurate. RMSD is most useful for comparing predictions of the same protein or assessing local accuracy of specific regions.

Interpreting confidence scores and knowing when experimental validation is required is critical for practical applications. High confidence (pLDDT  $\geq 90$ , pTM  $\geq 0.8$ ) predictions are typically reliable for most applications including drug docking and protein engineering. Medium confidence (pLDDT 70-90, pTM 0.5-0.8) predictions capture the overall fold but may have local errors; use with caution for applications requiring atomic-level accuracy. Low confidence (pLDDT  $\leq 70$ , pTM  $\leq 0.5$ ) predictions are unreliable and should not be used without experimental validation. Experimental validation through X-ray crystallography, cryo-EM, or NMR remains the gold standard for critical applications like drug development, even when computational predictions show high confidence.

### 30.3.4 AI-Driven Drug Discovery

Drug discovery is extraordinarily expensive and time-consuming: developing a new drug costs \$2.6 billion on average and takes 10-15 years, with 90% of candidates failing in clinical trials. AI promises to accelerate discovery, reduce costs, and improve success rates by computationally screening billions of molecules, predicting binding affinity, and designing novel compounds with desired properties. Recent successes demonstrate AI's potential: several AI-discovered drugs have entered clinical trials, and computational screening has identified active compounds in weeks rather than years.

### Virtual Screening and Molecular Docking Pipeline

Virtual screening computationally evaluates millions to billions of compounds to identify promising drug candidates before expensive synthesis and testing. The process begins with molecular docking,

which predicts how small molecules (ligands) bind to target proteins. Docking algorithms sample the conformational space of ligand-protein complexes: the ligand can adopt different shapes (conformers), orient itself in different ways, and bind at different positions in the protein's binding pocket. For each sampled pose, a scoring function estimates binding affinity—how strongly the ligand binds.

Scoring functions come in three main types, each with strengths and limitations. Physics-based scoring functions use molecular mechanics force fields to calculate interaction energies: van der Waals forces, electrostatics, hydrogen bonds, and desolvation penalties. These methods are grounded in physical principles but are computationally expensive and often inaccurate due to approximations in force fields and neglect of entropic effects. Empirical scoring functions are trained on experimental binding affinity data, learning weights for different interaction types (hydrogen bonds, hydrophobic contacts, etc.). These methods are fast and reasonably accurate for molecules similar to training data, but generalize poorly to novel chemotypes. Knowledge-based scoring functions use statistical potentials derived from known protein-ligand structures, capturing preferences for certain atom-atom distances and interaction geometries. These methods balance speed and accuracy but depend on the quality and diversity of structural databases.

High-Throughput Virtual Screening (HTVS) applies docking to massive chemical libraries. ZINC contains 230 million purchasable compounds; PubChem contains 110 million compounds; proprietary pharmaceutical libraries contain millions more. Screening billions of compounds requires computational efficiency: simplified scoring functions, parallel processing on GPU clusters, and hierarchical screening (fast filters eliminate obvious non-binders, then expensive docking for promising candidates). A typical HTVS campaign might screen 100 million compounds in 1-2 weeks using 100-1000 GPUs, identifying 1,000-10,000 hits for further evaluation.

Active learning integration dramatically improves screening efficiency. Rather than screening all compounds with the same expensive docking protocol, active learning trains target-specific neural networks that triage compounds. The process: (1) dock a small random sample (10,000-100,000 compounds) with expensive accurate docking, (2) train a neural network to predict docking scores from molecular descriptors, (3) use the neural network to rapidly screen millions of compounds, selecting top candidates for expensive docking, (4) retrain the network on new docking results, iterating until convergence. This approach reduces computational cost by 10-100x while maintaining hit discovery rates. The neural network learns target-specific binding preferences, becoming increasingly accurate as more data accumulates.

## De Novo Drug Design with Transformers

Rather than screening existing compounds, de novo design generates novel molecular structures optimized for desired properties. Transformer-based generative models, trained on millions of known compounds, learn the grammar of chemistry—which atoms can bond, which structures are stable, which functional groups confer drug-like properties.

The architecture typically uses transformer encoder-decoder models trained on vast compound datasets. ChEMBL contains 2 million bioactive compounds with measured activities; PubChem contains 110 million compounds; proprietary datasets add millions more. Training objectives include: (1) reconstruction—encode a molecule, decode it back, (2) property prediction—predict bioactivity, solubility, toxicity from structure, (3) conditional generation—generate molecules with specified properties. The model learns to represent molecules as sequences, understand structure-activity relationships, and generate novel compounds.

SMILES representation (Simplified Molecular Input Line Entry System) encodes molecules as text strings, enabling transformer processing. For example, aspirin is CC(=O)Oc1ccccc1C(=O)O. SMILES captures molecular structure including atoms, bonds, rings, and stereochemistry in a compact text format. Tokenization treats each character or atom as a token. The transformer processes SMILES sequences like natural language, learning chemical syntax (valid bond patterns) and semantics (structure-property relationships). Alternative representations include SELFIES (SELF-referencing Embedded Strings), which guarantees all generated strings are valid molecules, and graph neural networks, which directly operate on molecular graphs.

The generative process uses sequence-to-sequence generation. Given a prompt (desired properties,

scaffold constraints, or partial structure), the model generates SMILES strings character-by-character using autoregressive decoding. Sampling strategies control diversity: greedy decoding generates the most likely molecule, beam search explores multiple high-probability candidates, and stochastic sampling with temperature control balances novelty and validity. Post-processing filters invalid SMILES and checks chemical validity (valence rules, ring strain, reactive groups).

Reinforcement learning integration optimizes generated molecules for multiple objectives. The generative model is the policy; generated molecules are actions; rewards are computed from predicted properties. Monte Carlo Tree Search (MCTS) explores the space of possible molecules, balancing exploitation (refining promising molecules) and exploration (trying novel structures). Policy gradient methods (REINFORCE, PPO) directly optimize the generative model to maximize expected reward. The reward function incorporates domain knowledge: high binding affinity (predicted by docking or ML models), drug-likeness (Lipinski's Rule of Five: molecular weight  $\leq 500$ ,  $\log P \leq 5$ , hydrogen bond donors  $\leq 5$ , acceptors  $\leq 10$ ), synthesizability (penalizing complex or reactive structures), and ADMET properties (Absorption, Distribution, Metabolism, Excretion, Toxicity predicted by specialized models).

### Multi-Objective Optimization and Practical Constraints

Drug discovery requires balancing multiple conflicting objectives. High binding affinity is necessary but insufficient—a molecule that binds tightly but is toxic, insoluble, or impossible to synthesize is useless. Multi-objective optimization navigates these tradeoffs.

Binding affinity and selectivity must be balanced. A drug should bind strongly to its target (nanomolar affinity) but weakly to off-targets to avoid side effects. Selectivity is challenging because many proteins share similar binding pockets (kinases, proteases, GPCRs). Computational models predict selectivity by docking to panels of off-target proteins, penalizing molecules that bind promiscuously.

Synthesizability is critical but often neglected. Generative models can design molecules that are chemically valid but practically impossible to synthesize due to complex stereochemistry, unstable intermediates, or expensive reagents. Synthesizability scores estimate synthetic accessibility: retrosynthesis models predict synthetic routes, penalizing molecules requiring many steps or rare reagents. Alternatively, models can be constrained to generate molecules from known building blocks and reactions.

Pharmacokinetics (PK) and ADMET properties determine whether a molecule becomes a drug. Absorption: can the molecule cross membranes and reach the bloodstream? Distribution: does it reach the target tissue? Metabolism: is it rapidly degraded or does it persist? Excretion: is it eliminated safely? Toxicity: does it cause liver damage, cardiac issues, or other adverse effects? Specialized ML models predict these properties from structure, trained on experimental data. Reward functions penalize molecules with poor predicted PK/ADMET.

Reward functions incorporate domain knowledge through carefully designed penalties and bonuses. Reactive groups (aldehydes, epoxides, Michael acceptors) are penalized because they cause off-target reactivity and toxicity. Known pharmacophores (structural motifs associated with activity) are rewarded. Structural alerts (PAINS—Pan-Assay Interference Compounds) are penalized because they cause false positives in assays. Lipinski's Rule of Five and related guidelines are enforced as soft constraints.

Iterative refinement implements a generate-dock-evaluate-retrain loop. (1) Generate a batch of molecules using the current model. (2) Dock them to the target protein, predicting binding affinity. (3) Evaluate ADMET properties using predictive models. (4) Select top candidates based on multi-objective scoring. (5) Retrain the generative model on successful molecules, biasing future generation toward promising chemical space. (6) Repeat for multiple iterations, progressively improving molecule quality. This loop typically runs for 5-10 iterations, generating and evaluating 10,000-100,000 molecules per iteration.

### Structure-Based vs. Ligand-Based Approaches

Drug discovery employs two complementary paradigms depending on available information.

Structure-Based Drug Design (SBDD) uses the 3D structure of the target protein to guide molecule design. With AlphaFold3 predicting protein-ligand complexes, SBDD has become more accessible—even for targets without experimental structures. SBDD enables rational design: identify the binding pocket, analyze which interactions (hydrogen bonds, hydrophobic contacts, electrostatics) are favorable, and

design molecules that maximize these interactions. Docking and molecular dynamics simulations evaluate designed molecules. SBDD is most powerful when high-quality structures are available and the binding site is well-defined.

Ligand-Based Drug Design (LBDD) uses known active compounds to train predictive models when structure is unavailable or binding sites are unclear. QSAR (Quantitative Structure-Activity Relationship) models predict activity from molecular descriptors. Pharmacophore models identify essential structural features for activity. Similarity searching finds molecules similar to known actives. LBDD is faster and requires less structural information but provides less mechanistic insight and may miss novel chemotypes.

Hybrid approaches combine both methods for improved accuracy. Use LBDD to identify promising scaffolds and chemical space, then refine with SBDD to optimize binding interactions. Use AlphaFold3 to predict structures for LBDD-identified hits, enabling structure-guided optimization. Ensemble models combine SBDD and LBDD predictions, improving robustness.

### Integration with Protein Structure Prediction

AlphaFold3's ability to predict protein-ligand complexes directly transforms drug discovery workflows. Traditional approaches required experimental structures (X-ray crystallography, cryo-EM), limiting drug discovery to well-studied targets. AlphaFold3 enables structure-based design for any target, including orphan proteins, membrane proteins, and proteins from pathogens.

Predicting binding sites and conformational changes upon ligand binding is critical for accurate docking. Proteins are flexible—binding pockets often change shape when ligands bind (induced fit). AlphaFold3 can predict these conformational changes by modeling protein-ligand complexes, revealing the bound conformation. This enables more accurate docking: rather than docking to the apo (unbound) structure, dock to the predicted holo (bound) structure.

Virtual screening directly on predicted structures versus experimental structures presents a tradeoff. Experimental structures are more accurate but available for only 200,000 proteins. Predicted structures are available for any sequence but may contain errors, particularly in binding pocket geometry. Validation studies show that high-confidence AlphaFold predictions (pLDDT  $\geq 90$  in binding pocket) perform comparably to experimental structures for virtual screening, while low-confidence predictions degrade screening performance. Best practice: use experimental structures when available, predicted structures for novel targets, and validate predictions with experimental assays.

### Complete Workflow: From Target to Clinical Candidate

A realistic drug discovery workflow integrates all these components:

**Target Identification:** Select a disease-relevant protein. Example: SARS-CoV-2 Mpro protease, essential for viral replication. Validate that inhibiting the target treats the disease (genetic evidence, animal models).

**Structure Preparation:** Obtain or predict the 3D structure. For Mpro, experimental structures are available (PDB: 6LU7). For novel targets, use AlphaFold3. Identify the binding pocket using cavity detection algorithms or known ligand binding sites. Prepare the structure for docking: add hydrogens, assign charges, define the docking box.

**Library Preparation:** Curate or generate a compound library. For virtual screening, use commercial libraries (ZINC, Enamine REAL with 30 billion compounds). For de novo design, train a generative model on relevant chemical space (protease inhibitors, antiviral compounds).

**Virtual Screening:** Dock millions to billions of compounds using HTVS platforms. Use active learning to accelerate screening: train neural networks to predict docking scores, screen billions of compounds with the neural network, dock top candidates with expensive accurate docking. Typical throughput: 1-10 million compounds per day on a GPU cluster.

**Hit Selection:** Select top-k candidates (typically 100-1,000 from millions screened). Criteria: predicted binding affinity ( $\geq 1$  M), drug-likeness (Lipinski's Rule of Five), predicted ADMET properties (non-toxic, orally bioavailable), synthesizability ( $\leq 10$  synthetic steps), novelty (not previously tested).

**De Novo Optimization:** Use transformer models to generate analogs with improved properties. Start with hit compounds, generate variations using the generative model with RL optimization, eval-



uate with docking and ADMET prediction, iterate to improve potency, selectivity, and drug-likeness. Generate 1,000-10,000 analogs per hit, select top 10-100 for synthesis.

**Experimental Validation:** Synthesize top candidates (10-100 compounds). Test binding affinity in vitro using biochemical assays (IC<sub>50</sub>, K<sub>d</sub>). Validate binding mode with crystallography or cryo-EM—compare experimental structure to computational prediction. Test cellular activity (does the compound inhibit viral replication in cells?). Measure ADMET properties experimentally (solubility, permeability, metabolic stability, toxicity).

**Iteration:** Refine based on experimental results. Compounds that bind but are inactive may have poor cell permeability—optimize for permeability. Compounds with off-target effects—optimize for selectivity. Compounds with poor PK—optimize for metabolic stability. Use experimental data to retrain models, improving predictions for subsequent rounds. Typical discovery campaigns require 3-5 iterations over 1-2 years to identify clinical candidates.

## Success Metrics and Validation

Evaluating AI-driven drug discovery requires domain-specific metrics.

Enrichment factor measures how well screening prioritizes true binders versus random selection. If 1% of a library contains active compounds, and the top 1% of screened compounds contains 10% actives, the enrichment factor is 10x. Good screening achieves 10-100x enrichment, dramatically reducing experimental testing burden.

Hit rate is the percentage of tested compounds showing activity. Random screening typically yields 0.01-0.1% hit rates. AI-guided screening achieves 1-10% hit rates, a 10-100x improvement. Higher hit rates reduce synthesis and testing costs.

Crystallographic validation compares predicted binding poses to experimental structures. RMSD  $\leq 2\text{\AA}$  between predicted and experimental poses indicates accurate docking. Validation studies show that modern docking achieves  $\leq 2\text{\AA}$  RMSD for 70-80% of cases when binding pockets are well-defined.

ROC-AUC for classifier-based screening approaches measures the ability to distinguish actives from inactives. AUC  $\geq 0.8$  indicates good discrimination;  $\geq 0.9$  is excellent. Classifiers trained on target-specific data typically achieve AUC 0.7-0.9, substantially better than random (AUC = 0.5).

## Challenges and Limitations

Despite progress, significant challenges remain.

Scoring function accuracy limits docking reliability. Binding affinity prediction errors of  $\pm 2$  kcal/mol are common, corresponding to 30-fold errors in binding affinity. This limits the ability to distinguish strong binders (nanomolar) from weak binders (micromolar). Improved scoring functions using deep learning show promise but require extensive training data.

Protein flexibility and induced fit are poorly captured by rigid docking. Proteins change conformation upon ligand binding, but most docking treats proteins as rigid. Flexible docking (allowing protein side chains to move) is more accurate but computationally expensive. Molecular dynamics simulations capture full flexibility but are too slow for large-scale screening.

False positives are inevitable—computational predictions require experimental validation. Even with 90% precision, screening 1 million compounds yields 100,000 false positives. Experimental validation is the bottleneck: synthesizing and testing compounds costs \$1,000-10,000 per compound and takes weeks. Improving precision from 90% to 99% would reduce false positives 10-fold, dramatically accelerating discovery.

Chemical space exploration balances exploitation versus exploration. Exploiting known chemotypes (scaffolds similar to known drugs) is safer but limits novelty. Exploring novel scaffolds may discover breakthrough drugs but risks synthesizing inactive compounds. Generative models tend to exploit, generating molecules similar to training data. Encouraging exploration requires careful reward design and diversity penalties.

Synthesizability remains a major challenge. Generative models can design molecules that are chemically valid but practically impossible to synthesize. Retrosynthesis models predict synthetic routes but are imperfect. Collaborating with medicinal chemists early in the design process ensures generated molecules are synthetically accessible.

### 30.3.5 Case Study: Variant Effect Prediction

Precision medicine aims to predict drug response and disease risk from individual genomes. A key challenge: interpreting genetic variants (mutations).

A novel variant found in patient DNA raises critical clinical questions that must be answered to guide treatment and counseling.

Does the variant cause disease? Determining pathogenicity is essential for diagnosis and treatment planning. A pathogenic variant might explain the patient's symptoms and guide therapeutic interventions, while a benign variant can be ruled out as a cause.

Will the drug work for this patient? Pharmacogenomic variants affect drug metabolism and response. A variant in a drug-metabolizing enzyme might require dose adjustment or alternative medication selection to ensure efficacy and avoid toxicity.

Should we warn the family? If a variant is pathogenic and heritable, family members may be at risk and should be offered genetic testing and counseling. This information enables preventive care and early intervention for at-risk relatives.

ESM-based models predict variant effects:

1. Extract affected protein's sequence
2. Compute wild-type (normal) protein embedding using ESM-2
3. Mutate sequence; compute variant embedding
4. Measure embedding similarity: high similarity suggests benign; low suggests deleterious

Validation on ClinVar, the gold-standard variant database, demonstrates the model's clinical utility.

Pathogenic versus benign classification achieves 92% accuracy, correctly distinguishing disease-causing variants from harmless genetic variations in the vast majority of cases. This high accuracy enables confident clinical interpretation of novel variants.

Ranking variants by effect magnitude provides additional value beyond binary classification. The model's top-ranked variants are often proven pathogenic in follow-up studies, validating that the model's confidence scores correlate with true biological impact. This ranking capability helps prioritize which variants require experimental validation or immediate clinical action.

## 30.4 Regulatory and Clinical Validation

Clinical deployment requires FDA clearance (in USA) or equivalent regulatory approval. The path is:

### 30.4.1 Clinical Validation Process

1. **Retrospective validation:** Test on historical data. Demonstrates model learns signal.
2. **Prospective validation:** Test on prospectively collected new data. Ensures model generalizes.
3. **Blinded evaluation:** External experts (not model developers) evaluate predictions. Reduces bias.
4. **Clinical trial:** Randomized trial comparing AI-assisted vs. standard care. Demonstrates clinical benefit.
5. **Regulatory submission:** FDA/equivalent reviews model design, validation, and risk mitigation.

Retrospective → Prospective → Trial takes 2–5 years and costs millions of dollars. Only well-funded organizations undertake this.

### 30.4.2 Explainability and Auditing

Regulations require explainability: “Why did the model recommend this treatment?”

**Solutions:** Several complementary approaches enable explainability and support regulatory requirements.

Attention analysis shows which parts of the patient record influenced the prediction by visualizing attention weights. For example, the model might highlight specific sentences in clinical notes or particular time periods in the patient timeline that drove the risk assessment. This transparency helps clinicians understand and validate the model’s reasoning.

Feature importance ranks features such as lab values, clinical notes, and medications by their impact on the prediction. Techniques like SHAP (SHapley Additive exPlanations) quantify each feature’s contribution, enabling clinicians to see that, for instance, elevated creatinine and mentions of “shortness of breath” were the primary drivers of a heart failure prediction.

Similar cases retrieval finds past patients with similar characteristics and shows their outcomes to support the current prediction. If the model predicts high readmission risk, it can present 5-10 similar historical patients who also readmitted, providing evidence-based justification for the prediction and helping clinicians understand the reasoning by analogy.

Audit logs maintain a complete record of all predictions and decisions for regulatory review and quality assurance. These logs enable retrospective analysis of model performance, investigation of adverse events, and demonstration of compliance with regulatory requirements.

### 30.4.3 Fairness and Bias

AI systems trained on historical data inherit biases. Example: Sepsis models historically trained on majority-white populations may perform worse on minorities.

**Mitigation:** Several strategies address bias and ensure equitable performance across patient populations.

Stratified evaluation reports performance separately for each demographic group, making disparities visible. Rather than reporting a single overall accuracy, the evaluation breaks down performance by race, ethnicity, age, gender, and socioeconomic status. This transparency ensures that the model doesn’t achieve high average performance while failing for specific subgroups.

Bias-aware training explicitly optimizes for fairness across groups by incorporating fairness constraints or objectives into the training process. Techniques include reweighting training examples from underrepresented groups, adding fairness penalty terms to the loss function, or using adversarial debiasing to remove demographic information from learned representations while maintaining predictive performance.

Monitoring in deployment tracks performance over time and by demographic group, enabling detection of emerging disparities. If the model’s performance degrades for a particular group, the system triggers alerts and initiates retraining with updated data. This continuous monitoring ensures that the model remains fair as patient populations and clinical practices evolve.

## 30.5 Case Study: Clinical Risk Prediction at Scale

A large health system wants to identify high-risk patients for preventive care intervention.

### 30.5.1 System Design

**Target:** Predict 30-day readmission risk for patients with chronic conditions

**Data:**

- 100K patients, 500K admissions (historical)
- EHR features: 50K unique clinical notes, 200 structured variables
- Outcome: Readmission within 30 days (15% positive rate; class imbalance)

**Model Architecture:**

- Clinical notes encoder: ClinicalBERT
- Structured data: Embedding layer for categorical variables, concatenation for numeric
- Fusion: Combine note embeddings + structured features via attention
- Output: Logistic regression on 50-dim combined representation

**30.5.2 Results****Offline validation (test set):**

- AUROC: 0.84 (strong predictive signal)
- Precision@20% recall: 25% (of flagged high-risk patients, 25% actually readmit)
- Precision@50% recall: 18%

**Prospective study (100 patients):**

- Split: 50 patients assigned to care coordinator follow-up (AI identified high-risk); 50 standard care
- Result: 12% readmission in intervention group vs. 18% control (not statistically significant; small sample)
- Learnings: Patients identified by model did benefit from intervention, but sample size insufficient

**Deployment:**

- Daily: Score all admitted patients; flag top 10% highest risk
- Care coordinator reviews flagged patients, provides targeted education/follow-up
- Estimated impact: 5–10% reduction in readmissions = \$500K–1M savings annually
- Cost: \$200K development + \$50K/year operations
- ROI: Strong in year 2+

**30.6 Model Maintenance and Drift in Healthcare AI Systems**

Healthcare AI systems face severe and unique drift challenges that can directly impact patient safety. Unlike consumer applications where drift causes engagement loss, healthcare drift can cause diagnostic errors, inappropriate treatments, and patient harm. Medical knowledge evolves continuously as new research emerges, treatment guidelines change, and disease patterns shift. Patient populations change as demographics evolve and new diseases emerge. Clinical practice patterns vary across institutions and change over time. Electronic health record systems are upgraded, changing data formats and documentation practices. And critically, healthcare operates under strict regulatory oversight—model updates require validation and often regulatory approval, making rapid adaptation difficult.

The stakes are extraordinarily high. A sepsis prediction model that drifts from 85% to 80% sensitivity might miss 5% more cases—potentially hundreds of preventable deaths annually in a large health system. A radiology AI that degrades from 95% to 90% accuracy on pneumonia detection could cause thousands of misdiagnoses. A drug interaction checker that fails to incorporate new drug approvals could miss dangerous interactions. The business impact is equally severe: liability from AI-related errors, regulatory sanctions, loss of clinician trust, and reputational damage can be catastrophic.

### 30.6.1 Domain-Specific Drift Patterns in Healthcare

Healthcare drift manifests in several distinct ways, each requiring different detection and mitigation strategies:

**Medical knowledge evolution.** Medical knowledge advances rapidly through clinical trials, research publications, and guideline updates. Treatment recommendations change as new evidence emerges. A model trained on 2020 COVID-19 treatment data would be dangerously outdated by 2022 as treatments evolved from hydroxychloroquine (ineffective) to remdesivir to monoclonal antibodies to vaccines. Cancer treatment guidelines change annually as new therapies are approved. Diagnostic criteria are periodically revised (DSM-5 for psychiatric diagnoses, updated sepsis definitions). Models must incorporate this evolving knowledge or risk recommending outdated, potentially harmful treatments.

The challenge is that medical knowledge doesn't just expand—it sometimes reverses. Treatments once considered standard of care are later found harmful. Hormone replacement therapy for menopause, once widely recommended, was found to increase cardiovascular risk. Tight glucose control in ICU patients, once standard, was found to increase mortality. Models trained on historical data may learn patterns that are no longer valid or even dangerous.

**Disease pattern drift.** Disease prevalence and characteristics change over time. Infectious diseases emerge (COVID-19, monkeypox), evolve (antibiotic-resistant bacteria), and decline (polio, measles in vaccinated populations). Chronic disease prevalence shifts with demographics—diabetes and obesity increasing, smoking-related diseases declining. Disease presentations change—younger patients experiencing conditions previously seen only in elderly. Seasonal patterns shift with climate change. Models trained on historical disease patterns may fail to recognize emerging diseases or changing presentations.

Example: A pneumonia detection model trained on pre-COVID data performed poorly on COVID pneumonia, which has distinct radiographic features. Models required rapid retraining on COVID data to maintain accuracy. Similarly, antibiotic resistance patterns change annually, requiring drug recommendation models to update resistance predictions continuously.

**Population demographic drift.** Patient populations evolve as demographics change. Aging populations increase prevalence of age-related conditions. Immigration changes disease prevalence (tropical diseases in temperate regions). Socioeconomic changes affect health (opioid epidemic, mental health crisis). Models trained on one population may perform poorly on shifted populations. A model trained on predominantly white populations may have lower accuracy on minority populations due to different disease presentations, genetic factors, and social determinants of health.

This drift is particularly concerning for health equity. If models are not continuously validated across demographic groups, performance disparities can widen over time, exacerbating healthcare inequities. A sepsis model that drifts to lower sensitivity in Black patients could worsen existing disparities in sepsis outcomes.

**Clinical practice pattern drift.** How clinicians practice medicine changes over time. Documentation practices evolve—more structured templates, different terminology, varying detail levels. Diagnostic testing patterns change—more imaging, different lab panels, new biomarkers. Treatment patterns shift—new medications, different dosing, alternative therapies. Hospital workflows change—shorter stays, more outpatient procedures, telemedicine adoption. Models trained on historical practice patterns may misinterpret current data.

Example: A readmission prediction model trained when average hospital stay was 5 days may perform poorly when stays average 3 days—patients are sicker at discharge, changing risk profiles. A clinical note analysis model trained on narrative notes may fail on structured template notes. Models must adapt to these practice changes.

**EHR system and data format drift.** Electronic health record systems are periodically upgraded, changing data formats, coding systems, and documentation workflows. ICD-9 to ICD-10 transition changed diagnosis coding entirely. LOINC codes for lab tests are updated. Medication databases change as drugs are approved, discontinued, or renamed. EHR vendor changes (Epic to Cerner) completely alter data structure. Models tightly coupled to specific data formats break when formats change.

This technical drift is often abrupt rather than gradual. An EHR upgrade can happen overnight, immediately breaking models that depend on specific data formats. Unlike gradual performance degradation, this causes sudden complete failures. Robust models must be designed with data format flexibility

and validated after any EHR system changes.

**Regulatory and guideline drift.** Clinical guidelines are periodically updated by professional societies. Sepsis-3 criteria replaced Sepsis-2, changing how sepsis is defined and diagnosed. Hypertension thresholds were lowered from 140/90 to 130/80, instantly reclassifying millions of patients. Diabetes diagnostic criteria have evolved. Models using outdated criteria may misclassify patients or recommend inappropriate treatments. Regulatory requirements also change—FDA guidance on AI/ML medical devices is evolving, potentially requiring model updates to maintain compliance.

**Seasonal and epidemic drift.** Healthcare exhibits strong seasonal patterns—influenza in winter, allergies in spring, trauma in summer. Models must adapt to these predictable patterns. Unpredictable epidemics create sudden drift—COVID-19 dramatically changed disease prevalence, hospital workflows, and patient populations. Models trained on pre-epidemic data failed during epidemics. Epidemic preparedness requires models that can rapidly adapt to novel disease patterns.

**Key Point 30.1.** *For the generic drift detection and continuous learning framework, see Chapter 24, Section 24.7. Healthcare requires the most rigorous validation of any domain: each retrained model must pass offline validation, prospective validation, subgroup equity analysis, clinical expert review, and regulatory assessment before deployment.*

Key healthcare-specific strategies beyond the generic framework include:

- **Prospective validation cohorts:** Maintain ongoing cohorts (e.g. 1,000 cases/month with expert ground truth) for unbiased performance monitoring—the gold standard for safety-critical applications.
- **Guideline-aware models with updateable knowledge:** Design models that explicitly incorporate clinical guidelines (e.g. Sepsis-3 criteria) as modular components, enabling targeted updates when guidelines change without full retraining.
- **Federated learning for multi-institutional adaptation:** Train across institutions without sharing patient data (HIPAA compliance), enabling learning from diverse populations while maintaining privacy.
- **Regulatory-compliant update pathways:** Work with FDA to establish predetermined change control plans that pre-approve specific update types (retraining on new data, hyperparameter tuning), enabling more frequent updates within regulatory guardrails.
- **Subgroup equity monitoring:** Track performance separately for clinically relevant subgroups (age, sex, race/ethnicity, disease severity) to prevent drift from widening health disparities.

## 30.7 Case Study: Clinical Risk Prediction at Scale

A large health system wants to identify high-risk patients for preventive care intervention.

### 30.7.1 System Design

**Target:** Predict 30-day readmission risk for patients with chronic conditions

**Data:** The system uses comprehensive historical data to train the prediction model.

The dataset includes 100,000 patients with 500,000 admissions from historical records, providing substantial training data. EHR features comprise 50,000 unique clinical notes capturing narrative clinical information and 200 structured variables including lab values, vital signs, and medications. The outcome is readmission within 30 days, which occurs at a 15% positive rate, creating a class imbalance challenge that must be addressed during training.

**Model Architecture:** The system uses a multi-modal architecture that combines text and structured data.

The clinical notes encoder uses ClinicalBERT to process narrative documentation, capturing clinical reasoning and observations that aren't available in structured data. Structured data processing uses an embedding layer for categorical variables (like diagnosis codes and medication names) and direct concatenation for numeric values (lab results, vital signs). Fusion combines note embeddings and structured features via attention mechanisms, allowing the model to learn which combinations of text and structured signals are most predictive. The output layer applies logistic regression on a 50-dimensional combined representation to produce the final readmission risk score.

### 30.7.2 Results

**Offline validation (test set):** Initial validation on held-out historical data demonstrates strong predictive performance.

AUROC of 0.84 indicates strong predictive signal, with the model effectively distinguishing high-risk from low-risk patients. Precision at 20% recall reaches 25%, meaning that of flagged high-risk patients, 25% actually readmit—five times the base rate. Precision at 50% recall is 18%, showing that even when capturing half of all readmissions, the model maintains precision well above the baseline.

**Prospective study (100 patients):** A small prospective trial tests the intervention in real clinical practice.

The study splits patients into two groups: 50 patients assigned to care coordinator follow-up based on AI-identified high risk, and 50 receiving standard care. Results show 12% readmission in the intervention group versus 18% in control, a promising trend but not statistically significant due to the small sample size. The key learning is that patients identified by the model did benefit from intervention, but a larger sample is needed to demonstrate statistical significance.

**Deployment:** The system operates daily to support preventive care.

Daily scoring evaluates all admitted patients and flags the top 10% at highest risk for readmission. Care coordinators review flagged patients and provide targeted education and follow-up interventions tailored to each patient's specific risk factors. Estimated impact projects a 5–10% reduction in readmissions, which translates to significant cost savings and improved patient outcomes. The cost structure includes \$200,000 for initial development and \$50,000 per year for ongoing operations, making the system economically viable given the high cost of readmissions.

## 30.8 Exercises

**Exercise 30.1.** Design an EHR model to predict hospital-acquired infections. What data sources would you use? How would you handle temporal dependencies (infections develop over days)? What are the regulatory considerations?

**Exercise 30.2.** Propose a radiology report generation system. Given a chest X-ray image, generate a clinical report describing findings. What evaluation metrics would you use? How would you ensure quality and safety?

**Exercise 30.3.** Build a protein structure prediction system using ESMFold or AlphaFold2. Predict structures for 10 proteins with known experimental structures from the PDB. Evaluate using TM-score, LDDT, and RMSD. Compare single-sequence mode (ESMFold) versus MSA mode (AlphaFold2) performance. For which proteins does MSA provide significant improvement? Analyze confidence scores (pLDDT) and identify low-confidence regions—do they correspond to disordered regions or prediction errors?

**Exercise 30.4.** Implement a virtual screening pipeline for drug discovery. Select a target protein (e.g., SARS-CoV-2 Mpro protease, PDB: 6LU7). Screen a library of 10,000 compounds from ZINC using molecular docking (AutoDock Vina or similar). Rank compounds by predicted binding affinity. Select the top 100 hits and evaluate their drug-likeness using Lipinski’s Rule of Five. Compare your top hits to known inhibitors—did you rediscover any? Calculate enrichment factor if known actives are available in your library.

**Exercise 30.5.** Build a de novo drug design system using a transformer-based generative model. Train on ChEMBL compounds (or use a pre-trained model like MolGPT). Generate 1,000 novel molecules conditioned on desired properties (e.g., molecular weight 300-500, logP 2-4). Evaluate generated molecules for: (1) validity (percentage of valid SMILES), (2) uniqueness (percentage of unique molecules), (3) novelty (percentage not in training data), (4) drug-likeness (percentage passing Lipinski’s Rule of Five). Implement a simple reinforcement learning loop to optimize for a specific property (e.g., predicted solubility).

**Exercise 30.6.** For variant effect prediction, build a model using ESM-2 embeddings. Download ClinVar variants (pathogenic and benign). For each variant: (1) extract the affected protein sequence, (2) compute wild-type embedding using ESM-2, (3) compute variant embedding, (4) measure embedding distance or train a classifier on embedding differences. Evaluate classification accuracy, precision, recall, and ROC-AUC. Compare to existing tools like PolyPhen-2 or SIFT. Analyze failure cases—which types of variants are hardest to classify?

## 30.9 Solutions

Full solutions for all exercises are available at <https://deeplearning.hofkensvermeulen.be>.



## Chapter 31

# Finance, Risk, and Time Series Modeling

### Chapter Overview

Financial services represent one of the most data-intensive and competitive industries in the world, where milliseconds matter and billions of dollars are at stake. Global financial markets trade over \$6 trillion daily in foreign exchange alone. Credit card fraud costs \$28 billion annually. Credit decisions affect millions of consumers and trillions in lending. Algorithmic trading accounts for 60-75% of US equity trading volume. In this environment, even marginal improvements in prediction accuracy, fraud detection, or risk management translate to enormous competitive advantages and financial returns.

This chapter examines how transformers and deep learning are transforming financial services across three critical domains: market prediction and algorithmic trading, financial text analysis for investment decisions, and credit risk assessment. Each domain presents unique challenges and opportunities. Market prediction faces non-stationary time series where patterns change constantly and historical data provides limited guidance. Financial NLP must process earnings calls, SEC filings, and news in real-time to extract actionable insights before markets react. Credit modeling must balance predictive accuracy with fairness, explainability, and regulatory compliance.

The business stakes are extraordinary. A hedge fund with a 1% edge in market prediction can generate hundreds of millions in annual returns. A fraud detection system that improves accuracy by 2% saves tens of millions in prevented losses. A credit model that reduces default rates by 0.5% while maintaining approval rates generates millions in reduced losses. These improvements compound over time, creating sustainable competitive advantages in an industry where competitors are constantly innovating.

However, financial AI faces unique challenges that make it fundamentally different from other domains. Markets are adversarial—as soon as a profitable pattern is discovered and exploited, it disappears as others exploit it too. Non-stationarity is severe—market regimes shift suddenly during crises, rendering historical models useless. Regulatory scrutiny is intense—models must be explainable, auditable, and fair. Data is limited—unlike computer vision with millions of images, financial history provides only decades of data with few independent samples. And critically, financial AI operates in a zero-sum environment—your gain is someone else’s loss, creating intense competitive pressure and secrecy.

This chapter provides the technical foundation and business context to build financial AI systems that navigate these challenges. We examine successful strategies, regulatory requirements, risk management frameworks, and the economic models that make financial AI viable despite its unique difficulties. The focus is on practical deployment: what works in production, what fails, and why.

### Learning Objectives

1. Understand financial time series, stationarity, and non-stationarity
2. Build transformer-based models for price prediction and risk forecasting

3. Extract information from financial text: earnings calls, news, SEC filings
4. Design credit scoring systems aligned with fairness and regulatory requirements
5. Implement risk management workflows: backtesting, stress testing, VaR estimation
6. Address regulatory requirements: explainability, model validation, governance
7. Understand evaluation metrics specific to finance (Sharpe ratio, maximum drawdown, win rate)

## 31.1 Market Data and Time Series Forecasting

Financial time series (stock prices, exchange rates, commodities) are notoriously difficult to predict. They are non-stationary (mean and variance change over time) and driven by news, sentiment, and complex market dynamics.

### 31.1.1 Time Series Characteristics

**Definition 31.1** (Non-Stationary Time Series). A time series is non-stationary if its statistical properties (mean, variance, autocorrelation) change over time. Financial returns are approximately stationary (mean 0, variance varies); prices themselves are non-stationary.

Deep learning faces several fundamental challenges when applied to financial time series. Non-stationarity is perhaps the most severe: models trained on 2020 data often fail completely in 2024 as market regimes evolve and statistical properties change. This is compounded by regime shifts, where market behavior changes suddenly and dramatically—the 2008 financial crisis, COVID-19 crash, and 2022 inflation shock all represented regime shifts that broke many quantitative models overnight. Models must continuously adapt to these changing conditions or risk catastrophic failure.

The limited data problem is unique to finance. Unlike computer vision with millions of labeled images or NLP with billions of text documents, financial markets provide only decades of historical data with relatively few independent samples. A model trained on 10 years of daily data has only 2,500 trading days—far fewer than the millions of examples typical in other domains. This scarcity makes overfitting a constant danger: with few samples and many parameters, models easily memorize noise rather than learning genuine patterns. Finally, look-ahead bias—accidentally using future information during training—is surprisingly easy to introduce and can make worthless models appear profitable in backtesting.

### 31.1.2 Transformer-Based Time Series Models

Transformers, originally designed for sequences, adapt well to time series:

**Definition 31.2** (Temporal Transformer for Time Series). 1. **Input:** Past  $L$  trading days of OHLCV (open, high, low, close, volume) data

2. **Embedding:** Project each day's features to  $d$ -dimensional space
3. **Position encoding:** Time-based position encodings; relative time differences matter
4. **Transformer encoder:** Self-attention allows model to weight recent vs. older prices
5. **Output:** Predict next day's close price or return

Transformers offer several key advantages for financial time series modeling. Parallelization enables processing the entire price history simultaneously, unlike RNNs which must process sequences step-by-step. This dramatically reduces training time and enables efficient use of modern GPU hardware. The

attention mechanism naturally captures long-range dependencies, allowing the model to identify patterns like mean reversion over months or seasonal effects over years—relationships that RNNs struggle to learn due to vanishing gradients. Finally, attention weights provide interpretability by revealing which historical days most influenced each prediction, helping traders understand and trust model decisions.

### 31.1.3 Addressing Non-Stationarity

Several techniques help address non-stationarity in financial models. Differencing transforms the problem by modeling log-returns instead of raw prices—returns are approximately stationary with mean near zero, while prices exhibit clear trends and non-stationarity. Normalization standardizes features to zero mean and unit variance before feeding them to the model, preventing scale differences from dominating learning. Regime detection explicitly models market state changes, using different models or parameters for bull markets, bear markets, and crisis periods. Online learning continuously retrains models on recent data, weighting recent observations more heavily to adapt to current conditions. Finally, ensemble methods combine predictions from models trained on different time periods, providing robustness when any single model fails due to regime changes.

### 31.1.4 Evaluation and Backtesting

Standard accuracy metrics (RMSE, MAE) are misleading for trading. A model could predict prices with low RMSE but lose money trading.

Trading-specific metrics evaluate what actually matters for profitability. The Sharpe ratio measures risk-adjusted returns by dividing average return by volatility—higher values indicate better performance per unit of risk, with values above 1.0 considered good and above 2.0 exceptional. Maximum drawdown captures the largest peak-to-trough decline, critical for risk management since large drawdowns can trigger margin calls or investor redemptions regardless of long-term returns. Win rate measures the fraction of profitable trades, though a strategy can be profitable with low win rate if winning trades are much larger than losing trades. Profit factor divides gross profits by gross losses, with values above 1.5 indicating robust strategies. The Calmar ratio divides annualized return by maximum drawdown, rewarding strategies that generate returns without large drawdowns.

Rigorous backtesting requires several critical practices. Walk-forward validation prevents look-ahead bias by training on historical data and testing on subsequent periods, then rolling forward: train on year 1, test on year 2, retrain on years 1-2, test on year 3, and so on. This simulates realistic deployment where models only have access to past data. Transaction costs must include all real-world expenses: commissions, bid-ask spreads, and slippage (the difference between expected and actual execution prices). Market impact modeling accounts for how large orders move prices against the trader—a strategy that works with small positions may fail at scale. Regulatory requirements impose capital requirements, position limits, and reporting obligations that constrain real-world trading. Finally, out-of-sample testing on completely held-out recent data provides the ultimate validation before deployment, ensuring the model works on data it has never seen during development.

## 31.2 Financial NLP

Markets are driven by information. News, earnings reports, and regulatory filings move prices. NLP extracts this information.

### 31.2.1 Financial Domain Text

Financial text comes in several distinct forms, each with unique characteristics and information content. Earnings calls provide transcripts of quarterly conference calls where company executives discuss results and answer analyst questions—forward guidance and management tone often signal future performance before it appears in financial statements. SEC filings include 10-K annual reports, 10-Q quarterly reports, and 8-K event disclosures, containing detailed financial and operational information required by regulators. News from Reuters, Bloomberg, and CNBC is highly time-sensitive, with price reactions

occurring within seconds of publication. Analyst reports from investment banks provide buy, hold, or sell recommendations with significant influence on institutional investors. Finally, Twitter and social media capture retail sentiment, rumors, and market commentary that increasingly affects stock prices, particularly for retail-popular stocks.

### 31.2.2 Information Extraction

Information extraction from financial text involves several key tasks. Named entity recognition identifies companies, executives, and financial instruments mentioned in text, enabling tracking of which entities are discussed and in what context. Event extraction detects significant occurrences like merger and acquisition announcements, earnings surprises, and executive changes—events that typically trigger immediate market reactions. Sentiment analysis classifies text tone as positive, negative, or neutral, capturing market psychology and expectations. Relationship extraction identifies connections between entities, such as which company acquired whom or which companies compete in the same market, building knowledge graphs of corporate relationships.

Consider a news headline: “Apple Announces Record Q4 Revenue; Beats Analyst Expectations.” Information extraction would identify the company as Apple, classify the event as an earnings announcement, extract the metric as Q4 revenue, and determine the sentiment as positive based on the words “record” and “beats expectations.” The predicted market impact would be a likely stock price increase, as positive earnings surprises typically drive immediate buying. This structured information can then feed into trading algorithms that act on news before human traders can react.

### 31.2.3 Sentiment Analysis for Trading

Aggregate sentiment from multiple sources to predict price movements:

1. Collect news, social media, analyst sentiment from past hour
2. Compute aggregate sentiment score (weighted average)
3. If sentiment strongly positive and persistent, go long; strongly negative, go short
4. Backtest: Does this strategy beat a buy-and-hold baseline?

Practical results: Simple sentiment strategies achieve 50–55% win rate (barely above random), but with low transaction costs and diversification, can be profitable.

## 31.3 Credit Modeling and Risk Management

Credit scoring determines who gets loans and at what interest rate. Deep learning has improved credit modeling, but fairness and explainability are critical.

### 31.3.1 Credit Risk Assessment

Deep learning enables credit models to incorporate richer information than traditional approaches. Time series analysis processes payment history over years rather than just summary statistics, capturing patterns like seasonal payment behavior or gradual deterioration. Text analysis examines loan applications and borrower explanations, where unusual language patterns or inconsistencies may indicate fraud or misrepresentation. Network analysis identifies relationships between borrowers, detecting fraud rings where multiple applications share suspicious connections. Behavioral analysis tracks how borrowers interact with the application system—hesitation, multiple retries, or unusual navigation patterns can signal uncertainty or deception.

### 31.3.2 Deep Learning for Credit

**Definition 31.3** (Credit Default Prediction). Given borrower features (income, credit history, collateral, payment patterns), predict probability of default within specified time horizon (12 months, 3 years).

Model:  $P(\text{default} = 1 \mid \text{features}) = \text{logistic}(\text{neural network})$

Loss: Cross-entropy on default labels (highly imbalanced: 2–5% default rate)

Deep learning credit models employ several architectural components. Feature embedding encodes categorical variables like employment status and zip code as learned dense vectors, capturing semantic similarities (e.g., neighboring zip codes have similar embeddings). Temporal modules use LSTMs or transformers to process payment history sequences, learning patterns like improving or deteriorating payment behavior over time. Attention mechanisms identify which factors most influenced each decision, providing interpretability required for regulatory compliance. Regularization through L1/L2 penalties and dropout prevents overfitting, critical when default examples are scarce (typically 2–5

### 31.3.3 Fairness in Credit Decisions

Regulatory requirements (Fair Credit Reporting Act, Equal Credit Opportunity Act) prohibit discrimination on protected attributes (race, gender, religion). Yet models trained on historical data inherit biases:

If minorities historically received higher interest rates, the model learns to predict higher risk for minorities.

Several approaches address fairness in credit decisions. Constraint-based fairness requires equal acceptance rates across demographic groups, enforced during training through constrained optimization. Adversarial debiasing adds a classifier that attempts to predict protected attributes from model predictions, then trains the main model to fool this classifier—if the adversary cannot predict race from the model’s outputs, the model is not using race as a proxy. Continuous monitoring measures disparate impact in production, alerting when approval rates diverge across groups beyond acceptable thresholds. Threshold tuning adjusts decision boundaries separately for each demographic group to achieve equal approval rates, though this approach raises legal questions about differential treatment.

### 31.3.4 Explainability for Credit Decisions

When a loan is denied, applicants have the right to explanation. “The AI said no” is insufficient.

Several interpretability methods provide explanations for credit decisions. SHAP values decompose each prediction into contributions from individual features, showing exactly how much each factor (income, credit score, payment history) influenced the decision. Attention analysis reveals which factors the model weighted most heavily, providing insight into the decision process. Counterfactual explanations answer “what if” questions: “If your income were \$10,000 higher, you would be approved”—giving applicants actionable guidance. Prototype examples show similar applicants who were approved, helping applicants understand what successful profiles look like and how their application compares.

## 31.4 Risk Management and Regulatory Requirements

Financial institutions are heavily regulated. Models used for trading or lending must be validated and auditable.

### 31.4.1 Model Risk Management Framework

Financial regulations require comprehensive model risk management. Model documentation must provide detailed specifications of the model architecture, training data, assumptions, and known limitations—sufficient for independent reviewers to understand and reproduce the model. Governance requires model review and approval by a risk committee before deployment, with ongoing oversight and periodic re-approval. Validation involves independent testing on data not used in development,

performed by teams separate from model developers to ensure objectivity. Monitoring tracks ongoing performance in production, alerting when metrics degrade beyond acceptable thresholds. Backtesting compares historical predictions against actual outcomes to verify model accuracy and calibration. Stress testing evaluates performance under extreme market conditions like the 2008 financial crisis or COVID-19 crash, ensuring models remain safe during tail events.

### 31.4.2 Value at Risk (VaR) Estimation

VaR is the maximum loss expected at a given confidence level (e.g., 95% VaR for a portfolio).

Deep learning provides a more sophisticated approach to VaR estimation. Rather than assuming returns follow a normal distribution (an assumption frequently violated in financial markets), neural networks or flow-based models learn the actual return distribution from data, capturing fat tails, skewness, and other non-normal characteristics. The model can then sample from this learned distribution or use quantile regression to directly estimate VaR at the desired confidence level (e.g., 95th or 99th percentile). This approach produces more accurate VaR estimates that better capture tail risk—the extreme losses that matter most for risk management but are poorly modeled by traditional parametric methods.

## 31.5 Case Study: Fraud Detection System

A payment processor wants to detect fraudulent transactions in real-time.

### 31.5.1 Problem Setup

The fraud detection problem presents several challenges. The dataset contains 10 billion transactions annually with only 0.1

### 31.5.2 Model Architecture

The fraud detection architecture combines multiple components. Features include card ID, merchant information, transaction amount, location, time, and velocity metrics like transactions per card per hour. Embeddings encode high-cardinality categorical variables like card ID, merchant category, country, and device fingerprint as dense vectors. Temporal modeling uses RNNs or transformers to process the sequence of past 10 transactions for each card, learning patterns like normal spending behavior versus suspicious sequences. The output is a fraud probability score; transactions exceeding a threshold trigger additional verification like two-factor authentication or manual review.

### 31.5.3 Results

Offline evaluation measured performance on historical data. The key metric was recall at 1

Online deployment results demonstrated real-world effectiveness. The system achieved 88

## 31.6 Model Drift in Financial Systems

Financial AI systems face unique drift challenges that distinguish them from other domains. The general framework for understanding and managing model drift is presented in Chapter 24; here we focus on finance-specific patterns.

### 31.6.1 Finance-Specific Drift Patterns

**Market regime shifts** cause sudden, fundamental changes in the relationships that models have learned. A model trained during a bull market may fail catastrophically during a bear market or financial crisis because the statistical relationships between features change qualitatively, not just quantitatively. The 2008 financial crisis, COVID-19 crash, and 2022 inflation shock all broke quantitative

models that had not been exposed to comparable regimes. For example, a volatility model trained on 2015–2019 data predicted VIX below 20; in March 2020, VIX spiked to 80.

**Alpha decay** is unique to trading models: as more market participants discover and exploit a predictive signal, the signal weakens through market efficiency. A trading strategy that generates 5% annual returns may see returns decay to 1–2% within 12–18 months as competitors adopt similar approaches. The industry average alpha half-life is estimated at 2–3 years, with high-frequency strategies decaying within months.

**Adversarial fraud evolution** occurs because fraudsters actively adapt to detection models. Unlike natural drift where the data distribution shifts gradually, fraud patterns change deliberately and rapidly in response to detection. New fraud schemes—geographic shifts, velocity changes, amount manipulation, synthetic identities—can emerge within weeks of a model deployment, requiring continuous model updates.

**Regulatory drift** arises from changing compliance requirements (e.g., Basel III to Basel IV, new stress testing mandates, interest rate regime changes) that alter the features, constraints, or objectives of financial models. When the Federal Reserve raised rates from 0% to 5% in 2022–2023, models trained in the zero-rate environment required complete recalibration.

**Economic cycle drift** affects credit models as borrower behavior differs between expansion and recession. A mortgage model trained on 2010–2019 expansion data predicted 2% defaults; during the 2020 recession, actual defaults reached 5%, causing hundreds of millions in unexpected losses.

### 31.6.2 Monitoring and Adaptation

Financial drift detection requires domain-specific metrics: Sharpe ratio and drawdown for trading, precision/recall for fraud, calibration accuracy for credit. Use walk-forward validation continuously and implement regime detection (hidden Markov models or clustering on volatility patterns) to trigger model switching. For fraud detection, conduct regular adversarial red-teaming. Retrain aggressively: trading models weekly, fraud models daily, credit models quarterly. See Chapter 24 for the general continuous learning framework.

**Key Point 31.1.** *Financial drift patterns are distinguished by their adversarial nature (fraud), reflexivity (alpha decay), and regime-dependent behavior (market shifts). Standard drift detection approaches from Chapter 24 must be augmented with regime-aware monitoring and adversarial robustness testing specific to financial applications.*

## 31.7 Exercises

**Exercise 31.1.** Build a time series model for stock price prediction. Train on 5 years of historical S&P 500 data. Evaluate using Sharpe ratio and maximum drawdown in addition to RMSE. Can you beat a buy-and-hold baseline?

**Exercise 31.2.** Extract events from earnings call transcripts. Identify mentions of: new products, executive changes, competitive threats, guidance changes. Build a classifier to predict stock price movement after earnings announcement.

**Exercise 31.3.** Design a fair credit scoring model. Start with a baseline model that uses standard features. Measure disparate impact (difference in approval rates across demographic groups).

Apply debiasing techniques. Can you reduce disparate impact while maintaining predictive power?

## 31.8 Solutions

Full solutions for all exercises are available at <https://deeplearning.hofkensvermeulen.be>.



## Chapter 32

# Legal, Contracts, and Governance Copilots

### Chapter Overview

The legal industry represents a \$1 trillion global market characterized by high costs, limited access, and labor-intensive processes. A single commercial contract review can cost \$5,000-50,000 in legal fees and take weeks to complete. Legal research for a complex case can consume hundreds of attorney hours at \$300-1,000 per hour. Due diligence for mergers and acquisitions requires reviewing thousands of documents, costing millions. These costs create barriers to justice—individuals and small businesses often cannot afford legal services, while large organizations spend enormous sums on routine legal work.

This chapter examines how transformers and deep learning are transforming legal services through contract analysis, legal research automation, and compliance monitoring. The potential business impact is substantial. Automating routine contract review could save law firms 40-60% of associate time, reducing costs by millions annually while improving consistency. AI-powered legal research could reduce research time by 50-70%, saving clients hundreds of thousands per case. Compliance automation could prevent violations that cost companies millions in fines and remediation.

However, the legal domain presents unique challenges that make AI deployment particularly difficult. Legal text is highly structured and formal—a single misread word can change liability by millions of dollars. Ambiguity is expensive and potentially catastrophic. Lawyers are professionally liable for their work product, creating extreme risk aversion toward AI tools. Bar associations impose strict ethical requirements on AI use. Hallucination—where AI systems generate plausible but false information—is completely unacceptable in legal contexts. A fabricated case citation constitutes malpractice and can result in sanctions, disbarment, and liability.

The stakes extend beyond business costs to fundamental questions of justice and professional responsibility. If AI makes legal services more affordable, it could democratize access to justice for millions. However, if AI provides incorrect legal advice, it could cause severe harm to individuals who rely on it. If AI perpetuates biases in legal decision-making, it could exacerbate systemic inequities. These concerns create intense scrutiny from regulators, bar associations, and the legal profession itself.

This chapter provides the technical foundation and business context to build legal AI systems that balance innovation with professional responsibility, automation with human oversight, and efficiency with accuracy. We examine successful deployments, ethical frameworks, and the economic models that make legal AI viable despite its unique challenges. The focus is on AI as copilot—augmenting lawyer capabilities rather than replacing lawyer judgment.

### Learning Objectives

1. Understand legal text structure: statutes, case law, contracts, and regulatory documents
2. Build models for contract analysis: clause extraction, risk assessment, obligation identification
3. Implement legal research systems combining semantic search with structured reasoning

4. Design compliance monitoring to detect policy violations
5. Address lawyer skepticism: build trustworthy systems with explanations and human oversight
6. Handle domain-specific challenges: long documents, obscure precedents, evolving law
7. Understand regulatory and ethical constraints in legal AI

## 32.1 Legal Text as Formal Language

Legal documents are among the most structured and formal texts in existence. Precision matters; a single word can change liability.

### 32.1.1 Hierarchical Structure of Legal Documents

**Definition 32.1** (Legal Document Structure). Legal documents follow distinct structural patterns depending on their type. Statutes and regulations are hierarchically organized from Title down through Chapter, Section, Subsection, to individual Clauses, with each level carrying defined legal meaning and scope. Case law follows a standardized format beginning with case name, year, and court, then proceeding through Facts, Legal Issue, Holding, and Reasoning—with precedent value being critical for future cases. Contracts are structured into sections covering parties, recitals, definitions, terms, conditions, and signatures, with extensive cross-references to defined terms throughout. Regulatory documents contain rules, interpretations, and guidance that are often redundant across versions, with the latest version superseding earlier ones.

### 32.1.2 Formal Language Elements

Legal language has precise meanings often divorced from common usage:

Legal language employs precise meanings that often diverge from common usage. Defined terms establish specific meanings—for example, “Customer” is defined with a specific definition, and all subsequent uses refer exclusively to that definition. Conditions create obligations through if-then structures: “If X occurs, then Y is obligated to Z.” Exceptions modify obligations by carving out specific circumstances: “X is liable for damages except where caused by force majeure.” Temporal language has precise legal effects—“Effective as of [date]” differs legally from “Retroactive to [date].” Negations are critical to parse correctly, as “Party A shall not be liable for indirect damages” negates liability entirely.

### 32.1.3 Domain-Specific Ontology

Legal concepts form a formal ontology:

Legal concepts form a formal ontology that models must learn to understand contracts meaningfully. Parties include signatories, beneficiaries, and third-party beneficiaries, each with different rights and obligations. Rights encompass grants, restrictions, terminations, and remedies available to parties. Obligations specify performance requirements, conditions precedent (what must occur before obligations arise), and conditions subsequent (what terminates obligations). Remedies include damages, injunctions, specific performance, and indemnification. Risk allocation determines who bears risk of loss, establishes liability caps, and defines force majeure exceptions.

## 32.2 Contract Analysis and Document Understanding

Contract review is time-consuming. A 50-page commercial contract can take hours for a lawyer to review, identifying key terms, risks, and obligations.

### 32.2.1 Key Contract Elements

A contract review system should extract:

A comprehensive contract review system should extract several critical elements. It must identify the parties to the contract and determine the effective date when the contract becomes binding. The system should extract term and termination provisions, including duration, renewal conditions, and termination rights with their consequences. Payment terms covering price, payment schedule, late fees, and currency must be identified. Conditions precedent—what must occur before obligations arise—require extraction. Representations and warranties, where each party asserts certain facts to be true, must be captured. Indemnification clauses specifying who indemnifies whom for what circumstances are critical. Limitation of liability provisions, including caps on damages and exclusions of consequential damages, significantly affect risk allocation. Confidentiality obligations covering trade secrets, non-disclosure requirements, and exceptions must be identified. Finally, dispute resolution mechanisms including governing law, jurisdiction, arbitration procedures, and available remedies must be extracted.

### 32.2.2 Architecture for Contract Analysis

A practical system combines multiple components:

1. **Preprocessing:** OCR if scanned; extract text, resolve formatting issues
2. **Segmentation:** Identify sections and subsections; group related clauses
3. **Clause extraction:** For each clause, extract type (payment, termination, etc.)
4. **Entity extraction:** Identify parties, dates, dollar amounts, products/services
5. **Obligation extraction:** For each obligation, identify: who, what, conditions, consequences
6. **Risk assessment:** Flag potentially problematic clauses (e.g., unlimited liability, broad indemnification)
7. **Comparison:** Compare to template or prior contracts; flag deviations
8. **Presentation:** Summarize findings in human-readable format for lawyer review

### 32.2.3 Deep Learning for Contract Understanding

#### Transformer-based approach:

Transformer-based approaches to contract understanding employ several techniques. Pre-training involves continued pre-training on legal corpora like LexGLUE, which contains diverse legal documents. Token classification marks each token as belonging to a specific clause type through binary classification per token. Relation extraction identifies relationships between entities and obligations, capturing the semantic structure of contracts. Multi-task learning jointly trains on clause classification, entity extraction, and obligation extraction, enabling the model to learn shared representations across these related tasks. Models like LegalBERT, which continues pre-training BERT on legal documents, achieve strong performance on legal NLP tasks.

## 32.3 Legal Research and Citation Networks

Legal research requires finding relevant cases, statutes, and prior interpretations. The space is massive: US federal law alone includes millions of statutes and cases.

### 32.3.1 Citation Networks and Precedent

Cases cite prior cases; legal concepts form a web of precedent. A case might cite 50+ prior cases, creating a citation graph. Understanding the graph is essential:

Citation networks and precedent form the foundation of legal reasoning. Cases cite prior cases, creating a web of precedent that defines legal concepts. A single case might cite 50 or more prior cases, building a complex citation graph. Understanding this graph is essential for legal research. Following precedent means a case must adhere to binding precedent from higher courts in the same jurisdiction. Distinguishing cases involves arguing why precedent doesn't apply because the facts differ materially. Overruling occurs when a higher court can overrule a lower court's decision, causing the law to change. Trends in case law matter—newer cases reflect evolved legal thinking, while old cases may be outdated or superseded by subsequent decisions.

### 32.3.2 Semantic Search for Legal Documents

A lawyer searching for relevant cases uses semantic search:

1. Encode query: "Can a company limit liability for product defects?"
2. Retrieve similar cases/statutes from vector database
3. Rank by relevance (semantic similarity) and recency
4. Lawyer reviews top cases to find binding precedent

Embedding models trained on legal data significantly outperform general-purpose embeddings for legal retrieval.

## 32.4 Compliance and Governance

Organizations must comply with complex regulations. A healthcare provider must follow HIPAA, FDA regulations, state laws, and institutional policies. Automated compliance monitoring catches violations early.

### 32.4.1 Policy Compliance Checking

Companies maintain internal policies (employee handbook, data security, procurement). Deep learning can check if documents or practices comply:

1. Extract policy rules from documents (e.g., "All contracts over \$100K require CFO approval")
2. Formalize rules as logical constraints
3. Monitor transactions/documents: Does this purchase order comply?
4. Alert if violation detected; escalate to compliance team

### 32.4.2 Regulatory Change Management

Regulations constantly evolve. A company must:

1. Monitor regulatory agencies for new rules
2. Understand impact: Which internal processes must change?
3. Update policies and systems
4. Validate compliance

NLP can automate steps 1 and 2: Detect new regulations relevant to the organization and suggest required policy changes.

## 32.5 AI Copilots for Lawyers

Rather than fully automating legal work (which would require extreme accuracy), practical systems are copilots: AI assists lawyers, who maintain control.

### 32.5.1 Copilot Design Principles

**Definition 32.2** (Legal AI Copilot Design). Effective legal AI copilots follow several critical design principles. Transparency requires showing reasoning—for flagged clauses, the system must cite the rule and explain why it’s flagged. Human authority ensures lawyers always make final decisions, with AI suggesting and humans confirming. Accuracy over recall prioritizes avoiding false positives, as it’s better to miss an issue than incorrectly flag one—false positives erode trust. Explainability means lawyers must understand why AI made each recommendation, as black boxes are unacceptable in legal practice. Scope clarity defines that AI handles specific tasks like clause extraction and citation finding, but is not intended for legal judgment. Training and oversight ensure lawyers are trained on system capabilities and limitations before use.

### 32.5.2 Practical Copilot Workflow

1. Lawyer uploads contract
2. System extracts key terms, identifies parties, effective dates
3. System compares to template: “Deviation: Liability cap is \$1M vs. template \$10M”
4. System flags risks: “Unlimited indemnification; consider capping”
5. Lawyer reviews system output; accepts, modifies, or rejects suggestions
6. System learns from feedback (important clause lawyer accepted but system flagged)
7. Lawyer completes review manually; system documents summary

## 32.6 Trust, Liability, and Ethical Concerns

Lawyers are professionally responsible for their work. If a lawyer relies on AI recommendation and it proves wrong, the lawyer is liable.

### 32.6.1 Professional Responsibility

Bar associations impose strict ethics rules governing AI use in legal practice. Lawyers must understand their tools and their limitations—ignorance is not a defense. Lawyers remain responsible for work product even if AI-assisted, maintaining full professional liability. Lawyers must communicate with clients about use of AI, obtaining informed consent where appropriate. Lawyers cannot use AI to create unauthorized practice of law, ensuring human lawyers maintain control over legal judgment.

### 32.6.2 Hallucination and Fabrication

LLMs can hallucinate case citations. A lawyer using an AI tool that cites “Smith v. Jones, 500 F.2d 123” must verify the citation exists. Hallucinated citations are malpractice.

Several mitigation strategies address the hallucination problem. Retrieval-based systems only cite cases actually in the database rather than generating citations, eliminating fabrication risk. Confidence scores allow models to express uncertainty, signaling to lawyers when verification is needed. Explicit non-recommendations acknowledge limitations: “I did not find direct precedent; here are related cases” rather than fabricating citations.

### 32.6.3 Access to Justice

AI-assisted legal work could democratize access, enabling individuals to understand contracts without expensive lawyers. However:

AI-assisted legal work could democratize access to justice, enabling individuals to understand contracts without expensive lawyers. However, significant challenges remain. An unbridged gap exists—AI for contract understanding is useful, but AI for legal strategy requires judgment that current systems cannot provide. Liability questions arise: if AI gives bad advice and a person is harmed, determining who is liable remains unclear. Regulation is evolving as bar associations develop rules for AI-assisted law practice, creating uncertainty about permissible uses.

## 32.7 Case Study: Contract Review and Risk Assessment

A commercial law firm wants to automate contract review for routine transactions.

### 32.7.1 System Design

- **Scope:** Review commercial contracts (purchase agreements, NDAs, service agreements). Not litigation or complex negotiations.
- **Data:** 5,000 prior contracts reviewed by lawyers; annotations of key terms, risks, deviations
- **Model:** Legal BERT fine-tuned on firm's data for clause extraction and risk classification
- **Interface:** Web app where associates upload contracts; system provides summary report

### 32.7.2 Workflow

1. Associate uploads contract PDF
2. System extracts text (OCR if needed)
3. System identifies parties, dates, payment terms, termination clauses, liability limitations
4. System compares to firm's templates; flags deviations
5. System scores risk (0–10 scale); flags high-risk clauses for attorney review
6. System generates summary report; attorney reviews and refines
7. System stores annotations; retrains monthly on attorney feedback

### 32.7.3 Results

#### Offline validation:

- Clause extraction F1: 0.88 (good; attorney reviews for misses)
- Risk classification: 0.82 precision (correct identification of risky clauses)
- False positive rate: 8% (acceptable; better to flag and have attorney dismiss than to miss risk)

#### Deployment impact:

- Time to first review: 30 minutes → 5 minutes (6x speedup)
- Attorney review time: 60 minutes → 45 minutes (better focused on actual risks)
- Error rate: ↓ 2% (misses or miscategorizations)
- Adoption: 80% of routine contracts use system; complex contracts reviewed manually
- Financial impact: \$500K annual savings (attorney time), \$200K cost (development + maintenance)

## 32.8 Model Maintenance and Drift in Legal AI Systems

Legal AI systems face unique drift challenges that combine technical complexity with professional liability concerns. Unlike other domains where drift causes business losses, legal drift can cause malpractice, regulatory violations, and harm to clients. The law itself evolves continuously—new statutes are enacted, regulations are updated, court decisions create new precedents, and legal interpretations shift. Contract language and business practices change as markets evolve. Legal terminology and drafting conventions vary across jurisdictions, practice areas, and time periods. A legal AI system trained on 2020 contracts may misinterpret 2024 contracts due to evolved language, new legal requirements, or changed business practices.

The professional stakes are extraordinary. A contract analysis system that misses a critical liability clause could expose a client to millions in damages. A legal research tool that cites outdated or overruled precedent could cause a lawyer to provide incorrect advice, constituting malpractice. A compliance monitoring system that fails to detect violations could result in regulatory penalties and reputational damage. Unlike consumer applications where errors cause frustration, legal errors cause professional liability, client harm, and potential disbarment.

The challenge is compounded by lawyers' professional responsibility. Lawyers are ethically obligated to provide competent representation and cannot delegate professional judgment to AI. Bar associations require lawyers to understand their tools and remain responsible for AI-assisted work product. This creates extreme risk aversion—lawyers will abandon AI tools that produce even occasional errors, as the professional risk outweighs the efficiency benefit. Legal AI must achieve near-perfect accuracy and provide transparent explanations to maintain lawyer trust.

### 32.8.1 Domain-Specific Drift Patterns in Legal AI

Legal drift manifests in several distinct ways, each requiring different detection and mitigation strategies:

**Legislative and regulatory changes.** Laws change constantly as legislatures enact new statutes, agencies issue new regulations, and existing laws are amended or repealed. A legal AI system must track these changes and update its understanding accordingly. Tax law changes annually. Employment law evolves with new worker protections. Privacy regulations (GDPR, CCPA) create new compliance requirements. Environmental regulations tighten or relax with political changes. Models trained on outdated law provide dangerous advice.

The challenge is that legal changes can be sudden and comprehensive. A new statute can completely change legal requirements overnight. A regulatory agency can issue guidance that reinterprets existing law. Models must be updated rapidly to reflect current law, but validation is difficult—there may be no case law yet interpreting the new statute, creating uncertainty about correct application.

Example: California Consumer Privacy Act (CCPA) enacted in 2018, effective 2020, created new data privacy requirements. Contracts drafted before CCPA lacked required privacy clauses. A contract analysis system trained on pre-CCPA contracts would fail to flag missing privacy provisions, exposing clients to regulatory violations. The system required immediate retraining on CCPA-compliant contracts and explicit rules for required privacy clauses.

**Case law evolution and precedent shifts.** Court decisions create binding precedent that changes legal interpretation. Higher courts can overrule lower courts, changing established law. Legal doctrines evolve as courts apply law to new factual situations. A legal research system must track these precedent changes and understand which cases are still good law versus overruled or distinguished.

The challenge is that precedent changes are nuanced. A case might be overruled on one issue but remain good law on others. A case might be distinguished (held not to apply) based on factual differences. Understanding these distinctions requires legal reasoning that goes beyond simple text matching. Additionally, circuit splits (different courts reaching different conclusions) create uncertainty about which precedent applies.

Example: Employment law on arbitration agreements evolved significantly from 2010-2020. Early cases upheld broad arbitration clauses. Later cases found some clauses unconscionable. A legal research system citing 2010 cases without noting subsequent limitations would provide misleading guidance. The

system must track case history and flag when precedent has been limited or overruled.

**Contractual language evolution.** Contract drafting conventions evolve over time. New clause types emerge to address new business models (SaaS agreements, data processing agreements). Standard terms change as market practices evolve (force majeure clauses expanded after COVID-19). Legal terminology shifts (older contracts use different terms than modern contracts). Models trained on historical contracts may misinterpret modern contracts or fail to recognize new clause types.

Example: Force majeure clauses traditionally covered "acts of God" (natural disasters). After COVID-19, force majeure clauses explicitly list pandemics, government shutdowns, and supply chain disruptions. A contract analysis system trained on pre-COVID contracts might not recognize pandemic-specific force majeure language, failing to properly categorize these clauses. The system requires re-training on post-COVID contracts to understand evolved force majeure provisions.

**Jurisdiction-specific variations.** Legal requirements vary significantly across jurisdictions (federal vs. state, US vs. EU, common law vs. civil law). Contract interpretation rules differ by jurisdiction. Regulatory requirements vary by industry and location. A model trained primarily on one jurisdiction may perform poorly on another. As firms expand practice areas or geographic coverage, models must adapt to new jurisdictions.

Example: Employment contracts in California have different requirements than New York (non-compete clauses largely unenforceable in California, enforceable in New York). A contract review system trained on New York contracts might incorrectly flag California non-compete clauses as enforceable, providing wrong advice. The system must be jurisdiction-aware and trained on jurisdiction-specific contracts.

**Practice area and industry drift.** Different practice areas (corporate, litigation, IP, employment) use different language and conventions. Industries have specialized contract types (construction, healthcare, technology). As firms take on new practice areas or industries, models encounter unfamiliar contract types and terminology. Models must adapt to these new domains or risk misinterpretation.

**Firm-specific preferences and templates.** Law firms develop their own templates, preferred language, and risk tolerances. What one firm considers standard, another considers risky. A contract review system must learn firm-specific preferences to provide useful guidance. As firm preferences evolve (new partners, changed risk appetite, client feedback), models must adapt.

**Technology and business model changes.** New technologies and business models create new legal issues requiring new contract provisions. Cloud computing created data processing agreements. Cryptocurrency created digital asset clauses. AI created AI liability and IP provisions. Gig economy created independent contractor agreements. Models must continuously learn new contract types and provisions as business evolves.

**Key Point 32.1.** *For the generic drift detection and continuous learning framework, see Chapter 24, Section 24.7. Legal AI faces slower drift than consumer domains (law changes over months/years) but demands near-perfect accuracy due to professional liability.*

Key legal-specific strategies beyond the generic framework include:

- **Incremental updates for legal changes:** When significant legislation or court decisions occur, add explicit rules for new requirements and update retrieval databases without waiting for full retraining.
- **Hybrid learned + rule-based systems:** Combine learned models (pattern recognition, semantic analysis) with rule-based components (jurisdiction-specific requirements, regulatory mandates) that can be updated rapidly when law changes.
- **Retrieval-augmented generation:** Prevent hallucination of non-existent cases by requiring retrieval from an up-to-date case/statute database before generating responses.
- **Jurisdiction and practice area specialization:** Train separate models per jurisdiction and practice area (e.g. California employment, New York corporate) for higher accuracy and easier targeted updates.



- **Conservative deployment:** Start on low-risk cases (simple NDAs, routine contracts) and expand to higher-risk matters only after extensive validation, never deploying to complex litigation without thorough vetting.

## 32.9 Exercises

**Exercise 32.1.** Extract key terms from a contract: parties, effective date, payment terms, termination conditions, liability caps. Compare extraction accuracy to human-annotated labels.

**Exercise 32.2.** Build a clause classification system. Train a model to identify clause types (payment, termination, indemnification, confidentiality). Evaluate precision and recall.

**Exercise 32.3.** Design a legal research system. Given a legal question, retrieve relevant statutes and cases from a database. Rank by relevance and recency. Compare to online legal research tools (LexisNexis, Westlaw).

## 32.10 Solutions

Full solutions for all exercises are available at <https://deeplearning.hofkensvermeulen.be>.

## Chapter 33

# Data, Logs, and Observability: Models for Infrastructure and Operations

### Chapter Overview

Modern digital infrastructure generates an overwhelming torrent of data. A typical enterprise with 10,000 servers produces 10 billion log messages daily, 100 million metric data points hourly, and millions of distributed traces. This machine-generated data—logs, metrics, traces, configurations—forms a rich language describing system behavior, health, and failures. However, the volume far exceeds human capacity to analyze. A single on-call engineer cannot manually review billions of events to diagnose why a service failed at 3am.

The business stakes are enormous. System downtime costs enterprises \$5,600 per minute on average, with major outages costing millions per hour. Amazon loses \$220,000 per minute of downtime. Facebook loses \$90,000 per minute. Beyond direct revenue loss, downtime damages customer trust, violates SLAs (triggering financial penalties), and consumes engineering time in firefighting rather than feature development. For SaaS companies, reliability is a competitive differentiator—99.9% uptime (8.7 hours downtime annually) versus 99.99% uptime (52 minutes annually) can determine market leadership.

This chapter examines how transformers and deep learning are revolutionizing observability—the ability to understand system behavior from external outputs. Traditional monitoring relies on static thresholds and manual analysis, generating alert fatigue (hundreds of false alarms daily) while missing subtle failures. AI-powered observability enables: anomaly detection that adapts to changing baselines, root-cause analysis that diagnoses failures in minutes rather than hours, and automated remediation that fixes common problems without human intervention.

The business impact is measurable and substantial. Companies implementing AI-driven observability report 50-70% reduction in mean time to resolution (MTTR), 60-80% reduction in false positive alerts, and 30-50% reduction in on-call engineer workload. For a large enterprise, reducing MTTR from 30 minutes to 10 minutes saves millions annually in prevented downtime. Reducing false positives from 100 to 20 daily alerts prevents alert fatigue and improves engineer quality of life. Automating 40% of incident responses frees engineers to focus on strategic work rather than repetitive firefighting.

However, observability AI faces unique challenges. Systems must operate in real-time with sub-minute latency—slow anomaly detection means prolonged outages. False positives are costly—waking engineers at 3am for non-issues causes burnout and erodes trust. False negatives are catastrophic—missing critical failures causes extended outages. The data is massive, noisy, and constantly changing as systems evolve. And critically, observability systems must be more reliable than the systems they monitor—if the monitoring system fails during an outage, engineers are blind.

This chapter provides the technical foundation and business context to build observability AI systems that detect, diagnose, and remediate infrastructure failures. We examine successful deployments, operational requirements, and the economic models that make observability AI essential for modern infrastructure. The focus is on practical systems that work in production at scale, handling billions of events daily while maintaining engineer trust.

## Learning Objectives

1. Understand machine data: logs, metrics, traces, configurations
2. Parse semi-structured logs with variable formats
3. Build anomaly detection models for multi-dimensional time series (metrics)
4. Implement root-cause analysis using sequence models
5. Automate incident response and remediation
6. Design closed-loop systems: detect → diagnose → remediate → learn
7. Optimize for operational metrics: false positive rate, MTTR, accuracy of diagnostics

### 33.1 Machine Data as a Language

Machine data consists of events generated by software and hardware:

#### 33.1.1 Types of Machine Data

**Definition 33.1** (Machine Data Types). Machine data consists of several distinct types, each providing different insights into system behavior. Logs are unstructured or semi-structured text messages emitted by applications, capturing events, errors, and state changes—for example: `[ERROR] Connection timeout after 5000ms to database.example.com:5432`. Metrics are numeric time series tracking system health indicators like CPU usage, memory consumption, latency, and request counts, typically sampled at 1-minute or 1-hour granularity. Traces provide detailed request flows through distributed services, recording timestamps, service names, durations, and parent-child relationships between service calls. Events capture discrete occurrences such as deployments, configuration changes, and scaling operations, often accompanied by structured metadata. Configurations describe system state including service versions, feature flags, and environment variables, typically stored as text or structured formats like JSON or YAML.

#### 33.1.2 Machine Language Grammar

Machine data has structure, though not formal grammar:

Machine data exhibits structural patterns despite lacking formal grammar. Log templates follow consistent patterns where multiple logs share the same structure, typically formatted as `[LEVEL] Message with parameters`. Metric names use hierarchical naming conventions like `system.cpu.usage` or `app.request.latency`, enabling organized aggregation and querying. Trace structure forms directed acyclic graphs (DAGs) of service calls with associated timings, revealing request paths through distributed systems. Event sequences follow causal chains where actions trigger consequences—for example, a deployment leads to configuration updates, which trigger service restarts, culminating in system recovery.

#### 33.1.3 Data Collection and Storage

Production systems generate massive amounts of data:

Production systems generate massive volumes of data that challenge traditional analysis approaches. A single server typically generates 100-1,000 log messages per second during normal operation. Scaling to datacenter level, a facility with 10,000 servers produces 1-10 billion events per second, creating petabytes of data annually. Specialized databases handle this ingestion: Elasticsearch for logs, Prometheus for metrics, and Jaeger for traces. Retention policies typically maintain 3-30 days of detailed data for operational analysis, with historical data archived to cheaper storage for compliance requirements and long-term research.

## 33.2 Anomaly Detection

Most events are normal. A model trained on normal data learns baseline behavior; deviations are anomalies.

### 33.2.1 Metric Anomaly Detection

A metric time series (e.g., CPU usage over time) has structure:

$$\text{metric}(t) = \text{baseline} + \text{seasonality} + \text{trend} + \text{noise} \quad (33.1)$$

**Baseline:** Normal operating level (e.g., CPU averages 40%)

**Seasonality:** Predictable patterns (e.g., higher traffic 9am–5pm)

**Trend:** Long-term changes (e.g., growing traffic week-over-week)

**Anomaly:** Deviation from expected pattern (e.g., CPU spikes to 95% unexpectedly)

### Traditional Approaches

Traditional anomaly detection approaches vary in sophistication and effectiveness. Static thresholds provide the simplest approach—alerting when CPU exceeds 80

### Deep Learning Approaches

Transformers excel at multi-step prediction:

- Definition 33.2** (Transformer-Based Anomaly Detection).
1. **Input:** Metric values for past  $H$  hours (e.g., 24 hours)
  2. **Prediction:** Predict next hour's value given history
  3. **Anomaly:** If actual value differs significantly from prediction, it's anomalous
  4. **Advantage:** Model learns complex temporal patterns including seasonality and trend

### 33.2.2 Multivariate Anomaly Detection

Most alerts involve multiple metrics. CPU spike alone might be normal; CPU spike + disk I/O spike + context switch spike together indicate problem.

Multivariate anomaly detection recognizes that most meaningful alerts involve correlations across multiple metrics. While a CPU spike alone might represent normal burst activity, the combination of CPU spike, disk I/O surge, and elevated context switches together indicates a genuine problem. Univariate approaches analyze each metric independently, missing these critical correlations. Multivariate approaches learn the correlation matrix and joint distributions across all metrics, enabling detection of anomalous patterns that only emerge when considering multiple signals together.

A transformer encoder processes all metrics jointly, learning correlations:

$$\text{anomaly\_score} = \sum_{i=1}^N ||\text{actual}_i - \text{predicted}_i|| \quad (33.2)$$

Multivariate detection is more accurate but requires more data (training on normal behavior across all combinations).

### 33.2.3 Practical Challenges

Several practical challenges complicate anomaly detection in production. False positives from legitimate operational events—deployments, scheduled backups, batch jobs—trigger alerts that waste engineering time and erode trust in the monitoring system. Tuning thresholds to balance sensitivity (catching real problems) and specificity (avoiding false alarms) proves difficult and requires continuous adjustment. Data quality issues including missing values from sensor failures, measurement errors, and incomplete distributed traces confuse models and degrade accuracy. Concept drift occurs as system behavior evolves over time with growing user bases, architectural changes, and new deployment patterns, causing models trained on historical data to become stale and inaccurate. Alert fatigue results when excessive alerts desensitize on-call engineers, leading them to ignore or dismiss notifications—a dangerous situation where critical alerts may be missed among the noise.

## 33.3 Root-Cause Analysis and Diagnosis

Detecting an anomaly is step one. Diagnosing the cause is step two. A model can:

Root-cause analysis models perform several key functions to diagnose detected anomalies. They retrieve similar historical incidents from the incident database, leveraging past resolutions to inform current diagnosis. They identify temporal relationships between metric changes, distinguishing symptoms from root causes by determining which metrics changed first in the causal chain. They correlate anomalies with operational events like deployments and configuration changes, suggesting likely causes based on temporal proximity. Finally, they generate causal hypotheses ranked by likelihood, providing engineers with actionable starting points for investigation.

### 33.3.1 Architecture for RCA

1. **Anomaly detection:** Identify unusual pattern
2. **Signal correlation:** Which metrics changed together? In what order?
3. **Timeline:** Build timeline of events (metrics, logs, config changes)
4. **Similar incidents:** Retrieve similar past incidents from database
5. **Hypothesis generation:** Propose likely causes
6. **Explanation:** Generate human-readable explanation

### 33.3.2 Example: API Latency Spike

**Observed:** API latency jumped from 50ms to 500ms at 2am.

**RCA Process:**

1. Anomaly detected: Latency  $\uparrow$  3x baseline
2. Correlations: Database CPU also spiked; query count unchanged
3. Timeline: Database CPU spike occurred 2 minutes before latency spike
4. Hypothesis 1: Slow database queries (query count normal, but duration increased)
5. Investigation: Check slow query log  $\rightarrow$  Find expensive query running
6. Root cause: A data migration job ran at 2am, locking tables
7. Remediation: Kill migration job; reschedule for lower-traffic time

A system that automates this diagnosis reduces MTTR from 30 minutes (human detective work) to 2 minutes (system analysis + human confirmation).

## 33.4 Incident Automation and Remediation

Beyond diagnosis, systems can automatically remediate common incidents. Automated actions include restarting unhealthy services when health checks fail three consecutive times, scaling up by adding servers when CPU exceeds 80

### 33.4.1 Safety in Automated Remediation

Automated actions must incorporate multiple safety mechanisms. Conservative decision-making ensures actions are only taken when diagnosis confidence is high. Reversibility requires that all automated actions can be easily undone—restarting services is safe, but deleting data is not. Bounded execution limits the frequency of actions, preventing repeated restarts that could worsen problems. Human oversight provides notification before action execution, allowing cancellation within a grace period. Comprehensive audit logs record all automated actions for post-incident review and continuous improvement.

## 33.5 Log Parsing and Understanding

Logs are semi-structured: same template with variable values. Example:

```
[2024-01-30 10:23:45] [ERROR] Connection timeout to user_service:8080 after 5000ms
[2024-01-30 10:23:46] [ERROR] Connection timeout to user_service:8080 after 5000ms
[2024-01-30 10:23:47] [ERROR] Connection timeout to user_service:8080 after 5000ms
```

Log template: [TIME] [LEVEL] Connection timeout to HOST:PORT after {DURATION}ms

### 33.5.1 Log Parsing Models

Neural models can parse logs:

1. **Tokenization:** Split log into tokens
2. **Classification:** Each token is a constant or variable (e.g., “timeout” is constant; “5000” is variable)
3. **Template extraction:** Infer template from multiple logs
4. **Clustering:** Group logs by template; identify new template types

### 33.5.2 Anomalous Log Detection

A model can flag unusual logs:

1. Encode log as sequence of tokens
2. Compute probability under learned language model
3. Flag logs with very low probability (likely anomalous)

Example: [ERROR] Connection timeout to user\_service:999 after -5000ms  
This is anomalous (negative duration) and would have low probability.

## 33.6 Configuration and Policy Compliance

Infrastructure configuration models provide several capabilities. They parse and understand configurations, extracting what systems declare about desired state. They perform policy compliance checks, verifying that configurations adhere to organizational policies such as replica limits for cost control. They suggest improvements aligned with best practices, recommending additions like health checks, resource limits, and proper labeling.

### 33.6.1 Configuration Language Models

Configuration language models fine-tuned on infrastructure code provide intelligent assistance. They suggest missing configurations that improve reliability and observability, such as health checks, resource limits, and metadata labels. They detect risky patterns including overly permissive security groups, missing backup configurations, and single points of failure. They propose refactoring opportunities to deduplicate code, extract reusable modules, and improve maintainability.

## 33.7 AIOps: AI-Powered IT Operations (2024-2025)

AIOps (Artificial Intelligence for IT Operations) has emerged as a comprehensive framework for applying AI and machine learning to IT operations, moving beyond isolated anomaly detection to integrated, intelligent operations management. As of 2024-2025, AIOps platforms have matured significantly, incorporating advances in causal inference, automated remediation, and predictive maintenance.

### 33.7.1 AIOps Platform Architecture

Modern AIOps platforms integrate multiple AI capabilities into unified systems. Data ingestion and correlation collects and correlates data from multiple sources—metrics, logs, traces, events, configurations, and tickets—in real-time, building a unified timeline of system state and changes. Intelligent anomaly detection performs multi-signal analysis that correlates anomalies across different data types, reducing false positives by 60-80% compared to single-signal detection through context-aware analysis. Causal inference for root cause analysis uses advanced methods to distinguish correlation from causation, determining whether metric A causes metric B, B causes A, or both are caused by a hidden factor C through causal graphs and do-calculus. Predictive failure detection identifies early warning signs hours or days before complete failure by training machine learning models on historical failure patterns to recognize precursor signals like gradual memory leaks, increasing error rates, and degrading performance. Automated remediation and self-healing automatically executes remediation actions for common failure patterns, including restarting unhealthy services, scaling resources, rerouting traffic, and rolling back deployments, while implementing safety constraints to prevent automated actions from causing additional problems. Incident management and collaboration integrates with systems like PagerDuty and ServiceNow to automatically create tickets, assign to appropriate teams, suggest runbooks, track resolution, and provide collaboration tools for distributed teams responding to incidents.

### 33.7.2 Causal Inference for Root Cause Analysis

Traditional RCA relies on correlation—if metric A and metric B change together, assume relationship. However, correlation doesn't imply causation. Causal inference methods provide more accurate diagnosis:

**Causal graph construction:** Build directed acyclic graph (DAG) representing causal relationships between system components. Nodes are services, metrics, or resources. Edges represent causal dependencies (service A calls service B, CPU affects latency).

**Causal discovery algorithms:** Automatically learn causal graphs from observational data using algorithms like PC (Peter-Clark), FCI (Fast Causal Inference), or GES (Greedy Equivalence Search). These algorithms use conditional independence tests to infer causal structure.

**Interventional analysis:** When anomaly occurs, use causal graph to identify root causes through interventional reasoning. If intervening on metric A would fix metric B, then A is likely causing B. This is formalized through do-calculus and counterfactual reasoning.

**Example:** API latency spike occurs. Correlation analysis shows database CPU also spiked. Causal analysis determines: (1) Database CPU spike occurred 2 minutes before API latency spike (temporal precedence), (2) API latency is conditionally dependent on database CPU given other factors (statistical dependence), (3) Intervening on database CPU (reducing load) would fix API latency (interventional test). Conclusion: Database CPU is root cause. Action: Investigate database queries, find expensive query, optimize or kill it.

### 33.7.3 Predictive Failure Detection and Preventive Maintenance

Rather than reacting to failures, predict and prevent them:

Failure precursor detection trains models on historical failure data to identify patterns that precede failures. Common precursors include gradual memory leaks where memory usage increases 1% daily over weeks, increasing error rates that grow from 0.1% to 0.5% over days, degrading performance with latency increasing 10% weekly, and resource exhaustion trends as disk usage approaches 90%.

**Time-to-failure prediction:** Predict not just that failure will occur, but when. This enables scheduling maintenance during low-traffic periods rather than emergency response during peak hours. Use survival analysis and time-series forecasting to estimate time-to-failure distributions.

**Preventive actions:** When failure is predicted with high confidence and sufficient lead time, take preventive actions:

- Schedule maintenance window for service restart
- Gradually drain traffic from at-risk instances
- Provision additional capacity before resource exhaustion
- Alert teams to investigate and fix underlying issues

**Implementation Considerations:** Predictive models require careful calibration. False positives (predicting failures that don't occur) waste resources on unnecessary maintenance. False negatives (missing actual failures) defeat the purpose. Target 80-90% precision and 70-80% recall, with lead times of 4-24 hours for actionable predictions.

### 33.7.4 Automated Remediation and Self-Healing Systems

AIOps platforms increasingly incorporate automated remediation, moving from detection to resolution:

**Runbook automation:** Codify common remediation procedures as executable runbooks. When specific failure patterns are detected, automatically execute appropriate runbooks. Examples:

- Service health check failure → Restart service
- High CPU usage → Scale out (add instances)
- Disk space exhaustion → Clean up old logs
- Database connection pool exhaustion → Increase pool size

**Reinforcement learning for remediation:** Use reinforcement learning to learn optimal remediation strategies. The agent observes system state, takes actions (restart, scale, reroute), and receives rewards (system recovery, minimal disruption). Over time, the agent learns which actions work best for different failure scenarios.

**Safety constraints and human oversight:** Automated remediation must be safe:

- Whitelist of allowed actions (only safe, reversible actions)
- Rate limiting (max 1 restart per service per hour)
- Human approval for high-risk actions (database restarts, traffic rerouting)
- Automatic rollback if action makes situation worse
- Complete audit logs of all automated actions

**Adoption Challenges:** Engineers are often hesitant to trust automated remediation due to fear of automation causing additional problems. Gradual adoption is key: start with safest actions (service restarts), build trust through demonstrated reliability, gradually expand to more complex actions. Maintain human oversight and easy override mechanisms.



### 33.7.5 AIOps Platform Vendors and Ecosystem (2024-2025)

The AIOps market has matured significantly, with several established platforms:

#### Commercial platforms:

- **Datadog AIOps:** Integrated with Datadog's monitoring platform. Strong anomaly detection and correlation. \$500-5,000/month depending on scale.
- **Splunk IT Service Intelligence (ITSI):** Enterprise-focused. Advanced analytics and machine learning. \$10,000-100,000+/year.
- **Dynatrace Davis AI:** Automated root cause analysis and predictive analytics. Strong causal inference capabilities. \$5,000-50,000+/month.
- **Moogsoft:** Specializes in event correlation and noise reduction. Reduces alert volume by 90%. \$2,000-20,000/month.

#### Open-source and custom solutions:

- Many large tech companies (Google, Facebook, Amazon) build custom AIOps platforms tailored to their infrastructure
- Open-source components: Prometheus (metrics), Elasticsearch (logs), Jaeger (traces), Grafana (visualization)
- ML frameworks: TensorFlow, PyTorch for custom anomaly detection and RCA models

#### Selection criteria:

- Scale: Can platform handle your data volume (billions of events daily)?
- Integration: Does it integrate with your existing monitoring tools?
- Customization: Can you train custom models on your data?
- Cost: Total cost of ownership (licensing + infrastructure + personnel)
- Vendor lock-in: Can you migrate to alternative platforms if needed?

### 33.7.6 Future Directions and Research Frontiers

AIOps continues to evolve rapidly. Emerging trends as of 2024-2025:

**Large language models for operations:** Using LLMs (GPT-4, Claude) to understand natural language incident descriptions, generate remediation suggestions, and explain system behavior to engineers. Early results show 30-40% improvement in incident response time when engineers have LLM assistants.

**Federated learning for cross-organization insights:** Multiple organizations collaboratively train AIOps models without sharing sensitive data. This enables learning from broader failure patterns while preserving privacy. Particularly valuable for industry-specific platforms (healthcare, finance).

**Quantum-inspired optimization for resource allocation:** Using quantum-inspired algorithms to optimize resource allocation and capacity planning. Early research shows 10-20% improvement in resource utilization compared to classical optimization.

**Explainable AI for operations:** Improving interpretability of AIOps decisions. Engineers need to understand why the system flagged an anomaly or suggested a remediation. Research focuses on attention visualization, counterfactual explanations, and natural language generation for explanations.

## 33.8 Case Study: Intelligent Alerting and Incident Response

A SaaS company operates a large distributed system: 500 microservices, 10,000 servers. Manual monitoring is infeasible.

### 33.8.1 System Design

The system design handles massive scale with 10 billion events per day including logs, metrics, and traces. Storage uses specialized databases: Elasticsearch for logs, Prometheus for metrics, and Jaeger for traces. The models include an anomaly detector using a multivariate transformer on key metrics, an RCA engine that correlates metrics and queries logs to match similar incidents, and a recommendation engine that suggests fixes based on diagnosis.

### 33.8.2 Workflow

1. System detects anomaly in real-time
2. RCA engine analyzes metrics and logs
3. System generates incident summary: “API latency spike in payment service. Database CPU also elevated. Similar to 3 prior incidents.”
4. Suggested actions: “Restart payment service or check database slow query log”
5. On-call engineer reviews suggestion; approves auto-restart
6. Incident resolved in 2 minutes (vs. 30 minutes manual detective work)

### 33.8.3 Results

Performance metrics demonstrate the system’s effectiveness. Detection latency averages 2 minutes, faster than humans typically notice issues. MTTR is reduced to 5 minutes with auto-remediation compared to 30 minutes for manual resolution. The false positive rate is 5

Business impact is substantial across multiple dimensions. Uptime improved from 99.98

## 33.9 Model Maintenance and Drift in Observability Systems

Observability AI systems face a paradoxical drift challenge: they must monitor systems that are constantly evolving while themselves remaining stable and reliable. Infrastructure changes continuously—new services are deployed, traffic patterns shift, hardware is upgraded, and architectures evolve. Each change alters the “normal” behavior that anomaly detection models learn, causing drift. Yet observability systems cannot afford frequent retraining downtime or accuracy degradation—they must remain operational 24/7, detecting anomalies even as the definition of “normal” changes.

The business consequences of observability drift are severe and immediate. When anomaly detection models drift, two problems occur simultaneously: (1) False positives increase—normal behavior is flagged as anomalous, generating alert fatigue and eroding engineer trust, (2) False negatives increase—actual failures go undetected, causing prolonged outages and revenue loss. A 10% increase in false positives might generate 50 additional false alerts daily, waking on-call engineers unnecessarily and causing burnout. A 10% increase in false negatives might miss 2-3 critical incidents monthly, each costing \$100K-1M in downtime.

The challenge is compounded by the meta-monitoring problem: observability systems monitor other systems, but who monitors the observability system? If the anomaly detector itself fails or drifts during an outage, engineers lose visibility precisely when they need it most. This creates a requirement for extreme reliability—observability systems must be more reliable than the systems they monitor, typically targeting 99.99%+ uptime and <1% error rates.

### 33.9.1 Domain-Specific Drift Patterns in Observability

Observability drift manifests in several distinct ways, each requiring different detection and mitigation strategies:

**Infrastructure evolution and service changes.** Modern infrastructure evolves rapidly through continuous deployment. New services are added, old services are deprecated, service dependencies

change, and architectures are refactored. Each change alters system behavior and the patterns that anomaly detection models have learned. A model trained when the system had 300 services may perform poorly when it has 500 services with different interaction patterns.

**Example:** A company migrates from monolithic architecture to microservices over 6 months. The monolith had predictable resource usage patterns. Microservices have different patterns—more network traffic, different latency distributions, cascading failures. Anomaly detection models trained on monolith data generate thousands of false positives on microservices, causing alert fatigue. Models require complete retraining on microservices data.

**Traffic pattern drift and load changes.** User traffic patterns change over time due to business growth, seasonal variations, marketing campaigns, and user behavior evolution. A model trained when daily traffic was 1M requests may consider 2M requests anomalous, even though it's normal growth. Seasonal patterns shift—holiday traffic, back-to-school, tax season. Marketing campaigns create sudden traffic spikes that look like attacks but are legitimate.

**Example:** E-commerce platform experiences 10x traffic spike during Black Friday. Anomaly detection models trained on normal traffic flag this as attack, triggering rate limiting that blocks legitimate customers. Models must learn that Black Friday traffic patterns are normal, not anomalous. This requires either seasonal models or adaptive baselines that adjust to traffic growth.

**Deployment and configuration drift.** Every deployment changes system behavior slightly. New code has different performance characteristics, resource usage, and failure modes. Configuration changes (feature flags, scaling parameters, database settings) alter behavior. Models must distinguish between expected changes from deployments and unexpected failures.

The challenge is that deployments sometimes introduce bugs that cause failures. Models must detect deployment-related failures while not flagging every deployment as anomalous. This requires understanding deployment context—if latency increases after deployment, it might be a bug; if it increases randomly, it's likely a failure.

**Hardware and infrastructure drift.** Hardware ages and degrades. Disks slow down, network cards fail intermittently, CPUs throttle due to heat. Cloud providers change instance types, network configurations, and availability zones. These hardware changes alter performance characteristics that models have learned. A model trained on fast SSDs may consider slow HDD performance anomalous, even though HDDs are now the standard.

**Monitoring system changes.** The observability infrastructure itself evolves. Metrics are added, removed, or renamed. Log formats change. Sampling rates adjust. Monitoring agents are upgraded. Each change affects the data that models consume, potentially causing drift. A model trained on one log format may fail when log format changes.

**Example:** Company upgrades logging library, changing log format from plain text to JSON. Log parsing models trained on plain text fail completely on JSON logs. Models require immediate retraining or format-agnostic parsing.

**Concept drift in failure patterns.** Failure modes evolve as systems mature. Early in a system's life, failures are often configuration errors or resource exhaustion. As the system matures, failures become more subtle—race conditions, memory leaks, cascading failures. Models trained on early failures may not recognize mature failure patterns.

**Alert fatigue and threshold drift.** As engineers respond to alerts, they adjust thresholds to reduce false positives. This threshold drift changes what the system considers anomalous. Additionally, engineers become desensitized to frequent alerts (alert fatigue), effectively raising their personal threshold for action. Models must adapt to these changing expectations.

**Key Point 33.1.** *For the generic drift detection and continuous learning framework, see Chapter 24, Section 24.7. Observability systems face a meta-monitoring paradox: they must remain reliable 24/7 while adapting to constantly evolving infrastructure.*

Key observability-specific strategies beyond the generic framework include:

- **Online learning with conservative updates:** Use exponential moving averages (e.g. decay

factor 0.95) for baselines, allowing gradual adaptation to traffic growth while resisting sudden anomalous spikes.

- **Deployment-aware anomaly detection:** Integrate CI/CD deployment events to temporarily relax thresholds during expected change windows, reducing false positives from legitimate deployments.
- **Multi-signal correlation:** Correlate metrics, logs, traces, and deployment events rather than analyzing signals in isolation—multi-signal anomalies are far more likely to be real issues, reducing false positives by 50–70%.
- **Synthetic incident injection:** Inject synthetic failures in test environments to verify detection systems catch them—analogue to fire drills for monitoring infrastructure.
- **Adaptive percentile-based thresholds:** Use percentile thresholds (e.g. alert if metric exceeds 99th percentile of recent values) rather than absolute thresholds, automatically adjusting to growth and seasonal patterns.

## 33.10 Exercises

**Exercise 33.1.** Build an anomaly detection model for a metric time series (e.g., CPU usage, request latency). Use a transformer to predict next hour's value. Evaluate on test set with known anomalies. What is the false positive rate at different thresholds?

**Exercise 33.2.** Parse a corpus of application logs. Extract templates using a neural model. Identify new log types not in training. How well does the model generalize to unseen log types?

**Exercise 33.3.** Design a root-cause analysis system. Given an anomaly and historical incident database, retrieve similar incidents and suggest likely causes. Evaluate on test set of real incidents.

## 33.11 Solutions

Full solutions for all exercises are available at <https://deeplearning.hofkensvermeulen.be>.

## Chapter 34

# Domain-Specific Languages, Tools, and Agents

### Chapter Overview

This concluding chapter synthesizes the domain-specific applications explored throughout this book into a unified framework for building production AI systems. Across healthcare, finance, legal, recommendations, visual content, and observability, we observe recurring patterns: domains are formalized into structured representations, models learn to operate within these formalizations, and systems integrate models with tools to achieve business objectives. Understanding these patterns enables practitioners to systematically approach new domains rather than reinventing solutions.

The business imperative is clear. Organizations that successfully deploy domain-specific AI systems achieve measurable competitive advantages: 50-70% cost reductions (legal contract review, healthcare documentation), 10-30% revenue increases (recommendations, fraud detection), and 40-60% efficiency gains (observability, visual content creation). However, success requires more than technical capability—it demands understanding domain constraints, managing model drift, balancing accuracy with explainability, and navigating regulatory requirements. The patterns synthesized in this chapter provide a reusable playbook for these challenges.

This chapter examines the world-to-language-to-tool pattern that underlies successful AI deployments, explores how to design domain-specific languages that enable reliable model-system integration, and investigates tool-augmented agents that orchestrate complex workflows. We synthesize drift management patterns across domains, compare accuracy-cost-latency trade-offs, and provide a practical framework for building domain-specific systems from requirements through deployment.

The stakes extend beyond individual applications to the future of AI deployment. As AI systems become more capable, they will increasingly operate as autonomous agents—perceiving environments, making decisions, and taking actions to achieve goals. These agents will need robust domain formalizations, reliable tool integration, and continuous adaptation to changing conditions. The patterns established in this chapter provide the foundation for this agent-driven future while remaining grounded in today's practical deployment realities.

### Learning Objectives

1. Understand the general pattern of DSLs in deep learning applications
2. Design and formalize domain-specific languages for your application
3. Build tool-augmented language models that call APIs, databases, and calculators
4. Implement agents that plan and execute multi-step workflows
5. Design structured outputs (JSON, XML) for reliable model-to-system integration
6. Evaluate tool use, agent plans, and error recovery

7. Understand trade-offs between model capability and system reliability

## 34.1 The World-to-Language-to-Tool Pattern

Across domains, a consistent pattern emerges:

1. **World:** Messy, unstructured reality. Customer support tickets with varied formats. Code repositories with inconsistent styles. Video files with varying codecs and metadata.
2. **Formalization:** Transform the world into a DSL. Ticket schemas define fields (customer ID, issue type, priority, description). Event schemas standardize user interactions. Log formats structure machine events.
3. **Models learn DSLs:** Deep learning models trained on domain data learn to understand and generate within the formalized language.
4. **Tools operate on DSL:** Systems downstream of the model (databases, APIs, business logic) operate on the formalized language. Because the model outputs adhere to the DSL, tools can process outputs reliably.

**Definition 34.1** (World-Language-Tool Pattern). The most successful applications of deep learning to real domains follow this pattern:

1. Identify the core data representation in your domain
2. Formalize it into an explicit DSL (schema, grammar, format)
3. Train models on domain data to master the DSL
4. Build tools that operate on the DSL, providing model feedback and enabling automation
5. Iterate: improve DSL clarity based on model mistakes; improve models based on tool feedback

## 34.2 Designing Domain-Specific Languages

A well-designed DSL makes models easier to train and systems easier to build. Poor DSL design leads to model confusion and system brittleness.

### 34.2.1 Case Example: Support Ticket DSL

**Poor DSL (unstructured):**

```
{
  "text": "I can't login to my account. Tried resetting password
          but didn't receive the email. My email is johndoe@example.com.
          Account created 6 months ago. Very frustrated!"
}
```

A model must extract key information from unstructured text, error-prone.

**Better DSL (structured):**

```
{
  "customer_id": "123456",
  "issue_type": "authentication",
```

```

"severity": "high",
"description": "Cannot login; password reset email not received",
"email": "johndoe@example.com",
"account_age_days": 180,
"previous_interactions": 2,
"sentiment": "negative"
}

```

Structured DSL reduces model ambiguity. Models learn to extract and classify information reliably. Downstream tools (routing, priority assignment) consume structured data.

### 34.2.2 DSL Design Principles

DSL design follows several key principles. Clarity requires that every field be unambiguous, avoiding free-text fields where discrete categories exist. Completeness demands including all information relevant to the task, as missing fields create ambiguity that degrades model performance. Consistency enforces uniform types and units across examples—all dates in ISO 8601 format, all sizes in bytes, all currencies explicitly specified. Expandability designs for future extensions through versioning or optional fields, preventing breaking changes as requirements evolve. Human readability ensures that humans can understand the DSL format (JSON, YAML, structured text) for debugging, annotation, and quality assurance.

### 34.2.3 Formal DSL Specification

For complex domains, define the DSL formally using schemas:

**JSON Schema example:**

```

{
  "$schema": "http://json-schema.org/draft-07/schema#",
  "type": "object",
  "properties": {
    "issue_type": {
      "enum": ["billing", "technical", "account", "other"]
    },
    "severity": {
      "enum": ["low", "medium", "high", "critical"],
      "description": "Impact on customer operations"
    },
    "description": {
      "type": "string",
      "maxLength": 500,
      "description": "Concise description of the issue"
    }
  },
  "required": ["issue_type", "description"]
}

```

Formal specification enables several critical capabilities. Validation checks that model outputs conform to schema before use, preventing malformed data from reaching downstream systems. Code generation automatically produces parsing and serialization code from schema definitions, ensuring consistency between specification and implementation. Documentation uses the schema as the authoritative specification for data handling, reducing ambiguity and miscommunication. Testing generates comprehensive test cases covering all schema types and edge cases, improving system robustness.

### 34.3 Tool-Augmented Models

Large language models are powerful but limited. They hallucinate facts, struggle with math, and cannot access real-time information. Tool augmentation addresses these limitations by enabling models to call external systems.

#### 34.3.1 Tool Calling Architecture

A tool-augmented model has two components:

1. **Model (decision-maker):** A language model decides when and how to call tools
2. **Tools (executors):** External systems that perform actions (database lookups, API calls, computations)

Workflow:

1. User query: “What is the refund status of order 12345?”
2. Model generates: Tool call: `lookup_order(order_id=12345)`
3. System executes tool: Returns `{status: refunded, amount: $50, timestamp: 2024-01-15}`
4. Model generates response: “Your refund of \$50 was processed on January 15, 2024.”

#### 34.3.2 Function Calling in Modern LLMs

Modern APIs (OpenAI’s function calling, Anthropic’s tool use) formalize this. Models are provided with a tool schema:

```
{
  "name": "lookup_order",
  "description": "Retrieve order details by ID",
  "parameters": {
    "type": "object",
    "properties": {
      "order_id": {
        "type": "string",
        "description": "Order identifier"
      }
    }
  },
  "required": ["order_id"]
}
```

The model learns to produce outputs like:

Tool call: `lookup_order(order_id="12345")`

The system parses this, executes the tool, and returns results to the model for the next step.

#### 34.3.3 Tool Selection and Chaining

With multiple tools available, the model must select appropriate tools and chain them:

1. “What is the weather in Berlin tomorrow?”
2. Model calls: `get_weather(location=Berlin, days_ahead=1)`



3. System returns: {temperature: 5C, condition: rainy}
4. Model generates: “It will be rainy and 5 degrees Celsius tomorrow in Berlin.”

More complex example:

1. “Show me orders from customers in California last month.”
2. Model calls: `search_customers(state=California) → [customer_id1, customer_id2, ...]`
3. For each customer, calls: `get_orders(customer_id=..., month=last_month) → [order1, order2, ...]`
4. Aggregates results and generates summary

The model learns to decompose queries into tool calls and orchestrate them.

### 34.3.4 Reliability and Error Handling

Tool-augmented systems must handle errors gracefully through several mechanisms. Tool failures occur when APIs return errors such as customer not found or timeout—the model should acknowledge the failure and offer alternatives. Invalid parameters happen when the model generates tool calls with missing or incorrect parameters—validation catches these errors and prompts the model to retry with corrections. Hallucinated tools arise when the model calls non-existent tools—the system should list available tools and allow the model to try again. Infinite loops occur when the model repeatedly calls the same tool without making progress—implementing call limits and loop detection prevents this failure mode.

## 34.4 Agents and Workflow Orchestration

An agent is an autonomous system that perceives its environment, makes decisions, and takes actions to achieve goals. In the context of deep learning, an agent uses a language model to decide actions, tools to execute, and a planning loop to manage multi-step workflows.

### 34.4.1 Agent Loop

---

#### Algorithm 16: Agent Decision Loop

---

1. **Initialize:** Given user goal and available tools
  2. **Loop:**
    - (a) Model reads current state (user goal, previous actions, results)
    - (b) Model thinks: “What is the next action I should take?”
    - (c) Model decides: Calls a tool or generates response to user
    - (d) If tool call:
      - i. Execute tool, get result
      - ii. Append result to state
      - iii. Continue loop
    - (e) If response: Return to user, exit
  3. **Termination:** User goal achieved or max iterations exceeded
-

### 34.4.2 Planning and Reasoning

Advanced agents plan before executing. Chain-of-thought prompting helps:

Goal: Find the best laptop for a developer under \$2000

Thinking:

1. I need to understand developer needs: CPU, RAM, battery, build quality
2. I should search for laptops matching these criteria
3. I need to compare options and recommend the best

Actions:

- Tool: `get_laptop_specs(type="developer", max_price=2000)`  
Result: [Laptop A, Laptop B, Laptop C]
- Tool: `compare_laptops(laptop_ids=[A, B, C])`  
Result: Detailed comparison
- Response: Based on comparison, Laptop A is best because...

Planning increases accuracy and transparency. Users understand the agent's reasoning, improving trust.

### 34.4.3 Memory and State Management

Agents require memory across interactions to maintain context and continuity. State management includes several components. Interaction history tracks previous queries, actions, and results, enabling the agent to reference past conversations and avoid repeating work. User preferences learned from past interactions allow personalization and improved recommendations. Task progress tracking is essential for multi-step workflows that may span hours or days, requiring checkpoints to resume interrupted work.

Long-term memory requires careful management to remain effective. Summarizing old history prevents token explosion as conversations grow lengthy. Retrieving relevant past interactions through semantic search ensures important context is available when needed. Using structured state storage in databases rather than relying solely on the context window enables scalable memory management for production systems.

## 34.5 Structured Output and Validation

Models can generate free-form text, but for integration with systems, structured outputs are essential. Modern approaches:

### 34.5.1 JSON Output Mode

Some models support JSON output mode: model generates only valid JSON:

System prompt: You must output valid JSON matching this schema: {...}

User: Extract person and age from "My name is Alice and I'm 30"

Model output:

```
{
  "person": "Alice",
  "age": 30
}
```

JSON mode ensures outputs are syntactically valid, but not semantically correct. Validation still checks correctness.

### 34.5.2 Semantic Validation

Beyond syntax, validate semantic correctness:

- **Type validation:** Age is an integer in range  $[0, 150]$
- **Consistency:** If order status is “cancelled,” refund amount should be nonzero
- **Logic validation:** If customer is VIP, discount should be  $\geq 10\%$

When validation fails, prompt the model to retry with explanation of the error.

## 34.6 Practical Design Framework

Here is a step-by-step framework for building domain-specific systems:

### 34.6.1 Step 1: Analyze the Domain

- What are the key entities? (orders, customers, products)
- What are the key relationships? (customer has orders, orders contain items)
- What are the key operations? (search, aggregate, transform)
- What are the typical workflows? (customer inquiries  $\rightarrow$  lookup  $\rightarrow$  respond)

### 34.6.2 Step 2: Design the DSL

- Identify core data representations
- Formalize as schema (JSON, Protobuf, custom grammar)
- Ensure clarity, consistency, and completeness
- Version the DSL for evolution

### 34.6.3 Step 3: Choose Model and Training Approach

- Fine-tune a pretrained foundation model vs. few-shot prompting vs. from-scratch training
- Collect and annotate domain training data
- Evaluate on domain-specific metrics, not generic benchmarks

### 34.6.4 Step 4: Integrate Tools and APIs

- Identify external systems (databases, APIs, services)
- Wrap tools with clear interfaces (name, description, parameters)
- Test tool invocation and error handling

### 34.6.5 Step 5: Implement Validation and Feedback

- Validate model outputs against schema
- Log failures for analysis and retraining
- Collect user feedback on system responses
- Retrain models on failures and feedback

### 34.6.6 Step 6: Evaluate and Deploy

- Offline evaluation on test set
- Online A/B testing with real users
- Monitor performance metrics in production
- Plan rollback if metrics degrade

## 34.7 Exercises

**Exercise 34.1.** Design a DSL for a restaurant reservation system. What entities, relationships, and operations are critical? Write a JSON schema for the core data types.

**Exercise 34.2.** Build a tool-augmented chatbot for a weather service. Tools: `get_weather(location, days_ahead)`, `get_hourly_forecast(location, date)`. Design the tool schemas. Implement the chatbot with proper error handling.

**Exercise 34.3.** Implement an agent loop for a personal expense tracker. The agent can: ask clarifying questions, retrieve past expenses, categorize new expenses, and summarize spending. What tools would the agent need?

## 34.8 Solutions

Full solutions for all exercises are available at <https://deeplearning.hofkensvermeulen.be>.

## 34.9 Conclusion and Future Directions

This chapter presented a general design pattern for applying deep learning to domain-specific problems. The pattern—world-formalization-language-tools—is not new to AI; it mirrors how humans solve problems by creating abstractions and tools. What is new is that deep learning models can now learn to operate effectively within these formal systems, bridging the gap between unstructured human communication and structured computational systems.

The landscape of deep learning applications will continue to expand as models grow more capable and tools become more integrated. Future directions include:

- **Multimodal agents:** Agents reasoning over text, images, and code simultaneously
- **Self-improving systems:** Agents that learn from interactions and improve autonomously
- **Federated DSL standards:** Industry standards for common domains (finance, healthcare, e-commerce)
- **Trustworthy agents:** Formal verification and safety guarantees for high-stakes domains
- **Energy efficiency:** Reducing computational requirements for model training and inference

We hope this book has provided both the theoretical foundations and practical insights needed to build the next generation of deep learning systems. The principles and techniques covered—transformers, attention, scaling, training, and deployment—are tools. The true skill lies in recognizing your domain, formalizing it into a language, and building systems that leverage models and tools to solve real problems.

## 34.10 Synthesis: Patterns Across Domains

Having explored domain-specific AI systems across healthcare, finance, legal, recommendations, visual content, and observability, we can now synthesize the key patterns. The universal themes—drift inevitability, the accuracy-cost-latency trade-off, human-in-the-loop necessity, and explainability requirements—manifest differently in each domain. Table 34.1 summarizes these variations.

Table 34.1: Cross-domain comparison of production AI characteristics.

Domain	Drift Pace	Retrain Cadence	Validation Rigor	Key Constraint
Healthcare	Quarterly	Quarterly–annual	Extreme (FDA)	Patient safety
Finance	Daily	Daily–weekly	High (regulatory)	Latency + adversarial
Legal	Episodic	Quarterly–semi-annual	Very high (liability)	Professional responsibility
Recommendations	Weekly	Daily–weekly	Moderate (A/B tests)	Scale + freshness
Visual Content	Monthly	Monthly–weekly	Moderate	Trend velocity
Observability	Continuous	Online + monthly	High (reliability)	24/7 uptime

Three universal principles emerge across all domains:

1. **Drift is inevitable, not exceptional.** Every production AI system degrades over time. Successful deployments plan for drift from deployment day, budgeting for detection, retraining pipelines, and continuous maintenance. The retraining frequency must match the domain’s drift pace while respecting its validation requirements.
2. **Human oversight remains essential.** The form varies—physician review of diagnoses, lawyer review of contract analysis, trader oversight of algorithmic decisions, product manager oversight of recommendation changes—but no high-stakes domain deploys AI without human judgment in the loop.
3. **Explainability is a business requirement, not a technical luxury.** Stakeholders across all domains demand explanations for AI decisions. Attention mechanisms, retrieval-augmented generation, ensemble confidence estimates, and rule-based components all serve this need. Black-box models fail to achieve adoption regardless of accuracy.

### 34.10.1 Future Directions

Looking forward, four trends will shape domain-specific AI: (1) **multi-domain agents** that operate across healthcare, finance, and legal simultaneously, requiring cross-domain drift management; (2) **federated learning** enabling cross-organizational training while maintaining privacy; (3) **automated governance** that monitors performance, detects drift, and maintains compliance at scale; and (4) **energy-efficient architectures** as sustainability concerns grow alongside model scale.